Weed control by biological compounds identified in necrotizing plant pathogenic fungi

Dissertation

zur Erlangung des Doktorgrades der Naturwissenschaften
(Dr. rer. nat.)

der

Naturwissenschaftlichen Fakultät II
Chemie, Physik und Mathematik

der Martin-Luther-Universität
Halle-Wittenberg

vorgelegt von

Frau Dipl.-LMChem. Lea Maleen Schmitz

This dissertation has been created under the supervision of Prof. Dr. René Csuk (Martin-Luther University Halle-Wittenberg) and mentorship of Dr. Norbert Arnold at Leibniz Institute of Plant Biochemistry Halle (Saale).

1st Reviewer: Prof. Dr. René Csuk

2nd Reviewer: Prof. Dr. Veronika Hellwig

Date of public defense: 12.11.2024

Weed control by biological compounds identified in necrotizing plant pathogenic fungi

Table of Contents

Acknowledgements

List of Abbreviations

Ces.	Cesati
Col-0	Columbia-0
CM	complete medium
COSY	correlation spectroscopy
d	doublet
dd	doublet of doublet
DAD	diode array detector
DF	delayed fluorescence
DKP	diketopiperazine
ECD	eletronic circular dichroism
ESI	electrospray ionisation
HMBC	heteronuclear multiple bond correlation
HMG	Hefeextrakt-Malzextrakt-Glucose
HRAC	herbicide resistance action committee
HRMS	high resolution mass spectrometry
HSQC	heteronuclear single quantum correlation
J	coupling constant
m	multiplet
MOA	mode of action
m/z	mass-to-charge-ratio
NMR	nuclear magnetic resonance
NTSR	non-target site resistance
P	peak number
PC	principal component
PLS-DA	partial least-squares discriminant analysis
PS	photosystem
QC	quality control
QSAR	quantitative structure-activity relationship
RDB	ring double bond equivalent
Rt	retention time
RP	reversed phase
s	singlet
t	triplet
TLC	thin-layer chromatography
TOF	time of flight
TSR	target site resistance
(U)HPLC	(ultra) high performance liquid chromatography
UV	ultraviolet

Summary

There is an urgent need for new bio-based herbicides, driven by factors such as growing world population, crop losses due to pests, increasing resistances and controversial discussions about the safety of synthetic herbicides. In this context, natural substances (phytotoxins) are of increasing interest. Natural products offer a rich reservoir of unknown substances with unique structural scaffolds. There are also prospects for the discovery of phytotoxins that attack previously unknown targets in plants. At the same time, it is already known that many phytotoxins have multiple modes of action, which impede the development of plant resistances. However, the physiochemical properties and phytotoxic efficiency of the compounds are often not ideal, so that synthetic modifications of the molecules are required.

Colletotrichum graminicola (Ces.) Wilson (teleomorph: *Glomerella graminicola*) is a species in the class Ascomycota and is the causative agent of leaf and stem anthracnose in maize. Anthracnose is characterized by sunken necrotic tissue and is caused by enzymes and secondary metabolites (phytotoxins) produced by the fungus.

The aim of this work was the activity-guided isolation and characterization of phytotoxins causing necrosis from cultures of *C. graminicola*. The fungal strain was grown in semi-solid cultures in two different complete media (CM and HMG). By combining different chromatographic separation techniques (TLC, HPLC, classical column chromatography), the compounds were isolated and subsequently characterized by different analytical methods (1D-NMR, 2D-NMR, HR-ESI-MS, ECD, X-ray). A total of 33 compounds was isolated and characterized. Among the isolated compounds were 11 previously undescribed or new-to-nature compounds, including 3-(6-hydroxy-2,6-dimethyloctanoyl)-5-methylpyrrolidin-2-one (**3.1a/b**), 5-(2,3-dihydroxypentyl)-5,6-dihydro-2H-pyran-2-one (**4.2**) and three hexanoic acid derivatives (**4.9, 4.11, 4.13**).The known compounds include diketopiperazines (**3.2, 3.4 – 3.9, 3.15, 4.8** and **4.10**), anthraquinones (**4.3, 4.5**) and acetamides (**3.3, 3.13 – 3.14**).

To test phytotoxic activity, two bioassays - a leaf spot assay and a leaf disk assay - were established. The leaf-spot assay on *Arabidopsis thaliana* Col-0 is a simple and rapid test for the phytotoxicity of fractions and pure substances and was used for the activity-guided isolation. For this assay, the fractions or isolated compounds are dissolved in a mixture of methanol and water (1:1, *v:v*) and applied directly to the leaf surface without prior wounding. After an incubation period of 24 - 72 h, the leaves can be examined for the development of necrosis or chlorosis. The evaluation of this assay was purely by visual means. With this assay, phytotoxic activity was observed for 21 of the 33 isolated compounds at concentrations between 10 and 100 mM.

The non-destructive leaf disk assay was originally developed to determine the resistance of plants to various herbicides. In this assay delayed fluorescence is measured, which is an indicator of the photosynthesis rate of plants. Photosynthesis reacts very sensitively to various stress factors and is therefore ideal for determining the phytotoxicity of substances. The main advantages of this assay are the short duration (48 hours) and the high sample throughput.

In addition, a quantitative structure-activity analysis (QSAR) was performed for one of the isolated compounds (*N*-(4-hydroxybutyl)benzenesulfonamide (**5.1**)). Based on the natural substance **5.1**, approximately 130 synthetic derivatives (syntheses carried out by Toni Denner, Institute of Chemistry - Organic Chemistry, Prof. Dr. Csuk, Martin Luther University Halle-Wittenberg) were tested for their phytotoxic activity. The evaluation was carried out using the non-destructive leaf disk assay. *A. thaliana* Col-0 (and *Secale cereale,* data not shown) were used as test organisms to determine possible differences in the effect on monocotyledonous and dicotyledonous plants. However, none of the compounds tested showed a preference for any of the plants tested. The results of the QSAR showed that lipophilicity, molecular weight and a sterically hindering substituent are essential for the phytotoxic activity of this compound class. The best results were observed for compounds with a partition coefficient log *P* between 2.80 and 3.00 and a molecular weight of about 305 g/mol. However, not all observations could be explained within this study. Further computational methods will be necessary in the future to identify additional influencing factors.

At the same time, a 50-fold increase in activity was achieved by the derivatization of the natural product **5.1**. While the natural product **5.1** was only active up to a concentration of 20 mM in the non-destructive

leaf disk assay, the most active derivatives **6.10b**, **6.11e**, **6.12e** and 6.**13e** showed activity up to a concentration of 400 µM.

Zusammenfassung

Aufgrund verschiedenster Faktoren, wie der wachsenden Weltbevölkerung, Ernteverlusten durch Schädlingsbefall, zunehmender Resistenzbildung und kontroverser Diskussionen über die Sicherheit synthetischer Herbizide, besteht ein immenser Bedarf an neuen bio-basierten Wirkstoffen. In diesem Kontext sind besonders Naturstoffe (Phytotoxine) von wachsendem Interesse. Naturstoffe bieten ein großes Reservoir unbekannter Substanzen mit einzigartigen Strukturelementen. Dabei erhofft man sich Phytotoxine zu entdecken, die bisher unbekannte Angriffspunkte in Pflanzen angreifen. Zudem ist bereits bekannt, dass zahlreiche Phytotoxine mehrere Wirkmechanismen besitzen, womit eine Resistenzbildung erschwert wird. Oftmals sind die physiochemischen Eigenschaften sowie die phytotoxische Aktivität der Phytotoxine jedoch nicht optimal, sodass eine synthetische Modifikation des Moleküls notwendig ist.

Colletotrichum graminicola (Ces.) Wilson (teleomorph: *Glomerella graminicola*) ist ein Vertreter der Schlauchpilze (Ascomycota) und Erreger der Blatt- und Stängelanthraknose bei Mais. Anthraknosen zeichnen sich durch abgestorbenes (nekrotisches) Gewebe aus und werden durch Enzyme und Sekundärmetaboliten (Phytotoxine) des Pilzes verursacht.

Im Fokus dieser Arbeit stand die aktivitätsgeleitete Isolierung und Charakterisierung dieser Phytotoxine aus Kulturen von *C. graminicola*. Die Anzucht des Pilzes erfolgte in Emerskulturen in zwei verschieden Vollmedien (CM und HMG). Durch die Kombination verschiedener chromatographischer Methoden (DC, HPLC, klassische Säulenchromatographie) erfolgte die Isolierung von Substanzen, die anschließend anhand verschiedener analytischer Methoden (1D-NMR, 2D-NMR, HR-ESI-MS, ECD, Kristallstrukturanalyse) in ihrer Struktur aufgeklärt wurden. Insgesamt konnten 33 Verbindungen isoliert und charakterisiert werden. Darunter befanden sich 11 neuartige bzw. zuvor nicht in der Natur beschriebene Verbindungen. Darunter unter anderem 3-(6-hydroxy-2,6-dimethyloctanoyl)-5-methylpyrrolidin-2-one (**3.1**), 5-(2,3-dihydroxypentyl)-5,6-dihydro-2*H*-pyran-2-one (**4.2**) sowie drei Hexansäure-Derivate (**4.9**, **4.11** und **4.13**). Zudem konnten zahlreiche bereits bekannte Verbindungen, wie Diketopiperazine (**3.2**, **3.4** – **3.9**, **3.15**, **4.8** und **4.10**), Anthrachinone (**4.3**, **4.5**) und Acetamide (**3.3**, **3.13** – **3.14**) isoliert werden.

Zur Testung der phytotoxischen Aktivität wurden zwei Bioassays – ein Blatt-Tropfen Assay, sowie ein Blattscheiben-Assay – implementiert. Bei dem Blatt-Tropfen-Assay (leaf-spot assay) an *Arabidopsis thaliana* Col-0 handelt es sich um einen einfachen und schnellen Test auf Phytotoxizität von Fraktionen und Reinsubstanzen, der im Rahmen der aktivitätsgeleiteten Isolierung genutzt wurde. Für diesen Assay werden die Fraktionen oder Reinsubstanzen in einer Mischung aus Methanol und Wasser (1:1, *v:v*) gelöst und direkt auf die Blattoberfläche aufgetragen. Nach einer Inkubationszeit von 24 – 72 h können die Blätter auf die Entwicklung von Nekrosen oder Chlorosen geprüft werden. Die Auswertung erfolgt dabei rein qualitativ.
Mittels dieses Assays konnte für 21 der 33 isolierten Verbindungen eine phytotoxische Aktivität bei Konzentrationen zwischen 10 und 100 mM beobachtet werden.

Der Blattscheiben-Assay (non-destructive leaf disk assay) wurde ursprünglich entwickelt, um Resistenzen von Pflanzen gegen verschiedene Herbizide festzustellen. In diesem Assay wird die verzögerte Fluoreszenz gemessen, die ein Indikator für die Photosynthese-Rate von Pflanzen ist. Die Photosynthese wiederum reagiert sehr sensitiv auf verschiedenste Stressfaktoren und eignet sich daher hervorragend zur Bestimmung der Phytotoxizität von Substanzen. Wesentlich Vorteile dieses Assays sind die kurze Dauer (48 Stunden), sowie der hohe Probendurchsatz.

Weiterhin, konnte für eine der isolierten Verbindungen (*N*-(4-hydroxybutyl)benzenesulfonamid (**5.1**)) eine quantitative Struktur-Wirkungs-Analyse (QSAR) durchgeführt werden. Dazu wurden basierend auf dem Naturstoff **5.1** ca. 130 synthetisch hergestellte Derivate (Synthesen durchgeführt von Toni Denner, Institut für Chemie – Organische Chemie, Prof. Dr. Csuk, Martin-Luther-University Halle-Wittenberg) auf ihre phytotoxische Aktivität getestet. Die Evaluierung erfolgte hierbei mittels des Blattscheiben-Assays (non-destructive leaf disk assay). Als Testorganismus dienten dabei *A. thaliana* Col-0 (und *Secale cereale*, Ergebnisse nicht gezeigt), um eventuelle Unterschiede in der Wirkung auf mono- und dikotyle Pflanzen feststellen zu können. Jedoch zeigte keine der getesteten Verbindungen eine Präferenz für eine der getesteten Pflanzen. Die Ergebnisse der QSAR zeigten, dass für die phytotoxische Aktivität dieser

Verbindungsklasse die Lipophilie, das Molekulargewicht und ein sterisch-hindernder Substituent entscheidend sind. Die besten Ergebnisse konnten dabei für Verbindungen mit einem Verteilungskoeffizient zwischen 2.80 – 3.00 und einem Molekulargewicht um etwa 305 g/mol beobachtet werden. Jedoch ließen sich mittels dieser Untersuchung nicht alle Beobachtungen erklären. Dazu sind zukünftig weitere computergestützte Methoden notwendig, um weitere Einflussfaktoren zu identifizieren.

Gleichzeitig konnte durch die Derivatisierung des Naturstoffes **5.1** eine Aktivitätssteigerung um das 50-fache erreicht werden. Während der Naturstoff **5.1** lediglich eine Aktivität bis zu einer Konzentration von 20 mM aufweist, zeigten die aktivsten Derivate **6.10b**, **6.11e**, **6.12e**, sowie **6.13e** eine Aktivität im Blattscheiben-Assay bis zu einer Konzentration von 400 µM.

1   Introduction and objectives

Over the last century, the world's population has grown at a remarkable rate. In 2022, it reached the eight billion mark and is estimated to grow to 9.7 billion people by 2050. [1] Developing countries will account for almost all of this population growth. [2] In order to ensure sufficient harvests, crop productivity must be further increased. [3; 4] The Food and Agriculture Organization of the United Nations (FAO) estimates that in developing countries, 80% of the increase in food production – which is needed to keep pace with the population growth – will be reached by an increase in yields and in the number of times a crop can be grown on the same land. Only 20% of crops are expected to come from an expansion of cultivation areas. [2; 5]

In addition, there are severe crop losses due to pests, which reduce the yield and food security of agricultural products. [3; 6] A study by Savary et al. (2019) [6] showed that global crop losses due to pests and pathogens range between 20 and 30%, confirming earlier findings by Oerke (2006). [7] Of all pests, weeds produced the highest potential lost. [7] At the same time, climate change is increasingly affecting growing conditions and its consequences are difficult to predict. Possible impacts include changes in the geographical distribution of weeds (pathogens and insects), as well as alterations in life cycles and population dynamics. [8; 9]

Pesticides have been one of the main tools in pest management and also will remain essential in the future to meet increasing demands and upcoming challenges. The total consumption of pesticides in agriculture worldwide amounted to 2.7 million tons of active ingredients with a value of USD 41.1 billion. The share of herbicides was around 50%. [10] In Germany, inland sales of herbicides amounted to 48.269 tons in 2022. [11]

Herbicides are agrochemicals used to prevent or interrupt normal plant growth and development of unwanted vegetation (weeds). The use of chemicals as herbicides has been known since the end of the 19th century. Initially, inorganic compounds such as arsenic ores and copper salts were used. In 1892, sodium dinitrocresylate (DNOC, Sinox) was developed as the first synthetic insecticide and introduced to the market. From 1934 it was also used as a herbicide. The first compound developed specifically as an herbicide was 2,4-dichlorophenoxyacetic acid (2,4-D). The chemical synthesis was described by Pokorny in 1941. 2,4-D has been commercially available since 1947 and is still in use up to now. [12–14]

Probably the best-known herbicide today is glyphosate. Historically, in 1970, John Franz discovered the herbicidal effect of glyphosate, and only four years later the first formulated end-use product called Roundup was sold commercially by Monsanto. [15] While glyphosate consumption in the U.S. (agricultural use only) was 0.36 million kg (active ingredient) in 1974, it had risen to about 13 million kg by 1995. This made glyphosate the 7th most widely used herbicide in the U.S in 1995 according to the Environmental Protection Agency (EPA) after atrazine, metolachlor, metam-sodium, methyl-bromide, dichloropropene and 2,4-D. [16]

However, it was not until the introduction of genetically-engineered (GE) herbicide-tolerant (HT) crops – so-called "Roundup Ready" varieties – in 1996 that glyphosate could be used as a post-emergence herbicide. Prior to that, it was restricted to pre-emergence application due to its non-selective mode of action (Chapter 2.2.2). [15; 16] By 2000, when GE-HT crops were gaining market share, glyphosate use in the U.S. had increased to 36.0 million kg. In 2014, glyphosate consumption had risen to 113.3 million kg glyphosate in the U.S., of which 80% were only used for the three major GE-HT crops (soybean, maize, and cotton). The global consumption of glyphosate in 2014 was around 750 million kg. [16] Of the herbicides mentioned above, only glyphosate and 2,4-D are still authorized in Germany. In 2022, sales of the active ingredient glyphosate amounted to 3914 tons and those of 2,4-D to almost 79 tons. [17]

Over the decades, there has been an increasing reliance on glyphosate, which in turn promoted the spread of resistant weeds. [16] Since, glyphosate provided an economical and easy weed control, farmers introduced little diversity into their weed management. [15; 19] Even as the first signs became apparent that this weed management was not sustainable, little attention was paid to them, since the use of the

broadcast herbicide was too attractive and beneficial. [20] To control weeds less sensitive to glyphosate only the dose or the number of applications was increased, which only increased the selection pressure. [16; 21]

For the consumer, glyphosate has come into focus due to controversial criticisms. Numerous studies have been published in the last decade suggesting that glyphosate has an endocrine effect and is linked to rare liver and kidney tumors and non-Hodgkin lymphoma. [16; 22–25] In 2015 glyphosate was classified as a "probable human carcinogen" by the International Agency for Research on Cancer. [26] On this basis, a large and still ongoing class action lawsuit was filed in the U.S. against Bayer/Monsanto with about 150.000 claimants. Subsequently, in May 2021, a total prohibition of glyphosate was discussed in Germany and other EU member states. As glyphosate had an EU approval until December 2023 at the time, this was not feasible. Simultaneously, a process for the re-evaluation and re-authorization of glyphosate in the EU was ongoing. [27; 28] In this context, ECHA's Risk Assessment Committee (RAC) concluded in 2022 that there is insufficient scientific evidence to classify glyphosate as a specific target organ toxicant or as a carcinogen, mutagen or reproductive toxicant. [29] Finally, on November 28, 2023, the EU Commission published the implementing regulation to extend the approval of glyphosate by 10 years. [30]

The case of glyphosate clearly illustrates the need for new herbicide solutions. [20] On the one hand, herbicide resistance is becoming an increasingly drastic problem (currently 530 unique cases, as of 26.01.2024) [31], and on the other hand, the demand for more sustainable weed management is steadily increasing. [20; 32]

This problem is compounded by the fact that the number of newly registered herbicides with new molecular targets is very small. [33] In the period from 1980 to 2009, according to Gerwick, 137 new herbicide ingredients were introduced with well-known modes of action. [34] It was not until 2019 that the first approval of a herbicide (Luximo) with a new mode of action was granted by BASF. [35] Conversely, this means that no herbicides with new modes of action have been introduced for about 30 years. [36] This is probably partly a result of the introduction of GE-HT crops, as glyphosate has dominated the market and thus significantly reduced the overall value of the market, making it less attractive. [32; 37; 38]

In the development of new herbicides, natural products are increasingly becoming the focus of research. On the one hand, they are considered by the public to be safer than synthetic herbicides - although this remains to be verified - and on the other hand, their structural diversity is expected to lead to new mechanisms of action. [32; 39–42]

The general objective of the present thesis was thus the bio-guided isolation and identification of phytotoxic compounds from the phytopathogenic fungi *Colletotrichum graminicola* (Ces.) G.W. Wilson that can potentially serve as lead structures for the development of novel (bio-) herbicides. In particular, the investigations covered the following aspects:

- Isolation, characterization, and structural elucidation of phytotoxic secondary metabolites from *Colletotrichum graminicola*

- Evaluation of their phytotoxic activity

- Synthesis of derivatives for activity enhancement and quantitative structure-activity relationship (QSAR) studies

- Investigations of the influence of different cultivation media by metabolite profiling using LC-ESI-HRMS

References

[1] United Nations Deparment of Economic and Social Affairs, Population Division, *World Population Prospects 2022: Summary of Result.,* **2022**.

[2] FAO's Director General on How to Feed the World in 2050, *Population and Development Review* **2009**, *35,* 837–839.

[3] Perera, W.H.; Meepa, K. M.; Fronczek, F.R.; Cook, D.D.; Wedge, D.E.; Duke, S.O., Bioassay-Guided Isolation and Structure Elucidation of Fungicidal and Herbicidal Compounds from *Ambrosia salsola* (Asteraceae), *Molecules* **2019**, *24*, 835*,* doi: 10.3390/molecules24050835.

[4] Edgerton, M.D., Increasing crop productivity to meet global needs for feed, food, and fuel, *Plant Physiol.* **2009**, *149,* 7–13, doi: 10.1104/pp.108.130195.

[5] Pesticide residues in food*,* https://www.who.int/news-room/fact-sheets/detail/pesticide-residues-in-food, last access: **19.01.2024**.

[6] Savary, S.; Willocquet, L.; Pethybridge, S.J.; Esker, P.; McRoberts, N.; Nelson, A., The global burden of pathogens and pests on major food crops, *Nat. Ecol. Evol.* **2019**, *3,* 430–439, doi: 10.1038/s41559-018-0793-y.

[7] Oerke, E., Crop losses to pests, *J. Agric. Sci.* **2006**, *144,* 31–43, doi: 10.1017/S0021859605005708.

[8] Ramesh, K.; Matloob, A.; Aslam, F.; Florentine, S.K.; Chauhan, B.S., Weeds in a Changing Climate: Vulnerabilities, Consequences, and Implications for Future Weed Management, *Front. Plant Sci.* **2017**, *8,* 95, doi: 10.3389/fpls.2017.00095.

[9] Vilà, M.; Beaury, E.M.; Blumenthal, D.M.; Bradley, B.A.; Early, R.; Laginhas, B.B.; Trillo, A.; Dukes, J.S.; Sorte, C.J.B.; Ibánez, I., Understanding the combined impacts of weeds and climate change on crops, *Environ. Res. Lett.* **2021**, *16,* 34043, doi: 10.1088/1748-9326/abe14b.

[10] Food and Agriculture Organization of the United Nations (FAO), *Faostat Analytical Brief 46,* **2022**.

[11] BVL, Absatz an Pflanzenschutzmitteln in der Bundesrepublik Deutschland, Ergebnisse der Meldungen gemäß § 64 Pflanzenschutzgesetz für das Jahr 2022, korrigierte Version **31.01.2024**, www.bvl.bund.de/psmstatistiken, last access: 08.03.2024.

[12] Vats, S., (**2015**), Herbicides: History, classification and genetic manipulation of plants for herbicide resistance. In: Lichtfouse, E. (ed). Sustainable Agriculture Reviews, vol 15. Springer, Cham., doi:10.1007/978-3-319-09132-7_3

[13] Mesnage, R.; Székács, A.; Zaller, J.G. (**2021**), Herbicides: Brief history, agricultural use, and potential alternatives for weed control. In: Mesnage, R; Zaller, J.G. (eds.), Emerging Issues in Analytical Chemistry*,* Herbicides*,* Elsevier, doi: 10.1016/B978-0-12-823674-1.00002-X.

[14] Chauvel, B.; Gauvrit, C.; Guillemin, J.P., From sea salt to glyphosate salt: a history of herbicide use in France, *Adv. Weed Sci.* **2022**, *40,* e020220015, doi: 10.51694/AdvWeedSci/2022;40:seventy-five008.

[15] Duke, S.O.; Powles, S.B., Glyphosate: a once-in-a-century herbicide, *Pest Manag. Sci.* **2008**, *64,* 319–325, doi: 10.1002/ps.1518.

[16] Benbrook, C.M., Trends in glyphosate herbicide use in the United States and globally, *Environ Sci Eur.* **2016**, *28,* article 3, doi: 10.1186/s12302-016-0070-0.

[17] BVL, Absatzmengen von Wirkstoffen in Pflanzenschutzmitteln von 1987 bis 2022, **2023**, www.bvl.bund.de/psmstatistiken, last access: 08.03.2024.

[18] Heap, I., Global perspective of herbicide-resistant weeds, *Pest Manag. Sci.* **2014**, *70,* 1306–1315, doi: 10.1002/ps.3696.

[19] Powles, S.B., Evolved glyphosate-resistant weeds around the world: lessons to be learnt, *Pest Manag. Sci.* **2008**, *64,* 360–365, doi: 10.1002/ps.1525.

[20] Duke, S.O., Perspectives on transgenic, herbicide-resistant crops in the United States almost 20 years after introduction, *Pest Manag. Sci.* **2015**, *71,* 652–657, doi: 10.1002/ps.3863.

[21] Mortensen, D.A.; Egan, J.F.; Maxwell, B.D.; Ryan M.R.; Smith, R.G., *Biosci.* **2012**, *62,* 75–84, doi: 10.1525/bio.2012.62.1.12.

[22] Schinasi, L.; Leon, M.E., Non-Hodgkin lymphoma and occupational exposure to agricultural pesticide chemical groups and active ingredients: A systematic review and meta-analysis*, Int. J. Environ. Res. Public Health* **2014**, *11,* 4449–4527, doi: 10.3390/ijerph110404449.

[23] Thongprakaisang, S.; Thiantanawat, A.; Rangkadilok, N.; Suriyo, T.; Satayavivad, J., Glyphosate induces human breast cancer cells growth via estrogen receptors, *FCT,* **2013**, *59,* 129–136, doi: 10.1016/j.fct.2013.05.057.

[24] Gasnier, C.; Dumont, C.; Benachour, N., Clair, E.; Chagnon, M.-C.; Séralini, G.-E., Glyphosate-based herbicides are toxic and endocrine disruptors in human cell lines, *Toxicol.* **2009**, *262,* 184–191, doi: 10.1016/j.tox.2009.06.006.

7

[25] Robinson, C., Teratogenic Effects of Glyphosate-Based Herbicides: Divergence of Regulatory Decisions from Scientific Evidence, *J Environ. Anal Toxicol.* **2012**, S4, 006, doi*: 10.4172/2161-0525.S4-006.

[26] WHO, International Agency for Research on Cancer., IARC Monographs Volume 112: evaluation of five organophosphate insecticides and herbicides, **2015**.

[27] European Food Safety Authority (EFSA), Glyphosate*,* https://www.efsa.europa.eu/en/topics/topic/glyphosate, last access: 27.01.2024.

[28] Bayer, EU Glyphosate Renewal, https://www.bayer.com/en/agriculture/glyphosateeu, last access: 27.01.2024.

[29] European Chemicals Agency (ECHA), ECHA/NR/22/10: Glyphosate: no change proposed to hazard classification,https://echa.europa.eu/de/-/glyphosate-no-change-proposed-to-hazard-classification, **2022**, last access: 27.01.2024.

[30] European Commission, Commission Implementing Regulation (EU) 2023/2660, **2023**.

[31] Heap, I. The International Herbicide-Resistant Weed Database. Online.*,* https://www.weedscience.org/, last access: 27.01.2024.

[32] Duke, S.O.; Pan, Z.; Bajsa-Hirschel, J.; Boyette, C.D., The potential future roles of natural compounds and microbial bioherbicides in weed management in crops, *Adv. Weed Sci.* **2022**, *40*, e020210054, doi: 10.51694/AdvWeedSci/2022;40:seventy-five003.

[33] Qu, R.-Y.; He, B.; Yang, J.-F.; Lin, H.-Y.; Yang, W.-C.; Wu, Q.-Y.; Li, Q.X.; Yang, G.F., Where are the new herbicides?, *Pest Manag. Sci.* **2021**, *77*, 2620–2625, doi: 10.1002/ps.6285.

[34] Gerwick B.C, Thirty years of herbicide discovery: surveying the past and contemplating the future, *Agrow Report.*, Informa; London, UK, **2010**, VII–IX.

[35] BASF, New mode of action classification for BASF herbicide Luximo®, P168/20e, **02.06.2020**, http://www.basf.com/global/en/media/news-releases/2020/06/p168.html#:~:text=Due%20to%20its%20novel%20mode,control%20black%2Dgrass%20and%20ryegrass, last access: 27.01.2024

[36] Dayan, F.E., Current Status and Future Prospects in Herbicide Discovery, *Plants* **2019**, *8,* 341, doi*: 10.3390/plants8090341.

[37] Duke, S.O., Why have no new herbicide modes of action appeared in recent years?, *Pest Manag. Sci.* **2012**, *68,* 505–512, doi: 10.1002/ps.2333.

[38] Davis, A.S.; Frisvold, G.B., Are herbicides a once in a century method of weed control?, *Pest Manag. Sci.* **2017**, *73,* 2209–2220, doi: 10.1002/ps.4643.

[39] Dayan, F.E.; Duke, S.O., Natural compounds as next-generation herbicides, *Plant Physiol.* **2014**, *166,* 1090–1105, doi: 10.1104/pp.114.239061.

[40] Triolet, M.; Guillemin, J.-P.; Andre, O.; Steinberg, C., Fungal-based bioherbicides for weed control: a myth or a reality?, *Weed Res* **2020**, *60,* 60–77, doi: 10.1111/wre.12389.

[41] Dayan, F.E.; Owens, D.; Duke, S.O., Rationale for a natural products approach to herbicide discovery, *Pest Manag. Sci.* **2012**, *68,* 519–528, doi: 10.1002/ps.2332.

[42] Gerwick, B.C.; Sparks, T.C., Natural products for pest control: an analysis of their role, value and future, *Pest Manag. Sci.* **2014**, *70,* 1169–1185, doi: 10.1002/ps.3744.

2   General part

2.1   The genus *Colletotrichum* Corda

The fungal genus *Colletotrichum* (teleomorph: *Glomerella*) CORDA is the only member of *Glomerellaceae* (Glomerellales, Sordariomycetes) and comprises currently 257 accepted species (based on molecular data) grouped into 15 species complexes and 14 singleton species. [1–4] However, it is noteworthy that there have been tremendous taxonomic changes within the genus in recent years. Currently, a revision of the genus based on multi-locus sequence data is ongoing, since there have been many misidentifications in the past, mainly based on missing morphological characteristics and misunderstandings regarding host specifity. [1; 5] This explains the immense differences found in the literature. Thus, the database Species Fungorum [6] lists currently 547 epiphets, the database MycoBank [7] even 956.

The genus includes several economically important plant pathogens that infect a wide variety of crops in tropical, sub-tropical and temperate regions [8; 9]. The pathogens can be either host-specific or infect multiple hosts. [1; 10] The disease, caused by *Colletotrichum* species, is called anthracnose and is characterized by sunken necrotic tissues on leaves, stems, flowers, and fruits, as well as crown rot, stem rot, and seedling rot. [5; 11]

2.1.1   Lifestyles

Lifestyle patterns in *Colletotrichum* can be divided in four forms: endophytic (1), necrotrophic (2), hemibiotrophic (3), latent or quiescent (4). [1; 12; 13] *Colletotrichum* species show different lifestyles, with closely related species showing similar infection- and colonization characteristics. [12; 14; 15] The major differences exist between the individual species complexes. However, almost all species are able to change their lifestyle sequentially. [12; 16]

Endophytic lifestyle (1): Endophytes are plant inhabiting fungi that live within in the host plant cells without causing any disease symptoms. Most endophytic fungi have a mutualistic relationship with their hosts, with benefits for both sides. For example, the fungus gains access to nutrients while protecting the plant from herbivores or pathogens. [12; 17–19] However, the relationship between fungus and host can switch from mutualistic to antagonistic and pathogenic depending on several influences, like environmental conditions or physiological conditions of the host plant. [20; 21] Many *Colletotrichum* species are endophytes for the longest part of their life cylce. [5; 12; 14] The majority of endophytic Colletotrichum species belong to the *boninense*, *gloeosporioides* and *graminicola* complexes. [22–24]

Necrotrophic lifestyle (2): Necrotrophs actively infect and colonizes plant cells. The pathogens secret cell wall-degrading enzymes and toxins leading to cell death of the plants to feed subsequently as saprotrophs. [25–27] Formation of necrosis is a characteristic symptom of the infected tissue. [10] Almost all species of *Colletotrichum* develop a necrotrophic stage during their life cycles. [1; 12]

Hemibiotrophic lifestyle (3): A hemibiotrophic mode of life is characterized by a short biotrophic phase after infection of the host, followed by a necrotrophic phase. [1; 5; 25] During the biotrophic phase, the pathogen absorbs nutrients without killing the plant cells. [26] This requires various strategies as masking of the invading hyphae to suppress or evade plant defense mechanisms. [28; 29] This phase usually lasts a few days, after which the transition to necrotrophy occurs. [1; 16]

Quiescent lifestyle (4): Quiescence (latency) corresponds to a longer period of time during which the pathogen is dormant in the host. During this time, the pathogen does not grow, and no symptoms appear until it transitions to an active state. This mode of life is particularly important for pathogens that cause postharvest disease, such as *C. gloeosporioides* or *C. acutatum*. [12; 30] Studies by Talhinhas and co-workers (2011) have shown that in immature fruits only infection of the host takes place. [31] Colonization only occurred when the fruits began to ripen. [31]
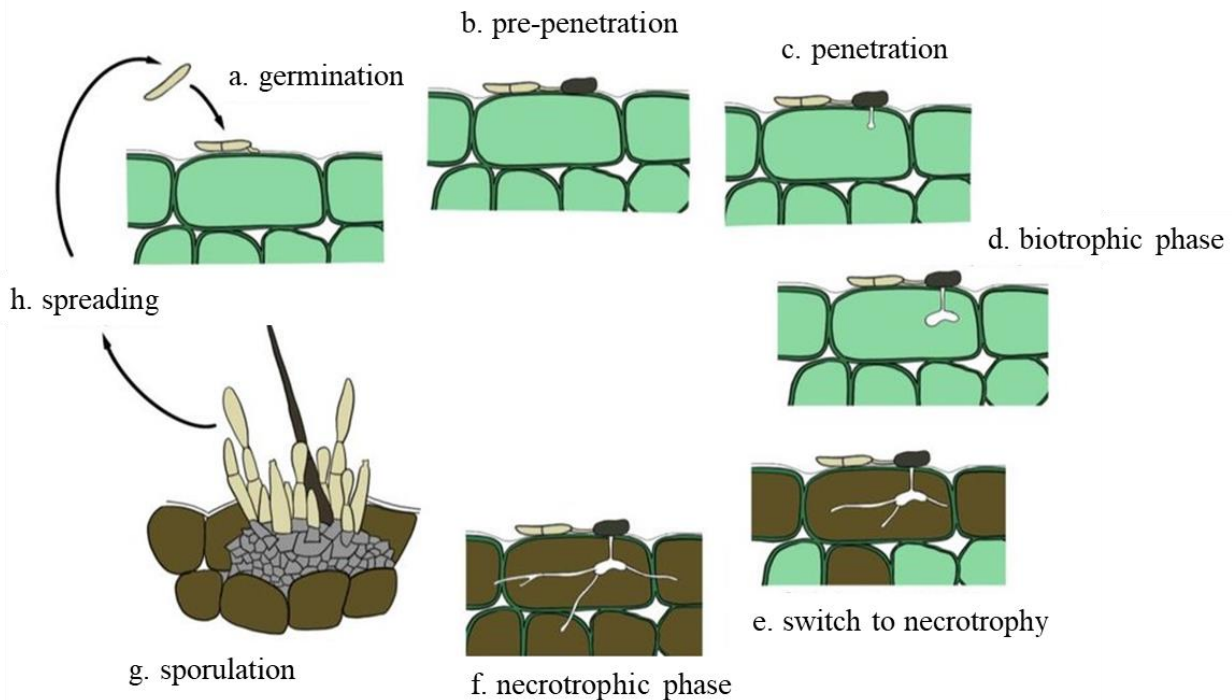
Figure 2-1 Life cycle of *Colletotrichum* adapted by Jayawardena and co-workers. [1]

2.1.2 Infection strategies

Pre-infection

The infection of plants starts with the adhesion of spores (conidia) and their germination. Conidia are produced in acervuli embedded in a glycoprotein-rich mucus. [25] The mucus also contains germination inhibitors and numerous enzymes.[32] The initial attachment of the conidia to the host cuticle occurs via hydrophobic interactions with proteins localized on the spore surface. [25; 33; 34] To initiate germination and the formation of the appressorium (specialized infection structure), the conidia need certain signals from the plant surface. These signals can be either chemical, such as a certain composition of the surface wax or the presence of the fruit ripening hormone ethylene or physical, like a required contact with hard surfaces to induce gene expression. [25; 35–37] Once the appressorium grows, a melanin layer is incorporated and osmolytically active compounds are synthesized, leading to an increase in the internal turgor pressure. Both factors are essential for penetration into the host cell with small penetration pegs. [28; 38–40]

Post-infection

Colletotrichum species can utilize either intracellular hemibiotrophy or subcuticular intramural necrotrophy.[41] Intracellular hemibiotrophic species use specialized infection structures called primary hyphae to invade host cells with or without prior formation of an infection vesicle. The primary hyphae are surrounded by a membrane that separates the fungal cell from the host cell. In this biotrophic stage, the plant cells remain alive, and the fungus evades defense mechanisms. In the transition to necrotrophy, thinner hyphae are formed that are not surrounded by a membrane and secrete lytic enzymes and toxins. [20; 25; 28; 41] At least three variants of intracellular hemibiotrophy can be distinguished. [13] **I**: The *C. destructivum* model has a very limited biotrophic phase. Only a single cell is colonized by primary hyphae before secondary hyphae are formed that kill host cells ahead of infection. [42] **II**: The second model is that of *C. orbiculare*. Multiple cells are colonized by primary hyphae. Infected cells gradually die, starting with the first infected cells. During the transition to necrotrophy, secondary hyphae are formed that kill host cells ahead of infection. [43] **III**: The third model is the *C. graminicola* model. Similar to *C. orbiculare*, multiple cells are colonized by primary hyphae. However, secondary hyphae are formed only as branches from primary hyphae behind the advancing biotrophic colony front. Thus, in this model, biotrophy and necrotrophy occur in parallel. [25; 44] In subcuticular intramural necrotrophy, the pathogen grows under the cuticle, in the periclinal and anticlinal wall of the epidermal cells and dissolves the cell wall. [41; 45]

2.1.3   *Colletotrichum graminicola* (Ces.) G.W. Wilson

Colletotrichum graminicola is an important member of the genus *Colletotrichum* and is part of the *graminicola* species complex which comprises 16 species associated with Poaceae (grasses). It is a hemibiotrophic species that uses intracellular hemibiotrophy and causes anthracnose leaf blight and anthracnose stalk rot on *Zea mays*. [1; 3; 46] *C. graminicola* is estimated to cause yearly damages of one billion USD in the USA alone. [47]

2.1.4   **Known metabolites**

Colletotrichum produces a wide range of secondary metabolites with different activities and functions. A review by Kim et al. published in 2018 records at least 109 metabolites. [48] However, they can be divided into four categories based on the key enzyme for their biosynthesis, namely polyketides (polyketide synthases), terpenes (terpene synthases), alkaloids (dimethylallyl tryptophan synthases) and peptides (non-ribosomal peptide synthases. [8]

Polyketides

Polyketides are a structurally diverse family of natural products with a broad spectrum of bioactivity. They are formed by repeated Claisen condensation of acyl-CoA with malonyl-CoA starter units catalyzed by multimodular polyketide synthases. Metabolites can be further subdivided according to the number of acetate units involved, e.g. into tri- or tetraketides. In addition, polyketides can be distinguished by the degree of keto processing. Unreduced or only partially reduced structures can lead to cyclic aromatic compounds, while largely reduced structures lead to linear or macrocyclic non-aromatic structures. [8; 49–51] Examples of this diverse structural class include monorden (**2.1**) and colletolactone A (**2.2**), both compounds were present in *C. graminicola* (see **Figure 2-2**). [52; 53]

Terpenes

Terpenoids are formed from repeating units of 5-carbon building blocks, isopentenyl diphosphate (IPP) and its isomer dimethylallyl diphosphate (DMAPP). The repetitive head-to-tail condensation of IPP and DMAPP catalyzed by prenyltransferases, results in the synthesis of prenyl diphosphates of increasing length: geranyl (C_{10}), farnesyl (C_{15}) and geranylgeranyl diphosphate (C_{20}). These, in turn, form the starting point for numerous downstream syntheses leading to a variety of derivatives such as sesquiterpenes, diterpenes, and others. [8; 54] Examples for previously reported terpenoids are the acorene-type sesquiterpene colletoic acid (**2.3**) and the monoterpene 5-hydroxy-α-terpinene (**2.4**) (**Figure 2-2**). [55; 56]

Alkaloids

Another important class of secondary metabolites are alkaloids. Based on their heterocyclic ring system and biosynthetic precursors they are divided in several subclasses including indoles, purines, quinolines and imidazoles. However, the vast majority of alkaloids detected in *Colletotrichum* belong to the indole alkaloids. Indole alkaloids are produced by dimethylallyl tryptophan synthases from tryptophan via the indole pathway. [8; 57] Indole-3-acetic acid (**2.5**) and colletotriauxin A (**2.6**) are shown in **Figure 2-2** as examples of the indole alkaloids previously identified in *Colletotrichum*. [58; 59]

Non-ribosomal peptides

Non-ribosomal peptides are small peptidic molecules with a wide range of bioactivities produced by nonribosomal peptide synthases (NRPS). NRPS are large multimodular enzymes (> 100 kDa). Within a single module are multiple catalytic domains catalyzing a cycle of amino acid activation, peptide bond formation and optional tailoring reactions. [60; 61] However, each NRPS can synthesize only one type of peptides. [62] A wide variety of structures such as the siderophore ferricrocin (**2.7**) [63], diketopiperazines such as brevianamide F (**2.8**) [64], and cyclic peptides such as tentoxin (**2.9**) [65] have already been described from *Colletotrichum*.
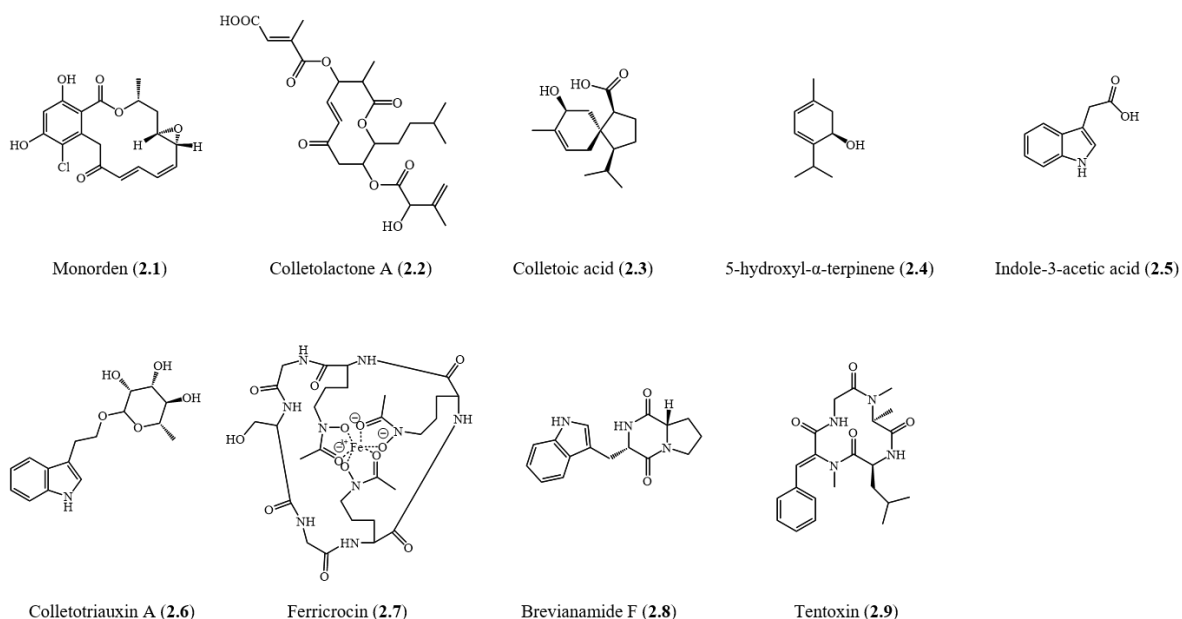
Monorden (**2.1**)   Colletolactone A (**2.2**)   Colletoic acid (**2.3**)   5-hydroxyl-α-terpinene (**2.4**)   Indole-3-acetic acid (**2.5**)

Colletotriauxin A (**2.6**)   Ferricrocin (**2.7**)   Brevianamide F (**2.8**)   Tentoxin (**2.9**)

Figure 2-2 Metabolites from the genus *Colletotrichum*.

2.1.4.1   Phytotoxic metabolites

Colletotrichum species produce phytotoxic metabolites, which induce symptoms on plants similar to those of the pathogen itself. [8] Phytotoxins can be further divided into host-specific and non-host-specific toxins. Host-specific toxins are considered to be metabolites that are phytotoxic only to the host of the pathogen, while non-host-specific toxins can affect different plants. [48; 66] However, host-specific toxins were rarely found in *Colletotrichum*. Alleyne and co-workers (1995) reported a host-specific toxin from *C. gloeosporioides* consisting of polysaccharides with one or more protein components. An exact structure was not reported. It was also found that phytotoxins were often falsely declared as host-specific, although no test was performed on plants other than the host plant. [67]

Nevertheless, numerous non-host specific phytotoxins from *Colletotrichum* have been identified so far. Phytotoxins from all four groups (see **2.1.4**) are known, including the compounds **2.5 – 2.9** (**Figure 2-2**). Other examples of phytotoxic compounds are shown in **Figure 2-3**, i.e. are colletotrichin A (**2.10**) isolated from *C. nicotianae* [68], colletochlorin A (**2.11**), 4-chloroorcinol (**2.12**) and colletopyrone (**2.13**) isolated from *C. higginsianum* [69], and mycosporin alanine (**2.14**) isolated from *C. graminicola*. [32]

Colletotrichin A (**2.10**)   Colletochlorin A (**2.11**)   4-Chloroorcinol (**2.12**)   Colletopyrone (**2.13**)   Mycosporine alanine (**2.14**)
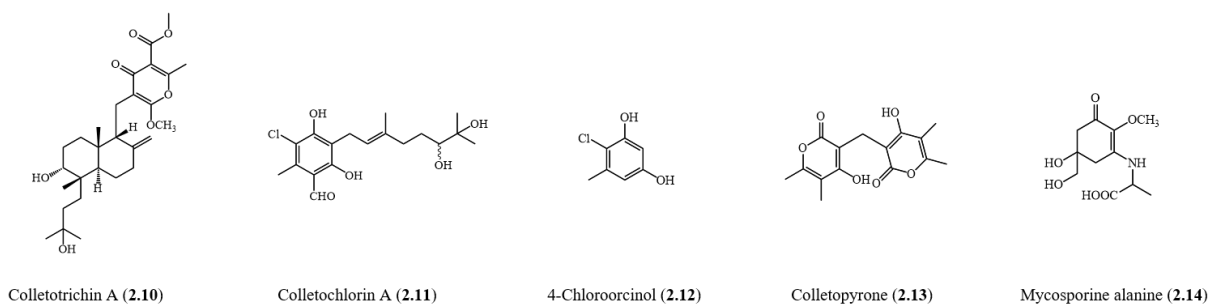
Figure 2-3 Phytotoxic metabolites from the genus *Colletotrichum*.

2.2 Herbicides

2.2.1 General

Herbicides are agrochemicals used to prevent or interrupt normal plant growth and development of unwanted vegetation (weeds). [70; 71] They can be classified according to various aspects, including translocation, time of application, method of application, specificity and mode of action (MOA). (Table 1)

Table 2-1 Classification of herbicides.

Classfication	Subdivision
Translocation	contact/ non-systemic
	systemic
Selectivity	selectivity
	non-selective
Time of application	preplant
	pre-emerge
	post-emerge
Method of application	soil
	leaf
Mode of action	see 2.2.2

Based on their translocation characteristics herbicides can be divided into contact agents and systemic agents. Contact agents are taken up by the plant surface but are not further translocated through the plant. Accordingly, their effect is limited to plant tissues that comes into contact with them. An example for a contact herbicide is paraquat. Systemic herbicides, on the other hand, are transported through the plant to their target site via the phloem or xylem. While contact herbicides act very quickly and show symptoms within hours, it can take several days to weeks for systemic herbicides to kill the plant. Glyphosate is an example of a systemic herbicide. [70; 71] Herbicides can also be classified according to their selectivity. While non-selective agents act on all plants, selective herbicides act only on certain plants species without affecting others. Selectivity may be due to differences in translocation, absorption morphology, or physiology. [71]

2.2.2 Mode of action (MOA)

Currently, the Herbicide Resistance Action Committee (HRAC) lists 25 different MOA for commercially available herbicides (**Table 2-2**). [72] In 2020, it was decided to switch from the alphanumeric system previously used in Germany to a numeric system in order to harmonize the classification globally. The classes are numbered from 1 to 34, based on the numerical system of the Weed Science Society of America (WSSA). Within this process of harmonization, the classification of active ingredients into chemical groups and/or mode of action has also changed, resulting in some missing numbers. [72]

The main targets for herbicides are amino acid biosynthesis, photosystem, pigment biosynthesis, lipid biosynthesis and microtubules. In addition, auxin mimics represent a large group of herbicides.

Table 2-2 HRAC classification of herbicides.

HRAC Classification	MOA	Target	Members
1	Inhibition of acetyl CoA carboxylase (ACCase)	Lipid biosynthesis	16
2	Inhibition of acetolactate synthase (ALS)	Amino acid biosynthesis	57
3	Inhibition of microtubule assembly	Microtubules	13
4	Auxin mimics	Auxin	21
5	Inhibition of PS II – others than hisitidine 215	Photosytem II	31
6	Inhibition of PS II – histidine 215	Photosytem II	4
7	-	-	-
8	-	-	-
9	Inhibition of enolpyruvyl shikimate phosphate synthase (ESPS)	Amino acid biosynthesis	1
10	Inhibition of glutamine synthetase (GS)	Amino acid biosynthesis	2
11	-	-	-
12	Inhibition of phytoene desaturase (PDS)	Pigment biosynthesis	7
13	Inhibition of deoxy-D-xylulose phosphate synthase (DOXP)	Isoprenyl biosynthesis	2
14	Inhibition of protoporphyrinogen oxidase (PPO)	Pigment biosynthesis	22
15	Inhibition of very long-chain fatty acid synthesis (VLCFAs)	Lipid biosynthesis	35
16	-	-	-
17	-	-	-
18	Inhibition of dihydropteroate synthase (DHP)	Amino acid biosynthesis	1
19	Inhibition of auxin transport	Auxin	2
20	-	-	-
21	-	-	-
22	PS I electron diversion	Photosystem I	2
23	Inhibition of microtuble organization	Microtubules	3
24	Uncouplers		2
25	-	-	-
26	-	-	-
27	Inhibition of hydroxyphenyl pyruvate dioxygenase (HPPD)	Pigment biosynthesis	14
28	Inhibition of dihydrooroate dehyhdrogenase	Pyrimidin biosynthesis	1
29	Inhibition of cellulose synthesis	Cellulose biosynthesis	6
30	Inhibition of fatty acid thioesterase	Lipid biosynthesis	2
31	Inhibition of serine threonine protein phosphatase	Protein phosphorylation	1
32	Inhibition of solanesyl diphosphate synthase	Plastoquinone	1
33	Inhibition of homogentisate solanesyltransferase	Plastoquinone	1
34	Inhibition of lycopene cyclase	Pigment biosynthesis	1
∅	Unknown MOA	-	16

Target amino acids

Three enzymes of the amino acid biosynthesis are important target sites of herbicides: 5-enolpyruvyl-shikimate-3-phosphate synthase (EPSP synthase), acetolactate synthase (ALS), and glutamine synthase (GS). [73] The EPSP synthase is an enzyme in the shikimate pathway required for the biosynthesis of aromatic amino acids (i.e. tryptophan, phenylalanine, and tyrosine). Inhibition of this enzyme leads to a deficiency of essential amino acids for protein biosynthesis. In addition, the biosynthesis of a variety of secondary metabolites important for plant growth and development, such as the plant hormone indole-3-acetic acid (**2.5**), is disrupted. The only herbicide that uses that target is glyphosate (**2.15**) (**Figure 2-4-A**). [73–75] ALS is an enzyme required in the synthesis of the branched chain amino acids leucine, isoleucine and valine. It catalyzes the condensation of two pyruvate molecules or of pyruvate with α-ketobutyrate to 2-acetolactate or 2-acetohydroxybutyrate, respectively. Inhibition of this enzyme leads to the accumulation of 2-oxybutyrate and its transamination product 2-amino butyrate, which seems to be toxic for the plant. Plants treated with these inhibitors stop growing, eventually wilt and turn red as stress-induced anthocyanins accumulate. [73; 76] ALS inhibitors are the largest group of commercial herbicides, including sulfonylureas, imidazolinone and triazolopyrimidine (**Figure 2-4-B**).

GS catalyzes the condensation of glutamate and ammonia to glutamine. Inhibition of this enzyme leads to an accumulation of ammonium ions which cause a rapid uncoupling of photophosphorylation, inhibition of photosynthetic carbon fixation and disruption of amino acid synthesis, upon which photorespiration depends. Symptoms are leaf wilting, followed by necrosis. [75; 76] The only representatives of this group are glufosinate ammonium (**2.19**) and bialaphos (**2.20**) (**Figure 2-4-C**).
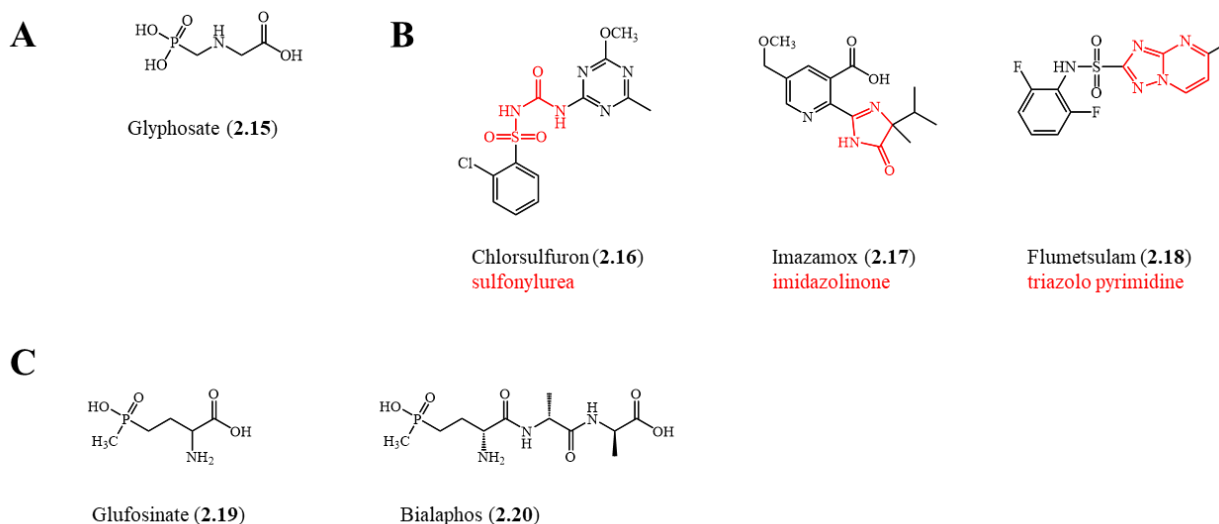
Figure 2-4 Examples of herbicides inhibiting the amino acid biosynthesis: **A**: EPSP synthase inhibitors, **B**: ALS inhibitors, **C**: GS inhibitors, highlighted in red is the core structure of the corresponding compound class.

Target Photosystem I and II

Photosystem I is an integral membrane protein complex that uses light energy to produce NADPH. The herbicides in this group, i.e. diquat (**2.21**) and paraquat (**2.22**) (**Figure 2-5-A**), can be reduced by PS I and subsequently form reactive superoxide radicals. These react to form numerous other radicals, including hydroxyl radicals, which rapidly lead to membrane destruction and cell death. This reaction occurs rapidly under daylight conditions when the redox strength of PS I is high, and PS II produces O_2 in large quantities. Symptoms of these herbicides are wilting, followed by necrosis. [76]

Photosystem II is a membrane protein complex that catalyzes the light-induced water oxidation in oxygenic photosynthesis. Through this reaction light energy is converted to electrochemical potential energy, which is used to produce ATP and NADPH in the following. Part of this electron transport chain are among other the D1 protein and the co-factor plastoquinone (PQ), which normally binds at the Q_B-binding site of the D1 protein. PSII-inhibiting herbicides act by competing with the PQ molecule for the Q_B site of the D1 protein and thus block the electron transfer. This will lead to many cellular dysfunctions, including deficient CO_2 binding, loss of carotenoids followed by the destruction of chlorophylls. In sunlight the treated plants wilt and turn brown, in less light the process is slower, the leaves turn white or necrotic. [76–78] Examples of photosystem II inhibitors are triazines, like atrazine (**2.23**) and ureas like monuron (**2.24**) (**Figure 2-5-B**).
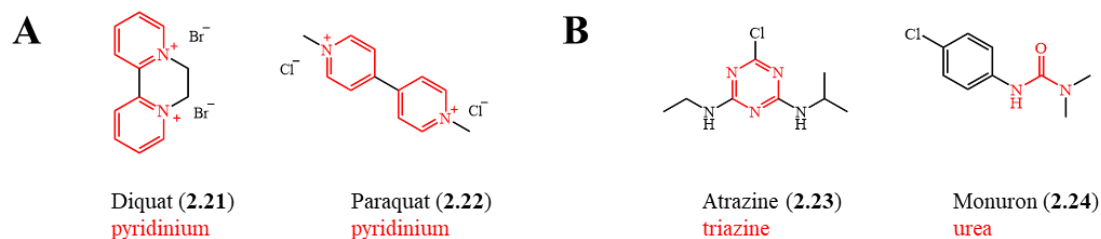
Figure 2-5 Examples of herbicides inhibiting the photosystem, **A**: photosystem I inhibitors, **B**: photosystem II inhibitors, highlighted in red is the core structure of the corresponding compound class.

Target pigment synthesis

Targets of inhibition of pigment synthesis include phytoene desaturase (PDS), hydroxyphenylpyruvate dioxygenase (HPPD) and protoporphyrinogen oxidase (PPO), which are important for the synthesis of carotenoids or chlorophyll.

PDS is an enzyme required for the biosynthesis of carotenoids. Carotenoids are important for quenching reactive oxygen species (ROS). Carotenoid deficiency leads to the destruction of chlorophyll, so plants are unable to perform photosynthesis. Characteristic symptom of PDS inhibitors is bleaching of the plant. [75; 76] An example is the phenylether derivative beflubutamin (**2.25**) (**Figure 2-6-A**)

HPPD is necessary for the synthesis of plastoquinone (PQ) and tocopherols. PQ is a co-factor of PDS. Therefore, a lack of PQ leads to the same symptoms as PDS inhibitors. Additionally, PQ is required for the electron transport in photosynthesis. In addition, PQ is required for electron transport in photosynthesis, so mature leaves are also affected by the treatment with HPPD inhibitors. Herbicides of this class are triketones like mesotrione and pyrazoles (**Figure 2-6-B**). [76]

PPO is an enzyme involved in porphyrin synthesis, a prerequisite for both heme and chlorophyll. Inhibition of this enzyme causes the release of its substrate protogen IX from the porphyrin pathway to cellular sites where it is oxidized to proto IX either non-enzymatically or by non-specific oxidases (e.g., peroxidases). Proto X is a photodynamic agent that generates reactive oxygen species in the presence of light, leading to cell destruction. PPO inhibitors cause rapid burning and necrosis of the plants. Several chemical classes of herbicides act on this enzyme. As a common feature of these herbicides, they possess at least two rings allowing them to bind to PPO. [76; 79] Bifenox (**2.28**) is an example of an PPO inhibiting herbicide.
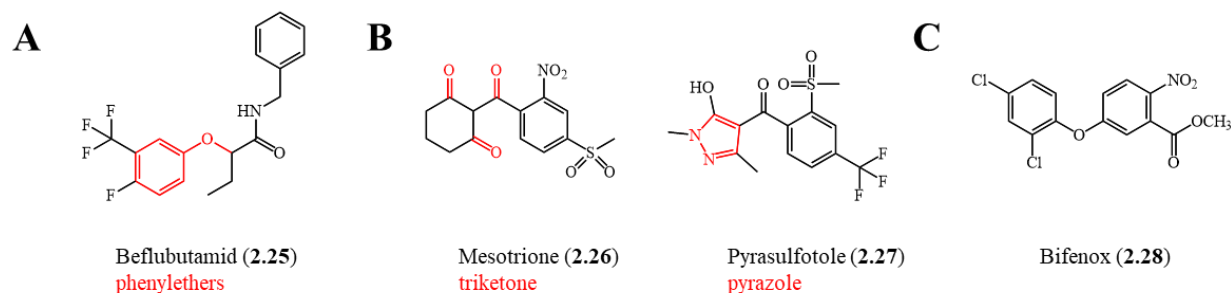
Figure 2-6 Examples of herbicides inhibiting the pigment synthesis, **A**: PDS inhibitors, **B**: HPPD inhibitors, **C**: PPO inhibitors, highlighted in red is the core structure of the corresponding compound class.

Target lipid biosynthesis

Targets involved in the lipid biosynthesis include the acetyl-CoA-carboxylase (ACCase) and the very-long-chain fatty acids elongases (VLCFAs).

ACCase catalyzes the first step in fatty acid synthesis, the carboxylation of acetyl-CoA to form malonyl-CoA. Inhibition blocks the formation of lipids and secondary metabolites and leads in consequence to a loss of cell membrane integrity, metabolites leakage and rapid plant death. [80; 81] Symptoms of treatment with ACCase inhibitors such as propachlor (**2.29**) are accumulation of anthocyanins followed by necrosis. Mature leaves are affected more slowly compared to young leaves. [76]

VLCFAs are necessary for the synthesis of waxes, cutins and suberins. Inhibition of this enzyme leads to the arrest of cell division, followed by slow dehydration of the plant and increased susceptibility to pathogens. Symptoms include reduced growth and curling and twisting of the leaves. [75; 76; 82] The cyclohexanedione sethoxydim (**2.30**) is an example of a VLCFA inhibiting enzyme.
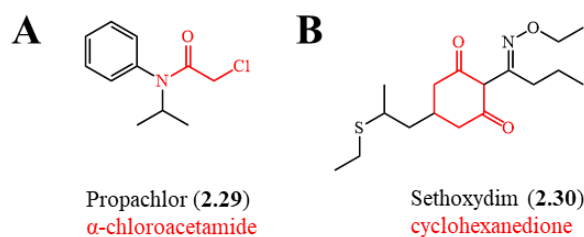
Figure 2-7 Examples of herbicides inhibiting the lipid biosynthesis, **A**: ACCase inhibitors, **B**: VLCFA inhibitors, highlighted in red is the core structure of the corresponding compound class.

Target microtubules

Microtubules are polymers of tubulin and are part of the cytoskeleton. The division and elongation of plant cells and the formation of cell walls require proper microtubule functioning. Herbicides such as dinitroaniline (**2.31**) can interfere with these processes by either binding tubulin or interfering with the centers of microtubule organization or proteins associated with microtubules. Characteristic symptom is swelling of the root tips. [76]
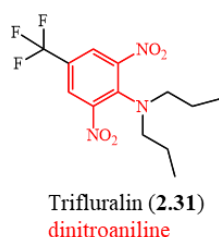
Figure 2-8 Example of herbicides inhibiting the microtubule assembly, highlighted in red is the core structure of the corresponding compound class.

Target auxin mimics

Auxins such as 3-indoleacetic acid (**2.5**) are plant hormones required for cell elongation and growth. Auxin-mimicking herbicides cause initial rapid growth associated with increased metabolism. This phase is characterized by curling of stems and leaves, swelling of tissue, and rapid length growth. Synthesis of ethylene and abscisic acid is also stimulated. High levels of abscisic acid inhibit growth and metabolism by closing stomata, which in turn leads to the formation of reactive oxygen species. The final stage is senescence and cell death. Important representatives of this group are 2,4-D (**2.32**) and dicamba (**2.33**).
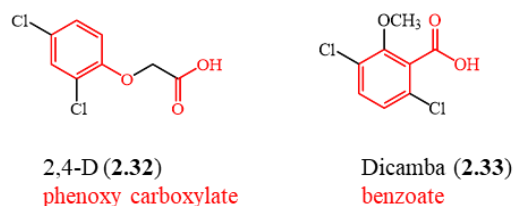
Figure 2-9 Examples of auxin mimicking herbicides, highlighted in red is the core structure of the corresponding compound class.

2.2.3 Resistances

The increasing number of herbicide resistances is a major topic in agriculture, especially since only few herbicides with a new mode of action have been introduced to the market for the last 30 years. [79; 83; 84] To date, there are 530 known cases of herbicide-resistant weeds worldwide, comprising 272 species (155 dicotyledons and 117 monocotyledons). Weeds have already developed resistance to 21 of the 34 known herbicide sites of action. [85]

Herbicide resistance is a natural result of the evolutionary process. However, many different factors influence the dynamics of this process. For instance, repeated use of herbicides with similar modes of action increases selection pressure on plants, accelerating the development of resistance. [83; 86; 87] According to the HRAC it can be distinguished between herbicide resistance and herbicide tolerance. [72] A plant is defined as herbicide resistant if the plant survives the use of an herbicide in the recommended concentration. An herbicide tolerant plant is also capable of reproduction after the treatment with the herbicide. Further, herbicide resistance mechanisms can be divided into target-site (TSR) and non-target-site (NTSR) resistances. [86; 88]

Target-site resistances

TSR mechanisms can be classified into two groups. TSR of the first group are caused by mutations in the amino acid sequence and result in the inability of the herbicide to bind to the enzyme. In some cases, the enzyme activity may also be reduced while others retain full enzyme function. TSR mechanisms are specific to a single site of action. However, cross-resistances with other chemical families within this site of action may also occur. [86–88] These different effects will be illustrated in the following two examples. The first example is a single amino acid substitution in the *psbA* gene, which encodes for the D1 protein of the photosystem II (see 2.2.2). Typically, a single amino acid change in this gene will lead to high-level resistance of herbicides of the same chemical family, but only moderate or no resistance to other families. For instance, substitution of glycine for serine at position 264 will prevent binding of triazines, but not of triazones or nitriles. However, this substitution also affects the binding of plastoquinone, which results in the impairment of the photosynthesis. [86; 88; 89] The second example is a mutation of the ALS (see 2.2.2). Several ALS mutations are known, and the strength of resistance as well as the spectrum of resistance across chemical families varies depending on the mutation. For example, the Trp-574 mutation leads to resistance to both sulfonylureas and imidazolinones because the binding sites of both classes of herbicides overlap on the enzyme. In addition, the activity of the enzyme is not affected by the mutation as it is not located at the substrate binding site. [88]

Both examples shown are caused by a non-synonymous single nucleotide polymorphism, the most common TSR mechanism. Further, multiple nucleotide polymorphism or complete codon deletion can occur.

TSR of the second group arise by increased expression of the gene at the target site. This can result from regulatory changes that increase transcription or from increased genomic copy number of the gene. In consequence, higher amounts of the herbicide are needed to inhibit the target enzyme. [86–88]

Non-target-site resistances

NTSRs involve a number of non-specific mechanisms that ensure that the herbicide concentration originally used is no longer sufficient to kill the plant. NTSRs include reduced absorption and/or translocation in the plant or increased sequestration on cell walls or in vacuoles, which reduces the concentration of active ingredients reaching their target enzyme. Reduced absorption for instance can be a result of changes in the physical and chemical properties of the cuticle. [90] Another mechanism is an increase in plant metabolism, which leads to increased degradation of the herbicide to less toxic compounds. [86–88] The detoxification of herbicide can be divided into three phases. Phase I involves the functionalization (e.g. hydroxylation, oxidation, reduction) of the molecule to increase its hydrophilicity mediated by cytochrome P450. In the second phase the molecules are conjugated to biomolecules such as glutathione or sugars, followed by the transport to vacuoles or cell walls where additional breakup or sequestration takes place (phase III). [88; 91]

2.2.4   Regulations in the European Union (EU)

The approval of pesticides is a two-stage process. In a first step the active substance must be approved by the EU. The legal basis is Regulation (EC) No 1107/2009, which lists the necessary approval criteria. Thus, in addition to demonstrating sufficient efficacy, criteria for persistence, toxicity and bioaccumulation must also be fulfilled. The dossier to be submitted must allow maximum residue levels (MRLs) and, where appropriate, acceptable daily intakes (ADIs) to be established based on available data. In addition, valid analytical methods for the determination of the substance must be specified. The evaluation is carried out by the member states, the European Food Safety Authority (EFSA) and the European Commission (EC). In Germany, the Federal Office of Consumer Protection and Food Safety (BVL), the Federal Environment Agency (UBA), the Julius Kühn Institute (JKI, Federal Research Centre for Cultivated Plants) and the German Federal Institute for Risk Assessment (BfR) are involved in this evaluation. The approval is usually valid for a period of 10 years, after which a re-evaluation has to be carried out. The subsequent step is the approval at the national level. The legal basis is Regulation (EC) No 1107/2009 and Directive 2009/128/EC, implemented in Germany in the law on the protection of cultivated plants (PflSchG). Since the respective pesticide usually contains not only the active ingredient but also a number of adjuvants such as solubilizers, spreading or wetting agents, again numerous criteria must be fulfilled, as was the case for the active ingredient alone. Applicants can also apply for simultaneous approval in several member states of a zone. In this case, the evaluation is carried out jointly by the countries involved (zonal approval). The EU member countries are divided into three zones based on their climatic conditions: South, Central and North. [92; 93]

2.2.5   Herbicides from natural sources

As mentioned earlier, the increasing incidence of resistance is leading to an urgent need for the development of herbicides with new mechanisms of action. In this context, natural phytotoxins are of increasing interest, either as herbicides used directly, as templates for the synthesis of better herbicides, or for the identification of new target sides. [94–96] Natural products have had a significant impact on the development of pesticides. Thus, Cantrell et al. (2012) categorized all pesticide registrations during the period 1997 – 2010 into synthetic, synthetic natural, natural product, and biological pesticides. [97] Interestingly, in the case of fungicides and insecticides, about 30 % were either natural products or natural product derived, while for herbicides only 8 % were natural product derived. [97] Considering all pesticides recognized by HRAC (Herbicide Action Resistance Committee), IRAC (Insecticide Action Resistance Committee) and FRAC (Fungal Resistance Action Committee) and adding all natural products, natural product derived compounds, and compounds that have (potentially) used natural products as a model, the percentage is 61 % compared to 39 % for purely synthetic compounds. [95] This clearly underlines the high potential of natural products in the development of pesticides.

In addition, public and political pressure on organic agriculture is growing. However, the direct use of natural products in commercial herbicides is very limited, in addition to their advantages they also have several limitations. While natural products offer a wide variety of unique scaffolds with oxygen- and nitrogen-rich molecules, this structural complexity in turn makes the synthesis of these compounds difficult and cost intensive. Another advantage and disadvantage in equal measure is the relatively short half-life in the environment. On the one hand, the absence of "unnatural" ring structures as well as the low content of heavy atoms makes these compounds much more environmentally friendly. On the other hand, however, the rate of degradation may be too rapid for them to be effective herbicides. Further, their physicochemical properties might be not ideal for an uptake or the translocation in the plant to cause effects at economic costs. [96] Nevertheless, natural products can be used as templates for efficient herbicides by simplification of the core structure to reduce the costs of the synthesis or by derivatization of the compound to improve its physiochemical properties. [96; 98]

Two examples of natural products used as commercial herbicides recognized by HRAC are pelargonic acid (**2.34**Figure 2-10) and bialaphos (**2.20**). Pelargonic acid (**2.34**) is a fatty acid used as a contact herbicide at high doses. It acts by disrupting the plasma membrane. [96; 99] Bialaphos (**2.20**), on the other hand, is a tripeptide produced by *Streptomyces hygroscopius* and *S. viridochromeogenes* that acts by inhibiting glutamine synthase, as described in chapter 2.2.2. [96] The phytotoxic properties are related to its phosphinothricin group. Thus, bialophos (**2.20**) gave rise to the synthetic herbicide glufosinate ammonium (**2.19**), which is a racemate of the aforementioned phosphinothricin. Another example is 3-indoleacetic acid (**2.5**) which served as a model for the development of several auxin-mimicking herbicides. [96] Additionally, numerous natural products have more than one MOA, which demonstrates another advantage of natural products as a basis for new herbicides. Examples are sarmentine (**2.35**) isolated from *Piper* sp. [100], sorgoleone (**2.36**) from *Sorgheum bicolor* (L.) Moench [101] and 3-acetyl-5-isopropyltetramic acid (**2.37**). [102] None of the commercially available herbicides exhibit this characteristic. However, the presence of multiple targets would make the development of resistance much less likely. [96; 103]
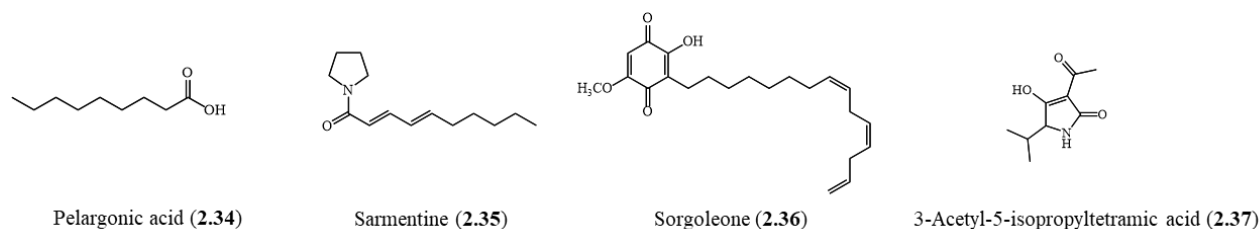

Pelargonic acid (**2.34**)   Sarmentine (**2.35**)   Sorgoleone (**2.36**)   3-Acetyl-5-isopropyltetramic acid (**2.37**)

Figure 2-10 Examples of natural products with herbicidal activity.

The classical approach to identify new natural products of interest is bioassay-guided isolation of crude extracts. After each separation step, all fractions are retested for bioactivity, and the active fractions are further purified. The structures of the isolated compounds are elucidated by NMR, HRMS and X-ray christallography. Another approach are structure-based tactics. Initially, the crude extract is screened for unique structural properties. Fractionation is based on the novelty of the compounds. [104] However, the classical approach of natural product isolation leads to increasing numbers of re-discoveries. [104; 105] Future prospects include genome-directed discovery of new natural products and their subsequent

expression from gDNA in heterologous hosts. To date, this approach has been limited due to bioinformatics challenges in identifying new gene clusters and subsequently predicting chemical structures. Especially since there are a number of natural products in which additional genes at distal loci to its biosynthetic gene cluster are involved. [104; 106; 107] Another approach is the combination of genomic analysis with metabolomics to verify biosynthetic gene clusters and to link them to natural product families. However, also this concept requires a large amount of data to allow this linkage. [104; 105]

2.2.6 Delayed fluorescence

Definition and delimitation
Delayed fluorescence is a type of luminescence. In general, luminescence is understood as the emission of light from an excited electronic state of molecules. Depending on its origin, luminescence can be divided into photoluminescence and chemoluminescence. In photoluminescence, molecules absorb energy by exciting electrons from the ground state to a higher state. Upon return to the ground state, the absorbed energy can be converted into radiation. [108] Three types of radiative transitions are known (**Figure 2-11-A-C**): fluorescence (**A**), phosphorescence (**B**) and delayed fluorescence (**C**).

Fluorescence (**A**) is the emission of photons from S_1 (first excited singlet state) to S_0 (singlet ground state of the molecule). A singlet state of a molecule is one in which all electrons are paired in up and down pairs. Thus, it is a radiative transition between two electronic states of the same spin multiplicity. Fluorescence occurs on a timescale of 10^{-10} to 10^{-7} s.

Phosphorescence (**B**) is the emission of photons from T_1 (first excited triplet state) to S_0 of the molecule. A triplet state is one in which one set of two electrons in different orbitals have the same orientation, up-up or down-down. Thus, it is a radiative transition between two electronic states of different spin multiplicity. Typical phosphorescence lifetimes are 10^{-6} to 10 s, well above those of fluorescence.

Delayed fluorescence (**C**) is the result of two intersystem crossings. An intersystem crossing is a non-radiative transition between two isoenergetic vibrational levels belonging to electronic states with different spin multiplicity. The intersystem crossing occurs first from S_1 to T_1, then from T_1 to S_1, followed by a radiative transition to S_0. The emission is identical in wavelength to standard fluorescence. [109; 110] Delayed fluorescence is caused by two different mechanisms: thermally activated delayed fluorescence and triplet-triplet-annihilation.

In thermally activated delayed fluorescence occurs a transition from T_1 to S_1 through reverse intersystem crossing. To do this, the molecule must have sufficient thermal energy to overcome the energy gap between the S_1 and T_1 states. In triplet-triplet annihilation, energy transfer occurs between two molecules in the T_1 state. In this process, one molecule is transferred to the S_1 state, while the other returns to the S_0 state.

| A | Fluorescence | B | Phosphorescence | C | Delayed Fluorescence |
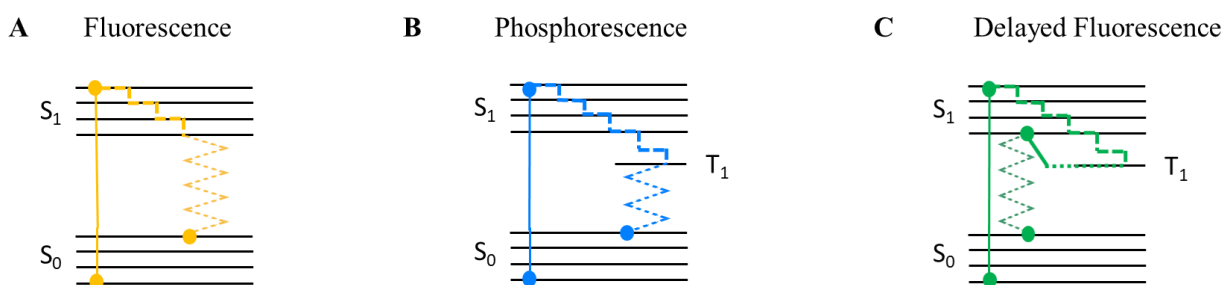
Figure 2-11 Jablonski diagram of **A**: fluorescence, **B**: phosphorescence, **C**: delayed fluorescence.

Delayed fluorescence in plants
Delayed fluorescence, also called afterglow, is a weak light emitted by green plants, algae and photosynthesizing bacteria for a short period of time after a preceding illumination. Delayed fluorescence follows the prompt fluorescence, which is extinguished after about 5 ns after illumination. [111; 112] Source of this emission is chlorophyll *a* in the light-harvesting antenna, associated with Photosystem II (PS II). [109]

When P680 (PS II chlorophyll) absorbs photon energy from the antenna complex, it transitions to an excited state P680*. [113] From this unstable state, an electron can be transferred, via a phaeophytin molecule, to the primary electron acceptor plastoquinone A (Q_A). The electron can then be further transferred to Q_B or transferred back to recombine with P680$^+$ (oxidized form of P680) and produce a re-exited P680*. [114; 115] The re-excited P680* can generate DF either by emitting a photon directly or after transfer back to the antennas. [113] Thus, it can be summarized that DF exists, because all redox reactions of the photosynthetic

electron transport are reversible. [109] Delayed fluorescence of plants was first discovered by Strehler and Arnold (1951) and since then had become a powerful tool to investigate environmental influences on plants. [116] Major advantages are the high sensitivity of photosynthesis to environmental factors, as well as the possibility to carry out measurements in native samples. [109] Various application of delayed fluorescence for the analysis of different chemical and physical factors have been described in the literature [117], including herbicides [118], drought stress [119; 120], heat stress [121], heavy metals [122], nutrient deficiencies [123] and many more.

References

[1] Jayawardena, R.S., *Colletotrichum*: Lifestyles, biology, morpho-species, species complexes and accepted species, *Mycosphere* **2021**, *12*, 519–669, doi: 10.5943/mycosphere/12/1/7.

[2] Hyde, K.D., Refined families of Sordariomycetes, *Mycosphere* **2020**, *11*, 305–1059, doi: 10.5943/mycosphere/11/1/7.

[3] Talhinhas, P.; Baroncelli, R., *Colletotrichum* species and complexes: geographic distribution, host range and conservation status, *Fungal Divers.* **2021**, *110*, 109–198, doi: 10.1007/s13225-021-00491-9.

[4] Réblová, M.; Gams, W.; Seifert, K.A., Monilochaetes and allied genera of the Glomerellales, and a reconsideration of families in the Microascales, *Stud. Mycol.* **2011**, *68*, 163–191, doi: 10.3114/sim.2011.68.07.

[5] Cannon, P.F.; Damm, U.; Johnston, P.R.; Weir, B.S., *Colletotrichum* - current status and future directions, *Stud. Mycol.* **2012**, *73*, 181–213, doi: 10.3114/sim0014.

[6] Species Fungorum, https://www.speciesfungorum.org/, last access: 09.01.2024.

[7] MycoBank, https://www.mycobank.org/, last access: 09.01.2024.

[8] Moraga, J.; Gomes, W.; Pinedo, C.; Cantoral, J.M.; Hanson, J.R.; M. Carbú, C.; Garrido, C.; Durán-Patrón, R.; Collado, I. G., The current status on secondary metabolites produced by plant pathogenic *Colletotrichum* species, *Phytochem. Rev.* **2019**, *18*, 215–239, doi: 10.1007/s11101-018-9590-0.

[9] Bailey, J.A. and Jeger, M.J. (eds.), *Colletotrichum: Biology, Pathology and Control*, C.A.B. International, Wallingford, Oxon, **1992**.

[10] Da Silva, L.L.; Moreno, H.L.A.; Correia, H.L.N.; Santana, M.F; de Queiroz, M.V., *Colletotrichum*: species complexes, lifestyle, and peculiarities of some sources of genetic variability, *Appl. Microbiol. Biotechnol.* **2020**, *104*, 1891–1904, doi: 10.1007/s00253-020-10363-y.

[11] Jeffries, P.; Dodd, J.C.; Jeger, M.J.; Plumbley, R.A., The biology and control of *Colletotrichum* species on tropical fruit crops, *Plant Pathol.* **1990**, *39*, 343–366, doi: 10.1111/j.1365-3059.1990.tb02512.x.

[12] De Silva, D.D.; Crous, P.W.; Ades, P.K.; Hyde, K.D.; Taylor, P.W., Life styles of *Colletotrichum* species and implications for plant biosecurity, *Fungal Biol. Rev.* **2017**, *31*, 155–168, doi: 10.1016/j.fbr.2017.05.001.

[13] Crouch, J.; O'Connell, R.; Gan, P.; Buiate, E.; Torres, M.F.; Beirn, L.; Shirasu, K.; Vaillancourt, L., *Genomics of Plant-Associated Fungi: Monocot Pathogens*, Dean, R.A., Lichens-Park, A.; Kole, C. (eds.), Springer Berlin Heidelberg, Berlin, Heidelberg, **2014**, 69–102.

[14] Jayawardena, R.S., Notes on currently accepted species of *Colletotrichum*, *Mycosphere* **2016**, *7*, 1192–1260, doi: 10.5943/mycosphere/si/2c/9.

[15] Damm, U.; O'Connell, R.J.; Groenewald, J.Z., Crous, P.W., The *Colletotrichum destructivum* species complex - hemibiotrophic pathogens of forage and field crops, *Stud. Mycol.* **2014**, *79*, 49–84, doi: 10.1016/j.simyco.2014.09.003.

[16] O'Connell, R.J.; Thon, M.R.; Hacquard, S.; Amyotte, S.G.; Kleemann, J.; Torres, M.F. et al., Lifestyle transitions in plant pathogenic *Colletotrichum* fungi deciphered by genome and transcriptome analyses, Nat. Genet. **2012**, *44*, 1060–1065, doi: 10.1038/ng.2372.

[17] Wippel, K., Plant and microbial features governing an endophytic lifestyle, *Curr. Opin. Plant Biol.* **2023**, *76*, 102483, doi: 10.1016/j.pbi.2023.102483.

[18] Busby, P.E.; Ridout, M.; Newcombe, G., Fungal endophytes: modifiers of plant disease, *Plant Mol. Biol.* **2016**, *90*, 645–655, doi: 10.1007/s11103-015-0412-0.

[19] Grabka, R.; d'Entremont, T.W.; Adams, S.J.; Walker, A.K.; Tanney, J.B.; Abbasi, P.A.; Ali, S., Fungal endophytes and their role in agricultural plant protection against pests and pathogens, *Plants* **2022**, *11*, 384, doi: 10.3390/plants11030384.

[20] Crouch, J.A.; Tredway, L.P.; Clarke, B.B.; Hillman, B.I., Phylogenetic and population genetic divergence correspond with habitat for the pathogen *Colletotrichum cereale* and allied taxa across diverse grass communities, *Mol. Ecol.* **2009**, *18*, 123–135, doi: 10.1111/j.1365-294X.2008.04008.x.

[21] Peres, N.A.; Timmer, L.W.; Adaskaveg, J.E.; Correll, J.C., Lifestyles of *Colletotrichum acutatum*, *Plant Dis.* **2005**, *89*, 784–796, doi: 10.1094/PD-89-0784.

[22] Damm, U.; Cannon, P.F.; Woudenberg, J.H.C.; Crous, P.W., The *Colletotrichum acutatum* species complex, *Stud. Mycol.* **2012**, *73*, 37–113, doi: 10.3114/sim0010.

[23] Weir, B.S.; Johnston, P.R.; Damm, U., The *Colletotrichum gloeosporioides* species complex, *Stud. Mycol.* **2012**, *73*, 115–180, doi: 10.3114/sim0011.

[24] Vieira, W.A.S.; Michereff, S.J.; de Morais, M.A.; Hyde, K.D.; Câmara, M.P.S., Endophytic species of *Colletotrichum* associated with mango in northeastern Brazil, *Fungal Divers.* **2014**, *67*, 181–202, doi: 10.1007/s13225-014-0293-6.

[25] Perfect, S.E., Hughes, H.B.; O' Connell, R.J.; Green, J.R., *Colletotrichum*: A model genus for studies on pathology and fungal–plant interactions, *Fungal Genet. Biol.* **1999**, *27*, 186-198, doi: 10.1006/fgbi.1999.1143.

[26] Mendgen, K.; Hahn, M., Plant infection and the establishment of fungal biotrophy, *Trends Plant Sci.* **2002**, *7*, 352–356, doi: 10.1016/s1360-1385(02)02297-5.

[27] van Kan, J.A.L., Licensed to kill: the lifestyle of a necrotrophic plant pathogen, *Trends Plant Sci.* **2006**, *11*, 247–253, doi: 10.1016/j.tplants.2006.03.005.

[28] Münch, S.; Lingner, U.; Floss, D.S.; Ludwig, N.; Sauer, N.; Deising, H.B., The hemibiotrophic lifestyle of *Colletotrichum* species, *J. Plant Physiol.* **2008**, *165,* 41–51, doi: 10.1016/j.jplph.2007.06.008.

[29] Vargas, W.A.; Martín, J.M.S.; Rech, G.E.; Rivera, L.P.; Benito, E.P.; Díaz-Mínguez, J.M., Thon, M.R.; Sukno, S.A., Plant defense mechanisms are activated during biotrophic and necrotrophic development of *Colletotricum graminicola* in maize, *Plant Physiol.* **2012**, *158,* 1342–1358, doi: 10.1104/pp.111.190397.

[30] Prusky, D., Pathogen quiescence in postharvest diseases, *Annu. Rev. Phytopathol.* **1996**, *34,* 413–434, doi: 10.1146/annurev.phyto.34.1.413.

[31] Talhinhas, P.; Mota-Capitão, C.; Martins, S.; Ramos, A.P.; Neves-Martins, J.; Guerra-Guimarães, L., Epidemiology, histopathology and aetiology of olive anthracnose caused by *Colletotrichum acutatum* and *C. gloeosporioides* in Portugal, *Plant Pathol.* **2011**, *60,* 483–495, doi: 10.1111/j.1365-3059.2010.02397.x.

[32] Leite, B.; Nicholson, R.L., Mycosporine-alanine: A self-inhibitor of germination from the conidial mucilage of *Colletotrichum graminicola*, *Exp. Mycol.* **1992**, *16,* 76–86, doi:: 10.1016/0147-5975(92)90043-Q.

[33] Rawlings, S.L.; O'Connell, R.J.; Green, J.R., The spore coat of the bean anthracnose fungus *Colletotrichum lindemuthianum* is required for adhesion, appressorium development and pathogenicity, *Physiol. Mol. Plant Pathol.* **2007**, *70,* 110–119, doi: 10.1016/j.pmpp.2007.07.007.

[34] Mercure, E.W.; Leite, B.; Nicholson, R.L., Adhesion of ungerminated conidia of *Colletotrichum graminicola* to artificial hydrophobic surfaces, *Physiol. Mol. Plant Pathol.* **1994**, *45,* 421–440, doi: 10.1016/S0885-5765(05)80040-2.

[35] Flaishman, M.A.; Kolattukudy, P.E., Timing of fungal invasion using host's ripening hormone as a signal, *Proc. Nat. Acad. Sci. U.S.A.* **1994**, *91,* 6579–6583, doi: 10.1073/pnas.91.14.6579.

[36] Hwang, C.S.; Kolattukudy, P. E., Isolation and characterization of genes expressed uniquely during appressorium formation by *Colletotrichum gloeosporioides* conidia induced by the host surface wax, *MGG* **1995**, *247,* 282–294, doi: 10.1007/BF00293196.

[37] Liu, Z.M.; Kolattukudy, P.E., Identification of a gene product induced by hard-surface contact of *Colletotrichum gloeosporioides* conidia as a ubiquitin-conjugating enzyme by yeast complementation, *J. Bacteriol.* **1998**, *180,* 3592–3597, doi: 10.1128/JB.180.14.3592-3597.1998.

[38] Latunde-Dada, A.O., *Colletotrichum*: tales of forcible entry, stealth, transient confinement and breakout, *Mol. Plant Pathol.* **2001**, *2,* 187–198, doi: 10.1046/j.1464-6722.2001.00069.x.

[39] Ludwig, N.; Löhrer, M.; Hempel, M.; Mathea, S.; Schliebner, I.; Menzel, M.; Kiesow, A.; Schaffrath, U.; Deising, H.B.; Horbach, R., Melanin is not required for turgor generation but enhances cell-wall rigidity in appressoria of the corn pathogen *Colletotrichum graminicola*, *IS-MPMI* **2014**, *27,* 315–327, doi: 10.1094/MPMI-09-13-0267-R.

[40] Deising, H.B.; Werner, S.; Wernitz, M., The role of fungal appressoria in plant infection, *Microbes Infect.* **2000**, *2,* 1631–1641, doi: 10.1016/S1286-4579(00)01319-8.

[41] Wharton P.S.; Diéguez-Uribeondo, J., The biology of *Colletotrichum acutatum*, *Anal. Jard. Bot. Madr.* **2004**, *61*, doi*:* 10.3989/ajbm.2004.v61.i1.61.

[42] Latunde-Dada, A.O.; Lucas, J.A., Localized hemibiotrophy in *Colletotrichum*: cytological and molecular taxonomic similarities among *C. destructivum*, *C. linicola* and *C. truncatum*, *Plant Pathol.* **2007**, *56,* 437–447, doi: 10.1111/j.1365-3059.2007.01576.x.

[43] Perfect, S.; Green, J.R., Infection structures of biotrophic and hemibiotrophic fungal plant pathogens, *Mol. Plant Pathol.* **2001**, *2*, 101-108, doi: 10.1046/j.1364-3703.2001.00055.x.

[44] Wharton, P.S.; Julian, A.M.; O'Connell, R.J., Ultrastructure of the Infection of *Sorghum bicolor* by *Colletotrichum sublineolum*, *Phytopathology* **2001**, *91,* 149–158, doi: 10.1094/PHYTO.2001.91.2.149.

[45] Moraes, S.R.G.; Tanaka, F.A.O.; Massola Júnior, N.S., Histopathology of *Colletotrichum gloeosporioides* on guava fruits (*Psidium guajava* L.), *Rev. Bras. Frutic.* **2013**, *35,* 657–664, doi: 10.1590/S0100-29452013000200039.

[46] Nordzieke, D.E.; Sanken, A.; Antelo, L.; Raschke, A.; Deising, H.B.; Pöggeler, S., Specialized infection strategies of falcate and oval conidia of *Colletotrichum graminicola*, *Fungal Genet. Biol.* **2019**, *133,* 103276, doi: 10.1016/j.fgb.2019.103276.

[47] Frey, T.J.; Weldekidan, T.; Colbert, T.; Wolters, P.; Hawk, J.A., Fitness evaluation of rcg1, a locus that confers resistance to *Colletotrichum graminicola* (Ces.) G.W. Wils. using near-isogenic maize hybrids, *Crop Sci.* **2011**, *51,* 1551–1563, doi: 10.2135/cropsci2010.10.0613.

[48] Kim, J.W.; Shim, S.H., The fungus *Colletotrichum* as a source for bioactive secondary metabolites, *Arch. Pharm. Res.* **2019**, *42,* 735–753, doi: 10.1007/s12272-019-01142-z.

[49] Wang, J.; Zhang, R.; Chen, X.; Sun, X.; Yan, Y.; Shen, X.; Yuan, Q., Biosynthesis of aromatic polyketides in microorganisms using type II polyketide synthases, *Microb. Cell Factories* **2020**, *19,* 110, doi: 10.1186/s12934-020-01367-4.

[50] Schümann, J.; Hertweck, C., Advances in cloning, functional analysis and heterologous expression of fungal polyketide synthase genes, *J. Biotechnol.* **2006**, *124,* 690–703, doi: 10.1016/j.jbiotec.2006.03.046

[51] Staunton, J.; Weissman, K. J., Polyketide biosynthesis: a millennium review, *Nat. Prod. Rep.* **2001**, *18,* 380–416, doi: 10.1039/a909079g.

[52] Wicklow, D.T.; Jordan, A.M.; Gloer, J.B., Antifungal metabolites (monorden, monocillins I, II, III) from

Colletotrichum graminicola, a systemic vascular pathogen of maize, *Mycol. Res.* **2009**, *113,* 1433–1442, doi: 10.1016/j.mycres.2009.10.001.

[53] Horbach, R.; Graf, A.; Weihmann, F.; Antelo, L.; Mathea, S.; Liermann, J.C; Opatz, T.; Thines, E.; Aguirre, J.; Deising, H.B., Sfp-type 4′-phosphopantetheinyl transferase is indispensable for fungal pathogenicity, *Plant Cell* **2009**, *21,* 3379–3396, doi: 10.1105/tpc.108.064188.

[54] Habtemariam, S., *Medicinal Foods as Potential Therapies for Type-2 Diabetes and Associated Diseases*, Academic Press, London, San Diego, CA, **2019**, doi: 10.1016/C2018-0-02257-4.

[55] Aoyagi, A.; Ito-Kobayashi, M.; Ono, Y.; Furukawa, Y.; Takahashi, M.; Muramatsu, Y.; Umetani, M.; Takatsu, T., Colletoic acid, a novel 11beta-hydroxysteroid dehydrogenase type 1 inhibitor from *Colletotrichum gloeosporioides* SANK 21404, *J. Antibiot.* **2008**, *61,* 136–141, doi: 10.1038/ja.2008.122.

[56] Wei, B.; Yang, Z.-D.; Chen, X.; Zhou, S.-Y.; Yu, H.-T.; Sun, J.-Y.; Yao, X.-J.; Wang, Y.; Xue, H.-Y., Colletotrilactam A-D, novel lactams from *Colletotrichum gloeosporioides* GT-7, a fungal endophyte of *Uncaria rhynchophylla*, *Fitoterapia* **2016**, *113,* 158–163, doi: 10.1016/j.fitote.2016.08.005.

[57] Dey, P.; Kundu, A.; Kumar, A.; Gupta, M.; Lee, B.M.; Bhakta, T.; Dash, S.; Kim, H.S., Analysis of alkaloids, *Recent Advances in Natural Products Analysis,* Silva, A.S.; Nabavi, S.F.; Nabavi, S.M. (eds.), Elsevier, **2020,** 505–567, doi: 10.1016/B978-0-12-816455-6.00015-9.

[58] Chung, K.R.; Shilts, T.; Ertürk, U.; Timmer, L.W.; Ueng, P.P., Indole derivatives produced by the fungus *Colletotrichum acutatum* causing lime anthracnose and postbloom fruit drop of citrus, *FEMS Microbiol. Lett.* **2003**, *226,* 23–30, doi: 10.1016/S0378-1097(03)00605-0.

[59] Zhou, J.; Wei, H.; Li, S.-M., Colletotriauxins A–D, New plant growth inhibitors from the phytopathogenic fungus *Colletotrichum gloeosporioides*, *J. Agric. Food Chem.* **2023**, *71,* 11104–11109, doi: 10.1021/acs.jafc.3c03143.

[60] Miller, B.R.; Gulick, A.M., Structural biology of nonribosomal peptide synthetases, *Methods Mol. Biol.* **2016**, *1401,* 3–29, doi: 10.1007/978-1-4939-3375-4_1.

[61] Borgman, P.; Lopez, R.D.; Lane, A.L., The expanding spectrum of diketopiperazine natural product biosynthetic pathways containing cyclodipeptide synthases, *Org. Biomol. Chem.* **2019**, *17,* 2305–2314, doi: 10.1039/c8ob03063d.

[62] Soltani, J., *New and future developments in microbial biotechnology and bioengineering,* Gupta, V.K (ed.), Elsevier, Amsterdam, **2016,** 275–292,

[63] Ohra, J.; Morita, K.; Tsujino, Y.; Tazaki, H.; Fujimori, T.; Goering, M.; Evans, S.; Zorner, P., Production of the phytotoxic metabolite, ferricrocin, by the fungus *Colletotrichum gloeosporioides*, *Biosci. Biotechnol. Biochem.* **1995**, *59,* 113–114, doi: 10.1271/bbb.59.113.

[64] Grundmann, A.; Li, S.-M., Overproduction, purification and characterization of FtmPT1, a brevianamide F prenyltransferase from *Aspergillus fumigatus*, *Microbiology* **2005**, *151,* 2199–2207, doi: 10.1099/mic.0.27962-0.

[65] Zhi-jun, Y.; Yu, Y.; Zhi-Quiang, W.; Tian, Y.; Dai-jie, C., Cytotoxic metabolites of endophytic fungus *Colletotrichum* sp. from *Aristolochia* spp., *Nat. Prod. Res. Dev.* **2012**, *23,* 329-332, https://www.trcw.ac.cn/EN/Y2012/V23/I3/329, last access 12.03.2024.

[66] Tsuge, T.; Harimoto, Y.; Akimitsu, K.; Ohtani, K.; Kodama, M.; Akagi, Y.; Egusa, M.; Yamamoto, M.; Otani, H., Host-selective toxins produced by the plant pathogenic fungus *Alternaria alternata*, *FEMS Microbiol. Rev.* **2013**, *37,* 44–66, doi: 10.1111/j.1574-6976.2012.00350.x.

[67] Alleyne, A.T.; O'Garro, L.; Delaunay, A.J., Host specificity of putative anthracnose toxins from *Colletotrichum gloeosporioides*, 31st Annual Meeting, **1995**, Dover, Barbados 257091, Caribbean Food Crops Society, doi: 10.22004/ag.econ.257091.

[68] Gan, P.; Ikeda, K.; Irieda, H.; Narusaka, M.; O'Connell, R. J.; Narusaka, Y.; Takano, Y.; Kubo, Y.; Shirasu, K., Comparative genomic and transcriptomic analyses reveal the hemibiotrophic stage shift of *Colletotrichum* fungi, *New Phytol.* **2013**, *197,* 1236–1249, doi: 10.1111/nph.12085.

[69] Masi, M.; Cimmino, A.; Boari, A.; Tuzi, A; Zonno, M.C.; Baroncelli, R.; Vurro, M.; Evidente, A., Colletochlorins E and F, new phytotoxic tetrasubstituted pyran-2-one and dihydrobenzofuran, isolated from *Colletotrichum higginsianum* with potential herbicidal activity, *J. Agric. Food Chem.* **2017**, *65,* 1124–1130, doi: 10.1021/acs.jafc.6b05193.

[70] Mesnage, R.; Székács, A.; Zaller, J.G., Herbicides: Brief history, agricultural use, and potential alternatives for weed control, *Herbicides,* Mesnage, R.; Zaller, J. G. (eds.), Elsevier, **2021,** 1–20, doi: 10.1016/B978-0-12-823674-1.00002-X.

[71] Vats, S., Herbicides: History, classification and genetic manipulation of plants for herbicide resistance, *Sustain. Agric. Res.* **2015**, *15,* 153–192, doi: 10.1007/978-3-319-09132-7_3.

[72] Herbicide Resistance Action Committee, *HRAC Mode of Action Classification 2022 Map*, https://hracglobal.com/tools/hrac-mode-of-action-classification-2022-map, last access: **09.01.2024**.

[73] Duke, S.O., Overview of herbicide mechanisms of action, *Environ. Health Perspect.* **1990**, *87,* 263, doi: 10.2307/3431034.

[74] Knaak, J.B. (ed.), *Reviews of Environmental Contamination and Toxicology – Glyphosate, Volume 255,* Springer International Publishing, Cham, **2021**, ISSN: 0179-5953.

[75] Reade, J.P.H.; Cobb, A.H., Herbicides: mode of action and metabolism, *Weed management handbook,* 9. Ed., Naylor, R.E.L (ed.), British Crop Protection Council, Oxford, Malden, MA, **2002**, ISBN: 978-0-632-05732-0.

[76] Duke, S.O.; Dayan, F.E, Bioactivity of herbicides, *Comprehensive Biotechnology* **2011**, *4*, 23-35, doi: 10.1016/B978-0-08-088504-9.00273-7.

[77] Battaglino, B.; Grinzato, A.; Pagliano, C., Binding properties of photosynthetic herbicides with the QB site of the d1 protein in plant photosystem II: A combined functional and molecular docking study, *Plants* **2021**, *10*, 1501, doi*:* 10.3390/plants10081501.

[78] Kawakami, K.; Shen, J.-R., Purification of fully active and crystallizable photosystem II from thermophilic cyanobacteria, *Methods Enzymol.* **2018**, *613*, 1-16. doi: 10.1016/bs.mie.2018.10.002.

[79] Dayan, F.E., Current status and future prospects in herbicide discovery, *Plants* **2019**, *8*, 341, doi*:* 10.3390/plants8090341.

[80] Délye, C., Weed resistance to acetyl coenzyme A carboxylase inhibitors: an update, *Weed Sci.* **2005**, *53*, 728–746, doi: 10.1614/WS-04-203R.1.

[81] Takano, H.K.; Ovejero, R.F.L.; Belchior, G.G.; Maymone G.P.L.; Dayan, F.E., ACCase-inhibiting herbicides: mechanism of action, resistance evolution and stewardship, *Sci. Agric* **2021**, *78*, e20190102, doi 10.1590/1678-992X-2019-0102.

[82] Babczinski, P.; Watanabe, Y.; Nakatani, M.; Yoshimura, T.; Hanai, R.; Tanetani, Y.; Shimizu, T., Herbicides disturbing the synthesis of very long-chain fatty acids, *Modern crop protection compounds,* Krämer, W.; Schirmer, U.; Jeschke, P. (eds.), Wiley-VCH, Weinheim, Germany, **2012,** 305–337, doi: 10.1002/9783527644179.ch6.

[83] Moss, S.; Ulber, L.; Den Hoed, I., A herbicide resistance risk matrix, *Crop Prot.* **2019**, *115*, 13–19, doi: 10.1016/j.cropro.2018.09.005.

[84] Duke, S.O., Why have no new herbicide modes of action appeared in recent years?, *Pest Manag. Sci.* **2012**, 68, 505–512, doi: 10.1002/ps.2333.

[85] Heap, I. *The International Herbicide-Resistant Weed Database. Online.,* https://www.weedscience.org/, last access: **27.01.2024**.

[86] Powles, S.B.; Yu, Q., Evolution in action: plants resistant to herbicides, *Annu. Rev. Plant Biol.* **2010**, *61*, 317–347, doi: 10.1146/annurev-arplant-042809-112119.

[87] Heap, I., Global perspective of herbicide-resistant weeds, *Pest Manag. Sci.* **2014**, *70*, 9, 1306–1315, doi: 10.1002/ps.3696.

[88] Gaines, T.A.; Duke, S.O.; Morran, S.; Rigon, C.A.G.; Tranel, P.J.; Küpper, A.; Dayan, F.E., Mechanisms of evolved herbicide resistance, *J. Biol. Chem.* **2020**, *295*, 10307–10330, doi: 10.1074/jbc.REV120.013572.

[89] Gronwald, J.W., Resistance to PS II inhibitor herbicides, *Weed and Crop Resistance to Herbicides*, De Prado, R.; Jorrín, J.; García-Torres, L. (eds). Springer, Dordrecht, **1997**, doi: 10.1007/978-94-011-5538-0_5

[90] Délye, C., Unravelling the genetic bases of non-target-site-based resistance (NTSR) to herbicides: a major challenge for weed science in the forthcoming decade, *Pest Manag. Sci.* **2013**, *69*, 176–187, doi: 10.1002/ps.3318.

[91] Nandula, V.K.; Riechers, D.E.; Ferhatoglu, Y.; Barrett, M.; Duke, S.O.; Dayan, F.E.; Goldberg-Cavalleri, A.; Tétard-Jones, C.; Wortley, D.J.; Onkokesung, N.; Brazier-Hicks, M.; Edwards, R.; Gaines, T.; Iwakami, S.; Jugulam, M.; Ma, R., Herbicide metabolism: crop selectivity, bioactivation, weed resistance, and regulation, *Weed Sci.* **2019**, *67*, 2, 149–175, doi: 10.1017/wsc.2018.88.

[92] Umweltbundesamt, *Zulassung von Pflanzenschutzmitteln,* https://www.umweltbundesamt.de/themen/chemikalien/pflanzenschutzmittel/zulassung-von-pflanzenschutzmitteln, last access: **09.01.2024**.

[93] Bundesministerium für Ernährung und Landwirtschaft (BMEL), *Pflanzenschutz - Zulassungsverfahren - Schutz von Gesundheit und Umwelt,* https://www.bmel.de/DE/themen/landwirtschaft/pflanzenbau/pflanzenschutz/zulassung.html, last access: **12.01.2023**.

[94] Dayan, F.E.; Duke, S.O., Natural compounds as next-generation herbicides, *Plant Physiol.* **2014**, *166*, 1090–1105, doi: 10.1104/pp.114.239061.

[95] Gerwick, B.C.; Sparks, T.C., Natural products for pest control: an analysis of their role, value and future, *Pest Manag. Sci.* **2014**, *70*, 1169–1185, doi: 10.1002/ps.3744.

[96] Duke, S.O.; Pan, Z.; Bajsa-Hirschel, J.; Boyette, C.D., The potential future roles of natural compounds and microbial bioherbicides in weed management in crops, *Adv. Weed Sci.* **2022**, e020210054, doi: 10.51694/AdvWeedSci/2022;40:seventy-five003.

[97] Cantrell, C.L.; Dayan, F.E.; Duke, S.O., Natural products as sources for new pesticides, *J. Nat. Prod.* **2012**, *75*, 1231–1242, doi: 10.1021/np300024u.

[98] Sparks, T.C.; Duke, S.O., Structure simplification of natural products as a lead generation approach in agrochemical discovery, *J. Agric. Food Chem.* **2021**, *69*, 8324–8346, doi: 10.1021/acs.jafc.1c02616.

[99] Dayan, F.E.; Watson, S.B., Plant cell membrane as a marker for light-dependent and light-independent herbicide mechanisms of action, *Pestic. Biochem. Phys.* **2011**, *101*, 182–190, doi: 10.1016/j.pestbp.2011.09.004.

[100] Dayan, F.E.; Owens, D.K.; Watson, S.B.; Asolkar, R.N.; Boddy, L.G., Sarmentine, a natural herbicide from *Piper* species with multiple herbicide mechanisms of action, *Front. Plant Sci.* **2015**, *6*, 222, doi: 10.3389/fpls.2015.00222.

[101]   Dayan, F.E.; Rimando, A.M.; Pan, Z.; Baerson, S.R.; Gimsing, A.L.; Duke, S.O., Sorgoleone, *Phytochemistry* **2010**, *71*, 1032–1039, doi: 10.1016/j.phytochem.2010.03.011.

[102] Chen, S.; Zhou, F.; Yin, C.; Strasser, R.J.; Yang, C.; Qiang, S., Application of fast chlorophyll a fluorescence kinetics to probe action target of 3-acetyl-5-isopropyltetramic acid, *Environ. Exp. Bot.* **2011**, *71*, 269–279, doi: 10.1016/j.envexpbot.2010.12.013.

[103] Gressel, J., Perspective: present pesticide discovery paradigms promote the evolution of resistance - learn from nature and prioritize multi-target site inhibitor design, *Pest Manag. Sci.* **2020**, *76*, 421–425, doi: 10.1002/ps.5649.

[104] Lorsbach, B.A.; Sparks, T.C.; Cicchillo, R.M.; Garizi, N.V.; Hahn, D.R.; Meyer, K.G., Natural products: a strategic lead generation approach in crop protection discovery, *Pest Manag. Sci.* **2019**, *75*, 2301–2309, doi: 10.1002/ps.5350.

[105] Doroghazi, J.R.; Albright, J.C.; Goering, A.W.; Ju, K.-S.; Haines, R.R.; Tchalukov, K.A.; Labeda, D.P.; Kelleher, N.L.; Metcalf, W.W., A roadmap for natural product discovery based on large-scale genomics and metabolomics, *Nat. Chem. Biol.* **2014**, *10*, 963–968, doi: 10.1038/nchembio.1659.

[106] Van der Lee, T.A.J.; Medema, M.H., Computational strategies for genome-based natural product discovery and engineering in fungi, *Fungal Genet. Biol.* **2016**, *89*, 29–36, doi: 10.1016/j.fgb.2016.01.006.

[107] Chan, A.N.; Santa Maria, K.C; Li, B., Direct capture technologies for genomics-guided discovery of natural products, *Curr. Top Med. Chem.* **2016**;*16,* 1695-704, doi: 10.2174/1568026616666151012111209.

[108] Omary, M.A.; Patterson, H.H., Luminescence, Theory, *Encyclopedia of spectroscopy and spectrometry*, Lindon, J.C.; Tranter, G.E. Koppenaal, D.W. (eds.), Elsevier, Oxford, **1999,** 1186–1207, doi:10.1016/B978-0-12-803224-4.00193-X.

[109] Goltsev, V.; Zaharieva, I.; Chernev, P.; Strasser, R.J., Delayed fluorescence in photosynthesis, *Photosynth. Res.* **2009**, *101*, 217–232, doi: 10.1007/s11120-009-9451-1.

[110] Arnold, W.; Davidson, J.B., The identity of the fluorescent and delayed light emission spectra in *Chlorella, J. Gen. Physiol.* **1954**, *37,* 677–684, doi: 10.1085/jgp.37.5.677.

[111] Jursinic, P.A., Delayed fluorescence: current concepts and status, *Light emission by plants and bacteria*, Govindjee; Amesz, J.; Fork, D.C. (eds.), Elsevier Science, Burlington, **2012,** 291–328, ISBN: 978-0124124622.

[112] Krause, G.H.; Weis, E., Chlorophyll fluorescence and photosynthesis: The basics, *Annu. Rev. Plant. Physiol. Plant. Mol. Biol.* **1991**, *42*, 313–349, doi: 10.1146/annurev.pp.42.060191.001525.

[113] Goltsev, V.; Zaharieva, I.; Lambrev, P.; Yordanov, I.; Strasser R., Simultaneous analysis of prompt and delayed chlorophyll a fluorescence in leaves during the induction period of dark to light adaptation, *J. Theor. Biol.* **2003**, *225,* 171–183, doi: 10.1016/S0022-5193(03)00236-4.

[114] Guo, Y.; Tan, J., A kinetic model structure for delayed fluorescence from plants, *Biosystems* **2009**, *95*, 98–103, doi: 10.1016/j.biosystems.2008.08.002.

[115] Guo, Y.; Wirth, B.; Tan, J., Observation of plastoquinone kinetics in photosystem II from delayed fluorescence measurements, *IET Syst. Biol.* **2010***, 4*, 90–98, doi: 10.1049/iet-syb.2008.0157.

[116] Strehler, B.L.; Arnold, W., Light production by green plants, *J. Gen. Physiol.* **1951**, *34,* 809–820, doi: 10.1085/jgp.34.6.809.

[117] Guo, Y.; Tan, J., Applications of delayed fluorescence from photosystem II, *Sensors* **2013**, *13*, 17332–17345, doi: 10.3390/s131217332.

[118] Wu, C.; Varanasi, V.; Perez-Jones, A., A nondestructive leaf-disk assay for rapid diagnosis of weed resistance to multiple herbicides, *Weed Sci.* **2021**, 69, 274–283, doi: 10.1017/wsc.2021.15.

[119] Guo, Y.; Tan, J., A biophotonic sensing method for plant drought stress, *Sens. Actuators B.* **2013**, *188*, 519–524, doi: 10.1016/j.snb.2013.07.020.

[120] Liu, J.; Guo, Y.Y.; Bai, Y.W.; Camberato, J.J.; Xue, J.Q.; Zhang, R.H., Effects of drought stress on the photosynthesis in maize, *Russ. J. Plant Physiol.* **2018**, *65*, 849–856, doi: 10.1134/S1021443718060092.

[121] Oukarroum, A.; Goltsev, V.; Strasser, R.J., Temperature effects on pea plants probed by simultaneous measurements of the kinetics of prompt fluorescence, delayed fluorescence and modulated 820 nm reflection, *PloS one* **2013**, *8*, e59433, doi: 10.1371/journal.pone.0059433.

[122] Razinger, J.; Drinovec, L.; Berden-Zrimec, M., Delayed fluorescence imaging of photosynthesis inhibitor and heavy metal induced stress in potato, *Open Life Sci.* **2012**, *7,* 531–541, doi: 10.2478/s11535-012-0038-z.

[123] Berden-Zrimec, M.; Drinovec, L.; Molinari, I.; Zrimec, A.; Umani, S.F.; Monti, M., Delayed fluorescence as a measure of nutrient limitation in *Dunaliella tertiolecta, J. Photochem. Photobiol. B* **2008**, *92*, 13–18, doi: 10.1016/j.jphotobiol.2008.03.007.

3 Isolation of phytotoxic compounds from *Colletotrichum graminicola* cultivated in HMG medium

Abstract

Bioactivity-guided isolation of cultures of *Colletotrichum graminicola* grown in HMG (Hefeextrakt-Malzextrakt-Glucose) is medium resulted in the isolation of 19 compounds. The compounds include six previously unknown compounds (**3.1**, **3.10** – **3.12**, **3.17** and **3.18**), eight diketopiperazines (**3.2**, **3.4** – **3.9** and **3.15**), three acetamides (**3.3**, **3.13** – **3.14**), lumichrome (**3.16**) and uracil (**3.19**). Their structures were determined by NMR spectroscopic analysis and ESI-HRMS measurements. Absolute configurations of the diketopiperazines were established by quantum chemical CD calculations. The phytotoxic activity was determined using a leaf spot test on *Arabidopsis thaliana* Col-0 at concentrations between 100 and 10 mM. 11 out of 16 tested compounds showed a phytotoxic activity. The highest rate of phytotoxic activity was achieved by the diketopiperazines *cyclo*-L-Leu-L-Pro (**3.2**) and *cyclo*-L-Trp-D-Pro (**3.9**), which caused necrosis up to a concentration 20 mM.

3.1 Introduction

HMG (Hefeextrakt-Malzextrakt-Glucose) is an undefined medium, also called complex medium, which consists of malt extract, yeast extract and glucose. It provides the organism rich carbon and nitrogen sources, but the exact composition, e.g. quantities of nutrients, is unknown. [1] The malt extract serves mainly as a source of carbohydrates (mainly maltose), while the yeast extract serves as a source of amino acids, peptides and water-soluble vitamins. [2]

In a previous study, Horbach and co-workers investigated *Colletotrichum graminicola* grown on HMG medium. [3] Part of the work deals with the isolation of secondary metabolites from the culture filtrate of the wild type and the subsequent biological evaluation of isolated secondary metabolites. As a result, 6 new secondary metabolites, including two pyrones, two anthraquinones, a 10-hydroxyanthrone, and an 11-membered macrolactone, as well as the known compounds orcinol and tryptophol (**Figure 3-1**) could be recognized. The isolated compounds were tested for their phytotoxic activity by applying 5 µL droplets (concentration 1 µg/µL) on the surface of wounded and non-wounded maize leaves. However, no necrosis could be observed, suggesting that the compounds are not phytotoxic. In addition, the siderophores coprogen B, 2-*N*-methyl coprogen B, and ferricrocin were detected, as well as indole-3-acetic acid, himanimide C and 2-phenylethanol (**Figure 3-1**). [3] Phytotoxic or growth inhibitory effects have already been described in the literature for ferricrocin and 2-*N*-methyl coprogen B [4], indole-3-acetic acid [5] and 2-phenylethanol [6].
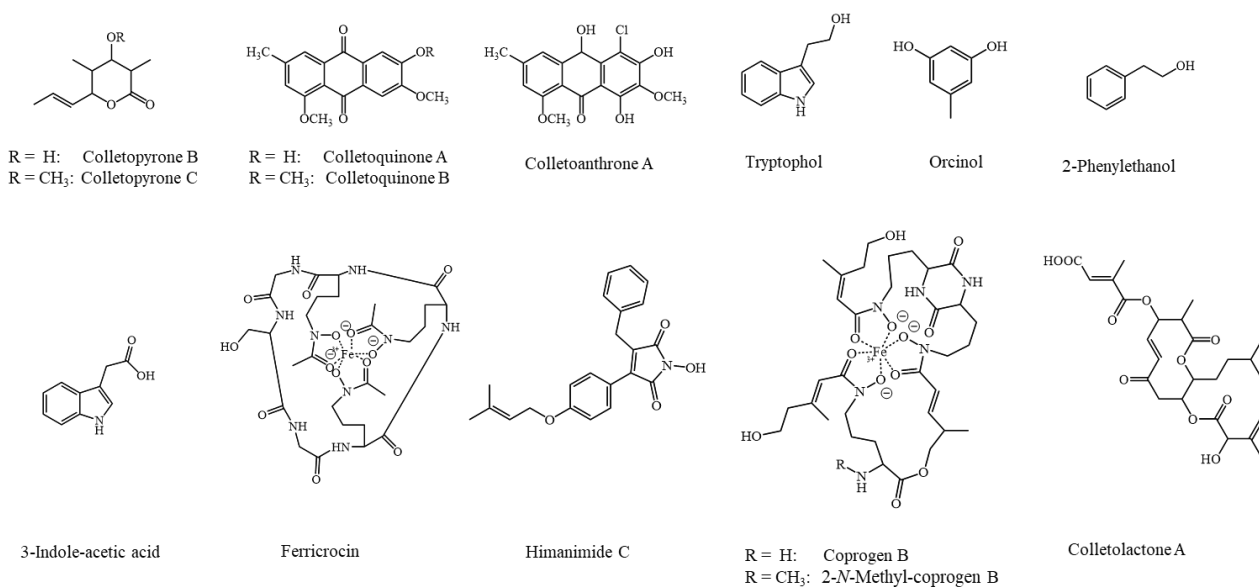
Figure 3-1 Compounds from *C. graminicola* grown in HMG medium. [3]

This chapter describes the bioassay-guided isolation and structure elucidation of six previously unknown, together with 15 known compounds from *C. graminicola* grown in HMG medium. All isolated compounds were tested for their phytotoxic activity using a leaf-spot assay on *Arabidopsis thaliana* Col-0.

3.2 Experimental

3.2.1 General experimental procedures

Column chromatography was performed on polyamide CC 6-Ac (Macherey Nagel, Germany), silica gel 60 (0.063 – 0.200 mm, Merck, Germany), silica gel 60 silanized (0.063 – 0.200 mm, Merck, Germany), Sephadex LH-20 (Fluka, Germany) and diol-functionalized silica gel (0.070 – 0.200 mm, Supelco, Germany), whereas analytical TLC was performed on pre-coated silica gel F_{254} aluminum sheets (Merck, Darmstadt, Germany).

HPLC

The analytical and semi-preparative HPLC was performed either on a Shimadzu prominence system (Shimadzu Europe, Germany) equipped with a CBM-20A communication bus module, a SPD-M20A diode array detector, a FRC-10A fraction collector, a DGU-20A5R degassing unit, a LC-20AT liquid chromatograph and a SIL-20A HT autosampler or on a Agilent Infinity 1260 system which consist of a autosampler (G1329B), a degasser (G1322A), a quaternary pump (G1311B), a thermostated column compartment (G1316A) with thermostat (G1330B), an analytical-scale fraction collector (G1364C) and a diode array detector (G1315C). Following columns were used: Zorbax Eclipse XDB column 1 (5 µM, 80 Å, 250 x 9.4 mm ID, Agilent, Germany), ODS-A column 2 (3 µM, 120 Å, 150 x 4.0 mm ID, YMC Europe, Germany), Triart C18 column 3 (5 µM, 120 Å, 150 x 10.0 mm ID, YMC Europe, Germany), Poroshell 120 EC column 4 (2.7 µM, 120 Å, 50 x 4.6 mm ID), ODS-A column 5 (5 µM, 120 Å, 150 x 4.6 mm ID, YMC Europe, Germany) or an ODS-A column 6 (5 µM, 120 Å, 150 x 10.0 mm ID, YMC Europe). The following solvent systems were used: H_2O (A) and CH_3CN (B) (solvent system I); H_2O (A) and methanol (B) (solvent system II); H_2O + 0.1 % TFA (A) and CH_3CN + 0.1 % TFA (B) (solvent system III) and H_2O + 0.1 % FA (A) and methanol + 0.1 % FA (B) (solvent system IV).

High-resolution mass spectrometry

The high-resolution mass spectrometry was either performed from an Orbitrap Elite mass spectrometer (Thermo Fisher Scientific, Germany) or from a QTOF MS instrument (TripleTOF 6600, Sciex, Canada). The used methods and parameters are listed below.

UHPLC-ESI-HRMS, Orbitrap Elite mass spectrometer

The negative ion high-resolution ESI mass spectra (*m/z* range 100-2000) were obtained from an Orbitrap Elite mass spectrometer (Thermo Fisher Scientific, Germany) equipped with a heated electrospray ion source (negative spray voltage 4 kV, capillary temperature 325 °C, source heater temperature 300 °C, FTMS resolution 15.000). Nitrogen was used as a sheath and auxiliary gas. The MS system was coupled to an ultra-high-performance liquid chromatography (UHPLC) system (Dionex UltiMate 3000, Thermo Fisher Scientific, Germany), equipped with a RP-18 column (particle size 1.7 µm, 50 × 2.1 mm ID, BEH-C18, Waters, Germany; column temperature 40 °C) connected with a C18 guard column (particle size 1.7 µm, 5 × 2.1 mm ID, BEH-C18, Waters, Germany). The mobile phases were H_2O (A; MilliQ-system Barnstead™ GenPure™ Pro (from Thermo Scientific, Germany)) and CH_3CN (B; Chromasolv™, for LC-MS, Honeywell Riedel de Haën, Germany) with 0.1% formic acid (additive for LC-MS, LiChropur®, Merck, Germany). Chromatographic separation was realized using a gradient system starting from 5% B (isocratic for 1 min) increasing to 95% B within 10 min, followed by further 3 min at 95% B (flow rate 0.4 mL/min, injection volume 3 µL). The re-equilibration time of the column was set to 3.5 min at 5% B. The wavelength range of the PDA measurements was set to λ = 190-600 nm. The CID mass spectra (buffer gas: helium) using data dependent acquisition were recorded using a normalized collision energy (NCE) of 35%. The CID mass spectra (buffer gas: helium) using data dependent acquisition were recorded using a normalized collision energy (NCE) of 35%. The instrument was externally calibrated by the Pierce ESI negative ion calibration solution (product no. 88324) from Thermo Fisher Scientific (Germany). The data were evaluated using the software Xcalibur 2.2 SP1.

Direct infusion (syringe), Orbitrap Elite mass spectrometer

The negative ion high resolution ESI mass spectra were obtained from a Orbitrap Elite mass spectrometer (Thermofisher Scientific, Germany) equipped with a HESI electrospray ion source (negative spray voltage 3.7 kV, capillary temperature 275 °C, source heater temperature 50 °C, FTMS resolution 30.000). Nitrogen was used as sheath gas. The sample solutions were introduced continuously via a 500 µl Hamilton syringe pump with a flow rate of 5 µl min^{-1}. The instrument was externally calibrated by the Pierce® ESI negative ion calibration solution (product number 88324) from Thermofisher Scientific, USA). The data were evaluated by the Xcalibur software 2.2 SP1.

Direct injection via autosampler, Orbitrap Elite mass spectrometer

The negative ion high resolution ESI mass spectra were obtained from a Orbitrap Elite mass spectrometer (Thermofisher Scientific, Bremen, Germany) equipped with a HESI electrospray ion source (negative spray voltage 4 kV, capillary temperature 325°C, source heater temperature 80 °C, FTMS resolution 60.000). Nitrogen was used as sheath gas. The sample solutions were injected through the autosampler (injection volume 5 µL) without chromatographic separation. H_2O (A; MilliQ-system Barnstead™ GenPure™ Pro (from Thermo Scientific, Germany)) and CH_3CN (B; Chromasolv™, for LC-MS, Honeywell Riedel de

Haën, Germany) with 0.1% formic acid (additive for LC-MS, LiChropur®, Merck, Germany) were used as eluents. The instrument was externally calibrated by the Pierce® ESI negative ion calibration solution (product number 88324) from Thermofisher Scientific, USA. The data were evaluated by the Xcalibur software 2.2 SP1.

UHPLC-ESI-HRMS + SWATH, TripleTOF 6600, Sciex
The UHPLC separation was performed using an Acquity UPLC system (Waters, Germany), configured in binary high pressure gradient mode. Eluent A consisted of ultrapure water (A, MilliQ-system Barnstead™ GenPure™ Pro (from Thermo Scientific, Germany)) and CH_3CN (B; Chromasolv™, for LC-MS, Honeywell Riedel de Haën, Germany) with 0.1% formic acid (additive for LC-MS, LiChropur®, Merck, Germany). The gradient profile for eluent B was as follows: 0.0–0.5 min 10%; 0.5–4.3 min increase to 95%; 4.3–4.7 min hold at 95%; 4.7–4.8 min decrease to 10%. For re-equilibration of the UHPLC column, the gradient was set to 10% eluent B for 0.5 min. The column oven was set at 40°C and the autosampler was cooled at 10°C. The flow rate was kept constant at 0.4 mL/min. A volume of 2 µL of the sample was injected onto a BEH RP-C18 column (50 mm × 2.1 mm i.d.; 1.7 µm particle size, 100 Å) (Waters, Germany) guarded with a C18 guard column (2.0 mm i.d. × 4.0 mm; Phenomenex). Mass spectrometric detection was performed using a QTOF MS instrument (TripleTOF 6600, Sciex, Canada) equipped with an ESI-DuoSpray-Ion-Source and a resolving power (full width at half-maximum, fwhm, at *m/z* 400) set of 30,000 in MS and 30,000 in Sequential Window Acquisition of all Theoretical Mass Spectra (SWATH) MS/MS (high resolution mode). The automated calibration device system performed an external calibration approximately every hour. The Turbo V ion drive source equipped with a stainless steel electrode (100 µm internal diameter) was operated with the following MS conditions: gas 1, nitrogen (40 psi); gas 2, nitrogen (40 psi); ion spray voltage, 5500 V; ion-source temperature, 450°C; curtain gas, nitrogen (35 psi); collision energy, 10 eV. The MS was operated in the SWATH acquisition mode, where one complete cycle consists of a survey scan and a Q1 isolation strategy. The survey scan covered a mass range of *m/z* 100 to 1000 with an accumulation time of 100 ms. The Q1 isolation strategy covered a mass range of *m/z* 100 to 650 with a 23 Da SWATH window for Q1 isolation (overlap 1 u). In each SWATH window, a collision energy of 35 eV with a spread of ±15 eV and an accumulation time of about 50 ms in high-resolution mode was used. The total cycle time was 1.4 s. All MS parameters were controlled by AnalystTF 1.7 Software (Sciex).

Direct injection via Autosampler, TripleTOF 6600, Sciex
The mass spectrometric detection in positive and negative ion mode was performed using a QTOF MS instrument (TripleTOF 6600, Sciex, Canada) equipped with an ESI-DuoSpray-Ion-Source and a resolving power (full width at half-maximum, fwhm, at *m/z* 400) set of 30,000 in MS. The automated calibration device system performed an external calibration. The Turbo V ion drive source equipped with a stainless steel electrode (100 µm internal diameter) was operated with the following MS conditions: gas 1, nitrogen (60 psi); gas 2, nitrogen (70 psi); ion spray voltage, 5500 V (positive ion mode), 4500 V (negative mode); ion-source temperature, 450°C; curtain gas, nitrogen (55 psi); collision energy 10 V. The TOF MS accumulation time was set to 50 ms and covered a mass range of *m/z* 100 to 2500. The sample solutions were injected through the autosampler (injection volume 5 µL) without chromatographic separation. H_2O (A; MilliQ-system Barnstead™ GenPure™ Pro (from Thermo Scientific)) and CH_3CN (B; Chromasolv™, for LC-MS, Honeywell Riedel de Haën™) with 0.1% formic acid (additive for LC-MS, LiChropur®, Merck) were used as eluents.

NMR
NMR spectra were obtained from an Agilent DD2-400 spectrometer using a 5-mm inverse detection cryoprobe (Agilent, Germany). The spectra were recorded at 399.917 (^{1}H) and 100.570 (^{13}C), respectively. 2D NMR spectra were recorded using standard CHEMPACK 8.1 pulse implemented in Varian VNMRJ 4.2 spectrometer software. For samples with low concentrations, NMR spectra were recorded on a Bruker Avance Neo 500 NMR spectrometer (Bruker, Germany) at 500.234 and 125.797 MHz, respectively, using a 5 mm prodigy probe with TopSpin 4.0.7 spectrometer software. Chemical shifts are reported relative to TMS.

CD
CD spectra were recorded on a Jasco J-815 CD spectrophotometer (Jasco, Germany).

3.2.2 Cultivation

The strain *Colletotrichum graminicola* M1.001 was provided by Prof. Dr. Deising, Institute of Agricultural and Nutritional Sciences, Martin-Luther University Halle-Wittenberg. *C. graminicola* was cultivated as semi-solid cultures in Erlenmeyer flasks (1 L) each containing 4 g cotton wool and 200 mL HMG medium (10 g/L malt extract, 10 g/L glucose, 4 g/L yeast extract) at 23°C for 13 days without agitation. In total, 260 flasks (52 L) were grown. Subsequently, the mycelium and the cotton wool were separated from the culture broth by vacuum filtration. The mycelium was frozen at -20°C prior to extraction. The culture filtrate was concentrated under reduced pressure to approximately 750 mL.

3.2.3 Extraction

The culture filtrate was extracted by partition with ethyl acetate (6 x 750 mL). The combined organic extracts were dehydrated by anhydrous sodium sulfate (Na_2SO_4) and evaporated to dryness *in vacuo* to obtain a crude extract (9.1 g).

The mycelium together with the cotton wool was extracted exhaustively with ethyl acetate (5 x 1.5 L) in an ultrasound bath for 60 minutes. The combined organic extracts were dehydrated by anhydrous sodium sulphate (Na_2SO_4) and reduced *in vacuo* to dryness to yield a crude extract (30 g).

3.2.4 Isolation

3.2.4.1 Culture filtrate

The organic extract from the culture filtrate (9.1 g) was separated on a polyamide CC 6-Ac column (34 x 8 cm) eluting with *n*-hexane → *n*-hexane: ethyl acetate (1:1, *v/v*) → ethyl acetate → acetone → methanol → acetone/H^+ to afford six fractions (A1 – A6).

Fraction A2 (*n*-hexane/ethyl acetate, 2.5 g) was subjected to size exclusion chromatography using Sephadex LH-20 (80 x 2.5 cm) eluting with chloroform : methanol (1:1, *v/v*). In total, 40 fractions (each 18 mL) were collected and combined based on their TLC pattern to get five fractions (B1 – B5). Fraction B2 (0.85 g) was further purified on silanized silica gel (20 x 4.5 cm) eluting with dichloromethane → dichloromethane : methanol (95:5, *v/v*) → methanol to afford four fractions (C1 – C4). Fraction C3 was purified by analytical HPLC using column 1 with solvent system I (1.8 mL/min; 2 – 22 min, 35 – 50 % B) to obtain **3.1a/b** (t_R= 13.9 min, 30 mg) as a mixture of isomers. Subsequently, the isomeric mixture was separated by HPLC using column 2 with solvent system I (0.6 mL/min; t_R= 7.5 and 8.3 min).

Fraction B3 (0.9 g) was subjected to a silica gel column (83 x 3.5 cm) using the following gradient system: chloroform: ethyl acetate (9:1→ 6:4, *v/v*) → ethyl acetate → methanol → methanol/H^+. 250 fractions (each 20 mL) were collected and combined to afford 24 fractions (D1 – D24). Fraction D15 contained the pure compound **3.2** (1.2 mg).

Fraction D13 (20 mg) was finally purified on a RP-18ec cartridge eluting with methanol : water (6:4, *v/v*) to yield compound **3.3** (10.3 mg).

Fraction D20 (26 mg) was subjected to column chromatography on a diol-functionalized silica gel column (80 x 3.1 cm) eluting with dichloromethane: ethyl acetate (9:1 → 4:6, *v/v*) → ethyl acetate → methanol. In total, 191 fractions (each 20 mL) were collected and combined to eight fractions (E1 – E8) according their TLC pattern. Fraction E1 containing **3.4** (t_R= 17.8 min, 1.1 mg) was finally purified by HPLC using column 1 with solvent system II (1.8 mL/min; 2 – 22 min, 5 – 100 % B).

Fraction D21 (82 mg) was further separated by size exclusion chromatography using Sephadex LH-20 (100 x 2.1 cm) eluting with methanol. 69 fractions (each 10 mL) were collected and combined according to their TLC pattern to seven fractions (F1 – F7). Fraction F4 was finally purified by HPLC using column 1 with solvent system II (1.8 mL/min; 2 – 22 min, 5 – 95 % B) to obtain **3.5 – 3.8** (**3.5**: t_R= 14.3 min, 1.3 mg; **3.6**: t_R= 16.6 min, 0.8 mg; **3.7** t_R= 17.6 min, 0.8 mg; **3.8**: t_R= 14.3 min, 1.0 mg). Fraction F6 contained the pure compound **3.9** (0.9 mg).

Fraction A3 (ethyl acetate, 3.5 g) was further purified on silanized silica (370 x 53 mm) eluting with *n*-hexane : ethyl acetate (4:1→7:3→1:1→3:7→1:9, *v/v*) → ethyl acetate : methanol (9:1→7:3→1:1→3:7, *v/v*) → methanol → methanol/H⁺. 520 fractions (each 18 mL) were collected and combined based on its TLC pattern to give 23 fractions (G1 – G23).

Fraction G3 (31 mg) was further separated on Sephadex LH-20 eluting with acetone : methanol (4:1). 32 fractions (each 7 mL) were collected and combined based on their TLC pattern to obtain four fractions (H1 – H4). Fraction H2 was separated by semi-preparative HPLC using column 3 with solvent system III (3.2 mL/min; 2 – 8 min, 75 – 100 % B (10 min)). The compounds in peak H2.1 (t_R= 6.1 min, 21 mg) were further separated by analytical HPLC II using column 4 and solvent system IV (0.8 mL/min; 1 – 10 min, 20 – 80 % B) to obtain **3.10a/b** (t_R= 3.9 min, 5.3 mg) as a mixture of isomers.

Fraction G8 (79 mg) was further purified on a silica gel column (32 x 2.1 cm) eluting with dichloromethane: isopropanol (39:1 → 29:1 → 19:1 → 9:1, *v/v*) → isopropanol → methanol. 132 fractions each 5 mL were collected and combined to nine fractions (I1 – I9). Final HPLC purification of I6 using column 1 with solvent system I (1.8 mL/min; 3 – 23 min, 20 – 40 % B) lead to the isolation of **3.11** (t_R= 8.7 min, 0.9 mg) and **3.12** (t_R= 11.5 min, 1.6 mg).

Fraction G9 (240 mg) was subjected to a silica gel column (32 x 2.1 cm) using the following gradient system: *n*-hexane : ethyl acetate (1:2→1:3→ 1:5, *v/v*) → ethyl acetate → methanol. In total, 130 (each 5 mL) were collected and combined to eight fractions (J1 – J8).

Fraction J5 and J6 containing **3.13** (t_R= 12.7 min, 1.3 mg) were finally purified by analytical HPLC using column 5 with solvent system I (0.8 mL/min; 2 – 10 min, 15 – 30 % B).

Fraction J7 was further separated on Sephadex LH-20 eluting with chloroform: methanol (1:1, *v/v*). 38 fractions (each 18 mL) were collected and combined to three fractions (K1 – K3). Final purification of K2 by semi-preparative HPLC using column 6 with solvent system I (3.7 mL/min; 2 – 10 min, 15 – 30 % B) afforded **3.2** (t_R= 13.5 min, 1.0 mg), **3.14** (t_R= 11.5 min, 1.3 mg), **3.15** (t_R= 13.1, 1.1 mg).

3-(6-hydroxy-2,6-dimethyloctanoyl)-5-methylpyrrolidin-2-one (3.1a): colorless oil; ¹H NMR (400 MHz, methanol-d₄) δ 2.34 (1H, dd, *J* = 13.0, 7.3 Hz, H-4a), δ 1.95 (1H, dd, *J* = 13.0, 6.8 Hz, H-4b), δ 3.71 (1H, sex, *J* = 6.6 Hz, H-5), δ 1.20 (3H, pt[a], *J* = 6.1 Hz, H-6), δ 2.94 – 3.06 (1H, m, H-2'), δ 1.32 (1H, m, H-3'a), δ 1.66 (1H, m, H-3'b), δ 1.32 (2H, m, H-4'), δ 1.40 (2H, m, H-5'), δ 1.45 (2H, m, H-7'), δ 0.83 – 0.90 (3H, dd, *J* = 4.0, 7.5 Hz, H-8'), δ 1.05 – 1.11 (6H, m, H-9', H-10'); ¹³C NMR (100 MHz, methanol-d₄) δ 175.5 (C-2), δ 54.2 (C-3)[b], δ 32.6 (C-4), δ 49.7 (C-5), δ 22.3 (C-6), δ 212.4 (C-1'), δ 47.1 (C-2'), δ 34.5 (C-3'), δ 22.5 (C-4'), δ 42.1 (C-5'), δ 73.4 (C-6'), δ 35.0 (C-7'), δ 8.5 (C-8'), δ 15.6 (C-9'), δ 26.1 (C-10').

[a] pseudotriplet by overlay of isomers, [b] assigned through HMBC.

¹H NMR (500 MHz, pyridine-d₅) δ 4.00 (1H, m, H-3), δ 2.25 (2H, m, H-4), δ 3.67 (1H, m, H-5), δ 1.17 (3H, m, H-6), δ 3.42 (1H, m, H-2'), δ 2.04 (2H, m, H-3'), δ 1.59 -1.70 (2H, m, H-4'), δ 1.59 -1.70 (2H, m, H-5'), δ 1.59 -1.70 (2H, m, H-7'), δ 1.01 (3H, m, H-8'), δ 1.24 (3H, m, H-9'), δ 1.27 (3H, m, H-10'); ¹³C NMR (125 MHz, pyridine-d₅) δ 173.1 (C-2), δ 53.8 (C-3), δ 31.8 (C-4), δ 47.9 (C-5), δ 22.3 (C-6), δ 210.7 (C-1'), δ 46.0 (C-2'), δ 33.0 (C-3'), δ 22.0 (C-4'), δ 42.2 (C-5'), δ 71.5 (C-6'), δ 35.2 (C-7'), δ 8.7 (C-8'), δ 15.5 (C-9'), δ 26.7 (C-10'); HRESIMS *m/z* 270.2080 ([M+H]⁺, calculated for $C_{15}H_{28}NO_3^+$, 270.2064); UV(CH₃CN) λₘₐₓ = 210, 284 nm.

3-(6-hydroxy-2,6-dimethyloctanoyl)-5-methylpyrrolidin-2-one (3.1b): colorless oil; ¹H NMR (400 MHz, methanol-d₄) δ 2.53 (1H, dd, *J* = 13.0, 7.4 Hz, H-4a), δ 1.78 (1H, dd, *J* = 13.0, 6.1 Hz, H-4b), δ 3.79 (1H, sex, *J* = 6.5 Hz, H-5), δ 1.20 (3H, pt[a], *J* = 6.1 Hz, H-6), δ 2.94 – 3.06 (1H, m, H-2'), δ 1.28 (1H, m, H-3'a), δ 1.69 (1H, m, H-3'b), δ 1.32 (2H, m, H-4'), δ 1.40 (2H, m, H-5'), δ 1.45 (2H, m, H-7'), δ 0.83 – 0.90 (3H, dd, *J* = 4.0, 7.5 Hz, H-8'), δ 1.05 – 1.11 (6H, m, H-10'); ¹³C NMR (100 MHz, methanol-d₄) δ 175.5 (C-2), δ 54.8 (C-3)[b], δ 33.1 (C-4), δ 50.3 (C-5), δ 22.3 (C-6), δ 212.4 (C-1'), δ 47.4 (C-2'), δ 33.6 (C-3'), δ 22.5 (C-4'), δ 42.1 (C-5'), δ 73.4 (C-6'), δ 35.0 (C-7'), δ 8.5 (C-8'), δ 16.8 (C-9'), δ 26.1 (C-10').

[a] pseudotriplet by overlay of isomers, [b] assigned through HMBC

¹H NMR (500 MHz, pyridine-d₅) δ 4.10 (1H, dd, *J* = 9.1, 5.0 Hz, H-3), δ 2.80 (2H, m, H-4), δ 3.87 (1H, m, H-5), δ 1.11 (3H, m, H-6), δ 3.45 (1H, m, H-2'), δ 1.87 (2H, m, H-3'), δ 1.59 -1.70 (2H, m, H-4'), δ 1.59 -1.70 (2H, m, H-5'), δ 1.59 -1.70 (2H, m, H-7'), δ 1.01 (3H, m, H-8'), δ 1.17 (3H, m, H-9'), δ 1.27 (3H, m,

H-10'); ^{13}C NMR (125 MHz, pyridine-d$_5$) δ 173.1 (C-2), δ 54.4 (C-3), δ 32.0 (C-4), δ 48.6 (C-5), δ 22.4 (C-6), δ 210.7 (C-1'), δ 46.2 (C-2'), δ 34.1 (C-3'), δ 21.9 (C-4'), δ 42.2 (C-5'), δ 71.5 (C-6'), δ 35.2 (C-7'), δ 8.7 (C-8'), δ 16.8 (C-9'), δ 26.7 (C-10'); HRESIMS *m/z* 270.2080 ([M+H]$^+$, calculated for C$_{15}$H$_{28}$NO$_3^+$, 270.2064); UV(CH$_3$CN) λ$_{max}$ = 210, 284 nm. (**Figure S 1** – **Figure S 9**).

Cyclo-**L**-**Leu**-**L**-**Pro** (3.2): white solid; ^{1}H NMR (500 MHz, methanol-d$_4$) δ 4.25 (1H, m, H-3), δ 4.10 (1H, m, H-6), δ 1.51 (1H, m, H-7a), δ 1.90 (1H, m, H-7b), δ 1.88 (1H, m, H-8), δ 0.96 (3H, dd, *J* = 6.5/2.5 Hz, H-9), δ 0.96 (3H, dd, *J* = 6.5/2.5 Hz, H-10), δ 3.50 (2H, m, H-11), δ 1.90 (1H, m, H-12a), δ 2.00 (1H, m, H-12b), δ 2.01 (1H, m, H-13a), δ 2.29 (1H, m, H-13b); ^{13}C NMR (125 MHz, methanol-d$_4$) δ 168.9 (C-2), δ 60.3 (C-3), δ 172.8 (C-5), δ 54.6 (C-6), δ 39.4 (C-7), δ 25.7 (C-8), δ 22.1 (C-9), δ 23.3 (C-10), δ 46.4 (C-11), δ 23.6 (C-12), δ 29.1 (C-13); HRESIMS *m/z* 211.1450 ([M+H]$^+$, calculated for C$_{11}$H$_{19}$N$_2$O$_2^+$, 211.1441); UV(MeOH) λ$_{max}$ = 210, 272 nm. (**Figure S 10** – **Figure S 15**).

N-**Phenethylacetamide** (3.3): white solid; ^{1}H NMR (400 MHz, methanol-d$_4$) δ 7.21 (2H, m, H-2/6), δ 7.26 (2H, m, H-3/5), δ 7.18 (1H, m, H-4), δ 2.77 (2H, t, *J* = 7.4 Hz, H-1'), δ 3.38 (2H, t, *J* = 7.4 Hz, H-2'), δ 1.90 (3H, s, H-5'); ^{13}C NMR (100 MHz, methanol-d$_4$) δ 140.5 (C-1), δ 129.8 (C-2/6), δ 129.5 (C-3/5), δ 127.3 (C-4), δ 36.5 (C-1'), δ 42.1 (C-2'), δ 173.2 (C-4'), δ 22.5 (C-5'); HRESIMS *m/z* 164.1083 ([M+H]$^+$, calculated for C$_{10}$H$_{14}$NO$_3^+$, 164.1070); UV(MeOH) λ$_{max}$ = 210, 258 nm. (**Figure S 16** – **Figure S 18**).

Cyclo-**L**-**Val**-**L**-**Pro** (3.4): white solid; ^{1}H NMR (500 MHz, methanol-d$_4$) δ 4.20 (1H, m, H-3), δ 4.03 (1H, t, *J* = 2.3 Hz, H-6), δ 1.91 (1H, m, H-7), δ 0.92 (3H, d, *J* = 6.8, H-8), δ 1.08 (3H, d, *J* = 7.3 Hz, H-9), δ 3.52 (2H, m, H-10), δ 1.91 (1H, m, H-11a), 2.04 (1H, m, H-11b), 2.31 (1H, m, H-12a), δ 2.48 (1H, m, H-12b); ^{13}C NMR (125 MHz, methanol-d$_4$) δ 172.8 (C-2), δ 61.4 (C-3), δ 167.5 (C-5), δ 58.2 (C-6), δ 29.8 (C-7), δ 16.4 (C-8), δ 18.7 (C-9), δ 45.9 (C-10), δ 22.8 (C-11), δ 29.7 (C-12); HRESIMS *m/z* 197.1288 ([M+H]$^+$, calculated for C$_{10}$H$_{17}$N$_2$O$_2^+$, 197.1285), UV(MeOH) λ$_{max}$ = 210 nm. (**Figure S 19** – **Figure S 22**)

Cyclo-**L**-**Ala**-**L**-**Pro** (3.5): white solid; ^{1}H NMR (400 MHz, methanol-d$_4$) δ 4.25 (1H, m, H-3), δ 4.18 (1H, m, H-6), δ 1.31 (3H, d, *J* = 6.9 Hz, H-7), δ 2.31 (1H, m, H-8a), δ 2.0 (1H, m, H-8b); δ 1.94 - 2.0 (2H, m, H-9), δ 3.51 (2H, m, H-10); ^{13}C NMR (100 MHz, methanol-d$_4$) δ 172.6 (C-2), δ 60.5 (C-3), δ 169.1 (C-5), δ 52.2 (C-6), δ 15.8 (C-7), δ 29.2 (C-8), δ 23.7 (C-9), δ 46.5 (C-10); HRESIMS *m/z* 169.0975 ([M+H]$^+$, calculated for C$_8$H$_{13}$N$_2$O$_2^+$, 169.0972); UV(MeOH) λ$_{max}$ = 210 nm. (**Figure S 23** – **Figure S 28**).

Cyclo-**L**-**Ala**-**D**-**Val** (3.6): white solid; ^{1}H NMR (500 MHz, methanol-d$_4$) δ 3.84 (1H, dd, *J* = 3.6, 1.4 Hz, H-3), δ 4.03 (1H, qd, *J* = 7.1, 1.4 Hz, H-6), δ 1.45 (3H, d, *J* = 7.1 Hz, H-7), δ 2.26 (1H, m, H-8), δ 1.04 (3H, d, *J* = 7.1 Hz, H-9), δ 0.95 (3H, d, *J* = 6.8 Hz, H-10); ^{13}C NMR (125 MHz, methanol-d$_4$) δ 170.3 (C-2), δ 61.5 (C-3), δ 171.4 (C-5), δ 51.5 (C-6), δ 21.5 (C-7), δ 33.4 (C-8), δ 19.2 (C-9), δ 17.3 (C-10); HRESIMS *m/z* 171.1132 ([M+H]$^+$, calculated for C$_8$H$_{15}$N$_2$O$_2^+$, 171.1128); UV(MeOH) λ$_{max}$ = 210, 273 nm. (**Figure S 29** – **Figure S 32**).

Cyclo-**L**-**Ala**-**D**-**Ile** (3.7): white solid; ^{1}H NMR (500 MHz, methanol-d$_4$) δ 3.83 (1H, dd, J = 1.4, 3.6 Hz, H-3), δ 4.03 (1H, qd, J = 1.5 , 7.1 Hz, H-6), δ 1.43 (3H, d, J = 7.1 Hz), δ 1.96 (1H, m, H-8), δ 1.25 (1H, m, H-9a), δ 1.52 (1H, m, H-9b), δ 0.96 (3H, d, J = 7.7 Hz, H-10), δ 1.02 (3H, d, J = 7.1 Hz, H-11); (125 MHz, methanol-d$_4$) δ 169.8 (C-2), δ 60.9 (C-3), δ 171.8 (C-5), δ 51.7 (C-6), δ 20.9 (C-7), δ 40.3 (C-8), δ 25.3 (C-9), δ 12.2 (C-10), δ 15.6 (C-11); HRESIMS m/z 185.1285 ([M+H]$^+$, calculated for C$_9$H$_{17}$N$_2$O$_2^+$, 185.1285) UV(MeOH) λ$_{max}$ = 210, 268 nm. (**Figure S 33**–**Figure S 35**).

Cyclo-**D**-**Ala**-**D**-**Leu** (3.8): white solid; ^{1}H NMR (400 MHz, methanol-d$_4$) δ 3.93 (1H, m, H-3), δ 4.00 (1H, m, H-6), δ 1.44 (3H, d, *J* = 7.1 Hz, H-7), δ 1.63 (1H, m, H-8a), δ 1.73 (1H, m, H-8b), δ 1.84 (1H, m, H-9), δ 0.96 (3H, t, *J* = 6.9 Hz, H-10), δ 0.96 (3H, t, *J* = 6.9 Hz, H-11); ^{13}C NMR (100 MHz, methanol-d$_4$) δ 170.9 (C-2), δ 54.6 (C-3), δ 171.4 (C-5), δ 52.0 (C-6), δ 20.9 (C-7), δ 45.1 (C-8), δ 25.3 (C-9), δ 22.1 (C-10), δ 23.6 (C-11); HRESIMS *m/z* 185.1290 ([M+H]$^+$, calculated for C$_9$H$_{17}$N$_2$O$_2^+$, 185.1285); UV(MeOH) λ$_{max}$ = 210, 275 nm. (**Figure S 36** – **Figure S 41**).

Cyclo-**L**-**Trp**-**D**-**Pro** (3.9): white solid; ^{1}H NMR (400 MHz, methanol-d$_4$) δ 3.99 (1H, m, H-3), δ 4.41 (1H, m, H-6), δ 2.31 (1H, m, H-7a), δ 1.97 (1H, m, H-7b), δ 1.94 - 2.0 (2H, m, H-8), δ 3.46 (1H, m, H-9a), δ

3.27 (1H, m, H-9b), δ 3.30 (2H, m, H-10), δ 7.10 (1H, m, H-2'), δ 7.57 (1H, d, J = 8.0 Hz, H-4'), δ 7.00 (1H, ddd, J = 1.1, 6.8, 8.0 Hz, H-5'), δ 7.08 (1H, m, H-6'), δ 7.33 (1H, d, J = 8.0 Hz, H-7'); ^{13}C NMR (100 MHz, methanol-d$_4$) δ 167.6 (C-2), δ 60.2 (C-3), δ 170.9 (C-5), δ 57.2 (C-6), δ 29.1 (C-7), δ 23.5 (C-8), δ 45.9 (C-9), δ 29.2 (C-10), δ 125.5 (C-2'), δ 109.6 (C-3'), δ 128.5 (C-3'a), δ 119.7 (C-4'), δ 119.8 (C-5'), δ 122.5 (C-6'), δ 112.4 (C-7'), δ 138.4 (C-7'a); HRESIMS m/z 284.1419 ([M+H]$^+$, calculated for C$_{16}$H$_{18}$N$_3$O$_2^+$, 284.1394). (**Figure S 42** – **Figure S 46**)

3-(2,6-dimethyloctanoyl)-5-methylpyrrolidin-2-one (3.10a): colorless oil; ^{1}H NMR (500 MHz, methanol-d$_4$) δ 1.76 (1H, dd, J = 7.3, 13.0 Hz, H-4a), δ 2.52 (1H, dd, J = 7.3, 13.0 Hz, H-4b), δ 3.79 (1H, m, H-5), δ 1.21 (3H, m, H-6), δ 2.99 (1H, m, H-2'), δ 1.33 (1H, m, H-3'a), δ 1.65 (1H, m, 3'b), δ 1.29 (2H, m, H-4'), δ 1.10 (1H, m, H-5'a), δ (1.30, m, H-5'b), δ 1.31 (1H, m, H-6'), δ 1.13 (1H, m, H-7'a), δ 1.33 (1H, m, H7'b), δ 0.87 (3H, m, H-8'), δ 1.05 (3H, d, J = 6.9 Hz, H-9'), δ 0.84 (3H, m, H-10'); ^{13}C NMR (125 MHz, methanol-d$_4$) δ 175.4 (C-2), δ 55.1 (C-3), δ 33.2 (C-4), δ 50.5 (C-5), δ 22.3 (C-6), δ 212.4 (C-1'), δ 47.2/ 47.4^a (C-2'), δ 34.1 (C-3'), δ 25.8/ 25.9^a (C-4'), δ 37.8/ 38.0^a (C-5'), δ 35.6 (C-6'), δ 30.5 (C-7'), δ 11.8 (C-8'), δ 15.6 (C-9'), δ 19.5 (C-10'); HRESIMS m/z 254.2113 ([M+H]$^+$, calculated for C$_{15}$H$_{28}$NO$_2^+$, 254.2115); UV(CH$_3$CN) λ_{max} = 210, 284 nm.

3-(2,6-dimethyloctanoyl)-5-methylpyrrolidin-2-one (3.10b): colorless oil; ^{1}H NMR (500 MHz, methanol-d$_4$) δ 1.97 (1H, m, H-4a), δ 2.33 (1H, m, H-4b), δ 3.72 (1H, m, H-5), δ 1.21 (3H, m, H-6), δ 2.99 (1H, m, H-2'), δ 1.29 (1H, m, H-3'a), δ 1.64 (1H, m, 3'b), 1.29 (2H, m, H-4'), δ 1.10 (1H, m,H-5'a), δ (1.30, m, H-5'b), δ 1.31 (1H, m, H-6'), δ 1.13 (1H, m, H-7'a), δ 1.33 (1H, m, H7'b), δ 0.87 (3H, m, H-8'), δ 1.09 (3H, d, J = 7.1 Hz, H-9'), δ 0.84 (3H, m, H-10'); ^{13}C NMR (125 MHz, methanol-d$_4$) δ 175.5 (C-2), δ 54.3 (C-3), δ 32.6 (C-4), δ 49.6 (C-5), δ 22.3 (C-6), δ 212.5 (C-1'), δ 47.2/ 47.4^a (C-2'), δ 33.1(C-3'), δ 25.8/ 25.9^a (C-4'), δ 37.8/ 38.0^a (C-5'), δ 35.6 (C-6'), δ 30.5 (C-7'), δ 11.8 (C-8'), δ 16.7 (C-9'), δ 19.5 (C-10'); HRESIMS m/z 254.2113 ([M+H]$^+$, calculated for C$_{15}$H$_{28}$NO$_2^+$, 254.2115); UV(CH$_3$CN) λ_{max} = 210, 284 nm. ^{a} no exact assignment was possible. (**Figure S 47** – **Figure S 52**).

1-(3,6-dihydro-2_H_-pyran-3-yl)pentane-2,3-diol (3.11): ^{1}H NMR (400 MHz, methanol-d$_4$) δ 3.48 (1H, m, H-2a), δ 3.88 (1H, t, J = 7.9 Hz, H-2b), δ 2.92 (1H, m, H-3), δ 5.64 (1H, m, H-4), δ 5.68 (1H, t, J = 5.3 Hz, H-5), δ 4.00 (2H, dd, J = 5.3, 1.2 Hz, H-6), δ 1.65 (1H, dt, J = 12.3, 9.9 Hz, H-1'a), δ 2.07 (1H, ddd, J = 12.8, 7.3, 6.1 Hz, H-1'b), δ 3.82 (1H, ddd, J = 9.5, 6.0, 5.2 Hz, H-2'), δ 3.48 (1H, m, H-3'), δ 1.33 (1H, m, H-4'a), δ 1.56 (1H, m, H-4'b), δ 0.97 (3H, t, J = 7.4 Hz, H-5'); ^{13}C NMR (100 MHz, methanol-d$_4$) δ 73.2 (C-2), δ 44.3 (C-3), δ 132.5 (C-4), δ 131.5 (C-5), δ 63.3 (C-6), δ 35.0 (C-1'), δ 84.2 (C-2'), δ 75.6 (C-3'), δ 27.5 (C-4'), δ 10.5 (C-5'); HRESIMS m/z 187.1334 [M+H]$^+$, calculated for C$_{10}$H$_{19}$O$_3^+$ 187.1329 UV(MeOH) λ_{max} = 210, 249 nm. (**Figure S 53** – **Figure S 58**).

5-(2,3-dihydroxypentyl)tetrahydro-2_H_-pyran-3,4-diol (3.12): ^{1}H NMR (400 MHz, methanol-d$_4$) δ 3.55 (1H, m, H-2a), δ 3.73 (1H, m, H-2b), δ 3.51 (1H, m, H-3), δ 3.30 (1H, m, H-4), δ 2.63 (1H, m, H-5), δ 3.66 (1H, d, J = 7.6 Hz, H-6a), δ 3.74 (1H, m, H-6b), δ 1.51 (1H, m, H-1'a), δ 1.91 (1H, d, J = 11.0 Hz, H-1'b), δ 3.95 (1H, d, J = 5.5 Hz, H-2'), δ 3.24 (1H, dd, H-3'), δ 1.40 (2H, m, H-4'), δ 0.94 (3H, t, J = 7.4 Hz, H-5'); ^{13}C NMR (100 MHz, methanol-d$_4$) δ 64.5 (C-2), δ 74.7 (C-3), δ 82.3 (C-4), δ 37.3 (C-5), δ 74.6 (C-6), δ 25.6 (C-1'), δ 80.3 (C-2'), δ 84.2 (C-3'), δ 27.4 (C-4'), δ 10.2 (C-5'); HRESIMS m/z 203.1277 [M-H$_2$O+H]$^+$, calculated for C$_{10}$H$_{19}$O$_4^+$ 203.1278; UV(MeOH) λ_{max} = 210, 234, 319 nm. (**Figure S 59** – **Figure S 63**).

_N_-[2-(2-hydroxyphenyl)-ethyl]-acetamide (3.13): white solid; ^{1}H NMR (500 MHz, methanol-d$_4$) δ 6.74 (1H, m, H-3), δ 7.00 (1H, m, H-4), δ 6.71 (1H, m, H-5), δ 7.04 (1H, m, H-6), δ 2.77 (2H, t, J = 7.3 Hz, H-1'), δ 3.36 (2H, t, J = 7.3 Hz, H-2'), δ 1.89 (3H, s, H-5'); ^{13}C NMR (125 MHz, methanol-d$_4$)^a δ 126.9 (C-1), δ 157.2 (C-2), δ 116.2 (C-3), δ 128.6 (C-4), δ 120.2 (C-5), δ 131.5 (C-6), δ 31.2 (C-1'), δ 41.0 (C-2'), δ 173.3 (C-4'), δ 22.6 (C-5'); HRESIMS m/z 180.1048 ([M+H]$^+$, calculated for C$_{10}$H$_{14}$NO$_2^+$, 180.1019); UV(MeOH) λ_{max} = 210, 272 nm. ^{a} determined by HSQC/HMBC. (**Figure S 64** – **Figure S 67**).

_N_-Acetyltyramine (3.14): white solid; ^{1}H NMR (500 MHz, methanol-d$_4$) δ 7.02 (2H, d, J = 8.3 Hz, H-2/6), δ 6.70 (2H, d, J = 8.3 Hz, H-3/5), δ 2.67 (2H, t, J = 7.3 Hz, H-1'), δ 3.32 (2H, m, H-2'), δ 1.89 (3H, s, H-

5'); ^{13}C NMR (125 MHz, methanol-d_4) δ 131.2 (C-1), δ 130.7 (C-2/6), δ 116.3 (C-3/5), δ156.9 (C-4), δ 35.7 (C-1'), δ 42.5 (C-2'), δ 173.2 (C-4'), δ 22.5 (C-5'); HRESIMS *m/z* 180.1030 ([M+H]$^+$, calculated for $C_{10}H_{14}NO_2^+$, 180.1019); UV(MeOH) λ_{max} = 210, 221, 276 nm. (**Figure S 68** – **Figure S 72**).

***Cyclo*-Ile-Pro (3.15):** white solid; ^{1}H NMR (500 MHz, methanol-d_4) δ 4.22 (1H, m, H-3), δ 4.06 (1H, q, *J* = 1.6/ 1.6/0.9 Hz, H-6), δ 2.16 (1H, *J* = 9.5/ 7.1/ 4.5/ 2.4 Hz, H-7), δ 1.31 (1H, m, H-8a), δ 1.46 (1H, m, H-8b), δ 0.94 (3H, m, H-9), δ 1.06 (3H, d, *J* = 7.0, H-10), δ 3.52 (2H, m, H-11), δ 1.92 (1H, m, H-12a), δ 2.02 (1H, m, H-12b), δ 1.94 (1H, m, H-13a), δ 2.31 (1H, m, H-13b); ^{13}C NMR (125 MHz, methanol-d_4) δ 172.4 (C-2), δ 60.3 (C-3), δ 167.6 (C-5), δ 54.6 (C-6), δ 37.1 (C-7), δ 25.4 (C-8), δ 12.6 (C-9), δ 15.5 (C-10), δ 46.1 (C-11), δ 23.2 (C-12), δ 29.5 (C-13); HRESIMS *m/z* 211.1471 ([M+H]$^+$, calculated for $C_{11}H_{19}N_2O_2^+$, 211.1441). (**Figure S 73** – **Figure S 78**).

3.2.4.2 Mycelium

The organic extract of the mycelium (30 g) was subjected to a polyamide CC 6-Ac column (26 x 8 cm) eluting with *n*-hexane → ethyl acetate → acetone → methanol → acetone/H$^+$ to get ten fractions (K1 – K10). Fraction K4 (2.5 g, ethyl acetate) was further separated on silica gel (30 x 3.5 cm) eluting with *n*-hexane : acetone (1:1) → *n*-acetone: methanol (9:1) → acetone: methanol (2:3) → methanol. 100 Fractions (each 10 mL) were collected and combined based on their TLC pattern to afford 13 fractions (L1- L12).

Fraction L3 (200 mg) was further separated by size exclusion chromatography using Sephadex LH-20 (100 x 1.5 cm) eluting with methanol. 65 fractions (each 10 mL) were collected and combined based on their TLC pattern to nine fractions (M1 – M9). M8 (2.5 mg) was finally purified by analytical HPLC using solvent system I (0.8 mL/min; 2 – 20 min, 2 – 100 % B (3 min)) to obtain **3.16** (t_R= 20.1 min, 0.6 mg). Fraction L4 (165 mg) was further separated on Sephadex LH-20 (100 x 1.5 cm) using methanol as eluent. 50 Fractions (each 15 mL) were collected and combined based on their TLC pattern to 6 fractions (N1 – N5). Fraction N1 was further purified on silica gel (35 x 1.5 cm) using a gradient system *n*-hexane : acetone (3:1) → *n*-hexane : acetone (2:1) → *n*-hexane : acetone (1:1) → *n*-hexane : acetone (1:2) → acetone → acetone : methanol (2:1) → acetone : methanol (1:1) → methanol → methanol/H$^+$. In total, 90 fractions (each 10 mL) were collected and combined based on their TLC pattern to afford five fractions (O1 – O5). Final purification of O2 was performed by semi-preparative HPLC using solvent system II (4.0 mL/min, 2 – 12 min, 70 – 85 % B, yielding **3.17** (t_R= 4.7 min, 10.0 mg) and **3.18** (t_R= 7.8 min, 2.0 mg). Fraction O4 contains the pure compound **3.19** (1.5 mg).

Lumichrome (3.16): slightly yellow solid with strong blue fluorescence in UV light (λ = 366 nm); ^{1}H NMR (500 MHz, DMSO-d_6) δ 11.84 (1H, s, H-1), δ 11.67 (1H, s, H-3), δ 7.93 (1H, s, H-6), δ 7.72 (1H, s, H-9), δ 2.47 (3H, s, H-10), δ 2.50 (3H, m, H-11); ^{13}C NMR (125 MHz, DMSO-d_6)^a δ 141.6 (C-5a), δ 128.7 (C-6), δ 139.1 (C-7), δ 144.6 (C-8), δ 125.9 (C-9), δ 137.7 (C-9a), δ 19.5 (C-10), δ 20.2 (C-11); HRESIMS m/z 243.0874 [M-H]$^-$, calculated for $C_{12}H_{11}N_4O_2^-$ 243.0882. ^{a} determined by HSQC/HMBC. (**Figure S 79** – **Figure S 82**).

7,8,16-trihydroxyoctadeca-9,12-dienoic acid (3.17): colorless oil; ^{1}H NMR (400 MHz, methanol-d_4) δ 2.18 (2H, t, *J* = 7.3 Hz, H-2), δ 1.48 (2H, m, H-3), δ 1.25 (2H, m, H-4), δ 1.23 (1H, m, H-5a), δ 1.39 (1H, m, H-5b), δ 1.19 (1H, m, H-6a), δ 1.39 (1H, m, H-6b), δ 3.20 (1H, m, H-7), δ 4.05 (1H, dd, *J* = 6.1, 8.0 Hz, H-8), δ 5.33 (1H, m, H-9), δ 5.32 (1H, m, H-10), δ 2.81 (2H, q, *J* = 6.8, 6.9 Hz, H-11), δ 5.30 (1H, m, H-12), δ 5.37 (1H, m, H-13), δ 2.07 (2H, m, H-14), δ 1.36 (2H, m, H-15), δ 3.31 (1H, m, H-16), δ 1.34 (2H, m, H-17), δ 0.85 (3H, t, *J* = 7.4 Hz, H-18); ^{13}C NMR (100 MHz, methanol-d_4) δ 174.5 (C-1), δ 33.6 (C-2), δ 24.5 (C-3), δ 28.7 (C-4), δ 25.2 (C-5), δ 32.0 (C-6), δ 73.8 (C-7), δ 69.9 (C-8), δ 129.2 (C-9), δ 131.0 (C-10), δ 25.9 (C-11), δ 127.4 (C-12), δ 130.1 (C-13), δ 23.2 (C-14), δ 36.5 (C-15), δ 70.4 (C-16), δ 29.8 (C-17), δ 10.2 (C-18); HRESIMS *m/z* 327.2171 [M-H]$^-$, calculated for $C_{18}H_{31}O_5^-$ 327.2177. (**Figure S 83** – **Figure S 89**).

(8*Z*,10*E*)-12,17-dihydroxyoctadeca-8,10-dienoic acid (3.18) colorless oil; ^{1}H NMR (500 MHz, methanol-d$_4$) δ 2.16 (2H, t, *J* = 7.4 Hz, H-2), δ 1.48 (2H, m, H-3), δ 1.21 – 1.26 (6H, m, H-4 – H-6), δ 2.12 (2H, m, H-7), δ 5.36 (1H, dt, *J* = 7.5, 11.0 Hz, H-8), δ 5.95 (1H, t, *J* = 11.0 Hz, H-9), δ 6.39 (1H, dd, *J* = 11.1, 15.2 Hz, H-10), δ 5.63 (1H, dd, *J* = 6.2, 15.2 Hz, H-11), δ 3.97 (1H, q, 6.2, 6.4 Hz, H-12), δ 1.37 (2H, m, H-13), δ 1.24 (1H, m, H-14a), δ 1.47 (1H, m, H-14b), δ 1.31-1.39 (2H, m, H-15), δ 1.30 (2H, m, H-16), δ 3.56 (1H, m, H-17), δ 1.02 (3H, d, *J* = 6.0 Hz, H-18); ^{13}C NMR (125 MHz, methanol-d$_4$) δ 174.5 (C-1), δ 33.9 (C-2), δ 24.5 (C-3), δ 28.5/ 28.8/ 28.9 (C-4 – C-6), δ 27.2 (C-7), δ 131.0 (C-8), δ 128.3 (C-9), δ 123.7 (C-10), δ 138.0 (C-11), δ 70.4 (C-12), δ 37.2 (C-13), δ 24.9 (C-14), δ 25.5 (C-15), δ 38.6 (C-16), δ 65.6 (C-17), δ 23.6 (C-18); HRESIMS *m/z* 311.2226 [M-H]$^-$, calculated for $C_{18}H_{31}O_4^-$ 311.2228 (**Figure S 90 – Figure S 95**).

Uracil (3.19): white solid; ^{1}H NMR (400 MHz, DMSO-d$_6$) δ 10.93 (2H, s, H-1/3), δ 5.44 (1H, d, *J* = 7.6 Hz, H-5), δ 7.39 (1H, d, *J* = 7.6 Hz, H-6); ^{13}C NMR (100 MHz, DMSO-d$_6$) δ 151.2 (C-2), δ 164.3 (C-4), δ 100.1 (C-5), δ 142.2 (C-6); HRESIMS *m/z* 111.0199 [M-H]$^-$, calculated for $C_4H_3N_2O_2^-$ 111.0200. (**Figure S 96 – Figure S 99**).

3.2.5   Leaf-spot bioassay

A modified leaf-spot bioassay by Evidente and co-workers was used to test fractions and pure compounds for their phytotoxic activity. [7] The samples were dissolved in methanol/ water (1:1, *v/v*) and droplets of 5 µL were placed on the leaf surface of undetached and fully expanded young leaves of *Arabidopsis thaliana* Col-0. Fractions were tested at concentrations of 5 – 10 µg/µL, pure compounds at concentrations from 10 mM – 100 mM. Plants were incubated in the greenhouse (19 °C, day/night cycle) for 72 h. Paraquat (100 µM, dissolved in methanol/ water 1:1, *v/v*) was used as a positive control. The pure solvent mixture of methanol/water (1:1, *v/v*) act as negative control. After 48 h the plants were observed for the occurrence of necrosis. Images were taken with CAMAG TLC visualizer (Camag, Switzerland). Only damage to the leaf in the form of chlorosis or necrosis was evaluated. The extent of the damage was not considered.

3.2.6   CD calculation

The molecular geometries of each molecule, including all possible stereoisomers, were obtained using a python script which transforms SMILES structures to SDF files with the RDKit python package. Based on these SDF files, gaussian input files were generated with the same script. The structures were then optimized with density functional theory (DTF) using CAM-B3LYP/6-31+G(d,p)[8-11] level of theory and the conductor-like polarizable continuum model (CPCM) solvent field for methanol[12] implemented in the Gaussian16 [13] program package. Electronic Circular Dichroism (ECD) calculation was performed for each optimized compound and conformation using TD-DFT calculations at the CAM-B3LYP/6-31+G(d,p) level and CPCM model, investigating the first 40 excited states. The calculated spectra were then compared with experimental data using the SpecDis software (version 1.71) [14] with a Gaussian distribution function at a half-bandwidth of σ = 0.3 eV and an allowed shift between +30 to -30 nm.

3.3   Results and discussion

3.3.1   Isolation and structure elucidation

Repeated column chromatography of the *C. graminicola* crude extracts on polyamide-CC-6Ac, Sephadex LH-20, silica gel, silanized silica and diol-functionalized silica gel in combination with analytical and semi-preparative HPLC yielded 19 compounds **3.1 – 3.19** (**Figure 3-1**).

3.1a/b   **3.2**   **3.3**   **3.4**   **3.5**   **3.6**

3.7   **3.8**   **3.9**   **3.10a/b**   **3.11**

3.12   **3.13**   **3.14**   **3.15**   **3.16**

3.17   **3.18**   **3.19**
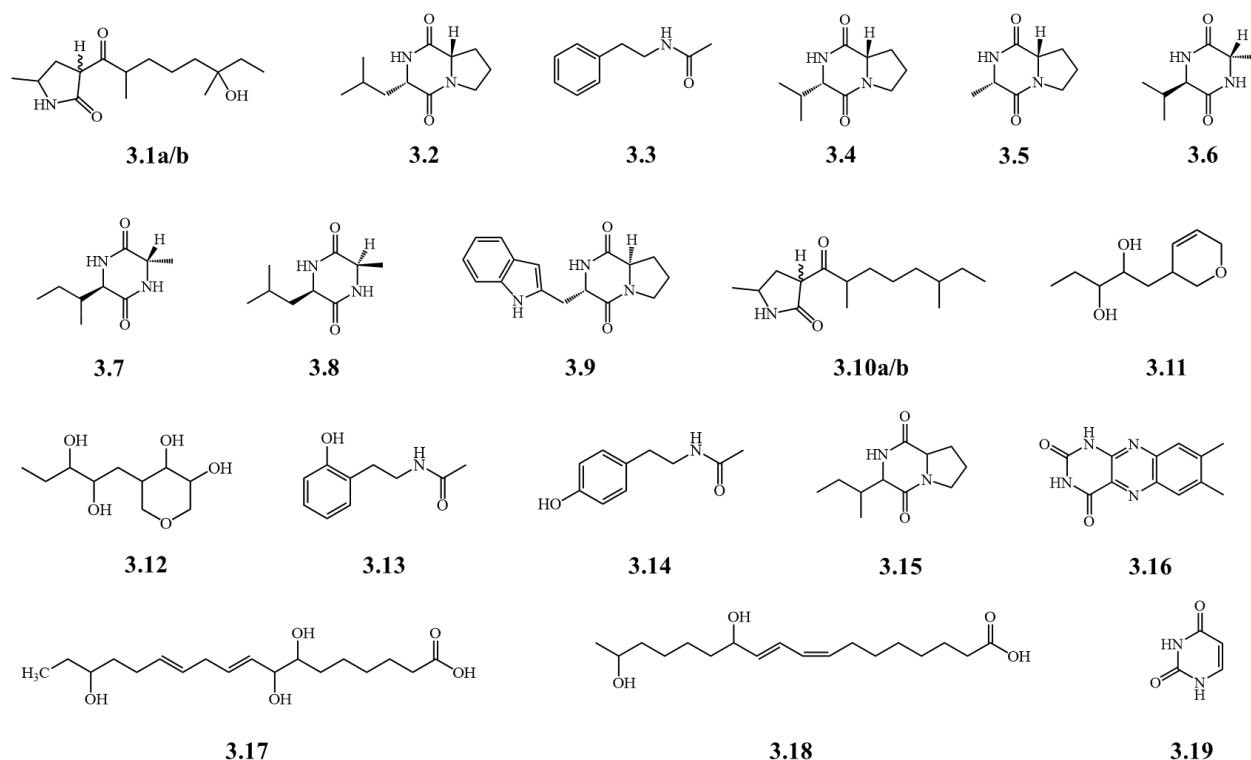
Figure 3-2 All isolated compounds.

The spectral data (MS and ^{1}H and ^{13}C NMR spectra) of compounds **3.2** – **3.9**, **3.13** – **3.16** and **3.19** were identical to those reported in literature. Accordingly, the isolated compounds were identified as *cyclo*-Leu-Pro (**3.2**) [15], *N*-phenylethylacetamid (**3.3**) [16], *cyclo*-Val-Pro (**3.4**) [17], *cyclo*-Ala-Pro (**3.5**) [18], *cyclo*-Ala-Val (**3.6**) [19], *cyclo*-Ala-Ile (**3.7**) [20], *cyclo*-Ala-Leu (**3.8**) [21], *cyclo*-Trp-Pro (**3.9**) [22], *N*-[2-(2-hydroxyphenyl)-ethyl]-acetamide (**3.13**) [23], *N*-acetyltyramine (**3.14**) [24], *cyclo*-Ile-Pro (**3.15**) [25], lumichrome (**3.16**) [26], uracil (**3.19**) [27]. Besides these known compounds, several new secondary metabolites could be isolated, and their structure elucidated by means of intense NMR-spectroscopic and MS-spectrometric measurements.

Compound **3.1a/b** was isolated as a colorless oil. Based on HRESIMS investigation the molecular formula was determined to be $C_{15}H_{27}NO_3$ (*m/z* 270.2079 [M+H]$^+$, calculated for $C_{15}H_{28}NO_3^+$, 270.2064) (**Figure S 1**). The NMR spectra of **3.1a/b** showed a double set of signals (ratio 1:1) which were slightly shifted. Thus, it can be concluded that the **3.1a/b** is as a mixture of diastereomers. A further separation of **3.1a/b** was achieved by HPLC. However, an equilibrium between the two isomers was quickly re-established. The ^{13}C NMR of **3.1a/b** measured in methanol-d$_4$ reveals 28 (of 30) carbon resonances, including four carbonyl-like carbons, eight methylenes, six methines and two quaternary carbons. Intense analysis of the COSY and HMBC correlations (**Figure 3-3**) revealed a octanone moiety with a hydroxy group and a methyl group at position 6'(quaternary carbon at δ$_C$ 73.4 ppm) and a second methyl group at position 2' in neighborhood to the carbonyl group at δ$_C$ 212.4 ppm. Additionally, the HMBC correlations from H-4 to C-2, C-3, C-5, C-6 and C-1'together with the correlations from H-5 to C-2, C-4 and C-6 revealed the presence of a methyl pyrrolidinone moiety, connected to the 6'-hydroxy-2',6'-dimethyl-octan-1'-one moiety via the methine group C-3. However, the methine groups at position 3 showed neither a carbon resonance nor a proton signal in methanol-d$_4$. An assignment could only be made via HMBC coupling from the neighboring methylene group (position 4). Interestingly, an additional NMR experiment with pyridine-d$_5$ as solvent the missing resonances could be detected. In total, compound **3.1a/b** possess 4 stereocenters, which means that 16 isomers are theoretically possible. However, the two isomers show the largest differences at position 4, making it likely that position 3 is present in different configurations. This assumption is confirmed by the NOESY experiment in pyridine-d$_5$. The proton at position 3a (δ$_H$ 4.00 ppm) showed a correlation with the methyl group at position 6a (δ$_H$ 1.17 ppm) and with the proton at position 2'(δ$_H$ 3.42 ppm). In contrary, the proton at position 3b (δ$_H$ 4.10 ppm) showed only a very weak correlation to the methyl group at position 6b (δ$_H$ 1.10 ppm) but a strong correlation to the proton at position 2'(δ$_H$ 3.45 ppm) and the methylene group at position 3'(δ$_H$ 1.86 ppm). Based on the above-mentioned experiments (**Figure S 2** – **Figure S 9**) the compound **3.1a/b** was determined as 3-(6-hydroxy-2,6-dimethyloctanoyl)-5-methylpyrrolidin-2-one.
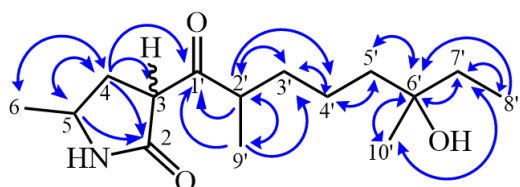
Figure 3-3 HMBC correlations of compound **3.1a/b.**

A similar compound containing a pyrrolidone moiety has already been described in the literature (**Figure 3-4**). [28] Here, the compound was present as a mixture of two epimers at position 3 (ratio 1:1). Additionally, the compound was reported to be present as the corresponding enol tautomer (ratio keto-enol = 2:1). Interestingly, the enol form is not detectable for **3.1a/b**.

keto epimers

enol tautomer
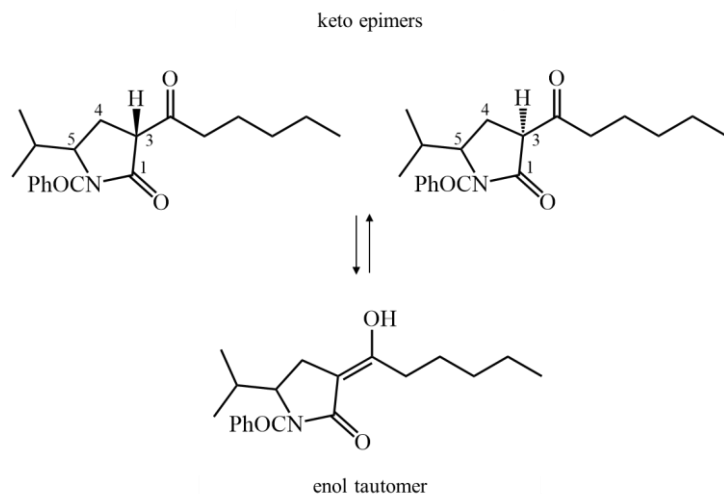
Figure 3-4 Pyrrolidone moiety (58) described by Thomas and Willis (2014). [28]

Compound **3.10a/b**, isolated as a colorless oil, possess the molecular formula $C_{15}H_{27}NO_2$, as deduced from HRESIMS data (m/z 254.2113 [M+H]$^+$, calculated for $C_{15}H_{28}NO_2^+$, 254.2115) (**Figure S 47**). Comparison with the molecular formula of **3.1a/b** indicated a difference in one hydroxy group and was identified as 3-(2,6-dimethyloctanoyl)-5-methylpyrrolidin-2-one. The NMR spectra likewise showed a double set of signals (ratio: 1:1). Intensive analysis of the NMR data (**Figure S 48 – Figure S 52**) confirmed that structure **3.10a/b** differs from **3.1a/b** only in the absence of the hydroxyl group at position 6'. The relative and absolute configuration of compound **3.1a/b** and **3.10a/b** could not be determined.

Compound **3.11** was isolated as a white solid. Based on HRESIMS data its molecular formula was deduced as $C_{10}H_{18}O_3$ (m/z 187.1331 [M+H]$^+$, calculated for $C_{10}H_{19}O_3^+$ 187.1329) (**Figure S 53**). The structure of **3.11** was determined on the basis of detailed NMR analysis (**Figure S 54 – Figure S 58**). The ^{1}H and ^{13}C NMR spectra show the occurrence of one methyl group (δ_H 0.97, t, $J = 7.4$ Hz), four methylenes (δ_C 27.5, 35.0, 63.3 and 73.2 ppm), three aliphatic methines (δ_C 44.3, 75.6 and 84.2 ppm), as well as two olefinic methines (δ_H 5.64 ppm, m and 5.68 ppm, t, $J = 5.3$ Hz). Intense analysis of the COSY spectra reveals the presence of a pentane-2,3-diol moiety connected to a 3,6-dihydro-2*H*-pyran. The pyran scaffold is confirmed by HMBC correlations from H-3 to C-2, C-4, C-5 and C-1' and from H-4 to C-2, C-3, C-5, C-6 and C-1'. Therefore, **3.11** was determined as 1-(3,6-dihydro-2*H*-pyran-3-yl)pentane-2,3-diol. The compound comprises three stereogenic centers at the positions C-3, C-2' and C-3', however, the relative and absolute configuration was not determined.

3.11 **3.12**
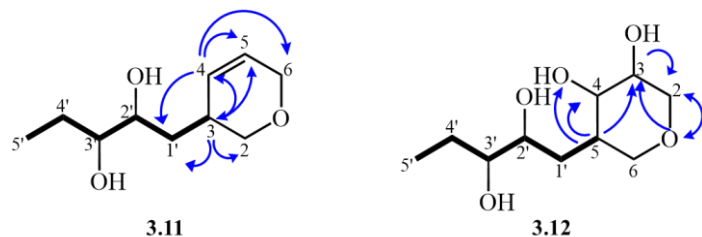
Figure 3-5 Structures of **3.11** and **3.12**, key COSY (bold) and HMBC (arrow) correlations.

Compound **3.12**, obtained as white solid, had the molecular formula $C_{10}H_{20}O_5$ as deduced from ESIHRMS data (*m/z* 203.1278 [M-H$_2$O]$^+$, calculated for $C_{10}H_{19}O_4^+$ 203.1278) (**Figure S *59***). Further, the NMR data (**Figure S 60** – **Figure S 63**) of **3.12** were very similar to those of **3.11**, except for the absence of olefinic methines (δ_H 5.64 and 5.68 ppm). Instead, the molecule has two aliphatic methines at the corresponding positions (δ_H 3.30 and 3.51 ppm), which carry two additional hydroxyl groups Thus, the 3,6-dihydro-2*H*-pyran moiety was substituted by a tetrahydro-2*H*-pyran-3,4-diol motif. Compound **3.12** was determined as 5-(2,3-dihydroxypentyl)tetrahydro-2*H*-pyran-3,4-diol.
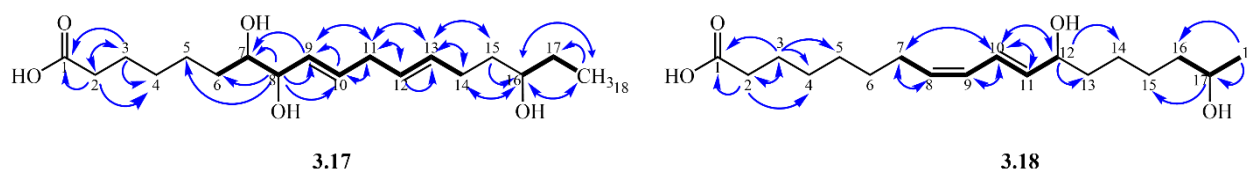
Figure 3-6 Structures of **3.17** and **3.18**, key COSY (bold) and HMBC (arrow) correlations.

A racemic mixture of compound **3.17** was isolated as a colorless oil. The molecular formula was determined to be $C_{18}H_{32}O_5$ based on HRESIMS data (*m/z* 327.2171 [M-H]$^-$, calculated for $C_{18}H_{31}O_5^-$ 327.2177), corresponding to three degrees of unsaturation (**Figure S 83**). The ^{13}C NMR spectrum of **3.17** reveals 18 carbon resonances including one signal for a carbonyl-like carbon (δ_C 174.5 ppm), four signals for sp^2 methines (δ_C 129.4 – 131.0 ppm), one methyl group (δ_C 10.2 ppm), eight shielded sp^3 methylenes (δ_C 23.2 – 36.5 ppm) and three signals for deshielded sp^3 methines (δ_C 69.9 – 73.8 ppm), which are linked to a hydroxy group. The aforementioned functionalities suggest a fatty acid. COSY correlations between H-11 and the olefinic protons (H-9, H-10, H-12 and H-13), together with the COSY correlation between H-9 and H-8 and H-8 and H-7 showed that the two double bounds (C9/10 and C12/13) are separated by a methylene group (C-11) and that two hydroxy groups are in direct neighborhood of the double bound (C-9/10). COSY correlation from H-18 to H-17 and from H-17 to H-16, allowed the localization of the third hydroxy group at position C-16. Based on above mentioned analyses (**Figure S 84** – **Figure S 89**) the structure of **3.17** was determined to be 7,8,16-trihydroxyoctadeca-9,12-dienoic acid. The compound contains three stereogenic centers at the positions C-7,-8 and -16. The ^{1}H NMR spectrum of **3.17** showed a pseudoquartet for the methylene group at position C-11 caused by the overlap of two triplets due to a slight change in chemical shift resulting from the different stereochemistry of the enantiomers. Further, this also makes it likely that a stereo center in close proximity (position C-7 or C-8) to position C-11 occurs in different configurations. The absolute configuration of the molecule was not determined.

Compound **3.18** purified as a colorless oil, had the molecular formula $C_{18}H_{32}O_4$, as deduced from HRESIMS data (*m/z* 311.2224 [M-H]$^-$, calculated for $C_{18}H_{31}O_4^-$, 311.2228) (**Figure S 90**). This suggests that **3.18** lacks a hydroxyl group compared to **3.17**. Detailed 1D and 2D NMR studies (**Figure S 91** – **Figure S 95**) confirmed that **3.18** is a derivative of octadecadienoic acid. In comparison with **3.17** the structure of **3.18** differs in the location of the hydroxyl groups as well as the position of the double bounds. The ^{1}H NMR spectrum displays four deshielded signals at δ_H 5.36 ppm (1H, dt, *J* = 7.5, 11.0 Hz, H-8), δ_H 5.95 ppm (1H, t, *J* = 11.0 Hz, H-9), δ_H 6.39 ppm (1H, dd, *J* = 11.1, 15.2 Hz, H-10) and δ_H 5.63 ppm (1H, dd, *J* = 6.2, 15.2 Hz, H-11). Based on the coupling constants the configuration of double bonds was determined to be 8*Z* and 10*E*. On the basis of the above analysis, the structure of **3.18** was determined as (8*Z*,10*E*)-12,17-dihydroxyoctadeca-8,10-dienoic acid.

3.3.2 Pyrrolidinone derivatives

Compounds with pyrrolidone moiety but bearing different side chains have been isolated previously. Two examples are the colletotrilactams A and B isolated from *Colletotrichum gleoeosporiodes* [29] and the berkeleyamide A isolated from *Penicillium rubrum* (**Figure 3-7**). [30] These compounds share the same pyrrolidone moiety connected to different side chains.

39
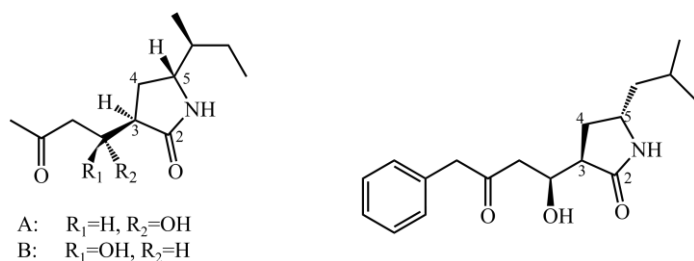
Figure 3-7 Structures of colletotrilactam A and B [29] and berkeleyamide A. [30]

Tetramic acid (pyrrolidine-2,4-dione) derivatives could be isolated from a variety of marine and terrestrial organisms. Examples of these are fusaridione A isolated from *Fusarium heterosporum* [31], tenuazonic acid from *Alternaria alternata* [32] or aminotenuazonic acid from *Laccaria bicolor*. [33]
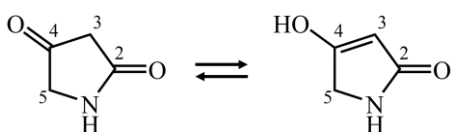
Figure 3-8 Core structure of tetramic acid derivatives. [33]

However, these compounds also carry an additional OH or carbonyl group (keto-enol tautomers) at position C-4. Mainly, position C-3 is substituted by acyl groups, substitution at C-5 usually derives from amino acids. [34] The biosynthesis of tetramic acid derivatives mostly takes place via hybrid polyketide synthase (PKS) and nonribosomal peptide synthetase (NRPS) machineries and is illustrated in **Figure 3-9**-**A** by the example of aspyridone. A deeper look inside reveals the close structural similarity between the pre-aspyridone and compound **3.10a/b**. The formation of aspyridone starts with the modification of phenylalanine, it can be suggested that in of **3.1a/b** and **3.10a/b** the modification process starts on alanine. [34; 35] After water is cleaved off, a further reduction step results in the formation of **3.10a/b**. For example, this would be possible with an associated reductase domain. Such motifs are known from liverworts such as *Marchantia paleacea* and their conversion of prelunularic acid to lunularic acid. [36] A proposed modified biosynthetic pathway is shown in **Figure 3-9**-**B**.

A
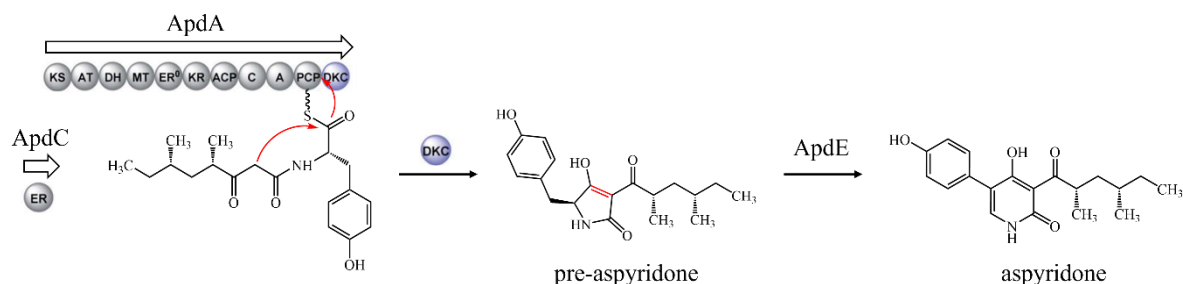
B
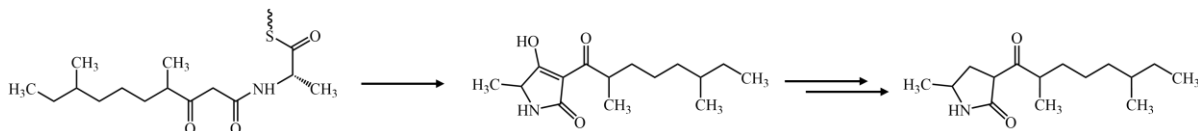
Figure 3-9 A: Biosynthetic pathway of aspyridone. Domain abbreviations: KS, ketosynthase; AT, acyltransferase; DH, dehydratase; MT, methyltransferase; ER, enoyl reductase; KR, ketoreductase; ACP, acyl carrier protein; C, condensation; A, adenylation; PCP, peptidyl carrier protein; DKC, Dieckmann cyclase. [34]; **B**: proposed biosynthetic pathway of **3.10**.

Tetramic acid derivatives have attracted considerable attention for their diverse promising bioactivities, like antimicrobial, antitumoral or antiviral properties. [37; 38] Tenuazonic acid and aminotenuazonic acid exhibit phytotoxic activity. [33] Unfortunately, during the structural elucidation of compound **3.10a/b**, the compound was degraded based on several changes of deuterated solvents, and no further testing was therefore possible.

Phytotoxic activity

compound	50 mM	20 mM	10 mM
3-(6-hydroxy-2,6-dimethyl-octanoyl)-5-methylpyrrolidin-2-one (**3.1a/b**)	+	(+)	-
3-(2,6-dimethyloctanoyl)-5-methylpyrrolidin-2-one (**3.10a/b**)	n.t.	n.t.	n.t.

+ formation of chlorosis/necrosis observed; - no effect; n.t. not tested.

The tested compound **3.1a**/**b** showed a phytotoxic activity up 20 mM in the leaf-spot assay on *A. thaliana* Col-0. The relatively low phytotoxicity of **3.1a**/**b** is relativized by the large amount produced by the fungus. The compounds **3.1a**/**b** and **3.10a**/**b** belong to the major metabolites produced in HMG medium (see Chapter 8). Therefore, the compound seems to be important for the pathogenicity of the fungus.

3.3.3 2,5-Diketopiperazines (DKPs)

In summary, eight known 2,5-diketopiperazines were isolated from the culture filtrate of *C. graminicola*. Four compounds (**3.2**, **3.4**, **3.5** and **3.9**) have been previously isolated from *Colletotrichum* spp.. [39–45] The DKPs **3.6**, **3.7**, **3.8** and **3.15** were identified for the first time in the genus *Colletotrichum*.

DKPs and natural products comprising a DKP scaffold are widely spread in nature and show a huge variety of biological activities, including antibacterial, antifungal, herbicidal, anticancer and anthelmintic properties. [39; 42–45] Especially proline-based DKPs are common in nature. Proline-based DKPs have special characteristics due to the DKP core is connected with the pyrrolidine ring, resulting in higher rigidity, structural stability and increased bioactivity. [45; 46]
Five (**3.2, 3.4, 3.5, 3.9, 3.15**) out of eight isolated DKPs contain proline. Additionally, strong biological properties are reported for several of them. [44; 47–50] For instance, Kumar and co-workers reported high antifungal activity of *cyclo*-L-Leu-L-Pro (**3.2**) against *Penicillium expansum* with MIC of 4 µg/ mL compared to the standard fungicide Bavistin with MIC of 50 µg/ mL. [44] Further, Castaldi and co-workers have demonstrated that *cyclo*-L-Val-L-Pro (**3.4**) has strong antibacterial effects similar to the positive control chloramphenicol. [48] Castaldi and co-workers observed a strong influence of the absolute configuration on the properties of the compounds. E.g., a *cyclo*-L-Pro-L-Tyr showed a 50 – 60 times higher activity than *cyclo*-D-Pro-L-Tyr. [48] This also demonstrates that studies without specification of the absolute configuration are not very comparable; at least four isomer forms can exist for the simplest DKP based on two amino acids.

Absolute configuration
Each of the isolated DKPs (**3.2**, **3.4** – **3.9** and **3.15**) possess two chiral centers at position C-3 and C-6, which corresponds to four possible stereoisomers.
By comparison of the experimental ECD spectra of **3.2** and **3.4** with the published ECD spectra, the compounds were identified as *cyclo*-L-Leu-L-Pro (**3.2**) and *cyclo*-L-Val-L-Pro (**3.4**). [51]

For the DKPs **3.5** – **3.9** the absolute configuration was determined by comparison of the experimental spectra with calculated ECD spectra (see 3.2.6). This is shown as an example for compound **3.7** in **Figure 3-10**. The comparative analysis of the calculated and experimental ECD spectra indicated the stereoisomer with the configuration D-L as the most suitable fit with a similarity factor (S = 0.973, sigma 0.3 eV and a shift of 21 nm). Therefore, **3.7** was unambiguously determined as *cyclo*-D-Ile-L-Pro. All other spectra can be found in the appendix (**Figure S 24**, **Figure S 30**, **Figure S 37**, **Figure S 43**).
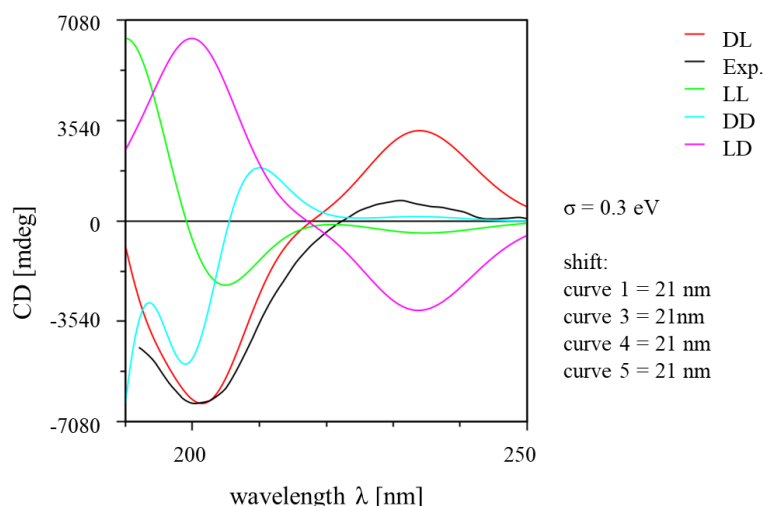
Figure 3-10 Calculated ECD spectra of compound **3.7** in comparison with the experimental one (black) in methanol. Red = *cyclo*-D-Ile-L-Ala, green = *cyclo*-L-Ile-L-Ala, blue = *cyclo*-D-Ile-D-Ala, purple = *cyclo*-L-Ile-D-Ala. Best similarity factor found for D-L (red) with 0.973 for sigma = 0.3 eV.

On this basis, the DKPs were identified as *cyclo*-L-Ala-L-Pro (**3.5**), *cyclo*-L-Ala-D-Val (**3.6**)*, cyclo*-L-Ala-D-Ile (**3.7**), *cyclo*-D-Ala-D-Leu (**3.8**), *cyclo*-L-Trp-D-Pro (**3.9**). For *cyclo*-Ile-Pro (**3.15**) the absolute configuration was not determined. Interestingly, numerous amino acids (leucine, alanine, valine and proline) occur in both configurations, making it essential to determine the absolute configuration of the molecules.

Phytotoxic activity
Table 3-1 Results of the leaf-spot bioassay of isolated DKP.

compound	100 mM	50 mM	20 mM	10 mM
cyclo-L-Leu- L-Pro (**3.2**)	+	+	+	-
cyclo-L-Val-L-Pro (**3.4**)	n.t.	+	-	n.t.
cyclo-L-Ala-L-Pro (**3.5**)	n.t.	+	-	-
cyclo-L-Ala-D-Val (**3.6**)	+	-	-	n.t.
cyclo-L-Ala-D-Ile (**3.7**)	+	+	-	-
cyclo-D-Ala-D-Leu (**3.8**)	-	-	-	-
cyclo-L-Trp-D-Pro (**3.9**)	n.t.	+	(+)	-
cyclo-Ile-Pro (**3.15**)	+	n.t.	n.t.	n.t.

+ formation of chlorosis/necrosis observed; - no effect; n.t. not tested.

The isolated DKPs (**3.2**, **3.4** – **3.9** and **3.15**) were tested in a modified leaf-spot assay on *A. thaliana* Col-0 in different concentrations (10, 20, 50 and 100 mM).[7] Due to the low yield of isolated DKP, some compounds could not be tested in the highest concentration of 100 mM. Above 50 mM all DKPs showed phytotoxic activity within 48 h, except **3.8**, which showed no phytotoxic activity at all. At 20 mM, only the two compounds **3.2** and **3.9** caused necrosis or chlorosis within 48 hours. However, the observed effects were only very weak. At the lowest concentration of 10 mM, none of the tested compounds showed any effect anymore.

The phytotoxic activity of three compounds (**3.2**, **3.4** and **3.15**) has already been described in the literature, however without specifying the bioassay and the concentrations used. [39] In contrast to this, Song et al. observed that *cyclo*-L-Leu-L-Pro (**3.2**) had only minor inhibiting effects on the root (5.6 ± 2.3 %) and shoot (3.7 ± 2.1%) growth of *Lolium perenne* at a concentration of 200 ppm. [52]
Guo et al. (2007) demonstrate the phytotoxic activity of *cyclo*-Val-Pro on black pine seedlings. At a test concentration of 20 µg/ mL 96% of the treated seedlings were wilted after an incubation time of 48 h. [49] No information was given on the absolute configuration of the compound. Interestingly, in the bioassay on *A. thaliana* Col-0, *cyclo*-L-Val-L-Pro (**3.4**) showed only very weak activity (100 mM).

In 2016 Wei and co-workers reported that Brevianamide F (*cyclo*-L-Trp-L-Pro) has strong inhibitory effect (inhibition > 60%) on the root growth of radish seedlings at a concentration of 100 ppm. The inhibition rate was comparable to that of the positive control glyphosate (55%). [50] The stereoisomer *cyclo*-L-Trp-D-Pro (**3.9**), however, only showed weak phytotoxic activity up to concentration of 20 mM in the leaf-spot assay.

Considering the results of the leaf spot bioassay, all DKP tested show phytotoxic effects at relatively high concentrations. However, it must be considered that the bioassays are not comparable as they were performed on different plants and, moreover, on different organs of the plants. As the leaf-spot assay used is performed on fully expanded leaves without prior wounding, the leaf cuticle could hinder the penetration of the quite polar compounds (log *P* between 0.25 and 1.50; consensus log *P* calculated by SwissADME webtool).[53]

3.3.4 Acetamides

In total, three known acetamides (**3.3**, **3.13**, **3.14**) could be identified from the culture filtrate of *C. graminicola*. *N*-phenethylacetamide (**3.3**) and *N*-acetyltyramine (**3.14**) have been previously reported from *C. fioriniae* [54] and *C. truncatum* [24], respectively, whereas *N*-[2-(2-hydroxyphenyl)-ethyl]-acetamide (**3.13**) could be detected for the first time in the genus *Colletotrichum*.

Phytotoxic activity

Table 3-2 Results of the leaf-spot bioassay of acetamides **3.3**, **3.13** and **3.14**.

compound	100 mM	50 mM	20 mM	10 mM
N-phenethylacetamide (**3.3**)	n.t.	+	+	-
N-[2-(2-hydroxyphenyl)-ethyl]-acetamide (**3.13**)	n.t.	-	-	n.t.
N-acetyltyramine (**3.14**)	-	-	n.t.	n.t.

+ formation of chlorosis/necrosis observed; - no effect; n.t. not tested.

Phytotoxic activity of *N*-phenethylacetamide (**3.3**) was previously demonstrated by Li and co-workers observing a growth inhibition of about 20 % for the macroalga *Ulva prolifera*. [55] The phytotoxic activity of the compound **3.3** was confirmed by the leaf-spot assay used resulting in necrosis up to a concentration of 20 mM. Masi and co-workers reported a phytotoxic activity of *N*-acetyltyramine (**3.14**) by inhibiting the germination of the soybean seed roots (29%) and a slight antifungal activity (20%) against *Macrophomina phaseolina* both at a concentration of 2.5 x10^{-3} mol/ L. [24] In opposite, no phytotoxic activity of *N*-acetyltyramine (**3.14**) could be observed in the leaf-spot assay used.

3.3.5 Further compounds

Phytotoxic activity

Table 3-3 Results of the leaf-spot bioassay

compound	100 mM	50 mM	20 mM	10 mM
1-(3,6-dihydro-*2H*-pyran-3-yl)pentane-2,3-diol (**3.11**)	(+)	(+)	-	n.t.
5-(2,3-dihydroxypentyl)tetrahydro-2*H*-pyran-3,4-diol (**3.12**)	n.t.	n.t.	n.t.	n.t.
lumichrome (**3.16**)	n.t.	n.t.	n.t.	n.t.
7,8,16-trihydroxyoctadeca-9,12-dienoic acid (**3.17**)	n.t.	+	+	-
(8Z,10E) -12,17-dihydroxyoctadeca-8,10-dienoic acid (**3.18**)	n.t.	+	-	-
uracil (**3.19**)	n.t.	-	n.t.	n.t.

+ formation of chlorosis/necrosis observed; - no effect; n.t. not tested.

Lumichrome (**3.16**) has previously been isolated from various plant and fungal sources, including *Colletotrichum gloeosporiodes* [56]. This is not surprising as lumichrome is a degradation product of vitamin B2 (riboflavin), which is ubiquitous in the plant and fungal kingdom. [57; 58] Due to the low

isolated amount of **3.16**, no bioassays could be performed. 7,8,16-trihydroxyoctadeca-9,12-dienoic acid (**3.17**) and (8*Z*,10*E*)-12,17-dihydroxyoctadeca-8,10-dienoic acid (**3.18**) could be recognized as two previously unknown oxylipins. Oxylipins originate from the oxidation or further conversion of polyunsaturated fatty acids and their production is widespread in the fungal kingdom. [59; 60] The oxidation itself can be either spontaneous in the presence of reactive oxygen species or catalyzed by enzymes. [61] Oxylipins play a versatile role as modulators of various metabolic pathways such as the induction of spore formation and the regulation of toxin production. [59; 61; 62] Moreover, a potential cross-kingdom communication by oxylipins is suggested. [61] Both compounds, **3.17** and **3.18** showed phytotoxic effects on *A. thaliana* Col-0. The observed phytotoxic effect could be based on the ability of fatty acids to penetrate and destabilize plasma membranes. [63; 64] Uracil (**3.19**) is a pyrimidine base and is one of the four nucleic acids of the ribonucleic acid (RNA). Uracil itself showed no phytotoxic activity, but there is a group of substituted synthetic uracil herbicides. These include, for example, 5-bromo-3-isopropyl-6-methyluracil, which acts as a photosynthesis inhibitor. [65; 66].

3.4 Conclusion

In summary, the bioassay-guided fractionation of crude extracts from the culture filtrate and mycelium of *C. graminicola* cultivated on HMG medium led to the isolation of 19 compounds. Among them, six previously undescribed compounds from different compound classes (**3.1**, **3.10 – 3.12**, **3.17** and **3.18**), eight diketopiperazines (**3.2**, **3.4 – 3.9** and **3.15**) and three acetamides (**3.3**, **3.13 – 3.14**) could be recognized. 11 out of 16 tested compounds showed a phytotoxic activity on *A. thaliana* in the modified leaf-spot assay. However, the activities could only be observed at relatively high concentrations (≥ 20 mM). However, as already mentioned, it must be taken into account that the bioassay on *A.thaliana* Col-0 was only carried out on the leaf surface without prior wounding. Thus, the hydrophobic cuticle impedes the penetration of polar substances. In addition, the pH value of the test substances was not adjusted. It can therefore not be ruled out that the tested substances were present in charged form. This would also make penetration into the plant more difficult. [53] Therefore, other test systems would also have to be used to obtain detailed information on the phytotoxicity of the compounds.

References

[1] Madigan M.T; Brock, T.D.; Martinko, J.M., *Brock biology of microorganisms,* 11. Ed., Pearson Prentice Hall, Upper Saddle River, **2006**.

[2] Zhang, J.; Reddy, J.; Buckland, B.; Greasham, R. Toward consistent and productive complex media for industrial fermentations: studies on yeast extract for a recombinant yeast fermentation process**,** *Biotechnol. Bioeng.* **2003**, *82,* 640–652, doi: 10.1002/bit.10608.

[3] Horbach, R.; Graf, A.; Weihmann, F.; Antelo, L.; Mathea, S.; Liermann, J.C.; Opatz, T.; Thines, E.; Aguirre, J.; Deising, H.B., Sfp-type 4′-phosphopantetheinyl transferase is indispensable for fungal pathogenicity, *Plant Cell* **2009**, *21,* 3379–3396, doi: 10.1105/tpc.108.064188.

[4] Ohra, J.; Morita, K.; Tsujino, Y.; Tazaki, H.; Fujimori, T.; Goering, M.; Evans, S.; Zorner, P., Production of the phytotoxic metabolite, ferricrocin, by the fungus *Colletotrichum gloeosporioides*, *Biosci. Biotechnol. Biochem.* **1995**, *59,* 113–114, doi: 10.1271/bbb.59.113.

[5] Zhou, J.; Wei, H.; Li, S.-M., Colletotriauxins A–D, New plant growth inhibitors from the phytopathogenic fungus *Colletotrichum gloeosporioides***,** *J. Agric. Food Chem.* **2023**, *71,* 11104–11109, doi: 10.1021/acs.jafc.3c03143.

[6] Tena, C.; Del Santiago, A. R.; Osuna, D.; Sosa, T., phytotoxic activity of *p*-cresol, 2-phenylethanol and 3-phenyl-1-propanol, phenolic compounds present in *Cistus ladanifer* L.**,** *Plants* **2021**, *10,* 1136, doi*:* 10.3390/plants10061136.

[7] Evidente, A.; Lanzetta, R.; Capasso, R.; Andolfi, A.; Bottalico, A.; Vurro, M.; Zonno, M.C., Putaminoxin, a phytotoxic nonenolide from Phoma putaminum, *Phytochemistry* **1995**, *40,* 6, 1637–1641, doi: 10.1016/0031-9422(95)00505-2.

[8] Yanai, T.; Tew, D.P; Handy, N.C., A new hybrid exchange-correlation functional using the Coulomb-attenuating method (CAM-B3LYP), *Chem. Phys. Lett.*, **2004**, *393*, 51-57, doi: 10.1016/j.cplett.2004.06.011.

[9] Hehre, W.J.; Ditchfield, R.; Pople, J.A., Self-consistent molecular orbital methods. XII. Further extensions of Gaussian-type basis sets for use in molecular orbital studies of organic molecules, *J. Chem. Phys.* **1972**, *56*, 2257-2261, doi: 10.1063/1.1677527.

[10] Hariharan, P.C.; Pople, J.A., The influence of polarization functions on molecular orbital hydrogenation energies, *Theor. Chim. Acta* **1973**, *28*, 213-222, doi: 10.1007/BF00533485.

[11] Clark, T.; Chandrasekhar, J.; Spitznagel, G.W.; Schleyer, P.V.R., Efficient diffuse function-augmented basis sets for anion calculations. III. The 3-21+G basis set for first-row elements, Li-F, *J. Comput. Chem.*, **1983**, *4*, 294-301, doi: 10.1002/jcc.540040303.

[12] Barone, V.; Cossi, M., Quantum calculation of molecular energies and energy gradients in solution by a conductor solvent model, *J. Phys. Chem. A* **1998**, *120*, 1995-2001, doi: 10.1021/jp9716997.

[13] Frisch, M.J.; Trucks, G.W.; Schlegel, H.B.; Scuseria, G.E.; Robb, M.A.; Cheeseman, J.R; Scalmani, G. et al., Gaussian 16 Revision A.03, Gaussian Inc. Walleingford CT **2016**.

[14] Bruhn, T.; Schaumlöffel, A.; Hemberger, Y.; Bringmann, G., SpecDis: Quantifying the comparison of calculated and experimental electronic circular dichroism spectra, *Chirality* **2013**, *25,* 243–249, doi: 10.1002/chir.22138.

[15] Zhai, Y.; Shao, Z.; Cai, M.; Zheng, L.; Li, G.; Yu, Z.; Zhang, J., *Cyclo*(L-Prol-L-Leu) of *Pseudomonas putida* MCCC 1A00316 isolated from antartic soil: identification and characterization of activity against *Meloidogyne incognita***,** *Molecules* **2019**, *24,* 768, doi*:* 10.3390/molecules24040768.

[16] Li, Z.; Zhang, B.-W.; Jiang, L.; Wang, H.; Ma, Q.-Y.; Wang, H.-F.; Zhang, J.; Chen, F.-L.; Zhao, Y.-X.; Luo, D.-Q., Two new alkaloids from the endophytic fungus *Schizophyllum* sp. HM230 isolated from *Vincetoxicum mongolicum* Maxim**,** *Nat. Prod. Res.* **2023,** 1–8, doi: 10.1080/14786419.2023.2176493.

[17] Lozano-González, M.; Ovalle-Magallanes, B.; Rangel-Grimaldo, M.; de La Torre-Zavala, S.; Noriega, L.G.; Tovar-Palacio, C. Tovar, A.R.; Mata, R., Antidiabetic *in vitro* and *in vivo* evaluation of cyclodipeptides isolated from *Pseudomonas fluorescens* IB-MR-66e, *New J. Chem.* **2019**, *43,* 7756–7762, doi: 10.1039/C9NJ00645A.

[18] Danh, C.D.; Dao, P.T.; Huong, D.T. M.; Thach, T.D.; Anh, N.M.; Minh, L.T.H., Anh, T.T.; Cuong, P.V., Cyclopeptides from marine actinomycete *Streptomyces* sp. G261, *Vietnam J. Chem.* **2018**, *56,* 570–573, doi: 10.1002/vjch.201800049.

[19] Liu, Y.; Wang, M.; Cao, Y.; Zeng, M.; Zhang, Q.; Ren, Y.; Chen, X.; He, C.; Fan, X.; Zheng, X.; Feng, W., Chemical constituents from the flowers of *Carthamus tinctorius* L. and their lung protective activity**,** *Molecules* **2022**, *27,* 3573, doi*:* 10.3390/molecules27113573.

[20] Chen, J.; Shao, J.; Zhao, C.; Shen, J.; Dong, Z.; Liu, W.; Zhao, M.; Fan, J., Chemical constituents from *Viburnum fordiae* Hance and their anti-inflammatory and antioxidant activities, *Arch. Pharmacal Res.* **2018**, *41,* 625–632, doi: 10.1007/s12272-018-1026-2.

[21] Tian, S.; Yang, Y.; Liu, K.; Xiong, Z.; Xu, L.; Zhao, L., Antimicrobial metabolites from a novel halophilic actinomycete *Nocardiopsis terrae* YIM 90022, *Nat. Prod. Res.* **2014**, *28,* 344–346, doi: 10.1080/14786419.2013.858341.

[22] Grundmann, A.; Li, S.-M., Overproduction, purification and characterization of FtmPT1, a brevianamide F prenyltransferase from *Aspergillus fumigatus, Microbiology* **2005**, *151,* 2199–2207, doi: 10.1099/mic.0.27962-0.

[23] Cheng, M.-J.; Wu, M.-D.; Aung, T.; Than, N.N; Hsieh, S.-Y.; Chen, J.J., Metabolite from the Endophytic Fungus of *Rosellinia* sp., *Chem. Nat. Compd.* **2021**, *57,* 171–173, doi: 10.1007/s10600-021-03310-4.

[24] Masi, M.; Castaldi, S.; Sautua, F.; Pescitelli, G.; Carmona, M.A.; Evidente, A., Truncatenolide, a bioactive disubstituted nonenolide produced by *Colletotrichum truncatum*, the causal agent of anthracnose of soybean in argentina: fungal antagonism and SAR studies, *J. Agric. Food Chem.* **2022**, *70,* 9834–9844, doi: 10.1021/acs.jafc.2c02502.

[25] Park, A.R.; Jeong, S.-I.; Jeon, H.W.; Kim, J.; Kim, N.; Ha, M. et al., A diketopiperazine, *Cyclo*-(L-Pro-L-Ile), derived from *Bacillus thuringiensis* JCK-1233 controls pine wilt disease by elicitation of moderate hypersensitive reaction, *Front. Plant Sci.* **2020**, *11,* 1023, doi: 10.3389/fpls.2020.01023.

[26] Cheng, M.-J.; Wu, M.-D.; Chen, J.-J.; Chen, C.-Y.; Aung, T.; Wu, H.-C. et al., Compounds from *Monascus sanguineus*, *Chem. Nat. Compd.* **2021**, *57,* 545–547, doi: 10.1007/s10600-021-03410-1.

[27] Xiao, T.; Cheng, X.; Huang, J.; Guo, Z.; Tao, L.; Shen, X., Bioactive substances inhibiting COX-2 and cancer cells isolated from the fibrous roots of *Alangium chinense* (Lour.) Harms, *RSC Adv.* **2023**, *13,* 3346–3363, doi: 10.1039/d2ra06931h.

[28] Thomas,E.J.; Willis, M., Approaches to the total synthesis of chaetochalasin A**,** *Org. Biomol. Chem.* **2014**, *12,* 7537–7550, doi: 10.1039/c4ob01308e.

[29] Wei, B.; Yang, Z.D.; Chen, X.-W.; Zhou, S.-Y.; Yu, H.-T.; Sun, J.-Y.; Yao, X.-J.; Wang, Y.-G.; Xue, H.-X., Colletotrilactam A-D, novel lactams from *Colletotrichum gloeosporioides* GT-7, a fungal endophyte of *Uncaria rhynchophylla*, *Fitoterapia* **2016**, *113,* 158–163, doi: 10.1016/j.fitote.2016.08.005.

[30] Stierle, A.A.; Stierle, D.B.; Patacini, B., The Berkeleyamides, amides from the acid lake fungus *Penicillum rubrum*, *J. Nat. Prod.* **2008**, *71,* 856–860, doi: 10.1021/np0705054.

[31] Kakule, T.B.; Sardar, D.; Lin, Z.; Schmidt, E.W., Two related pyrrolidinedione synthetase loci in *Fusarium heterosporum* ATCC 74349 produce divergent metabolites, *ACS Chem. Biol.* **2013**, *8,* 1549–1557, doi: 10.1021/cb400159f.

[32] Meronuck, R.A.; Steele, J.A.; Mirocha, C.J.; Christensen, C.M., Tenuazonic acid, a toxin produced by *Alternaria alternata*, *Appl. Microbiol.* **1972**, *23,* 613–617, doi: 10.1128/am.23.3.613-617.1972.

[33] Schrey, H.; Backenköhler, J.; Kogler, H.; Plaumann, M.; Spiteller, P., Aminotenuazonic acid: isolation, structure elucidation, total synthesis and herbicidal activity of a new tetramic acid from fruiting bodies of *Laccaria* species, *Chemistry* **2019**, *25,* 10333–10341, doi: 10.1002/chem.201901405.

[34] Mo, X.; Gulder, T.A.M, Biosynthetic strategies for tetramic acid formation, *Nat. Prod. Rep.* **2021**, *38,* 1555–1566, doi: 10.1039/d0np00099j.

[35] Bergmann, S.; Schümann, J.; Scherlach, K.; Lange, C.; Brakhage, A.A.; Hertweck, C., Genomics-driven discovery of PKS-NRPS hybrid metabolites from *Aspergillus nidulans*, *Nat. Chem. Biol.* **2007**, *3,* 213–217, doi: 10.1038/nchembio869.

[36] Ohta, Y.; Abe, S.; Komura, H.; Kobayashi, M., Prelunularic acid in liverworts, *Phytochemistry* **1984**, *23,* 1607–1609, doi: 10.1016/S0031-9422(00)83450-0.

[37] Mo, X.; Li, Q.; Ju, J., Naturally occurring tetramic acid products: isolation, structure elucidation and biological activity, *RSC Adv* **2014**, *4,* 50566–50593, doi: 10.1039/C4RA09047K.

[38] Jiang, M.; Chen, S.; Li, J.; Liu, L., The biological and chemical diversity of tetramic acid compounds from marine-derived microorganisms, *Mar. Drugs* **2020**, *18,* 114, doi: 10.3390/md18020114.

[39] Trigos, A.; Reyna, S.; Galindo, G.; Ramos, J. M., Diketopiperazines from cultures of fungus *Pestalotia palmarum*, *Nat. Prod. Lett.* **1996**, *8,* 199–205, doi: 10.1080/10575639608044894.

[40] Chapla, V.M.; Zeraik, M.L.; Cafeu, M.; Silva, G.; Cavalheiro, Bolzani, A.V.; Young, M.C.M.; Pfenning, L.H.; Araujo, A.R., Griseofulvin, diketopiperazines and cytochalasins from endophytic fungi *Colletotrichum crassipes* and *Xylaria* sp., and their antifungal, antioxidant and anticholinesterase activities, *J. Braz. Chem. Soc.* **2018**, *29*, 1707-1713, doi**:** 10.21577/0103-5053.20180045.

[41] Chapla, V. M.; Zeraik, M.L.; Leptokarydis, I.H.; Silva, G.H.; Bolzani, V.S.; Young, M.C.M.; Pfenning, L.H.; Araújo, A.R., Antifungal compounds produced by *Colletotrichum gloeosporioides*, an endophytic fungus from *Michelia champaca, Molecules* **2014**, *19,* 19243–19252, doi: 10.3390/molecules191119243.

[42] Borthwick, A.D., 2,5-Diketopiperazines: Synthesis, Reactions, Medicinal Chemistry, and Bioactive Natural Products, *Chem. Rev.* **2012**, *112,* 3641–3716, doi: 10.1021/cr200398y.

[43] Jia, J.; Yao, J.; Kong, J.; Yu, A.; Wei, J.; Dong, Y; Song, R.; Shan, D.; Zhong, X.; Lv, F.; Fan, Q.; She, G., 2,5-Diketopiperazines: A review of source, synthesis, bioactivity, structure, and MS fragmentation, *Curr. Med. Chem.* **2023**, *30,* 1060–1085, doi: 10.2174/0929867329666220801143650.

[44] Nishanth Kumar, S.; Mohandas, C.; Siji, J.V.; Rajasekharan, K.N.; Nambisan, B., Identification of antimicrobial compound, diketopiperazines, from a *Bacillus* sp. N strain associated with a rhabditid entomopathogenic nematode against major plant pathogenic fungi, *J. Appl. Microbiol.* **2012**, *113,* 914–924, doi: 10.1111/j.1365-2672.2012.05385.x.

[45] Bojarska, J.; Mieczkowski, A.; Ziora, Z.M.; Skwarczynski, M.; Toth, I.; Shalash, A.O.; Parang, K.; El-Mowafi, S. A.; Mohammed, E. H. M.; Elnagdy, S.; Al Khazindar, M.; Wolf, W. M., Cyclic Dipeptides: The Biological and Structural Landscape with Special Focus on the Anti-Cancer Proline-Based Scaffold, *Biomolecules* **2021**, *11,* 1515, doi: 10.3390/biom11101515.

[46] Bojarska, J.; Remko, M.; Breza, M.; Madura, I.; Fruziński, A.; Wolf, W.M., A proline-based tectons and supramolecular synthons for drug design 2.0: A case study of ACEI, *Pharmaceuticals* **2020**, *13,* 338, doi*:* 10.3390/ph13110338.

[47] Nishanth Kumar, S.; Mohandas, C.; Nambisan, B., Purification of an antifungal compound, cyclo(l-Pro-d-Leu) for cereals produced by *Bacillus cereus* subsp. *thuringiensis* associated with entomopathogenic nematode, *Microbiol. Res.* **2013**, *168,* 278–288, doi: 10.1016/j.micres.2012.12.003.

[48] Castaldi, S.; Cimmino, A.; Masi, M.; Evidente, A., Bacterial lipodepsipeptides and some of their derivatives and cyclic dipeptides as potential agents for biocontrol of pathogenic bacteria and fungi of agrarian plants, *J. Agric. Food Chem.* **2022**, *70,* 4591–4598, doi: 10.1021/acs.jafc.1c08139.

[49] Guo, Q.; Guo, D.; Zhao, B.; Xu, J.; Li, R., Two cyclic dipeptides from *Pseudomonas fluorescens* GcM5-1A carried by the pine wood nematode and their toxicities to japanese black pine suspension cells and seedlings in vitro, *J. Nematol.* **2007**, *39,* 243–247, PMCID: PMC2586505.

[50] Wei, J.; Zhang, X.-Y; Deng, S.; Cao, L.; Xue; Q.-H.; Gao, J.-M., α-Glucosidase inhibitors and phytotoxins from *Streptomyces xanthophaeus*, *Nat. Prod. Res.* **2017**, *31,* 2062–2066, doi: 10.1080/14786419.2016.1269100.

[51] Domzalski, A.; Margent, L.; Vigo, V.; Dewan, F.; Pilarsetty, N.V.K.; Xu, Y.; Kawamura, A., Unambiguous stereochemical assignment of cyclo(Phe-Pro), cyclo(Leu-Pro), and cyclo(Val-Pro) by electronic circular dichroic spectroscopy, *Molecules* **2021**, *26,* 5981, doi*:* 10.3390/molecules26195981.

[52] Song, Q.-Y.; Nan, Z.-B; Gao, K.; Song, H.; Tian, P.; Zhang, X.-X.; Li, C.-J.; Xu, W.-B.; Li, X.-Z., Antifungal, Phytotoxic, and Cytotoxic Activities of Metabolites from *Epichloë bromicola,* a Fungus Obtained from *Elymus tangutorum* Grass, *J. Agric. Food Chem.* **2015**, *63,* 8787–8792, doi: 10.1021/acs.jafc.5b04260.

[53] Schreiber, L., Polar paths of diffusion across plant cuticles: new evidence for an old hypothesis, *Ann. Bot.* **2005**, *95,* 1069–1073, doi: 10.1093/aob/mci122.

[54] Wang, H.-H.; Li, G.; Peng, X.-P.; Lou, H.-X., Secondary metabolites from *Colletotrichum fioriniae* F18, an endophytic fungus isolated from the medicinal plant *Mahonia fortune*, *Acta Pharmacol. Sin.* **2018,** 1862–1867.

[55] Li, N.; Zhang, J.; Zhao, X.; Wang, P.; Tong, M.; Glibert, P.M., Allelopathic Inhibition by the bacteria *Bacillus cereus* BE23 on growth and photosynthesis of the macroalga *Ulva prolifera*, *JMSE* **2020**, *8,* 718, doi: 10.3390/jmse8090718.

[56] Zou, W.X.; Meng, J.C.; Lu, H.; Chen, G.X.; Shi, G.X; Zhang, T.Y.; Tan, R.X., Metabolites of *Colletotrichum gloeosporioides*, an endophytic fungus in *Artemisia mongolica*, *J. Nat. Prod.* **2000**, *63,* 1529–1530, doi: 10.1021/np000204t.

[57] Kino, K.; Kobayashi, T.; Arima, E.; Komori, R.; Kobayashi, T.; Miyazawa, H., Photoirradiation products of flavin derivatives, and the effects of photooxidation on guanine, *Bioorganic Med. Chem. Lett.* **2009**, *19,* 2070–2074, doi: 10.1016/j.bmcl.2009.01.112.

[58] Bacher, A.; Eberhardt, S.; Fischer, M.; Kis, K.; Richter, G., Biosynthesis of vitamin b2 (riboflavin), *Annu. Rev. Nutr.* **2000**, 20, 153–167, doi: 10.1146/annurev.nutr.20.1.153.

[59] Tsitsigiannis, D.I.; Keller, N.P., Oxylipins as developmental and host-fungal communication signals, *Trends Microbiol.* **2007**, *15,* 109–118, doi: 10.1016/j.tim.2007.01.005.

[60] Fox, S.R.; Akpinar, A.; Prabhune, A.A.; Friend, J.; Ratledge, C., The biosynthesis of oxylipins of linoleic and arachidonic acids by the sewage fungus *Leptomitus lacteus*, including the identification of 8R-hydroxy-9Z,12Z-octadecadienoic acid, *Lipids* **2000**, *35,* 23–30, doi: 10.1007/s11745-000-0490-5.

[61] Beccaccioli, M.; Pucci, N.; Salustri, M.; Scortichini, M.; Zaccaria, M.; Momeni, B.; Loreti, S.; Reverberi, M.; Scala, V., Fungal and bacterial oxylipins are signals for intra- and inter-cellular communication within plant disease, *Front Plant Sci.* **2022**, *13,* 823233, doi: 10.3389/fpls.2022.823233.

[62] Scarpari, M.; Punelli, M.; Scala, V.; Zaccaria, M.; Nobili, C.; Ludovici, M.; Camera, E.; Fabbri, A.A.; Reverberi, M.; Fanelli, C., Lipids in *Aspergillus flavus*-maize interaction, *Front. Microbiol.* **2014**, *5,* 74, doi: 10.3389/fmicb.2014.00074.

[63] Lederer, B.; Fujimori, T.; Tsujino, Y.; Wakabayashi, K.; Böger, P., Phytotoxic activity of middle-chain fatty acids II: Peroxidation and membrane effects, *Pestic. Biochem. Phys.* **2004**, *80,* 151–156, doi: 10.1016/j.pestbp.2004.06.010.

[64] Gruber, H.J.; Low, P.S., Interaction of amphiphiles with integral membrane proteins. I. Structural destabilization of the anion transport protein of the erythrocyte membrane by fatty acids, fatty alcohols, and fatty amines, *Biochim. Biophys. Acta* **1988**, *944,* 414–424, doi: 10.1016/0005-2736(88)90512-3.

[65] Bucha, H.C.; Cupery, W.E.; Harrod, J.E.; Loux, H.M.; Ellis, L.M., Substituted uracil herbicides, *Science* **1962**, *137,* 537–538, doi: 10.1126/science.137.3529.537.

[66] Hilton, J.L.; Monaco, T.J.; Moreland, D.E.; Gentner, W.A., Mode of action of substituted uracil herbicides, *Weeds* **1964**, *12,* 129, doi: 10.2307/4040613.

4 Isolation of phytotoxic compounds from *Colletotrichum graminicola* cultivated in CM medium

Abstract

From cultures of *Colletotrichum graminicola* grown in CM medium (complete medium) 13 compounds could be isolated according to their phytotoxic activity. Isolated compounds comprise the new dehydropyranone derivative named graminolactone (**4.2**), the new anthraquinone derivative named 5-chloro-colletoquinone A (**4.4**), beside three hexanoic acid derivatives new to nature (**4.9**, **4.11** and **4.13**), as well as the eight known compounds, trans-anhydro-mevalonic acid (**4.1**), colletoquinone A (**4.3**), colletoquinone B (**4.5**), azelaic acid (**4.6**), (*E*)-dec-2-enedioic acid (**4.7**), *cyclo*-Ala-Pro (**4.8**), *cyclo*-L-Phe-D-Pro (**4.10**) and *N*-5-hydroxypentylacetamide (**4.12**). The structures were determined by intense NMR spectroscopic analysis, ESI-HRMS measurements and X-ray crystallography. In addition, the absolute configuration of graminolactone (**4.2**) and *cyclo*-L-Phe-D-Pro (**4.10**) were established by quantum chemical CD calculation. The phytotoxic activity was tested using a leaf spot test on *Arabidopsis thaliana* Col-0 at concentrations between 100 and 10 mM. Nine out of twelve compounds exhibit phytotoxic activity.

4.1 Introduction

This chapter describes the bioassay-guided isolation and structure elucidation of five previously unknown compounds comprising the anthraquinone derivative named 5-chloro-colletoquinone A (**4.4**) and three new hexanoic acid derivatives new to nature (**4.9**, **4.11** and **4.13**), together with the known compounds *trans*-anhydro-mevalonic acid (**4.1**), colletoquinone A (**4.3**), colletoquinone B (**4.5**), azelaic acid (4.6), (*E*)-dec-2-enedioic acid (**4.7**), *cyclo*-Ala-Pro (**4.8**), *cyclo*-L-Phe-D-Pro (**4.10**) and *N*-5-hydroxypentylacetamide (**4.12**). from *C. graminicola* grown on CM medium. All isolated compounds were tested for their phytotoxic activity using a leaf-spot assay on *Arabidopsis thaliana* Col-0.

The Complete Medium (CM) is a medium, which consist of casein hydrolysate, yeast extract, calcium nitrate, glucose with additional minerals (K, Na, Mg, Cl, P, S). Caseins is a family of related phosphoproteins in mammalian milk that precipitate at pH = 4.6. [1] Smaller peptides arising from hydrolysis of casein are used as a source of amino acids in culture media. Also, the yeast extract serves as a source of amino acids, peptides, and water-soluble vitamins. [2] In addition, the glucose (carbohydrates) provides a rich source of carbon, while the calcium nitrate is an additional source of nitrogen. Thus, the CM medium covers all the necessary nutrients for the fungal cultivation.

4.2 Experimental

4.2.1 General experimental procedures

Column chromatography was performed on polyamide CC 6-Ac (Macherey Nagel, Germany), silica gel 60 silanized (0.063 – 0.200 mm, Merck, Germany) and Sephadex LH-20 (Fluka, Germany), whereas analytical TLC was performed on pre-coated silica gel F_{254} aluminum sheets (Merck, Germany).

HPLC
The analytical and semi-preparative HPLC were performed on a Shimadzu prominence system (Shimadzu Europe, Germany) which consists of a CBM-20A communication bus module, a SPD-M20A diode array detector, a FRC-10A fraction collector, a DGU-20A5R degassing unit, a LC-20AT liquid chromatograph and a SIL-20A HT autosampler. Following columns were used: ODS-A column 1 (5 µM, 120 Å, 150 x 4.6 mm ID, YMC Europe, Germany), an ODS-A column 2 (5 µM, 120 Å, 150 x 10.0 mm ID, YMC Europe) and a Zorbax Eclipse XDB column 3 (5 µM, 80 Å, 250 x 9.4 mm ID, Agilent, Germany).
The solvent systems H_2O + 0.1 % FA (A) and CH_3CN + 0.1 % FA (B) (solvent system I) or H_2O (A) and methanol (B) (solvent system II) were used for the HPLC separation of target compounds.

High-resolution mass spectrometry
The high-resolution mass spectrometry was either performed from an Orbitrap Elite mass spectrometer (Thermo Fisher Scientific, Germany) or from a QTOF MS instrument (TripleTOF 6600, Sciex, Canada).

UHPLC-ESI-HRMS, Orbitrap Elite mass spectrometer
The positive ion high-resolution ESI mass spectra (*m/z* range 100-2000) were obtained from an Orbitrap Elite mass spectrometer (Thermo Fisher Scientific, Germany) equipped with a heated electrospray ion source (spray voltage 4 kV, capillary temperature 325 °C, source heater temperature 300 °C, FTMS resolution Full scan 30.000, MS/MS 15.000). Nitrogen was used as a sheath and auxiliary gas. The MS system was coupled to an ultra-high-performance liquid chromatography (UHPLC) system (Dionex UltiMate 3000, Thermo Fisher Scientific, Germany), equipped with a RP-18 column (particle size 1.7 µm, 50 × 2.1 mm ID, BEH-C18, Waters, Germany; column temperature 40 °C) connected with a C18 guard column (particle size 1.7 µm, 5 × 2.1 mm ID, BEH-C18, Waters, Germany). The mobile phases were H_2O (A; MilliQ-system Barnstead GenPure Pro (from Thermo Scientific, Germany)) and CH_3CN (B; Chromasolv, for LC-MS, Honeywell Riedel de Haën, Germany) with 0.1% formic acid (additive for LC-MS, LiChropur, Merck, Germany). Chromatographic separation was realized using a gradient system starting from 5% B (isocratic for 1 min) increasing to 95% B within 10 min, followed by further 3 min at 95% B (flow rate 0.4 mL/min, injection volume 3 µL). The re-equilibration time of the column was set to 3.5 min at 5% B. The wavelength range of the PDA measurements was set to 190-600 nm. The CID mass spectra (buffer gas: helium) using data dependent acquisition were recorded using a normalized collision energy (NCE) of 35%. The instrument was externally calibrated by the Pierce ESI positive ion calibration

solution (product no. 88323) from Thermo Fisher Scientific (Germany). The data were evaluated using the software Xcalibur 2.2 SP1.

Direct injection via autosampler, Orbitrap Elite mass spectrometer
The negative ion high resolution ESI mass spectra were obtained from a Orbitrap Elite mass spectrometer (Thermofisher Scientific, Germany) equipped with a HESI electrospray ion source (negative spray voltage 4 kV, capillary temperature 325°C, source heater temperature 80 °C, FTMS resolution 60.000). Nitrogen was used as sheath gas. The sample solutions were injected through the autosampler (injection volume 5 µL) without chromatographic separation. The instrument was externally calibrated by the Pierce® ESI negative ion calibration solution (product number 88324) from Thermofisher Scientific, USA. The data were evaluated by the Xcalibur software 2.2 SP1.

UHPLC-ESI-HRMS + SWATH, TripleTOF 6600, Sciex
The UHPLC separation was performed using an Acquity UPLC system (Waters, Germany), configured in binary high pressure gradient mode. Eluent A consisted of ultrapure water (A, MilliQ-system Barnstead GenPure Pro (from Thermo Scientific, Germany)) and CH_3CN (B; Chromasolv, for LC-MS, Honeywell Riedel de Haën, Germany) with 0.1% formic acid (additive for LC-MS, LiChropur, Merck, Germany). The gradient profile for eluent B was as follows: 0.0–0.5 min 10%; 0.5–4.3 min increase to 95%; 4.3–4.7 min hold at 95%; 4.7–4.8 min decrease to 10%. For re-equilibration of the UHPLC column, the gradient was set to 10% eluent B for 0.5 min. The column oven was set at 40°C and the autosampler was cooled at 10°C. The flow rate was kept constant at 0.4 mL/min. A volume of 2 µL of the sample was injected onto a BEH RP-C18 column (50 mm × 2.1 mm i.d.; 1.7 µm particle size, 100 Å) (Waters, Canada) guarded with a C18 guard column (2.0 mm i.d. × 4.0 mm; Phenomenex). Mass spectrometric detection was performed using a QTOF MS instrument (TripleTOF 6600, Sciex, Canada) equipped with an ESI-DuoSpray-Ion-Source and a resolving power (full width at half-maximum, fwhm, at *m/z* 400) set of 30,000 in MS and 30,000 in Sequential Window Acquisition of all Theoretical Mass Spectra (SWATH) MS/MS (high resolution mode). The automated calibration device system performed an external calibration approximately every hour. The Turbo V ion drive source equipped with a stainless-steel electrode (100 µm internal diameter) was operated with the following MS conditions: gas 1, nitrogen (40 psi); gas 2, nitrogen (40 psi); ion spray voltage, 5500 V (positive mode) 4500 V (negative mode); ion-source temperature, 450°C; curtain gas, nitrogen (35 psi); collision energy, 10 eV. The MS was operated in the SWATH acquisition mode, where one complete cycle consists of a survey scan and a Q1 isolation strategy. The survey scan covered a mass range of *m/z* 100 to 1000 with an accumulation time of 100 ms. The Q1 isolation strategy covered a mass range of *m/z* 100 to 650 with a 23 Da SWATH window for Q1 isolation (overlap 1 u). In each SWATH window, a collision energy of 35 eV with a spread of ±15 eV and an accumulation time of about 50 ms in high-resolution mode was used. The total cycle time was 1.4 s. All MS parameters were controlled by AnalystTF 1.7 Software (Sciex, Canada).

Direct injection via autosampler, TripleTOF 6600, Sciex
The mass spectrometric detection in positive ion mode was performed using a QTOF MS instrument (TripleTOF 6600, Sciex, Canada) equipped with an ESI-DuoSpray-Ion-Source and a resolving power (full width at half-maximum, fwhm, at *m/z* 400) set of 30,000 in MS. The automated calibration device system performed an external calibration. The Turbo V ion drive source equipped with a stainless steel electrode (100 µm internal diameter) was operated with the following MS conditions: gas 1, nitrogen (60 psi); gas 2, nitrogen (70 psi); ion spray voltage, 5500 V (positive mode); ion-source temperature, 450°C; curtain gas, nitrogen (55 psi); collision energy 10 V. The TOF MS accumulation time was set to 50 ms and covered a mass range of *m/z* 100 to 2500. The sample solutions were injected through the autosampler (injection volume 5 µL) without chromatographic separation.

NMR
NMR spectra were obtained from an Agilent DD2-400 spectrometer (Agilent, Germany) using a 5-mm inverse detection cryoprobe. The spectra were recorded at 399.917 (^{1}H) and 100.570 (^{13}C), respectively. 2D NMR spectra were recorded using standard CHEMPACK 8.1 pulse implemented in Varian VNMRJ 4.2 spectrometer software. For samples with low concentrations, NMR spectra were recorded on a Bruker Avance Neo 500 NMR spectrometer (Bruker, Germany) at 500.234 and 125.797 MHz, respectively, using a 5 mm prodigy probe with TopSpin 4.0.7 spectrometer software. Chemical shifts are reported relative to TMS.

CD

CD spectra were recorded on a Jasco J-815 CD spectrophotometer (Jasco, Germany).

4.2.2 Cultivation

The strain *Colletotrichum graminicola* M1.001 was provided by Prof. Dr. Deising, Institute of Agricultural and Nutritional Sciences, Martin-Luther University Halle-Wittenberg. *C. graminicola* was cultivated as semi-solid cultures in Erlenmeyer flasks (1 L) containing 4 g cotton wool and 200 mL CM medium (10 g/ L glucose, 1 g/ L Ca(NO$_3$)$_2$, 1 g/ L yeast extract, 1 g/ L casein hydrolysate, 0.2 g/ L KH$_2$PO$_4$, 0.25 g/ L MgSO$_4$, 0.05 g/ L NaCl) at 23°C for 13 days without agitation. In total, 200 flasks (40 L) were grown. Subsequently, the mycelium and the cotton wool were separated from the culture broth by vacuum filtration. The mycelium was frozen at -20°C prior to extraction.

4.2.3 Extraction

The culture filtrate was extracted by partition first with ethyl acetate (3 x 1 L) followed by *n*-butanol (3 x 0.75 L) to obtain two crude extracts (ethyl acetate = **1**, *n*-butanol = **2**). The ethyl acetate phases were combined and dehydrated by adding anhydrous sodium sulfate (Na$_2$SO$_4$).

The mycelium together with the cotton wool was exhaustively extracted with ethyl acetate (6 x 3 L) in an ultrasound bath for 15 minutes. The organic phases were combined, dehydrated by adding anhydrous sodium sulfate (Na$_2$SO$_4$), filtered and concentrated under reduced pressure to obtain the ethyl acetate crude extract **3**. Both ethyl acetate crude extracts (**1** and **3**) were combined based on their TLC pattern and subsequently subjected to a liquid-liquid partition with acetonitrile (extract **4**) and *n*-hexane (extract **5**).

4.2.4 Isolation

The *n*-butanol crude extract **2** was separated by size exclusion chromatography on Sephadex LH-20 (50 x 4.5 cm) eluting with water : methanol (1:1, *v/v*) → methanol. Twelve fractions (each approximately 150 mL, A1 – A12) were collected. Based on their phytotoxic activity to *A. thaliana* Col-0 the fractions A5 – A9 (2.8 g) were combined and further separated on silanized silica (41 x 3.1 cm) using a chloroform : methanol gradient (15:1 → 9:1 → 6:1 → 3:1 → 1:1 → 0:1, *v/v*) followed by acidified methanol. In total, 22 fractions à 80 mL were collected and combined based on their TLC pattern to afford five fractions (B1 – B5).

Fraction B1 (300 mg) was further separated on silanized silica (column size 41 x 3.1 cm) using a chloroform : methanol gradient (100:1 → 30:1 → 10:1 → 5:1 → 3:1 → 1:1 → 0:1, *v/v*) followed by acidified methanol. Thirty fractions each 150 mL were collected and subsequently combined into six fractions (C1 – C6) according to the TLC pattern. Subsequently, fraction C5 (110 mg) was separated on Sephadex LH-20 (86 x 2.1 cm) using methanol as eluent. 130 fractions (each 10 mL) were collected and combined into 10 fractions (D1 – D10). Final isolation of **4.1** (t_R = 7.7 min, 1.1 mg) was achieved by analytical HPLC of fraction D5 (12.1 mg) using column 1 with solvent system I (0.8 mL/min; 2 – 20 min, 5 – 100 % B).
Fraction B3 (10 mg) was further separated by semi-preparative HPLC using column 2 with solvent system I (3.0 mL/min; 2 – 15 min; 10 – 50 % B) to afford **4.2** (t_R = 10.2 min, 2.3 mg).

The acetonitrile extract **4** (2.5 g) was separated on a polyamide CC 6-Ac column (80 x 2.5 cm) eluting with *n*-hexane : ethyl acetate (4:1 → 3:1 → 2:1 → 1:1, *v/v*) → ethyl acetate → ethyl acetate : acetone (1:1, *v/v*) → acetone → acetone : methanol (2:1 → 1:1, *v/v*) → methanol to give ten fractions (E1 – E10). From fraction E6 compound **4.3** precipitated in form of crystals. The crystals were separated and analyzed by X-ray crystallography (see 4.2.5).
Fraction E7 (270 mg) was subjected to column chromatography on silanized silica (70 x 2.5 cm) using the gradient system *n*-hexane : ethyl acetate (2:1 → 1:1 → 0:1, *v/v*) → ethyl acetate : methanol (1:1 → 0:1, *v/v*) followed by acidified methanol to afford seven fractions (F1 – F7) each fraction 300 mL.
Fraction F1 (67 mg) was further separated on Sephadex LH-20 (10 x 2.5 cm) eluting first with ethyl acetate and changing to ethyl acetate : methanol (1:1, *v/v*) to afford four fractions (G1 – G4, each fraction 40 mL).
Fraction G2 was purified by semi-preparative HPLC using column 3 with solvent system II (1.8 mL/min; 2 – 12 min, 80 – 100 % B) to afford **4.3** (t_R = 10.7 min, 4.5 mg), **4.4** (t_R = 12.4 min, 4.7 mg) and **4.5**;(t_R = 14.0, 3.2 mg). Compound **4.4** precipitated in form of crystals from the fraction. The crystals were separated and analyzed by X-ray crystallography.

HPLC separation of fraction G3 using the same conditions as described for G2 afforded **4.6** (t_R = 16.8 min, 2.1 mg) and **4.7** (t_R = 18.9 min, 1.8 mg).

Semi-preparative HPLC of fraction F6 using column 3 with solvent system II (1.8 mL/min; 3 – 23 min, 5 – 100 % B) yielded compound **4.8** (t_R = 15.6 min, 0.9 mg), **4.9** (t_R = 21.7 min, 1.6 mg), and **4.10** (t_R = 22.4 min, 1.1 mg)

HPLC separation of fraction F7 using column 3 with solvent system II (1.8 mL/min; 3 – 23 min, 5 – 100 % B) resulted in the isolation of **4.11** (t_R = 15.8 min, 1.3 mg), **4.10** (t_R = 16.4 min, 1.2 mg), and **4.13** (t_R = 21.8 min, 1.3 mg).

trans-Anhydromevalonic acid (**4.1**): colorless oil; ^{1}H NMR (400 MHz, methanol-d_4) δ 5.72 (1H, d, J = 1.3 Hz, H-2), δ 2.37 (2H, t, J = 6.5 Hz, H-4), δ 3.70 (2H, t, J = 6.5 Hz, H-5), δ 2.15 (3H, d, J = 1.3 Hz, H-6); ^{13}C NMR (100 MHz, methanol-d_4) δ 170.5 (C-1), δ 119.0 (C-2), δ 157.0 (C-3), δ 44.5 (C-4), δ 60.5 (C-5), δ 18.8 (C-6); HRESIMS m/z 129.0560 [M-H]$^-$, calculated for $C_6H_9O_3$, 129.0557. (**Figure S 101 – Figure S 105**).

Graminolactone (**4.2**): colorless oil; ^{1}H NMR (400 MHz, methanol-d_4) δ 5.87 (1H, d, J = 15.6 Hz, H-3), δ 6.84 (1H, dd, J = 8.2, 15.6 Hz, H-4), δ 3.08 (1H, q, J = 8.3 Hz, H-4), δ 3.60 (1H, t, J = 8.2 Hz, H-5a), δ 3.92 (1H, t, J = 8.2 Hz, H-5b), δ 2.15 (1H, m, H-1'a), δ 1.74 (1H, dt, J = 9.4, 12.4 Hz, H-1'b), δ 3.84 (1H, dt, J = 5.7, 9.2 Hz, H-2'), δ 3.51 (1H, ddd, J = 3.8, 5.2, 9.0 Hz, H-3'), δ 1.33 (1H, m, H-4'a), δ 1.57 (1H, m, H-4'b), δ 0.97 (3H, t, J = 7.4 Hz, H-5'); ^{13}C NMR (100 MHz, methanol-d_4) δ 170.0 (C-2), δ 123.5 (C-3), δ 149.7 (C-4), δ 43.9 (C-5), δ 73.2 (C-6), δ 34.5 (C-1'), δ 84.2 (C-2'), δ 75.4 (C-3'), δ 27.6 (C-4'), δ 10.6 (C-5'); HRESIMS m/z 199.0990 [M-H]$^-$, calculated for $C_{10}H_{15}O_4^-$ 199.0976. (**Figure S 106 – Figure S 110**).

Colletoquinone A (**4.3**): orange needles; ^{1}H NMR (400 MHz, DMSO-d_6) δ 7.35 (1H, s, H-2), δ 7.54 (1H, d, J = 1.6 Hz, H-4), δ 7.03 (1H, s, H-5), δ 13.45 (1H, s, 8-OH), δ 3.95 (3H, s, H-11), δ 2.46 (3H, s, H-12), δ 3.85 (3H, s, H-13); ^{13}C NMR (100 MHz, methanol-d_4) δ 156.4 (C-1), δ 119.4 (C-2), δ 145.9 (C-3), δ 119.9 (C-4), δ 134.6 (C-4a), δ 110.9 (C-5), δ 156.8 (C-6), δ 140.0 (C-7), δ 160.5 (C-8), δ 107.5 (C-8a), δ 186.7 (C-9), δ 117.6 (C-9a), δ 181.6 (C-10), δ 127.9 (C-10a), δ 56.4 (C-11), δ 21.7 (C-12), δ 59.9 (C-13); HRESIMS m/z 313.0716 ([M-H]$^-$, calculated for $C_{17}H_{13}O_6^-$, 313.0707). (**Figure S 111 – Figure S 114**).

5-Chloro-colletoquinone A (**4.4**): orange solid; ^{1}H NMR (600 MHz, DMSO-d_6) δ 7.36 (1H, s, H-2), δ 7.55 (1H, d, J = 1.5 Hz, H-4), δ 11.15 (1H, br, 6-OH), δ 14.18 (1H, s, 8-OH), δ 3.95 (3H, s, H-11), δ 2.48 (3H, s, H-12), δ 3.87 (3H, s, H-13); ^{13}C NMR (125 MHz, DMSO-d_6)[a] δ 160.1 (C-1), δ 118.7 (C-2), δ 146.4 (C-3), δ 119.9 (C-4), δ 147.3 (C-4a), δ 139.8 (C-7), δ 155.8 (C-8), δ 110.9 (C-8a), δ 181.2 (C-10), δ 116.9 (C-9a), δ 56.4 (C-11), δ 21.9 (C-12), δ 59.8 (C-13); HRESIMS m/z 347.0327 [M-H]$^-$, calculated for $C_{17}H_{12}ClO_6^-$, 347.0328. [a] ^{13}C shifts obtained from HSQC and HMBC (**Figure S 115 – Figure S 119**).

Colletoquinone B (**4.5**): orange solid; ^{1}H NMR (400 MHz, DMSO-d_6) δ 7.46 (1H, s-H-2), δ 7.64 (1H, d, J = 1.5 Hz, H-4), δ 7.33 (1H, s, H-5), δ 13.25 (1H, s, 8-OH), δ 3.97 (3H, s, H-11), δ 2.50 (3H, m, H-12), δ 3.99 (3H, s, H-13), δ 3.85 (3H, s, H-14); ^{13}C NMR (100 MHz, DMSO-d_6) δ 160.7 (C-1), δ 119.6 (C-2), δ 147.4 (C-3), δ 120.0 (C-4), δ 134.5 (C-4a), δ 102.7 (C-5), δ 157.3 (C-6), δ 141.3 (C-7), δ 155.8 (C-8), δ 112.5 (C-8a), δ 187.1 (C-9), δ 117.5 (C-9a), δ 181.5 (C-10), δ 127.9 (C-10a), δ 56.5 (C-11), δ 21.7 (C-12), δ 56.3 (C-13), δ 60.2 (C-14); HRESIMS m/z 329.1039 ([M+H]$^+$, calculated for $C_{18}H_{17}O_6^+$, 329.1020). (**Figure S 120 – Figure S 124**).

Azelaic acid (**4.6**): pale yellow needles; ^{1}H NMR (400 MHz, methanol-d_4) δ 2.27 (4H, t, J = 7.4 Hz, H-2/8), δ 1.61 (4H, quint, J = 7.4 Hz, H-3/7), δ 1.35 (6H, m, H-4/5/6); ^{13}C NMR (100 MHz, methanol-d_4) δ 177.8 (C-1/9), δ 35.0 (C-2/8), δ 26.0 (C-3/7), δ 30.0 (C-4/5/6); HRESIMS m/z 189.1144 [M+H]$^+$, calculated for $C_9H_{33}O_4^+$ 189.1121. (**Figure S 125 – Figure S 129**).

(_E_)-dec-2-enedioic acid (**4.7**): colorless oil; ^{1}H NMR (500 MHz, methanol-d_4) δ 5.77 – 5.82 (1H, dt, J = 1.6, 15.6 Hz, H-2), δ 6.93 (1H, dt, J = 7.0, 15.6 Hz, H-3), δ 2.22 (2H, qd, J = 1.6, 7.0 Hz, H-4), δ 1.48 (2H, m, H-5), δ 1.36 (4H, m, H-6/7), δ 1.60 (2H, m, H-8), δ 2.27 (2H, t, J = 7.4 Hz, H-9); ^{13}C NMR (150 MHz, methanol-d_4) δ 170.6 (C-1), δ 122.9 (C-2), δ 150.9 (C-3), δ 32.8 (C-4), δ 29.0 (C-5), δ 29.8 (C-6/7), δ 25.9 (C-8), δ 34.9 (C-9), δ 177.6 (C-10); HRESIMS m/z 201.1143 ([M+H]$^+$, calculated for $C_{10}H_{17}O_4^+$,

201.1121). (**Figure S 130** – **Figure S 134**).

***Cyclo*-Ala-Pro** (**4.8**): white solid; ^{1}H NMR (500 MHz, methanol-d$_4$) δ 4.18 (1H, m, H-3), δ 4.25 (1H, m, H-6), δ 2.30 (1H, m, H-7a), δ 2.00 (1H, m-7b), δ 1.93 (1H, m, H-8a), δ 2.00 (1H, m, H-8b), δ 3.51 (2H, m, H-9), δ 1.38 (3H, d, *J* = 6.9 Hz, H-10); ^{13}C NMR (125 MHz, methanol-d$_4$)^a δ 169.4 (C-2), δ 52.3 (C-3), δ 172.8 (C-5), δ 60.7 (C-6), δ 29.3 (C-7), δ 23.7 (C-8), δ 46.5 (C-9), δ 15.7 (C-10); HRESIMS *m/z* 169.0976 ([M+H]$^+$, calculated for C$_8$H$_{13}$N$_2$O$_2^+$, 169.0972).^{a} ^{13}C shifts obtained from HSQC and HMBC (**Figure S 135** – **Figure S 139**).

Methyl-6-acetamidohexanoate (**4.9**): white solid; ^{1}H NMR (400 MHz, methanol-d$_4$) δ 2.32 (2H, t, *J* = 7.4 Hz, H-2), δ 1.62 (2H, p, *J* = 7.5 Hz, H-3), δ 1.35 (2H, m, H-4), δ 1.49 (2H, m, H-5), δ 3.13 (2H, t, *J* = 7.0 Hz, H-6), δ 1.91 (3H, s, H-2'), δ 3.64 (3H, s, H-3'); ^{13}C NMR (100 MHz, methanol-d$_4$) δ 175.8 (C-1), δ 34.6 (C-2), δ 25.6 (C-3), δ 27.4 (C-4), δ 30.0 (C-5), δ 40.3 (C-6), δ 173.2 (C-1'), δ 22.5 (C-2'), δ 51.9 (C-3'); HRESIMS *m/z* 188.1282 ([M+H]$^+$, calculated for C$_9$H$_{18}$NO$_3^+$, 188.1281); HRESIMS/MS 156.1025 (30), 146.1175 (8), 114.0942 (100). (**Figure S 140** – **Figure S 145**).

***Cyclo*-L-Phe-D-Pro** (**4.10**): white solid; ^{1}H NMR (500 MHz, methanol-d$_4$) δ 4.18 (1H, t, *J* = 4.8 Hz, H-3), δ 2.60 (1H, dd, *J* = 6.5, 10.7 Hz, H-6), δ 1.63 (1H, m, H-7a), δ 2.03 (1H, m, H-7b), δ 1.63 (1H, m, H-8a), δ 1.89 (1H, m, H-8b), δ 3.31 (1H, m, H-9a), δ 3.52 (1H, m, H-9b), δ 2.97 (1H, dd, *J* = 4.7, 13.6 Hz, 10-a), δ 3.19 (1H, dd, *J* = 4.7, 13.6 Hz, H-10b), δ 7.18 (2H, m, H-12/16), δ 7.28-7.31 (3H, m, H-13/14/15); ^{13}C NMR (125 MHz, methanol-d$_4$) δ 167.4 (C-2), δ 59.7 (C-3), δ 171.3 (C-5), δ 59.1 (C-6), δ 29.8 (C-7), δ 22.4 (C-8), δ 46.1 (C-9), δ 40.9 (C-10), δ 136.7 (C-11), δ 131.2 (C-12/16), δ 129.6 (C-13/15), δ 128.5 (C-14); HRESIMS *m/z* 245.1282 [M+H]$^+$, calculated for C$_{14}$H$_{17}$N$_2$O$_2^+$, 245.1285). (**Figure S 146** – **Figure S 151**).

6-Acetamidohexanamid (**4.11**): colorless oil; ^{1}H NMR (400 MHz, methanol-d$_4$) δ 2.19 (2H, t, *J* = 7.0 Hz, H-2), δ 1.60 (2H, p, *J* = 7.6 Hz, H-3), δ 1.37 (2H, m, H-4), δ 1.50 (2H, m, H-5), δ 3.15 (2H, t, *J* = 7.5 Hz, H-6), δ 1.92 (3H, s, H-2'); ^{13}C NMR (100 MHz, methanol-d$_4$) δ 179.0 (C-1), δ 36.2 (C-2), δ 26.5 (C-3), δ 27.5 (C-4), δ 30.0 (C-5), δ 40.3 (C-6), δ 173.2 (C-1'), δ 22.5 (C-2'); HRESIMS *m/z* 173.1283 ([M+H]$^+$, calculated for C$_8$H$_{15}$N$_2$O$_2^+$, 173.1281); HRESIMS/MS 156.1017 (8), 114.0924 (100). (**Figure S 152** – **Figure S 157**).

***N*-(5-hydroxypentyl)acetamide** (**4.12**): colorless oil; ^{1}H NMR (400 MHz, methanol-d$_4$) δ 3.15 (2H, t, *J* = 7.0 Hz, H-1), δ 1.51 (2H, m, H-2), δ 1.37 (2H, m, H-3), δ 1.53 (2H, m, H-4), δ 3.54 (2H, t, *J* = 6.5 Hz, H-5), δ 1.91 (3H, s, H-2'); ^{13}C NMR (100 MHz, methanol-d$_4$) δ 40.4 (C-1), δ 30.1 (C-2), δ 24.2 (C-3), δ 33.2 (C-4), δ 62.7 (C-5), δ 173.2 (C-1'), δ 22.5 (C-2'); HRESIMS *m/z* 146.1179 ([M+H]$^+$, calculated for C$_7$H$_{16}$NO$_2^+$, 146.1176); HRESIMS/MS 128.1059 (100), 114.0924 (27). (**Figure S 158** – **Figure S 163**).

6-Pentanamidohexanamid (**4.13**): white solid; ^{1}H NMR (400 MHz, methanol-d$_4$) δ 2.20 (2H, m, H-2), δ 1.63 (2H, m, H-3), δ 1.35 (2H, m, H-4), δ 1.51 (2H, m, H-5), δ 3.15 (2H, m, H-6), δ 2.16 (2H, m, H-8), δ 1.56 (2H, m, H-9), δ 1.36 (2H, m, H-10), δ 0.93 (3H, t, *J* = 7.4 Hz, H-11); ^{13}C NMR (100 MHz, methanol-d$_4$) δ 179.1 (C-1), δ 36.3 (C-2), δ 26.5 (C-3), δ 27.5 (C-4), δ 30.1 (C-5), δ 40.2 (C-6), δ 176.3 (C-7), δ 36.9 (C-8), δ 29.3 (C-9), δ 23.4 (C-10), δ 14.1 (C-11); HRESIMS *m/z* 215.1760 ([M+H]$^+$, calculated for C$_{11}$H$_{23}$N$_2$O$_2^+$, 215.1754); HRESIMS/MS 114.0930 (100). (**Figure S 164** – **Figure S 169**).

4.2.5   X-ray crystallography

Crystals of sufficient quality enabled X-ray structural analysis of compound **4.3** and **4.4**. A suitable crystal of each compound was selected and mounted on a STOE IPDS 2 diffractometer. The crystal was kept at 170 K during data collection. Using Olex2 [3], the structure was solved with the ShelXT [4] structure solution program using Intrinsic Phasing and refined with the ShelXL [5] refinement package using Least Squares minimization. Crystallographic data for **4.3** and **4.4** have been deposited with the Cambridge Crystallographic Data Centre (**4.3**: CCDC 2348292; **4.4**: CCDC 2348291). Copies of these data can be obtained free of charge from the Cambridge Crystallographic Data Centre on application to the Director, CCDC, 12, Union Road, Cambridge CB2 1 EZ, UK (e-mail: deposit@ccdc.cam.uk).

Crystal data

4.3: $C_{17}H_{14}O_6$ (M =314.28 g/mol): monoclinic system, space group P 1 2_1/c 1. a = 7.5723 (5) Å, b = 14.4127 (10) Å, c = 12.7547 (9) Å, V = 1385.58(17) Å^3, Z = 4, d = 1.507 g/cm^3, crystal size: 0.36 × 0.09 × 0.08 mm^3, number of independent reflections = 2708, R(int)= 0.0469, completeness to Θ = 25.999°: 99.6 %. The final R1 was 0.0559 (I > 2σ(I)) and wR2 was 0.1630 (all data). (**Figure S 114**).

4.4: $C_{17}H_{13}ClO_6$, C_2H_6OS (M= 426.85 g/mol): triclinic system, space group P -1, a = 7.2720(5) Å, b = 10.6557 (7) Å, c = 12.5971 (8) Å, V = 913.75 (11) Å^3, Z = 2, d = 1.551 g/cm^3, crystal size: 0.49 × 0.217 × 0.03 mm^3, number of independent reflections: 4897, R(int) = 0.0393, completeness to Θ = 29.262°: 98.2 %. The final R1 was 0.0511 (I > 2σ(I)) and wR2 was 0.1085 (all data). (**Figure S 119**).

4.2.6 Calculation of CD spectra

Graminolactone **4.2**

All possible four stereo isomers with S5-configuration (S2', S3'), (SR), (RS), (RR) of compound **4.2** were constructed using MOE (Molecular Operating Environment) software. [6] Subsequently a conformational search was performed. The resulting most stable conformation of each isomer was optimized by applying the density functional theory (DFT) using the B3LYP functional with the SV (P) basis set [7–10] implemented in the *ab initio* ORCA 3.0.3 program package [11]. The influence of the experimentally used methanol solvent was included in the DFT calculations using the conductor-like polarizable continuum model, CPCM. [12] For the quantum chemical simulations of the CD spectra the first 30 excited triplet states of the structures were calculated by applying the long-range corrected hybrid function TD B3LYP/G with SV (P) basis set. The CD spectra of the corresponding four enantiomers with R5-configuration were obtained by mirroring from the calculated spectra with S5-configuration. The CD curves were visualized and compared with the experimental spectra with the help of the software SpecDis 1.64. [13]

Diketopiperazine **4.10**

The molecular geometries of the molecule, including all possible stereoisomers, were obtained using a python script which transforms SMILES structures to SDF files with the RDKit python package. Based on these SDF files, gaussian input files were generated with the same script. The structures were then optimized with density functional theory (DTF) using CAM-B3LYP/6-31+G(d,p)[14-17] level of theory and the conductor-like polarizable continuum model (CPCM) solvent field for methanol[12] implemented in the Gaussian16 [18] program package. Electronic Circular Dichroism (ECD) calculation was performed for each optimized compound and conformation using TD-DFT calculations at the CAM-B3LYP/6-31+G(d,p) level and CPCM model, investigating the first 40 excited states. The calculated spectra were then compared with experimental data using the SpecDis software (version 1.71) [13] with a Gaussian distribution function at a half-bandwidth of σ = 0.3 eV and an allowed shift between +30 to -30 nm.

4.2.7 Leaf-spot bioassay

A modified leaf-spot bioassay by Evidente et al. (1995) [19] was used for all fractions and pure compounds tested for their phytotoxic properties. The samples were dissolved in methanol/ water (1:1, *v/v*) and droplets of 5 µL were placed on the leaf surface of undetached and fully expanded young leaves of *Arabidopsis thaliana* Col-0. Fractions were tested at concentrations of 5 – 10 µg/ µL; pure compounds at concentrations from 5 mM – 100 mM. Plants were incubated in the greenhouse (19 °C, day/night cycle) for 24 – 72 h. Paraquat (100 µM, dissolved in methanol/ water 1:1, *v/v*) was used as a positive control. The pure solvent mixture of methanol/water (1:1, *v/v*) served as the negative control. After 72 h the plants were observed for the formation of necrosis. Images were taken with CAMAG TLC visualizer (Camag, Switzerland). Only the damage to the leaf in the form of chlorosis or necrosis was evaluated. The extent of the damage was not considered.

4.3   Results and discussion

4.3.1   Isolation and structure elucidation

Repeated column chromatography of the *C. graminicola* crude extracts on polyamide CC 6-Ac, Sephadex LH-20, silanized silica in combination with semi-preparative HPLC yielded the compounds **4.1 – 4.13** (**Figure 4-1**).
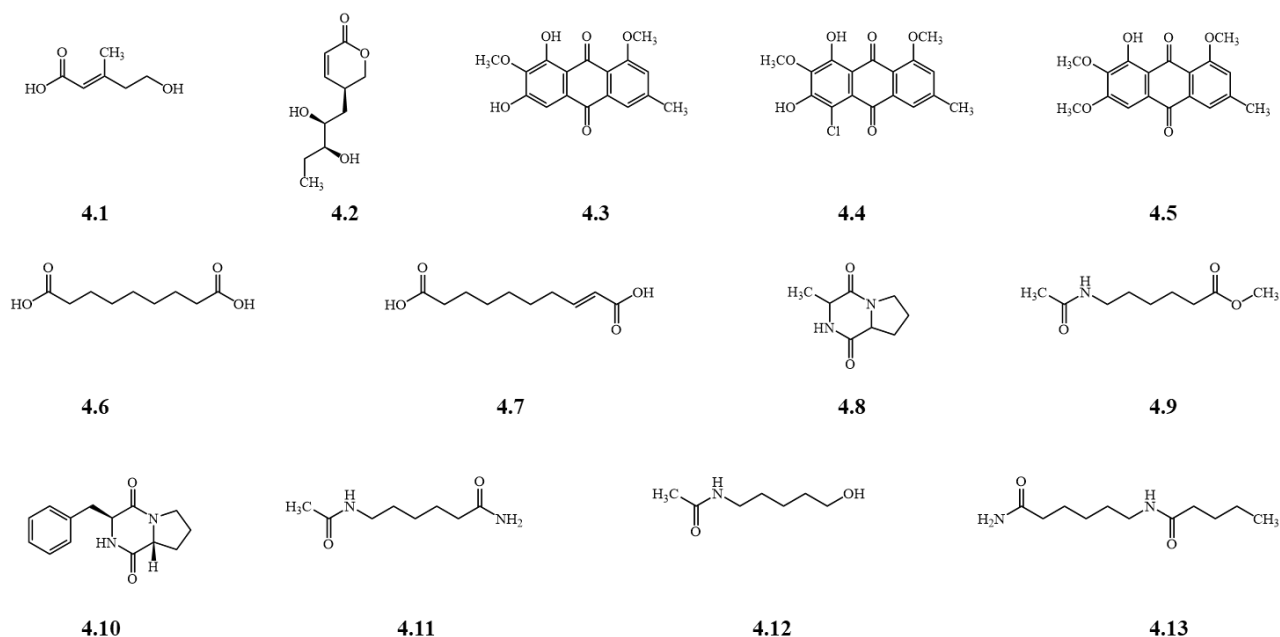
Figure 4-1 Structure of compounds **4.1** - **4.13**.

The spectral data (MS and ^{1}H and ^{13}C NMR spectra) of compounds **4.1**, **4.5 – 4.8**, **4.10** and **4.12** were identical to those reported in the previous literature. Accordingly, their structures were identified as *trans*-anhydromevalonic acid (**4.1**) [20], colletoquinone B (**4.5**) [21], azelaic acid (**4.6**) [22], (*E*)-dec-2-enedioic acid (**4.7**) [23], *cyclo*-Ala-Pro [24] (**4.8**), *cyclo*-Phe-Pro (**4.10**) [25] and *N*-(5-hydroxy-pentyl)acetamide (**4.12**). [26] Besides these known compounds, several new secondary metabolites could be isolated.

Compound **4.2** was isolated as a white solid. Its molecular formula was determined to be $C_{10}H_{16}O_4$, based on HRESIMS data of the molecular ion at *m/z* 199.0990 ([M-H]$^-$, calculated for $C_{10}H_{15}O_4^-$ 199.0976) (**Figure S 106**). The ^{13}C NMR spectrum of **4.2** reveals ten carbon signals, classified as one methyl group (δ_C 10.6 ppm), three aliphatic methylenes (δ_C 27.6, 34.5 and 73.2 ppm), five methines (two olefinic – δ_C 123.5 and 149.7 ppm – and three aliphatic – δ_C 43.9, 75.4 and 84.2 ppm) and a carbonyl-like carbon (δ_C 170.0 ppm). Intense analysis of the COSY exhibits the presence of a pentane-2,3-diol moiety connected to a 5,6-dihydro-2*H*-pyran-2-one moiety. This scaffold is confirmed by HMBC correlations from H-3 to C-2, C-4 and C-5 and from H-4 to C-2, C-3, C-5, C-6 and C-1'. (**Figure S 107** – **Figure S 110**) Compound **4.2** contains three stereogenic centers at C-5, C-2' and C-3', corresponding to eight possible stereoisomers. In order to figure out the absolute configuration of **4.2**, the experimental electronic circular dichroism (ECD) spectrum was compared with the ECDs for the possible isomers calculated by quantum chemical methods. The isomer with 5*S*, 2'*S*, 3'*S* configurations was found to fit best with the experimental spectrum showing a similarity factor of 0.9448 (sigma = 0.3 eV, shift = 3 nm). The isomer with 5*S*, 2'*S*, 3'*R* configurations shows a similarity factor of 0.8911 (sigma = 0.3 eV, shift = 9 nm). On the basis of the analysis, the structure of compound **4.2** was suggested to be 5*S*-(2*S*,3*S*-dihydroxypentyl)-5,6-dihydro-2*H*-pyran-2-one and trivially named graminolactone (**Figure 4-2**).
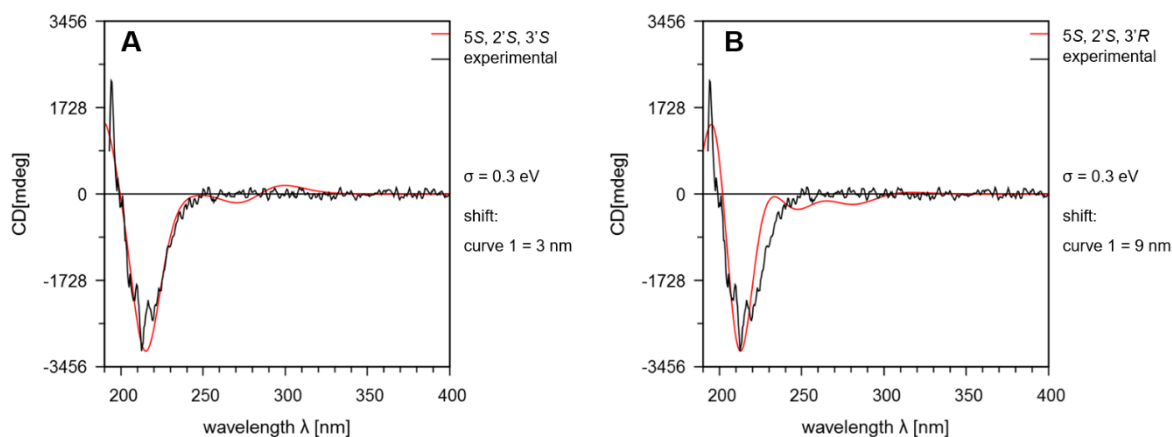
Figure 4-2 A: Calculated CD spectra of the 5*S*,2'*S*,3'*S* isomer (red) of compound **4.2** in comparison with the experimental one (black line); similarity factor = 0.9448 (sigma = 0.3 eV, shift = 3 nm) **B:** Calculated CD spectra of the 5*S*,2'*S*,3'*R* isomer (red) of compound **4.2** in comparison with the experimental one (black line); 0.8911 (sigma = 0.3 eV, shift = 9 nm.

Compound **4.3** was identified as colletoquinone A by comparison of its spectral data with published HRMS and NMR data. [21] Since the compound **4.3** precipitated in large quantities as crystals from methanolic solutions during isolation procedure, additional X-ray crystallographic analysis was carried out, which clearly confirmed the proposed structure.
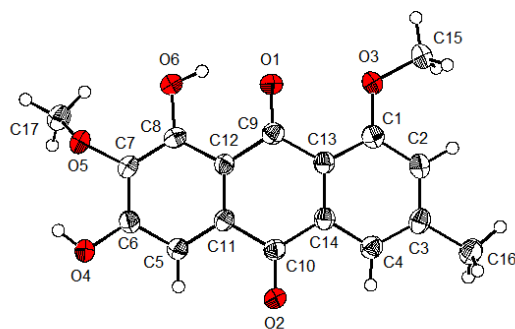
Figure 4-3 Molecular structure of colletoquinone A (**4.3**).

Compound **4.4** was isolated as a yellow-orange solid. On the TLC **4.4** showed a reversible bathochromic shift from orange to red when treated with ammonia vapor. Based on HRESIMS the molecular formula was determined to be $C_{17}H_{13}ClO_6$ (*m/z* 347.0327 [M-H]$^-$, calculated for $C_{17}H_{12}ClO_6{}^-$, 347.0328). The occurrence of chlorine in **4.4** is supported by the presence of an isotope peak at *m/z* 349.0298 with an intensity of 30 % in the MS spectrum (**Figure S 115**). Further structural elucidation was performed by intense NMR analysis. However, the yield of **4.4** was too low to record a ^{13}C spectrum. Therefore, all ^{13}C shifts were only determined indirectly through HSQC and HMBC experiments. The ^{1}H NMR spectrum of **4.4** revealed seven proton resonances including two resonances of hydroxyl groups (δ_H 11.1 and 14.1 ppm), two resonances of aromatic protons (δ_H 7.55 and 7.40 ppm), two resonances of methoxy groups (δ_H 3.95 and 3.87 ppm) and one of a methyl group (δ_H 2.48 ppm). Both aromatic protons (δ_H 7.55 and 7.40 ppm) showed a coupling constant of 1.5 Hz and are thus in meta-position to each other. Together with the HMBC correlations of H-2 to C-1, C-4, C-9, C-9a and C-12 and H-4 to C-2, C-9, C-9a and C-12 the substitution pattern of the C-ring was determined indicating a 1,3- substitution. Further, one of the hydroxy signals (δ_H 14.18 ppm) showed a sharp singlet, whereas the hydroxy signal at δ_H 11.15 ppm showed a broad singlet. On the basis of the NMR experiments (**Figure S 116** –
Figure S 118) compound **4.4** was determined to be 5-chloro-6,8-dihydroxy-1,7-dimethoxy-3-methylanthracene-9,10-dione (anthraquinone numbering). Crystals of sufficient quality of the new compounds named 5-chloro-colletoquinone A (**4.4**) verified the proposed structure through X-ray analysis.
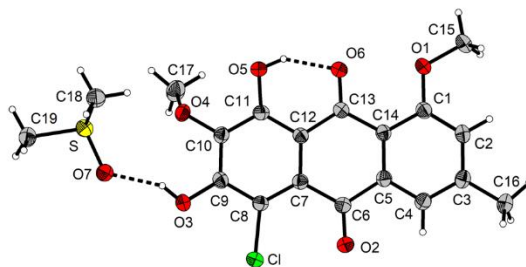
Figure 4-4 Molecular structure of 5-chloro-colletoquinone A.

The isolated 5-chloro-colletoquinone A (**4.4**) can be interpreted as the oxidized form of colletoanthrone (**4.14**), which was previously recognized by Horbach and co-workers. [21] Colletoanthrone belongs to the chemical class of oxanthrones. Oxanthrones and their tautomeric anthrahydroquinones are generally quite labile intermediates and are easily oxidized to the stable anthraquinones. [27]
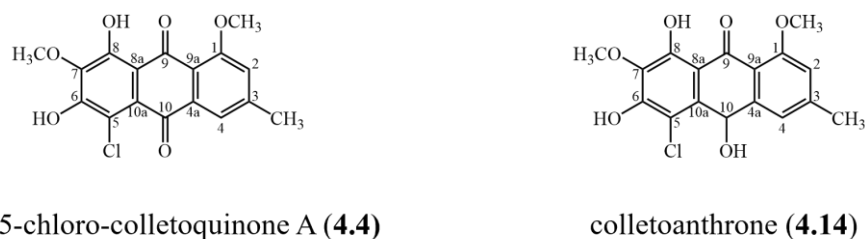
5-chloro-colletoquinone A (**4.4**)   colletoanthrone (**4.14**)

Figure 4-5 Structures of 5-chloro-colletoquinone A (**4.4**) and colletoanthrone (**4.14**).

Compound **4.9** was isolated as a white solid. The molecular formula was determined to be $C_9H_{17}NO_3$, based on HRESIMS data of the molecular ion at *m/z* 188.1278 ([M+H]$^+$, calculated for $C_9H_{18}NO_3^+$, 188.1281), corresponding to two degrees of unsaturation (**Figure S 140**). The ^{13}C NMR analysis revealed the presence of nine carbon atoms, classified as two carbonyl-like carbons (δ_C 173.2 and 175.8 ppm), five aliphatic methylenes (δ_C 25.6 – 40.3 ppm), one methyl group (δ_C 22.5 ppm) and a methoxy group (δ_C 51.9 ppm). Intense NMR analysis revealed the presence of an acetamide moiety, characterized by the HMBC correlation of C-2' to C-1' and from C-6 to C-1'. Additionally, a HMBC correlation from C-3'to C-1 indicated the presence of a carboxylic acid ester, which was supported by HRESIMS/MS measurements, as the first fragmentation observed is the cleavage of the methoxy group. By detailed analysis of the COSY spectra the compound **4.9** could be determined as methyl-6-acetamidohexanoate. (**Figure S 141** – **Figure S 145**).

Compound **4.11**, purified as a white solid, was determined as $C_8H_{14}N_2O_2$ as deduced from HRESIMS data ([M+H]$^+$ at *m/z* 173.1283, calculated for calculated for $C_8H_{15}N_2O_2^+$, 173.1185) (**Figure S *152***). The NMR spectroscopic data (**Figure S 153** – **Figure S 157**) of **4.11** were closely resemble that of **4.9**, with the exception that a carboxamide is present instead of a methyl carboxylate. Therefore, compound **4.11** was determined as 6-acetamidohexanamide.

Compound **4.13** obtained as a white solid, had the molecular formula $C_{11}H_{22}N_2O_2$, as deduced from HRESIMS data (*m/z* 215.1760 ([M+H]$^+$ calculated for $C_{11}H_{23}N_2O_2^+$, 215.1754) (**Figure S *164***). The NMR data (**Figure S 165** – **Figure S 169**) showed similarity to those of **4.9**, **4.11** and **4.12**. The ^{13}C NMR spectra revealed 11 carbon resonances, including two carboxamides (δ_C 176.3 and 179.1 ppm), one methyl groups (δ_C 14.1 ppm) and eight aliphatic methylenes (δ_C 23.4 – 40.2 ppm). Intensive investigations of the COSY and HMBC spectra exhibit the presence of a hexanamide and a pentanamide moiety. The HMBC correlations from C-6 to C-7 and from C-8 to C-7 show that the two structural elements are connected by the nitrogen of the pentanamide. Therefore, compound **4.13** was identified as 6-pentanamidohexanamid.

Absolute configuration of diketopiperazines

The isolated DKP **4.8** and **4.10** each possess two chiral centers at position C-3 and C-6, which corresponds to four possible stereoisomers. The yield of compound **4.8** was too low to measure sufficient ECD spectra (data not shown), resulting in poor similarity factors. Therefore, the absolute configuration of **4.8** could not be determined.

For the **4.10** the absolute configuration was determined by comparison of the experimental spectra with calculated ECD spectra (see 3.2.6) as shown in **Figure 4-6**. The most suitable fit with a similarity factor of 0.973 (sigma 0.3 eV, shift -28 nm) was found for the stereoisomer with D-L configuration. Thus, **4.10** was identified as *cyclo*-L-Phe-D-Pro, which is in accordance with the literature. [28]
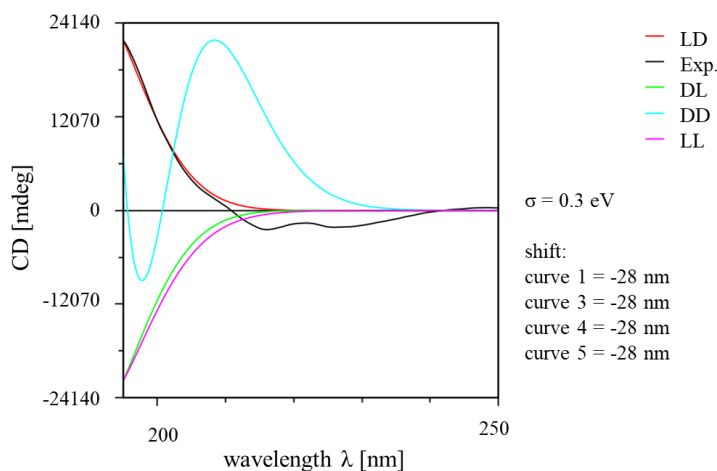
Figure 4-6 Calculated ECD spectra of compound **4.10** in comparison with the experimental one (black). Red = *cyclo*-L-Phe-D-Pro, green = *cyclo*-D-Phe-L-Pro, blue = *cyclo*-D-Phe-D-Pro, purple = *cyclo*-L-Phe-L-Pro. Best similarity factor found for L, D (red) with 0.959 for sigma = 0.3 eV.

4.3.2   Hexanoic acids 4.9, 4.11– 4.13

A total of four (partially) new-to-nature hexanoic acid derivatives (**4.9**, **4.11 – 4.13**) were isolated from the crude extract of *C. graminicola*. Compound **4.12** was previously reported as a natural product isolated from the fungus *Neodidymelliopsis sp.*.[26] The isolates **4.9**, **4.11** and **4.13** have not yet been reported from natural sources. Structural, the isolated compounds exhibit a high similarity with polyamide monomers (**Figure 4-7**).

ε-caprolactam   ε-aminocaproic acid   polycaprolactam (polyamide 6)
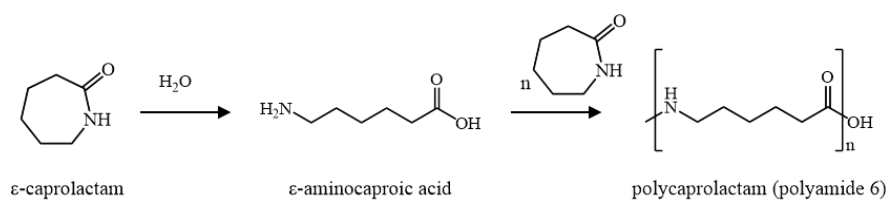
Figure 4-7 Synthesis of polyamide 6.

Since polyamide 6-Ac was used in the isolation process, it was investigated, if the isolated compounds are degradation products of polyamide 6-Ac. Therefore, the native occurrence of the isolated compounds **4.9**, **4.11 – 4.13** in the crude extract prior to its column chromatographic processing was verified by LC-HRESIMS measurements (comparison of retention time and high-resolution mass).

Compounds **4.9** and **4.12** could be detected in the crude extract, while no signal was obtained for **4.11** and **4.13**. It can therefore be assumed that **4.9** and **4.12** are secondary metabolites of the fungus. However, it is likely that **4.11** and **4.13** are also native natural products, as they are structurally closely related. The lack of signals could be due to numerous factors, such as ion suppression, poor ionizability or the low content in the extract, e.g. the highest amount of a hexanoic acid derivatives isolated from the crude extract was only 1.9 mg from 200 flasks (40 l culture filtrate) for compound **4.9**.

4.3.3 Natural occurrence and biological activity

4.3.3.1 Phytotoxic activity

All isolated compounds were tested for their phytotoxic activity in a leaf-spot bioassay on *A. thaliana* Col-0 in concentrations of 100, 50, 20 and 10 mM. Compound **4.3** was additionally tested at 5 mM.

Table 4-1 Results of the leaf-spot assay.

Compound	100 mM	50 mM	20 mM	10 mM	5 mM
trans-Anhydro mevalonic acid (**4.1**)	n.t.	n.t.	n.t.	n.t.	n.t.
Graminolactone (**4.2**)	+	n.t.	n.t.	n.t.	n.t.
Colletoquinone A (**4.3**)	+	+	+	+	-
5-Chloro-colletoquinone A (**4.4**)	n.t.	-	-	-	n.t.
Colletoquinone B (**4.5**)	-	-	-	-	n.t.
Azelaic acid (**4.6**)	+	+	+	-	n.t.
(*E*)-dec-2-enedioic acid (**4.7**)	+	+	+	-	n.t.
cyclo-Ala-Pro (**4.8**)	n.t.	-	n.t.	n.t.	n.t.
Methyl-6-acetamidohexanoate (**4.9**)	+	-	-	-	n.t.
cyclo-L-Phe-D-Pro (**4.10**)	-	-	-	-	n.t.
6-Acetamidohexanamid (**4.11**)	+	+	-	-	n.t.
N-5-hydroxypentylacetamid (**4.12**)	+	-	-	-	n.t.
6-Pentanamidohexanamid (**4.13**)	+	-	-	-	n.t.

+ formation of chlorosis/necrosis observed; - no effect; n.t. not tested.

Trans-anhydromevalonic acid (**4.1**) has been described from many fungal sources like *Phaeosphaeria* sp. [29], *Trichoderma polysporum* [30] and *Xylaria* sp. [31]. The compound **4.1** is a derivative of mevalonate, which act as a building block of several siderophores like fusarinines and coprogens. [32–34] Coprogens were also identified in *C. graminicola* and exhibit phytotoxic effects. [21] Kamo and co-workers describe a weak antifungal activity of *trans*-anhydromevalonic acid (**4.1**) against *Pythium iwayamae* (snow rot pathogen), but so far there is no hint regarding phytotoxic effects. [30] Due to the low amount isolated, **4.1** could not be tested for phytotoxic activity.

Graminolactone (**4.2**) showed a strong phytotoxic effect at a concentration of 100 mM. Unfortunately, no further tests at lower concentrations were possible due to the small yield of the isolated compound **4.2**. Phytotoxic effects have already been described in the literature for the related compound (*R*)-5,6-dihydro-6-pentyl-2*H*-pyran-2-one (**4.15**, **Figure 4-8**). In a wheat coleoptile test, the compound **4.15** showed activity up to a concentration of 10^{-4} M. [35]
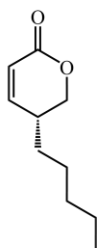
Figure 4-8 Structure of (*R*)-5-pentyl-5,6-dihydro-2*H*-pyran-2-one (**4.15**).

Anthraquinones are a large and ubiquitous family of aromatic polyketides occurring in fungi, bacteria, plants, and animals with diverse biological activities including antibacterial, antiviral, anticancer and antioxidative activities. [36] There are also some examples for phytotoxic anthraquinones, like catenarin [37] and lentisone [38]. Also, colletoquinone A (**4.3**) was found to exhibit a phytotoxic activity up to 10 mM on *A*. thaliana Col-0. Previously, Horbach and co-workers had tested colletoquinone A (**4.3**) for phytotoxic activity without positive results. [21] However, they tested the compound at much lower concentrations (5 µL with a concentration of 1µg/µL). [21] Interestingly, **4.4** bearing an additional chlorine atom at position C-5, showed no phytotoxic activity.

Further, for colletoquinone B (**4.5**) with an additional methoxy group on C-3, instead of a hydroxy group no more phytotoxic activity could be observed. The presence of phenolic OH groups - which are

characterized by their acidity - therefore appears to be important for the bioactivity. Phenolic herbicides inhibit photosynthetic electron transport by binding to the QB site of the D1 protein of photosystem II (see 2.2.2). [39] Further, they can act as uncouplers of photophosphorylation. This activity is due to a protonophoric property that allows protons to be transported across the thylakoid membrane. It has also been shown that anthraquinones can act as inhibitors of photosystem II. [40] This mode of action could also explain the observation by Andolfi and co-workers who recognized that lentisone (**4.16**) only exhibits a phytotoxic effect in day light. [38] For **4.3**, a further test in the dark would also show whether the compound attacks photosystem II and thus acts according to the same mode of action as other anthraquinones.
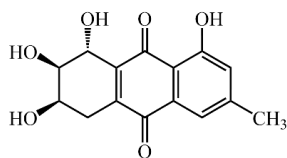
Figure 4-9 Structure of lentisone (**4.16**). [37]

From the two tested diketopiperazines (**4.8** and **4.10**) none showed phytotoxic activity on *A. thaliana*. For **4.8** no phytotoxic activity was reported so far, however the stereoisomer cyclo-L-Ala-L-Pro (Chapter 3), showed phytotoxic activity up to a concentration of 50 mM. Compound *cyclo*-L-Phe-L-Pro (**4.10**) did not show any effects in the leaf-spot assay. Interestingly, its stereoisomer *cyclo*-L-Phe-L-Pro, also known as maculosin-2 was shown to have a broad-spectrum herbicidal activity. [41; 42] This result once again underlines the importance of determining the absolute configuration of isolated natural compounds.

Azelaic acid (**4.6**) has been described from numerous plants such as *Triticum durum.* [43] and *Chaenomeles sinensis* [44] in response to biotic and abiotic stress conditions. Further, **4.6** is also known from fungal sources including *Macrophomina phaseolina* [45] and for its bacteriostatic and bactericidal properties. [46] However, to the best of our knowledge, no phytotoxic activity has been described for azelaic acid (**4.6**) so far. Compound **4.6** causes necrosis in the leaf-spot assay on *A. thaliana* up to a concentration of 20 mM.

(*E*)-dec-2-enedioic acid (**4.7**) has been reported from several natural sources like *Aspergillus rugulosa* [47] and *Morchella sextelata* [48] but could not be detected in *Colletotrichum* spp. so far. Also, a phytotoxic activity was previously not described.

All isolated hexanoic acid derivatives **4.9**, **4.11** – **4.13** showed phytotoxic activity at the highest test concentration of 100 mM. The strongest activity was observed for 6-acetamidohexanamid (**4.11**), which caused up to 50 mM necrosis.

4.4 Conclusion

Bioactivity-guided isolation of crude extracts of *C. graminicola* grown in CM medium led to isolation of 13 compounds. The compounds included five previously undescribed compounds, including a dihydropyranone derivative (**4.2**), an anthraquinone (**4.4**) and three hexanoic acid derivatives (**4.9**, **4.11** and **4.13**), besides eight known compounds. 9 out of 12 compounds showed phytotoxic activity in the leaf-spot assay on *A. thaliana* Col-0. The highest phytotoxic activity was observed for the anthraquinone colletoquinone A (**4.3**), which caused strong necrosis even at 10 mM. According to initial assumptions, **4.3** could act by inhibition of the photosystem II. However, further tests are necessary for conformation.

References

[1] Fischer, M.; Glomb, M. (eds.) *Moderne Lebensmittelchemie,* Behr, Hamburg, **2015**, ISBN: 978-3-89947-864.8.

[2] Zhang, J.; Reddy, J.; Buckland, B.; Greasham, R., Toward consistent and productive complex media for industrial fermentations: studies on yeast extract for a recombinant yeast fermentation process, *Biotechnol. Bioeng.* **2003**, *82,* 640–652, doi: 10.1002/bit.10608.

[3] Dolomanov, O.V.; Bourhis, L.J.; Gildea, R.J.; Howard, J.A.K.; Puschmann, H., *OLEX*2: a complete structure solution, refinement and analysis program, *J. Appl. Crystallogr.* **2009**, *42,* 339–341, doi: 10.1107/S0021889808042726.

[4] Sheldrick, G.M., *SHELXT* - Integrated space-group and crystal-structure determination, *Acta Cryst. A* **2015**, *71,* 3–8, doi: 10.1107/S2053273314026370.

[5] Sheldrick, G.M., Crystal structure refinement with *SHELXL, Acta Cryst. C* **2015**, *71,* 3–8, doi: 10.1107/S2053229614024218.

[6] Moleular Operating Eniroment (MOE), **2021**, Chemical Computing Group Inc., Quebec, Canada.

[7] Becke, A.D., Density-functional exchange-energy approximation with correct asymptotic behavior, *Phys. Rev. A* **1988**, *38,* 3098–3100, doi: 10.1103/physreva.38.3098.

[8] Karton, A.; Tarnopolsky, A.; Lamère, J.-F.; Schatz, G.C.; Martin, J.M.L., Highly accurate first-principles benchmark data sets for the parametrization and validation of density functional and other approximate methods. derivation of a robust, generally applicable, double-hybrid functional for thermochemistry and thermochemical kinetics, *J. Phys. Chem. A* **2008**, *112,* 12868–12886, doi: 10.1021/jp801805p.

[9] Schäfer, A.; Horn, H.; Ahlrichs, R., Fully optimized contracted Gaussian basis sets for atoms Li to Kr, *J. Chem. Phys.* **1992**, *97,* 2571–2577, doi: 10.1063/1.463096.

[10] Weigend, F.; Ahlrichs, R., Balanced basis sets of split valence, triple zeta valence and quadruple zeta valence quality for H to Rn: Design and assessment of accuracy, *Phys. Chem. Chem. Phys.* **2005**, *7,* 3297–3305, doi: 10.1039/B508541A.

[11] Neese, F., The ORCA program system, *Wiley Interdiscip. Rev. Comput. Mol. Sci.* **2012**, *2,* 1, 73–78, doi: 10.1002/wcms.81.

[12] Takano, Y.; Houk, K.N., Benchmarking the conductor-like polarizable continuum model (CPCM) for aqueous solvation free energies of neutral and ionic organic molecules, *J. Chem. Theory Comput.* **2005**, *1,* 70–77, doi: 10.1021/ct049977a.

[13] Bruhn, T.; Schaumlöffel, A.; Hemberger, Y.; Bringmann, G., SpecDis: Quantifying the comparison of calculated and experimental electronic circular dichroism spectra, *Chirality* **2013**, *25,* 243–249, doi: 10.1002/chir.22138.

[14] Yanai, T.; Tew, D.P; Handy, N.C., A new hybrid exchange-correlation functional using the Coulomb-attenuating method (CAM-B3LYP), *Chem. Phys. Lett.*, **2004**, *393*, 51-57, doi: 10.1016/j.cplett.2004.06.011.

[15] Hehre, W.J.; Ditchfield, R.; Pople, J.A., Self-consistent molecular orbital methods. XII. Further extensions of Gaussian-type basis sets for use in molecular orbital studies of organic molecules, *J. Chem. Phys.* **1972**, *56*, 2257-2261, doi: 10.1063/1.1677527.

[16] Hariharan, P.C.; Pople, J.A., The influence of polarization functions on molecular orbital hydrogenation energies, *Theor. Chim. Acta* **1973**, *28*, 213-222, doi: 10.1007/BF00533485.

[17] Clark, T.; Chandrasekhar, J.; Spitznagel, G.W.; Schleyer, P.V.R., Efficient diffuse function-augmented basis sets for anion calculations. III. The 3-21+G basis set for first-row elements, Li-F, *J. Comput. Chem.*, **1983**, *4*, 294-301, doi: 10.1002/jcc.540040303.

[18] Frisch, M.J.; Trucks, G.W.; Schlegel, H.B.; Scuseria, G.E.; Robb, M.A.; Cheeseman, J.R; Scalmani, G. et al., Gaussian 16 Revision A.03, Gaussian Inc., Walleingford ,CT **2016**.

[19] Evidente, A.; Lanzetta, R.; Capasso, R.; Andolfi, A.; Bottalico, A.; Vurro, M.; Zonno, M.C., Putaminoxin, a phytotoxic nonenolide from *Phoma putaminum*, *Phytochemistry* **1995**, *40,* 1637–1641, doi: 10.1016/0031-9422(95)00505-2.

[20] Nakayama, A.; Yasuno, Y.; Yamamoto, Y.; Saito, K.; Kitsuwa, K.; Okamura, H.; Shinada, T., Stereoselective syntheses of trans-anhydromevalonic acid and trans-anhydromevalonyl group-containing natural products, *J. Nat. Prod.* **2022**, *85,* 1052–1058, doi: 10.1021/acs.jnatprod.1c01176.

[21] Horbach, R.; Graf, A.; Weihmann, F.; Antelo, L.; Mathea, S.; Liermann, J.C.; Opatz, T.; Thines, E.; Aguirre, J.; Deising, H.B., Sfp-type 4′-phosphopantetheinyl transferase is indispensable for fungal pathogenicity, *Plant Cell* **2009**, *21,* 3379–3396, doi: 10.1105/tpc.108.064188.

[22] Zimmermann, F.; Meux, E.; Mieloszynski, J.-L.; Lecuire, J.-M.; Oget, N., Ruthenium catalysed oxidation without CCl4 of oleic acid, other monoenic fatty acids and alkenes, *Tetrahedron Lett.* **2005**, *46,* 3201–3203, doi: 10.1016/j.tetlet.2005.03.052.

[23] Xu, Q.; Qiao, Y.; Zhang, Z.; Deng, Y.; Chen, T.; Tao, L.; Xu, Q.; Liu, J.; Sun, W.; Ye, Y.; Lu, Y.; Qi, C.; Zhang, Y., New polyketides with anti-inflammatory activity from the fungus *Aspergillus rugulosa, Front. Pharmacol.* **2021**, *12,* 700573, doi: 10.3389/fphar.2021.700573.

[24] Danh, C.D.; Dao, P.T.; Huong, D.T.M.; Thach, T.D.; Anh, N.M.; Minh, L.T.H.; Anh, T.T.; Van Cuong, P., Cyclopeptides from marine actinomycete *Streptomyces* sp. G261, *Vietnam J. Chem.* **2018**, *56,* 570–573, doi: 10.1002/vjch.201800049.

[25] Domzalski, A.; Margent, L.; Vigo, V.; Dewan, F.; Pilarsetty, N.V.K.; Xu, Y.; Kawamura, A., Unambiguous stereochemical assignment of cyclo(Phe-Pro), cyclo(Leu-Pro), and cyclo(Val-Pro) by electronic circular dichroic spectroscopy, *Molecules* **2021**, *26,* 5981, doi*:* 10.3390/molecules26195981.

[26] Cadelis, M.M.; Gordon, H.; Grey, A.; Geese, S.; Mulholland, D.R.; Weir, B.S.; Copp, B.R.; Wiles, S., Isolation of a novel polyketide from *Neodidymelliopsis* sp., *Molecules* **2021**, *26,* 3235, doi*:* 10.3390/molecules26113235.

[27] Teuscher, E., *Reihe Wissenschaft - Pharmazeutische Biologie,* 2. Ed., Vieweg & Teubner, Wiesbaden, ISBN 978-3-528-06844-8.

[28] Domzalski, A.; Margent, L.; Vigo, V.; Dewan, F.; Pilarsetty, N.V.K.; Xu, Y.; Kawamura, A., Unambiguous stereochemical assignment of cyclo(Phe-Pro), cyclo(Leu-Pro), and cyclo(Val-Pro) by electronic circular dichroic spectroscopy, *Molecules* **2021**, *26,* 5981, doi*:* 10.3390/molecules26195981.

[29] Xiao, Y.; Liang, W.; Zhang, Z.; Wang, Y.; Zhang, S.; Liu, J.; Chang, J.; Ji, C.; Zhu, D., Polyketide derivatives from the endophytic fungus *Phaeosphaeria* sp. LF5 isolated from *Huperzia serrata* and their acetylcholinesterase inhibitory activities, *J. Fungi* **2022**, *8,* 232, doi*:* 10.3390/jof8030232.

[30] Kamo, M.; Tojo, M.; Yamazaki, Y.; Itabashi, T.; Takeda, H.; Wakana, D.; Hosoe, T., Isolation of growth inhibitors of the snow rot pathogen *Pythium iwayamai* from an arctic strain of *Trichoderma polysporum*, *J. Antibiot.* **2016**, *69,* 451–455, doi: 10.1038/ja.2015.130.

[31] Mo, T.-X.; Liu, X.-B.; Duan, L.-H.; Zhang, X.-M.; Xu, Z.-L.; Qin, X.-Y.; Li, B.-C.; Li, J.; Yang, R.-Y., Secondary metabolites of the endophytic fungus *Xylaria* sp. GDG-102 from *Sophora tonkinensis*, *Chem Nat. Compd.* **2021**, *57,* 764–766, doi: 10.1007/s10600-021-03470-3

[32] Pecoraro, L.; Wang, X.; Shah, D.; Song, X.; Kumar, V.; Shakoor, A.; Tripathi, K.; Ramteke, P.W.; Rani, R., Biosynthesis pathways, transport mechanisms and biotechnological applications of fungal siderophores, *J. Fungi* **2021**, *8,* 21, doi: 10.3390/jof8010021.

[33] Liras, P.; Martín, J.F., Interconnected set of enzymes provide lysine biosynthetic intermediates and ornithine derivatives as key precursors for the biosynthesis of bioactive secondary metabolites, *Antibiotics* **2023**, *12,* 159, doi: 10.3390/antibiotics12010159.

[34] Van der Helm, D.; Hossain, M.B.; Jalal, M.A.F.; Benson, B.; Barnes, C.L., The molecular structure of a novel siderophore, neocoprogen I, *Acta Cryst. A* **1984**, *40,* C92-C92, doi: 10.1107/S0108767384097117.

[35] Parker, S.R.; Cutler, H.G.; Jacyno, J.M.; Hill, R.A., Biological activity of 6-pentyl-2*H*-pyran-2-one and its analogs, *J. Agric. Food Chem.* **1997**, *45,* 2774–2776, doi: 10.1021/jf960681a.

[36] Sang, M.; Feng, P.; Chi, L.-P.; Zhang, W., The biosynthetic logic and enzymatic machinery of approved fungi-derived pharmaceuticals and agricultural biopesticides, *Nat. Prod. Rep.* 2024, Advance Article, doi:10.1039/d3np00040k.

[37] Bouras, N.; Strelkov, S.E., The anthraquinone catenarin is phytotoxic and produced in leaves and kernels of wheat infected by *Pyrenophora tritici-repentis*, *Physiol. Mol. Plant Pathol.* **2008**, *72,* 87–95, doi: 10.1016/j.pmpp.2008.06.001.

[38] Andolfi, A.; Cimmino, A.; Villegas-Fernández, A.M.; Tuzi, A.; Santini, A.; Melck, D.; Rubiales, D.; Evidente, A., Lentisone, a new phytotoxic anthraquinone produced by *Ascochyta lentis*, the causal agent of ascochyta blight in *Lens culinaris*, *J. Agric. Food Chem.* **2013**, *61,* 7301–7308, doi: 10.1021/jf4026663.

[39] Oettmeier, W.; Kude, C.; Soll, H.-J., Phenolic herbicides and their methylethers: Binding characteristics and inhibition of photosynthetic electron transport and photophosphorylation, *Pestic. Biochem. Phys.* **1987**, *27,* 50–60, doi: 10.1016/0048-3575(87)90095-2.

[40] Oettmeier, W.; Masson, K.; Donner, A., Anthraquinone inhibitors of photosystem II electron transport, *FEBS Lett.* **1988**, *231,* 259–262, doi: 10.1016/0014-5793(88)80743-9.

[41] Bobylev, M.M.; Bobyleva, L.I.; Strobel, G.A., Synthesis and bioactivity of analogs of maculosin, a host-specific phytotoxin produced by *Alternaria alternata* on spotted knapweed (*Centaurea maculosa*), *J. Agric. Food Chem.* **1996**, *44,* 3960-3964, doi:10.1021/jf960091c.

[42] Bobylev, M.M.; Bobyleva, L.I.; Strobel, G.A., Natural products containing phenylalanine as potential bioherbicides, *Biologically active natural products,* Cutler, H.G.; Cutler, S.J. (eds.), CRC Press, Boca Raton, **1999**, ISBN: 9781420048629.

[43] Spaggiari, C.; Annunziato, G.; Spadini, C.; Montanaro, S.L.; Iannarelli, M.; Cabassi, C.S.; Costantino, G., Extraction and quantification of azelaic acid from different wheat samples (*Triticum durum* Desf.) and evaluation of their antimicrobial and antioxidant activities, *Molecules* **2023**, *28,* 2134, doi*:* 10.3390/molecules28052134.

[44] Kim, C.S.; Kwon, O.W.; Kim, S.Y.; Choi, S.U.; Kim, K.H.; Lee, K.R., Five new oxylipins from *Chaenomeles sinensis*, *Lipids* **2014**, *49,* 1151–1159, doi: 10.1007/s11745-014-3953-0.

[45] Salvatore, M.M.; Félix, C.; Lima, F.; Ferreira, V.; Naviglio, D.; Salvatore, F.; Duarte, A.S.; Alves, A.; Andolfi, A.; Esteves, A.C., Secondary metabolites produced by *Macrophomina phaseolina* isolated from *Eucalyptus globulus*, *Agriculture* **2020**, *10,* 72, doi: 10.3390/agriculture10030072.

[46] Fitton, A.; Goa, K.L., Azelaic acid. A review of its pharmacological properties and therapeutic efficacy in acne and hyperpigmentary skin disorders, *Drugs* **1991**, *41,* 780–798, doi: 10.2165/00003495-199141050-00007.

[47] Xu, Q.; Qiao, Y.; Zhang, Z.; Deng, Y.; Chen, T.; Tao, L.; Xu, Q.; Liu, J.; Sun, W.; Ye, Y.; Lu, Y.; Qi, C.; Zhang, Y., New polyketides with anti-inflammatory activity from the fungus *Aspergillus rugulosa, Front. Pharmacol.* **2021**, *12*, doi: 10.3389/fphar.2021.700573.

[48] Li, D.-X.; Cheng, X.; Ma, F.-P.; Chen, J.-Y.; Chen, Y.-P.; Zhao, X.-S.; Luo, Q., Identification of metabolites from edible mushroom *Morchella sextelata* and their biological evaluation **2023**, *37*, 1774-1781, doi: 10.1080/14786419.2022.2119389.

5 Phytotoxic sulfonamide from *Colletotrichum graminicola*: isolation and synthesis

Abstract

From crude extracts of *Colletotrichum graminicola* grown in complete medium (CM) *N*-(4-hydroxybutyl)benzenesulfonamide (**5.1**) could be recognized by bioactivity-guided isolation. To our knowledge, this is the first time that **5.1** has been isolated from natural sources. *N*-(4-hydroxybutyl)benzenesulfonamide (**5.1**) and four derivatives **5.2 – 5.5**, which differ in the length of the alkyl chain (C2 – C6) could be successfully synthesized. Compounds **5.1 – 5.5** were tested for their phytotoxic potential in a leaf-spot bioassay and a non-destructive leaf disc assay on *Arabidopsis thaliana* Col-0. Based on the results, first structure-activity relationships were determined, showing that the phytotoxic activity increases with enhancement of the alkyl chains. The phytotoxic activity could be increased from 20 mM of the natural product **5.1** to up to 5 mM by the synthesized compound **5.5**.

5.1   Introduction

Due to the rapidly increasing number of resistances to commercial herbicides, there is an urgent need in the development of herbicides with new mode of action. [1–3] In this context, phytopathogenic fungi are increasingly becoming focus of research as a source of new phytotoxins that can be either directly used in bio-compatible weed management or indirectly as templates for the development of new herbicides. [1; 4; 5]

Several studies have already focused on the isolation of phytotoxins of the genus *Colletotrichum*. [6–8] The genus *Colletotrichum* (Glomerellales, Sordariomycetes) comprises around 250 currently accepted species among them numerous economically important plant pathogens. [9; 10] One important member is *Colletotrichum graminicola* which causes leaf blight and stalk rot of maize. [11; 12] A large number of secondary metabolites of various classes are already known from *Colletotrichum,* including pyrones, phenols, sterols, terpenes, amides and many more. None of these natural products, however, contains an nitrogen-sulfur bond. [13; 14]

In nature, only relatively few compounds are known to contain a nitrogen-sulfur (N-S) bond. To date, only about 100 natural compounds containing a nitrogen-sulfur (N-S) bond are known. Most of them, about 75%, are sulfamates ($-O-SO_2-NH_2$). Sulfonamides, characterized by a hexacoordinated sulfur (oxidation state: +IV), are less common with 8 natural products known to date. [15]

Compounds that containing a nitrogen-sulfur (N-S) bond have diverse biological activities, making them of great industrial importance. Their applications include herbicides, insecticides, pharmaceuticals and antimicrobials. [16–18]

According to the Herbicide Resistance Action Committee (HRAC) classification of mode of action [19], a total of 46 compounds contain a nitrogen-sulfur (N-S) bond. The vast majority of this compounds belongs to the compound classes of sulfonylureas (34), triazolopyrimidines (7) and sulfonanilides (2), which all act as acetolactate synthase (ALS) inhibitors. Examples for each chemical class are shown in Figure 5-1. ALS is a key enzyme in the biosynthetic pathway of the branched-chain amino acids valine, leucine and isoleucine. [20] Symptoms caused by this type of herbicides usually occur several days after application and include a slowing of plant growth and the formation of chlorosis or a purple coloration of the leaves. These type of herbicides are systemic and non-selective. [21; 22]

Further representatives containing a nitrogen-sulfur (N-S) bond are the herbicides asulam and bensulide (**Figure 5-1**). Asulam acts as an inhibitor of the dihydropteroate synthase, an enzyme involved in the folate metabolism in plants, bacteria and fungi. [20] Thus, the antibacterial effect of numerous sulfonamides can also be explained by this mechanism. [23] Herbicidal symptoms develop slowly and include chlorosis formation and stunned growth of new tissues. Asulam is a systemic and selective herbicide with its selectivity based on different metabolic degradation processes.[24] The organophosphate bensulide inhibits root growth and cell division. However, the exact mechanism of action is not yet known. Bensulide is applied before the plants emerge and thus prevents weeds from germinating. [21]

Additionally, a new herbicide, dimesulfazet (**Figure 5-1**), is currently under development. The compound belongs to trifluoromethansulfonanilides and is assumed to act on the biosynthesis of very long chain fatty acid (VLCFA) in plants. The same mechanism is known from mefluidide. [25; 26] VLCFA are fatty acids consisting of more than 20 carbon atoms. They are essential for the vitality of plants since they serve as precursors of cuticle waxes and as components of sphingo- and phospholipids. [25; 27] Symptoms caused by dimesulfazet include decreased growth and leaf curling. [24]
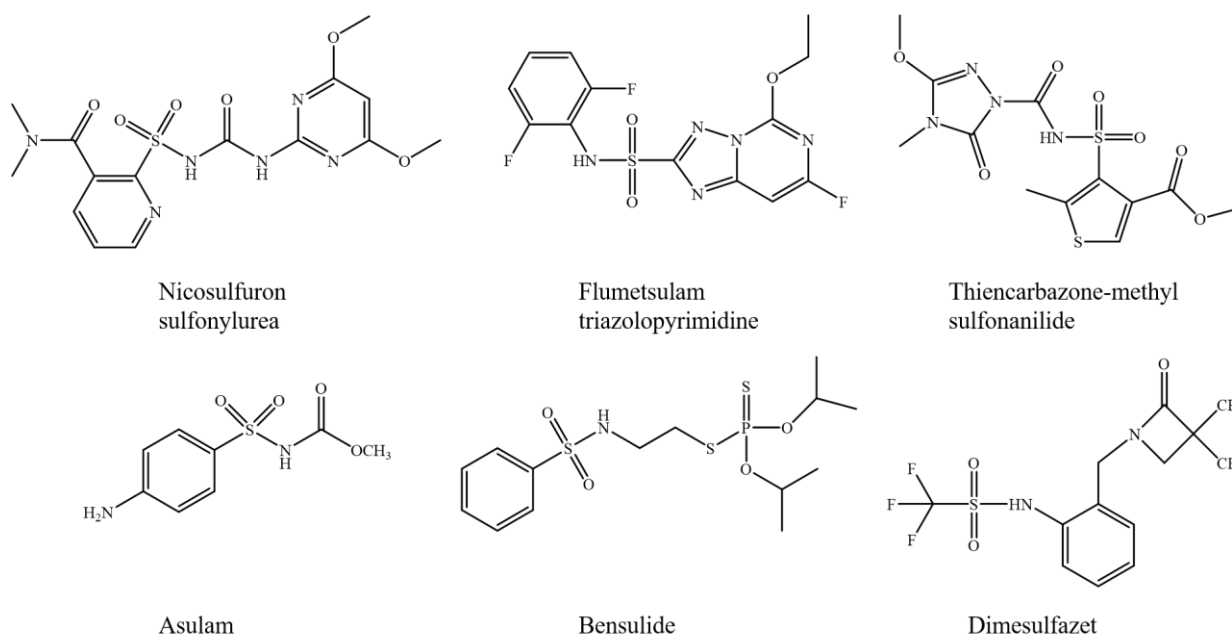
Figure 5-1 Examples of herbicides containing a nitrogen-sulphur bond.

This chapter describes the bioassay-guided isolation and structure determination of *N*-(4-hydroxybutyl)-benzenesulfonamide (**5.1**) from *Colletotrichum graminicola.* To the best of our knowledge, this is the first time that *N*-(4-hydroxybutyl)-benzenesulfonamide (**5.1**) has been reported as a natural product. Further the synthesis of **5.1** as well as of four derivatives (**5.2 – 5.5**) differing in alkyl chain length to get first insights into the structure – activity relationship, is presented. The phytotoxic activity of all compounds was evaluated using two different test systems, including a leaf-spot assay and a non-destructive leaf disk assay. In addition, the compounds **5.1 – 5.5** were tested for their antibacterial, antifungal and anticarcinogenic properties.

5.2   Experimental

5.2.1   General experimental procedures

Column chromatography was performed on polyamide CC 6-Ac (Macherey Nagel, Germany), silica gel 60 silanized (0.063 – 0.200 mm, Merck, Germany), whereas analytical TLC was performed on pre-coated silica gel F_{254} aluminium sheets (Merck, Germany). The compound spots were detected by their absorbance at $\lambda = 254$ nm.

The analytical HPLC was performed on a Shimadzu prominence system (Shimadzu Europe, Germany) which consists of a CBM-20A communication bus modul, a SPD-M20A diode array detector, a FRC-10A fraction collector, a DGU-20A5R degassing unit, a LC-20AT liquid chromatograph and a SIL-20A HT autosampler using an ODS-A column (5 µM, 120 Å, 150 x 4.6 mm ID, YMC Europe, Germany).

Direct injection via autosampler, Orbitrap Elite mass spectrometer
The negative ion high resolution ESI mass spectra were obtained from a Orbitrap Elite mass spectrometer (Thermofisher Scientific, Germany) equipped with a HESI electrospray ion source (negative spray voltage 3.7 kV, capillary temperature 325°C, source heater temperature 80 °C, FTMS resolution 60.000). Nitrogen was used as sheath gas. The sample solutions were injected through the autosampler (injection volume 5 µL) without chromatographic separation. H_2O (A; MilliQ-system Barnstead GenPure Pro (from Thermo Scientific, Germany)) and CH_3CN (B; Chromasolv, for LC-MS, Honeywell Riedel de Haën, Germany) with 0.1% formic acid (additive for LC-MS, LiChropur, Merck, Germany) were used as eluents. The instrument was externally calibrated by the Pierce ESI negative ion calibration solution (product number 88324) from Thermofisher Scientific, Rockford, IL, 61105 USA. The data were evaluated by the Xcalibur software 2.2 SP1. The collision induced dissociation (CID) MSn measurements were performed using the relative collision energies given in the appendix.

^{1}H and ^{13}C NMR spectra were recorded on an Agilent DD2 400 NMR (Agilent, Germany) spectrometer at 399.917 and 100.570 MHz, respectively. The 2D NMR spectra were recorded using standard CHEMPACK 8.1 pulse sequences implemented in Varian VNMRJ 4.2 spectrometer software. Chemical shifts are reported relative to TMS.

Delayed fluorescence was measured with a NightShade LB 985 fluorescence imaging instrument (Berthold Technologies, Germany). Samples were irradiated for 10 minutes with a halogen lamp. Subsequently, the light was turned off for 3 s before the delayed fluorescence measurement started. The camera (Peltier/air-cooled slow scan CCD camera, resolution: 1024 x 1024 pixels, 13.6 µm) was set in high scan mode with (x-binning: 2, y-binning: 2). Background correction and cosmic suppression were enabled. Delayed fluorescence was measured for 60 s. The photo was taken with an illumination intensity of 10%. The sample was exposed for 0.1 s for the photo. The sample size corresponded to the dimensions of a 96-well plate (w= 130 mm, h= 15 mm).

5.2.2 Fungal material and cultivation conditions

Colletotrichum graminicola (strain M1.001, provided by Prof. Dr. Deising, Institute of Agricultural and Nutritional Sciences, Martin-Luther-University Halle-Wittenberg) was cultivated as semi-solid cultures in Erlenmeyer flasks (1 L) containing 4 g cotton wool and 200 mL CM medium (10 g/ L glucose, 1 g/ L Ca(NO$_3$)$_2$, 1 g/ L yeast extract, 1 g/ L casein hydrolysate, 0.2 g/ L KH$_2$PO$_4$, 0.25 g/ L MgSO$_4$, 0.05 g/ L NaCl) at 23°C for 13 days without agitation. In total, 260 flasks (52 L) were grown. Subsequently, the mycelium and the cotton wool were separated from the culture broth by vacuum filtration. The mycelium was frozen at -20°C prior to extraction.

5.2.3 Extraction and isolation

The culture filtrate was extracted by partition with ethyl acetate (3 x 1 L) and subsequently dehydrated by anhydrous sodium sulfate (Na$_2$SO$_4$), filtered and evaporated to dryness *in vacuo*.

The mycelium with cotton wool was exhaustively extracted with ethyl acetate (6 x 3 L) in ultrasound bath for 15 minutes, dehydrates by anhydrous sodium sulfate (Na$_2$SO$_4$), filtered, and evaporated to dryness *in vacuo*. Both ethyl acetate crude extracts were combined based on their TLC pattern and subsequently subjected to a liquid-liquid partition with acetonitrile and *n*-hexane.

The acetonitrile extract (2.5 g) was subjected to a polyamide CC 6-Ac column (2.5 x 80 cm) eluting with *n*-hexane : ethyl acetate (4:1 → 3:1 → 2:1 → 1:1, *v:v*) → ethyl acetate → ethyl acetate : acetone (1:1, *v:v*) → acetone → acetone : methanol (2:1 → 1:1) → methanol. Fractions à 30 mL were collected and combined based on their TLC pattern to give ten fractions (A1 – A10). Fraction A4 was further separated by column chromatography on silanized silica (35 x 2cm) eluting with chloroform : ethanol (100:1) → chloroform : methanol (1:1). In total, 26 fractions (each 10 mL) were collected and combined based on their TLC pattern to obtain ten fractions (B1 – B10). Fractions B6 and B7 were finally separated by analytical HPLC with H$_2$O (A) and methanol (B) as solvents (2 – 22 min, 5 – 100% B) to afford **5.1a** (t$_R$ =17.3 min, 0.5 mg).

N-(4-hydroxybutyl)benzenesulfonamide (**5.1a**): colorless oil, R$_f$ = 0.27 (SiOH, *n*-hexane/ethyl acetate, 1:1); ^{1}H-NMR (400 MHz, methanol-d$_4$) δ 7.84 (m, 2H, H-2/6), δ 7.56 (m, 2H, H-3/5), δ 7.61 (m, 1H, H-4), δ 2.86 (m, 2H, H-7), δ 1.50 (m, 2H, H-8), δ 1.50 (m, 2H, H-9), δ 3.49 (m, 2H, H-10); ^{13}C-NMR (100 MHz, Mmethanol-d$_4$) δ 141.9 (C-1), δ 127.7 (C-2/6), δ 129.9 (C-3/5), δ 133.2 (C-6), δ 43.6 (C-7), δ 26.9 (C-8), δ 30.3 (C-9), δ 62.1 (C-10). HRESIMS *m/z* 228.0696 [M-H]$^-$, calculated for C$_{10}$H$_{13}$NO$_3$S$^-$ *m/z* 228.0689. (**Figure S 171** – **Figure S 178**).

5.2.4 Synthesis
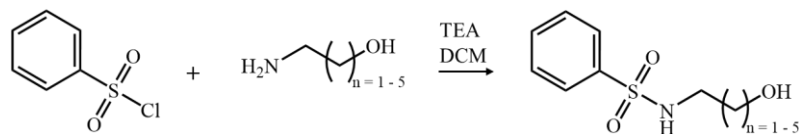
Figure 5-2 Synthesis scheme of 5.1b – 5.5; TEA= triethylamine, DCM= dichloromethane.
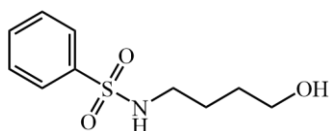
Figure 5-3 Structure of compound **5.1**.

N-(4-hydroxybutyl)benzenesulfonamide (**5.1b**): The synthesis was carried out according to Schafroth et al. [28] 0.184 mL (2 mmol) 4-hydroxybutylamine were solved in 10 mL dichloromethane. The solution was cooled to 0 °C and 0.28 mL (2 mmol) triethylamine followed by 0.256 mL benzenesulfonyl chloride (2 mmol) were added. The reaction mixture was allowed to warm to room temperature and was stirred until consumption of the educts. The reaction was tracked by TLC on silica with *n*-hexane/ethyl acetate (1:1) under UV-light (λ = 254 nm and λ = 366 nm). The compound was obtained as a colorless oil (394 mg, 1.72 mmol, 86%).

R_f =0,27 (SiOH, *n*-hexane/ethyl acetate, 1:1); ^{1}H-NMR (400 MHz, methanol-d$_4$) δ 7.84 (m, 2H, H-2/6), δ 7.58 (m, 2H, H-3/5), δ 7.58 (m, 1H, H-4), δ 2.86 (m, 2H, H-7), δ 1.50 (m, 2H, H-8), δ 1.50 (m, 2H, H-9), δ 3.49 (m, 2H, H-10)); ^{13}C (100 MHz, methanol-d$_4$) δ 141.9 (C-1), δ 127.9 (C-2/6), δ 130.2 (C-3/5), δ 133.5 (C-4), δ 43.9 (C-7), δ 27.1 (C-8), δ 30.6 (C-9), δ 62.3 (C-10) HRESIMS *m/z* 228.0695 [M-H]⁻, calculated for C$_{10}$H$_{14}$NO$_3$S⁻ *m/z* 228.0689. (**Figure S 179** – **Figure S 183**).

All spectroscopic data are in accordance with those of the natural product **5.1a**.
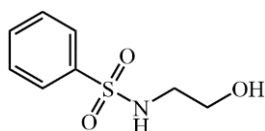
Figure 5-4 Structure of compound **5.2**.

N-(2-hydroxyethyl)benzenesulfonamide (**5.2**): The synthesis was performed as described above using 0.120 mL of ethanolamine instead of 4 hydroxybutylamine. The target compound was obtained as colorless oil (395 mg, 1.95 mmol, 98%).

R_f =0,40 (SiOH, *n*-hexane/ethyl acetate, 1:4); ^{1}H (400 MHz, methanol-d$_4$) δ 7.86 (m, 2H, H-2/6), δ 7.55 (m, 2H, H-3/5), δ 7.59 (m, 1H, H-4), δ 2.95 (t, *J* = 6.0 Hz, 2H, H-7), δ 3.53 (t, *J* = 5.9 Hz, 2H, H-8); ^{13}C (400 MHz, methanol-d$_4$) δ 141.8 (C-1), δ 127.9 (C-2/6), δ 130.2 (C-3/5), δ 133.6 (C-4), δ 46.2 (C-7), δ 61.8 (C-8); HRESIMS *m/z* 200.0386 [M-H]⁻, calculated for C$_8$H$_{10}$NO$_3$S⁻ 200.0387. (**Figure S 184** – **Figure S 188**).
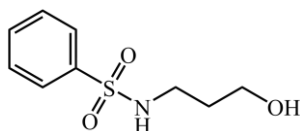
Figure 5-5 Structure of compound **5.3**.

N-(3-hydroxypropyl)benzenesulfonamide (**5.3**): The synthesis was performed as described above using 0.152 mL of 3-amino-1-propanol instead of 4 hydroxybutylamine. The target compound was obtained as colorless oil (377 mg, 1.75 mmol, 87%).

R_f =0,43 (SiOH, *n*-hexane/ethyl acetate, 1:4); ^{1}H (400 MHz, methanol-d$_4$) δ 7.84 (m, 2H, H-2/6), δ 7.57 (m, 2H, H-3/5), δ 7.61 (m, 1H, H-4), δ 2.93 (t, *J* = 7.0 Hz, 2H, H-7), δ 1.65 (m, 2H, H-8), δ 3.55 (t, *J* = 6.2 Hz, 2H, H-9); ^{13}C (400 MHz, methanol-d$_4$) δ 141.8 (C-1), δ 127.9 (C-2/6), δ 130.1 (C-3/5), δ 133.5 (C-4), δ 41.2 (C-7), δ 33.4 (C-8), δ 60.1 (C-9); HRESIMS *m/z* 214.0543 [M-H]⁻, calculated for C$_9$H$_{12}$NO$_3$S⁻ 214.0543. (**Figure S 189** – **Figure S 193**).
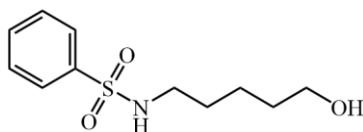
Figure 5-6 Structure of compound **5.4**.

N-(5-hydroxypentyl)benzenesulfonamide (**5.4**): The synthesis was performed as described above using 0.217 mL of 5-amino-1-pentanol instead of 4 hydroxybutylamine. The target compound was obtained as colorless oil (340 mg, 1.40 mmol, 70%).

R_f =0,45 (SiOH, *n*-hexane/ethyl acetate, 1:4); ^{1}H (400 MHz, methanol-d$_4$) δ 7.84 (m, 2H, H-2/6), δ 7.56 (m, 2H, H-3/5), δ 7.59 (m, 1H, H-4), δ 2.84 (t, J = 6.9 Hz, 2H, H-7), δ 1.45 (m, 2H, H-8), δ 1.34 (m, 2H, H-9), δ 1.45 (m, 2H, H-10), δ 3.49 (t, J = 6.5 Hz, 2H, H-11); ^{13}C (400 MHz, methanol-d$_4$) δ 142.0 (C-1), δ 127.9 (C-2/6), δ 130.1 (C-3/5), δ 133.5 (C-4), δ 43.9 (C-7), δ 30.4 (C-8), δ 23.9 (C-9), δ 33.0 (C-10), δ 62.6 (C-11); HRESIMS *m/z* 242.0858 [M-H]$^-$, calculated for $C_{11}H_{16}NO_3S^-$ 242.0856. (**Figure S 194 – Figure S 198**).
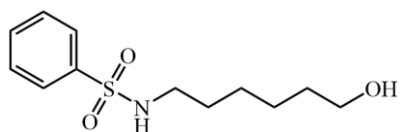
Figure 5-7 Structure of compound **5.5**.

N-(6-hydroxyhexyl)benzenesulfonamide (**5.5**): The synthesis was performed as described above using 0.234 g of 6-amino-1-hexanol instead of 4 hydroxybutylamine. The target compound was obtained as colorless oil (317 mg, 1.23 mmol, 62%).

R_f =0,50 (SiOH, *n*-hexane/ethyl acetate, 1:4); ^{1}H (400 MHz, methanol-d$_4$) δ 7.84 (m, 2H, H-2/6), δ 7.56 (m, 2H, H-3/5), δ 7.59 (m, 1H, H-4), δ 2.84 (t, J = 7.0 Hz, 2H, H-7), δ 1.44 (m, 2H, H-8), δ 1.29 (m, 2H, H-9), δ 1.29 (m, 2H, H-10), δ 1.47 (m, 2H, H-11), δ 3.50 (t, J = 6.6 Hz, 2H, H-12); ^{13}C (400 MHz, methanol-d$_4$) δ 142.1 (C-1), δ 127.9 (C-2/6), δ 130.1 (C-3/5), δ 133.5 (C-4), δ 43.9 (C-7), δ 30.6 (C-8), δ 27.4 (C-9), δ 26.4 (C-10), δ 33.4 (C-11), δ 62.8 (C-12); HRESIMS *m/z* 256.1012 [M-H]$^-$, calculated for $C_{12}H_{18}NO_3S^-$ 256.1013. (**Figure S 199 – Figure S 203**).

5.2.5 Leaf-spot bioassay

A modified leaf-spot bioassay [29] was used to test fractions and pure compounds for their phytotoxic activity. The samples were dissolved in methanol : water (1:1, *v/v*) and droplets of 5 µL were placed on the leaf surface of undetached and fully expanded young leaves of *Arabidopsis thaliana* Col-0. Fractions were tested at concentrations of 5 – 10 µg/ µL, pure compounds at concentrations from 1 mM – 50 mM. Plants were incubated in the greenhouse (19 °C, day/night cycle) for 24 – 72 h. Paraquat (100 µM, dissolved in methanol : water 1:1, *v/v*) was used as a positive control. The pure solvent mixture of methanol/water (1:1, *v/v*) served as the negative control. Every 24 h the plants were observed for the formation of necrosis. Images were taken with CAMAG TLC visualizer (Muttenz, Switzerland).

5.2.6 Non-destructive leaf disk assay

A modified non-destructive leaf disk assay [30] was used to determine the phytotoxic activity of the pure compounds. As test organism *Arabidopsis thaliana* Col-0 was used. The assay was performed in a 96-well plate (cat. no. 92096, 96F, TPP Techno Plastic Products AG, Trasadingen, Switzerland), each well containing 200 µL of test solution consisting of a leaf disk buffer and stock solutions of the test substances. The leaf disk buffer contains 1 mM MES and 1 g/L sucrose adjusted to pH = 6.5. Stock solutions of the test substances were prepared in methanol. The concentrations of these stock solutions were selected in such a way that a maximum of 5 µL per well had to be added to achieve the desired concentration. The maximum concentration of methanol was therefore 2.5% per well. The pure solvent (methanol) served as the negative control; Paraquat (5 µM) was chosen as positive control.

Leaf punches were taken from fully unfolded green leaves using 5-mm biopsy punches with plunger system (WellTech Rapid-Core 5.0 mm). The leaves were placed on the surface of the test solution, the adaxial surface facing upwards. The 96-well plate was incubated in the greenhouse for 48 h, every 24 h delayed fluorescence was measured. Before measurement, the plates were wrapped in aluminum foil and adapted to darkness for 20 min. Daylight images were taken with CAMAG TLC visualizer (Camag, Switzerland).

5.3 Results and discussion

5.3.1 Isolation and synthesis

The crude ethyl acetate extract prepared from the mycelium of *C. graminicola* caused severe necrosis when applied to leaves of *A. thaliana* Col-0 and was accordingly subjected to bioassay-guided fractionation. Liquid-liquid extraction followed by repeated column chromatography on polyamide CC 6-Ac and silanized silica in combination with analytical HPLC resulted in the isolation of *N*-(4-

hydroxybutyl)benzenesulfonamide (**5.1a**).

Compound **5.1a** was isolated as colorless oil. Its molecular formula was determined to be $C_{10}H_{14}NO_3S$, based on the molecular ion m/z 228.0696 [M-H]⁻, calculated for $C_{10}H_{14}NO_3S^-$ m/z 228.0689.

The presence of sulfur in **5.1a** is confirmed by the isotopic pattern, as ^{34}S has a relative abundance of 4.21%. (**Figure S 171**) HRESIMS^n analysis (**Figure S 172** – **Figure S 174**) in negative ion mode displayed three fragment ions at m/z 210 [M-H-H$_2$O]⁻, m/z 156 [M-H-C$_4$H$_8$O]⁻ and m/z 141 [M-H-C$_4$H$_9$NO]⁻. Furthermore, the MS^3 spectrum of the [M-H-C$_4$H$_8$O]⁻ ion shows a characteristic fragment at m/z 92 [M-H-C$_4$H$_8$O- SO$_2$]⁻. In the MS^3 of the [M-H-C$_4$H$_9$NO]⁻ three fragments at m/z 93 [M-H-C$_4$H$_9$NO-SO]⁻, m/z 77 [M-H-C$_4$H$_9$NO-SO$_2$]⁻ and [M-H-C$_4$H$_9$NO-C$_6$H5]⁻. The proposed fragmentation pattern is shown in **Figure 5-8**.
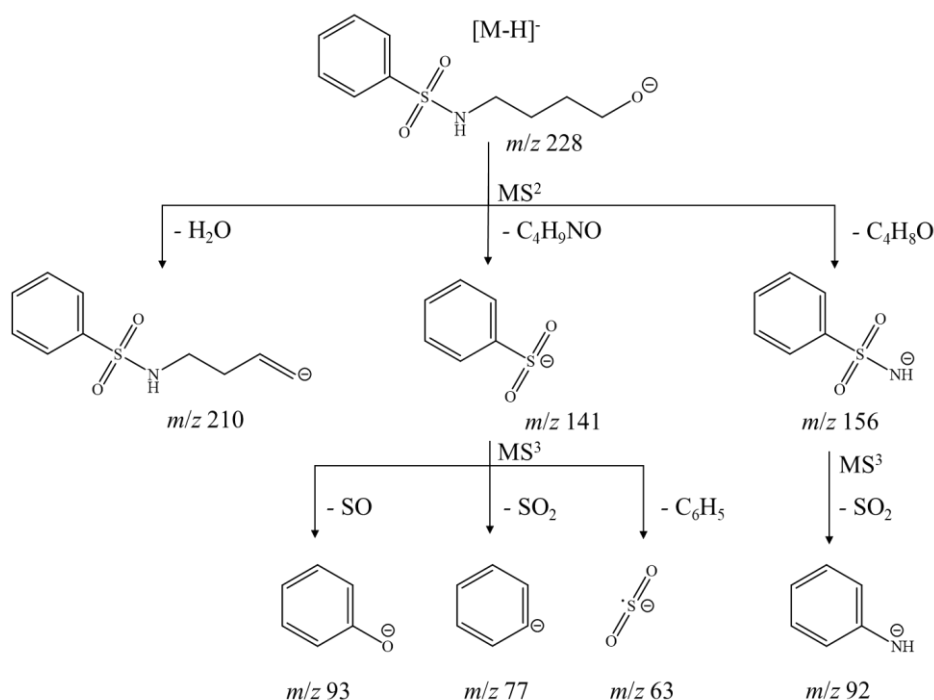
Figure 5-8 Proposed fragmentation pattern of **5.1a**.

The structure of **5.1a** was further determined on the basis of 1D and 2D NMR. The NMR data agreed with data described in literature. [31]

To verify the structure of **5.1a** and to obtain sufficient amounts for further biological studies, the synthesis was performed and named **5.1b**. In addition, further four derivatives **5.2 – 5.5** differing in chain length of the alkyl chain were synthesized to obtain initial insights into structure-activity relationships. The synthesis was performed according to Schafroth and co-workers [28] and is shown schematically in **Figure 5-2**. The reaction follows a nucleophilic substitution as the amino alcohol act as a nucleophile. Compound **5.2** [32], **5.3** and **5.4** [33], and **5.5** [34] were already described in the literature. However, NMR spectroscopic data were only available for **5.2**.[32]

This is the first time that isolation of **5.1a** from natural sources has been described. In the context of natural products, **5.1a** was previously known only as a transformation product. In 2013, Yamada et al. showed that *Streptomyces* sp. are able to transform *N*-benzenesulfonylpyrrolidines into the corresponding amino alcohol by adding to the culture broth. [31]

5.1   **5.6**
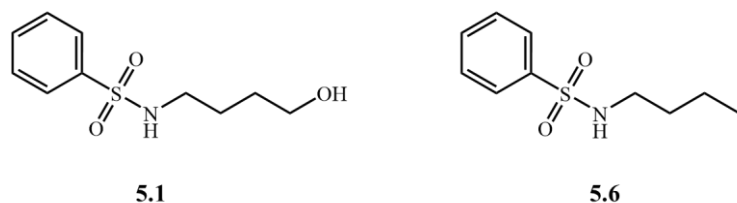
Figure 5-9 Structures of **5.1** and NBBS (**5.6**).

There are however some studies describing the isolation of *N*-butylbenzenesulfonamide (NBBS, **5.6**) from various natural sources, including *Pseudomonas* sp. [35], *Angelica sinensis* [36] and *Pygeum africanum.* [37; 38] NBBS (**5.6**) is structurally very similar to compound **5.1**, lacking only the hydroxy group at the alkyl chain (**Figure 5-9**). In this context, it should be noted that NBBS (**5.6**) is frequently used in industry as a plasticizer [39] and in the synthesis of sulfonyl carbamate herbicides. [37] Furthermore, it is very stable in the environment, so that at the current state of research it cannot be ruled out that it has solely accumulated in organisms as a contaminant. [15; 40]

Therefore, a new batch of cultures was grown under the same conditions as before. Contact with plastics was avoided as much as possible during cultivation and extraction processes. The culture filtrate was separated and extracted with ethyl acetate as described above. The compound **5.1a** was detected by LC-HRESIMS by comparing retention time and high-resolution mass spectrometric data. IT could clearly demonstrate, that *N*-(4-hydroxybutyl)benzenesulfonamide (**5.1a**) is a native and not a xenobiotic constituent of *C. graminicola*.

5.3.2 Phytotoxic activity

Two different test systems were used to evaluate the phytotoxic properties of compounds **5.1a/b** – **5.5**.

5.3.2.1 Leaf-spot assay

Using a modified leaf spot test [29], the dissolved test substances were applied directly to the leaf surface. The evaluation was purely visual based on the formation of necrosis that were characterized by a light to slightly brownish discoloration of the leaves at the application site.

Conc.	5.1 (C4)	5.2 (C2)	5.3 (C3)	5.4 (C5)	5.5 (C6)	Control	Blank
25 mM							
50 mM							
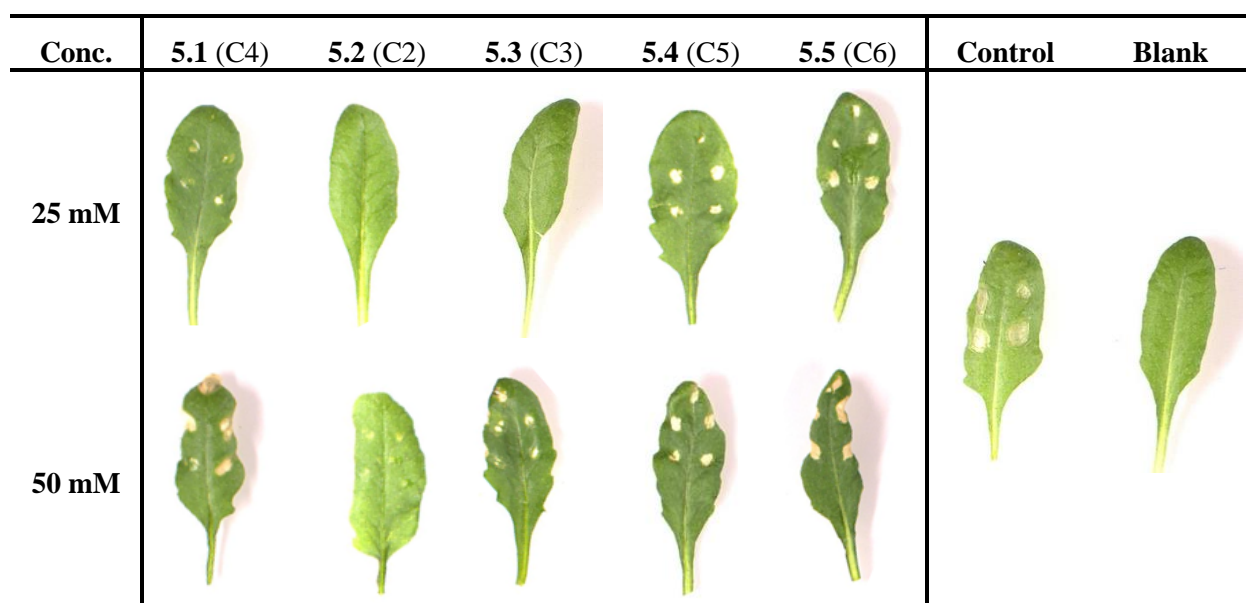
Figure 5-10 Leaf-spot biossay of the synthesized compounds **5.1b - 5.5** after an incubation period of 72 h; positive control: paraquat (100 µM in methanol/water 1:1 *v/v*; negative control: methanol: water 1:1 *v/v*.

All compounds were tested in two different concentrations: 25 and 50 mM. Pictures of treated leaves after an incubation period of 72 hours are shown in Figure 5-10.

At a concentration of 50 mM, all tested substances showed phytotoxic activity. The intensity of necrosis increased with increasing chain length. Thus, compound **5.2** with C2-alkyl side chain formed only very small, barely visible necrotic areas, while *N*-(6-hydroxyhexyl)benzenesulfonamide (**5.6**) with C6 alkyl side chain caused very strong brownish necrosis. At a concentration of 25 mM, only for the derivatives **5.1a/b**, **5.4** and **5.5** an effect was recognized, whereby stronger necroses were observed with increasing length of the alkyl side chain.

Additionally, it was recognized that the formation of necrosis in the leaf spot test was limited to the application sites even with longer exposure duration (> 2 weeks). This indicates that the compounds act as contact herbicides and are not distributed in the plant.

5.3.2.2 Non-destructive leaf-disk assay

The modified non-destructive leaf disc test used is based on the measurement of delayed fluorescence (DF) and was originally described by Wu and co-workers [30] for the identification of herbicide-tolerant plants. DF is a weak light emitted by chlorophyll *a* (P680) in the light harvesting antenna, associated with photosystem II (see 2.2.6). Due to the high sensitivity of photosynthesis to environmental factors, DF can be used as a stress parameter for plants. [41]A high photosynthetic rate is associated with a strong DF, represented by a red to yellow-green color of the leaf disks. A low DF is indicated by a blue-purple coloration of the leaf disks. If only gray leaf disks are visible, the plant is no longer perfo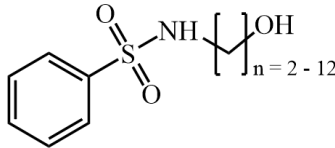rming photosynthesis, i.e. the plant is dead. All compounds were tested at two different concentrations (10 and 15 mM) in four biological replicates each. **Figure 5-11** shows the measurement of DF at t = 0 h and t = 48 h as well as in daylight.
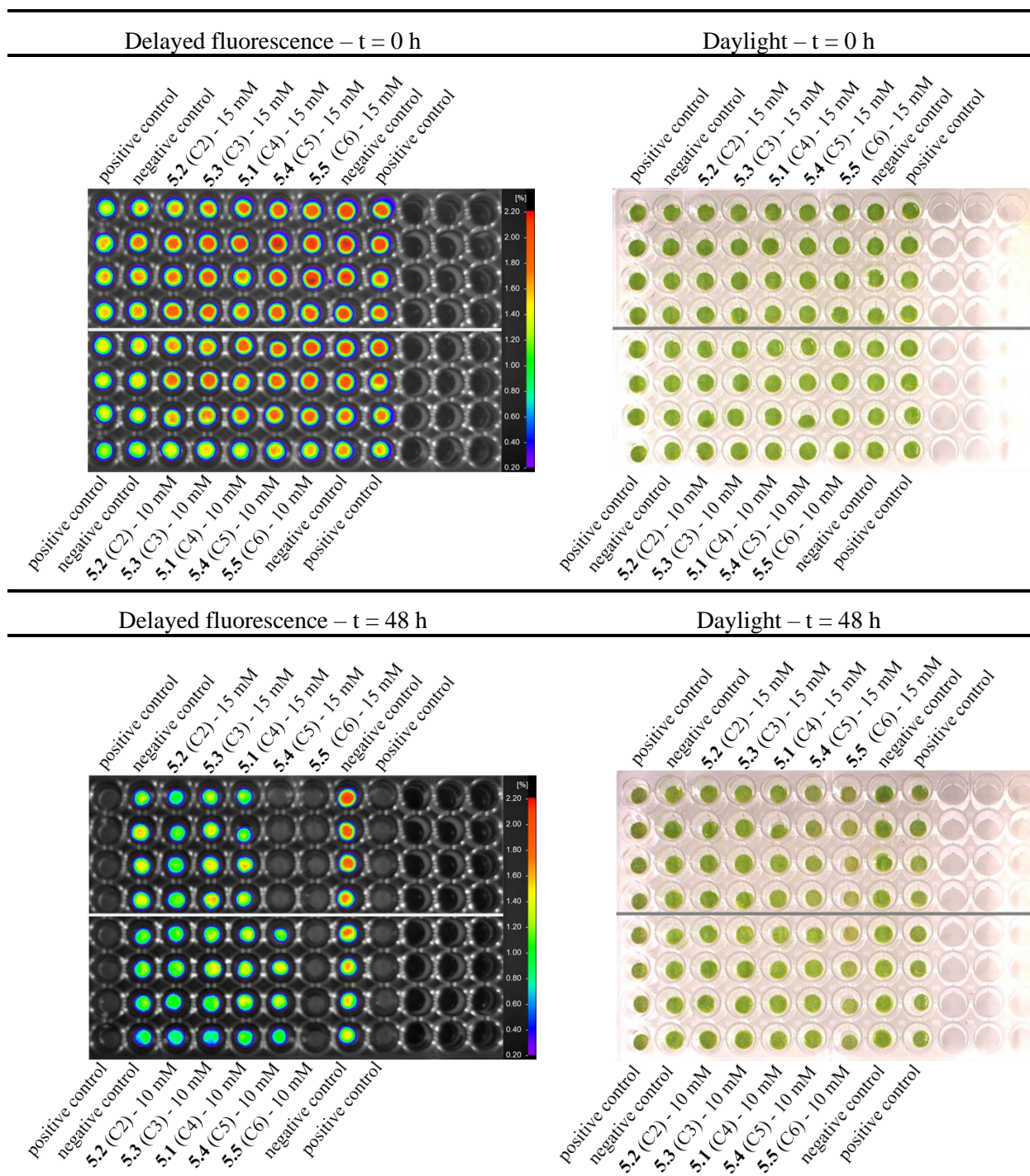
Figure 5-11 Non-destructive leaf-disk assay of synthesized compounds **5.1b** – **5.5** at t = 0 h and t = 48 h.

The dependence of the alkyl chain length in **5.1a/b – 5.5** on the phytotoxic activity observed in the leaf-spot assay was confirmed by the non-destructive leaf disk test. Here, compounds **5.4** and **5.5** showed strong phytotoxic effects on *A. thaliana* Col-0 at a concentration of 15 mM, leading to plant death indicated by gray leaf discs. Only compound **5.5** showed a phytotoxic effect even at 10 mM. Compounds **5.1a/b – 5.4** do not affect the photosynthetic activity, as still a rather high value of DF could be observed. However, it is worthful to mention that the leaf discs show at time point zero a decreased rate of DF, which is based on the stress reaction of the plant caused by cutting of the leaf discs.

On the one hand, enhancement of the alkyl chain length may increase the activity of the molecule in the leaf-spot assay by facilitating penetration into and through the hydrophobic plant cuticle. [42] On the other hand, the results of the non-destructive leaf disk assay suggest that the nonpolar character is also required to cause phytotoxicity, as the cuticle does not have to be crossed when leaf-disks are used. If the ability to penetrate through the cuticle were the only reason, the shorter chain derivatives in the non-destructive leaf disk assay should have significantly higher activity compared to the leaf-spot assay. However, this phenomenon was not observable.

Regarding the mode of action to known herbicides with nitrogen-sulfur bonds as structural feature, some mechanisms of action can already be excluded for the tested compounds **5.1a/b – 5.5**. It can be excluded that compounds **5.1a/b – 5.5** act as ALS inhibitors, as their phytotoxic effect is observable after some days as it is typical for systemic herbicides. This is supported by the fact, that a purple coloration of the leaves due to the accumulation of anthocyanins was not observed. [20–22] Inhibition of dihydropteroate synthase cannot be assumed either, as the phytotoxic effects would also only be visible after a few days. To proof this hypothesis, antibacterial tests should be carried out because dihydropteroate synthase is also present in bacteria. [20; 23]

VLCFA inhibitors are mainly absorbed by plants via the soil and lead to an arrest of cell division. The symptoms are growth arrest, curled leaves and dehydration of the plant. Pre-existing tissue is often not affected. Since compounds **5.1a/b – 5.5** only have an direct effect on existing tissue and only in direct contact, it cannot be assumed that they act as VLCFA inhibitors. However, all these assumptions need to be confirmed by further experiments. Molecular docking studies could also provide insights on the target of the compounds.

5.4   Conclusion and outlook

The phytotoxic *N*-(4-hydroxybutyl)benzenesulfonamide **5.1a** could be isolated from the mycelium and culture filtrate of *Colletotrichum graminicola* by a bioactivity-guided approach. This compound and its derivatives (**5.1b – 5.5**) were subsequently synthesized and biologically evaluated by means of a leaf-spot assay and a non-destructive leaf-disk assay in order to identify initial structural activity relationships. Here, the activity was found to increase with enhancement of the alkyl chain length of the molecule. By comparing the symptoms, clear deviations from those of known herbicides with nitrogen-sulphur bonds in the structure were observed, which indicates that the compounds (**5.1a/b – 5.5**) could have a different mechanism of action. Whether this is the case or to what extent these compounds have a previously unknown mode of action must be investigated in further studies.

Further derivatives are to be synthesized in follow up work in order to further increase the activity and to gain more detailed insights into the structure-activity relationships of the compounds, e.g. derivatives with longer alkyl chains will be synthesized to see at which point the activity decreases again.

References

[1]   Dayan, F.E.; Duke, S.O., Natural compounds as next-generation herbicides, *Plant Physiol.* **2014**, *166,* 1090–1105, doi: 10.1104/pp.114.239061.

[2]   Peterson, M.A.; Collavo, A.; Ovejero, R.; Shivrain, V.; Walsh, M.J., The challenge of herbicide resistance around the world: a current summary, *Pest Manag. Sci.* **2018**, *74,* 2246–2259, doi: 10.1002/ps.4821.

[3]   Qu, R.-Y.; He, B.; Yang, J.-F.; Lin, H.-Y.; Yang, W.-C.; Wu, Q.-Y.; Li, Q. X.; Yang, G.-F., Where are the new herbicides?, *Pest Manag. Sci.* **2021**, *77,* 2620–2625, doi: 10.1002/ps.6285.

[4]   Duke, S.O.; Pan, Z.; Bajsa-Hirschel, J.; Boyette, C.D.; The potential future roles of natural compounds and microbial bioherbicides in weed management in crops, *Adv. Weed Sci.* **2022**, *40, ,* e020210054*,* doi*:* 10.51694/AdvWeedSci/2022;40:seventy-five003.

[5]   Cimmino, A.; Masi, M.; Evidente, M.; Superchi, S.; Evidente, A., Fungal phytotoxins with potential herbicidal activity: Chemical and biological characterization, *Nat. Prod. Rep.* **2015**, *32,* 1629–1653, doi: 10.1039/c5np00081e.

[6]   Masi, M.; Cimmino, A.; Boari, A.; Tuzi, A.; Zonno, M. C.; Baroncelli, R.; Vurro, M.; Evidente, A., Colletochlorins E and F, new phytotoxic tetrasubstituted pyran-2-one and dihydrobenzofuran, isolated from *Colletotrichum higginsianum* with potential herbicidal activity, *J. Agric. Food Chem.* **2017**, *65,* 1124–1130, doi: 10.1021/acs.jafc.6b05193.

[7]   Masi, M.; Castaldi, S.; Sautua, F.; Pescitelli, G.; Carmona, M. A.; Evidente, A., Truncatenolide, a bioactive disubstituted nonenolide produced by *Colletotrichum truncatum*, the causal agent of anthracnose of soybean in Argentina: Fungal antagonism and SAR studies, *J. Agric. Food Chem.* **2022**, *70,* 9834–9844, doi: 10.1021/acs.jafc.2c02502.

[8]   Xu, Z.; Shi, M.; Tian, Y.; Zhao, P.; Niu, Y.; Liao, M.; Dirhamnolipid produced by the pathogenic fungus *Colletotrichum gloeosporioides* BWH-1 and its herbicidal activity, *Molecules* **2019**, *24,* 2969, doi*:* 10.3390/molecules24162969.

[9]   Jayawardena, R.S., *Colletotrichum*: Lifestyles, biology, morpho-species, species complexes and accepted species, *Mycosphere* **2021**, *12,* 519–669, doi: 10.5943/mycosphere/12/1/7.

[10] Cannon, P.F.; Damm, U.; Johnston, P.R.; Weir, B.S., *Colletotrichum* - current status and future directions, *Stud. Mycol.* **2012**, *73,* 181–213, doi: 10.3114/sim0014.

[11] Frey, T.J.; Weldekidan, T.; Colbert, T.; Wolters, P.; Hawk, J.A., Fitness evaluation of Rcg1, a locus that confers resistance to *Colletotrichum graminicola* (Ces.) G.W. Wils. using near-isogenic maize hybrids, *Crop Sci.* **2011**, *51,* 1551–1563, doi: 10.2135/cropsci2010.10.0613.

[12] Sukno, S.A.; García, V.M.; Shaw, B.D.; Thon, M.R., Root infection and systemic colonization of maize by *Colletotrichum graminicola*, *Appl. Environ. Microbiol.* **2008**, *74,* 823–832, doi: 10.1128/AEM.01165-07.

[13] Kim, J.W.; Shim, S.H., The fungus *Colletotrichum* as a source for bioactive secondary metabolites, *Arch. Pharmacal Res.* **2019**, *42,* 735–753, doi: 10.1007/s12272-019-01142-z.

[14] Moraga, J.; Gomes, W.; Pinedo, C.; Cantoral, J.M.; Hanson, J.R.; Carbú, M.; Garrido, C.; Durán-Patrón, R.; Collado, I.G., The current status on secondary metabolites produced by plant pathogenic *Colletotrichum* species, *Phytochem. Rev.* **2019**, *18,* 215–239, doi: 10.1007/s11101-018-9590-0.

[15] Petkowski, J.J.; Bains, W.; Seager, S., Natural products containing a nitrogen–sulfur bond, *J. Nat. Prod.* **2018**, *81,* 423–446, doi: 10.1021/acs.jnatprod.7b00921.

[16] Thiele-Bruhn, S.; Pharmaceutical antibiotic compounds in soils – a review, *J. Plant. Nutr. Soil Sci.* **2003**, *166,* 145–167, doi: 10.1002/jpln.200390023.

[17] Rohilla, S.; Sharma, D., Sulfonamides, quinolones, antiseptics, and disinfectants, *Medicinal Chemistry of Chemotherapeutic Agents,* Acharya, P. C.; Kurosu, M. (eds.), Elsevier, **2023,** 21–63, doi: 10.1016/B978-0-323-90575-6.00015-6.

[18] Devendar, P.; Yang, G.-F., Sulfur-containing agrochemicals, *Top. Curr. Chem.* **2017**, *375,* 82, doi: 10.1007/s41061-017-0169-9.

[19] Herbicide Resistance Action Committee, *HRAC Mode of Action Classification 2022 Map,* https://hracglobal.com/tools/hrac-mode-of-action-classification-2022-map, last access: **09.01.2024**.

[20] Duke, S.O., Overview of herbicide mechanisms of action, *Environ. Health Perspect.* **1990**, *87,* 263–271, doi: 10.1289/ehp.9087263.

[21] Zimdahl, R.L., Properties and uses of herbicides, *Fundamentals of Weed Science,* 5. Ed., Zimdahl, R. L. (ed.), Elsevier, **2018,** 463–499, ISBN: 978-0-12-811143-7.

[22] Gunsolus, J.L.; Curran, W.S., *Herbicide mode of action and injury symptoms (Revised 1991)*, University of Minnesota. Agricultural Extension Service, https://hdl.handle.net/11299/207555, **1991**.

[23] Achari, A.; Somers, D.O.; Champness, J.N.; Bryant, P.K.; Rosemond, J.; Stammers, D.K., Crystal structure of the anti-bacterial sulfonamide drug target dihydropteroate synthase, *Nat. Struct. Biol.* **1997**, *4,* 490–497, doi: 10.1038/nsb0697-490.

[24] Duke, S.O.; Dayan, F.E., Bioactivity of herbicides, *Comprehensive Biotechnology,* 2. Ed., Moo-Young, M. (ed.), Elsevier, Amsterdam, **2011,** 23–35, doi: 10.1016/B978-0-08-088504-9.00273-7.

[25] Tresch, S.; Heilmann, M.; Christiansen, N.; Looser, R.; Grossmann, K., Inhibition of saturated very-long-chain fatty acid biosynthesis by mefluidide and perfluidone, selective inhibitors of 3-ketoacyl-CoA synthases, *Phytochemistry* **2012**, *76,* 162–171, doi: 10.1016/j.phytochem.2011.12.023.

[26] Umetsu, N.; Shirai, Y., Development of novel pesticides in the 21st century, *J. Pest. Sci.* **2020**, *45,* 54–74, doi: 10.1584/jpestics.D20-201.

[27] Bach, L.; Faure, J.-D., Role of very-long-chain fatty acids in plant development, when chain length does matter, *C. R. Biol.* **2010**, *333,* 361–370, doi: 10.1016/j.crvi.2010.01.014.

[28] Schafroth, M.A.; Rummelt, S.M.; Sarlah, D.; Carreira, E.M., Enantioselective iridium-catalyzed allylic cyclizations, *Org. Lett.* **2017**, *19,* 3235–3238, doi: 10.1021/acs.orglett.7b01346.

[29] Evidente, A.; Lanzetta, R.; Capasso, R.; Andolfi, A.; Bottalico, A.; Vurro, M.; Zonno, M.C., Putaminoxin, a phytotoxic nonenolide from *Phoma putaminum*, *Phytochemistry* **1995**, *40,* 1637–1641, doi: 10.1016/0031-9422(95)00505-2.

[30] Wu, C.; Varanasi, V.; Perez-Jones, A., A nondestructive leaf-disk assay for rapid diagnosis of weed resistance to multiple herbicides, *Weed Sci.* **2021**, 69, 274–283, doi: 10.1017/wsc.2021.15.

[31] Yamada, S.; Miyagawa, T.-A.; Yamada, R.; Shiratori-Takano, H.; Sayo, N.; Saito, T.; Takano, H.; Beppu, T.; Ueda, K., Amide-transforming activity of *Streptomyces:* possible application to the formation of hydroxy amides and aminoalcohols, *Appl. Microbiol. Biotechnol.* **2013**, *97,* 6223–6230, doi: 10.1007/s00253-013-4952-4.

[32] Aslan, H.G.; Özcan, S.; Karancan, N., The antibacterial activity of some sulfonamides and sulfonyl hydrazones, and 2D-QSAR study of a series of sulfonyl hydrazones, *Spectrochim. Acta A Mol. Biomol. Spectrosc.* **2012**, *98,* 329-336, doi: 10.1016/j.saa.2012.08.043.

[33] Van Gysel, A.; Van Overvelt, J.-C.; Godard, P.; Nannan, A.; Biebuyck, J.-J.; De Groote, P., Plasticised polymer compositions, International Patent No. WO1998014513A1, **1998**.

[34] Yasuyoshi, U.; Hiroshi, K.; Naoki, K., Nitro Compound, Japanese Patent No. JPH09202764, **1997**.

[35] Kim, K.K.; Kang, J.G.; Moon, S.S.; Kang, K.Y., Isolation and identification of antifungal *N*-butylbenzenesuphonamide produced by *Pseudomonas* sp. AB$_2$, *J. Antibiot.* **2000**, *53,* 131-136, doi: 10.7164/antibiotics.53.131.

[36] Deng, S.; Chen, S.-N.; Yao, P.; Nikolic, D.; Van Breemen, R.B.; Bolton, J.L.; Fong, H.H.S.; Farnsworth, N.R.; Pauli, G.F., Serotonergic activity-guided phytochemical investigation of the roots of *Angelica sinensis*, *J. Nat. Prod.* **2006**, *69,* 536–541, doi: 10.1021/np050301s.

[37] Schleich, S.; Papaioannou, M.; Baniahmad, A.; Matusch, R., Extracts from *Pygeum africanum* and other ethnobotanical species with antiandrogenic activity, *Planta Med.* **2006**, *72,* 807–813, doi: 10.1055/s-2006-946638.

[38] Papaioannou, M.; Schleich, S.; Roell, D.; Schubert, U.; Tanner, T.; Claessens, F.; Matusch, R.; Baniahmad, A., NBBS isolated from *Pygeum africanum* bark exhibits androgen antagonistic activity, inhibits AR nuclear translocation and prostate cancer cell growth, *Invest. New Drugs* **2010**, *28,* 729–743, doi: 10.1007/s10637-009-9304-y.

[39] Rider, C.V.; Janardhan, K.S.; Rao, D.; Morrison, J.P.; McPherson, C.A.; Harry, G.J., Evaluation of *N*-butylbenzenesulfonamide (NBBS) neurotoxicity in Sprague-Dawley male rats following 27-day oral exposure, *Neurotoxicology* **2012**, *33,* 1528–1535, doi: 10.1016/j.neuro.2012.07.002.

[40] Huppert, N.; Würtele, M.; Hahn, H.H., Determination of the plasticizer *N*-butylbenzenesulfonamide and the pharmaceutical Ibuprofen in wastewater using solid phase microextraction (SPME), *Fresenius J. Anal. Chem.* **1998**, *362,* 529–536, doi: 10.1007/s002160051119.

[41] Goltsev, V.; Zaharieva, I.; Chernev, P.; Strasser, R.J., Delayed fluorescence in photosynthesis, *Photosynth. Res.* **2009**, *101,* 217–232, doi: 10.1007/s11120-009-9451-1.

[42] Schönherr, J.; Riederer, M., Foliar penetration and accumulation of organic chemicals in plant cuticles, *Reviews of Environmental Contamination and Toxicology*, Ware, G.W. (ed.), Springer, New York, **1989,** 1–70.

6   Studies on quantitative structure-activity relationship (QSAR) of phytotoxic sulfonamides

Abstract

Based on the natural product N-(4-hydroxybutyl)benzenesulfonamide (**6.1-c**), previously isolated from the phytopathogenic fungus *Colletotrichum graminicola*, a total of 127 derivatives were synthesized and tested for their phytotoxic activity to gain insight into the structure-activity relationship. The phytotoxic activity was determined using a non-destructive leaf-disk assay with *Arabidopsis thaliana* Col-0 and *Secale cereale* as test organisms. The QSAR study is based on the evaluation of the bioactivity as a function of various physiochemical parameters. The parameters include molecular weight (M), partition coefficient log P, parachor (P_C), molar refractivity (A), density (ρ), molecular volume (V_m), Taft's steric parameter (E_s), Charton's steric parameter (v) and the substituent hydrophobicity parameter (Hansch π). The lipophilicity of the molecule, expressed by the partition coefficient log P, and the molecular weight were identified as variables that influences the phytotoxicity. In addition, an increase in phytotoxic activity was observed in the presence of sterically hindering substituents. However, it should also be mentioned that the molar refractive index (A), the parachor (P_C) and the molar volume (V_m) are linearly dependent on the partition coefficient log P and therefore cannot be considered individually. Moreover, the observed activities could not be explained by these three variables alone. The highest phytotoxic activity was achieved at a mean value of log P 2.80 and 302.4 g/mol. The sterically demanding substituents *tert*-butyl and cyclohexane showed the best results. Overall, the bioactivity of 20 mM of the natural substance (**6.1-c**) was increased to 0.4 mM (**6.10**-**b**, **6.11-e**, **6.12-e** and **6.13-a-e**).

6.1   Introduction

The structure activity relationship (SAR) is defined as the relationship between the chemical structure of a molecule and its bioactivity. SAR aims to identify structural characteristics, which are associated with the activity. Therefore, SAR is an important tool in drug discovery, from primary screening to lead optimization. [1] SAR studies can be carried out either qualitatively or quantitatively. Qualitative SAR studies are based exclusively on binary information. This means that a distinction is only made between the presence of bioactivity and its absence. This approach allows the identification of structural elements that are essential for bioactivity. [2] Quantitative SAR (QSAR) studies on the other hand, are used to find a mathematical correlation between the biological activity and quantitative chemical attributes that define the properties of the analyzed molecules. These physicochemical descriptors include parameters that account for hydrophobicity, topology, electronic parameters, and steric effects and are determined empirically by computational methods. [3;4]

A quantitative structure-activity relationship (SAR) analysis based on several physicochemical descriptors was applied to find a correlation between the chemical structures of 127 sulfonamide derivatives and their respective phytotoxic activity. Synthesized compounds **6.1** – **6.32** were provided by Prof. Dr. Csuk and co-worker Toni Denner, Institute of Chemistry – Organic Chemistry, Martin-Luther University Halle-Wittenberg.

Methodology

The physicochemical descriptors used in this study are molecular weight (M), partition coefficient (log P), molar refractivity (A), parachor (Pc), density (ρ) and molar volume (V_m). The partition coefficient and the molar refractivity were obtained by the web tool "SwissADME" [5], all other properties were obtained using "Chemsketch 2018.2.5". [6]

*Partition coefficient (*log P)
The partition coefficient between *n*-octanol and water (log $P_{o/w}$) is a classical descriptor for the lipophilicity of a molecule. Several methods for the estimation of log $P_{o/w}$ values - with diverse performances on different chemical sets - were developed. For this study consensus log $P_{o/w}$ obtained from SwissADME [5] was chosen to increase the prediction accuracy. The consensus log $P_{o/w}$ is the arithmetic mean of the values predicted by the following five methods: XLOGP3 (atomistic method and knowledge-based method) [7], WLOGP (purely atomistic method implemented from Wildman and Crippen [8]) MLOGP (topological method implemented from Morguchi [9; 10]), SILICOS-IT (hybrid fragmental/topological method) [11] and iLOGP (physics-based method implemented from Daina and co-workers. [12]

Molar refractivity (A)
Molar refractivity is related to the polarizability of a mole of a substance calculated by the Lorenz-Lorenz formula:

$$A = \frac{n^2 - 1}{n^2 + 2} \times \frac{M}{\rho}$$

Where M is the molecular weight, n is the refraction index and ρ the density. Its value depends on the temperature, pressure and the wave longitude of the light used to measure the refraction index. For radiation with infinite wavelength, the molar refractivity can be used to measure the real volume of the molecules. Further molar refractivity is related to the London dispersive forces that are important for drug-receptor interactions. [3; 13; 14]

Parachor (Pc)

The parachor is a parameter introduced by Sugden [15] related to the surface tension and the molecular volume of a molecule. It is defined by the following equitation as the product of the molar volume and the fourth root of the surface tension:

$$Pc = \frac{M}{\rho} \times \gamma^{1/4}$$

Where M is the molecular weight, ρ the density and γ the surface tension. [16; 17]

Density (ρ)

$$\rho = \frac{m}{V}$$

Where m is the mass and V is the volume.

Molar volume

$$V_m = \frac{M}{\rho}$$

Where M is the molar mass and ρ is the density.

Taft's steric parameter

The Taft equation allows the correlation of steric parameter with the reaction rate. The equation reflects the steric influence of substituents on the hydrolysis rate, where k_s is the rate of ester hydrolysis for a given substrate and k_{CH_3} is the methyl acetate hydrolysis rate, which is used a standard. δ is a proportionality constant, which is a measure of sensitivity. [18-20] The used E_s values were taken from Sigman and co-workers. [20]

$$\delta E_s = \log\left(\frac{k_s}{k_{CH_3}}\right)$$

Charton's steric parameter

Charton's steric parameter is a modification of the Taft parameter. Charton correlated the E_s values with the corresponding van der Waals radii of the groups in order to eliminate inductive and resonance effects [20; 21] The used v values were taken from Sigman and co-workers. [20]

$$\psi v = \log\left(\frac{k_s}{k_{CH_3}}\right)$$

Where the log of the relative rate (k_s/k_{CH_3}) is proportional to the product of ψ (sensitivity factor) and v, and v is the adjusted E_s value based on the van der Waals radii.

Hansch parameter

Hansch and Fujita [22] introduced a new hydrophobic scale, with π as the relative hydrophobicity of a substituent, which is defined by the following equation:

$$\pi_x = \log\left(\frac{P_x}{P_H}\right)$$

Where P_H is the partition coefficient of the parent compound and P_X is the value for the derivative. [22; 23] π values were calculated using the web tool "Calculation of Substituent Properties v2024.02" (https://bitly.com/getsigmas). [24]

6.2 Experimental

6.2.1 General experimental procedures

Delayed fluorescence was measured with a NightShade LB 985 fluorescence imaging instrument (Berthold Technologies, Germany). Samples were irradiated for 10 minutes with a halogen lamp. Subsequently, the light was turned off for 3 s before the delayed fluorescence measurement started. The camera (Peltier/air-cooled slow scan CCD camera, resolution: 1024 x 1024 pixels, 13.6 µm) was set in high scan mode with (x-binning: 2, y-binning: 2). Background correction and cosmic suppression were enabled. Delayed fluorescence was measured for 60 s. The photo was taken with an illumination intensity of 10%. The sample was exposed for 0.1 s for the photo. The sample size corresponded to the dimensions of a 96-well plate (w= 130 mm, h= 15 mm).

6.2.2 Non-destructive leaf disk assay

A modified non-destructive leaf disk assay [25] was used to determine the phytotoxic activity of the pure compounds. The assay was performed with *Arabidopsis thaliana* Col-0 as a dicotyledonous plant and with *Secale cereale* as a monocotyledonous plant. The assay was performed in a 96-well plate (cat. no. 92096, 96F, TPP Techno Plastic Products AG, Switzerland), each well containing 200 µL of test solution consisting of a leaf disk buffer and stock solutions of the test substances. The leaf disk buffer was made up with 1 mM MES and 1 g/L sucrose with a pH of 6.5. Stock solutions of the test substances were prepared in methanol. The concentration of these stock solutions was selected in such a way that a maximum of 5 µL per well had to be added to achieve the desired concentration. The maximum concentration of methanol was therefore 2.5 % per well. The pure solvent (methanol) served as the negative control; Paraquat (5 µM) was chosen as the positive control.

Leaf punches were taken from fully unfolded green leaves using 5 mm biopsy punches with plunger system (WellTech Rapid-Core 5.0 mm). The leaves were placed on the surface of the test solution, the adaxial surface facing upwards. The 96-well plate was incubated in the greenhouse for 48 h, every 24 h delayed fluorescence (DF) was measured. Before measurement, the plates were wrapped in aluminum foil and adapted to darkness for 20 min. Daylight images were taken with CAMAG TLC visualizer (Camag, Switzerland).

A high photosynthetic rate is associated with a strong DF, represented by a red to yellow-green color of the leaf disks. A low DF is indicated by a blue-purple coloration of the leaf disks. Only grey leaf discs are visible when the plant is no longer performing photosynthesis, i.e. when it is dead.
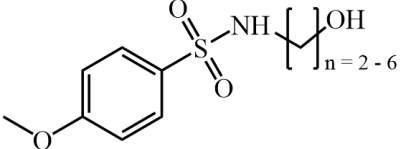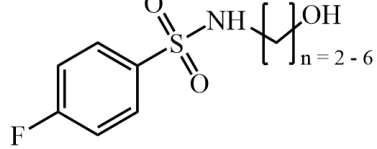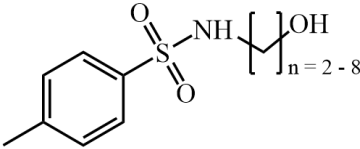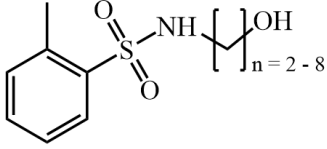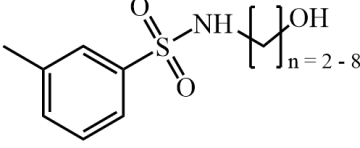
Each compound was tested in four replicates per concentration. The compounds were classified as active "+" if all four replicates died during the observation period (only grey leaf discs visible). When not all four replicates (but at least two replicates) died and the others showed only a weak DF, the activity was rated as "(+)".
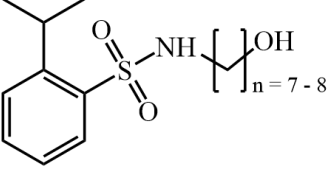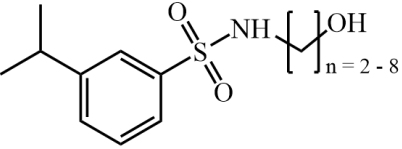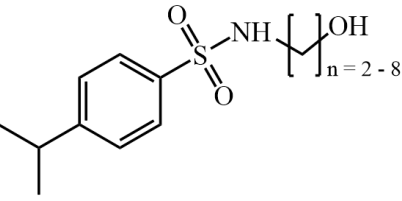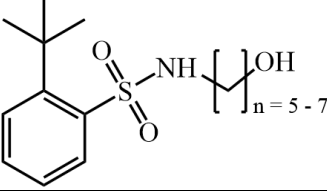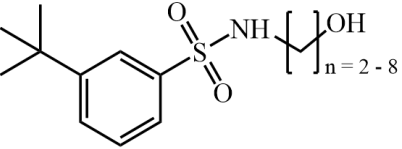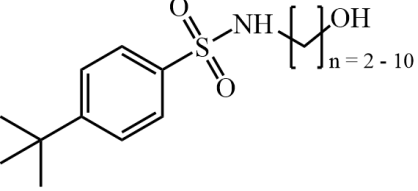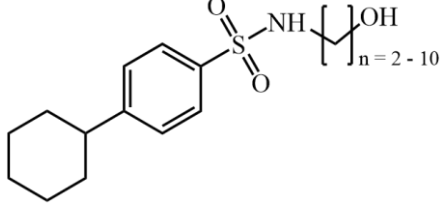
6.3 Results and discussion

6.3.1 Phytotoxicity tests of all derivatives
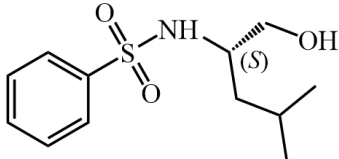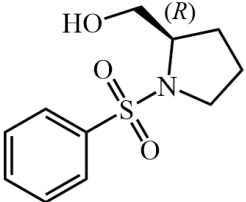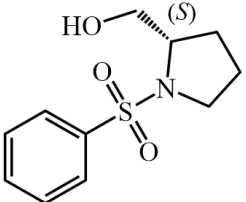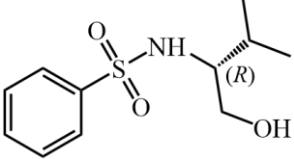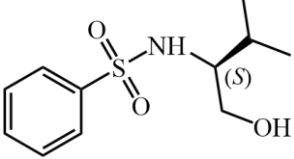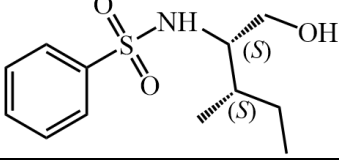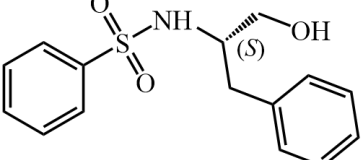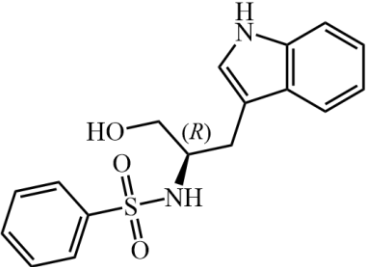
Table 6-1 Phytotoxic activity of derivatives **6.1 - 6.32** in the non-destructive-leaf-disk assay.
Legend: + = all replicates showed no DF; (+) = at least two replicates showed no more DF; - = no phytotoxic activity; n.t. = not tested.
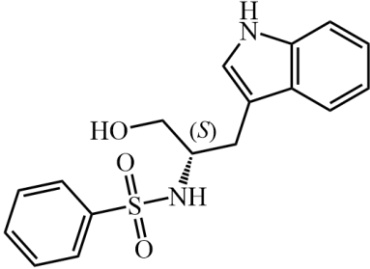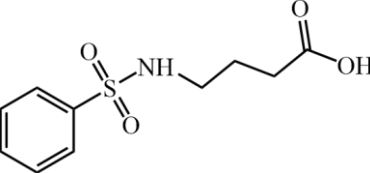
No	structure + identifier			5 mM	2 mM	1 mM	0.4 mM
6.1		a	n = 2	-	-	n.t.	n.t.
		b	n = 3	-	-	n.t.	n.t.
		c	n = 4	-	-	n.t.	n.t.
		d	n = 5	-	-	n.t.	n.t.
		e	n = 6	+	-	n.t.	n.t.
		f	n = 7	+	+	-	-
		g	n = 8	+	+	-	-
		h	n = 9	+	-	n.t.	n.t.
		i	n = 10	-	-	n.t.	n.t.
		j	n = 11	-	-	n.t.	n.t.
		k	n = 12	-	-	n.t.	n.t.
6.2		a	n = 2	-	-	n.t.	n.t.
		b	n = 3	-	-	n.t.	n.t.
		c	n = 4	-	-	n.t.	n.t.
		d	n = 5	-	-	n.t.	n.t.
		e	n = 6	+	-	n.t.	n.t.
6.3		a	n = 2	-	-	n.t.	n.t.
		b	n = 3	-	-	n.t.	n.t.
		c	n = 4	-	-	n.t.	n.t.
		d	n = 5	-	-	n.t.	n.t.
		e	n = 6	-	-	n.t.	n.t.
6.4		a	n = 2	-	-	n.t.	n.t.
		b	n = 3	-	-	n.t.	n.t.
		c	n = 4	-	-	n.t.	n.t.
		d	n = 5	(+)	(+)	n.t.	n.t.
		e	n = 6	+	+	-	-
		f	n = 7	+	+	-	-
		g	n = 8	+	+	(+)	-
6.5		a	n = 2	-	-	n.t.	n.t.
		b	n = 3	-	-	n.t.	n.t.
		c	n = 4	-	-	n.t.	n.t.
		d	n = 5	(+)	(+)	n.t.	n.t.
		e	n = 6	+	+	-	-
		f	n = 7	+	+	-	-
		g	n = 8	+	+	(+)	-
6.6		a	n = 2	-	-	n.t.	n.t.
		b	n = 3	-	-	n.t.	n.t.
		c	n = 4	-	-	n.t.	n.t.
		d	n = 5	(+)	(+)	n.t.	n.t.
		e	n = 6	+	+	-	-
		f	n = 7	+	+	-	-
		g	n = 8	+	+	(+)	-

Compound		n				
6.7 (2-isopropylbenzenesulfonamide, n = 7–8)	a	n = 7	+	+	(+)	-
	b	n = 8	+	(+)	-	-
6.8 (3-isopropylbenzenesulfonamide, n = 2–8)	a	n = 2	+	-	n.t.	n.t.
	b	n = 3	+	-	n.t.	n.t.
	c	n = 4	+	-	n.t.	n.t.
	d	n = 5	+	+	-	-
	e	n = 6	+	+	+	-
	f	n = 7	+	+	+	-
	g	n = 8	+	+	-	-
6.9 (4-isopropylbenzenesulfonamide, n = 2–8)	a	n = 2	+	-	n.t.	n.t.
	b	n = 3	+	-	n.t.	n.t.
	c	n = 4	+	(+)	n.t.	n.t.
	d	n = 5	+	+	-	-
	e	n = 6	+	+	(+)	-
	f	n = 7	+	+	n.t.	n.t.
	g	n = 8	+	(+)	n.t.	n.t.
6.10 (2-tert-butylbenzenesulfonamide, n = 5–7)	a	n = 5	+	+	+	(+)
	b	n = 6	+	+	+	+
	c	n = 7	+	+	-	-
6.11 (3-tert-butylbenzenesulfonamide, n = 2–8)	a	n = 2	+	(+)	n.t.	n.t.
	b	n = 3	+	(+)	n.t.	n.t.
	c	n = 4	+	+	-	-
	d	n = 5	+	+	+	(+)
	e	n = 6	+	+	+	+
	f	n = 7	+	(+)	n.t.	n.t.
	g	n = 8	(+)	(+)	n.t.	n.t.
6.12 (4-tert-butylbenzenesulfonamide, n = 2–10)	a	n = 2	+	+	n.t.	n.t.
	b	n = 3	+	+	n.t.	n.t.
	c	n = 4	+	+	-	-
	d	n = 5	+	+	+	(+)
	e	n = 6	+	+	+	+
	f	n = 7	+	(+)	n.t.	n.t.
	g	n = 8	(+)	(+)	n.t.	n.t.
	h	n = 9	-	-	n.t.	n.t.
	i	n = 10	-	-	n.t.	n.t.
6.13 (4-cyclohexylbenzenesulfonamide, n = 2–10)	a	n = 2	+	+	+	+
	b	n = 3	+	+	+	+
	c	n = 4	+	+	+	+
	d	n = 5	+	+	+	(+)
	e	n = 6	+	+	+	(+)
	f	n = 7	+	(+)	n.t.	n.t.
	g	n = 8	+	(+)	n.t.	n.t.
	h	n = 9	-	-	n.t.	n.t.
	i	n = 10	-	-	n.t.	n.t.

6.14		a	n = 8	-	-	n.t.	n.t.
		b	n = 9	-	-	n.t.	n.t.
		c	n = 10	-	-	n.t.	n.t.
6.15		a	n = 2	-	-	n.t.	n.t.
		b	n = 3	-	-	n.t.	n.t.
		c	n = 4	-	-	n.t.	n.t.
		d	n = 5	-	-	n.t.	n.t.
		e	n = 6	-	-	n.t.	n.t.
		f	n = 7	-	-	n.t.	n.t.
		g	n = 8	-	-	n.t.	n.t.
6.16		a	n = 2	-	-	n.t.	n.t.
		b	n = 3	-	-	n.t.	n.t.
		c	n = 4	-	-	n.t.	n.t.
		d	n = 5	-	-	n.t.	n.t.
		e	n = 6	-	-	n.t.	n.t.
		f	n = 7	-	-	n.t.	n.t.
		g	n = 8	-	-	n.t.	n.t.
6.17		a	n = 2	(+)	-	n.t.	n.t.
		b	n = 3	(+)	-	n.t.	n.t.
		c	n = 4	+	-	n.t.	n.t.
		d	n = 5	+	-	n.t.	n.t.
		e	n = 6	-	-	n.t.	n.t.
		f	n = 7	-	-	n.t.	n.t.
		g	n = 8	-	-	n.t.	n.t.
6.18		a	n = 5	-	-	n.t.	n.t.
		b	n = 8	-	-	n.t.	n.t.
6.19		a	n = 5	-	-	n.t.	n.t.
		b	n = 8	+	+	+	-
6.20		-	-	-	-	n.t.	n.t.
6.21		-	-	-	-	n.t.	n.t.
6.22		-	-	+	(+)	n.t.	n.t.

No.	Structure						
6.23		-	-	+	(+)	n.t.	n.t.
6.24		-	-	-	-	n.t.	n.t.
6.25		-	-	-	-	n.t.	n.t.
6.26		-	-	+	(+)	n.t.	n.t.
6.27		-	-	+	(+)	n.t.	n.t.
6.28		-	-	+	(+)	n.t.	n.t.
6.29		-	-	+	+	-	-
6.30		-	-	(+)	-	n.t.	n.t.

6.31		-	-	(+)	-	n.t.	n.t.
6.32		-	-	+	-	n.t.	n.t.

Based on the natural product *N*-(4-hydroxybutyl)benzenesulfonamide (**6.1c**), a total of 127 derivatives were obtained by convergent synthesis in 1 – 3 steps (syntheses performed by Toni Denner, Institute of Chemistry – Organic Chemistry, Prof. Dr. Csuk, Martin-Luther-University Halle-Wittenberg; data not shown). All synthesized derivatives were first tested for their phytotoxic activity in a non-destructive leaf disk test on *A. thaliana* Col-0 (**Figure S 205**) and *S. cereale* (data not shown) at a concentration of 5 mM and 2 mM. The selected two test organism were chosen in order to determine any differences in the effect on monocotyledonous and dicotyledonous plants. However, none of the substances showed any preference for a representative of the plant class. Therefore, only results from the non-destructive leaf disk assay with *A. thaliana* Col-0 are shown in **Table 6-1**. Derivatives that exhibited phytotoxic activity at 2 mM were tested in a follow-up leaf disk assay at concentrations of 1 mM and 0.4 mM. Structure-activity relationships were deduced from the achieved results.

Derivatives 6.1 a – k

In a first approach, 11 derivatives (**6.1a-b, 6.d-k**) including the natural product **6.1c** with different chain lengths ($n = 2$-12) were synthesized. In Chapter 5 it was already demonstrated that the phytotoxic activity increases with growing alkyl chain length from $n = 2$ to $n = 6$. In addition, it has now been found that the highest activity (2 mM) was achieved at a chain length of $n = 7$-8. With increasing chain length ($n = 9$-12), the activity decreases again.
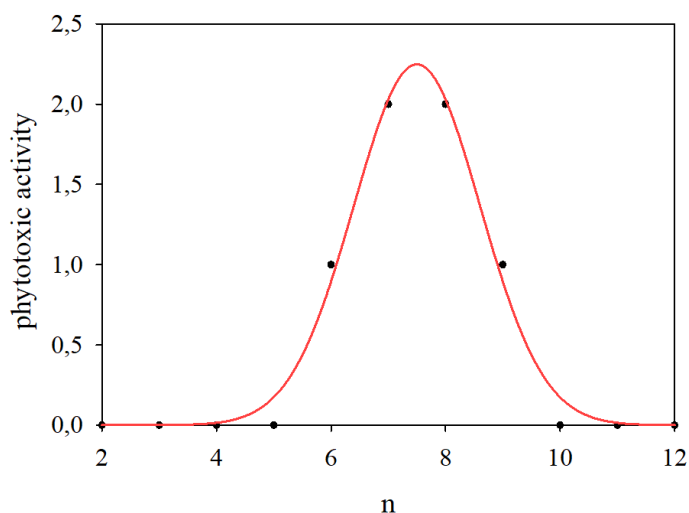
Figure 6-1 Plotting of phytotoxic activity as a function of chain length n; phytotoxic activity, where 0 = no activity, 1 = 5 mM and 2 = 2 mM.

Derivatives 6.2 – 6.14
A total of 78 derivatives with different substitutions at the benzene moiety were tested. Phytotoxic activity was found to increase as follows:

-F (**6.2**) < -OMe (**6.3**) < -Me (**6.4 – 6.6**) < -*i*Pr (**6.7 – 6.9**) < -*t*Bu (**6.10 – 6.12**) = -cyclohexane (**6.13**) > -adamantane (**6.14**)
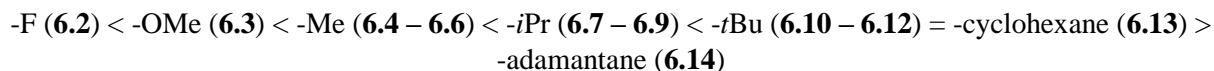
At first sight, bioactivity appears to depend on the size of the substituent (steric effects) and the lipophilicity of the molecule. These relationships are examined in more detail below based on various physiochemical descriptors of the molecules.
At the same time, the position of the substituent at the benzene moiety appears to be less relevant for the activity. The tests carried out did not reveal a preferred position (*o*, *m* or *p*) of the substituent on the benzene moiety. Only the derivatives with an isopropyl substituent (**6.7** - **6.9**) exhibited a higher activity by insertion at the meta-position compared to the ortho- and para-position.

Derivatives 6.15 – 6.16
Substitution of the benzene ring by pyridine or cyclopropane results in a complete loss of phytotoxic activity.

Derivatives 6.17
The insertion of a double bond between the benzene moiety and the sulfonamide core structure led to a drastic decrease in phytotoxic activity. Only the derivatives **6.17a-d** showed a phytotoxic effect up to a maximum of 5 mM. In comparison, derivatives **6.1f-g** showed a phytotoxic effect up to 2 mM.

Derivatives 6.18 - 6.19
The elimination of the benzene ring and substitution with a methyl group (**6.18a/b)** led to a complete loss of phytotoxic activity. However, the formation of the methanesulfonic ethers (**6.19a/b**) showed phytotoxic activity up to 1 mM.

Derivatives 6.20 – 6.31
A total of twelve derivatives **6.20** – **6.31** with the benzene sulfonamide core structure linked to different proteinogenic amino acids were synthesized.

Table 6-2 Amino acid derivatives **6.20 – 6.31**.

derivative	amino acid	derivative	amino acid
6.20	D-alanine	6.26	D-valine
6.21	L-alanine	6.27	L-valine
6.22	D-leucine	6.28	L-phenylalanine
6.23	L-leucine	6.29	L-isoleucine
6.24	D-proline	6.30	D-tryptophane
6.25	L-proline	6.31	L-tryptophane

Above the synthesized amino acid derivatives, the highest phytotoxic activity was achieved by the L-phenylalanine derivative **6.29**, which showed activity up to 2 mM.

Derivative 6.32

The carboxylic acid derivative **6.32** based on the alcoholic natural product (**6.1c**) showed a higher phytotoxic activity (5 mM) than **6.1c**. Since compounds bearing a carboxylic acid moiety are more water soluble and enable salt formation - which would be of interest for a field application - further derivatives with an acid function are to be synthesized and tested.

6.3.2 Studies on structure-activity correlations

To confirm the first ideas that the bioactivity of the molecules is related to the lipophilicity and the size of the substituents, the following physiochemical parameters were investigated in more detail: molecular weight (M), partition coefficient log P, molecular refractivity (A), parachor (Pc), density (ρ), molecular volume (V_m).

Those parameters refer to the entire molecule and were calculated using various programs (see **Methodology**). All values are given in **Table 6-3**.

Table 6-3 Physiochemical descriptors of derivatives **6.1 - 6.32**.
Legend: n.a. – no value could be generated by Chemsketch.

No	Structural identifier		M [g/mol]	log P	A [cm³]	Pc [cm³]	ρ [g/cm³]	V_m [cm³/mol]
6.1	a	n = 2	201.24	0.53	48.3	408.6	1.306	154.0
	b	n = 3	215.27	0.85	53.1	448.7	1.262	170.5
	c	n = 4	229.29	1.16	57.9	488.8	1.225	187.0
	d	n = 5	243.32	1.52	62.7	528.9	1.195	203.5
	e	n = 6	257.35	1.81	67.5	568.9	1.169	220.0
	f	n = 7	271.38	2.19	72.3	609.0	1.147	236.5
	g	n = 8	285.39	2.54	77.2	649.1	1.127	253.0
	h	n = 9	299.43	2.91	82.0	689.2	1.110	269.5
	i	n = 10	313.46	3.27	86.8	729.2	1.095	286.0
	j	n = 11	327.48	3.66	91.6	769.3	1.082	302.6
	k	n = 12	341.51	4.02	96.4	n.a.	n.a.	n.a.
6.2	a	n = 2	231.27	0.51	54.8	467.2	1.298	178.0
	b	n = 3	245.30	0.84	59.6	507.3	1.260	194.5
	c	n = 4	259.32	1.19	64.4	547.4	1.228	211.0
	d	n = 5	273.35	1.51	69.2	587.5	1.201	227.5
	e	n = 6	287.38	1.85	74.0	627.5	1.177	244.0
6.3	a	n = 2	219.23	0.78	48.3	416.0	1.385	158.2
	b	n = 3	233.26	1.19	53.1	456.1	1.334	174.7
	c	n = 4	247.29	1.48	57.9	496.1	1.292	191.2
	d	n = 5	261.31	1.78	62.7	536.2	1.257	207.7
	e	n = 6	275.34	2.25	67.5	576.3	1.227	224.2
6.4	a	n = 2	215.27	0.86	53.3	446.9	1.263	170.3
	b	n = 3	229.29	1.20	58.1	487.0	1.227	186.8
	c	n = 4	243.32	1.52	62.9	527.1	1.196	203.3
	d	n = 5	257.35	1.82	67.7	567.1	1.170	219.8
	e	n = 6	271.38	2.18	72.5	607.2	1.148	236.3
	f	n = 7	285.39	2.54	77.3	647.3	1.128	252.8
	g	n = 8	299.43	2.91	82.1	687.4	1.111	269.3

No	Structural identifier		M [g/mol]	log P	A [cm³]	Pc [cm³]	ρ [g/cm³]	V_m [cm³/mol]
	a	n = 2	215.27	0.88	53.3	446.9	1.263	170.3
	b	n = 3	229.29	1.17	58.1	487.0	1.227	186.8
	c	n = 4	243.32	1.50	62.9	527.1	1.196	203.3
6.5	d	n = 5	257.35	1.95	67.7	567.1	1.170	219.8
	e	n = 6	271.38	2.16	72.5	607.2	1.148	236.3
	f	n = 7	285.39	2.54	77.3	647.3	1.128	252.8
	g	n = 8	299.43	2.90	82.1	687.4	1.111	269.3
	a	n = 2	215.27	0.86	53.3	446.9	1.263	170.3
	b	n = 3	229.29	1.18	58.1	487.0	1.227	186.8
	c	n = 4	243.32	1.50	62.9	527.1	1.196	203.3
6.6	d	n = 5	257.35	1.83	67.7	567.1	1.170	219.8
	e	n = 6	271.38	2.17	72.5	607.2	1.148	236.3
	f	n = 7	285.39	2.55	77.3	647.3	1.128	252.8
	g	n = 8	299.43	2.78	82.1	687.4	1.111	269.3
6.7	a	n = 7	313.46	3.16	86.9	725.4	1.093	286.6
	b	n = 8	327.48	3.54	91.7	765.5	1.080	303.1
	a	n = 2	243.32	1.56	62.9	525.0	1.192	204.1
	b	n = 3	257.35	1.83	67.7	565.1	1.166	220.6
	c	n = 4	271.38	2.21	72.5	605.2	1.144	237.1
6.8	d	n = 5	285.40	2.53	77.3	645.2	1.125	253.6
	e	n = 6	299.43	2.85	82.1	685.3	1.108	270.1
	f	n = 7	313.46	3.20	86.9	725.4	1.093	286.6
	g	n = 8	327.48	3.52	91.7	765.5	1.080	303.1
	a	n = 2	243.32	1.49	62.9	525.0	1.192	204.1
	b	n = 3	257.35	1.80	67.7	565.1	1.166	220.6
	c	n = 4	271.38	2.16	72.5	605.2	1.144	237.1
6.9	d	n = 5	285.40	2.48	77.3	645.2	1.125	253.6
	e	n = 6	299.43	2.80	82.1	685.3	1.108	270.1
	f	n = 7	313.46	3.13	86.9	725.4	1.093	286.6
	g	n = 8	327.48	3.54	91.7	765.5	1.080	303.1
	a	n = 5	299.43	2.74	82.0	683.6	1.107	270.2
6.10	b	n = 6	313.46	3.06	86.8	723.7	1.093	286.7
	c	n = 7	327.48	3.47	91.6	763.8	1.079	303.2
	a	n = 2	257.35	1.76	67.6	563.4	1.165	220.7
	b	n = 3	271.38	2.08	72.4	603.5	1.143	237.2
	c	n = 4	285.40	2.42	77.2	643.5	1.124	253.7
6.11	d	n = 5	299.43	2.68	82.0	683.6	1.107	270.2
	e	n = 6	313.46	3.02	86.8	723.7	1.093	286.7
	f	n = 7	327.48	3.29	91.6	763.8	1.079	303.2
	g	n = 8	341.51	3.84	96.4	803.8	1.067	319.7
	a	n = 2	257.35	1.76	67.6	563.4	1.165	220.7
	b	n = 3	271.38	2.15	72.4	603.5	1.143	237.2
	c	n = 4	285.40	2.41	77.2	643.5	1.124	253.7
	d	n = 5	299.43	2.75	82.0	683.6	1.107	270.2
6.12	e	n = 6	313.46	2.98	86.8	723.7	1.093	286.7
	f	n = 7	327.48	3.44	91.6	763.8	1.079	303.2
	g	n = 8	341.51	3.74	96.4	803.8	1.067	319.7
	h	n = 9	355.54	4.14	101.2	843.9	1.057	336.2
	i	n = 10	369.56	4.52	106.0	884.0	1.047	352.7

No	Structural identifier		M [g/mol]	log P	A [cm³]	Pc [cm³]	ρ [g/cm³]	V_m [cm³/mol]
6.13	**a**	n = 2	283.39	2.34	75.2	615.8	1.204	235.2
	b	n = 3	297.41	2.57	80.0	655.8	1.181	251.7
	c	n = 4	311.44	2.90	84.8	695.9	1.160	268.2
	d	n = 5	325.47	3.25	89.6	736.0	1.142	284.7
	e	n = 6	339.49	3.58	94.4	776.1	1.126	301.2
	f	n = 7	353.52	3.92	99.2	816.1	1.112	317.7
	g	n = 8	367.55	4.26	104.0	856.2	1.099	334.2
	h	n = 9	381.57	4.64	108.8	896.3	1.087	350.7
	i	n = 10	395.60	4.95	113.7	936.4	1.077	367.2
6.14	**a**	n = 8	419.62	4.60	119.0	949.4	1.142	367.2
	b	n = 9	433.65	5.07	123.8	989.4	1.129	383.7
	c	n = 10	447.67	5.46	128.7	1029.5	1.118	400.2
6.15	**a**	n = 2	202.23	-0.24	46.1	404.2	1.373	147.2
	b	n = 3	216.26	0.10	50.9	444.3	1.320	163.7
	c	n = 4	230.28	0.43	55.7	484.3	1.277	180.2
	d	n = 5	244.31	0.75	60.5	524.4	1.241	196.7
	e	n = 6	258.34	1.03	65.3	564.5	1.211	213.4
	f	n = 7	272.36	1.40	70.1	604.6	1.185	229.7
	g	n = 8	286.39	1.76	74.9	644.6	1.162	246.3
6.16	**a**	n = 2	165.21	-0.30	37.0	323.5	1.39	118.7
	b	n = 3	179.24	0.01	41.8	363.6	1.32	135.3
	c	n = 4	193.26	0.28	46.6	403.6	1.27	151.7
	d	n = 5	207.29	0.62	51.4	443.7	1.23	168.2
	e	n = 6	221.32	0.97	56.2	483.8	1.19	184.6
	f	n = 7	235.34	1.32	61.0	523.9	1.17	200.9
	g	n = 8	249.37	1.72	65.8	563.9	1.14	217.3
6.17	**a**	n = 2	227.28	0.93	59.1	477.8	1.304	174.2
	b	n = 3	241.31	1.27	63.9	517.6	1.264	190.7
	c	n = 4	255.33	1.54	68.7	557.4	1.231	207.2
	d	n = 5	269.36	1.94	73.5	597.2	1.203	223.7
	e	n = 6	283.39	2.26	78.3	637.0	1.179	240.2
	f	n = 7	297.41	2.59	83.1	676.8	1.158	256.8
	g	n = 8	311.44	2.92	87.9	716.6	1.139	273.3
6.18	**a**	n = 5	181.25	0.13	43.9	398.7	1.169	154.9
	b	n = 8	223.33	1.24	58.3	518.0	1.092	204.4
6.19	**a**	n = 5	259.34	0.45	57.6	524.6	1.288	201.3
	b	n = 8	301.42	1.47	71.4	644.0	1.201	250.8
6.20	-	-	215.27	0.81	53.1	446.7	1.259	170.9
6.21	-	-	215.27	0.84	53.1	446.7	1.259	170.9
6.22	-	-	257.35	1.68	67.5	564.8	1.165	220.8
6.23	-	-	257.35	1.83	67.5	564.8	1.165	220.8
6.24	-	-	241.31	1.15	64.6	495.4	1.300	185.6
6.25	-	-	241.31	1.13	64.6	495.4	1.300	185.6
6.26	-	-	243.32	1.48	62.7	524.8	1.190	204.3
6.27	-	-	243.32	1.50	62.7	524.8	1.190	204.3
6.28	-	-	257.35	1.76	67.5	564.8	1.165	220.8
6.29	-	-	323.43	1.94	85.2	620.5	1.257	231.6
6.30	-	-	330.40	2.24	89.5	686.8	1.353	244.0
6.31	-	-	330.40	2.18	89.5	686.8	1.353	244.0
6.32	-	-	243.28	0.96	58.5	439.9	1.320	184.1

To recognize correlations between a physiochemical parameter and the phytotoxic activity, all observed bioactivity rates of the tested sulfonamide derivatives **6.1** – **6.32** were plotted against the corresponding values of the given parameters – molecular weight (M), partition coefficient log P, molecular refractivity (A), parachor (P_c), density (ρ) and molecular volume (V_m). In **Figure 6-2** each dot (•) represents one tested compound. The phytotoxic activity was expressed in levels: no phytotoxic activity (0), 1 represents activity at 5 mM, 2 activity at 2 mM, 3 activity at 1 mM, and 4 activity at 0.4 mM. If not all four replicates, but at least two replicates, show no more DF, the phytotoxic activity was assigned as "(+)" in **Table 6-1** and intermediate steps were used, e.g. if a compound was assigned with "(+)" at a concentration of 1 mM it was plotted as 2.5 (higher activity than 2 but lower than 3).

A = phytotoxic activity plotted against molecular weight M
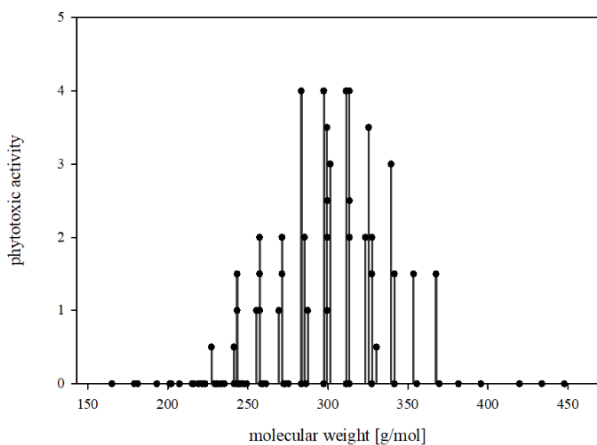
B = phytotoxic activity plotted against partition coefficient log P
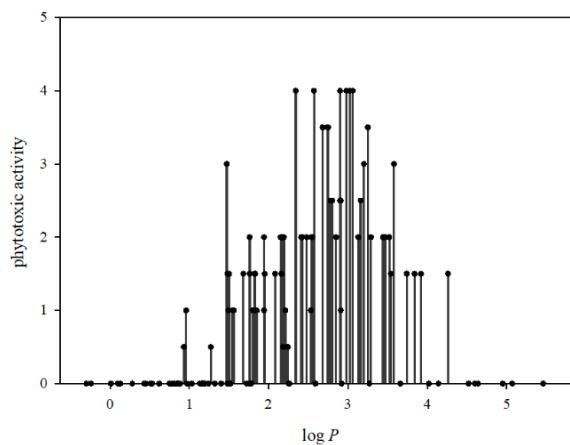
C = phytotoxic activity plotted against molecular refractivity A
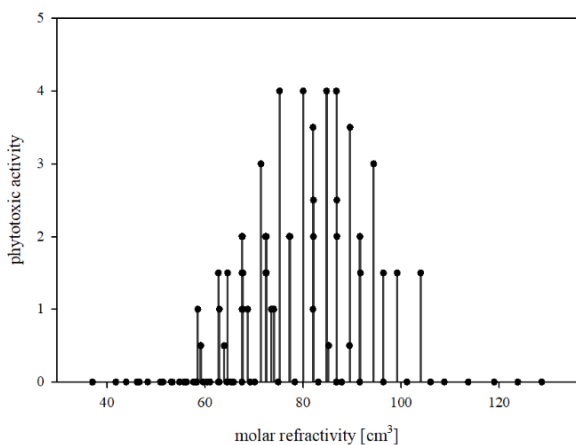
D = phytotoxic activity plotted against parachor P_c
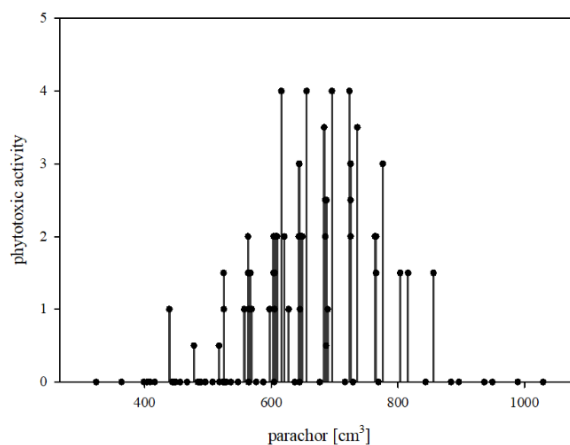
E = phytotoxic activity plotted against density ρ **F** = phytotoxic activity plotted against molar volume V_m
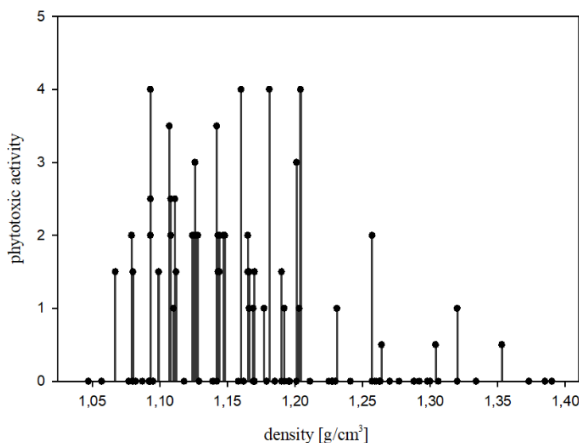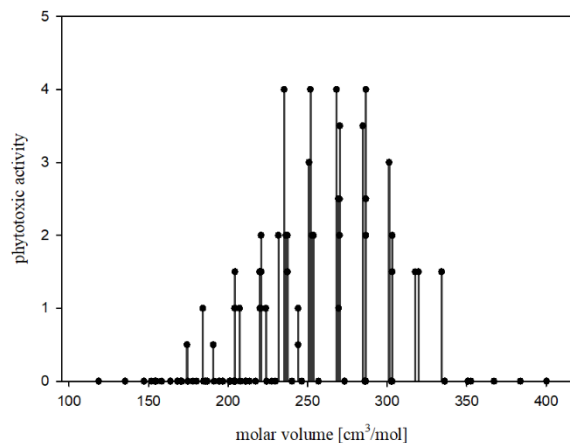
Figure 6-2 Phytotoxic activity of all tested 127 substances **6.1** – **6.32** plotted against **A**: molecular weight (*M*), **B**: partition coefficient log *P*, **C**: molecular refractivity (*A*), **D**: parachor (*Pc*), **E**: density (ρ), **F**: molar volume (V_m); each dot (•) represents one substance; phytotoxic activity, where 0 = no activity, 1 = 5 mM, 2 = 2 mM, 3 = 1 mM, 4 = 0.4 mM; when not all four replicates (but at least two replicates) showed no more DF, activity was assigned as "(+)" in **Table 6-1**. Here steps of 0.5 were used, e.g. if a compound was assigned with "(+)" at a concentration of 1 mM it was plotted as 2.5 (higher activity than 2 but lower than 3).

The plot of bioactivity of the sulfonamide derivatives against the various parameters (**Figure 6-2**) show a correlation for five out of selected six parameters with the bioactivity, which can be described by a Gaussian-like distribution. Only for the parameter "density(ρ)" no correlation could be determined. At the same time, however, the data also show that several variables are responsible for the observed bioactivity. For example, from **Figure 6-2**-**B**, it can be concluded that different sulfonamide derivatives with the same log *P* value nevertheless exhibit different levels of bioactivity.

In a following step, two selected parameters of the sulfonamide derivatives were plotted against each other (**Figure 6-3**). The bioactivity - represented by the coloration in **Figure 6-3** - was considered as a third parameter. If a cluster is formed between the parameters taken in account, these parameters are significant for the phytotoxic activity. The plot of molecular volume (V_m), molar refractivity (*A*) and parachor (*Pc*) against partition coefficient log *P* (**Figure 6-3A**) showed a linear dependence, so that an independent consideration of these parameters is not possible. Moreover, no linear relationship exists between molecular weight (*M*) and partition coefficient log *P* (**Figure 6-3B**). Furthermore, clustering was observed depending on the level of phytotoxic activity.

A= molar refractivity (*A*), parachor (*P$_c$*) and molar volume (*V$_m$*) plotted against partition coefficient log *P*

B= molecular weight (*M*) plotted against partition coefficient log *P*
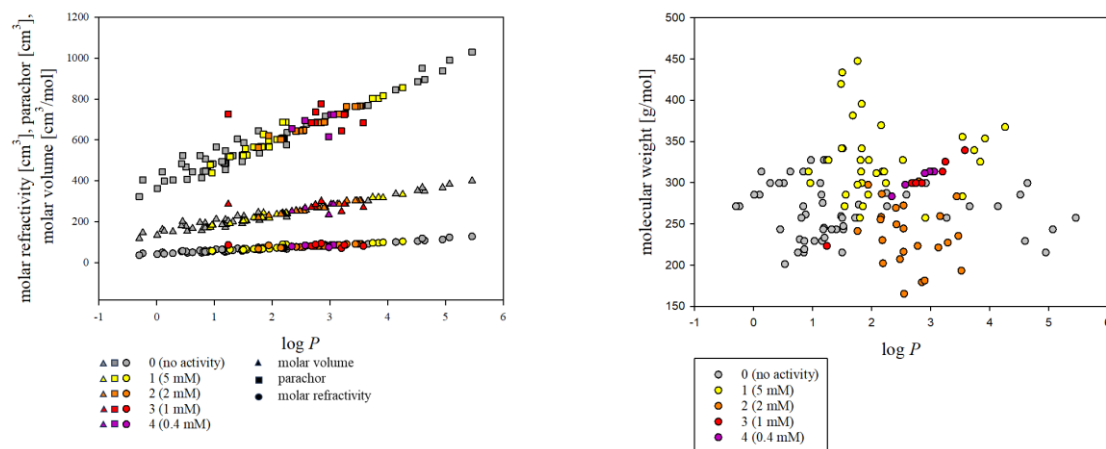
Figure 6-3 A: Plot of molar refractivity (*A*), parachor (*P$_c$*) and molar volume (*V$_m$*) plotted against partition coefficient log *P*, phytotoxic activity indicated by coloration, where grey = no activity (0), yellow = 5 mM (1), orange = 2 mM (2), red = 1 mM (3), purple = 0.4 mM (4); **B**: Plot of molecular weight (*M*) against partition coefficient log *P*, phytotoxic activity indicated by coloration where grey = no activity (0), yellow = 5 mM (1), orange = 2 mM (2), red = 1 mM (3), purple = 0.4 mM (4).
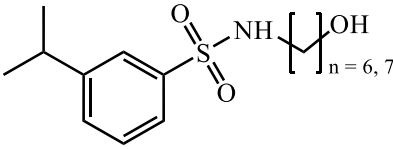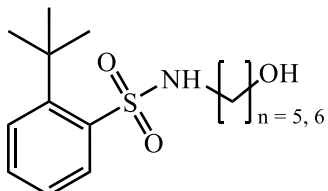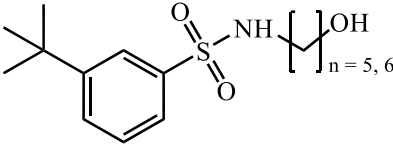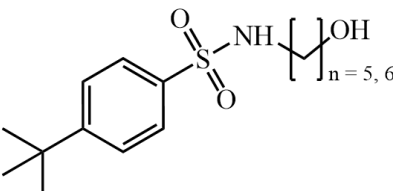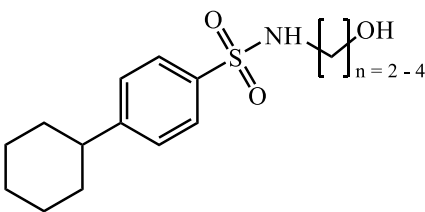
To proof this observation, the mean, the median and the 25% and 75% quartiles of four activity intervals (I1= no activity, I2 = 5 mM, I3 = 2 mM and I4 = 0.4 − 1 mM) were calculated for the partition coefficient log *P* and molecular weight (*M*) (**Table 6-4**). Sulfonamide derivatives showing the highest phytotoxic activity between 0.4 mM and 1 mM were combined in interval I4.

Table 6-4 Median and quartiles (25 and 75%) of partition coefficient log *P* and molecular weight (*M*).

Phytotoxic activity	I1 (no activity)	I2 (5 mM)	I3 (2 mM)	I4 (0.4 – 1mM)
median (log *P*)	1.19	1.83	2.54	2.88
25% quartile (log *P*)	0.83	1.68	2.19	2.70
75% quartile (log *P*)	1.77	2.24	2.91	3.03
mean	1.18	2.17	2.65	2.80
median (M)	261.3	325.5	241.3	305.4
25% quartile (M)	243.3	299.4	216.3	299.4
75% quartile (M)	286.4	353.5	269.4	313.5
mean	266.0	328.9	240.5	302.3

The highest phytotoxic activity (I4) of the sulfonamide derivatives **6.1** – **6.32** was mainly observed for compounds with a partition coefficient log *P* between 2.88 and 3.03 and a molecular weight (*M*) between 299.4 and 313.5 g/mol. Comparison of the derivatives in activity interval I3 with those in interval I4 shows that the median of the molecular weight (*M*) and partition coefficient (log *P*) are significantly lower (241.3 vs. 305.4 and 2.54 vs. 2.88). In activity interval I2, the molecular weight range of the sulfonamide derivatives **6.1** – **6.32** is comparable to that of activity interval I4, but the partition coefficient (log *P*) is significantly lower. However, the derivatives in activity interval I2 exhibit only moderate phytotoxic activity, which demonstrate the importance of a certain degree of lipophilicity for the phytotoxic activity.

Table 6-5 Sulfonamide derivatives with the highest phytotoxic activity. Phytotoxic activity (based on DF), where 0 = no activity, 1 = activity at 5 mM, 2 = activity at 2 mM, 1 = activity at 1 mM, 4 = activity at 0.4 mM and intermediate steps (0.5) when not all four but at least two replicates showed no more DF.

No	sturucture + identifier			M [g/mol]	log P	phytotoxic activity
6.8		e	n = 6	299.43	2.85	3
		f	n = 7	313.46	3.20	3
6.10		a	n = 5	299.43	2.74	3.5
		b	n = 6	313.46	3.06	4
6.11		d	n = 5	299.43	2.68	3.5
		e	n = 6	313.46	3.02	4
6.12		d	n = 5	299.43	2.75	3.5
		e	n = 6	313.46	2.98	4
6.13		a	n = 2	283.39	2.34	4
		b	n = 3	297.41	2.57	4
		c	n = 4	311.44	2.90	4
		d	n = 5	325.47	3.25	3.5
		e	n = 6	339.49	3.58	3

On closer analysis of **Table 6-5** with the most active compounds shows that molecular weight (*M*) and partition coefficient log *P* are not the only variables required for the phytotoxic activity. For example, compounds **6.10b** and **6.13a** exhibit strong phytotoxic activity up to 0.4 mM (I4). But the partition coefficient (log *P)* and molecular weights (*M*) of the two compounds differ significantly (**6.10b**: 3.06 vs. **6.13a**: 2.34 and **6.10b**: 313.5 vs. **6.13a**: 289.4 g/mol). The partition coefficient (log *P*) of compound **6.13a** is also significantly lower than the median of the activity intervals I3 and I4 (**Table 6-4**), in other words, such a high level of phytotoxic activity would not have been expected if these two parameters (*M,* log *P*) had been the only ones to be taken into account.

Therefore, the steric effects of the substituents at the benzene moiety and the hydrophobicity parameter of the substituents (Hansch π) itself are also considered in the following

Table 6-6. The Taft (*E$_s$*) and Charton (*v*) steric parameters were taken from Sigman and co-workers. [20] Hansch (π) parameters were calculated with the web tool "Calcuation of Substituent Properties v2024.02". [24]

Table 6-6 Taft (*E$_s$*) and Charton (*v*) steric- and Hansch (π) hydrophobicity parameter.

substituent	Taft (*E$_s$*)	Charton (*v*)	Hansch (π)
-H	-1.24	0	0.174
-Me	0	0.52	0.256
-*i*Pr	0.47	0.76	0.995
-cyclohexane	0.79	0.87	2.162
-*t*Bu	1.54	1.24	1.442
-adamantyl	-	1.33	3.180

Steric effects of the substituents at the benzene sulfonamide moiety seem to be essential for the observed phytotoxic activity of the tested compounds **6.1** – **6.32** and can explain the observed increase in activity in the series: -Me (**6.4 – 6.6**) < -*i*Pr (**6.7 – 6.9**) < -*t*Bu (**6.10 – 6.12**) = cyclohexane (**6.13**). However, the Taft (*E$_s$*) and Charton (*v*) parameter cannot explain the equal activity of the *tert*-butyl (**6.10** – **6.12**) and cyclohexane (**6.13**) derivatives, as the *tert*-butyl substituents have significantly higher steric effects. On the other hand, the cyclohexane substituent at the benzene sulfonamide has a much higher hydrophobic character, which is expressed by a higher Hansch (π) parameter. This might also be relevant for the activity. All these is speculative. Further computer-aided quantitative structure-activity relationships (QSAR) are required to gain more precise insights into the influencing factors for the observed phytotoxic activities and to summarize all individual factors in a comprehensive model. For this purpose, the Hansch equation is often used, which relates biological activity to hydrophobic, steric and electronics parameters. In this context, additional attention should be given to the Hammet parameters, which consider the electronic effects of the substituents. [23; 26; 27] In addition, molecular docking studies can provide further insight into compound requirements by revealing the interactions between the compound and the target enzyme. [28; 29]

6.4   Conclusion

Starting with the natural product *N*-(4-hydroxybutyl)benzenesulfonamide (**6.1c**), a total of 127 sulfonamide derivatives were tested for their phytotoxic activity in a non-destructive leaf-disk assay on *A. thaliana* Col-0 (and *S. cereale,* data not shown). The compounds showed almost identically activity in species representing both plant classes of Dicotyledons and Monocotyledons, so only the *A. thaliana* Col-0 test results were considered. Increasing activity was observed for the following substituents series: -F (**6.2**) < -

OMe (**6.3**) < -Me (**6.4 – 6.6**) < -*i*Pr (**6.7 – 6.9**) < -*t*Bu (**6.10 – 6.12**) = -cyclohexane (**6.13**) > -adamantane (**6.14**). By analyzing the phytotoxic activity in correlation to the different physiochemical parameters, the partition coefficient log P and the molecular weight (M) were identified influencing the phytotoxic activity. On average, the highest activity was obtained from compounds with a molecular weight of 305.4 g/mol and a log P = 2.80. In addition, sterically hindering substituents were found to increase the activity. The best results were obtained for *tert*-butyl (**6.10 – 6.12**) and cyclohexane (**6.13**) substituents at the benzene sulfonamide moiety. However, it was not possible, to fully explain the relationship between observed phytotoxic activity and the chemical structure on the basis of the molecular weight (M), partition coefficient log P and steric parameters (E_s, v). Further computational work is necessary to determine all parameters that have an influence on the phytotoxic activity. Moreover, by derivatization of the natural product *N*-(4-hydroxybutyl)benzenesulfonamide (**6.1c**), it was also possible to increase the phytotoxic activity from 20 mM up to 0.4 mM (**6.10b**, **6.11-**, **6.12e** and **6.13-a-e**) in the non-destructive leaf disk assay.

References

[1] Guha, R., On exploring structure activity relationships, *Methods Mol. Biol.* **2013**, *993*, 81-94, doi: 10.1007/978-1-62703-342-8_6.

[2] McKinney, J.D.; Richard, A.; Waller, C.; Newman, M.C.; Gerberick, F., The practive of structure activity relationships (SAR) in toxicology, *Toxicol. Sci.* **2000**, *56*, 8-17, doi: 10.1093/toxsci/56.1.8.

[3] Yadav, M., 2 D - QSAR studies on CYP26A1 inhibitory activity of 1-[benzofuran-2-yl-(4-alkyl/aryl-phenyl)-methyl]- 1 H-triazoles, *Bioinformation* **2011**, *7*, 388-392, doi: 10.6026/97320630007388.

[4] Roy, K.; Kar, S.; Das, R.N., QSAR/QSPR Modeling: Introduction, Roy, K.; Kar, S.; Das, R.N. (Eds.), *A Primer on QSAR/QSPR Modeling*, Springer, Cham. **2015**, doi: 10.1007/978-3-319-17281-1_1.

[5] Swiss Institute of Bioinformatics, SwissADME, www.swissadme.ch, last access: 27.03.2024

[6] Chemsketch version 2018.2.5, ACD/Labs, Canada.

[7] Cheng, T.; Zhao, Y.; Li, X.; Lin, F.; Xu, Y.; Zhang, X.; Li, Y.; Wang, R; Lai, L., Computation of octanol−water partition coefficients by guiding an additive model with knowledge, *J. Chem. Inf. Model.* **2007**, *47*, 2140-2148, doi: 10.1021/ci700257y.

[8] Wildmann, S.A.; Crippen, G., Prediction of physiocochemical parameters by atomic contributions, *J. Chem. Inf. Compout. Sci.* **1999**, *39*, 868-873, doi: 10.1021/ci9903071.

[9] Moriguchi, I.; Hirono, S.; Liu, Q.; Nakagome, I.; Matsushita, Y., Simple method of calculating octanol/water partition coefficient, *Chem. Pharm. Bull.* **1992***, 40*, 127-139, doi: 10.1248/CPB.40.127.

[10] Moriguchi, I.; Hirono, S.; Liu, Q.; Nakagome, I.; Hirano, H., Comparison of reliability of log *P* values for drugs calculated by several methods, *Chem. Pharm. Bull.* **1994**, *42*, 976-978, doi: 10.1248/CPB.42.976.

[11] Silicos-IT, Silicos-it.be.s3-website-eu-west-1.amazonaws.com.

[12] Daina, A.; Michielin, O.; Zoete, V., iLOGP: A simple, robust, and efficient description of n-octanol/water partition coefficient for drug design using the GB/SA approach, *J. Chem. Inf. Model.* **2014**, 54, 3284-3301, doi: 10.1021/ci500467k.

[13] Padrón, J.A.; Carrasco, R.; Pellón, R.F, Molecular descriptor based on a molar refractivity partition using Randic-type graph-theoretical invariant, *J. Pharm. Pharmaceut. Sci.* **2002**, *5*, 258-265, https://sites.ualberta.ca/~csps/JPPS5(3)/R.Carrasco/molecular.htm.

[14] Berinde, Z.M., QSPR models for the molar refraction, polarizability and refractive index of aliphatic carboxylic acids using the ZEP topological index, *Symmetry* **2021**, *13*, 2359. doi: 10.3390/sym13122359.

[15] Sugden, S., A relation between surface tension, density, and chemical composition, *J. Chem. Soc., Trans.* **1924**, *125*, 1177-1189, doi: 10.1039/CT9242501177.

[16] Ahmad, P.; Fyfe, C.A.; Mellors, A., Parachors in drug design, *Biochem. Pharamcol.* **1975**, *24*, 1103-1109, doi: 10.1016/0006-2952(75)90198-7.

[17] Van Krevelen, D.W., Te Nijenhuis, K., Interfacial energy properties, Van Krevelen, D.W., Te Nijenhuis, K. (eds.) *Properties of Polymers* (Fourth Edition), Elsevier, **2009**, 229-244, doi: 10.1016/B978-0-08-054819-7.00008-X.

[18] Taft Jr, R.W.., Linear free energy relationsships from rates of esterification and hydrolysis of aliphatic and ortho-substituted benzoate esters, *J. Am. Chem. Soc,* **1952**, *74*, 2729-2732, doi:10.10211/ja01131a010.

[19] Taft Jr., R.W., Linear steric energy relationships, *J. Am. Chem. Soc.*, **1953**, *75*, 4538-4539, doi: 10.1021/ja01114a044.

[20] Sigman, M.S.; Miller, J.J., Examination of the role of Taft-type steric parameters in asymmetric catalysis, *J. Org. Chem.* **2009**, *74*, 7633-7643, doi: 10.1021/jo901698t.

[21] Charton, M., The nature of the ortho effect. II. Composition of the Taft steric parameter, *J. Am. Chem. Soc.* **1969**, *91*, 615–618, doi: 10.1021/ja01031a016.

[22] Hansch, C.; Fujita, T., p-σ-π Analysis. A method for the correlation of biological activity and chemical structure, *J. Am. Chem. Soc.* **1964**, *86*, 1616-1626, doi: 10.1021/ja01062a035.

[23] Jhanwar, B.; Sharma, V.; Singla, R. K.; Shrivastava, B., QSAR-Hansch analysis and related approaches in drug design, *Pharmacologyonline* **2011**, Newsletter, 1, 306-344, https://pharmacologyonline.silae.it/files/newsletter/2011/vol1/030.singla.pdf.

[24] Ertl, P., A web tool for calculating substituent descriptors compatible with Hammett Sigma constants, *Chemistry-Methods* **2022**, *2*, 12, doi: 10.1002/cmtd.202200041.

[25] Wu, C.; Varanasi, V.; Perez-Jones, A., A nondestructive leaf-disk assay for rapid diagnosis of weed resistance to multiples herbicides, *Weed Sci.* **2021**, *69*, 274-283, doi: 10.1017/wsc.2021.15.

[26] Hansch, C., A quantitative approach to biochemical structure-activity relationships, *Acc. Chem. Res.* **1969**, *2*, 232-239, doi: 10.1021/ar50020a002.

[27] Hansch, C.; Hoekman, D.; Gao, H., Comparative QSAR: Toward a deeper understanding of chemicobiological

interactions, *Chem. Rev.* **1996**, *96*, 1045-1076, doi: 10.1021/cr9400976.

[28] Hawkins, P.C.D.; Skillman, A. G.; Nicholls, A., Comparison of shape-matching and docking as virtual screening tools, *J. Med. Chem.* **2007**, *50*, 74-82, doi: 10.1021/jm0603365.

[29] Lill, M.A.; Danielson, M.L., Computer-aided drug design platform using PyMOL, *J. Comput. Aided Mol. Des.* **2011**, *25*, 13-19, doi: 10.1007/s10822-010-9395.8.

7   LC-HR-ESI-MS based comparison of extracts of *Colletotrichum graminicola* grown in different cultivation media

Abstract

Colletotrichum graminicola was grown in five different cultivation media, including three minimal media and two complete media (CM, HMG). The extracts obtained were compared in terms of their yield, phytotoxicity and metabolite profiles using TLC and LC-HR-ESI-MS measurements. Fungal cultivation in the minimal media resulted in significantly lower yields compared to the full media, with approximately 1 g of mycelium being obtained from one culture containing 200 mL liquid culture medium. The crude extracts of fungi grown in minimal media showed significantly higher effects in a leaf-spot assay on *Arabidopsis thaliana* Col-0. Formation of necrosis was observed for 20 µg crude extract per application spot, whereas crude extracts of fungi grown in complete media caused only weak necrosis even at 50 µg per spot.

TLC and LC-HR-ESI-MS measurements were used to study the chemical variances of the metabolite profiles. Based on the mass spectrometrical data PLS-DA were performed to identify major changes in secondary metabolite pattern.

7.1 Introduction

Secondary metabolites have a broad spectrum of biological activities and are therefore of high interest for the development of new drugs, agrochemicals, etc. [1–4] Fungi have the potential to produce several metabolites from one single strain, however many of them are not characterized as they contain silent gene clusters, which are not expressed under standard laboratory conditions. The OSMAC approach ("one strain – many compounds") is a cultivation-based approach to activate hidden metabolic pathways. [5–7] Numerous parameters such as ingredients in cultivation medium, pH, temperature, light, and stress influence on the production of secondary metabolites. [1; 8–11]

In general, cultivation media can be divided into minimal and complete media based on their nutrient content. Minimal media only contain the minimum amount of nutrients required for growth of the strain. Complete media, on the other hand, contain complex components such as yeast extract, casein hydrolysate or malt extract. These components provide additional vitamins, growth factors and trace elements, which results in higher growth rates. [11–13]

Aim of this study was to investigate the influence of the media on the profile of secondary metabolites produced by *C. graminicola*, also with respect to the phytotoxicity of the obtained crude extracts.

7.2 Experimental

7.2.1 General

7.2.2 Cultivation

Colletotrichum graminicola (strain M1.001, provided by Prof. Dr. Deising, Institute of Agricultural and Nutritional Sciences, Martin-Luther University Halle-Wittenberg) was cultivated in five different media (**Table 7-1**). Three replicates were prepared for each medium. Erlenmeyer flasks (1 L) with 200 ml medium each were inoculated with two 1 cm^2 mycelium plugs and incubated at 23°C for 13 days without agitation.

Table 7-1 Composition of media 1 - 5.

No	Name	Ingredients per L
1	+N, +Glc	10 mL stock solution A, 10 mL stock solution B, 10 g glucose
2	+N, -Glc	10 mL stock solution A, 10 mL stock solution B
3	-N, +Glc	10 mL stock solution B, 10 g glucose
4	CM	10 g glucose, 1 g $Ca(NO_3)_2$, 1 g yeast extract, 1 g casein hydrolysate, 0.2 g KH_2PO_4, 0.25 g $MgSO_4$, 0.05 g NaCl
5	HMG	10 g glucose, 10 g malt extract, 4 g yeast extract

Stock solution A: 50 g $Ca(NO_3)_2$
                     ad 500 ml aqua dest.

Stock solution B: 10 g KH_2PO_4
                     12.5 g $MgSO_4$
                     2.7 g NaCl
                     ad 500 mL

7.2.3 Sample preparation

Mycelium

The mycelia were separated by filtration from the culture filtrate and immediately frozen at -20°C. After lyophilization (72 h) and weighing, three stainless steel balls (5 mm) were added and all samples were powdered using a ball mill (Retsch, Germany). The samples were grinded four times for 30 s with 30 Hz. A break of 15 s in between avoided heating of the samples.

For the production of a representative quality control sample (QC), fungal material of all cultures was mixed in equal parts. The QC samples was extracted as described in 7.2.6.

Culture filtrate

The culture filtrates were evaporated *in vacuo* to dryness and immediately frozen at -20°C. Prior to the LC-HRESIMS measurement, a SPE (1mL, C18ec, Machery Nagel, Germany) was carried out to enrich the methanol-soluble secondary metabolites and to remove sugars, proteins, etc.. The cartridges were activated with methanol and rinsed with 3.0 mL water. The dried samples were dissolved in 4.0 mL water in ultrasonic bath for 3 minutes and subsequently centrifuged for 5 min at 14.000 rpm (Eppendorf, Germany) to separate the insoluble residue. The supernatant was applied on the activated SPE cartridge and washed with 3.0 mL H_2O. The eluate was discarded. In parallel, the insoluble residues were extracted with 1.0 mL methanol. After mixing the samples for 30 s with a vortex an extraction in ultrasonic bath followed for 3 minutes. The samples were centrifuged for 5 minutes at 14.000 rpm to remove insoluble residues and the supernatant was applied to the SPE previously used. The SPE was rinsed with 3.0 mL methanol and the obtained eluates were evaporated to dryness.

7.2.4 Thin-layer chromatography (TLC)

From each cultivar, 50 mg powdered fungal material was mixed with 2 mL distilled methanol. After brief mixing on a vortex, samples were sonicated for 15 minutes, followed by centrifugation for 10 minutes at 14 000 rpm (Eppendorf, Germany). The supernatant was used for TLC analysis. From each sample, 10 µL extract was applied on pre-coated silica gel F_{254} aluminum sheets (0.063 – 0.200 mm, Merck, Germany). The analysis was performed with a mobile phase containing toluene : ethyl formate : formic acid (10:5:3, *v/v/v*). Documentation images were taken with CAMAG TLC visualizer (Camag, Switzerland) at daylight, λ = 254 nm, λ = 366 nm and after derivatization with spray reagent (vanillin-sulfuric acid).

7.2.5 Leaf-spot bioassay

A modified leaf-spot bioassay by Evidente et al. (1995) [14] was used to test the crude extracts for their phytotoxic activity. The samples were dissolved in methanol/ water (1:1, *v/v*) and droplets of 5 µL were placed on the leaf surface of undetached and fully expanded young leaves of *Arabidopsis thaliana* Col-0. Fractions were tested at concentrations of 4 – 10 µg/µL. Plants were incubated in the greenhouse (19 °C, day/night cycle) for 72 h. Paraquat (100 µM, dissolved in methanol/ water 1:1, *v/v*) was used as a positive control. The pure solvent mixture of methanol/water (1:1, *v/v*) served as the negative control. After 72 h the plants were observed for the formation of necrosis. Images were taken with CAMAG TLC visualizer (Muttenz, Switzerland). Only damage to the leaf in the form of chlorosis or necrosis was evaluated. The extent of the damage was not considered.

7.2.6 UHPLC-ESI-HRMS

For UHPLC-ESI-HRMS of the mycelium 20 mg of powdered fungal material was mixed with 1 mL LC-MS grade methanol (Honeywell, Riedel de Haën, Germany). After brief mixing for 30 s on a vortex, were sonicated for 15 minutes. Subsequently, the samples were centrifuged for 10 minutes at 14.000 rpm (Eppendorf, Germany). The supernatant was diluted to a final concentration of 15 mg extract per mL methanol and applied to UHPLC-ESI-HRMS. The injection volume was 2 µL.

For UHPLC-ESI-HRMS of the culture filtrates the samples were dissolved in LC-MS grade methanol (Honeywell, Riedel de Haën, Germany) : water (1:1, *v/v*) and the concentration was adjusted to 1 mg/ mL. For the production of a representative quality control sample (QC), 100 µL of each sample were combined.

The MS system was coupled to an ultra-high-performance liquid chromatography (UHPLC) system (Dionex UltiMate 3000, Thermo Scientific, Germany), fitted with a RP-C18 column (1,9 µm; 50 x 2.1 mm; column temperature: 40 °C). For UHPLC separation a water: acetonitrile gradient solvent system (each containing 0.1% formic acid) at a flow rate of 400 µl/min was applied (95:5 for 1 min, 10 min gradient to a ratio of 0:100, hold for 5 min, returning to 95:5 in 1 min, isocratic hold for 4 min).
Positive ion high-resolution ESI mass spectra were obtained from an Orbitrap Elite mass spectrometer (Thermofisher Scientific, Germany) equipped with a HESI electrospray ion source (spray voltage 4.0 kV; source heater temperature: 300 °C; capillary temperature 325 °C; FTMS resolution 15.000). Nitrogen was used as sheath and auxiliary gas. The CID mass spectra (buffer gas: helium) were recorded in data dependent acquisition mode (dda) using normalized collision energies (NCE) of 35%. The data were evaluated with the Xcalibur software 2.7 SP1 (Thermo Fisher, Germany).

7.2.7 Processing of the acquired LC-ESI-HRMS data

Data processing was performed using MS-Dial (Version 4.90) [15] and included (1) determination of monoisotopic mass. The mass of a peak was determined when at least two adduct ions matched the adduct dictionary, that was defined as: $[M+H]^+$, $[M+Na]^+$, $[M+K]^+$, $[M-H_2O+H]^+$, $[2M+H]^+$. (2) Peak list alignment. The MS tolerance was set as 0.01 Da, the minimum peak height was set as 1 x 10^4, and the maximum charge was set to 2. (3) Gap-filling. The statistical interpretation of the acquired data relied on Metaboanalyst 5.0 [16] The aligned data were uploaded to Metaboanalyst, normalized by sum and auto-scaled. The data where analyzed with partial-least-square discriminant analysis (PLS-DA).

7.3 Results and discussion

7.3.1 General observations

To investigate the influence of the medium on the secondary metabolism pattern of *C. graminicola*, the fungus was cultivated on five different media, each with three replicates. The media comprised three minimal media - including one with a nitrogen and carbon source (medium 1), one with a nitrogen source only (medium 2) and one with a carbon source (medium 3) only - as well as two full media (medium 4 and medium 5). The pH value of the media was not adjusted; the pH values of the individual media are given in **Table 7-2**. The extent to which differences in pH values influence the (secondary) metabolism cannot be assessed in this experiment. Overall, however, it is noticeable that the pH value of the minimum media 1 – 3 tested, with a pH value of approximately 5, is significantly more acidic than that of the full media 4 and 5, which have pH values between 6 and 6.5.

Table 7-2 pH values of media 1 - 5.

Medium	pH value
1	4.8
2	4.7
3	4.9
4	6.0
5	6.5

Figure 7-1 shows the optical differences between the media before (**A**) and after incubation (13 days) (**B**). Media 1 - 3 are clear, colorless liquids, medium 4 (CM) shows a slight yellow coloration and medium 5 (HMG) a strong yellow coloration. After incubation time (13 days), there are clear differences between all media. Particularly noticeable is culture filtrate 3, which shows a strong red coloration, while all others show a yellowish to slightly orange coloration in various intensities. Surprisingly, the red coloration of medium 3 is not stable. After 24 h, a color change of culture filtrate 3 from red to yellow can be observed.

A **B**

Figure 7-1 Optical comparison of the media (**A**) and the culture filtrate after 13 days of incubation (**B**).

In addition, the fungal mycelium was balanced after lyophilization (**Table 7-3**) As expected, the fungi cultivated in the complete media 4 and 5 (CM and HMG) had the highest weights. The weights differed by nearly one gram compared to the minimal media 1-3.

Table 7-3 Average balances of fungal mycelium grown in different media.

Medium	Average balance [g]
1	0.20
2	0.36
3	0.17
4	1.01
5	1.32

7.3.2 TLC

To get a first impression of the effects of the different growing conditions, a TLC of all 15 mycelial extracts was prepared (**Figure 7-2**). In daylight, the raw extracts show only a few faint yellowish and orange spots. Medium 3 also shows a striking purple spot (R_f = 0.53) associated with the red coloration of the extract, which is also faintly visible in medium 1. Observing the TLC at λ= 366 nm and after derivatization with vanillin-sulfuric acid, numerous spots are visible. At first glance, the chromatograms of the extracts do not seem to differ too much from each other. However, medium 3 shows some additional spots in comparison, especially at λ = 366 nm. Further characteristic differences are the spots at R_f = 0.3 in media 1, 2 and 5 at λ = 254 nm, which are barely visible in media 3 and 4, the spots at R_f = 0.17 (λ = 366 nm), which are mainly visible in full media 4 and 5, as well as the spots at R_f =0.38 (derivatized), which are most prominent in medium 5.
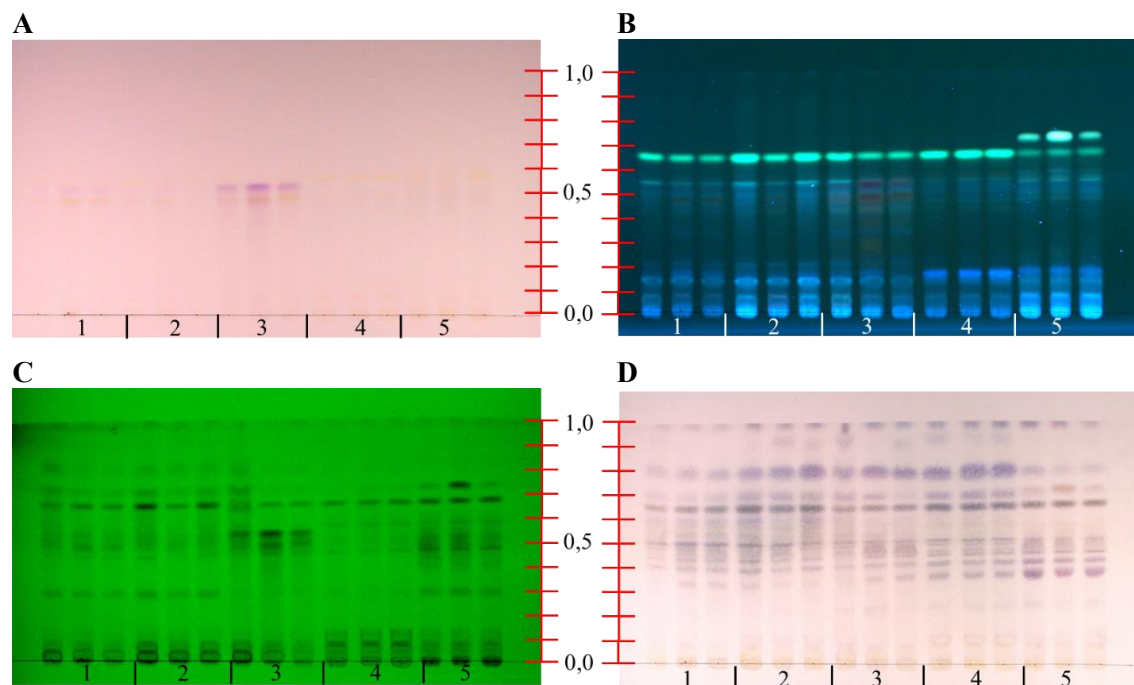
Figure 7-2 TLC of *C. graminicola* grown in five different media (1 - 5); **A**: daylight; **B**: λ= 366 nm; **C**: λ= 254 nm; **D**: daylight after derivatization with vanillin-sulfuric acid.

7.3.3 Phytotoxic activity

The phytotoxic activity of all crude extracts of the mycelia was evaluated using a modified leaf-spot assay [14] on *A. thaliana* Col-0 to determine possible differences in activity levels. The concentrations of 4 µg/µL (= 20 µg per spot) and 10 µg/µL (= 50 µg per spot) were chosen relatively low - especially in comparison to the tested concentrations of the isolated pure compounds (see chapter 3 – 5). For example, a test concentration of 20 mM at a molecular weight of 300 g/mol corresponds to an absolute amount of 30 µg per spot or 6 µg/µL. Moreover, out of 21 isolated compounds, only 9 showed activity at a concentration of 20 mM (see chapter 3 – 5).

Figure 7-3 shows the leaves of *A. thaliana* Col-0 after an incubation time of 72 h. In both concentrations tested, it is noticeable that the fungus cultivated in medium 1 causes the strongest necrosis. The fungus cultivated on the other minimal media (2 and 3) showed significantly weaker necrosis formation. The presence of both a nitrogen and a carbon source in medium 1 may be important for the formation of highly active phytotoxic metabolites, whereas a nitrogen and carbon deficiency in minimal media 2 und 3 leads to reduced phytotoxic activity. Further, the fungus cultivated in complete media 4 and 5 show only very weak activity. Even in the higher concentration of the applied extract, no necrosis is visible, only yellowing of the leaves. While a minimal medium only provides the essential nutrients, the complete medium often contains several nitrogen and carbon sources as well as numerous non-essential compounds that the organism can produce itself. The growth rates of the organism in the complete medium are therefore higher. [11;13] Kim and Kim showed for *Escherichia coli* and *Saccharomyces cerevisiae* that in the minimal medium energy-storing metabolites such as fatty acids, sugars and sugar alcohols were formed predominantly, while amino acids, essential for protein synthesis and rapid cell growth, were highly abundant in the complete medium. [11] The lower activity of extracts 4 and 5 can probably be explained by the lower proportion of phytotoxic substances in the total extract, which would be consistent with the significantly different yields of the extracts. However, it should be noted that in chapters 3 -5 the fungus

was cultivated on the complete media 4 and 5 (despite the lower phytotoxicity), because the yield from the cultures in minimal media were significantly lower.

A

B

Figure 7-3 Leaf-spot assay of crude extracts 1 – 5 from mycelium after 72 h of incubation; **A**: 20 µg per spot; **B**: 50 µg per spot.

LC-ESI-HRMS

LC-ESI-HRMS measurements were performed to gain further insight into the chemical composition of the fungal crude extracts 1 – 5. The high sensitivity enables the detection of compounds with low concentrations with respect to their ionization properties.

Mycelium

Figure 7-4 shows the chromatogram of the QC sample of the mycelium. Peaks (P_M) were tentatively assigned by their accurate mass and MS/MS fragmentation, also in comparison with the previously isolated compounds (Chapter 3 – 5). The results are listed in **Table 7-4**.
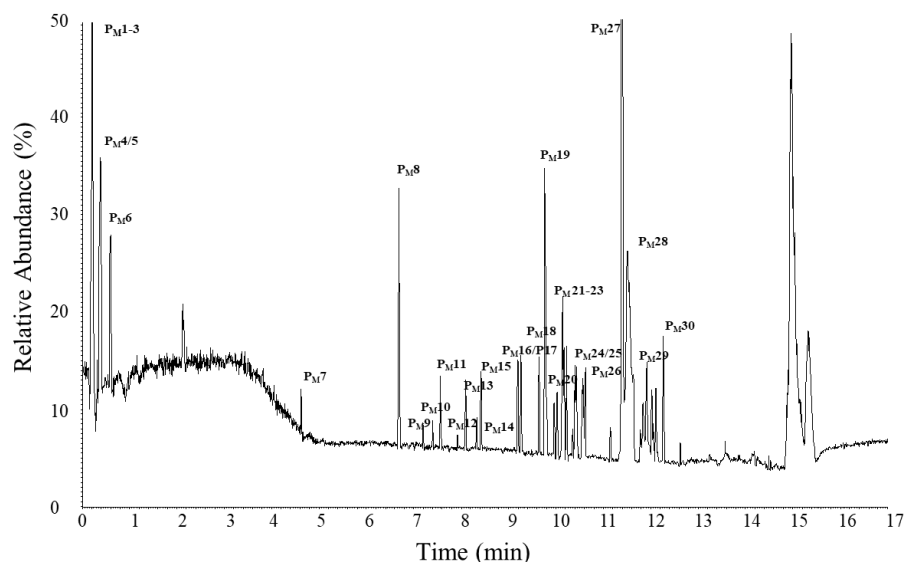
Figure 7-4 (+)-HR-ESI-MS chromatogram (base peak) of the QC sample of the mycelium.

Table 7-4 Peak table of compounds (P_M) annotated in the QC sample (mycelium) of *C. graminicola.*

No	$[M+H]^+$	Rt (min)	Molecular formula	Δ ppm	Fragments (Intensity)	Annotation/ Compound Class
P_M1	175.1189	0.17	$C_6H_{15}N_4O_2$	-0.235	158.0920 (100), 130.0972 (42), 116.0703 (64)	Arginine
P_M2	258.1095	0.20	$C_8H_{21}NO_6P$	-0.610	104.1067 (100)	Glycero-phosphocholine
P_M3	104.1069	0.22	$C_5H_{14}NO$	-1.351	87.0439 (100), 86.0599 (55)	Choline
P_M4	268.1037	0.33	$C_{10}H_{14}N_5O_4$	-1.351	136.0615 (100)	Adenosine
P_M5	132.1016	0.35	$C_6H_{14}NO_2$	-0.426	86.0961 (100)	(Iso-) Leucine
P_M6	166.0863	0.60	$C_9H_{14}NO_2$	-0.874	120.0805 (100)	Phenylalanine
P_M7	727.3866	4.63	$C_{28}H_{55}N_8O_{15}$	4.640	709.3757 (100), 691.3655 (62), 615.3341 (56), 597.3195 (90), 467.2492 (34), 355.1966 (59), 243.1322 (19)	Unknown
P_M8	270.2063	6.67	$C_{15}H_{28}NO_3$	-0.151	252.1954 (100), 234.1850 (68)	3-(6-hydroxy, 2,6-dimethyl-octanonyl)-5-methylpyrrolidin-2-one (**3.10**)
P_M9	285.0754	7.20	$C_{16}H_{13}O_5$	-3.222	267.0650 (59), 257.0807 (100), 239.0701 (36)	Unknown Anthraquinone
P_M10	195.1015	7.40	$C_{11}H_{15}O_3$	-0.512	163.0751 (28), 149.0958 (42), 135.0802 (43), 107.0852 (100)	Colletopyrone C [17]
P_M11	315.0862	7.56	$C_{17}H_{15}O_6$	-0.237	300.0624 (100), 282.0519 (94)	Colletoquinone A (**4.3**)
P_M12	365.0783	7.93	$C_{18}H_{18}O_6Cl$	-0.993	334.0600 (100)	Monorden [18]
P_M13	319.0363	8.10	$C_{16}H_{12}O_5Cl$	-1.654	301.0258 (100), 291.0415 (89), 273.0310 (45)	Unknown
P_M14	567.1276	8.32	$C_{29}H_{18}O_9N$	-0.442	552.1047 (29), 535.1020 (100)	Unknown
P_M15	329.1015	8.41	$C_{18}H_{17}O_6$	-1.412	314.0780 (40), 296.0674 (100), 285.0757 (32), 268.0726 (63)	Colletoquinone B (**4.5**)

No	[M+H]$^+$	Rt (min)	Molecular formula	Δ ppm	Fragments (Intensity)	Annotation/ Compound Class
P$_M$16	254.2110	9.20/ 9.26	C$_{15}$H$_{28}$NO$_3$	-1.918	236.2002 (100), 211.2051 (9)	3-(2,6-dimethyl-octanonyl)-5-methylpyrrolidin-2-one (**3.1**)
P$_M$17	254.2110	9.20/ 9.26	C$_{15}$H$_{28}$NO$_3$	-1.918	236.2002 (100), 211.2051 (9)	3-(2,6-dimethyl-octanonyl)-5-methylpyrrolidin-2-one (**3.1**)
P$_M$18	520.3394	9.64	C$_{29}$H$_{42}$O$_2$N$_7$	-0.182	502.3283 (63), 184.0731 (100)	Unknown
P$_M$19	1009.5316	9.76	C$_{44}$H$_{73}$O$_{15}$N$_{12}$	-0.343	979.5211 (20), 897.4794 (11)	Unknown
P$_M$20	391.2452	9.96	C$_{21}$H$_{33}$O$_4$N$_3$	-3.369	373.2340 (24), 317.2079 (100), 279.1608 (5), 149.0231 (8)	Unknown
P$_M$21	454.2921	10.14	C$_{23}$H$_{40}$O$_6$N$_3$	0.879	436.2819 (100), 393.2399 (5), 313.2736 (36)	Unknown
P$_M$22	496.3387	10.17	C$_{26}$H$_{46}$O$_6$N$_3$	-0.022	478.3284 (100), 184.0732 (33)	Unknown
P$_M$23	933.6255	10.22	C$_{47}$H$_{83}$O$_{10}$N$_9$	-0.856	915.6158 (53), 821.5743 (40), 803.5635 (100), 677.3860 (6), 577.4210 (41), 548.3079 (13)	Unknown Peptide
P$_M$24	277.2159	10.41	C$_{18}$H$_{29}$O$_2$	-0.953	259.2056 (89), 167.1067 (100), 151.1118 (92)	Unknown
P$_M$25	1018.5273	10.41	C$_{55}$H$_{76}$O$_{15}$N$_3$ C$_{54}$H$_{70}$O$_{10}$N$_{10}$	0.231 0.236	1000.5165 (100), 888.4643 (42), 665.3453 (30), 489.2771 (28)	Unknown
P$_M$26	277.2161	10.60	C$_{18}$H$_{29}$O$_2$	-0.513	259.2056 (89), 167.1067 (100), 151.1118 (92)	Unknown
P$_M$27	524.3704	11.15	C$_{28}$H$_{50}$O$_6$N$_3$	1.807	506.3594 (100), 184.0731 (28)	Unknown
P$_M$28	889.5620	11.51	C$_{44}$H$_{75}$O$_{10}$N$_9$	-1.339	855.5584 (100), 760.4852 (54), 647.4013 (26), 613.4170 (74), 486.3173 (22)	Unknown Peptide
P$_M$29	481.2916	11.92	C$_{25}$H$_{41}$O$_7$N$_2$	0.392	355.2240 (100)	Unknown
P$_M$30	292.2631	12.27	C$_{19}$H$_{34}$ON	-0.372	-	Unknown

Further, chemometric tools were used to reveal patterns in the profile changes. Therefore, PLS-DA as was chosen as a supervised method and the different media (1-5) were defined as a responsible variable.

The chemical variance of *C. graminicola* grown in different media is described in the PLS-DA (**Figure 7-5**). The first three components explain only 49.2 % of the total variance, with component 2 already showing a variance of only 10.7 %. This shows that the samples do not differ fundamentally from each other. However, this is also to be expected, as the fungal strain was always the same.

A   **B**
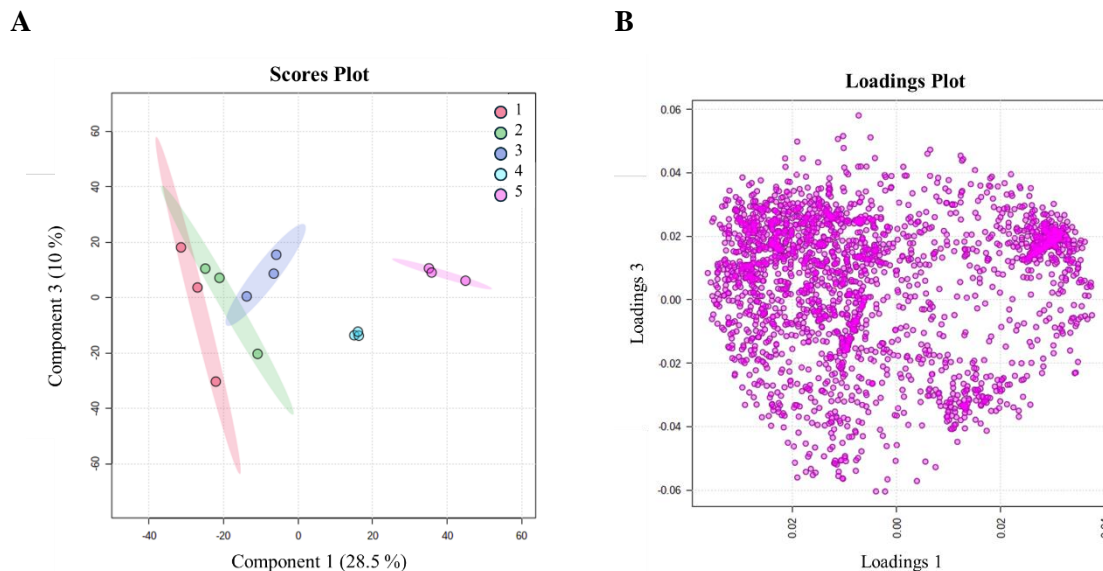
Figure 7-5 PLS-DA analysis of LC-ESI-HRMS of the mycelium of *C. graminicola* grown on different media (1-5); **A**: scores plot, **B**: loadings plot.

Nevertheless, the PLS- DA shows a clear separation between the minimal media (1-3) and the complete media (4-5) in component 1 (28.5 %). The minimal media are located in the negative direction of component 1, whereas the complete media are located in the positive direction, with medium 4 and 5 also clearly separated from each other. A closer look at the chromatograms of the crude extracts of *C. graminicola* grown in the different media (**Figure 7-6**) shows that the compound composition during the time span 11.0 to 12.4 minutes differs significantly between the minimal media (1-3) and the full media (4-5). In the complete media, no resolution into individual peaks can be observed here. In particular, peptide compounds like P_M28 are present.

Component 2 (10 %) mainly separates medium 4 from the other four media. While medium 4 is oriented in the negative direction, all other media are mainly located in the positive direction. Especially the time span between 4 – 5 minutes is responsible for this separation. During this period, several compounds elute that are unique in medium 4.
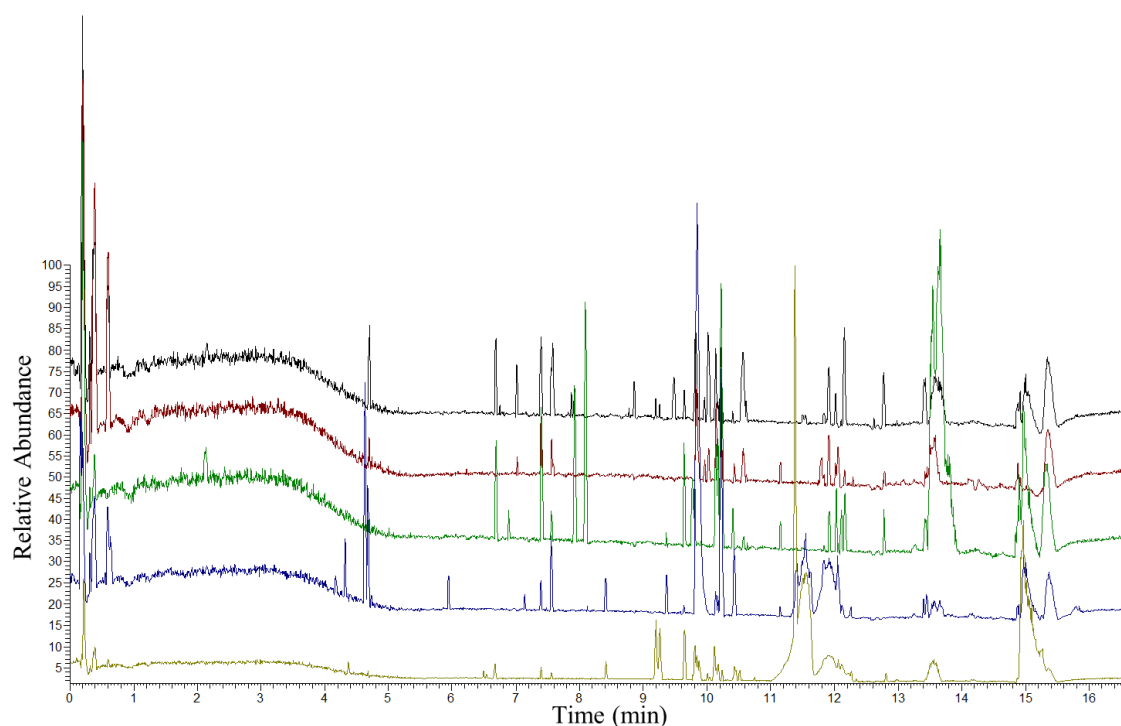
Figure 7-6 (+)-HR-ESI-MS chromatograms (base peak) of *C. graminicola* crude extracts (mycelium) grown in five different media: black line – medium 1 , red line – medium 2, green line – medium 3, blue line – medium 4, yellow line – medium 5.

A closer look at the peak table (**Figure S 208**) of fungal extracts cultivated in minimal medium 3 showed that chlorinated compounds such as colletoanthrone (**S 210-**P9) [17] and monorden (**S 210-**P12) [18], as well as **S 210-**P13, are particularly present in this medium. While colletoanthrone ((**S 210-**P9) has also been detected in other media, monorden (**S 210-**P12) and **S 210-**P13 are unique for medium 3. For monorden (**Table 7-4** P_M12/ **S 210-**P12), Wicklow and co-workers demonstrated a phytotoxic effect in the form of necrosis formation on maize plants in a leaf puncture assay at 10 µg per spot. [18]

In addition, medium 3 showed a characteristic red coloration probably caused by anthraquinones or anthrones as already indicated by the TLC (violet on the DC, Rf = 0.53). The red coloration may be caused by a pH shift of the medium to basic due to the formation of mesomerically stabilized phenolate anions. Colletoquinone A (P_M11, **4.3**), for example, showed a yellow coloration in acidic/neutral medium and a red coloration in the basic medium. The pH value of the culture filtrate after incubation (13 days) was not measured. However, the fact that the red coloration was degraded after a short time (24 h) suggests that not (only) a pH shift is responsible for the color but an oxidation process of the responsible compounds. The presence of red anthrones, which are oxidized to the yellow anthraquinones, could explain this color change. In general, a strong red coloration of anthraquinones/ anthrones can be observed by introducing auxochromic groups (such as NH_2 or OH) especially in position 1, 4, 5 or 8. [19]

A deeper look at the chromatograms of medium 5 also shows that numerous compounds of the same mass - i.e. stereoisomers (**Figure S 210**) – are found in this medium. This was also shown in Chapter 3 for the isolation of the pyrrolidone derivatives **3.1a/b** and **3.10a/b**. The reason for the apparent formation of isomers in this medium is unknown.

107

Culture filtrate

Figure 7-7 shows the chromatogram of the QC sample of the culture filtrate. Peaks (P$_C$) were tentatively assigned by their accurate mass and MS/MS fragmentation, also in comparison with the previously isolated compounds (Chapter 3 – 5). The results are listed in **Table 7-6**.
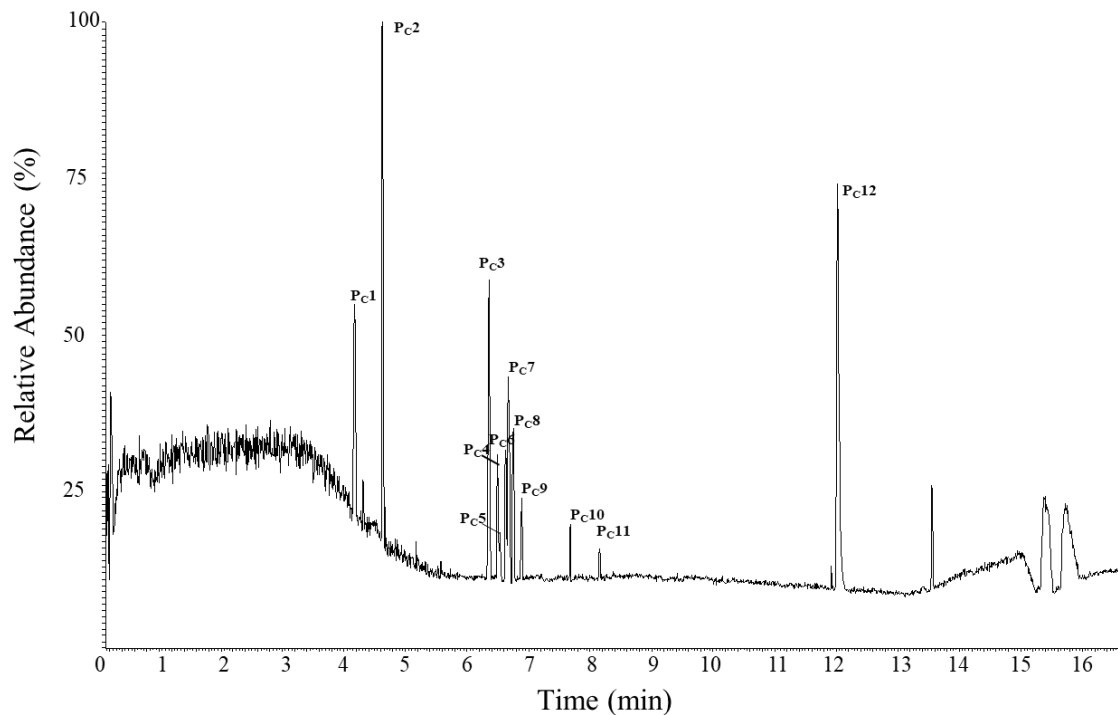
Figure 7-7 (+)-ESI-HR-MS chromatogram (base peak) of the QC sample of the culture filtrates.

Comparing the two chromatograms of the QC samples (**Figure 7-4** and **Figure 7-7**), it is noticeable that significantly fewer peaks were detected in the culture filtrate than in the mycelium.
Considering the corresponding masses, it can be seen that there are also numerous stereoisomers among the peaks (**P$_C$4** – **P$_C$8**, **Table 7-5**).

Table 7-6 Peak table compounds identified in the QC sample (culture filtrate) of *C. graminicola*.

No	$[M+H]^+$	Rt (min)	Molecular formula	Δ ppm	Fragments (Intensity)	Annotation/ Compound Class
P_C1	252.1224	4.17	$C_{13}H_{18}O_4N$	2.47	206.1170 (100), 192.1014 (89)	Unknown
P_C2	727.3854	4.63	$C_{28}H_{55}N_8O_{14}$	2.95	709.3745 (100), 615.3331 (52), 597.3185 (86), 582.3116 (28), 485.2596 (34), 467.2439 (36), 355.1948 (60)	Unknown
P_C3	258.1152	6.36	$C_{18}H_{14}N_2$	0.31	240.1044 (100)	Unknown
P_C4	252.1952	6.49	$C_{15}H_{26}O_2N$	2.57	-	Pyrrolidone derivative
P_C5	252.1951	6.54	$C_{15}H_{26}O_2N$	2.78	-	Pyrrolidone derivative
P_C6	268.1900	6.63	$C_{15}H_{26}O_3N$	2.68	250.1792 (100), 232.1687 (52), 208.1688 (18)	Pyrrolidone derivative
P_C7	252.1951	6.68	$C_{15}H_{26}O_2N$	2.78	-	Pyrrolidone derivative
P_C8	268.1898	6.75	$C_{15}H_{26}O_3N$	3.25	250.1792 (100), 232.1687 (52), 208.1688 (18)	Pyrrolidone derivative
P_C9	351.0620	6.88	$C_{17}H_{16}O_6Cl$	2.79	336.0384 (73), 334.0591 (65), 333.0514 (39), 319.0356 (100), 315.0853 (65)	Colletoanthrone [17]
P_C10	328.2112	7.68	$C_{17}H_{30}O_5N$	1.95	310.2006 (100)	Unknown
P_C11	272.2213	8.15	$C_{15}H_{30}O_3N$	2.72	254.2106 (100)	Pyrrolidone derivative
P_C12	425.2864	12.02	$C_{22}H_{39}O_5N_3$	4.73	-	Unknown
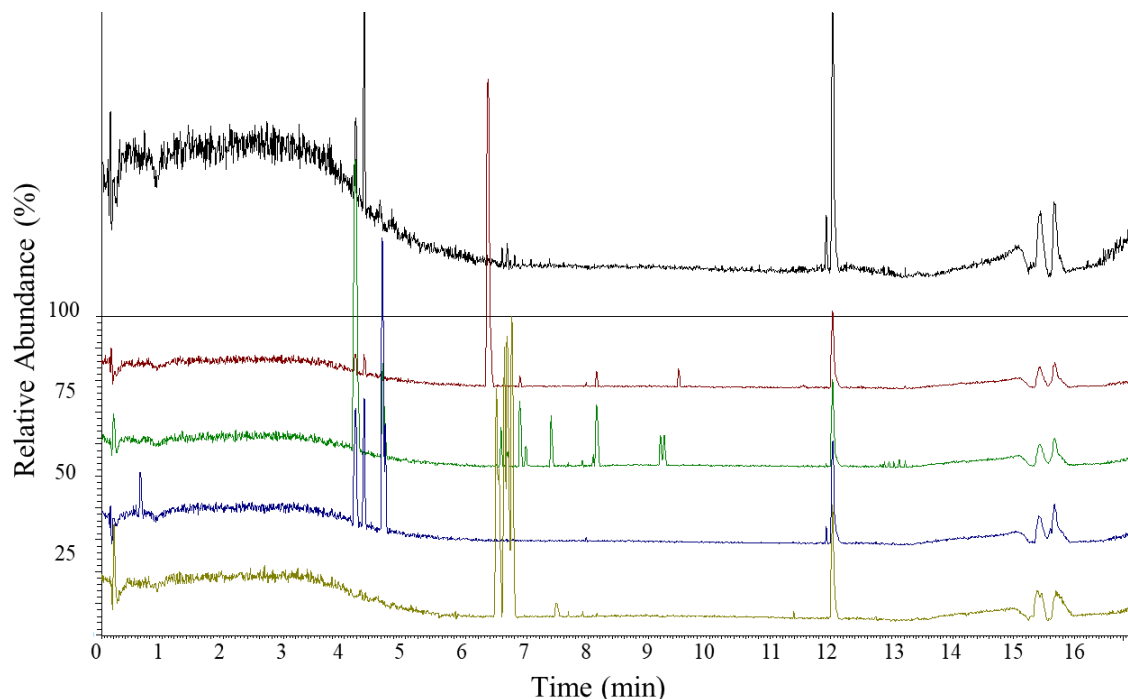
Figure 7-8 (+)-HR-ESI-MS chromatograms (base peak) of *C. graminicola* crude extracts (culture filtrate) grown in five different media: black line – medium 1 , red line – medium 2, green line – medium 3, blue line – medium 4, yellow line – medium 5.

Analysis of the chromatograms of the individual culture filtrates shows that most of the peaks were detected in medium 3. Moreover, the substances detected in the medium and in the mycelium differ significantly from each other. Only colletopyrone (**S 210**-P10, S 215-P13) and colletoanthrone (**S 210**-P9, **S 215**-P11) were detected in both the mycelium and the culture filtrate (**Figure S 208**, **Figure S 213**).
In contrast, all peaks in the culture filtrate of medium 4 were also detected in the mycelium. In the culture filtrate of medium 5, almost exclusively the metabolites present in the form of stereoisomers – presumably derivatives of **3.1a/b** (P_M17) and **3.10a/b** (P_M8) as suggested by the fragmentation pattern – were detected. This occurrence of stereoisomeric compounds was already observed in the mycelium.

A common feature of all 5 culture filtrates is the feature **Table 7.6** P_c12 at 12.02 minutes. Interestingly, it was only detected in the culture filtrates and not in the mycelia.

However, it is also noteworthy that the chromatograms of the culture filtrate in medium 2 looked different each time in the triplicate. This could possibly be due to the fact that medium 2 is a medium without a carbon source, which means that the stress level for the organism could be the highest.

7.4   Conclusion

The present study showed that *C. graminicola* produces different phytotoxic metabolites depending on the growth medium. The fungus produced biologically active compounds both in minimal media with missing carbon or nitrogen sources and in complete media. In addition, the investigations indicated that *C. graminicola* has great potential for previously unknown compounds that could have other promising biological activities in addition to possible phytotoxicity. It should be noted that only LC-HR-ESI-MS measurements in positive mode were performed in this study, as numerous nitrogen-containing compounds were obtained during isolation. To achieve a more comprehensive image, negative measurements should also be considered, as macrolides, fatty acids, terpenes, etc. are better ionized in negative mode. However, studies in negative mode could not be performed in this study due to time constrains.

These results could be the starting point for more in-depth analyses, for more comprehensive OSMAC studies on the media, but also on the influence of light, pH, temperature, etc. on the formation of secondary metabolites or on phytotoxicity. Additionally, metabolomics tools such as MS-Finder [20], MetFrag [21] and GNPS [22] should be used to better identify metabolites and substance classes. However, it must also be taken into account that many of the signals cannot be annotated, as only few data for fungal metabolites are available in databases. [23]

A similar study has already been performed by Reveglia and co-workers for *Colletotrichum truncatum* and *Colletotrichum trifolii*. [24] They found clear differences in the phytotoxicity of the extracts grown in different media. Using the above-mentioned tools, they were able to tentatively assign numerous metabolites. Thus, this approach could also be used in the future to find a promising medium for subsequent activity-guided isolation.

References

[1] Pan, R.; Bai, X.; Chen, J.; Zhang, H; Wang, H., Exploring structural diversity of microbe secondary metabolites using OSMAC strategy: A literature review. *Front. Microbiol.* **2019**, *10*, 294. doi: 10.3389/fmicb.2019.00294.

[2] Martins, A.; Vieira, H.; Gaspar, H.; Santos, S., Marketed marine natural products in the pharmaceutical and cosmeceutical industries: Tips for success, *Mar. Drugs* **2014**, *12*, 1066-1101, doi: 10.3390/md12021066.

[3] Hüter, O.F., Use of natural products in the crop protection industry, *Phytochem. Rev.* **2011**, *10*, 185-194, doi: 10.1007/s11101-010-9168-y.

[4] David, B.; Wolfender, J.L.; Dias, D.A., The pharmaceutical industry and natural products: historical status and new trend, *Phytochem. Rev.* **2015**, *14*, 299-315, doi: 10.1007/s11101-014-9367-z.

[5] Wei, H.; Lin, Z.; Li, D.; Gu, Q.; Zhu, T., OSMAC (one strain many compounds) approach in the research of microbial metabolites – a review, *Acta Microbiol. Sin.* **2010**, *50*, 701-709,

[6] Bode, H.B.; Bethe, B.; Höfs, R.; Zeeck, A., Big effects from small changes: possible ways to explore nature's chemical diversity, *ChemBioChem* **2002**, *3*, 619-627, doi: 10.1002/1439-7633(20020703)3:7<619::AID-CBIC619>3.0.CO;2-9.

[7] Romano, S., Jackson, S.A.; Patry, S.; Dobson, A.D.W., Extending the "one strain many compounds" (OSMAC) principle to marine microorganisms, *Mar. Drugs* **2018**, *16*, 244, doi: 10.3390/md16070244.

[8] Schmidt-Heydt, M.; Magan, N.; Geisen, R., Stress induction of mycotoxin biosynthesis genes by abiotic factors, *FEMS Microbiol. Lett.* **2008**, *284*, 142-149, doi: 10.1111/j. 1574-6968.2008.01182.x.

[9] Sørensen, L.M.; Lametsch, R.; Andersen, M.R.; Nielsen, P.V.; Frisvad, J.C., Proteome analysis of *Aspergillus niger*: Lactate added in starch-containing medium can increase production of the mycotoxin fumonisin B2 by modifying acetyl-CoA metabolism, *BMC Microbiol.* **2009***, 9*, 255, doi: 10.1186/1471-2180-9-255.

[10] Frisvad, J.C., Media and growth conditions for induction of secondary metabolite production, *Methods Mol. Biol.* **2012**, *944*, 47-58, doi: 10.1007/978-1-62703-122-6_3.

[11] Kim, J.; Kim, K.H., Effects of minimal media vs. complex media on the metabolite profiles of *Escherichia coli* and *Saccharomyces cerevisiae, Process Biochem.* **2017**, *57*, 64-71, doi: 10.1016/j.procbio.2017.04.003.

[12] Speretto, G.; Stasiak, L.G.; Godoi, J.P.M.G.; Gabiatti, N.C.; de Souza, S.S., A review of culture media for bacterial cellulose production: complex, chemically defined and minimal media modulations, *Cellulose* **2021**, *28*, 2649-2673, doi: 10.1007/s10570-021-03754-5.

[13] Tao, H.; Bausch, C.; Richmond, C.; Blattner, F.R.; Conway, T., Functional genomics: expression analysis of *Escherichia coli* growing on minimal and rich media, *J. Bacteriol.* **1999** , *181*, doi: 10.1128/jb.181.20.6425-6440.1999.

[14] Evidente, A.; Lanzetta, R.; Capasso, R. Andolfi, A.; Bottalico, A.; Vurro, M.; Zonno, M.C.; Putaminoxin, a phytotoxic nonenolide from *Phoma putaminum*, *Phytochemistry* **1995**, *40*, 1637-1641, doi: 10.1016/0031-9422(95)00505-2.

[15] Tsuwaga, H.; Cajka, T.; Ma, Y.; Higgins, B.; Ikeda, K.; Kanazawa, M.; van der Gheynst, J.; Fiehn, O.; Arita, M., MS-DIAL: data independent MS/MS deconvolution for comprehensive metabolome analysis, *Nat. Methods* **2015**, *12*, 523-526, doi: 10.1038/nmeth.3393.

[16] Pang, Z.; Chong, J.; Zhou, G.; de Lima Morais, D.A.; Chang, L.; Barrette, M.; Gauthier, C.; Jacques, P.-E.; Li, S.; Xia, J., MetaboAnalyst 5.0: narrowing the gap between raw spectra and functional insights, *Nucleic Acids Res.* **2021**, *49*, 388-396, doi:10.1093/nar/gkab382.

[17] Horbach, R.; Graf, A.; Weihmann, F.; Antelo, L.; Mathea, S.; Liermann, J.C.; Opatz, T.; Thines, E.; Aguirre, J.; Deising, H.B., Sfp-type 4'-phosphopantetheinyl transferase is indispensable for fungal pathogenicity, *Plant Cell* **2009**, *21*, 3379-3396, doi: 10.1105/tpc.108.064188.

[18] Wicklow, D.T.; Jordan, A.M.; Gloer, J.B., Antifungal metabolites (monorden, monocillins I, II, III) from *Colletotrichum graminicola*, a systemic vascular pathogen of maize, *Mycol. Res.* **2009**, *113*, 1433-1442, doi: 10.1016/j.mycres.2009.10.001.

[19] Gregory, P.; *Industrial dyes: Chemistry, properties, applications*, Hunger, K. (ed), Wiley-VCH, Weinheim, **2003**, 35, ISBN: 978-3527304264.

[20] Tsuwaga, H.; Kind, T.; Nakabayashi, R.; Yukihira, D.; Tanaka, W.; Cajka, T.; Saito, K.; Fiehn, O.; Arita, M., Hydrogen rearrangement rules: Computational MS/MS fragmentation and structure elucidation using MS-FINDER software, *Anal. Chem.* **2016***, 88*, 7946-7958, doi: 10.1021/acs.analchem.6b00770.

[21] Ruttkies, C.; Schymanski, E.L.; Wolf, S.; Hollender, J.; Neumann, S., MetFrag relaunched: Incorporating strategies beyond in silico fragmentation, *J. Cheminform.* **2016**, *8*, doi: 10.1186/s13321-016-0115-9

[22] Wang, M.; Carver, J.; Pheland, V.V.; Sanchez, L.M.; Garg, N.; Peng, Y.; Nguyen, D.D. et al., Sharing and community curation of mass spectrometry data with global natural products social molecular networking, *Nat.*

Biotechnol. **2016**, *34*, 828-837, doi: 10.1018/nbt.3597.

[23] Li, G.; Jian, T.; Liu, X.; Lv, Q.; Zhang, G.; Ling, J., Application of metabolomics in fungal research, *Molecules* **2002**, *27*, 7365, doi: 10.3390/molecules27217365.

[24] Reveglia, P.; Agudo-Jurado, F.J.; Barilli, E.; Masi, M.; Evidente, A.; Rubiales, D., Uncovering phytotoxic compounds produced by *Colletotrichum* spp. involved in legume diseases using an OSMAC-metabolomics approach, *Fungi* **2023**, *9*, 610, doi: 10.3390/jof9060610.
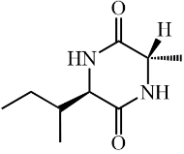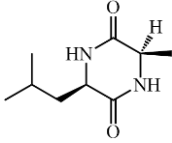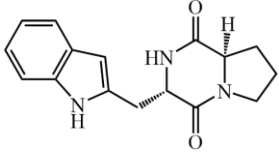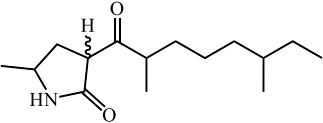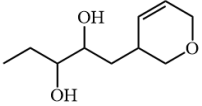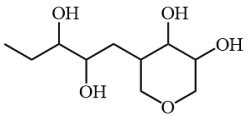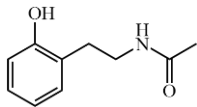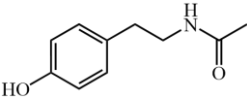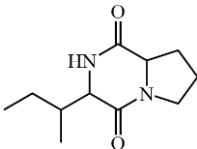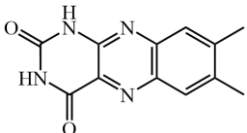
8   Conclusion

The aim of this work was the isolation of phytotoxic secondary metabolites produced by the fungus *Colletotrichum graminicola* M1.001. The fungus was cultivated on two different complete media (HMG (Chapter 3) and CM (Chapter 4 and 5)) as semi-solid cultures. HMG and CM were chosen, as they are established media from the working group of Prof. Dr. H. Deising (Institute of Agricultural and Nutritional Sciences, Martin-Luther University Halle-Wittenberg), who also provided the fungal strain   .

The isolation of phytotoxic secondary metabolites was carried out using the classical approach of activity-guided isolation. By this, a total of 33 substances was purified and characterized. **Table 8-1** and **Table 8-2** show all isolated compounds produced by *C. graminicola* growing on the two complete media HMG and CM.

Table 8-1 Compounds isolated from *C. graminicola* cultivated on HMG medium.

HMG medium (Chapter 3)		
no.	name	structure
3.1	3-(6-hydroxy-2,6-dimethyloctanoyl)-5-methylpyrrolidin-2-one	
3.2	*cyclo*-L-Leu- L-Pro	
3.3	*N*-phenethylacetamide	
3.4	*cyclo*-L-Val-L-Pro	
3.5	*cyclo*-L-Ala-L-Pro	
3.6	*cyclo*-L-Ala-D-Val	

HMG medium (Chapter 3) - continued

no.	name	structure
3.7	*cyclo*-L-Ala-D-Ile	
3.8	*cyclo*-D-Ala-D-Leu	
3.9	*cyclo*-L-Trp-D-Pro	
3.10	3-(2,6-dimethyloctanoyl)-5-methylpyrrolidin-2-one	
3.11	1-(3,6-dihydro-*2H*-pyran-3-yl)pentane-2,3-diol	
3.12	5-(2,3-dihydroxypentyl)-tetrahydro-2H-pyran-3,4-diol	
3.13	*N*-[2-(2-hydroxyphenyl)-ethyl]-acetamide	
3.14	*N*-Acetyltyramine	
3.15	*cyclo*-Ile-Pro	
3.16	lumichrome	

HMG medium (Chapter 3) - continued		
no.	name	structure
3.17	7,8,16-trihydroxyoctadeca-9,12-dienoic acid	
3.18	(8Z,10E)-12,17-dihydroxyoctadeca-8,10-dienoic acid	
3.19	uracil	

Table 8-2 Compounds isolated from *C. graminicola* cultivated on CM medium.

CM medium (Chapter 4 and 5)		
no.	name	structure
4.1	*trans*-anhydromevalonic acid	
4.2	graminolactone	
4.3	colletoquinone A	
4.4	5-chloro-colletoquinone A	
4.5	colletoquinone B	
4.6	azelaic acid	

CM medium (Chapter 4 and 5) - continued		
no.	**name**	**structure**
4.7	(*E*)-dec-2-enedioic acid	
4.8	*cyclo*-Ala-Pro	
4.9	methyl-6-acetamidohexanoate	
4.10	*cyclo*-L-Phe-D-Pro	
4.11	6-acetamidohexanamid	
4.12	*N*-(5-hydroxypentyl)-acetamide	
4.13	6-pentanamidohexanamide	
5.1	*N*-(4-hydroxybutyl)-benzenesulfonamide	

Of these, 21 exhibited a phytotoxic effect in the leaf spot test on *A. thaliana* Col-0 in the range between 10 – 100 mM. Thus, the basic principle of activity-guided isolation was successful. At the same time, however, this approach also revealed some problems and challenges already known in the literature. Especially the re-isolation of already known compounds has become an increasing problem in recent years. [1; 2]

Having a closer look at the isolated substances, most of them were already isolated before. Out of all 33 isolated compounds, 19 compounds, comprising **3.2**, **3.4 – 3.9**, **3.13 – 3.16**, **3.19**, **4.1**, **4.3**, **4.5 – 4.8** and **4.10** were already described from natural sources.

In parallel, HR-ESI-MS/MS analyses of the extracts or fractions might help to identify known compounds to avoid their re-isolation. However, it is really hard or basically impossible to decide whether an extract or fraction that contains already known phytotoxins alongside completely unknown compounds will lead to success in the search of new active compounds through further purification/ isolation.

Preliminary OSMAC studies ("one strain many compounds") can help to select a promising cultivation media of the fungal strain. In Chapter 7, the influence of different minimal and complete media on yield, bioactivity and secondary metabolite profiles were investigated. For crude extracts obtained from

cultivation on minimal media, a high phytotoxic activity in the leaf-spot assay on *Arabidopsis thaliana* Col-0 was observed. However, the obtained yields from minimal media were very low, so cultivation was only performed in complete media. The investigation of the different metabolite patterns in the extracts also demonstrated that there is still a great potential for the isolation of new compounds with new structures from *C. graminicola*.

Another challenge of activity-guided isolation is the choice of the bioassay. First of all, the plant organ for the bioassay must be selected, whether leaves, roots, seeds, or whole plants. In addition, decisive factors must be considered, e.g. whether the uptake of the substances should be facilitated by prior wounding of the leaves. To obtain a truly comprehensive picture of the phytotoxic effect of the compounds, it would be necessary to perform different test systems in order to take the various possible mechanisms of action or physicochemical properties of the compounds into account.
An example may be a substance that is absorbed via the roots. Its phytotoxic effect would not be recognized in leaf assays, like the leaf spot assay used in this work. Nevertheless, for reasons of time, costs and manageability, it is not reasonable to concentrate on all these aspects simultaneously. This mainly concerns the required amounts of extracts/fractions/substances, which leads to another challenge that will be discussed in more detail below.

The assay chosen for this work for the activity-guided isolation was a modified leaf spot assay. [3] In this assay, the fractions were dissolved in a mixture of methanol/water (1:1, *v/v*) and then applied directly to the leaf surface of the test plant (*A. thaliana* Col-0) without any prior wounding. The greatest advantage of this bioassay is its simplicity. It does not require time-consuming preparation or follow-up times. The results can be read out quickly by simply observing the leaves. The maximum sample quantity of 250 µg per spot is relatively high compared with other bioassays but was chosen in order to keep the number of false negative results as low as possible. Nevertheless, an amount of $1-2$ mg extract/fraction/substance is enough to allow initial determination of the activity.
However, the chosen leaf spot test also has some disadvantages. On the one hand, the phytotoxicity of the polar toxins appears much weaker than it possibly is, as no prior wounding of the leaves was chosen, and the substances therefore have to overcome the hydrophobic plant cuticle as a barrier. On the other hand, the test is also limited by the solubility of the test compounds. Very non-polar substances that can no longer be dissolved in the solvent mixture cannot be tested with this assay under the selected conditions.
In the context of activity-guided isolation, the fact that the leaf-spot assay is a purely qualitative and not a quantitative test is of secondary importance, as substance mixtures are usually influenced by many more factors, such as additive/subtractive or (anti-) synergistic effects, as well as the proportion of phytotoxin in relation to the other substances contained.

Nevertheless, the leaf-spot assay without prior wounding was chosen in this work, as the aim was the isolation of phytotoxic compounds that could be used directly as a potential bioherbicide. Ideally, sufficient amounts of an active substances (with high activity) should be isolated that simple up-scaling techniques can be used to obtain the substance on a large scale. Therefore, a test system was needed that comes closest to the application methods used in practice. Accordingly, a test without wounding was chosen and a solvent mixture with a high-water content was selected.

However, no phytotoxic secondary metabolites fulfilling both requirements could be isolated in the frame of this work. Regarding the yield, almost all pure compounds were in the lower milligram range (< 3 mg) from a batch of 200 - 250 L culture filtrate. This could be due to the choice of the media or the cultivation conditions. Extended OSMAC studies could help to find a more suitable growth media. However, it could also be possible that additional factors are required for the up regulation of the responsible genes. For instance, some *Colletotrichum* species are known to require external stimuli to enter the necrotrophic phase, such as the presence of ethylene in *C. gloeosporioides* [4] or *C. graminicola* which need contact with hard surfaces to induce gene expression. Therefore, it is possible that are large part of the responsible gene

clusters is not active under the selected conditions (silent gene clusters). [5]

Also, the activities observed in the leaf spot test are not suitable for a direct use. The compound **4.3** showed the highest phytotoxic activity of all tested compounds up to a concentration of 10 mM. Often the physicochemical properties, such as solubility, adhesion to the plant surface, penetration, and distribution in the plant, are not ideal. [6] However, this is hardly surprising as these compounds do not have to fulfill these requirements in nature. For example, if the fungus releases the secondary metabolites directly into the lumen of the plant cell, they do not have to (be able to) penetrate the plant membranes. At the same time, it should be noted that the fungus produces a large number of different metabolites, and additive or synergistic effects can also be relevant in this context.

It is therefore often necessary to synthesize and modify the structure of recognized phytotoxic compounds. In many cases, however, this can be difficult due to complexity or stereochemistry of the natural product or is only possible through multi-step and cost-intensive syntheses. As part of this work, the phytotoxic compound *N*-(hydroxybutyl)-benzenesulfonamide (**5.1**) was isolated from culture filtrate and mycelium of *C. graminicola* cultivated on CM medium as shown in Chapter 5. The compound **5.1** as well as around 130 derivatives of it could be synthesized by a simple 1 – 3 step synthesis (syntheses performed by Toni Denner, Institute of Chemistry – Organic Chemistry, Prof. Dr. Csuk, Martin-Luther-University Halle-Wittenberg) to perform initial quantitative structure-activity relationship studies (QSAR) (Chapter 6).

The phytotoxic activity of the sulfonamide derivatives (**6.1** – **6.32**) were tested using a modified non-destructive leaf disk assay. [7] This assay was originally described by Wu and co-workers [7] for detecting resistance to various commercial herbicides in different plants. The non-destructive leaf disk assay is based on the measurement of delayed fluorescence of chlorophyll (Chapter 2.2.6), which can be considered as an indicator of photosynthetic activity. Since the photosynthesis is highly sensitive, delayed fluorescence has become an important tool to study environmental influences on plants.

For the non-destructive leaf disk assay, stock solutions of the compounds are prepared in methanol an added to prefilled 96-well plates containing a buffer solution (MES, pH = 6.5). Leaf disks of the test plants (*A. thaliana* Col-0 and *Secale cereale*) are placed on the surface of the solution and delayed fluorescence is measured at different time points (t = 0 h, t = 24 h and t = 48 h) to determine the phytotoxic activity of the compounds. The greatest advantage of this bioassay is that it enables high throughput of test substances, while at the same time the amount of required test plants is low. Other advantages include the simplicity of performing dilution series and the short time needed to obtain results (48 hours).

However, the non-destructive leaf disk assay has also some disadvantages. One the one hand, the required amount of compounds is higher than for the leaf-spot assay, as stock solutions need to be prepared at first, which are diluted up to 39 times in the 96-well plate with the buffer solution, ensuring that a maximum of 2.5 % of methanol is present per well. Due to this higher demand of compound, this assay could not be performed during the isolation process. One the other hand, the solubility of the compounds is also a limiting factor, as it was in the leaf-spot assay since the assay is performed in an aqueous buffer.
Finally, the obtained results need to be interpreted with appropriate care, as in this assay compounds can enter the plant other ways, than via the plant cuticle. It is therefore not possible to assess the suitability of the compounds on the basis of this bioassay alone. Whole-plant experiments are necessary, to show if further modification of the molecule or the use of additives is required to observe a phytotoxic effect on the plants or to facilitate the uptake into the plants. This in turn highlights the difficulties of the development of new herbicides with new mode of action.

The synthesized derivatives were selected in such a way that structural elements relevant to the phytotoxic activity could be identified. For example, the replacement of benzene (**6.1**) with pyridine (**6.15**) led to a complete loss of activity. The derivatives cover a broad range of polarity (log *P* between -0.30 (**6.16a**) and

5.46 (**6.14**)). Additionally, the influence of sterically hindering substituents bound to the benzene sulfonamide moiety on the phytotoxic activity was analyzed.

On average, the best results were obtained for sulfonamide derivatives with a molecular weight of 305.4 g/mol and a log P of 2.80. It was also shown that the substituents have a strong influence on the activity. An increase in activity was observed along the following series of substituents: -F (**6.2**) < -OMe (**6.3**) < -Me (**6.4 – 6.6**) < -iPr (**6.7 – 6.9**) < -tBu (**6.10 – 6.12**) = -cyclohexane (**6.13**) > -adamantane (**6.14**). However, further computational chemistry is required to fully explain the relationship of the observed bioactivity and the chemical structure.

In addition, derivatization led to a 50-fold increase in phytotoxic activity compared to the natural product **5.1** in the non-destructive leaf disc test, which showed an activity of up to 20 mM. The most active compounds (**6.10-b**, **6.11-e**, **6.12-e** and **6.13-a-e**) were already active at a concentration of 0.4 mM.
These results show that conventional bioassay-guided isolation is a powerful tool for the discovery and development of new active ingredients. Whether the compounds have a so far undescribed mode of action was not part of the studies and can therefore not be answered. Further experiments and computational molecular modeling studies are necessary to identify the target of the phytotoxic compounds, e.g. the mechanisms of the molecular recognition between proteins and inhibitors.

References

[1] Lorsbach, B.A.; Sparks, T.C.; Cicchillo, RM.; Garizi, N. .V.; Hahn, D.R.; Meyer, K.G., Natural products: a strategic lead generation approach in crop protection discovery, *Pest Manag. Sci.* **2019**, *75*, 2301–2309, doi: 10.1002/ps.5350.

[2] Doroghazi, J.R.; Albright, J.C.; Goering, A.W.; Ju, K.-S.; Haines, R.R.; Tchalukov, K.A.; Labeda, D.P.; Kelleher, N.L.; Metcalf, W.W., A roadmap for natural product discovery based on large-scale genomics and metabolomics, *Nat. Chem. Biol.* **2014**, *10*, 963–968, doi: 10.1038/nchembio.1659.

[3] Evidente, A.; Lanzetta, R.; Capasso, R.; Andolfi, A.; Bottalico, A.; Vurro, M.; Zonno, M.C., Putaminoxin, a phytotoxic nonenolide from *Phoma putaminum*, *Phytochemistry* **1995**, *40,* 6, 1637–1641, doi: 10.1016/0031-9422(95)00505-2.

[4] Flaishman, M.A.; Kolattukudy, P.E., Timing of fungal invasion using host's ripening hormone as a signal, *Proc. Nat. Acad. Sci. U.S.A.* **1994**, *91,* 6579–6583, doi: 10.1073/pnas.91.14.6579.

[5] Liu, Z. M.; Kolattukudy, P.E., Identification of a Gene Product Induced by Hard-Surface Contact of *Colletotrichum gloeosporioides* Conidia as a ubiquitin-conjugating enzyme by yeast complementation, *J. Bacteriol.* **1998**, *180,* 3592–3597, doi: 10.1128/JB.180.14.3592-3597.1998.

[6] Duke, S.O.; Pan, Z.; Bajsa-Hirschel, J.; Boyette, C.D., The potential future roles of natural compounds and microbial bioherbicides in weed management in crops, *Adv. Weed Sci.* **2022**, *40*, e020210054, doi: 10.51694/AdvWeedSci/2022;40:seventy-five003.

[7] Wu, C.; Varanasi, V.; Perez-Jones, A., A nondestructive leaf-disk assay for rapid diagnosis of weed resistance to multiple herbicides, *Weed Sci.* **2021**, 69, 274–283, doi: 10.1017/wsc.2021.15.

Appendix
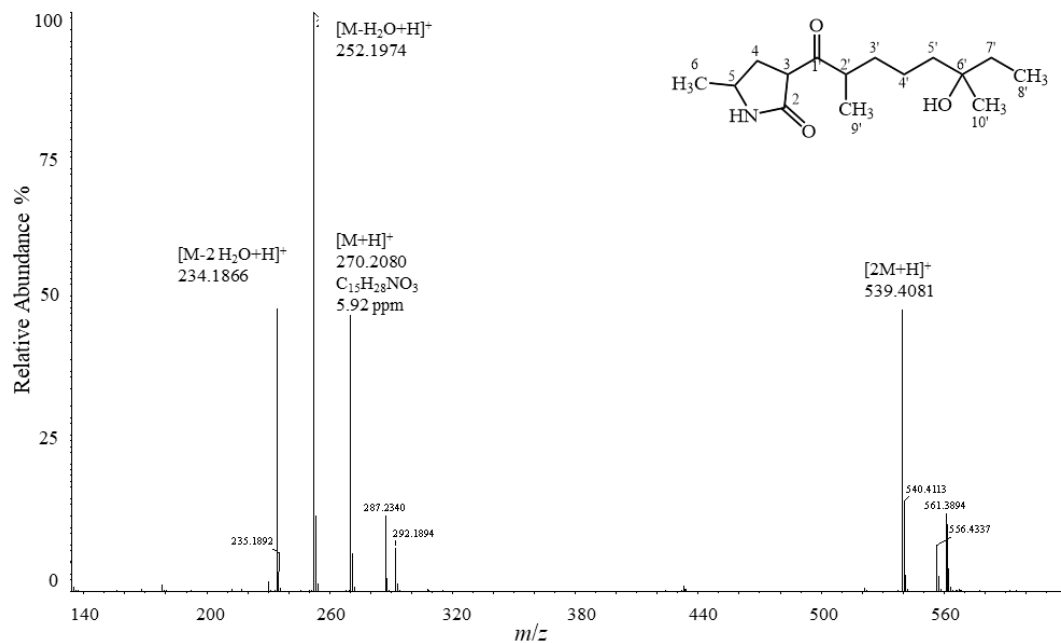
Figure S 1 (+)-ESI-HRMS spectrum of compound **3.1a/b**.
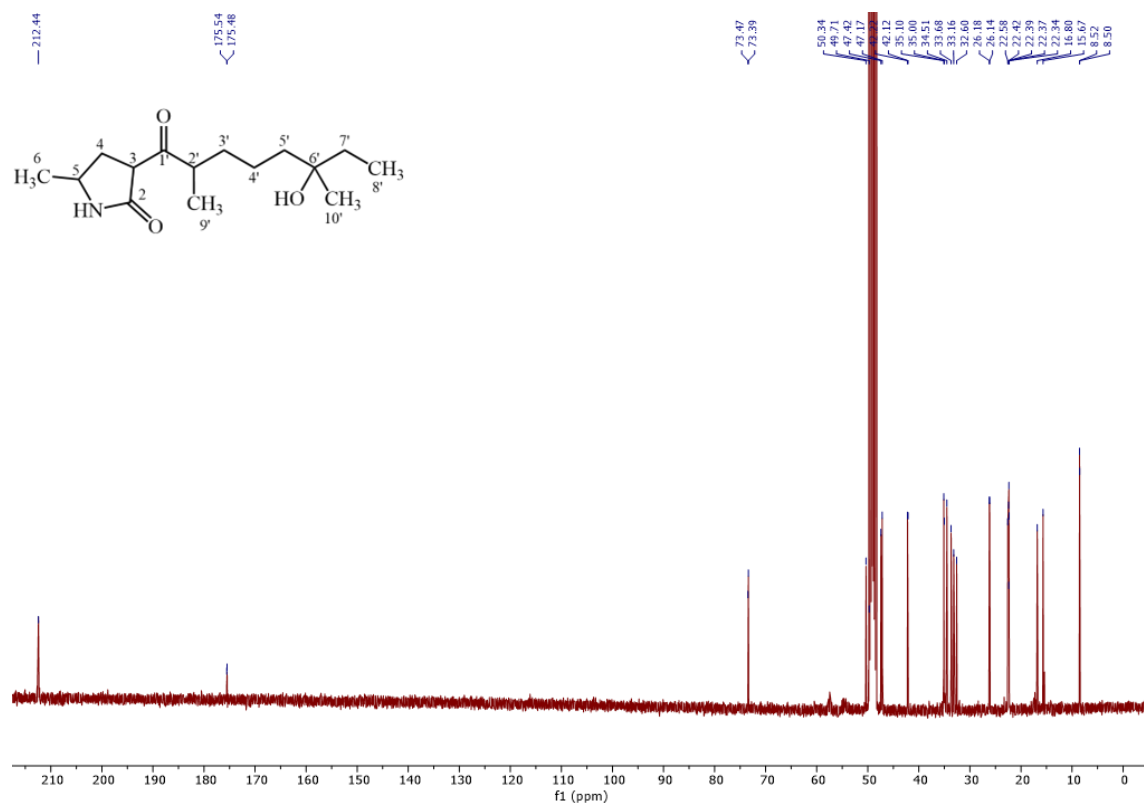
Figure S 2 ^{13}C NMR spectrum of compound **3.1a/b** in methanol-d$_4$, 100 MHz.
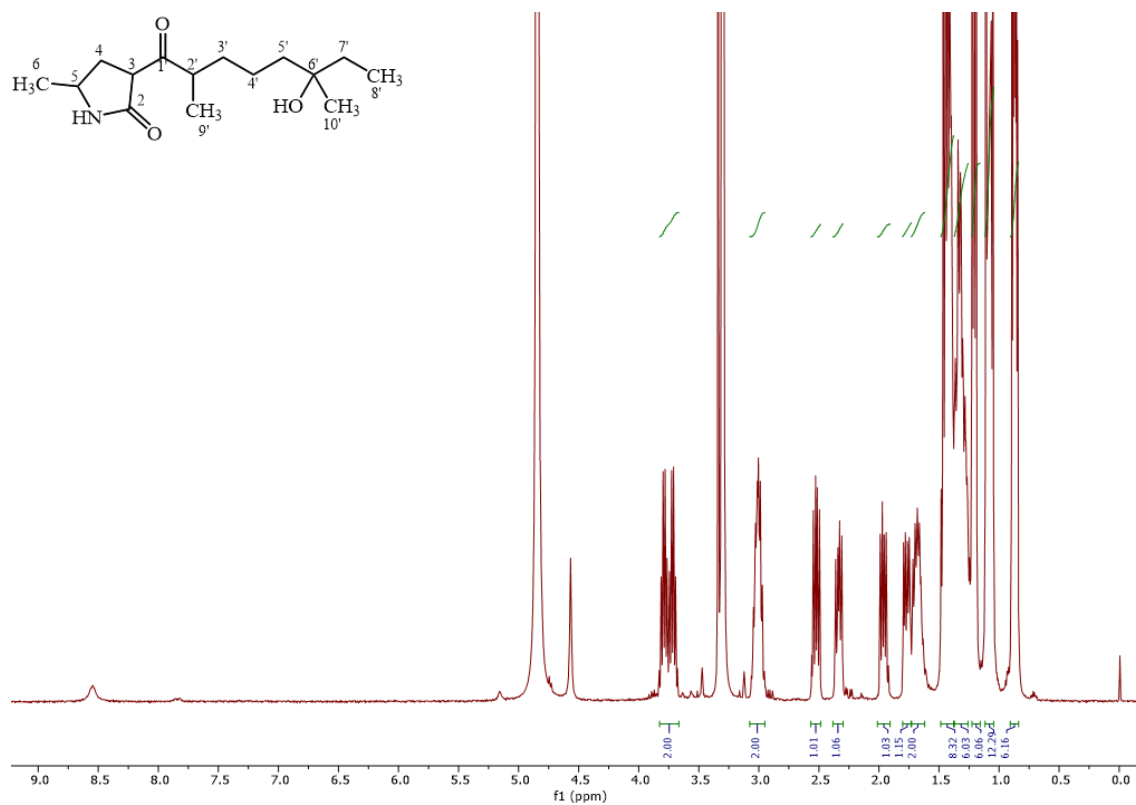
Figure S 3 ^{1}H NMR spectrum of compound **3.1a/b** in methanol-d$_4$, 400 MHz.
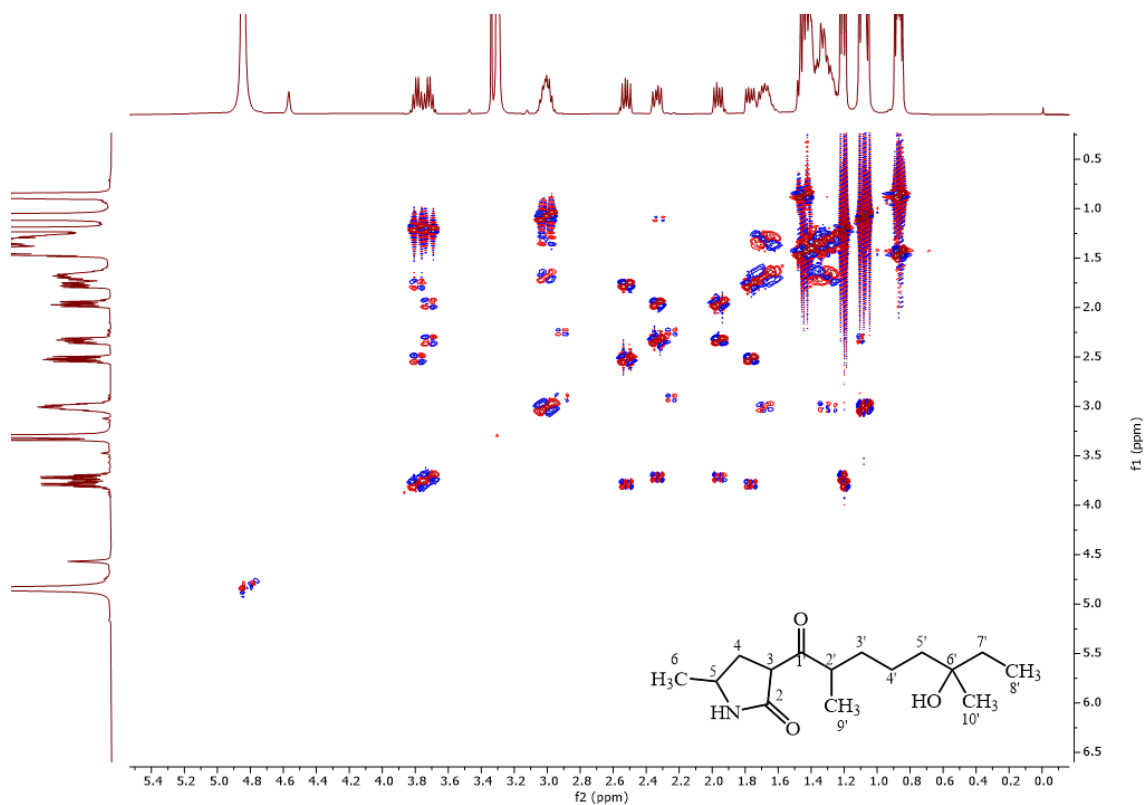
Figure S 4 COSY spectrum of compound **3.1a/b** in methanol-d$_4$, 400 MHz.
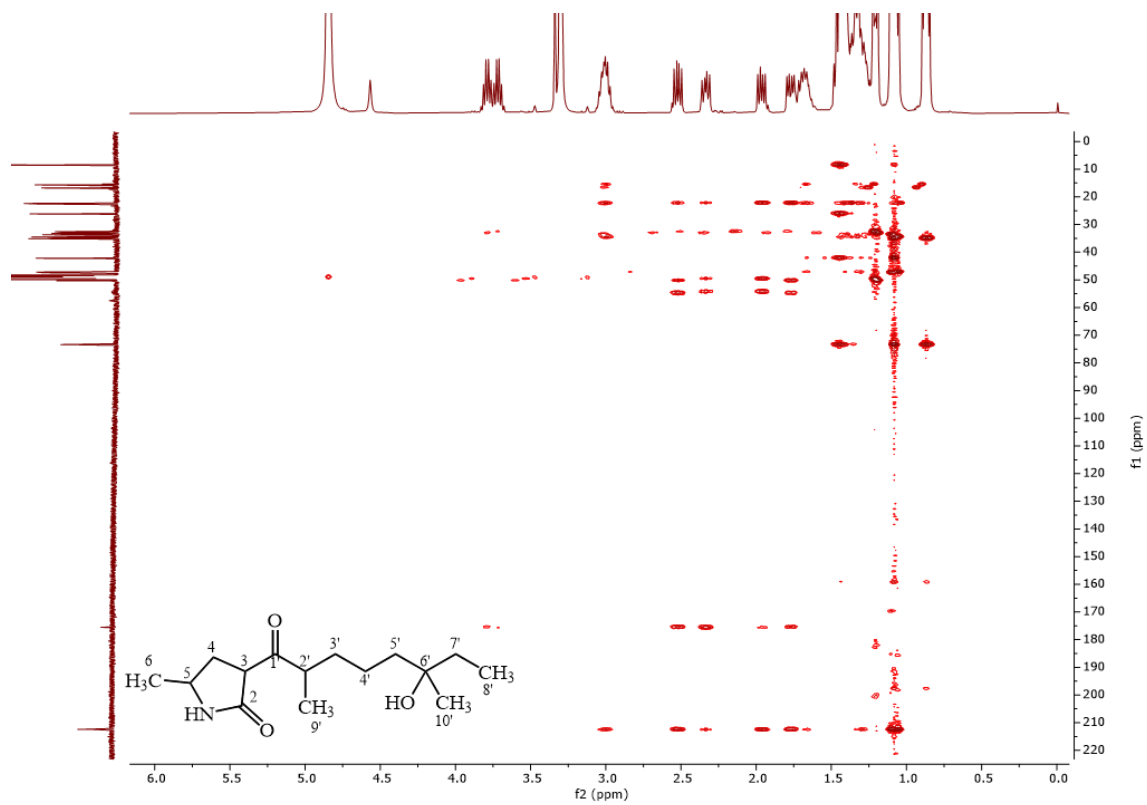
Figure S 5 HMBC spectrum of compound **3.1a/b** in methanol-d4, 400/100 MHz.
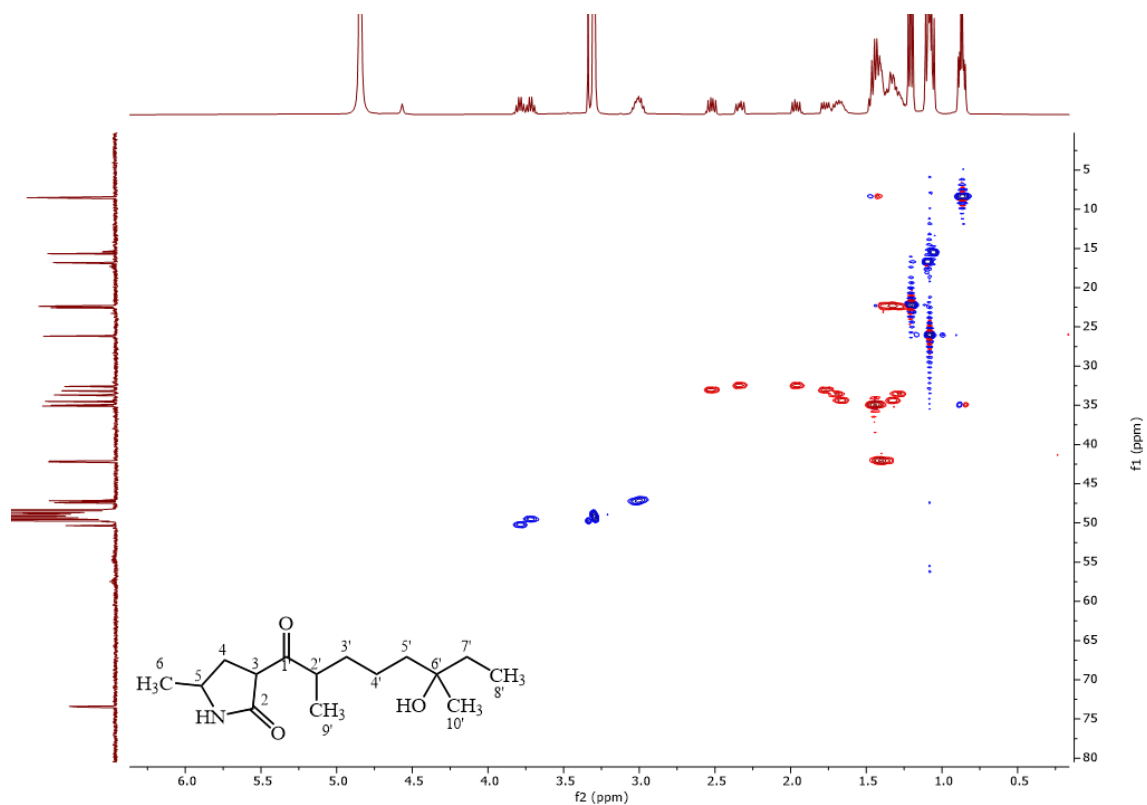
Figure S 6 HSQC spectrum of compound **3.1a/b** in methanol-d4, 400/100 MHz.
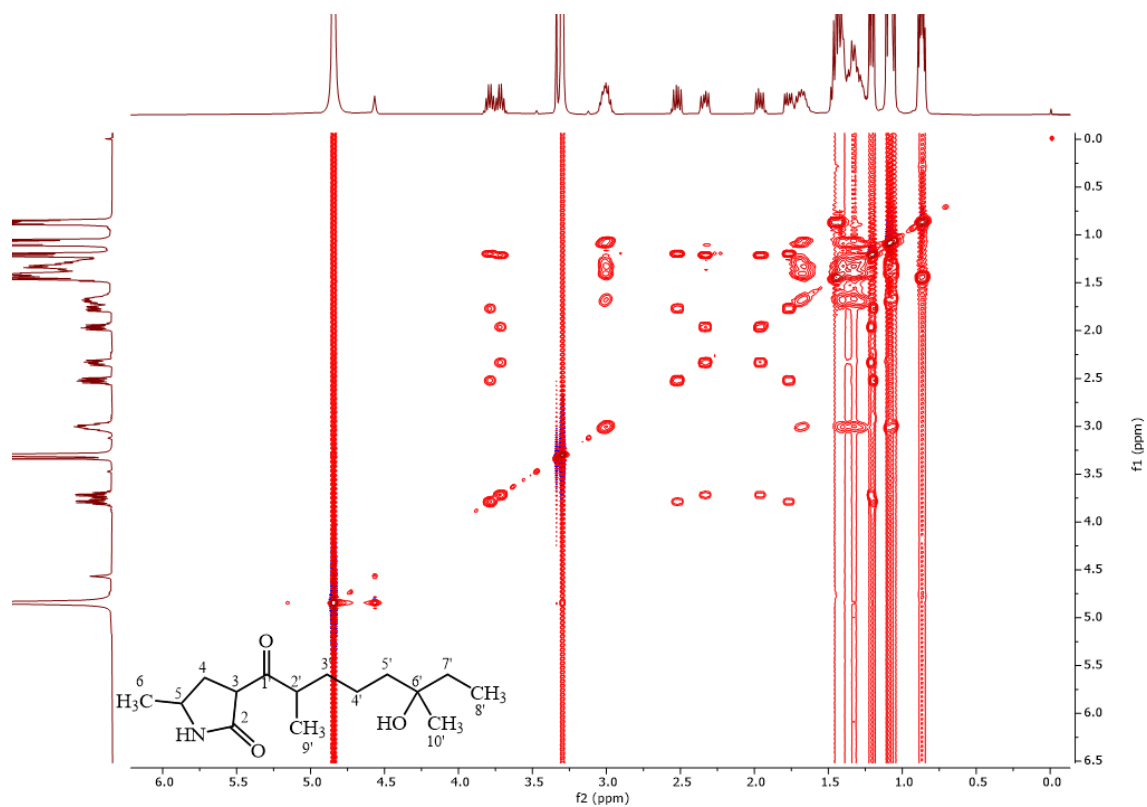
Figure S 7 TOCSY spectrum of compound **3.1a/b** in methanol-d$_4$, 400/100 MHz.
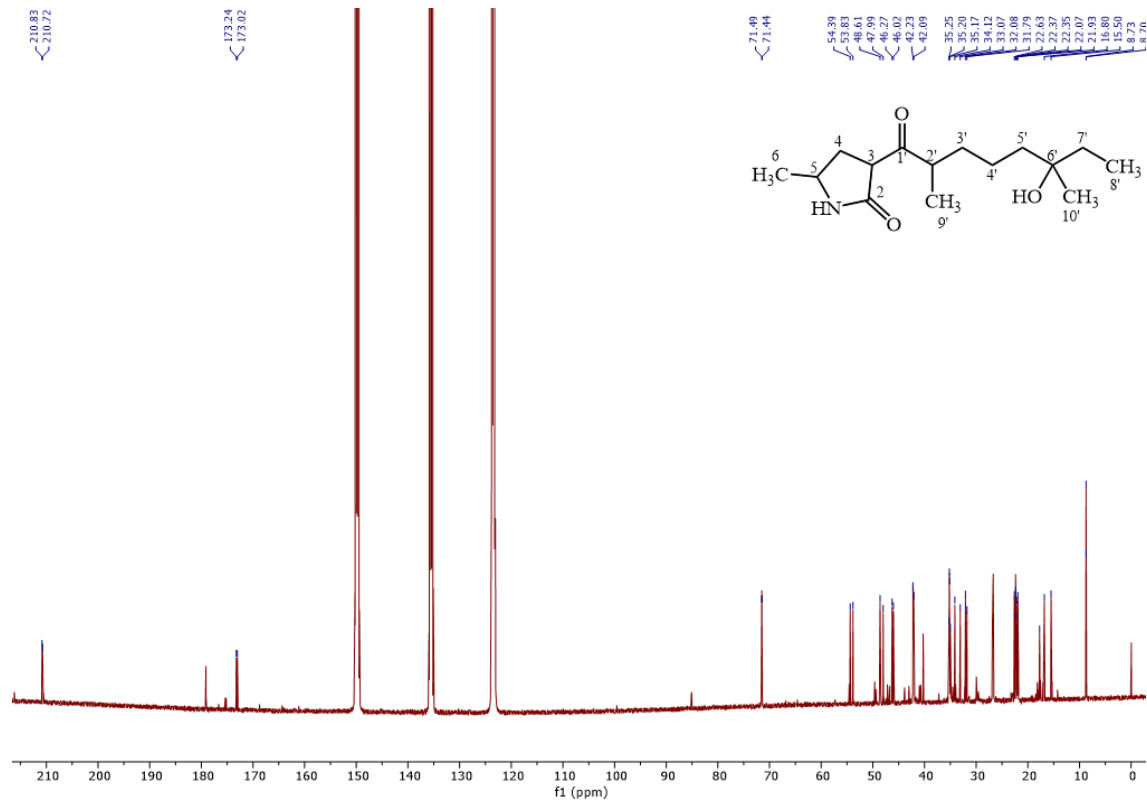
Figure S 8 ^{13}C spectrum of compound **3.1a/b** in pyridine-d$_5$, 125 MHz.

Figure S 9 ^{1}H spectrum of compound **3.1a/b** in pyridine-d$_5$, 500 MHz.

[M+H]$^+$
185.1290
C$_9$H$_{17}$N$_2$O$_2$
2.70 ppm

Figure S 10 (+)-ESI-HRMS spectrum of compound **3.2**.

126
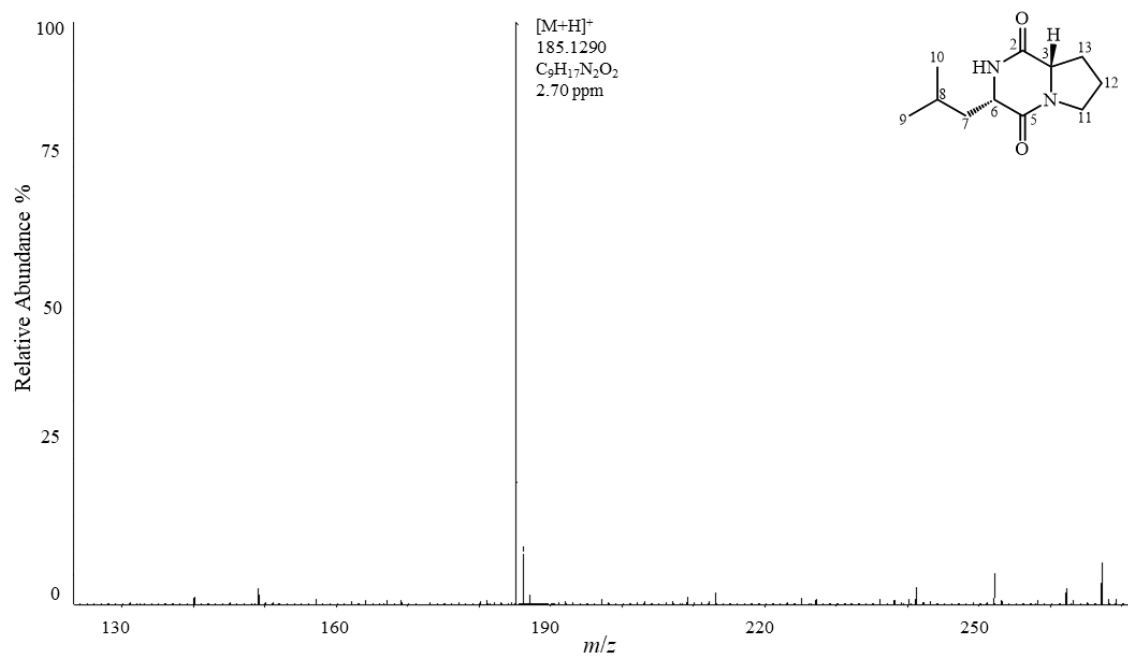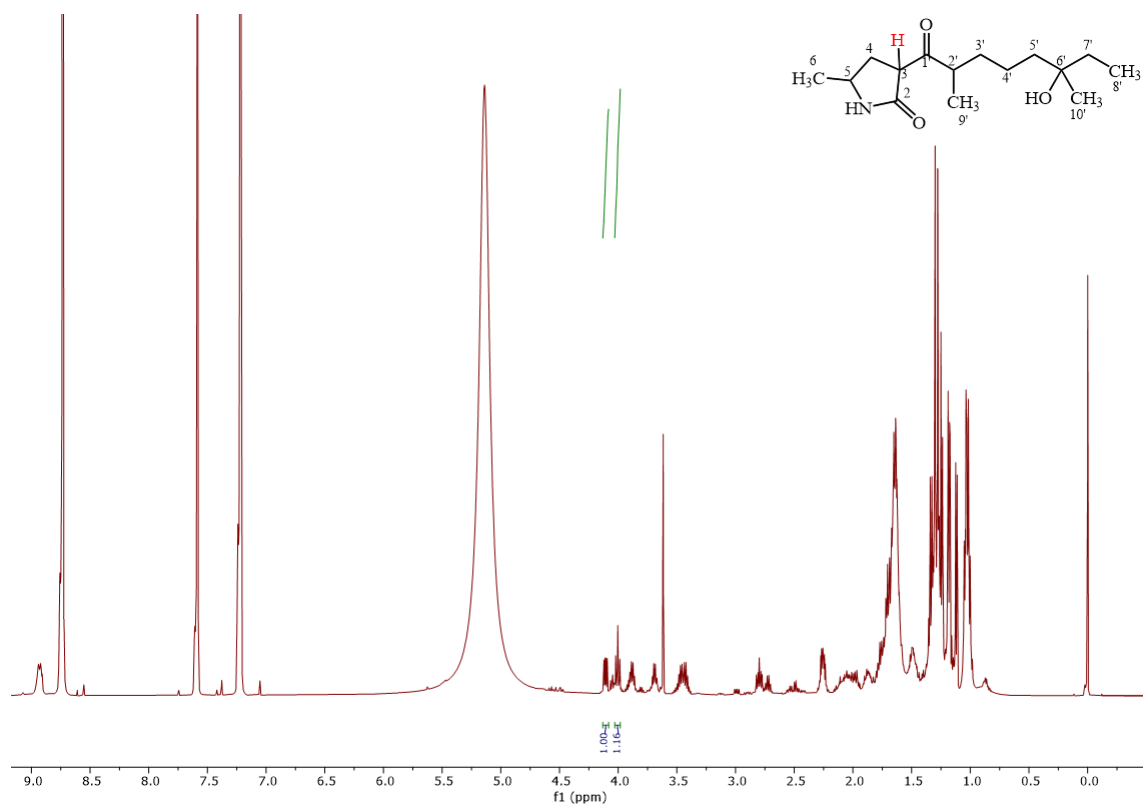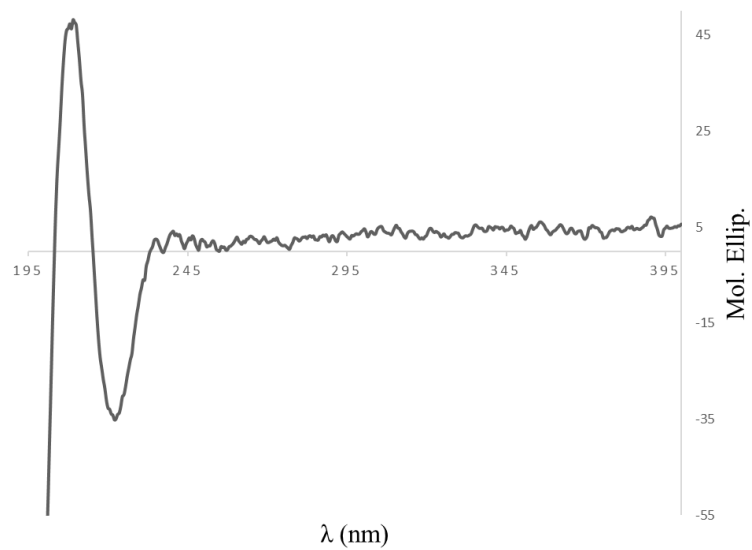
Figure S 11 ECD spectrum of *cyclo*-L-Leu-L-Pro (**3.2**) in methanol.
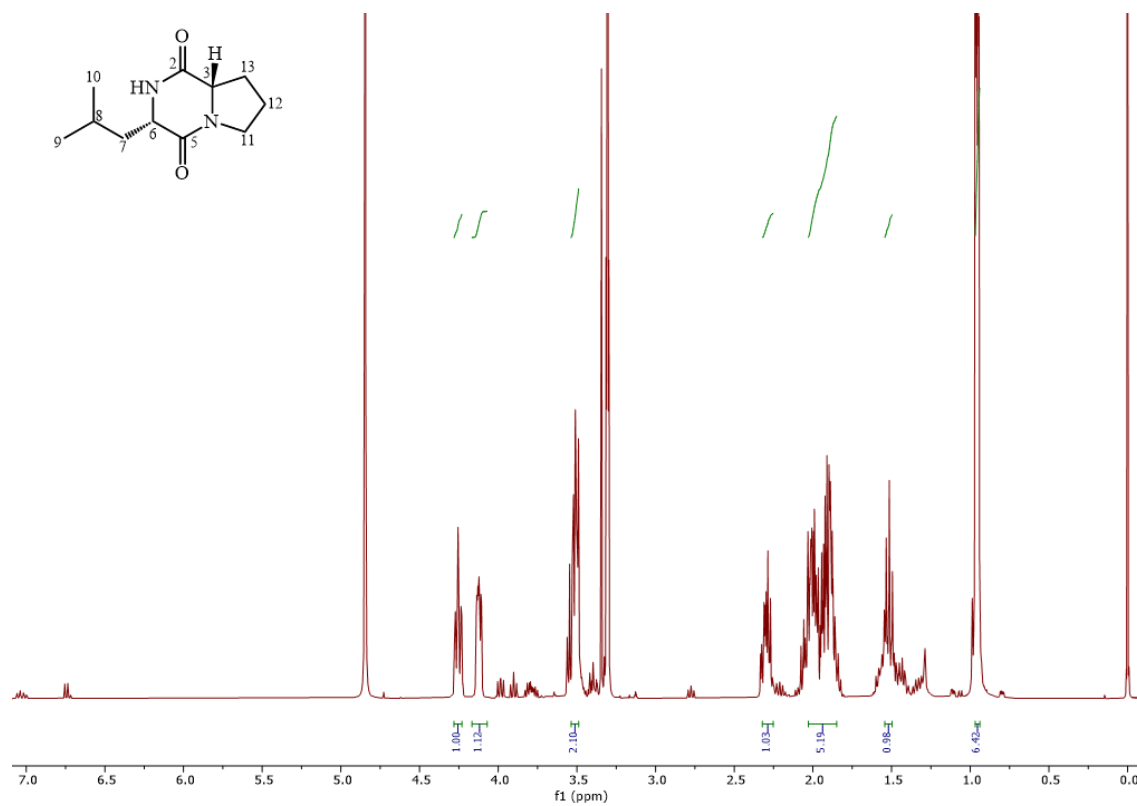
Figure S 12 ^{1}H NMR spectrum of compound **3.2** in methanol-d4, 400 MHz.
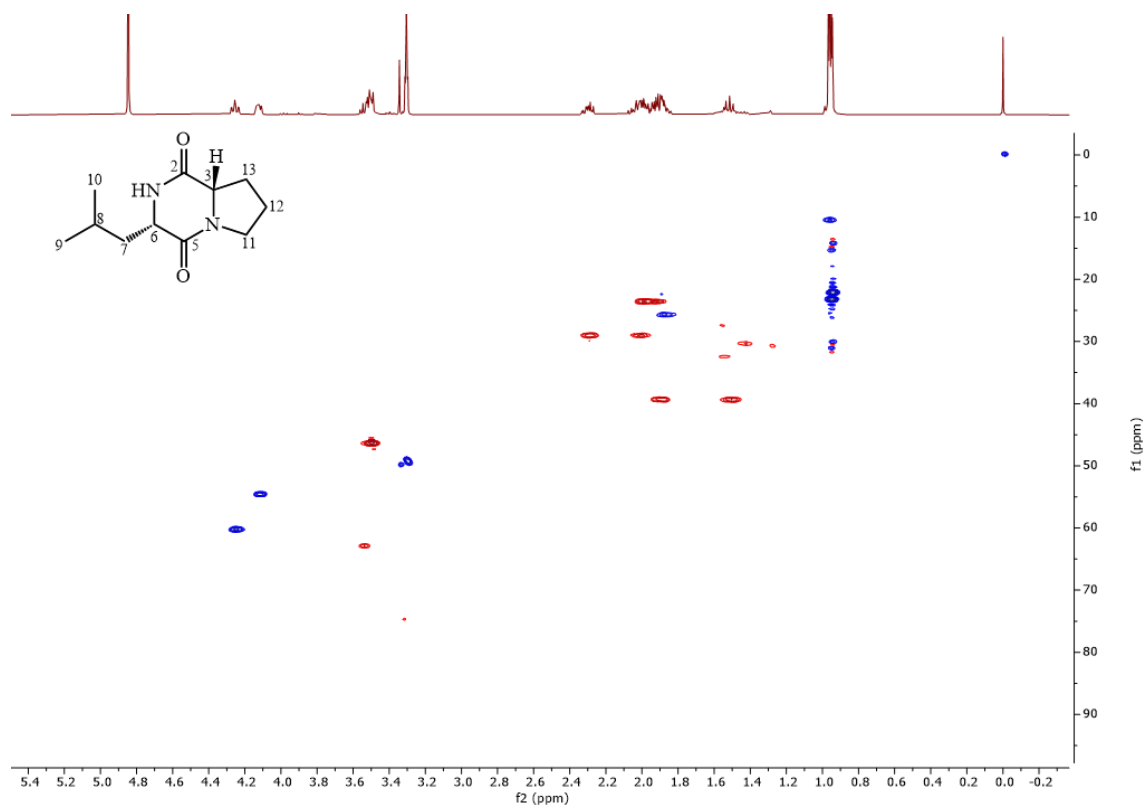
Figure S 13 HSQC spectrum of compound **3.2** in methanol-d₄, 400/100 MHz.
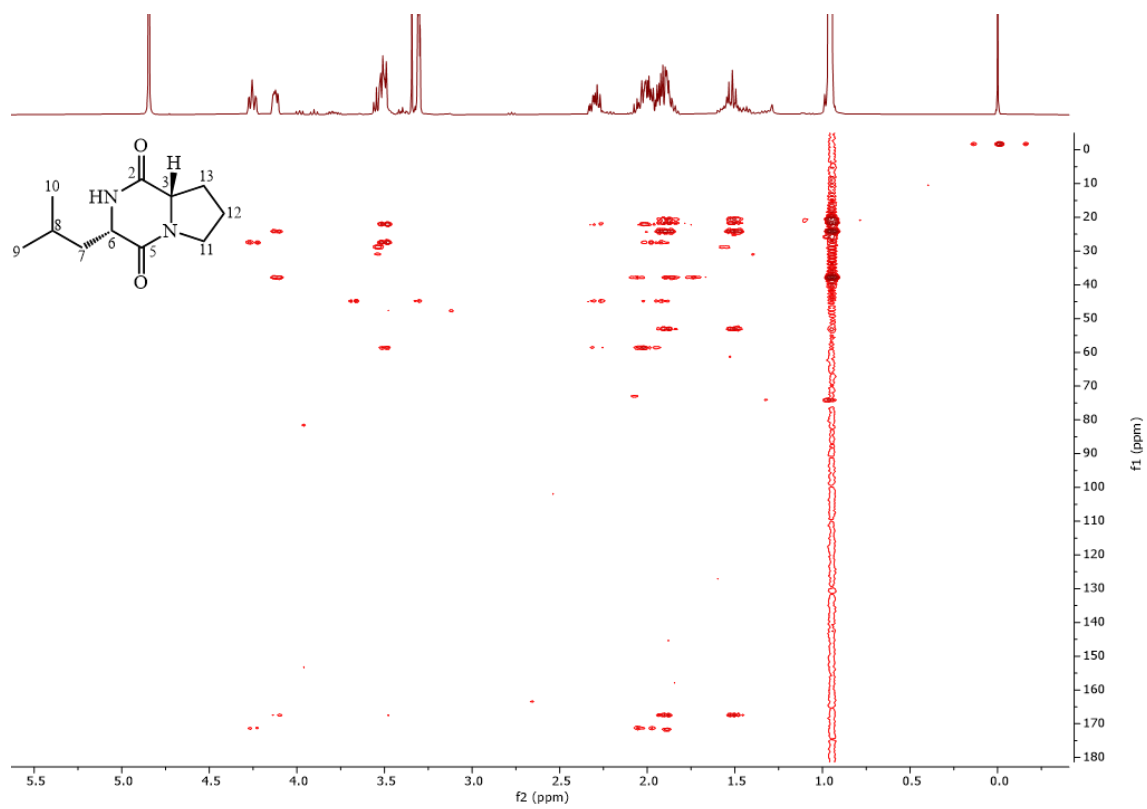
Figure S 14 HMBC spectrum of compound **3.2** in methanol-d₄, 400/100 MHz.
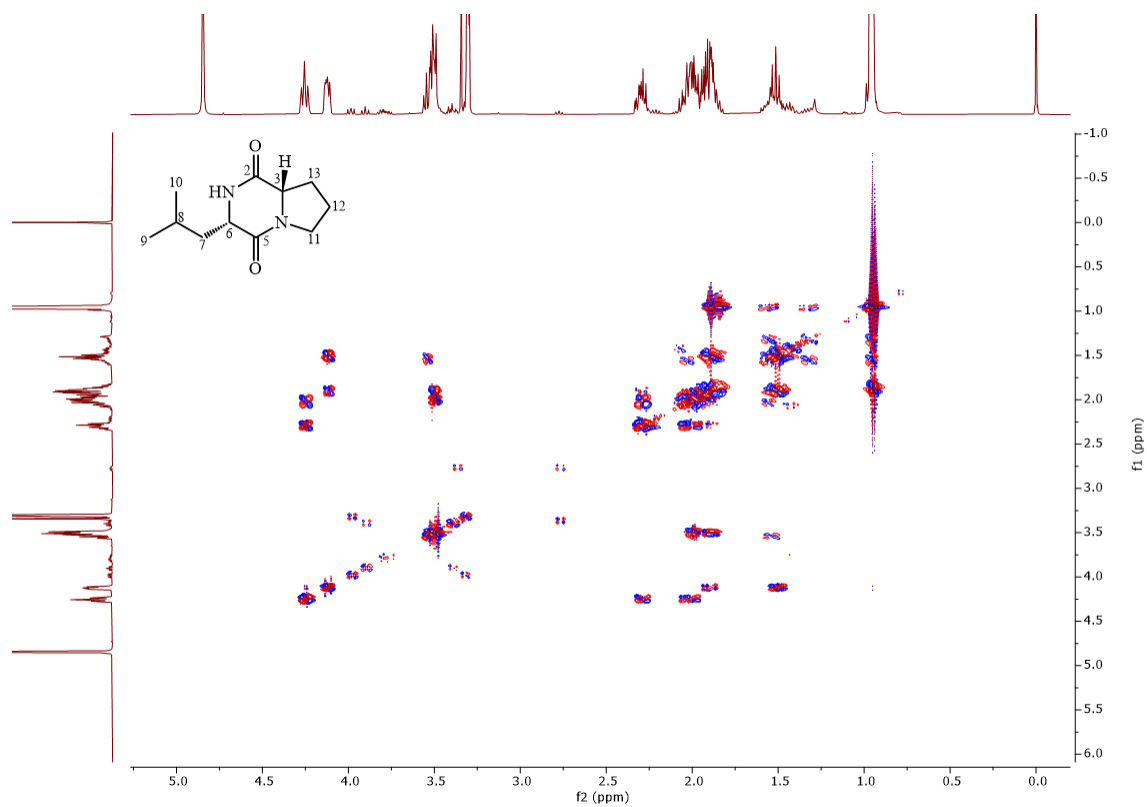
Figure S 15 COSY spectrum of compound **3.2** in methanol-d4, 400 MHz.

[M+H]⁺
164.1082
$C_{10}H_{14}NO_3$
7.31 ppm
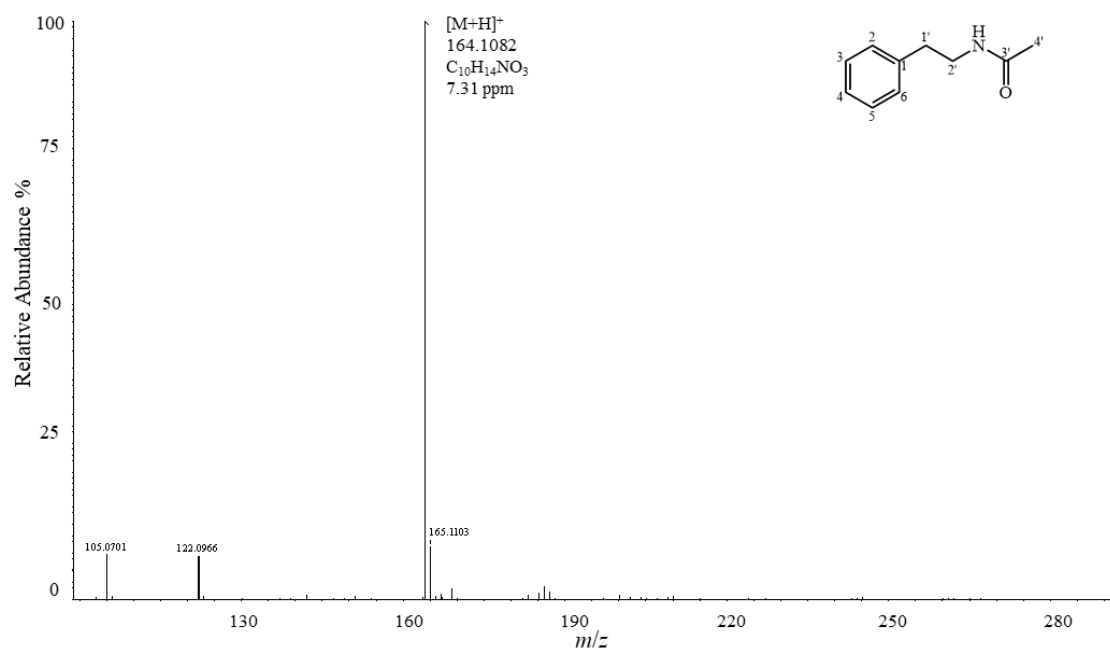
Figure S 16 (+)-ESI-HRMS spectrum of compound **3.3**.
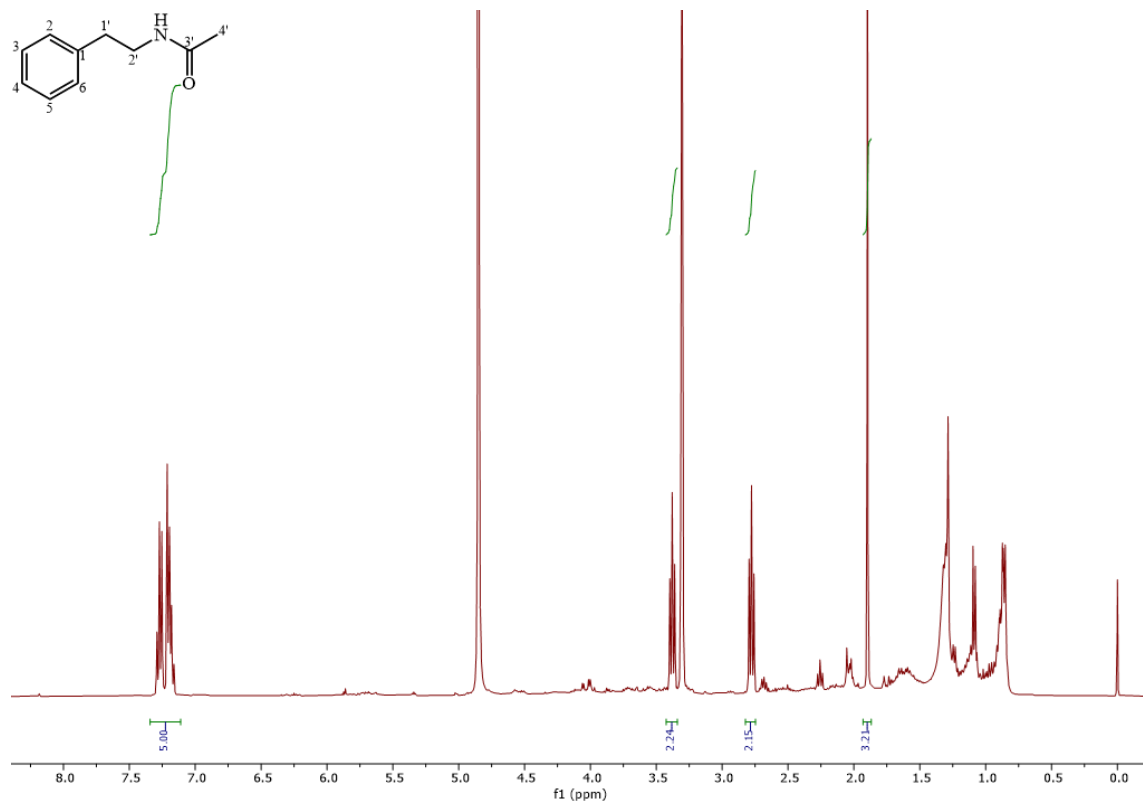
Figure S 17 ^{1}H NMR spectrum of compound **3.3** in methanol-d$_4$, 400 MHz.
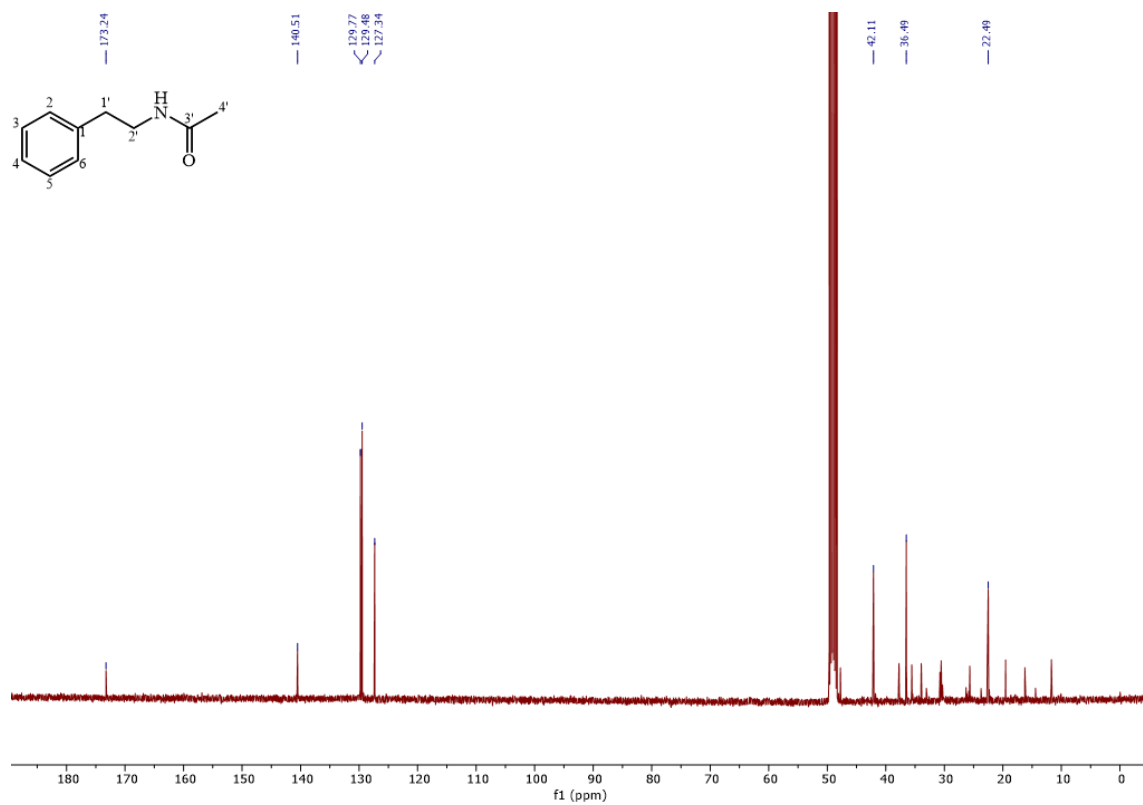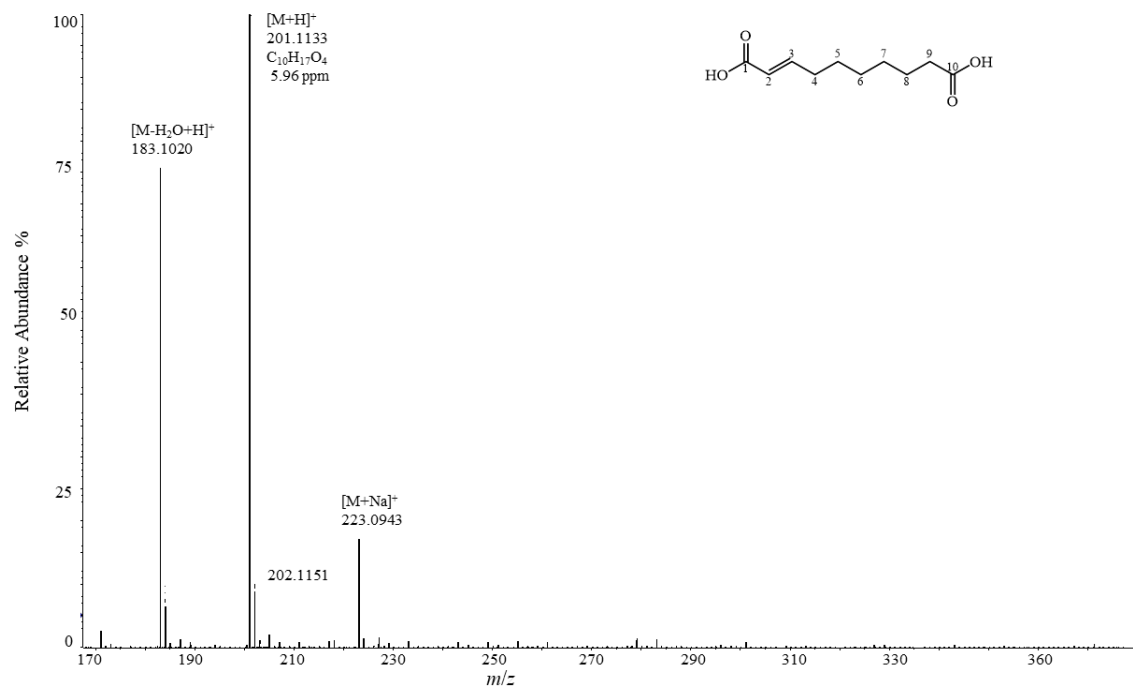

Figure S 18 ^{13}C NMR spectrum of compound **3.3** in methanol-d$_4$, 100 MHz.
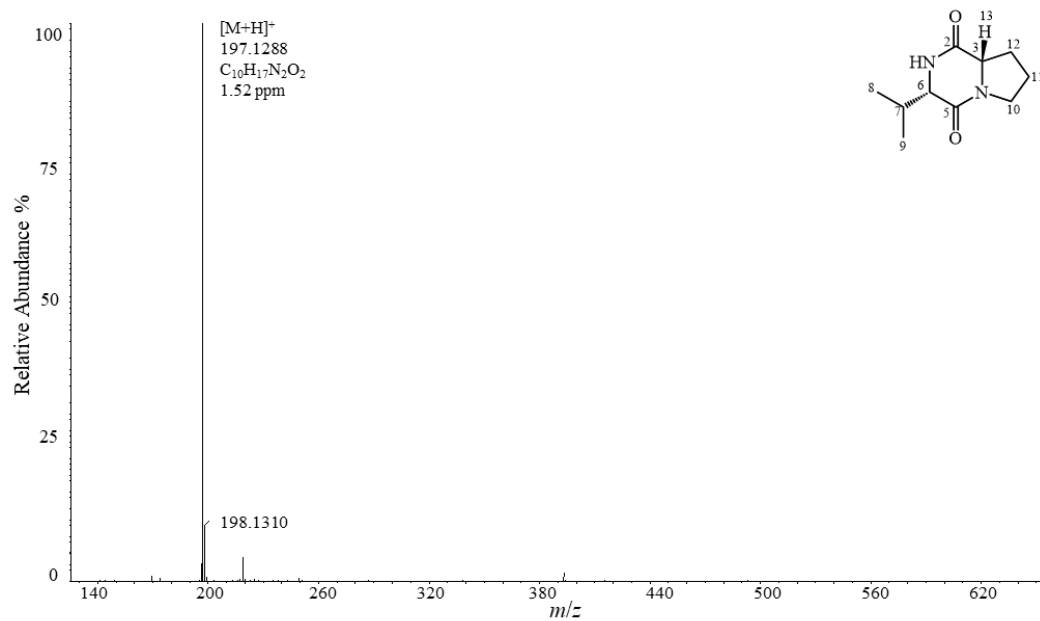
Figure S 19 (+)-ESI-HRMS spectrum of compound **3.4**.
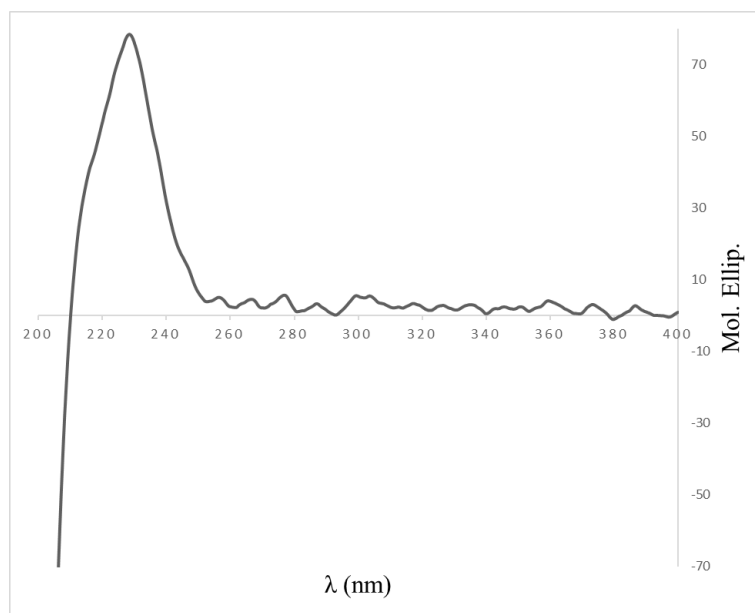
Figure S 20 Experimental ECD spectrum of *cyclo*-L-Val-L-Pro (**3.4**) in methanol.
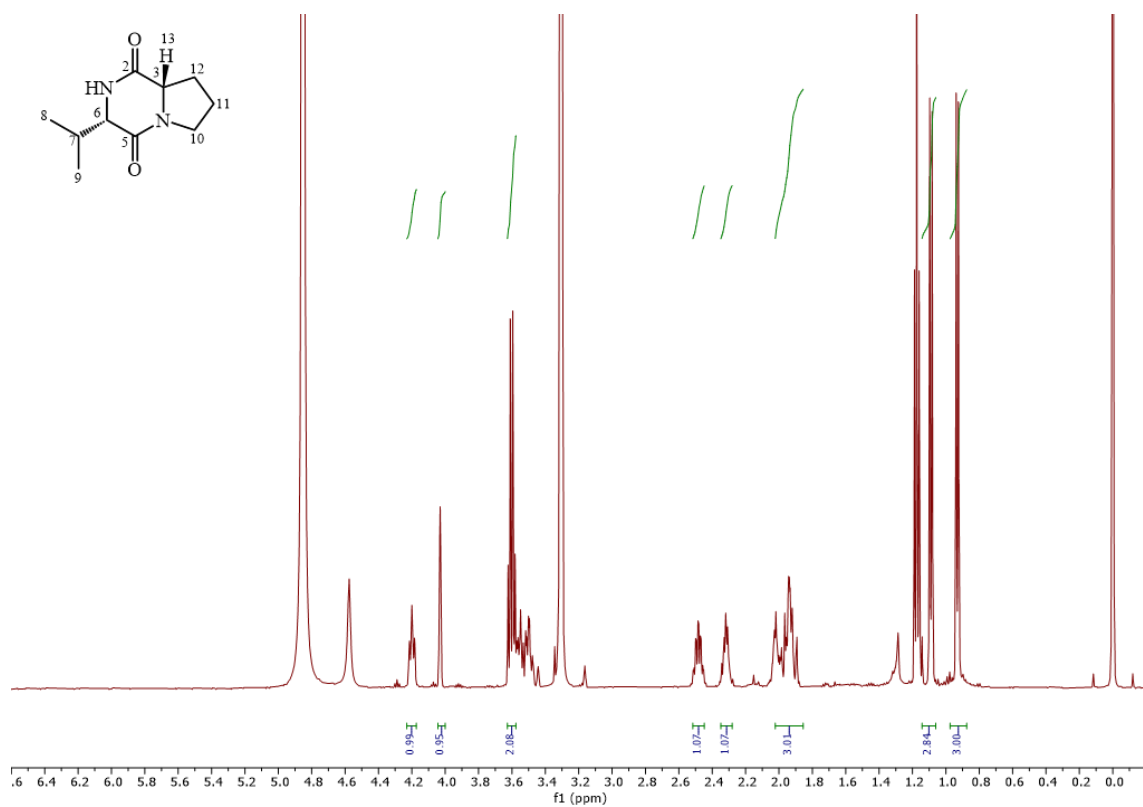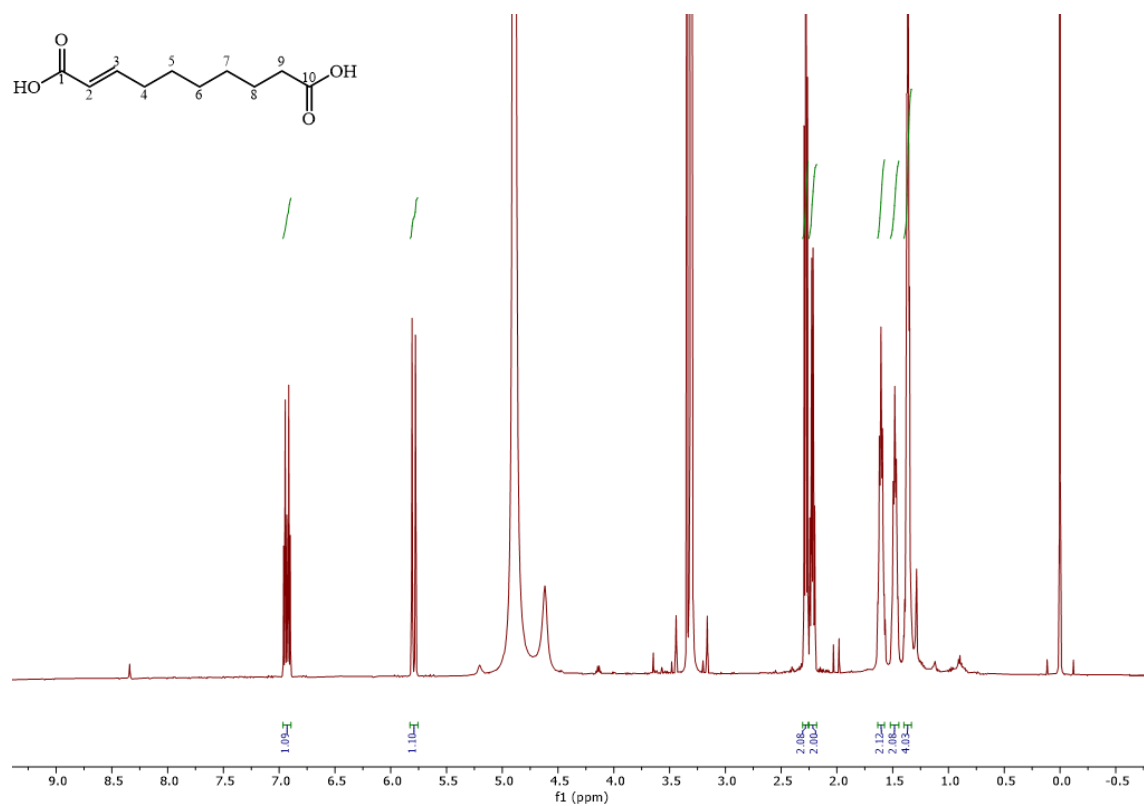
Figure S 21 ^{1}H NMR spectrum of compound **3.4** in methanol-d$_4$, 500 MHz.
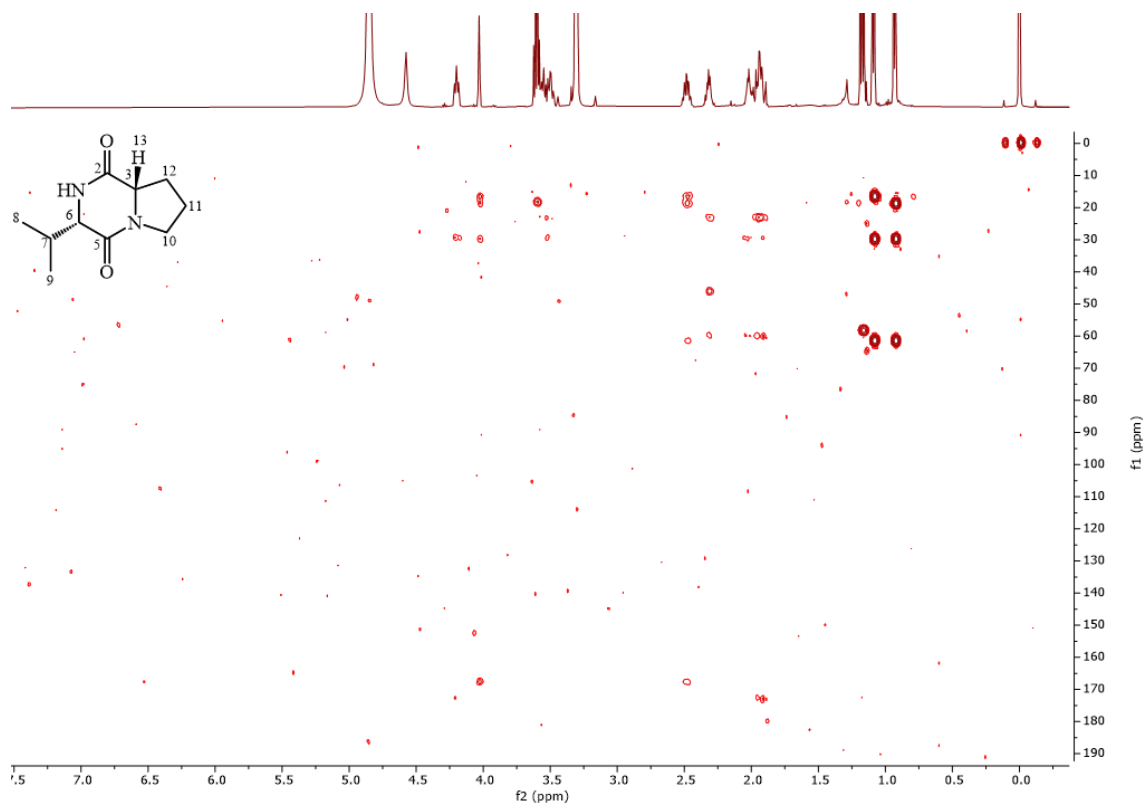
Figure S 22 HMBC spectrum of compound **3.4** in methanol-d$_4$, 500/125 MHz.

132
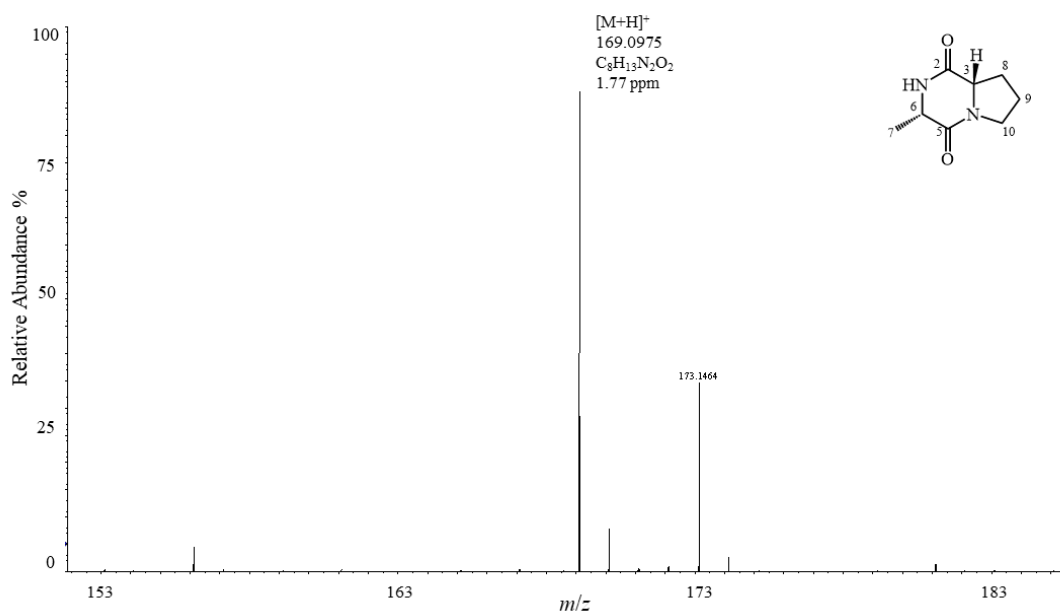
Figure S 23 (+)-ESI-HRMS spectrum of compound **3.5**.
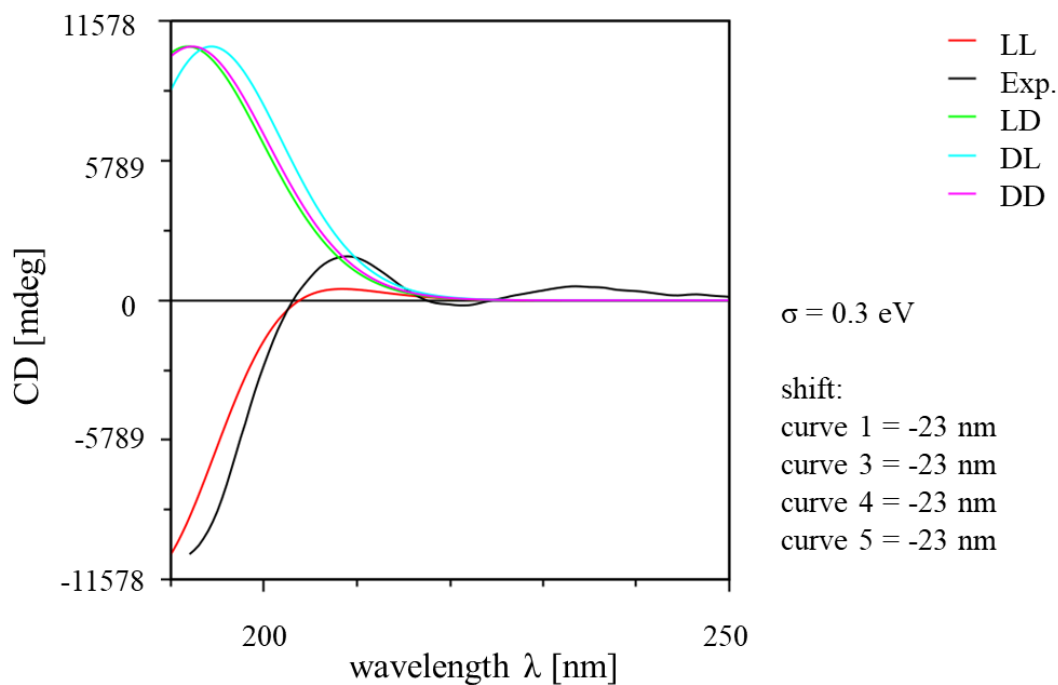
Figure S 24 Calculated ECD spectra of compound **3.5** in comparison with the experimental one. Red = *cyclo*-L-Ala-L-Pro, green = *cyclo*-L-Ala-D-Pro, blue = *cyclo*-D-Ala-L-Pro, purple = *cyclo*-D-Ala-D-Pro. Best similarity factor found for SS (red) with 0.955 at sigma = 0.3 eV.

133
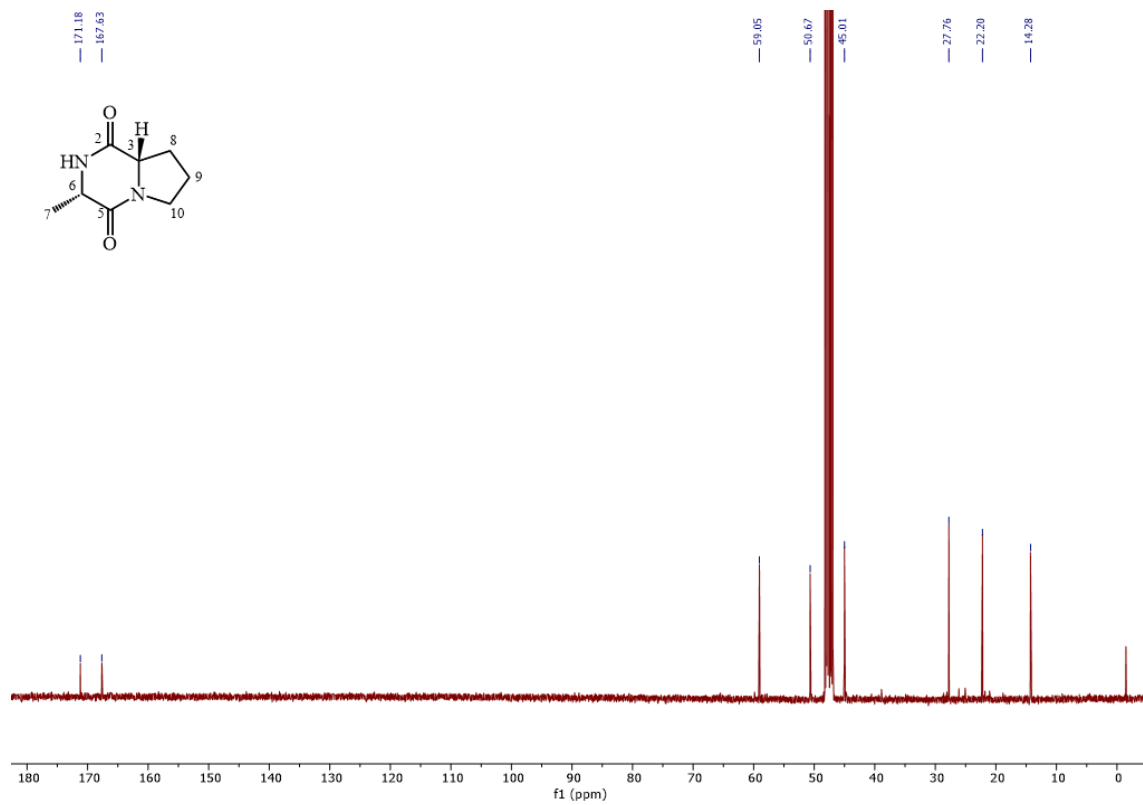
Figure S 25 ¹³C spectrum of compound **3.5** in methanol-d₄, 100 MHz.
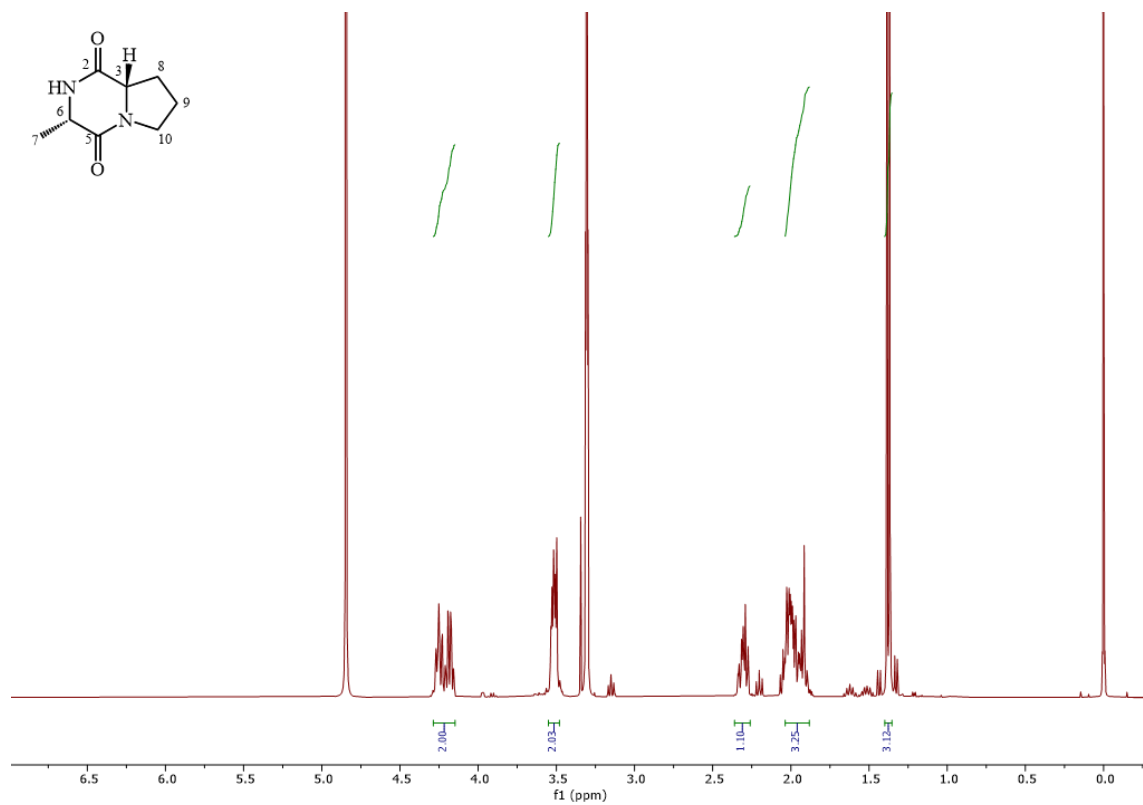
Figure S 26 ¹H NMR spectrum of compound **3.5** in methanol-d₄, 400 MHz.
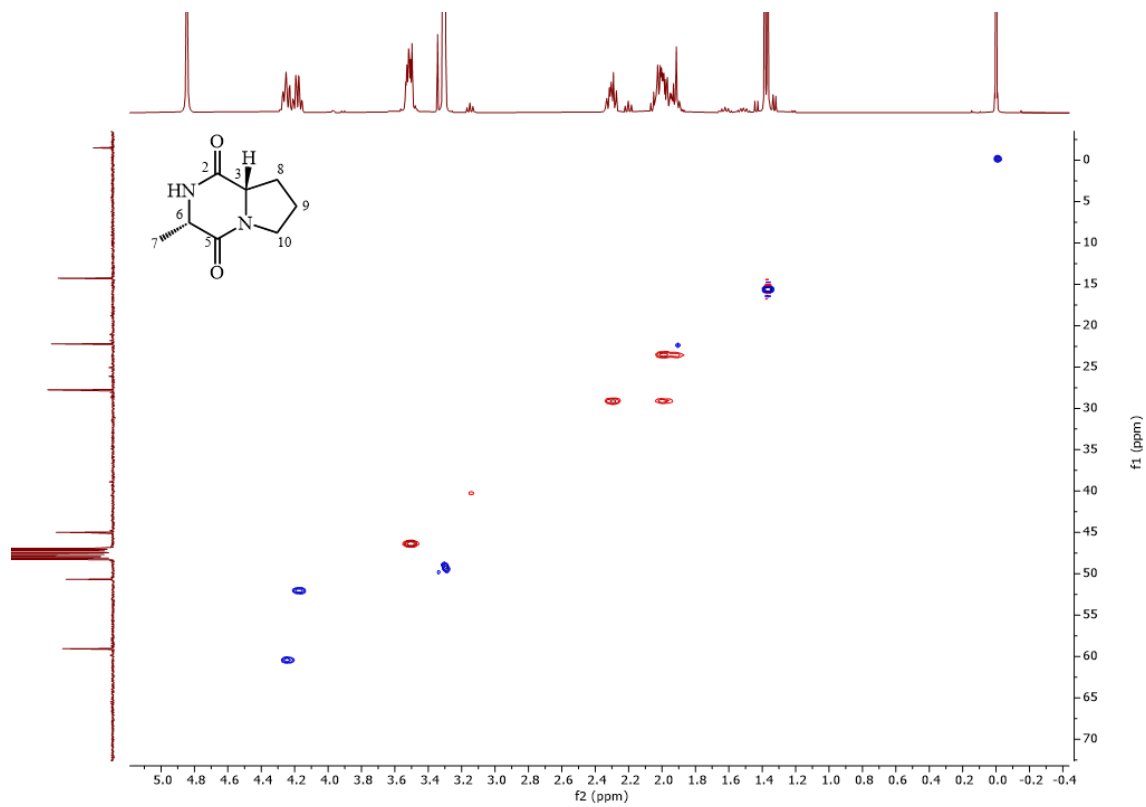
Figure S 27 HSQC spectrum of compound **3.5** in methanol-d$_4$, 400/100 MHz.
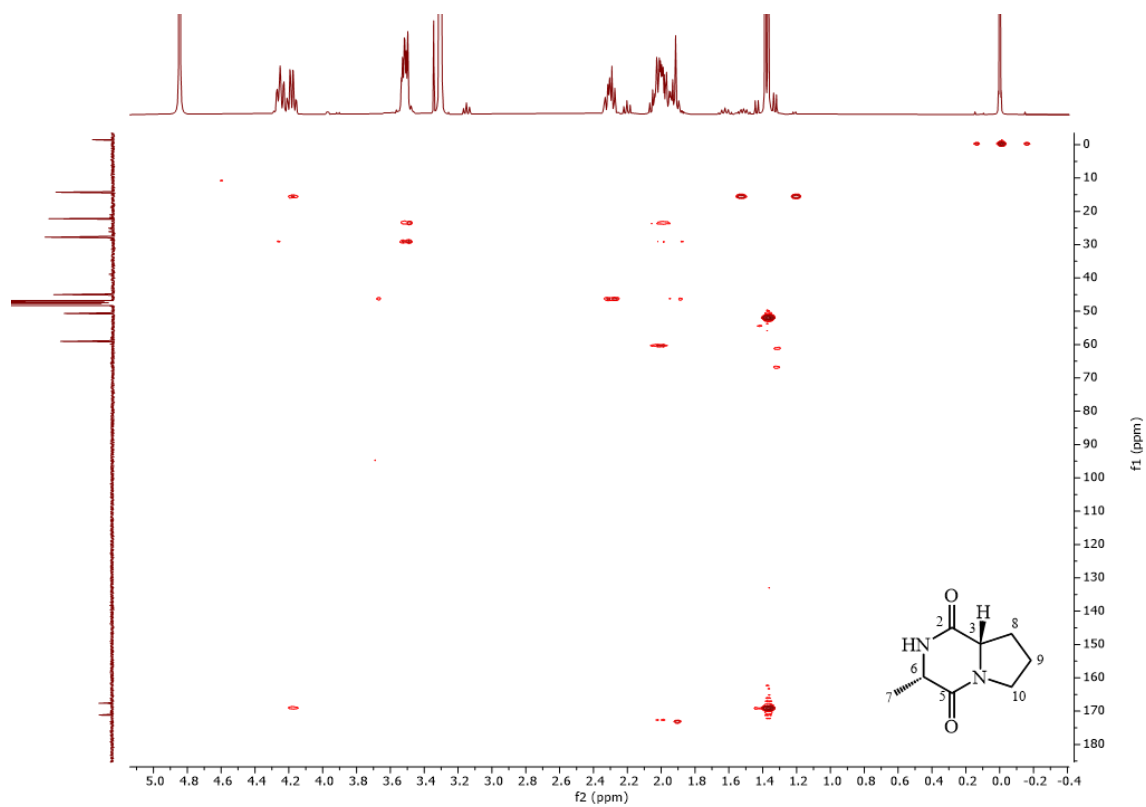
Figure S 28 HMBC spectrum of compound **3.5** in methanol-d$_4$, 400/100 MHz.

135
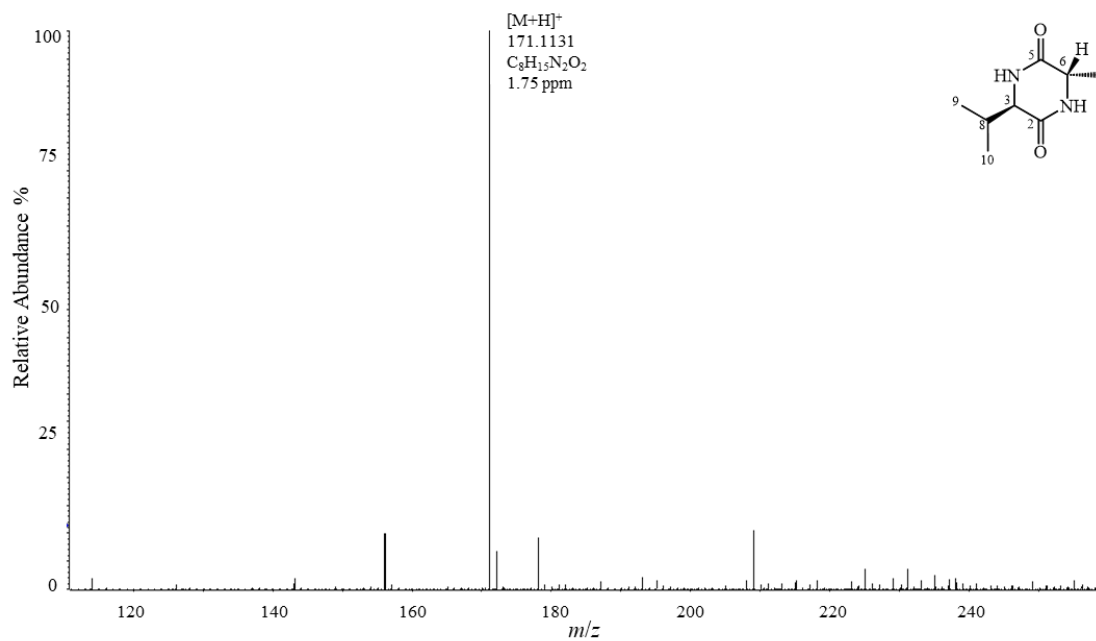
Figure S 29 (+)-ESI-HRMS spectrum of compound **3.6**.
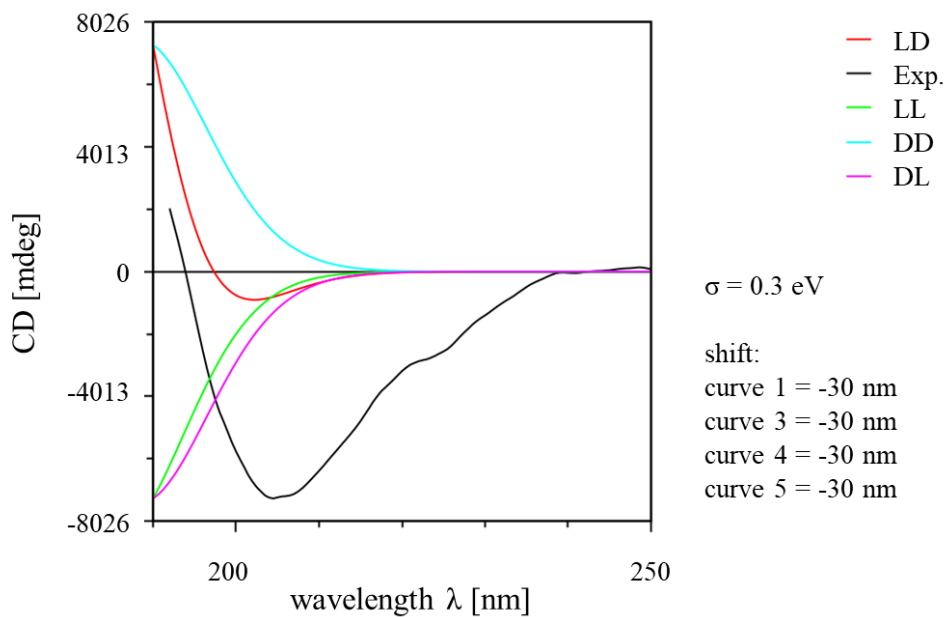
Figure S 30 Calculated ECD spectra of compound **3.6** in comparison with the experimental one. Red = *cyclo*-L-Ala-D-Val, green = *cyclo*-L-Ala-L-Val, blue = *cyclo*-D-Ala-D-Val, purple = *cyclo*-D-Ala-L-Val. Best similarity factor found for SR (red) with 0.864 at sigma = 0.3 eV.
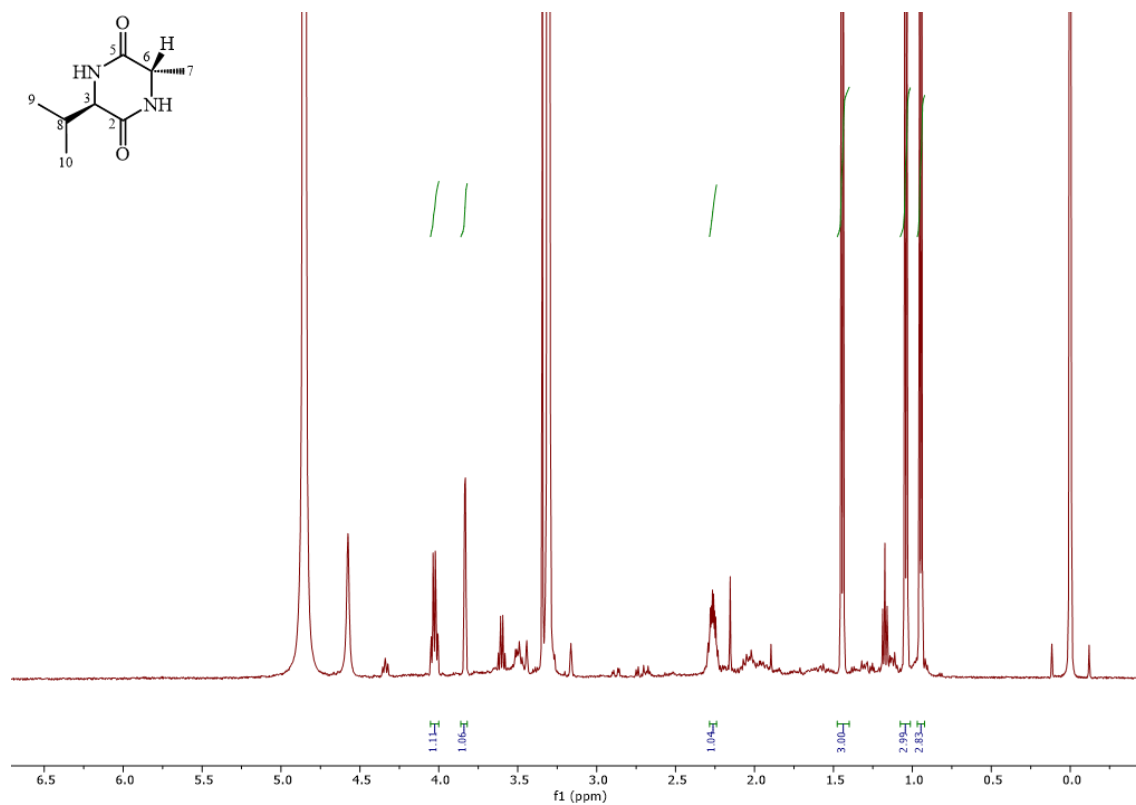
Figure S 31 ^{1}H NMR spectrum of compound **3.6** in methanol-d$_4$, 500 MHz.
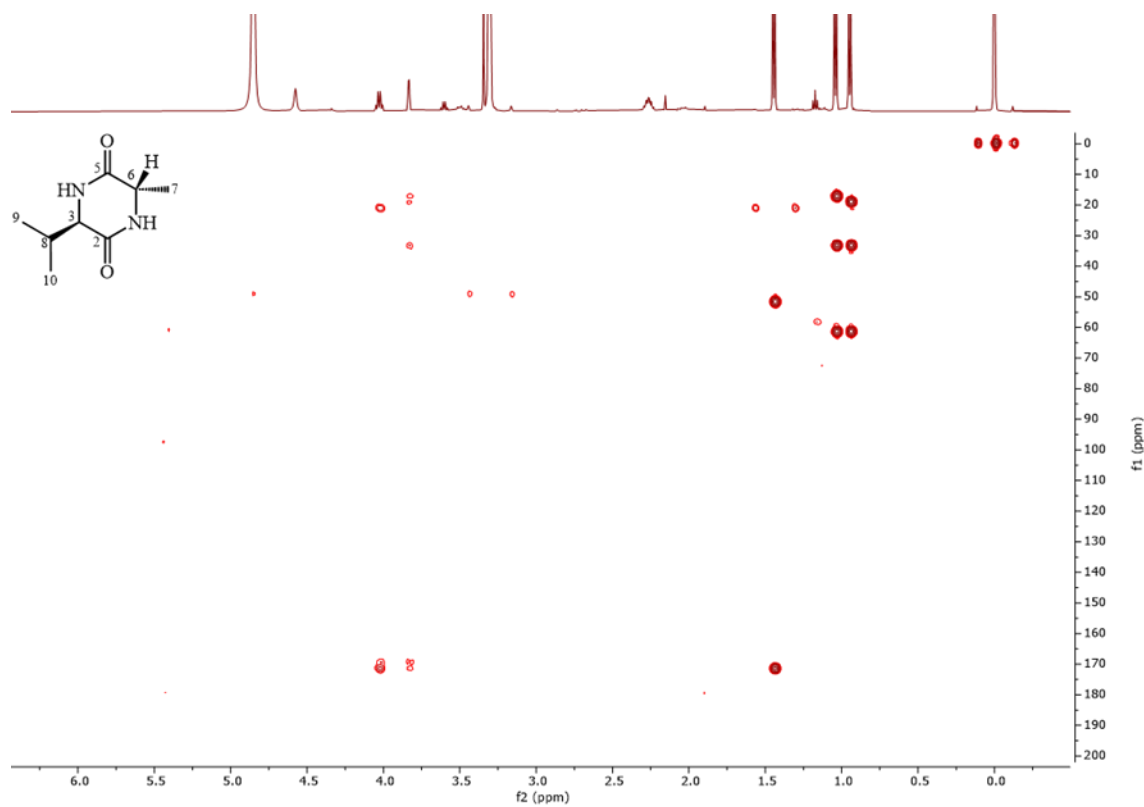
Figure S 32 HMBC spectrum of compound **3.6** in methanol-d$_4$, 500/125 MHz.
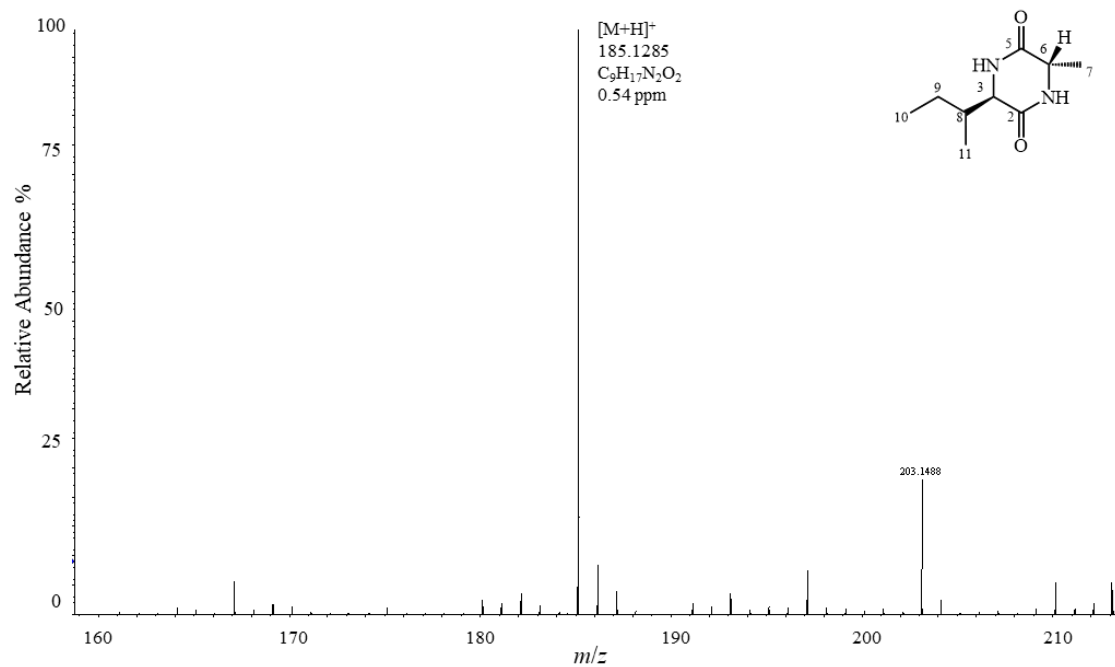
Figure S 33 (+)-ESI-HRMS spectrum of compound **3.7**.
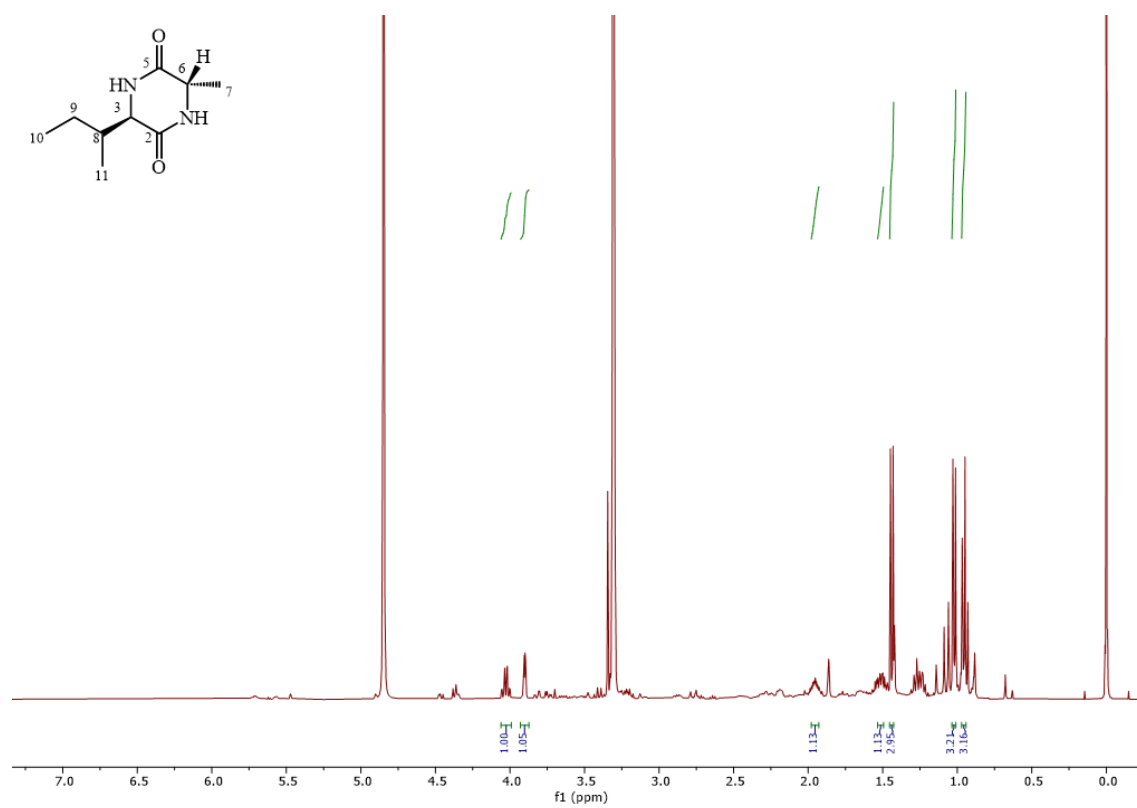
Figure S 34 ^{1}H NMR spectrum of compound **3.7** in methanol-d4, 500 MHz.
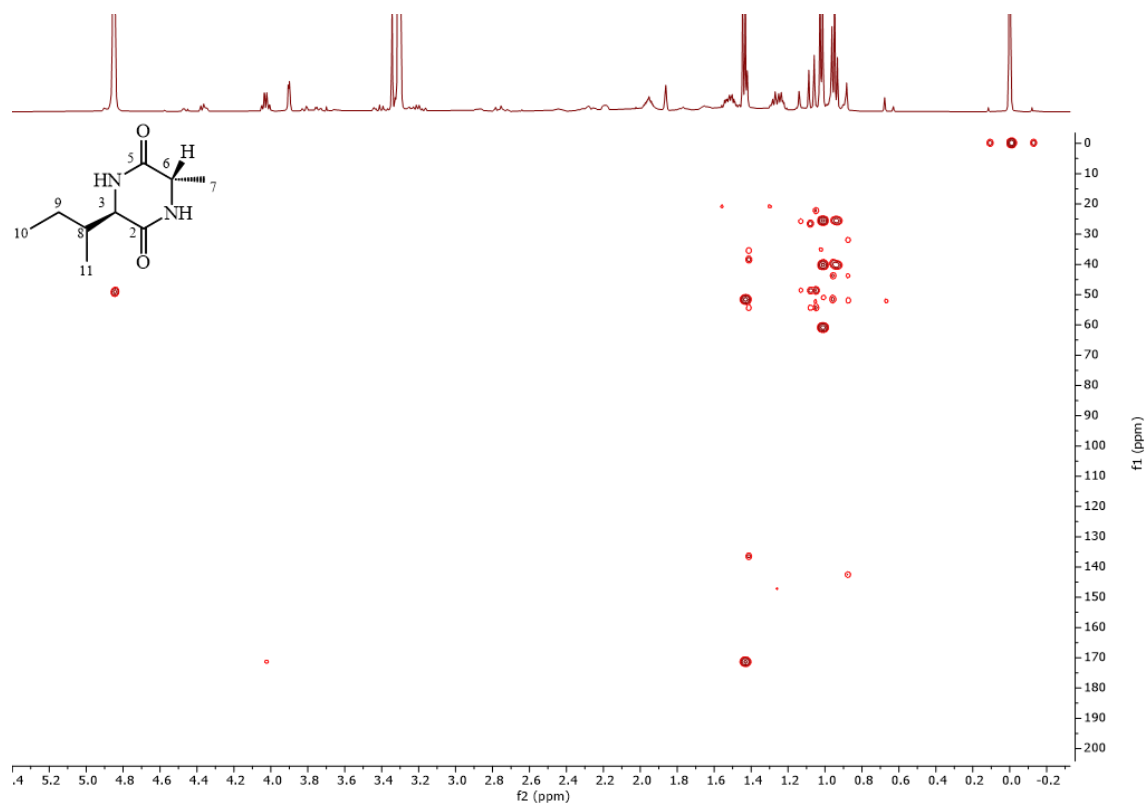
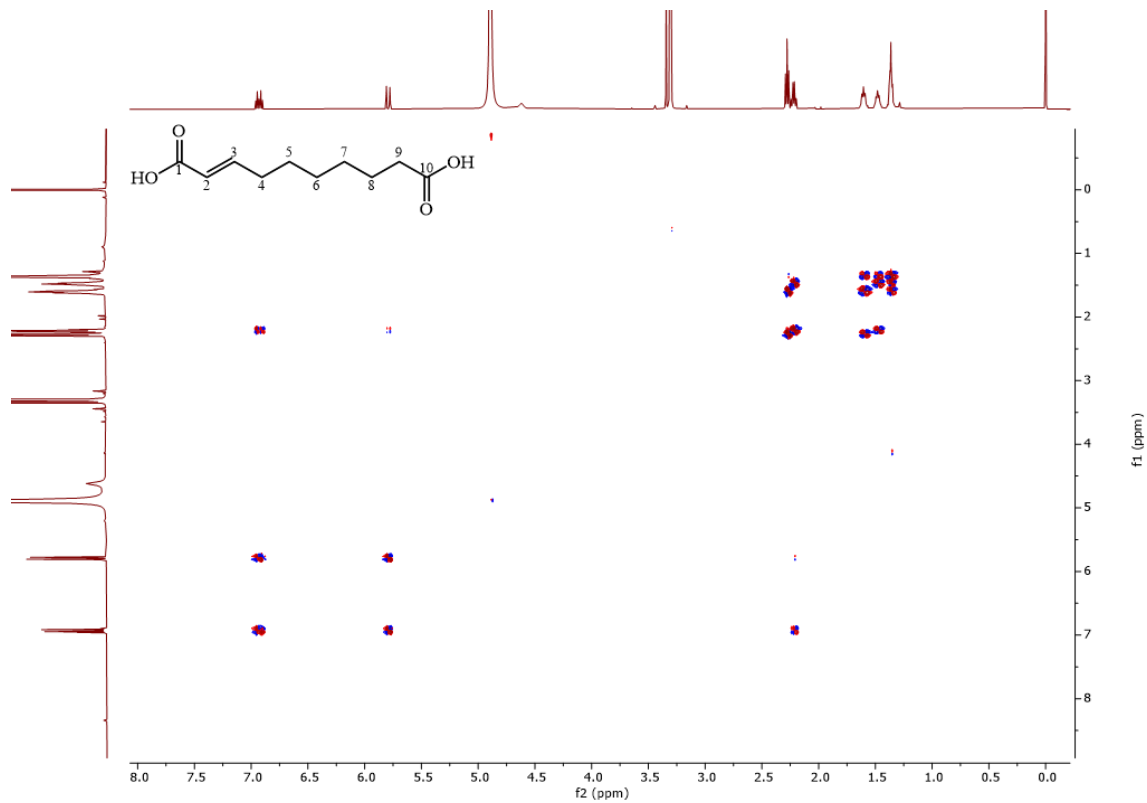**Figure S 35** HMBC spectrum of compound **3.7** in methanol-d₄, 500/125 MHz.

[M+H]⁺
185.1285
C₉H₁₇N₂O₂
0.54 ppm

203.1488
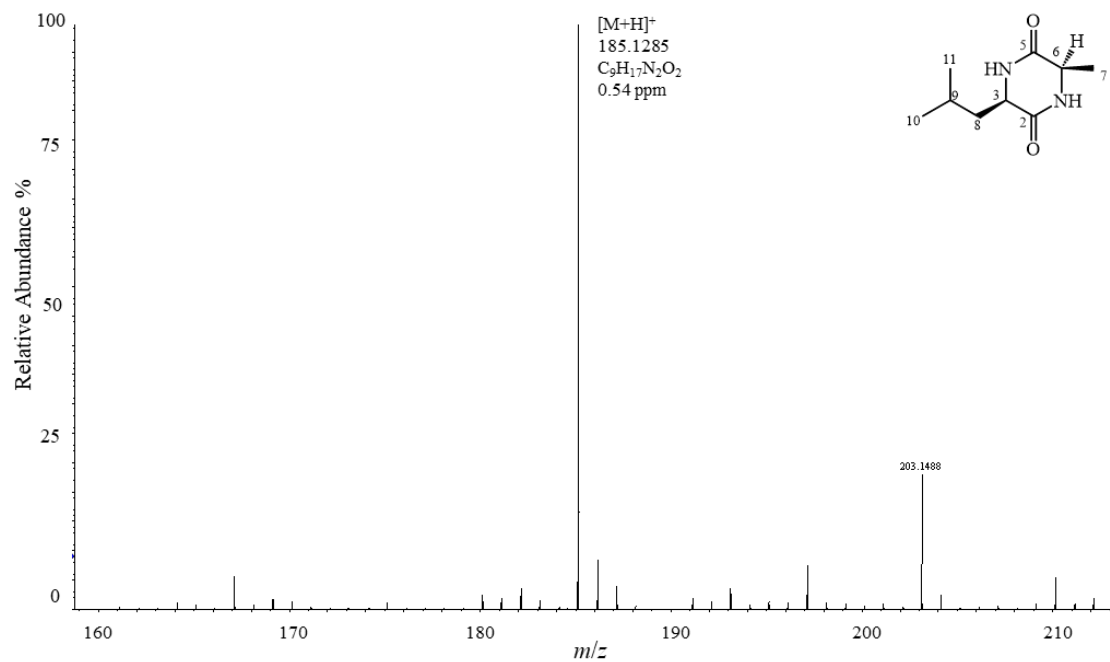
Figure S 36 (+)-ESI-HRMS spectrum of compound **3.8**.
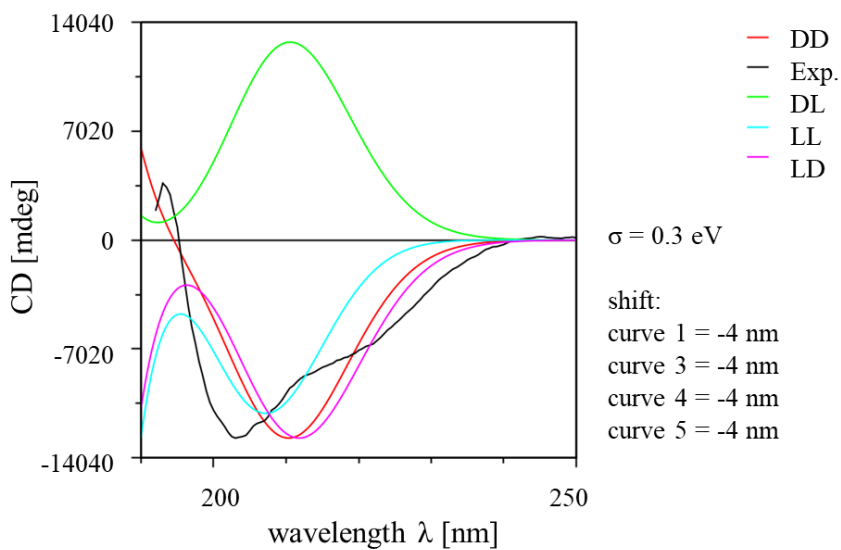
Figure S 37 Calculated ECD spectra of compound **3.8** in comparison with the experimental one (black). Red = *cyclo*-D-Ala-D-Leu, green = *cyclo*-D-Ala-L-Leu, blue = *cyclo*-L-Ala-D-Leu, purple = *cyclo*-L-Ala-D-Leu. Best similarity factor found for RR (red) with 0.919 at sigma = 0.3 eV.
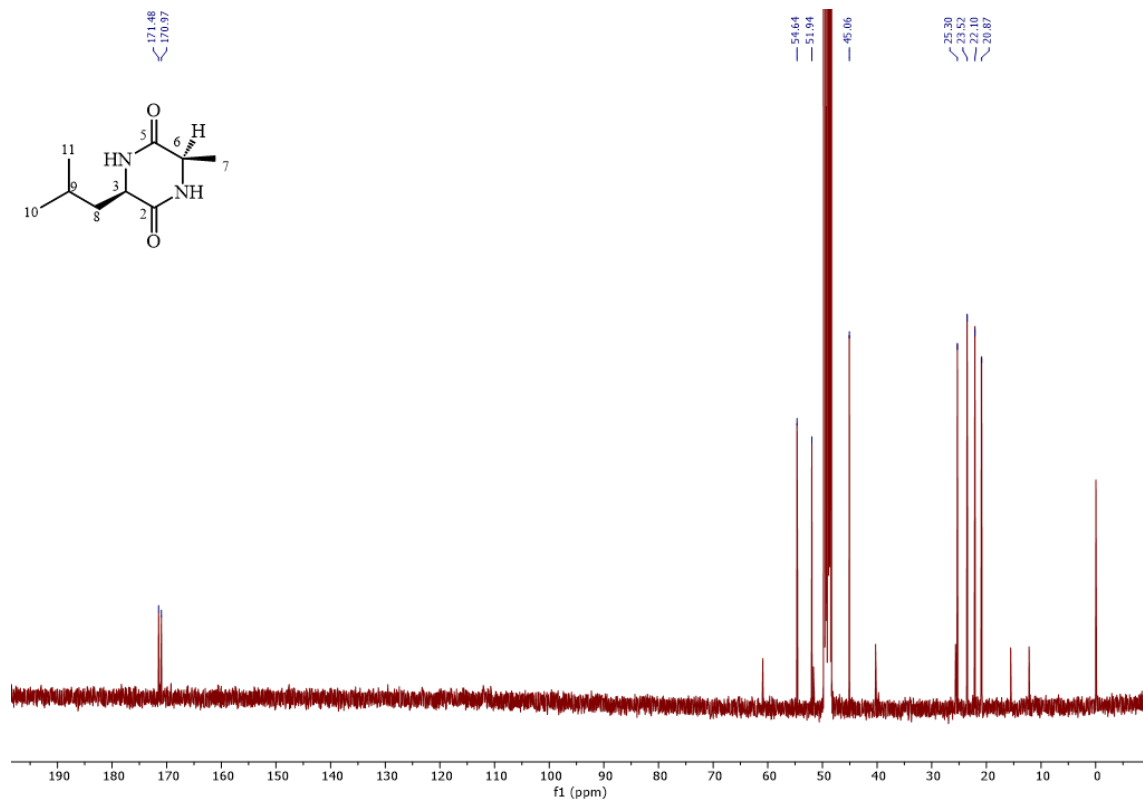
Figure S 38 ^{13}C NMR spectrum of compound **3.8** in methanol-d₄, 100 MHz.
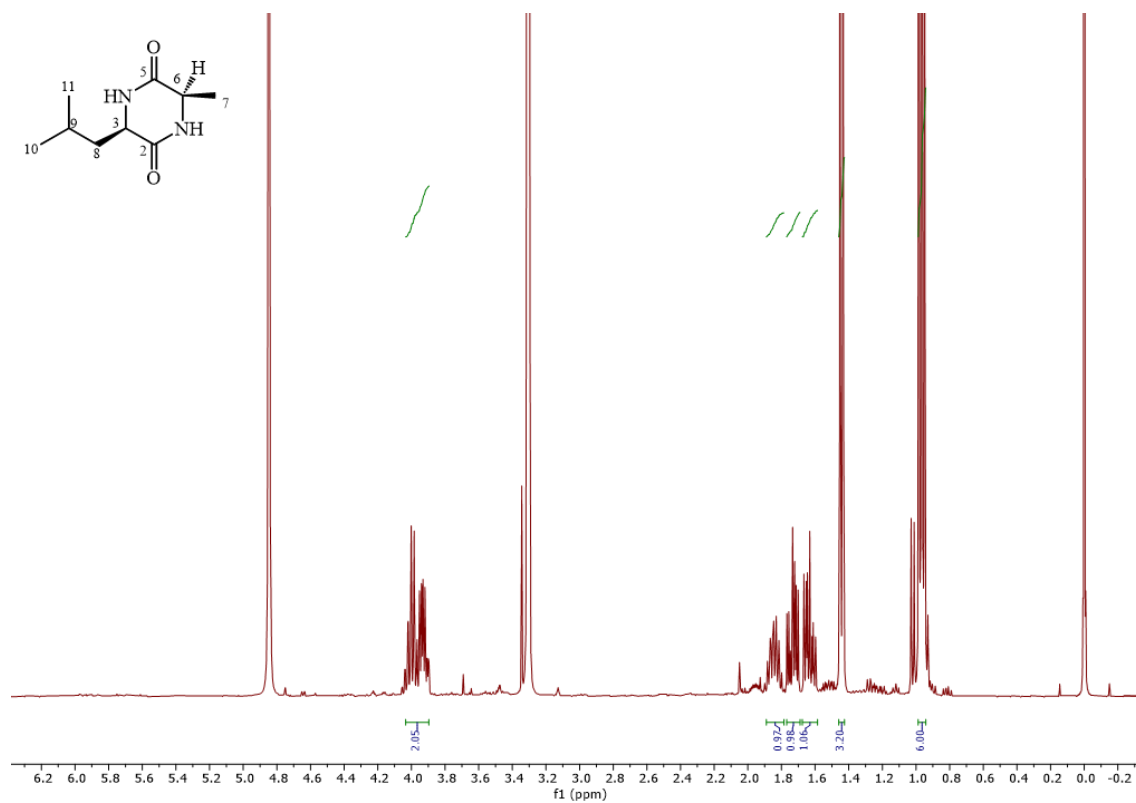
Figure S 39 ^{1}H NMR spectrum of compound **3.8** in methanol-d$_4$, 400 MHz.
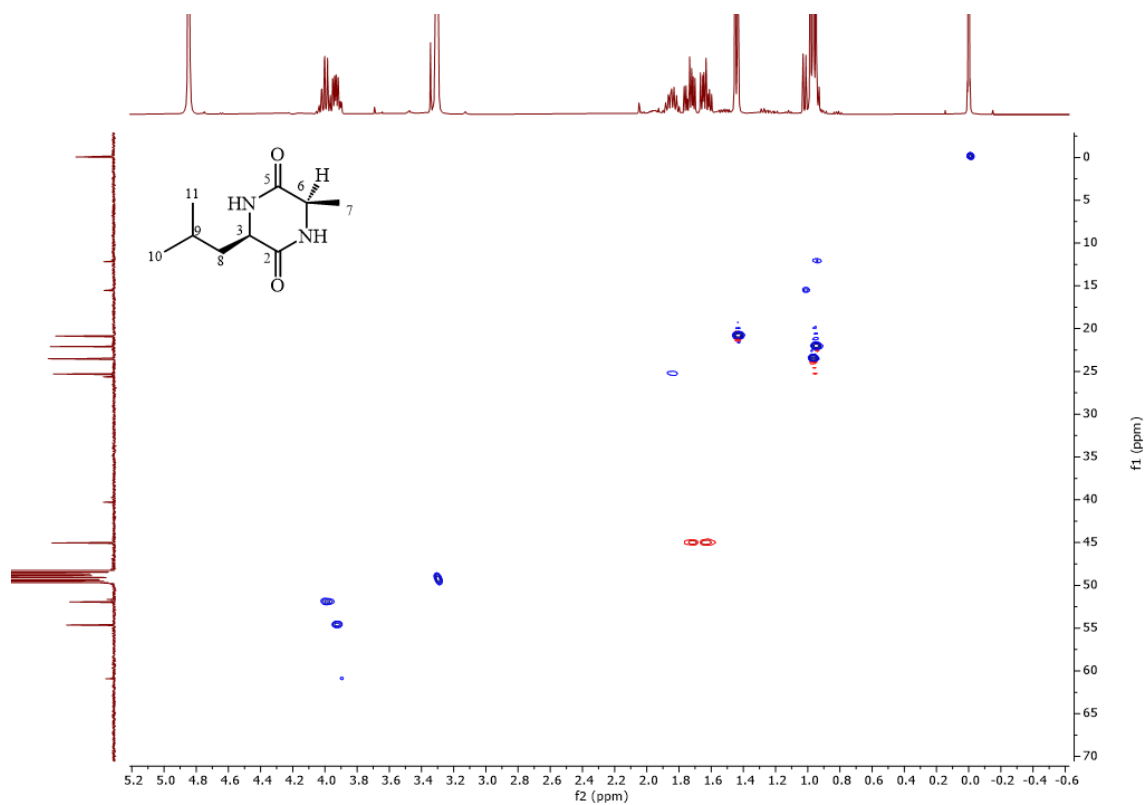
Figure S 40 HSQC spectrum of compound **3.8** in methanol-d$_4$, 400/100 MHz.
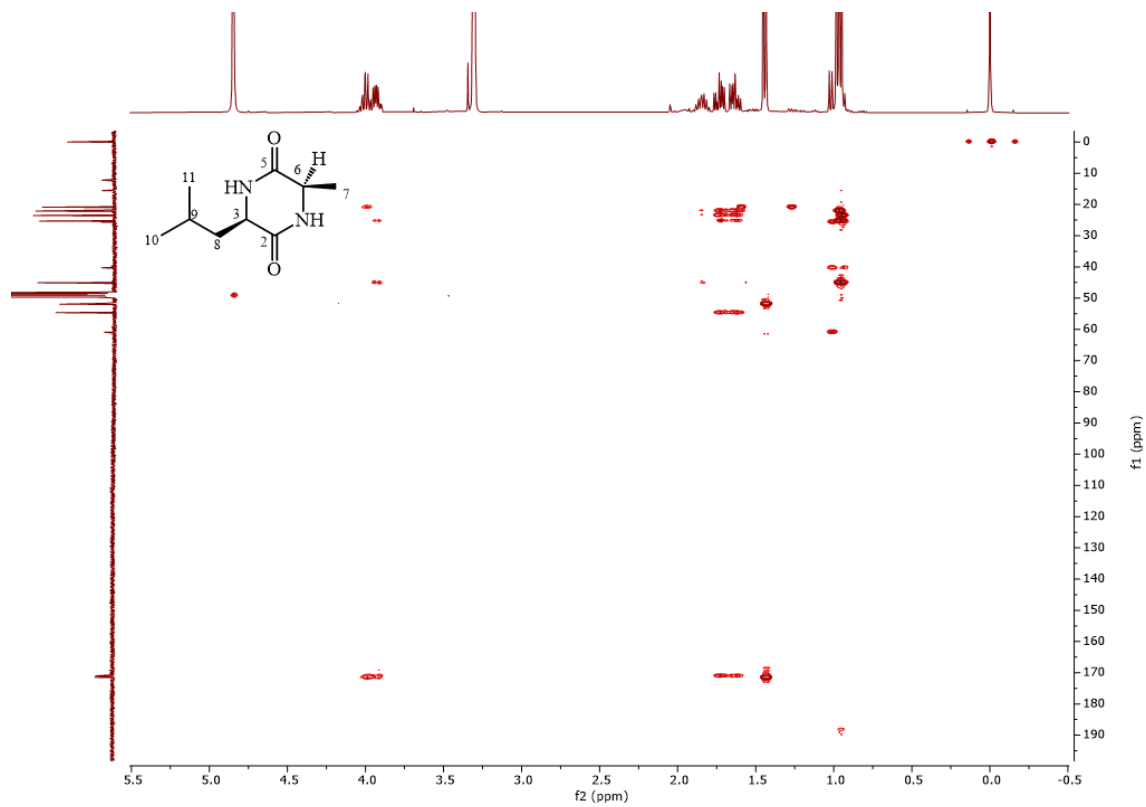
Figure S 41 HMBC spectrum of compound **3.8** in methanol-d₄, 400/100 MHz.
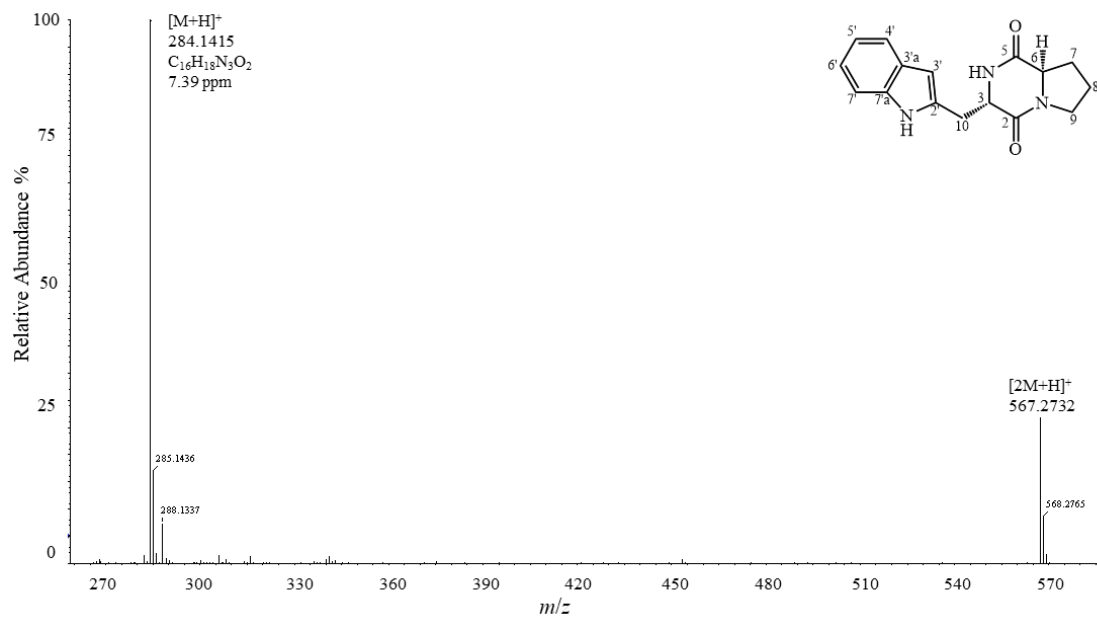
Figure S 42 (+)-ESI-HRMS spectrum of compound **3.9**.
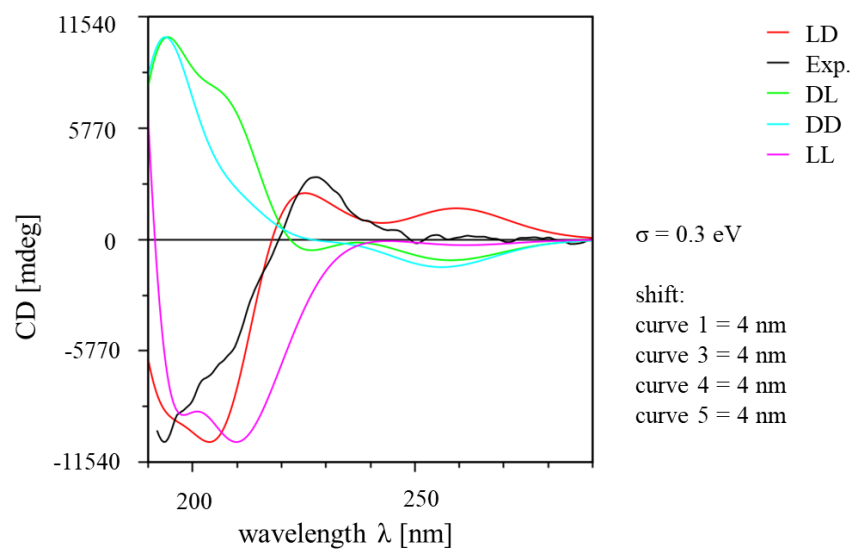
Figure S 43 Calculated ECD spectra of compound **3.9** in comparison with the experimental one (black). Red = *cyclo*-L-Trp-D-Pro, green = *cyclo*-D-Trp-L-Pro, blue = *cyclo*-D-Trp-D-Pro, purple = *cyclo*-L-Trp-L-Pro. Best similarity factor found for SR (red) with 0.918 for sigma = 0.3 eV.
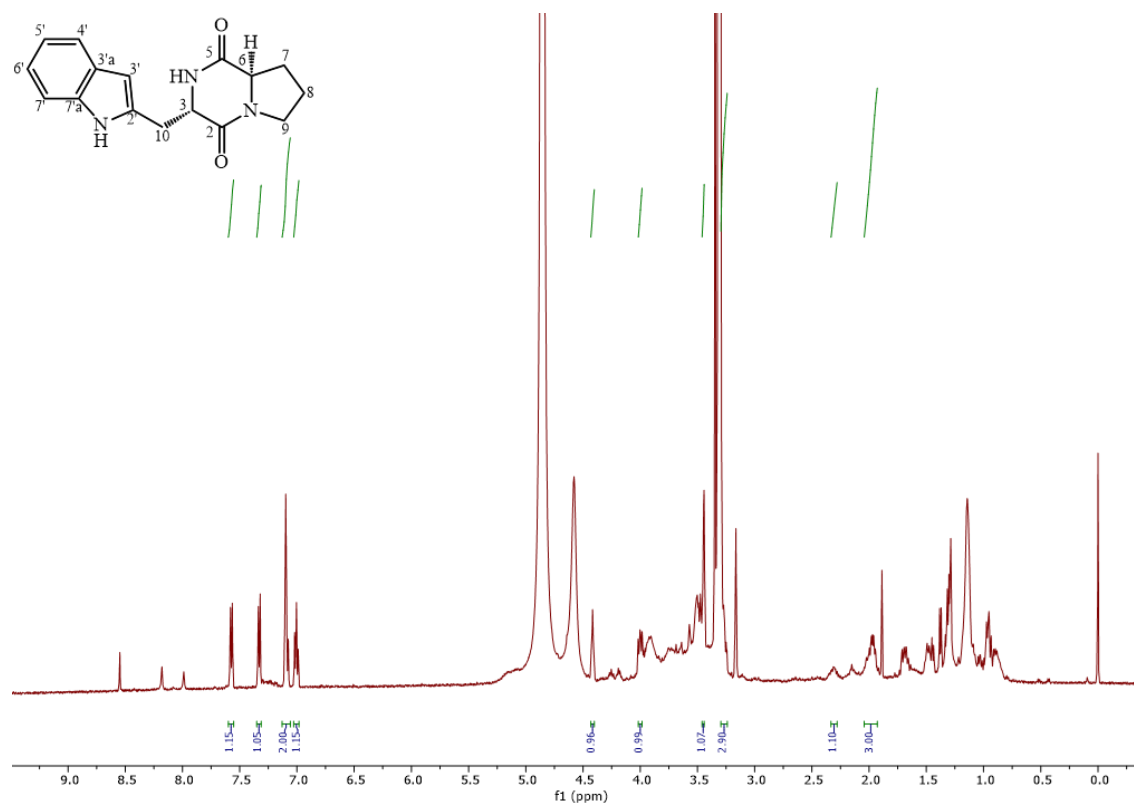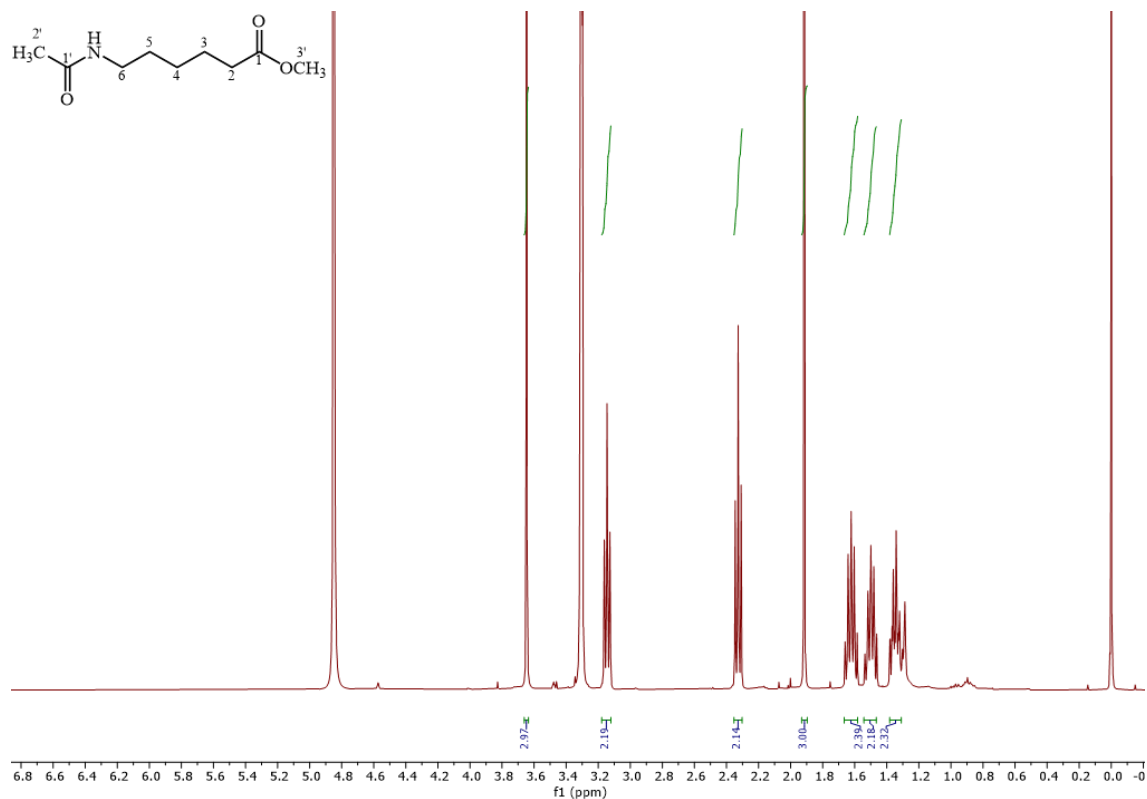

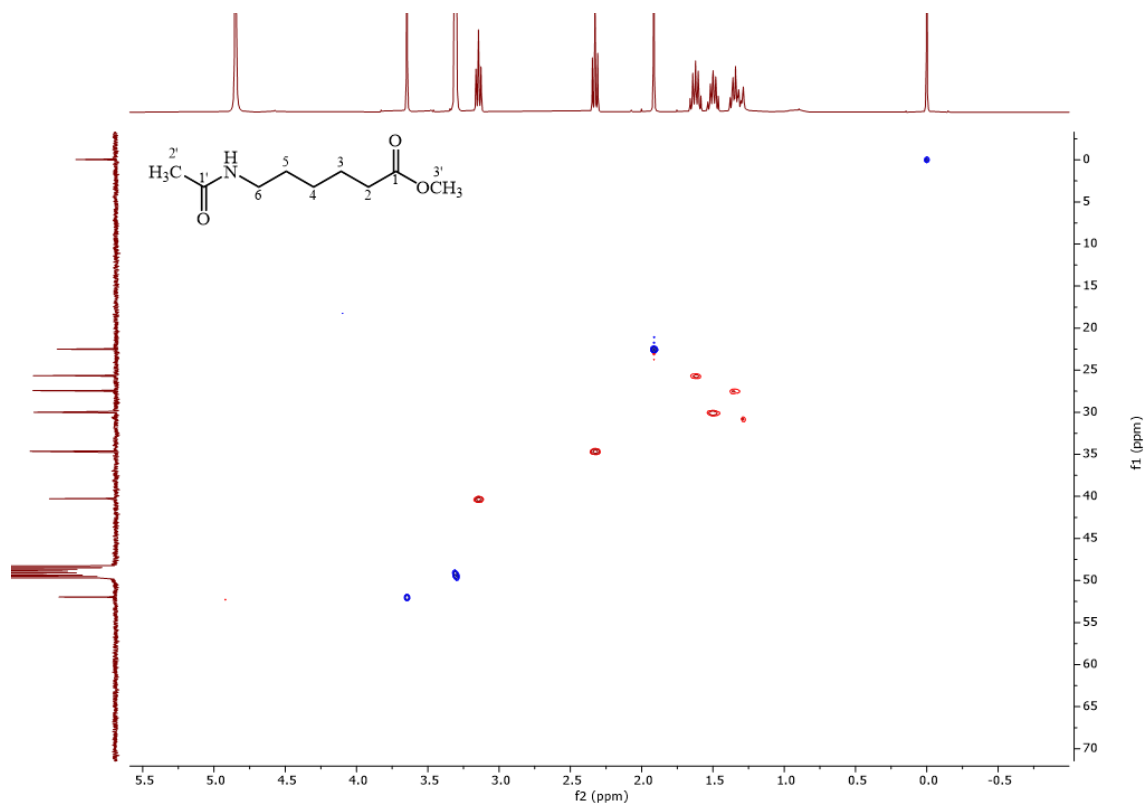**Figure S 44** ^{1}H NMR spectrum of compound **3.9** in methanol-d$_4$, 500 MHz.
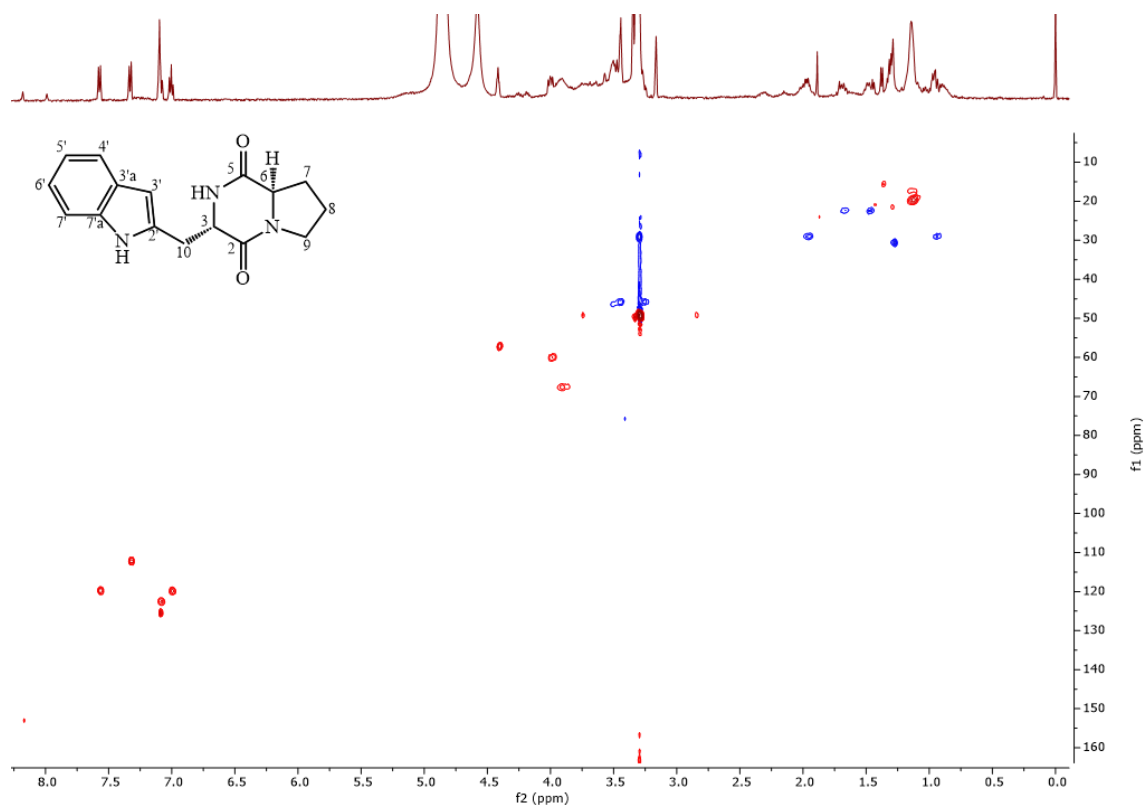
Figure S 45 HSQC spectrum of compound **3.9** in methanol-d4, 500/125 MHz.
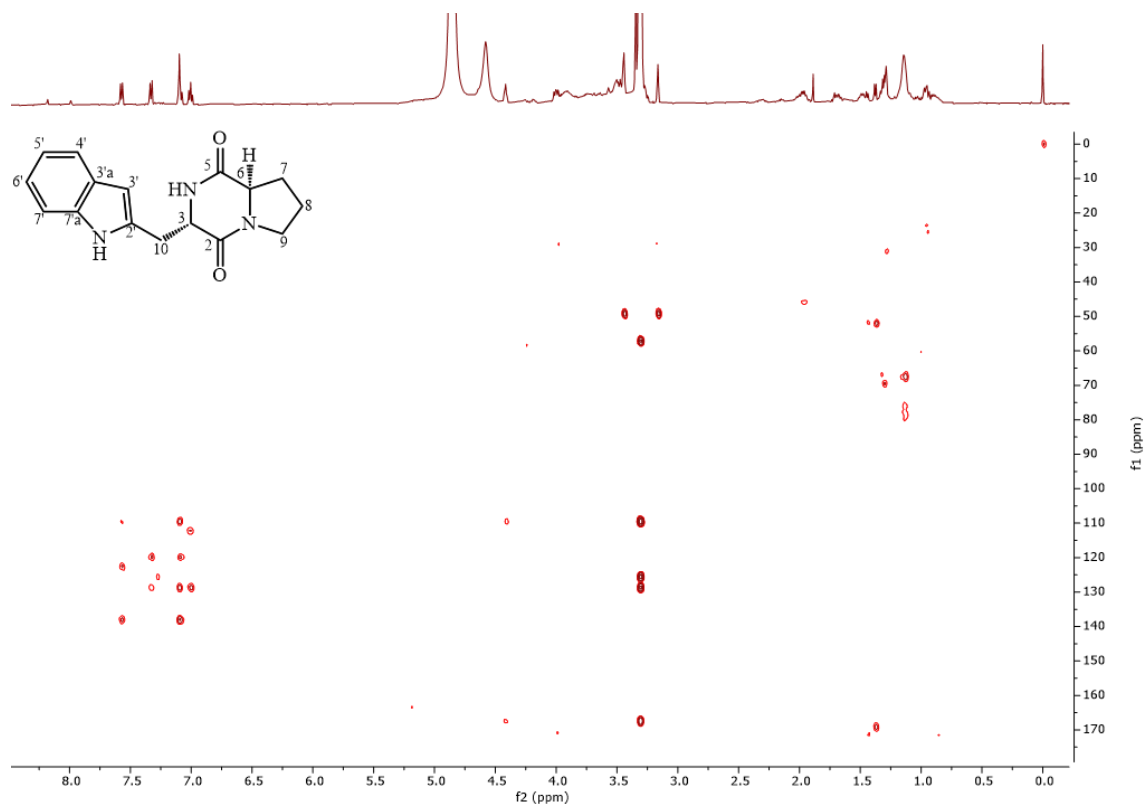
Figure S 46 HMBC spectrum of compound **3.9** in methanol-d4, 500/125 MHz.

144
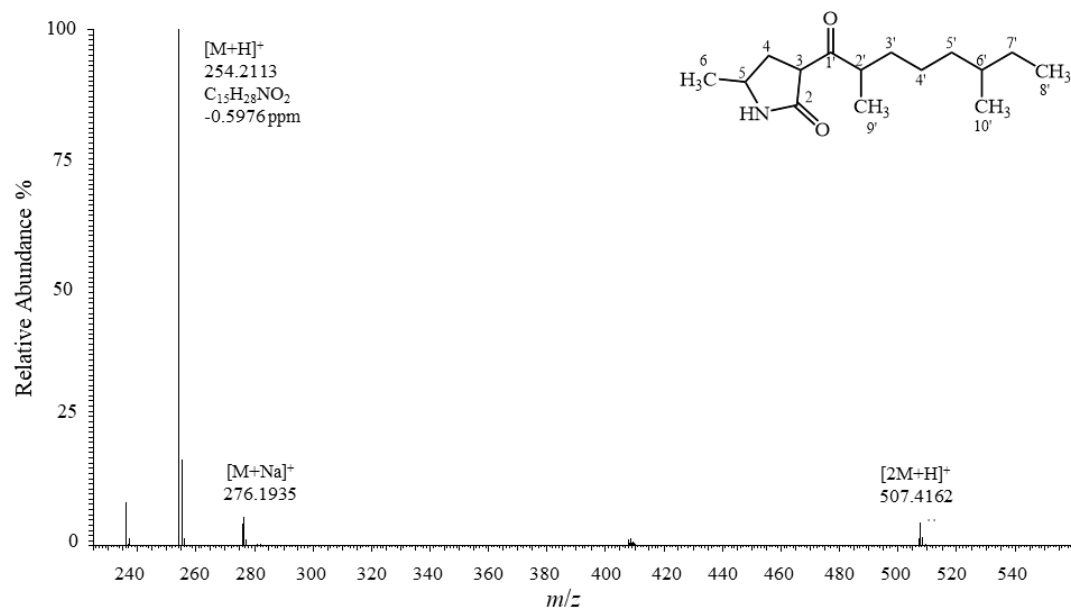
Figure S 47 (+)-ESI-HRMS spectrum of compound **3.10a/b**.
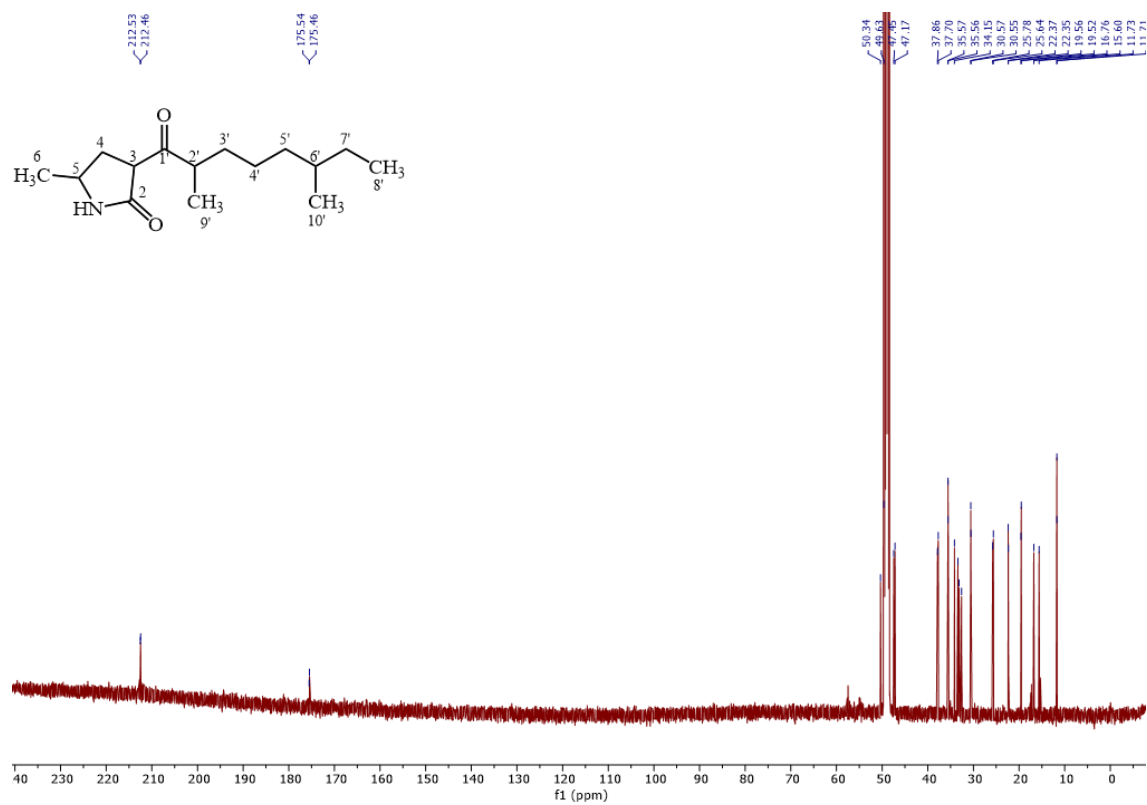
Figure S 48 ^{13}C NMR spectrum of compound **3.10a/b** in methanol-d$_4$, 125 MHz.
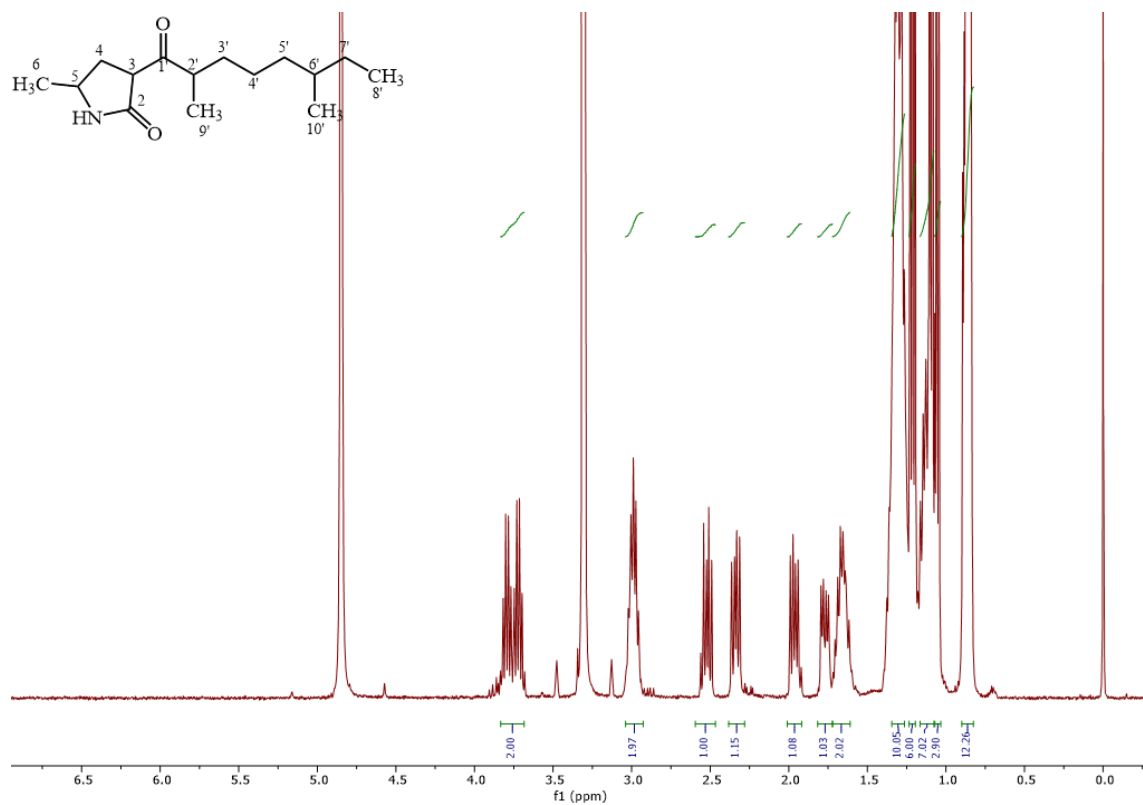
Figure S 49 ^{1}H NMR spectrum of compound **3.10a/b** in methanol-d$_4$, 400 MHz.
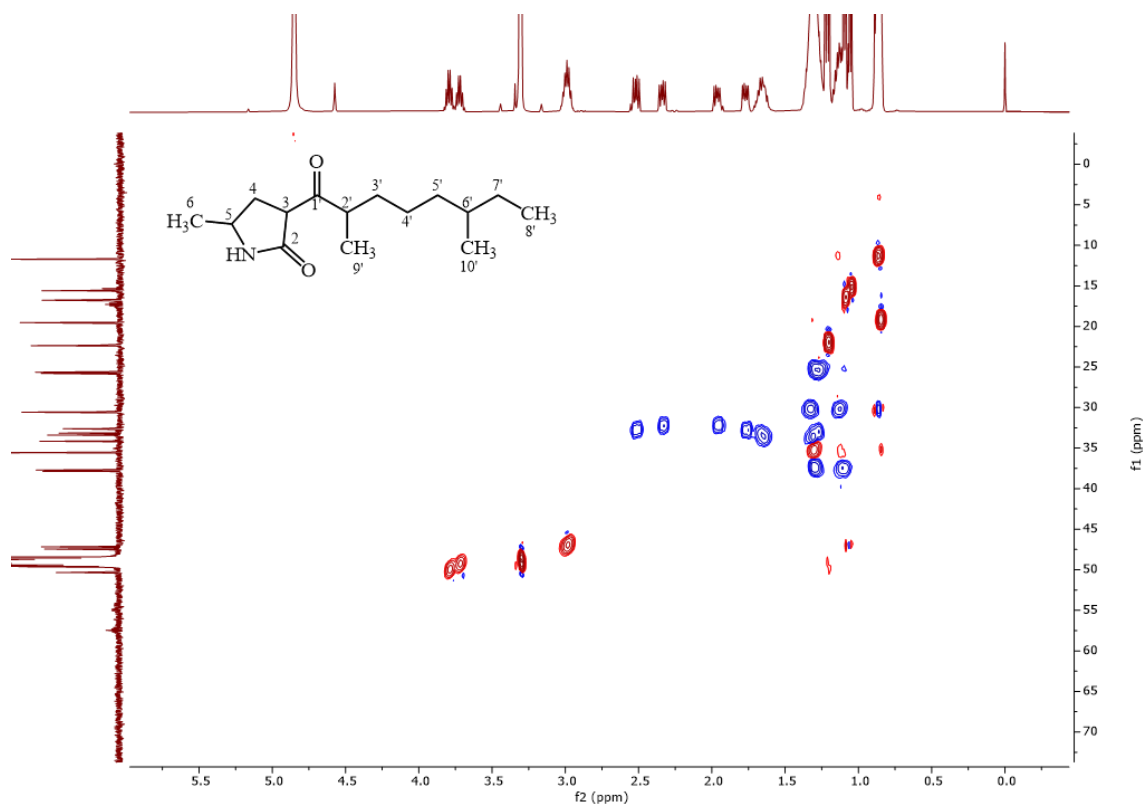
**Figure S 50** HSQC spectrum of compound **3.10a/b** in methanol-d$_4$, 400/100 MHz.
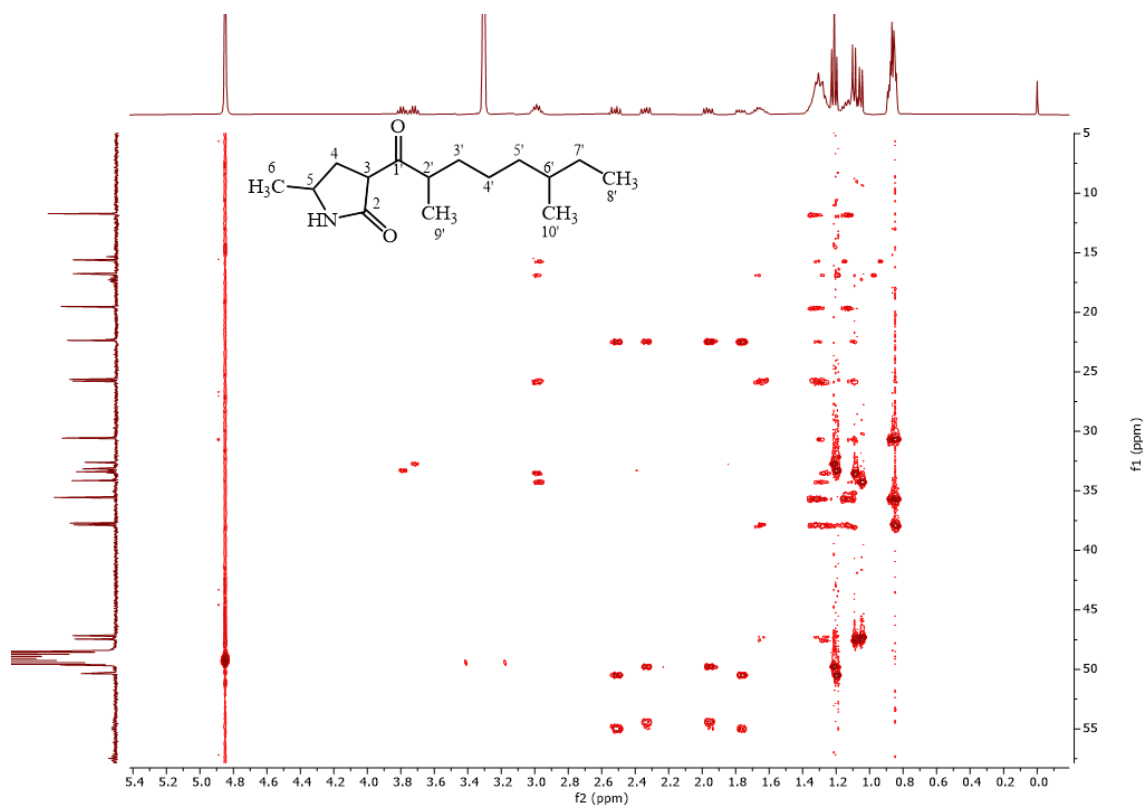
Figure S 51 Band-selective HMBC spectrum (0 -55 ppm) of compound **3.10a/b** in methanol-d$_4$, 400/100 MHz.
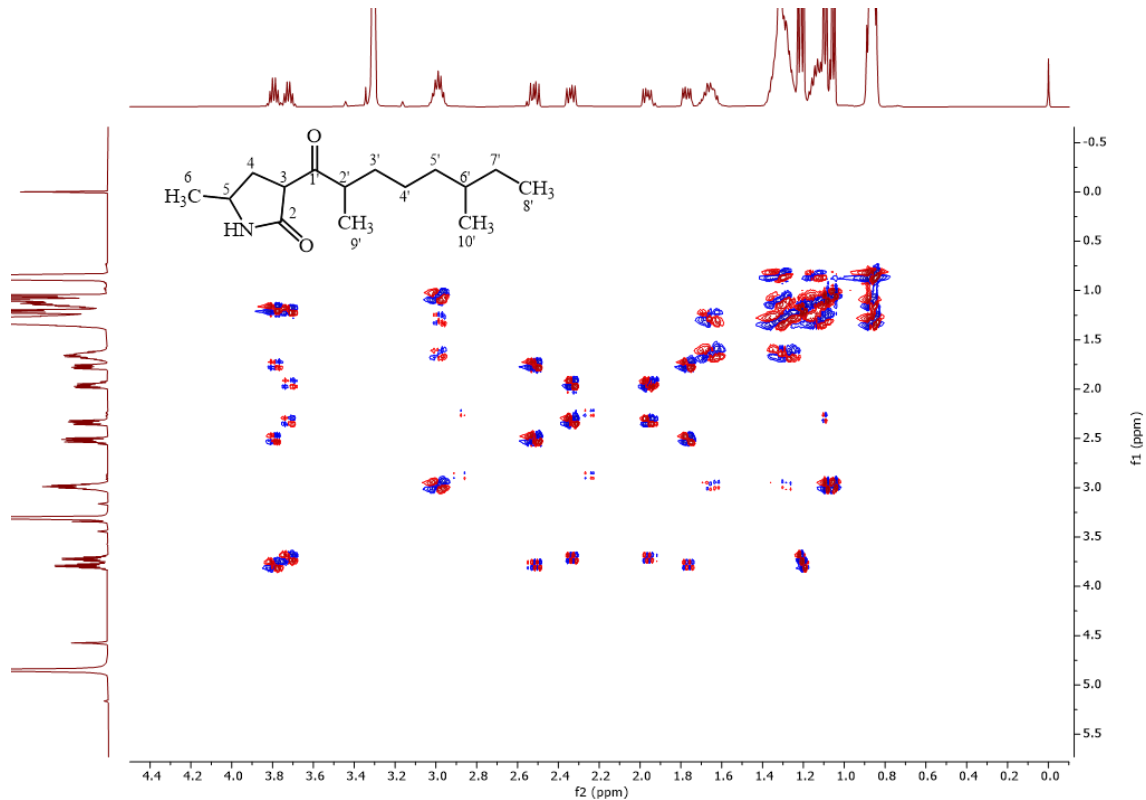
Figure S 52 COSY spectrum of compound **3.10a/b** in methanol-d$_4$, 400 MHz.
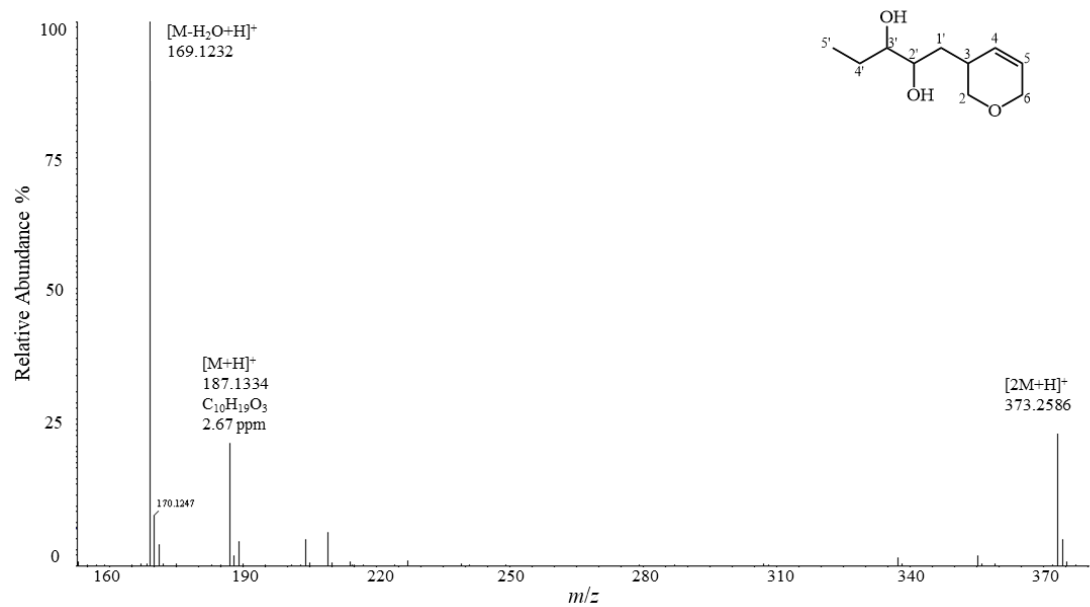
Figure S 53 (+)-ESI-HRMS spectrum of compound **3.11**.
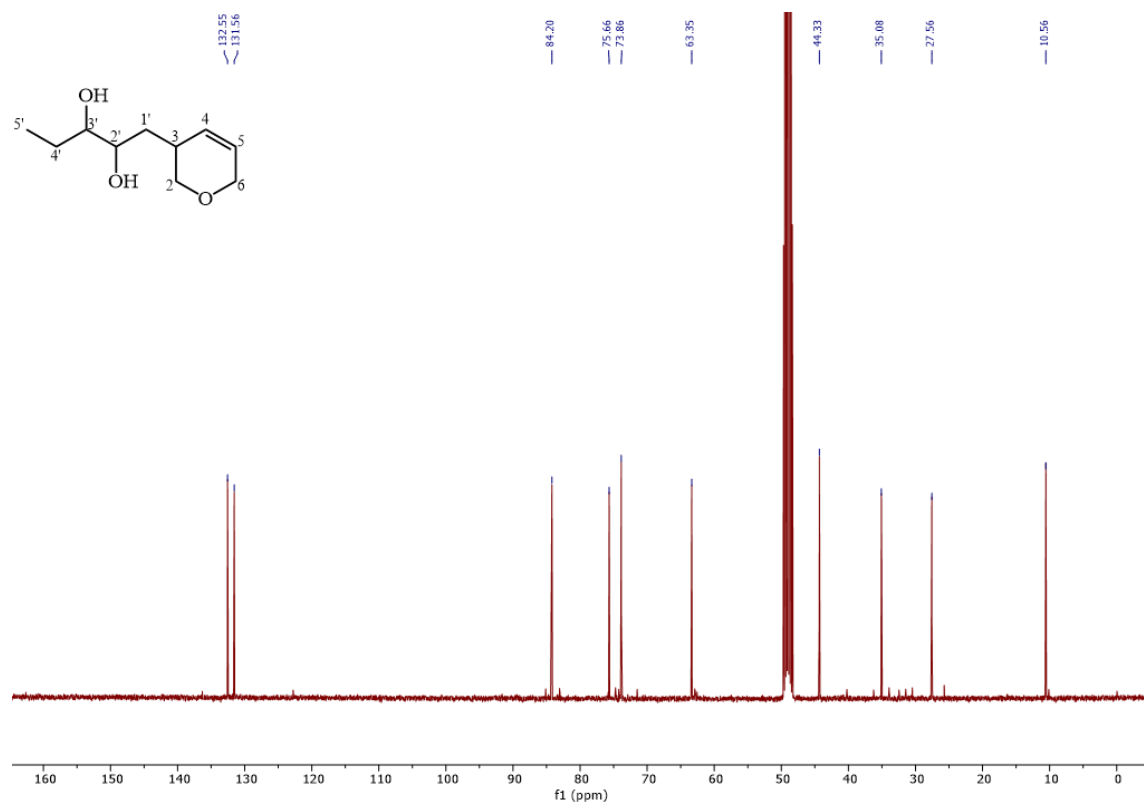
Figure S 54 ^{13}C NMR spectrum of compound **3.11** in methanol-d$_4$, 100 MHz.
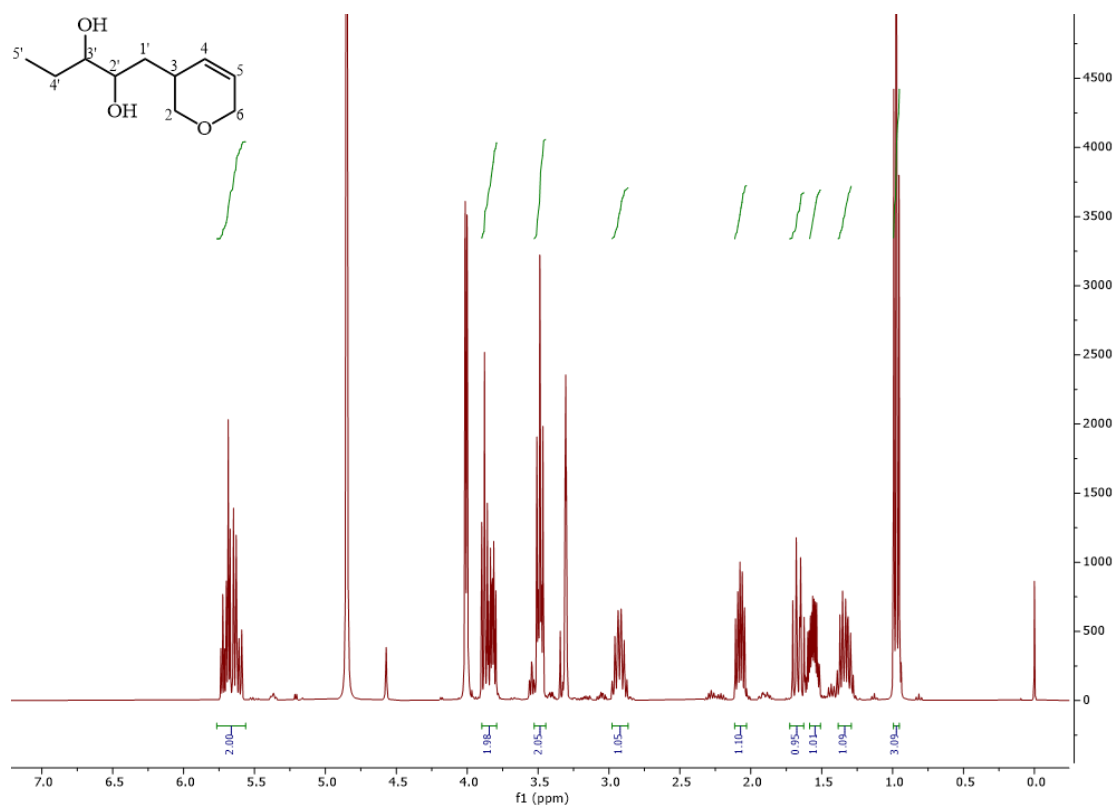
Figure S 55 ^{1}H NMR spectrum of compound **3.11** in methanol-d4, 400 MHz.
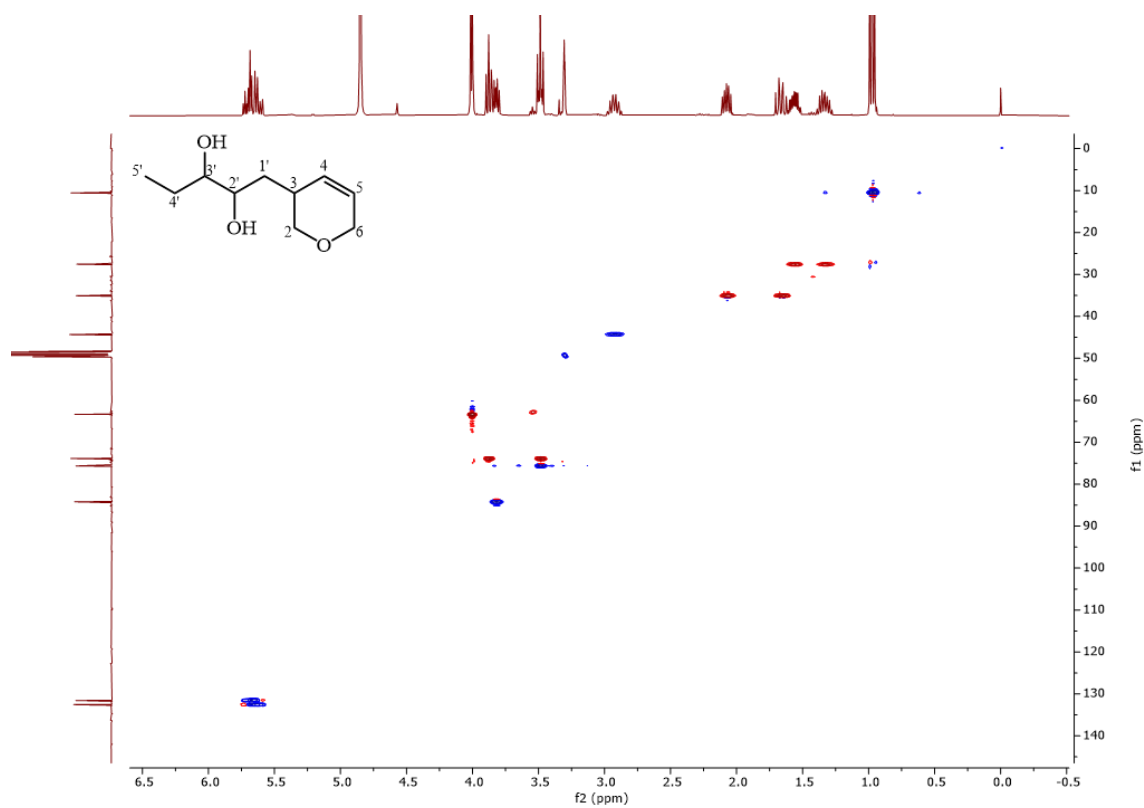
Figure S 56 HSQC spectrum of compound **3.11** in methanol-d4, 400/100 MHz.
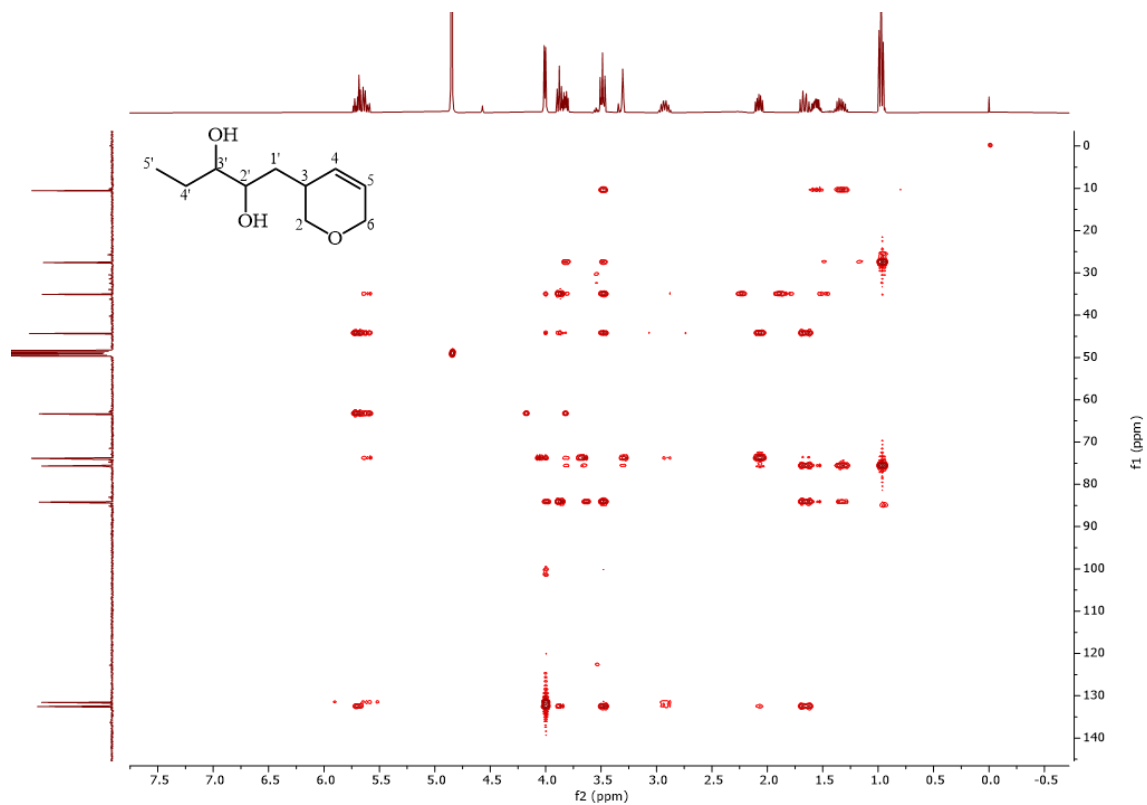
Figure S 57 HMBC spectrum of compound **3.11** in methanol-d₄, 400/100 MHz.
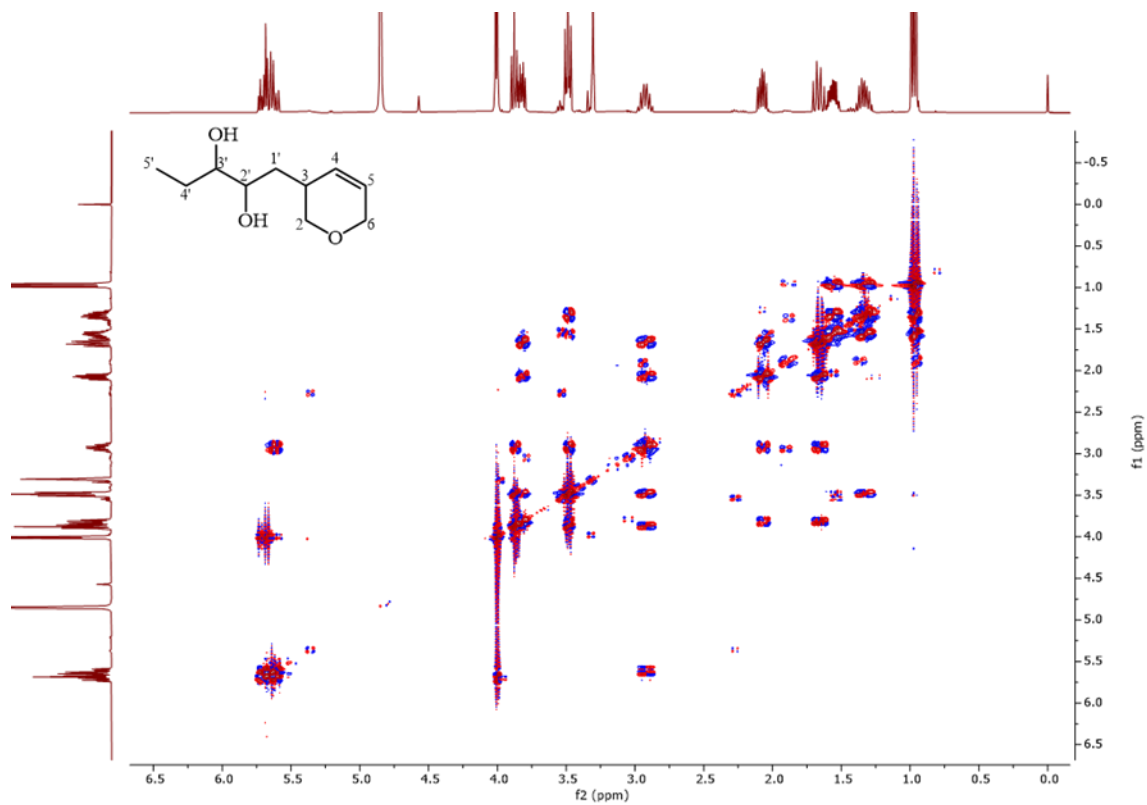
Figure S 58 COSY spectrum of compound **3.11** in methanol-d₄, 400 MHz.
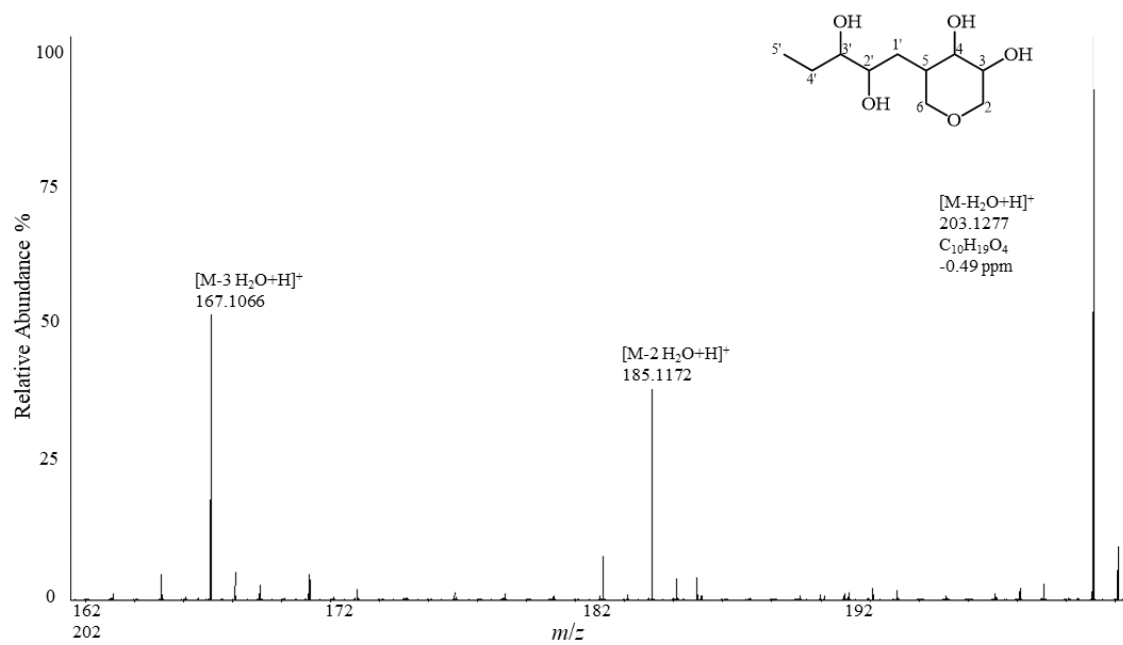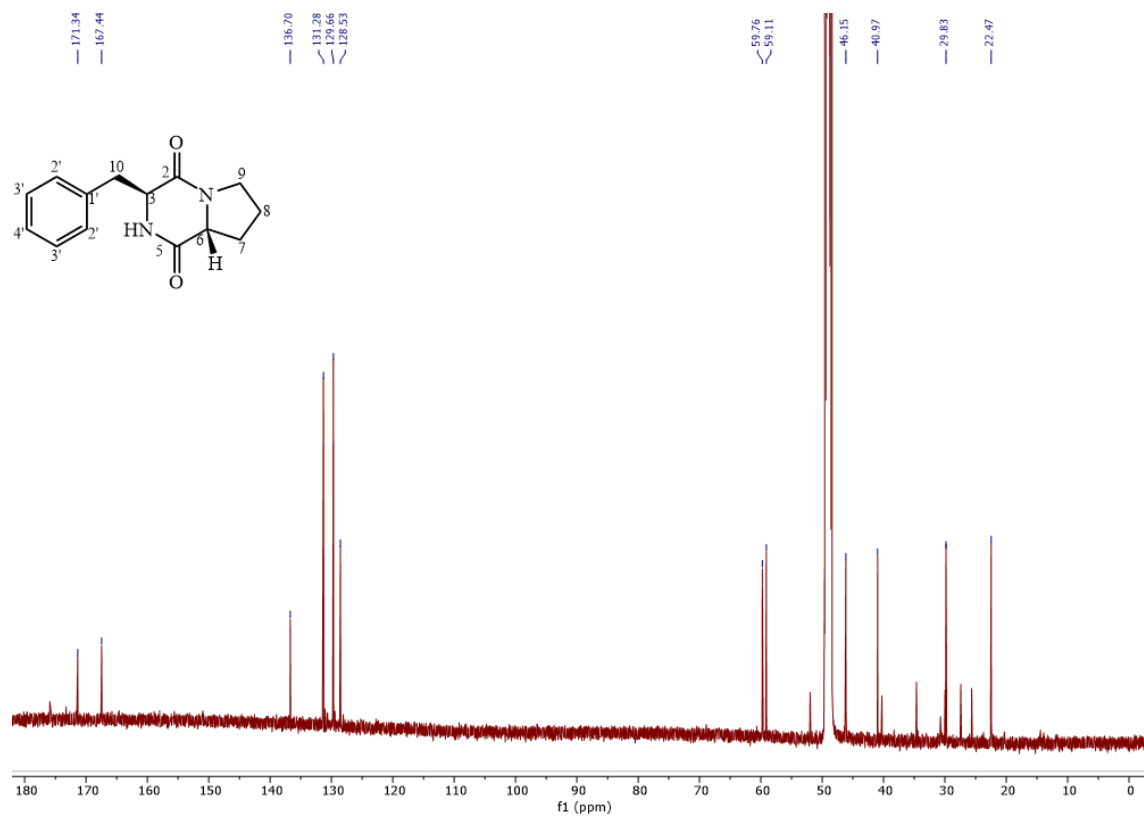
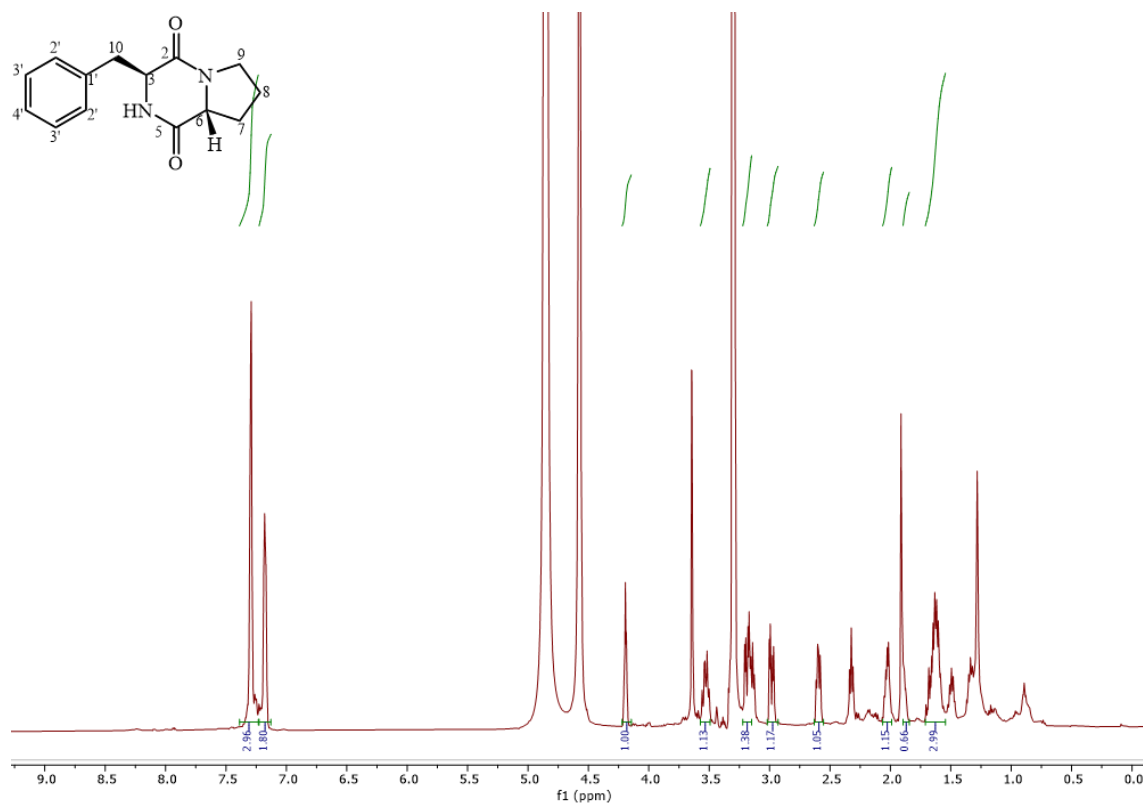**Figure S 59** (+)-ESI-HRMS spectrum of compound **3.12**.
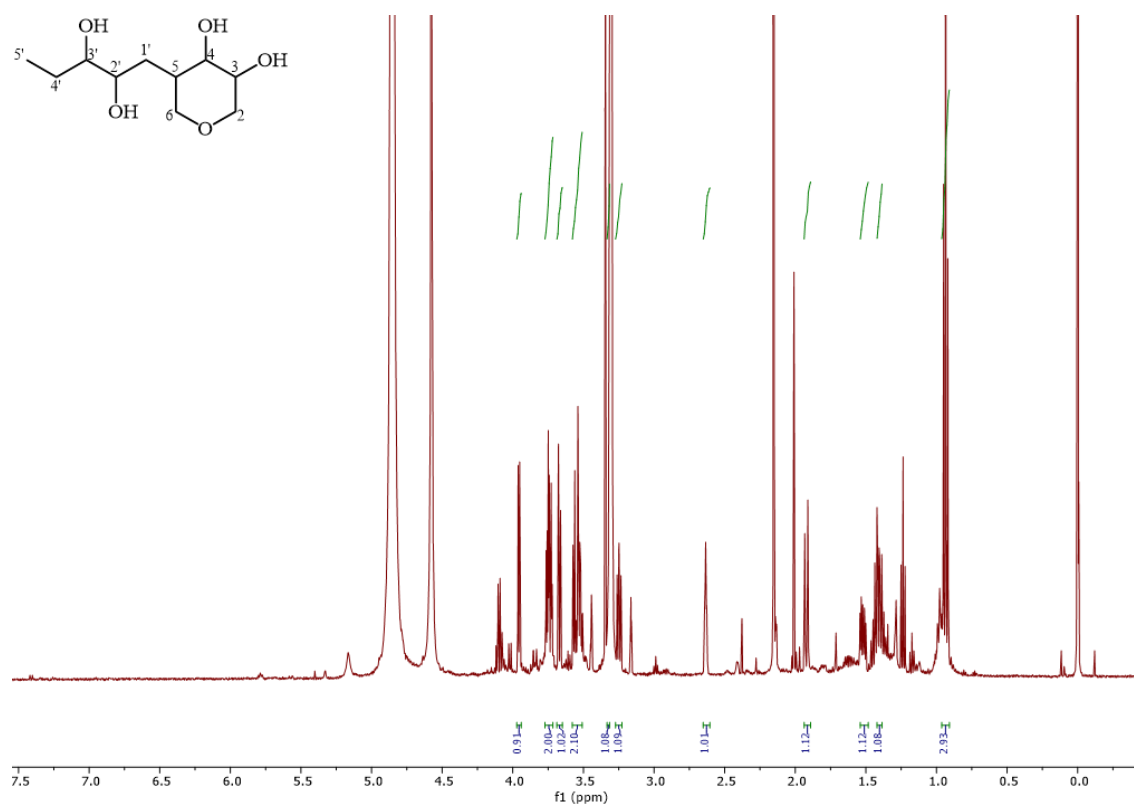
Figure S 60 ^{1}H NMR spectrum of compound **3.12** in methanol-d$_4$, 500 MHz.
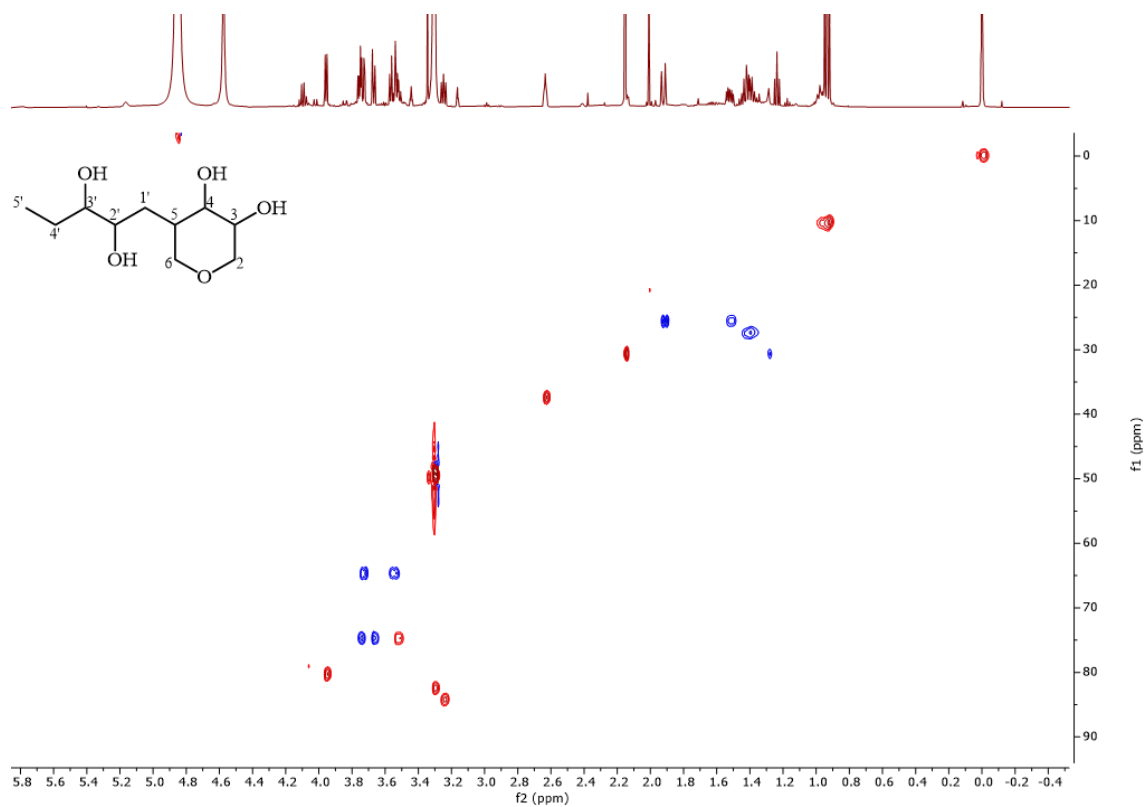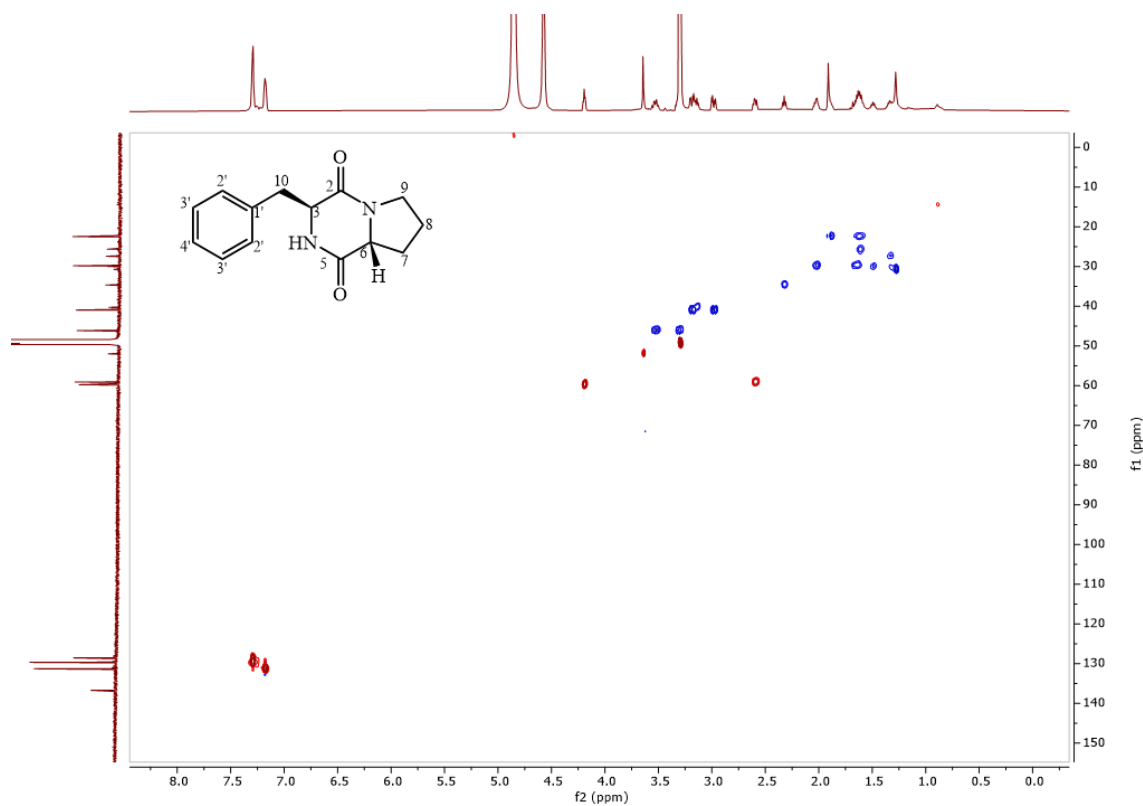
Figure S 61 HSQC spectrum of compound **3.12** in methanol-d4, 500/125 MHz.
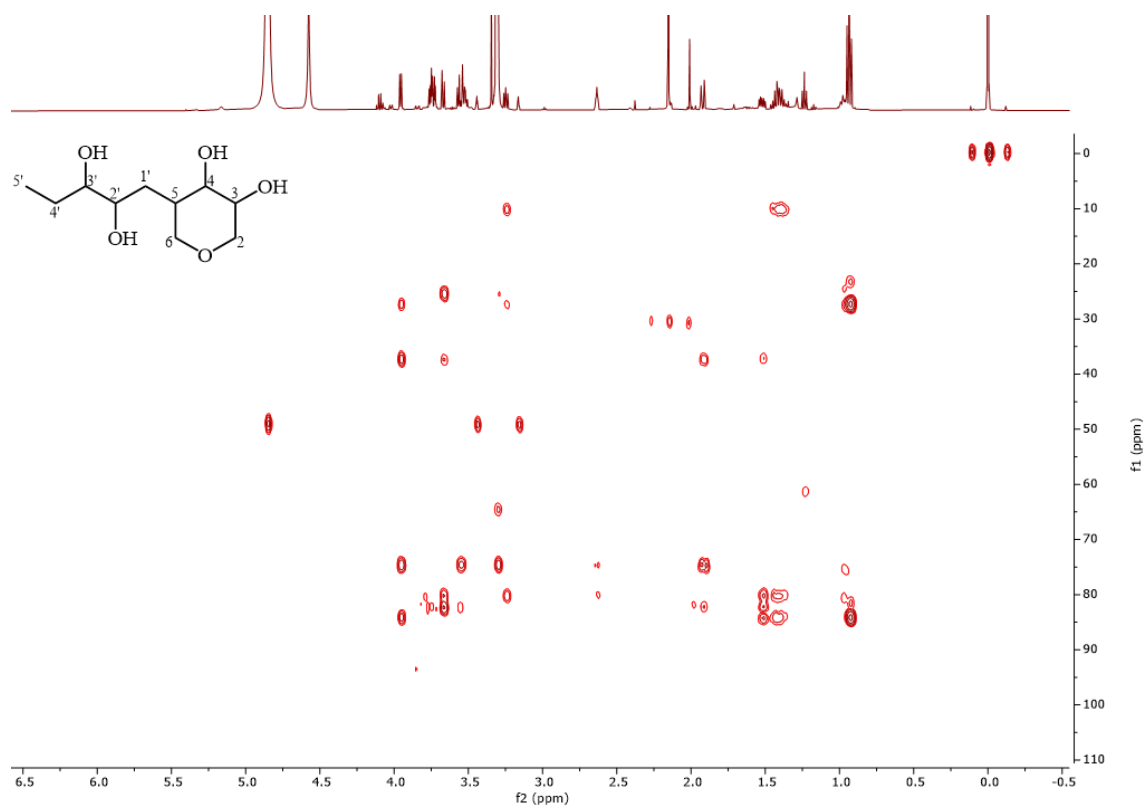
Figure S 62 HMBC spectrum of compound **3.12** in methanol-d4, 500/125 MHz.
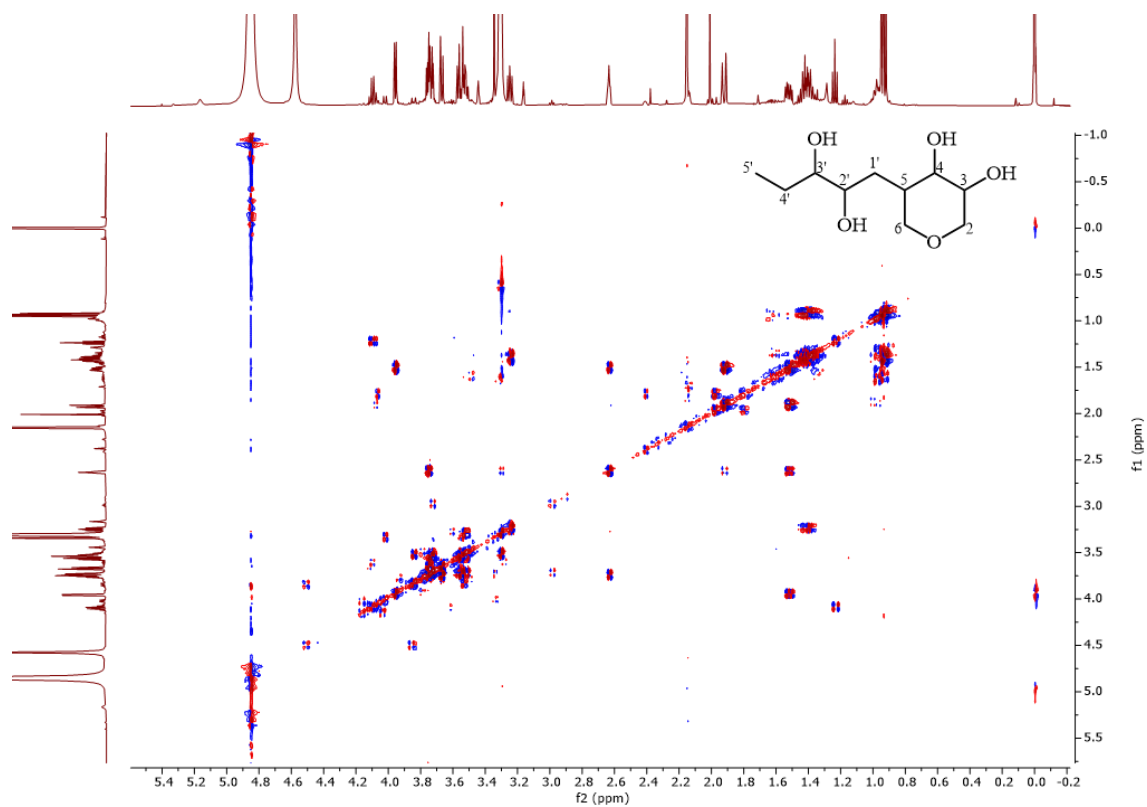
Figure S 63 COSY spectrum of compound **3.12** in methanol-d$_4$, 500 MHz.

[M+H]$^+$
180.1030
C$_{10}$H$_{14}$NO$_2$
6.10 ppm

181.1062
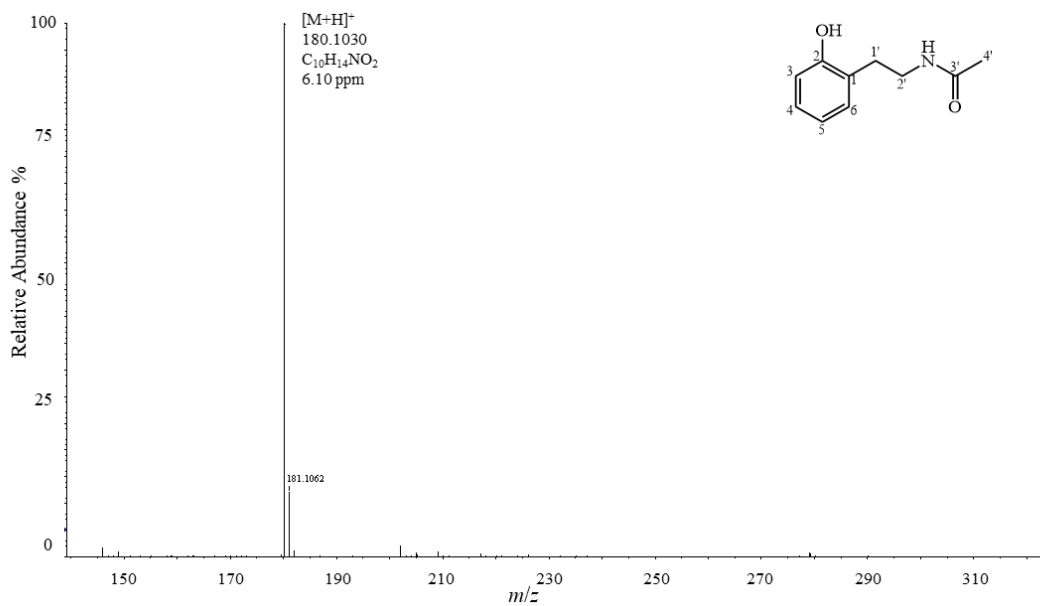
Figure S 64 (+)-ESI-HRMS spectrum of compound **3.13**.
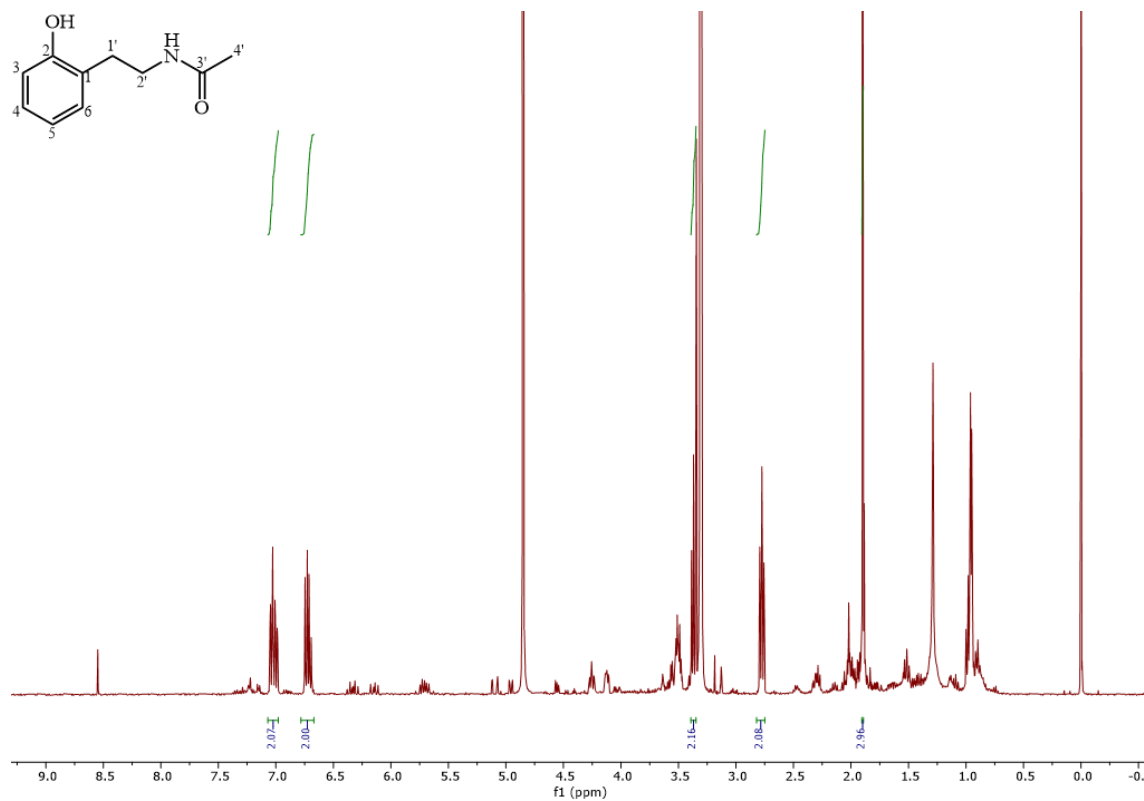
Figure S 65 ^{1}H NMR spectrum of compound **3.13** in methanol-d$_4$, 500 MHz.
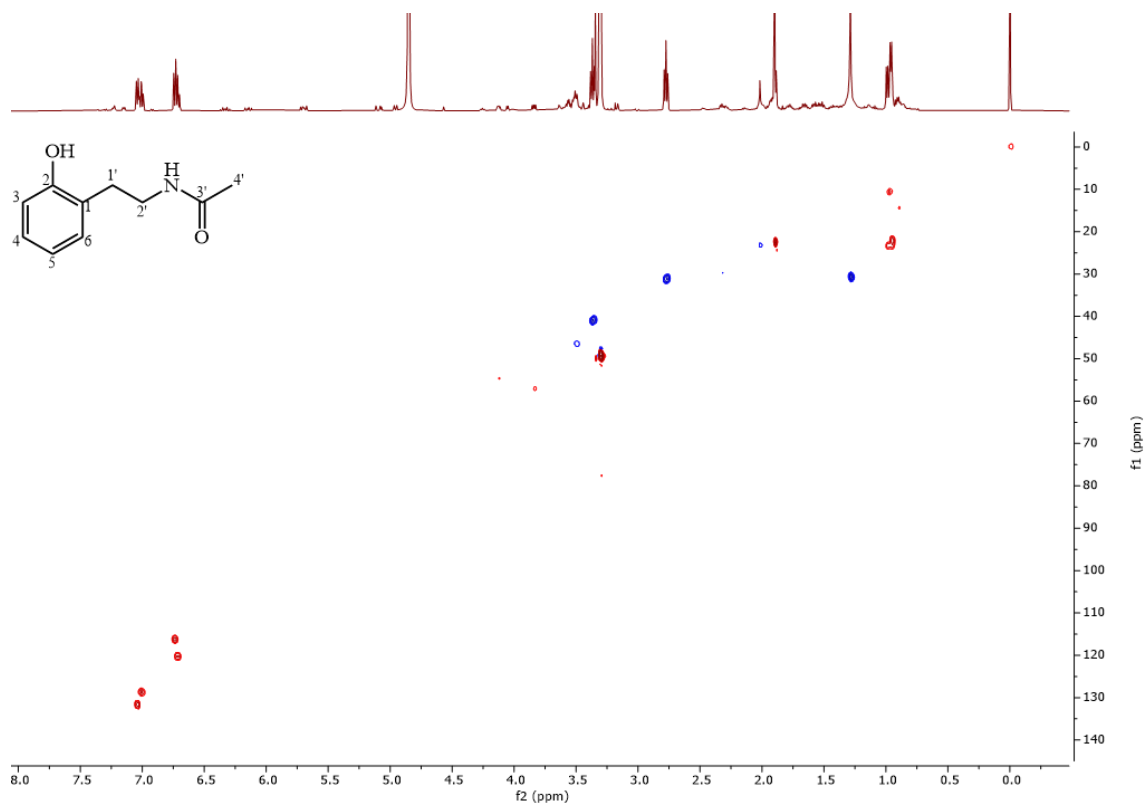
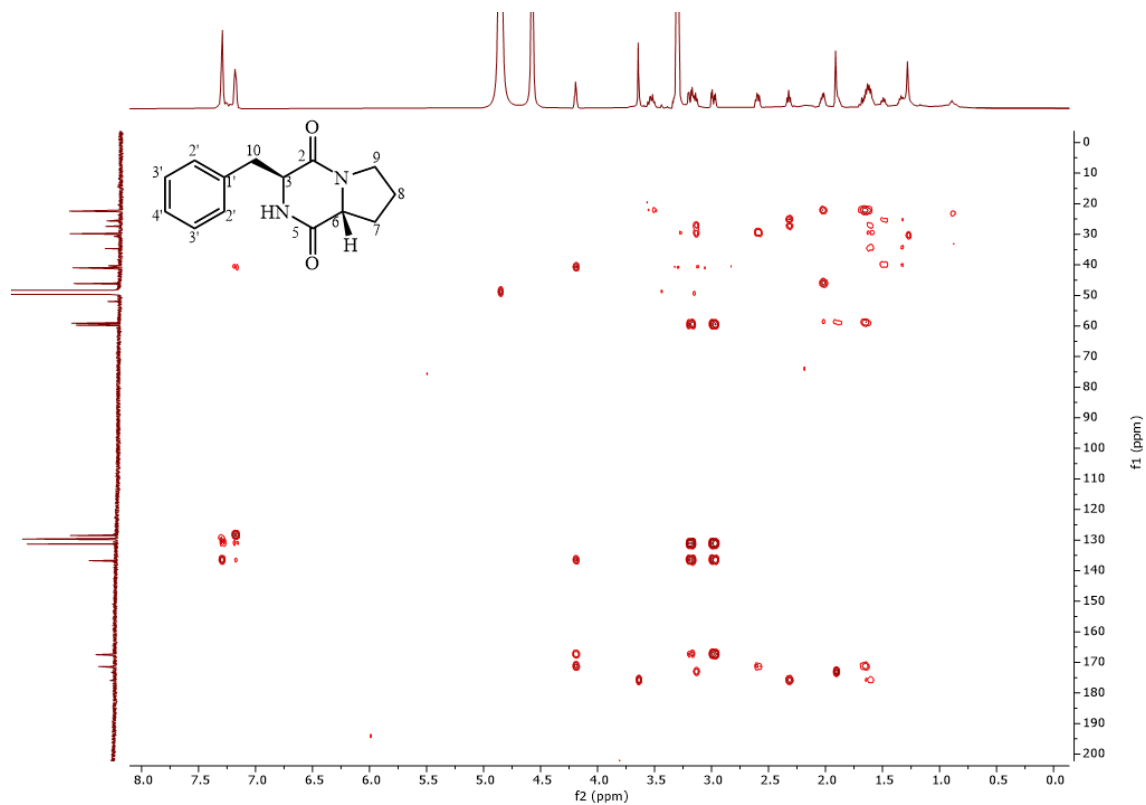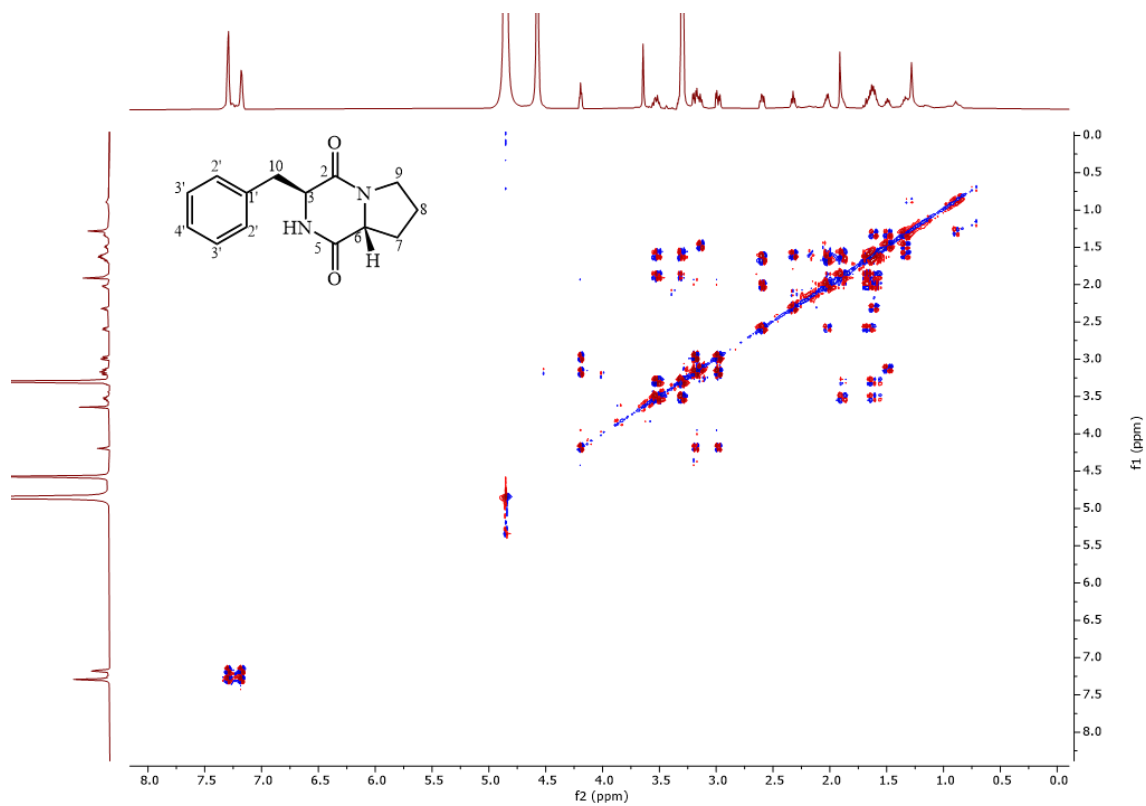**Figure S 66** HSQC spectrum of compound **3.13** in methanol-d$_4$, 500/125 MHz.

154
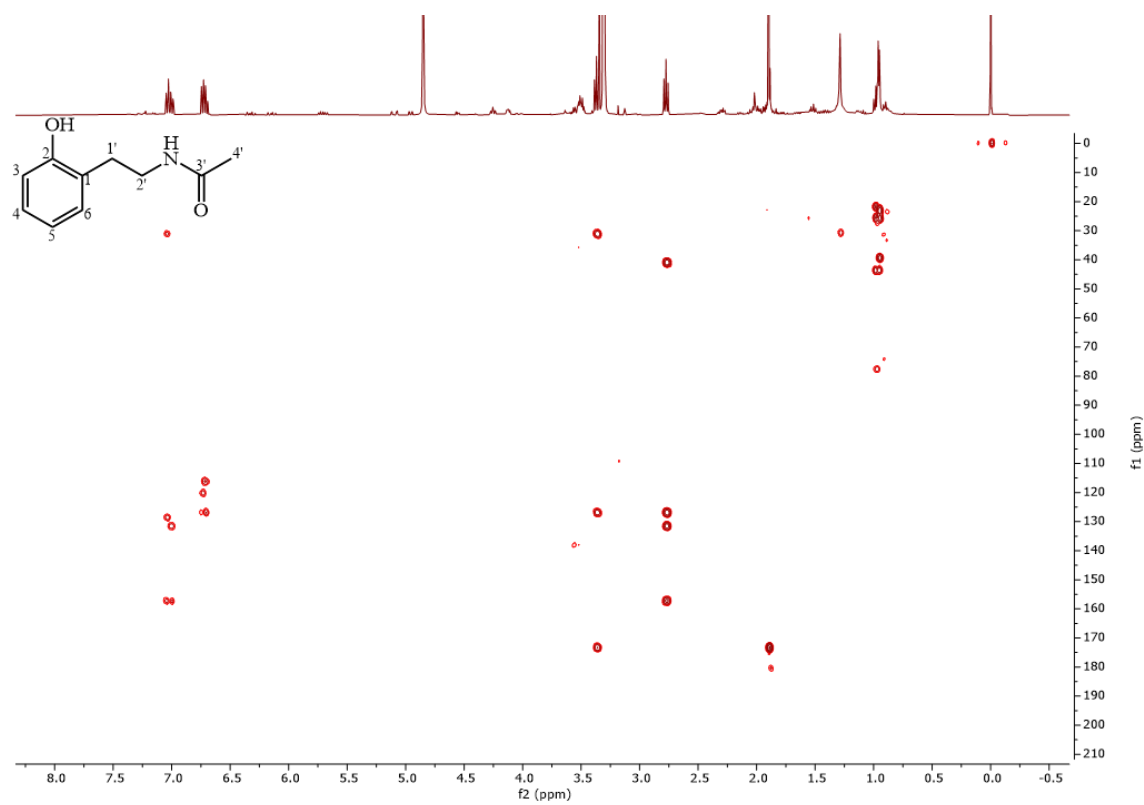
Figure S 67 HMBC spectrum of compound **3.13** in methanol-d$_4$, 500/125 MHz.
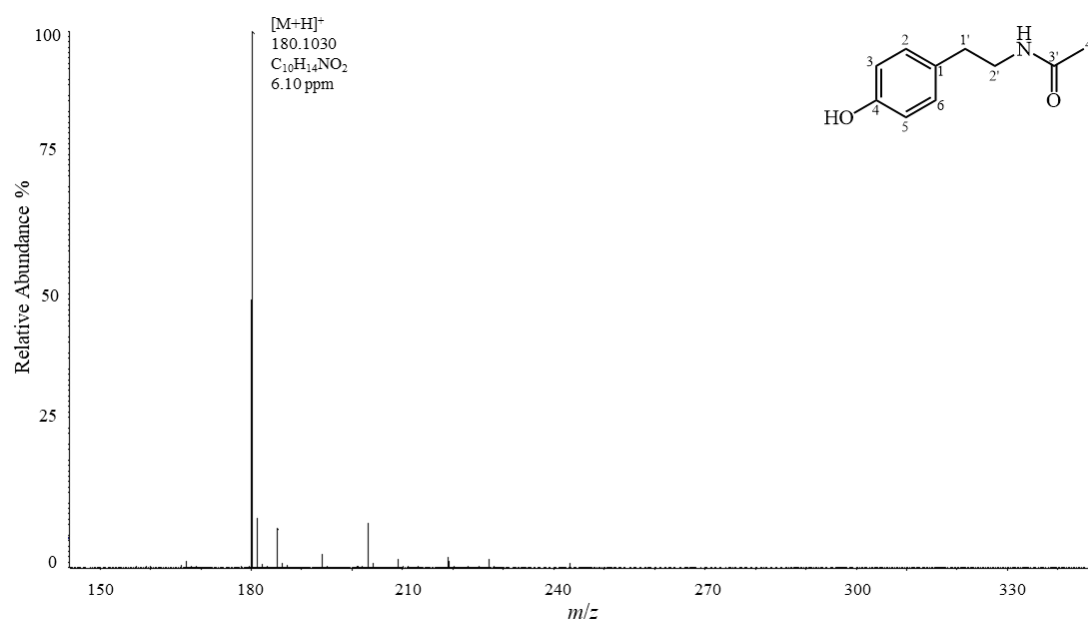
Figure S 68 (+)-ESI-HRMS spectrum of compound **3.14**.

155
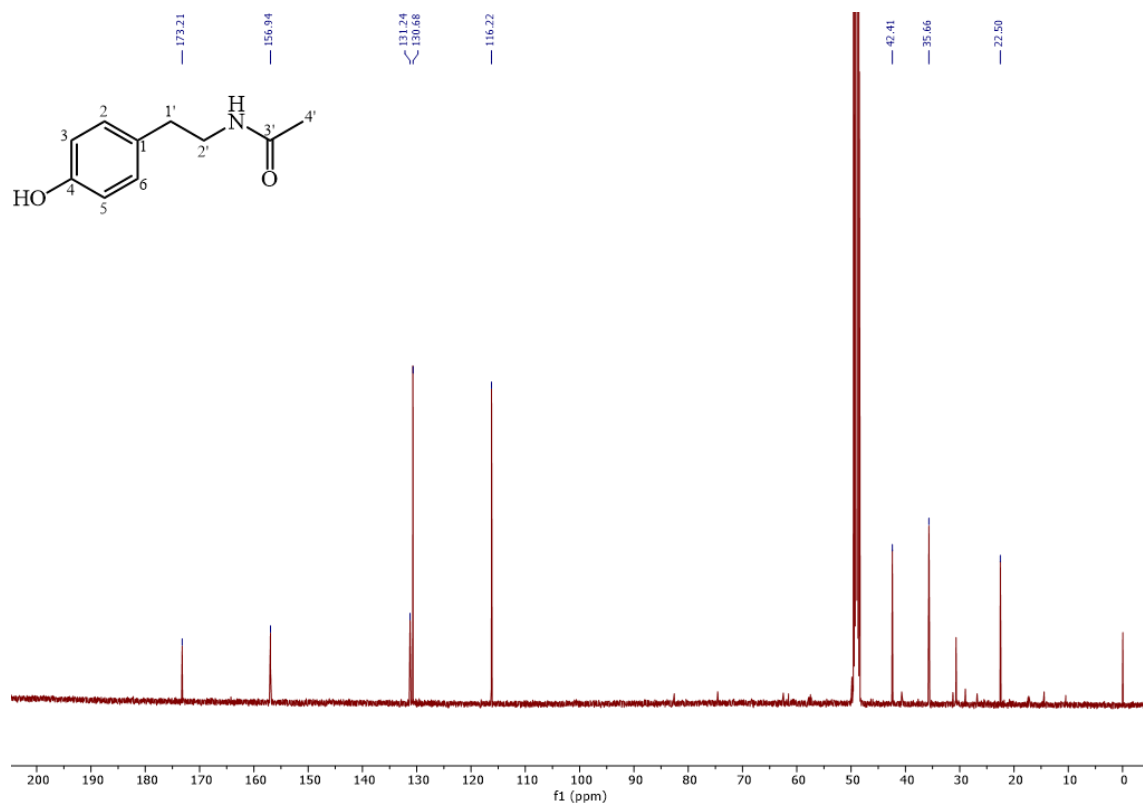
Figure S 69 ^{13}C NMR spectrum of compound **3.14** in methanol-d$_4$, 125 MHz.
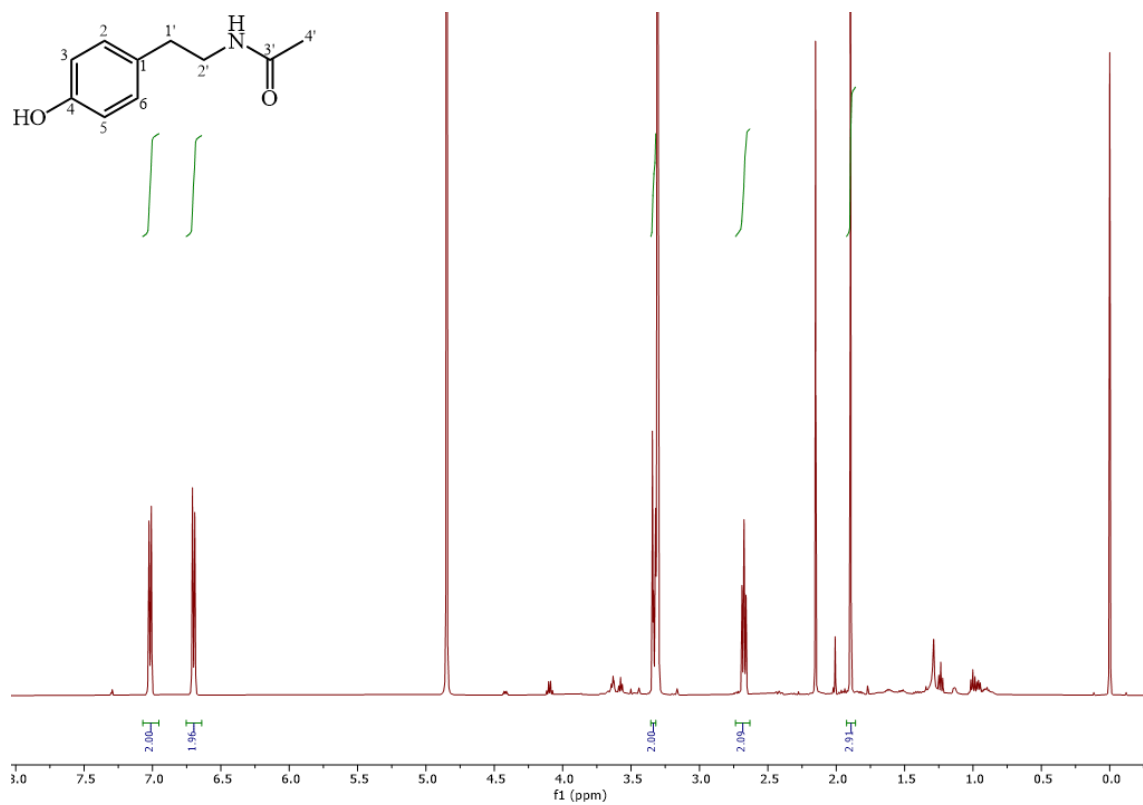
Figure S 70 ^{1}H NMR spectrum of compound **3.14** in methanol-d$_4$, 500 MHz.

Figure S 71 HSQC spectrum of compound **3.14** in methanol-d$_4$, 500/125 MHz.

Figure S 72 HMBC spectrum of compound **3.14** in methanol-d$_4$, 500/125 MHz.
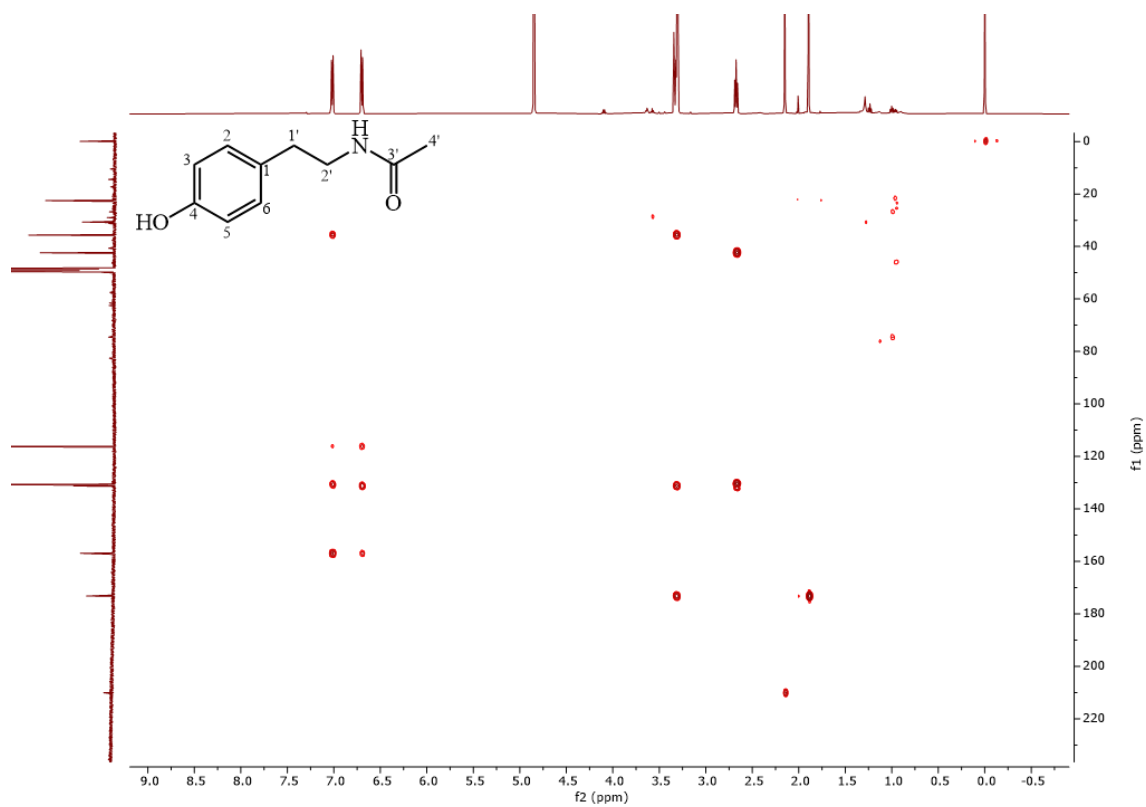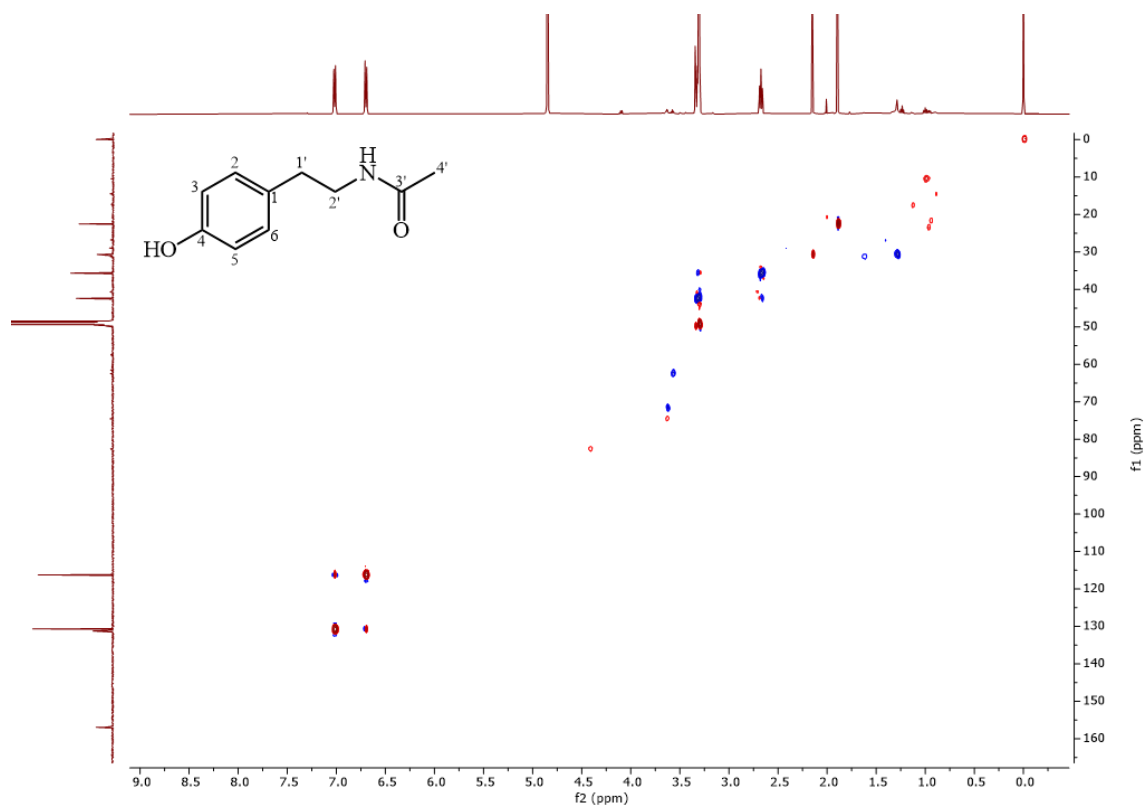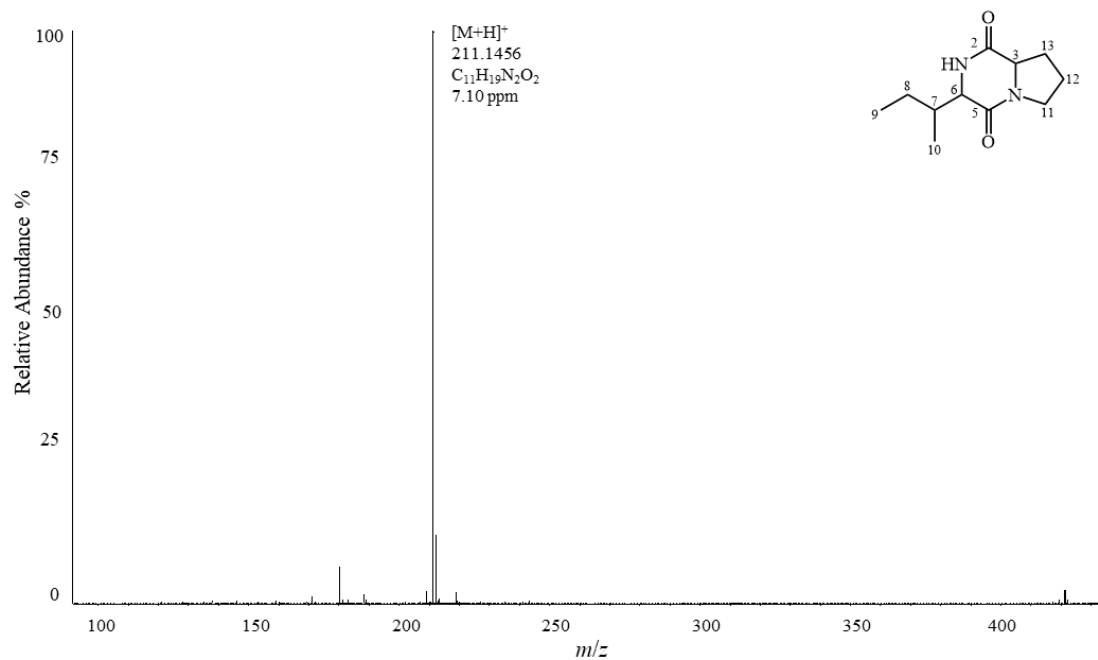
Figure S 73 (+)-ESI-HRMS spectrum of compound **3.15**.

[M+H]+
211.1456
$C_{11}H_{19}N_2O_2$
7.10 ppm
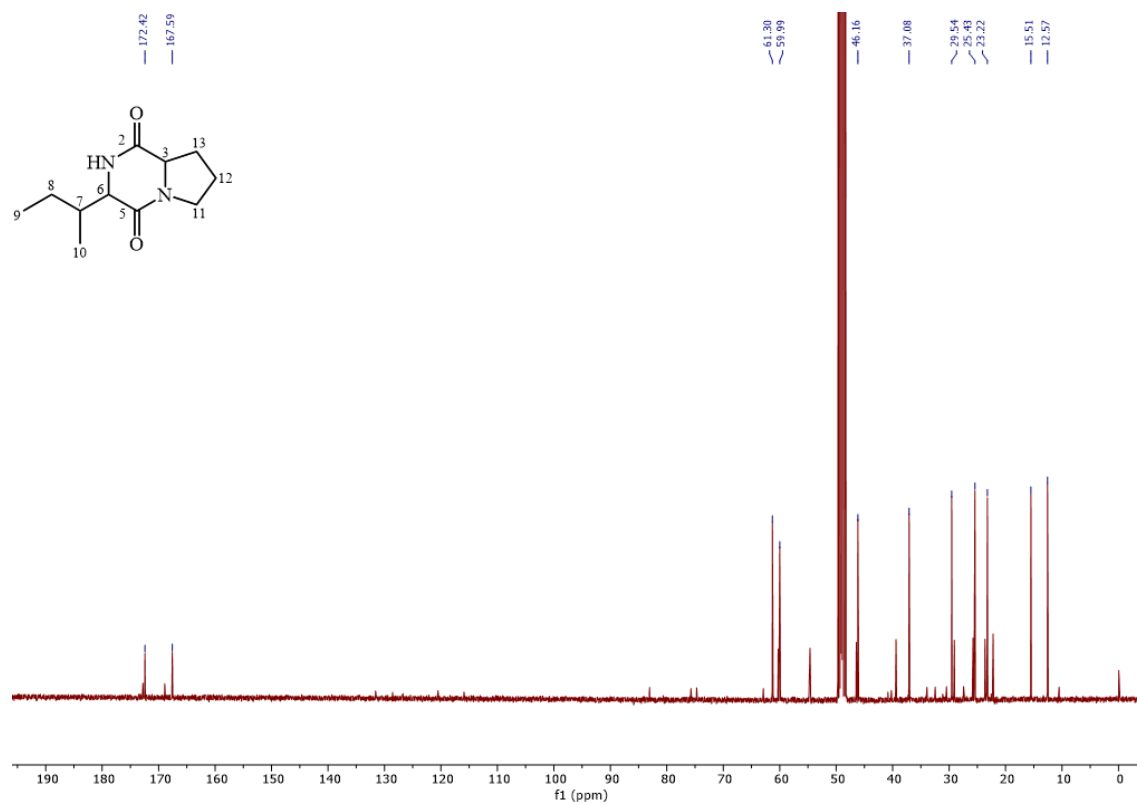
Figure S 74 ^{13}C NMR spectrum of compound **3.15** in methanol-d4, 100 MHz.
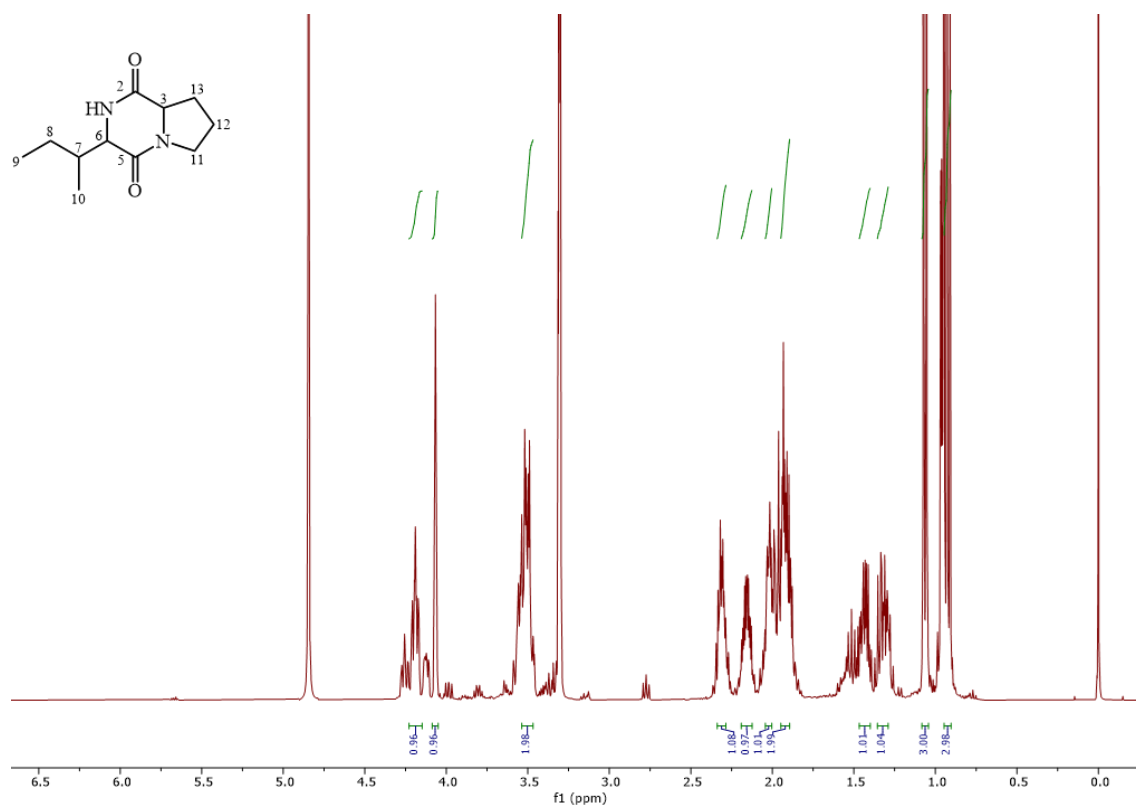
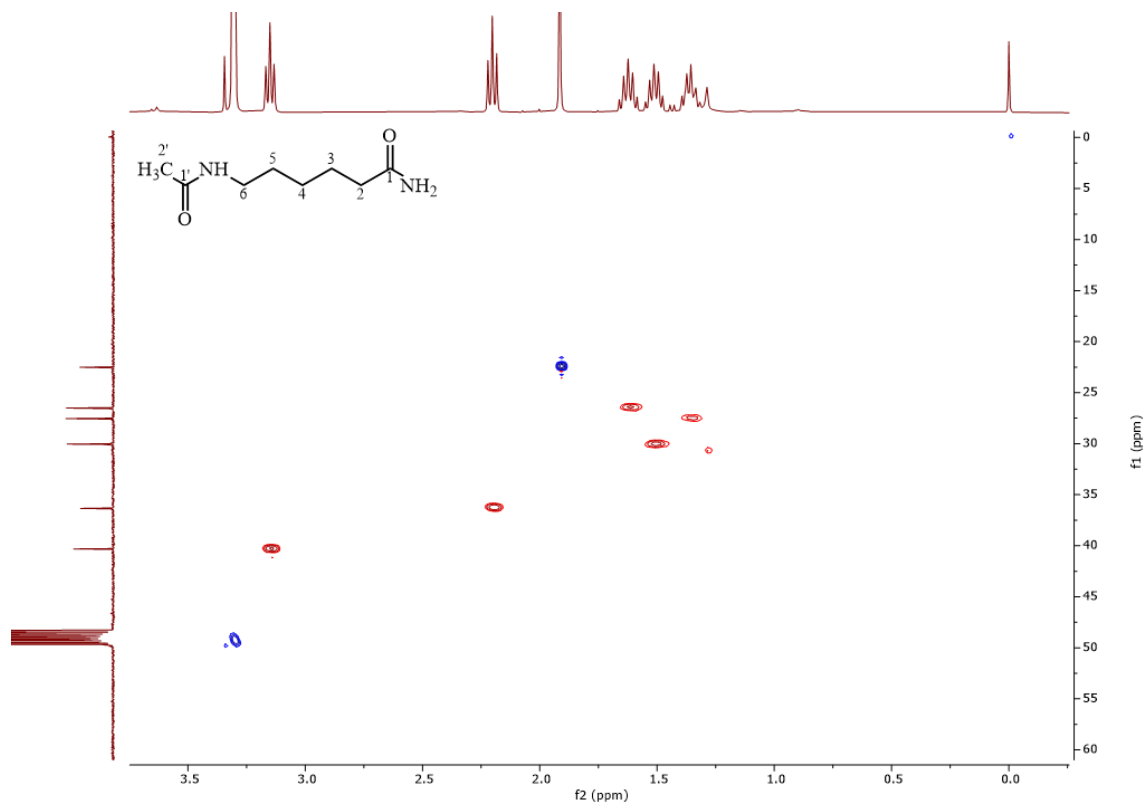**Figure S 75** ^{1}H NMR spectrum of compound **3.15** in methanol-d$_4$, 400 MHz.
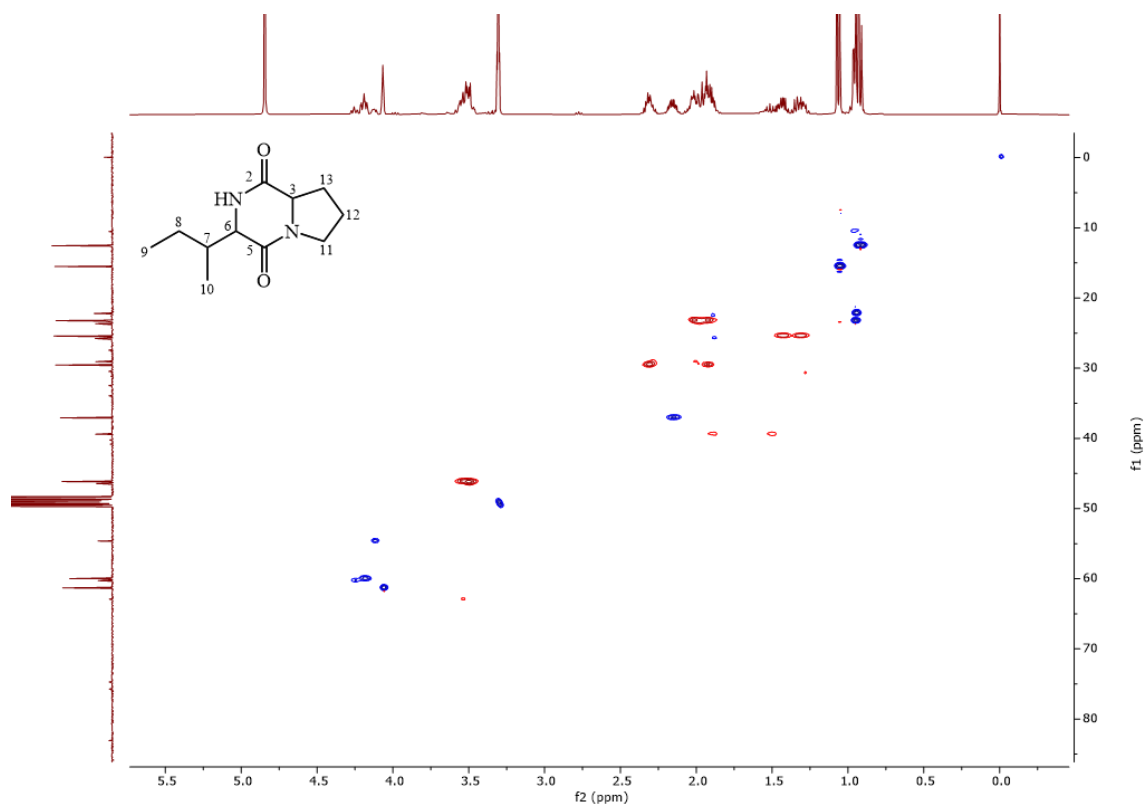
Figure S 76 HSQC spectrum of compound **3.15** in methanol-d$_4$, 400/100 MHz.
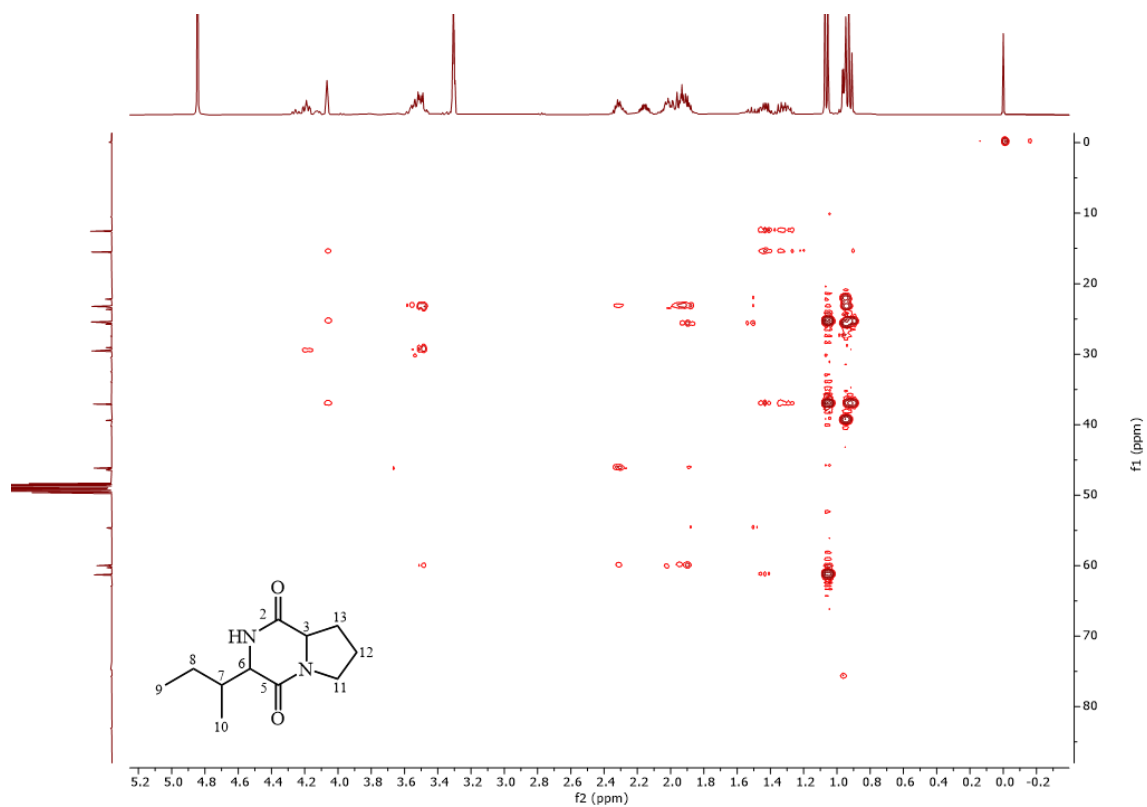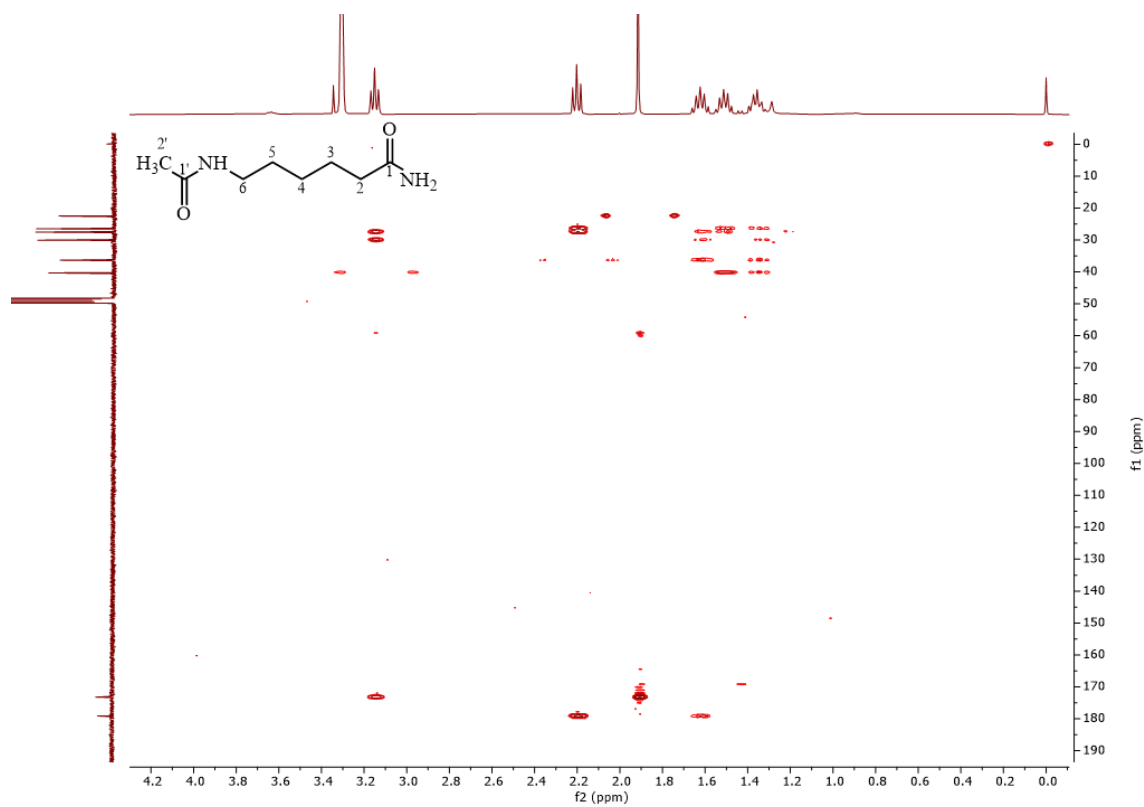
Figure S 77 HMBC spectrum of compound **3.15** in methanol-d₄, 400/100 MHz.
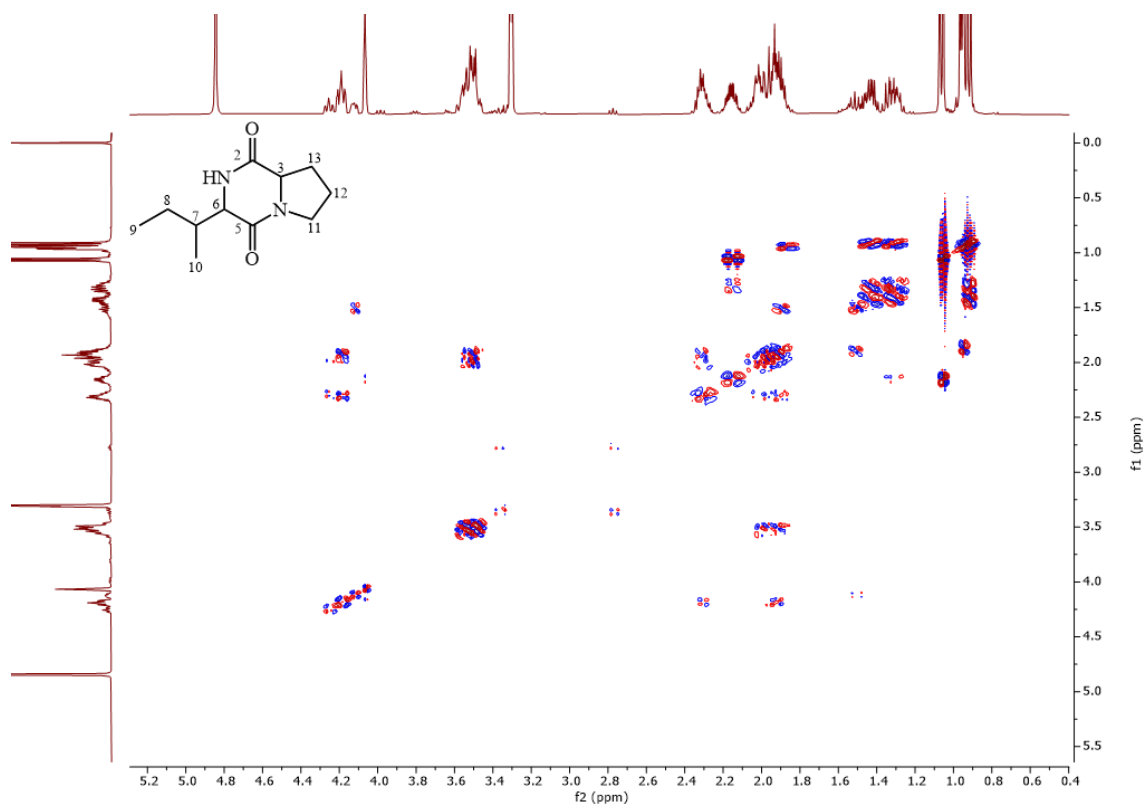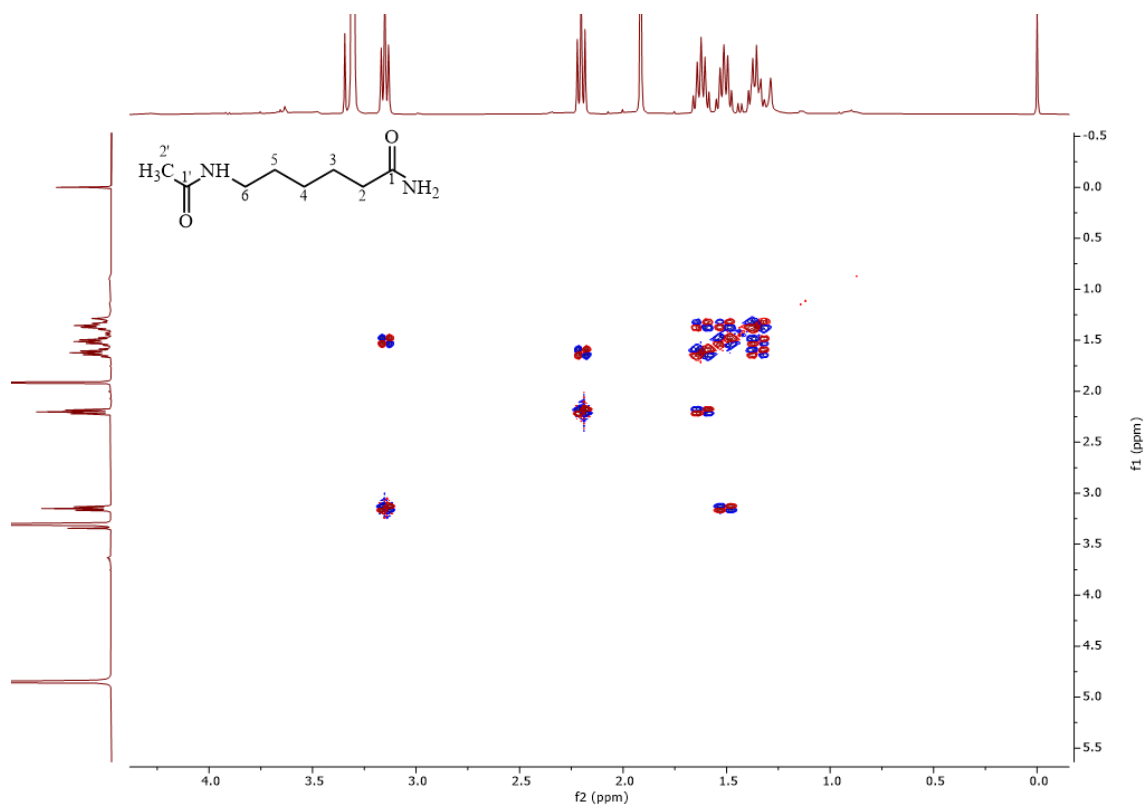

Figure S 78 COSY spectrum of compound **3.15** in methanol-d₄, 100 MHz.
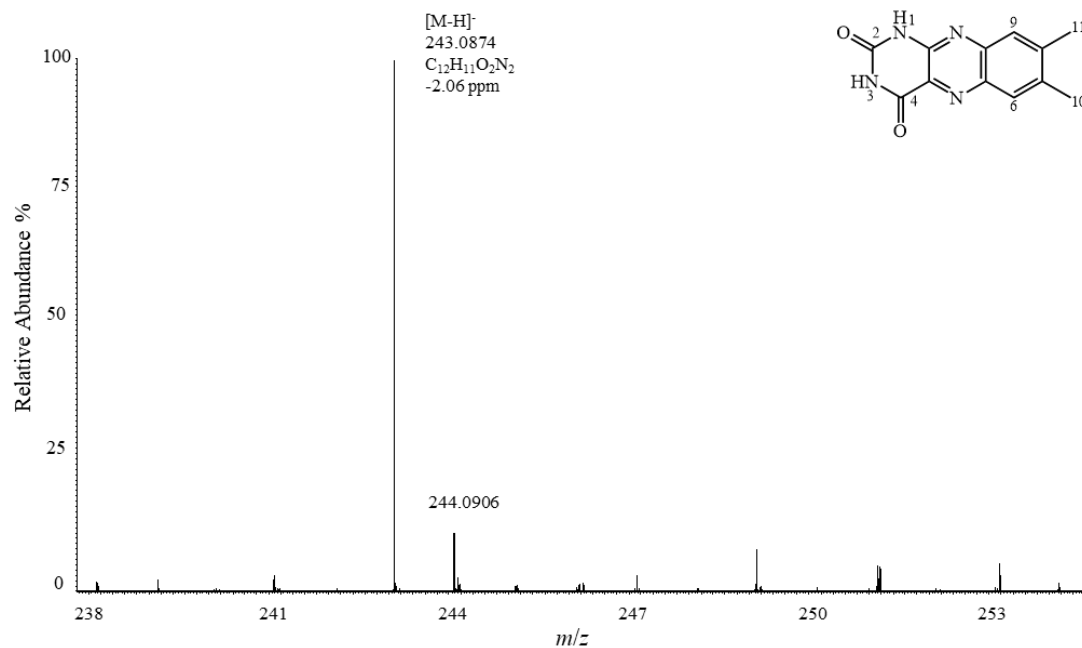
Figure S 79 (-)-ESI-HRMS spectrum of compound **3.16**.
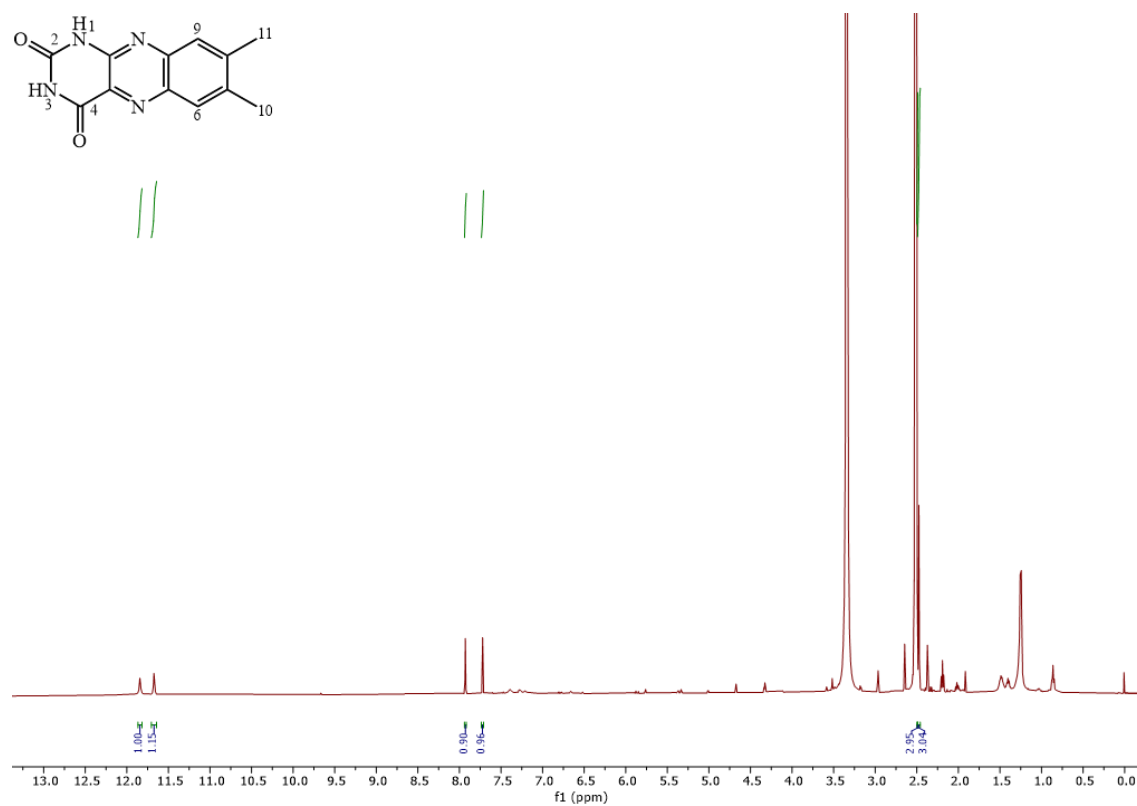
Figure S 80 ¹H NMR spectrum of compound **3.16** in DMSO-d₆, 500 MHz.
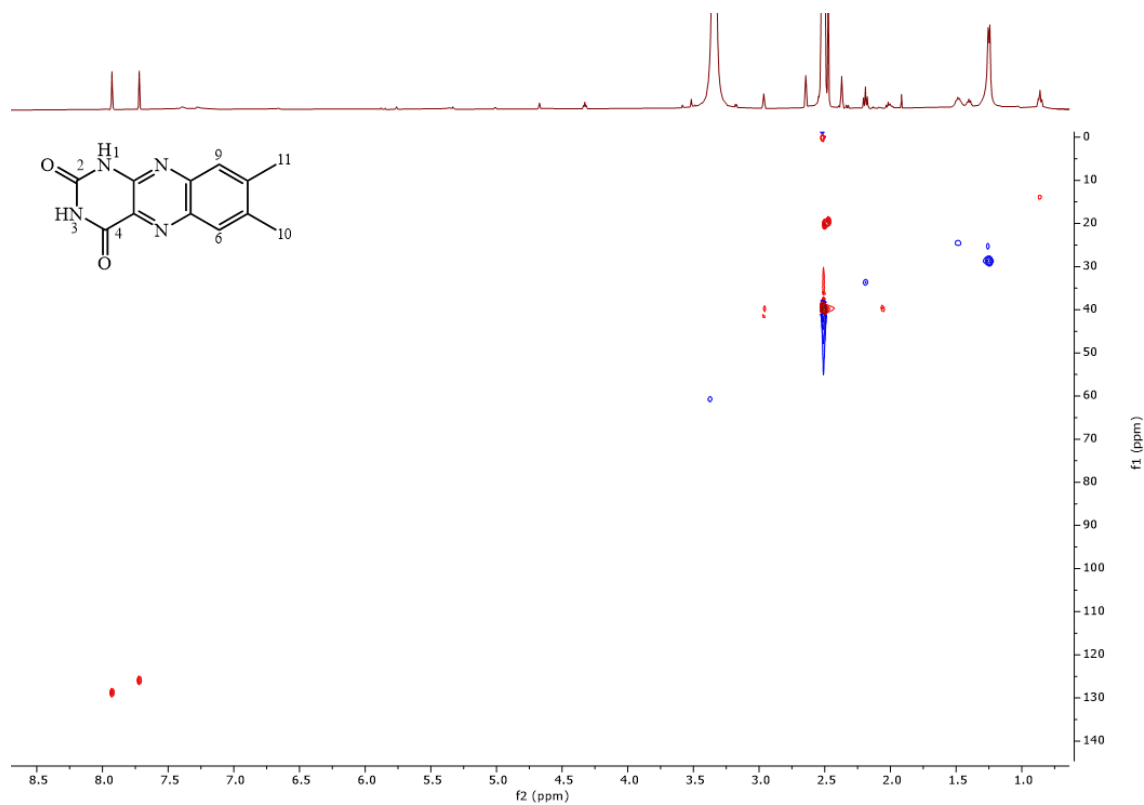
Figure S 81 HSQC spectrum of compound **3.16** in DMSO-d$_6$, 500/125 MHz.
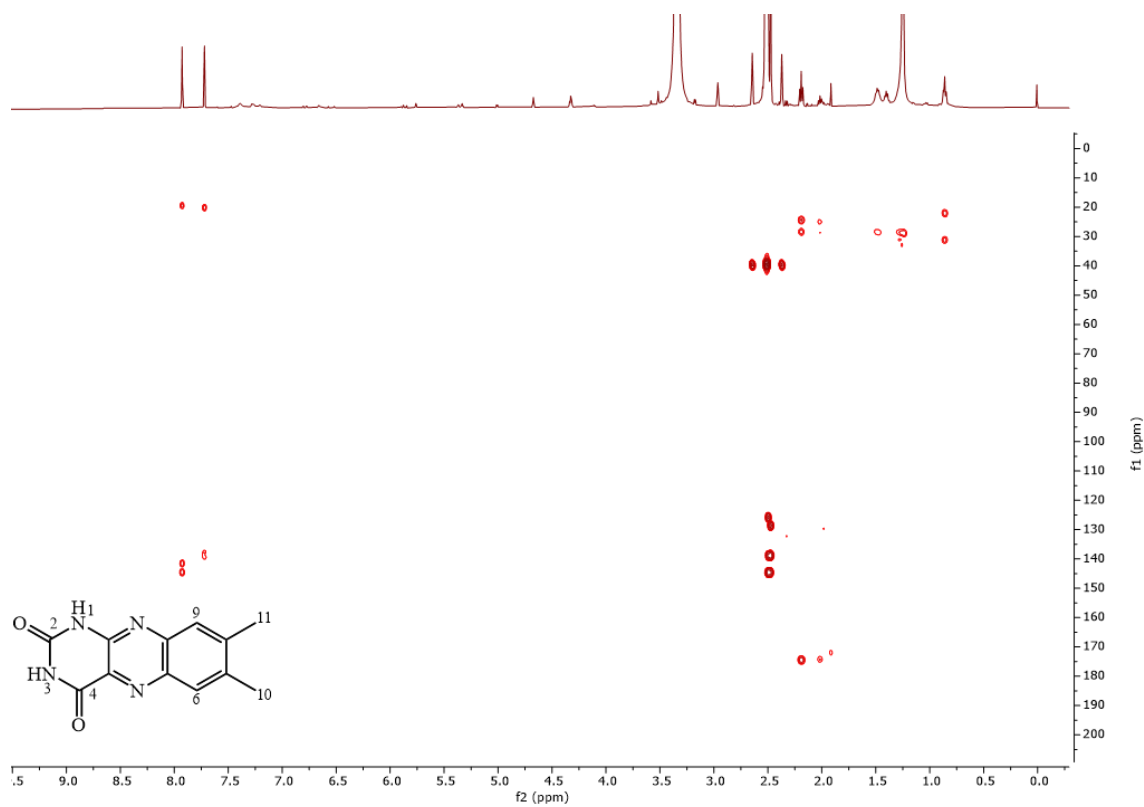
Figure S 82 HMBC spectrum of compound **3.16** in DMSO-d$_6$, 500/125 MHz.
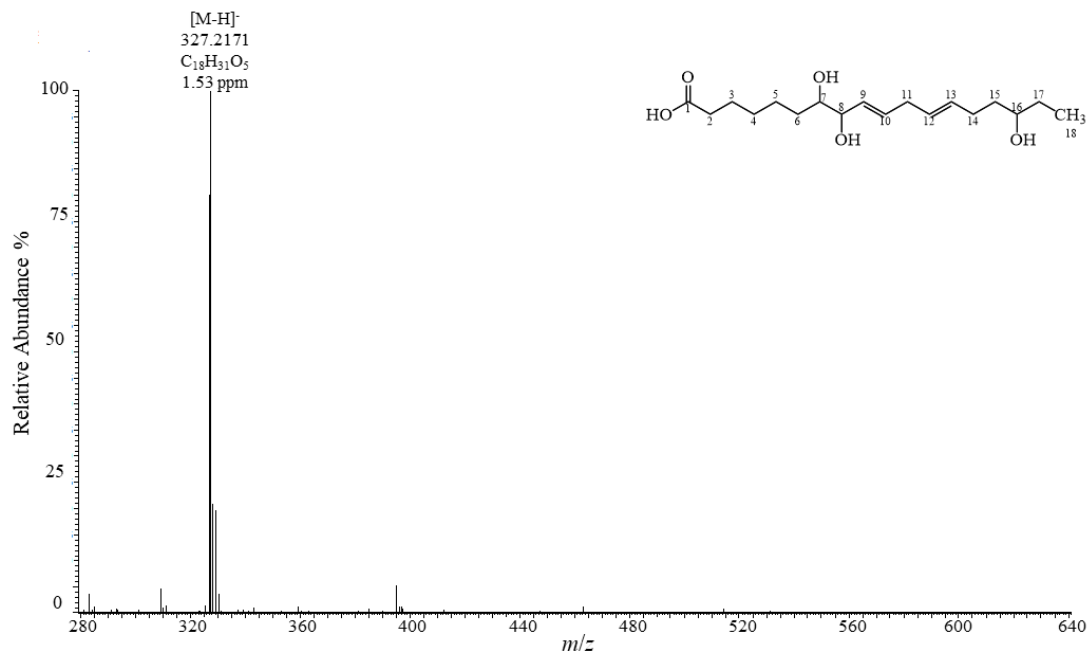
Figure S 83 (-)-ESI-HRMS spectrum of compound **3.17**.
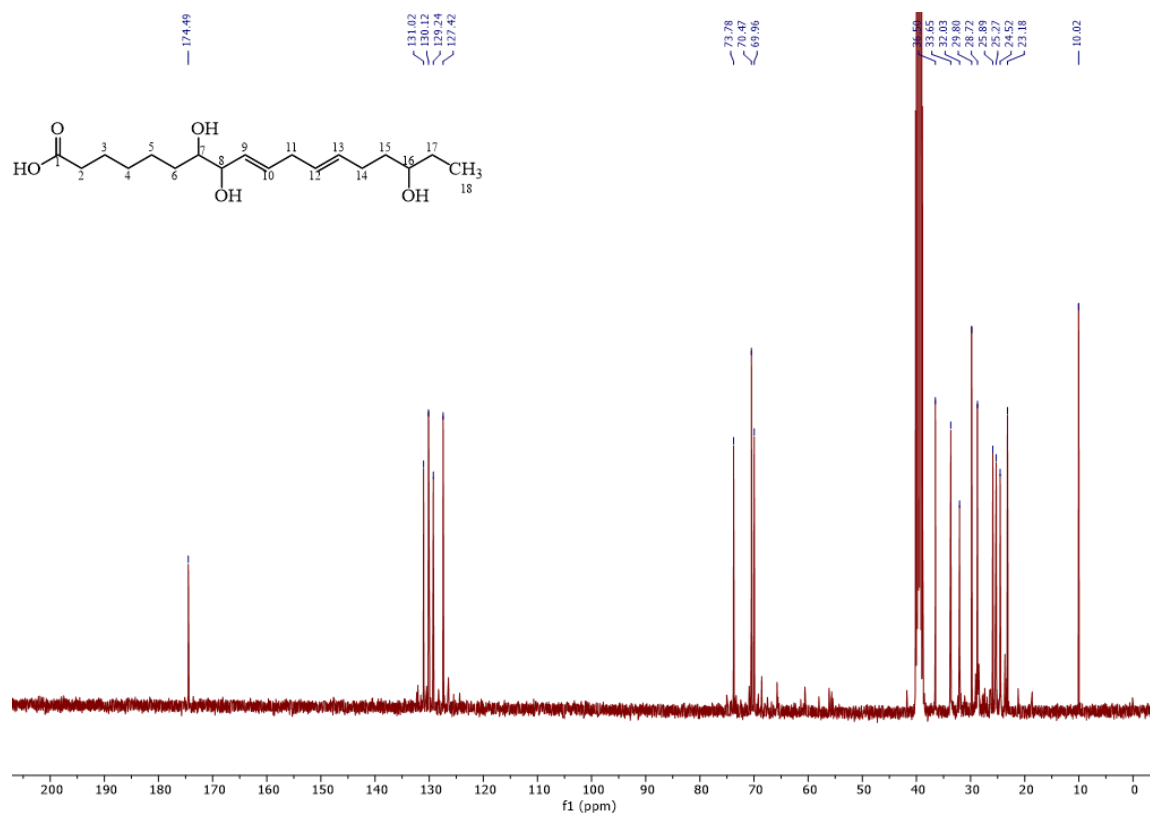
Figure S 84 ^{13}C NMR spectrum of compound **3.17** in DMSO-d$_6$, 100 MHz.
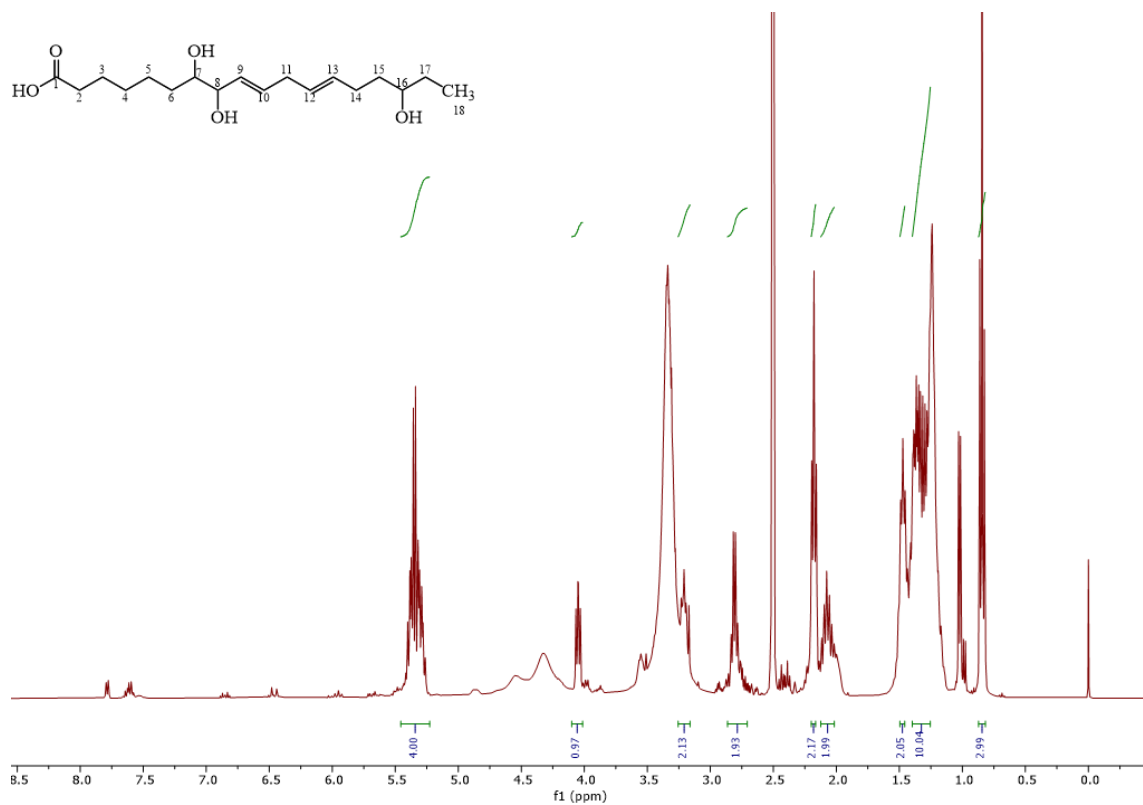
Figure S 85 ^{1}H NMR spectrum of compound **3.17** in DMSO-d$_6$, 400 MHz.
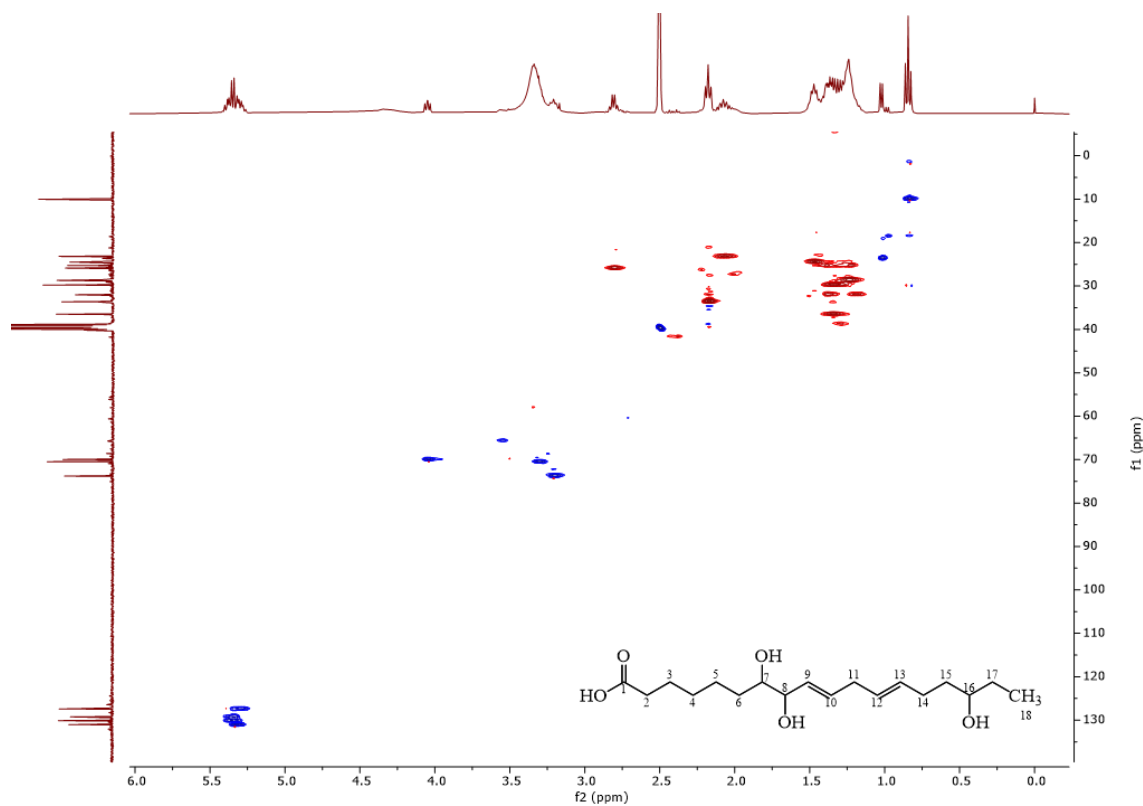
Figure S 86 HSQC spectrum of compound **3.17** in DMSO-d$_6$, 400/100 MHz.
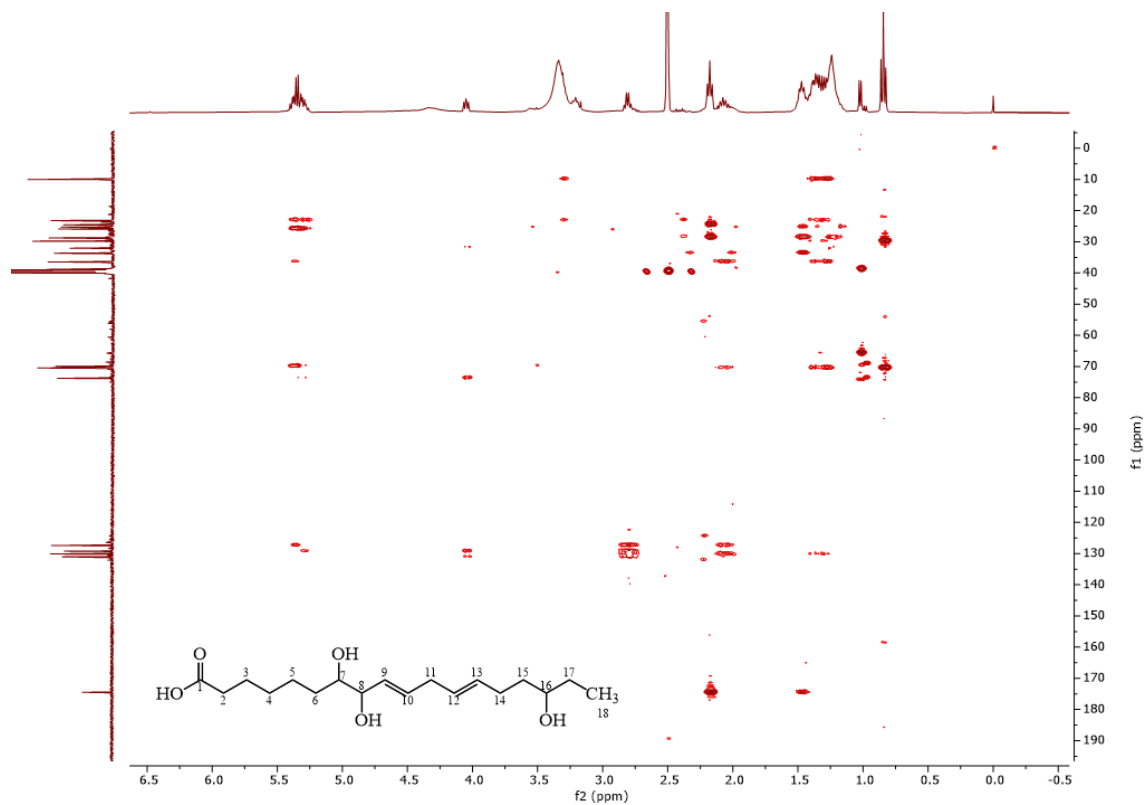
Figure S 87 HMBC spectrum of compound **3.17** in DMSO-d₆, 400/100 MHz.
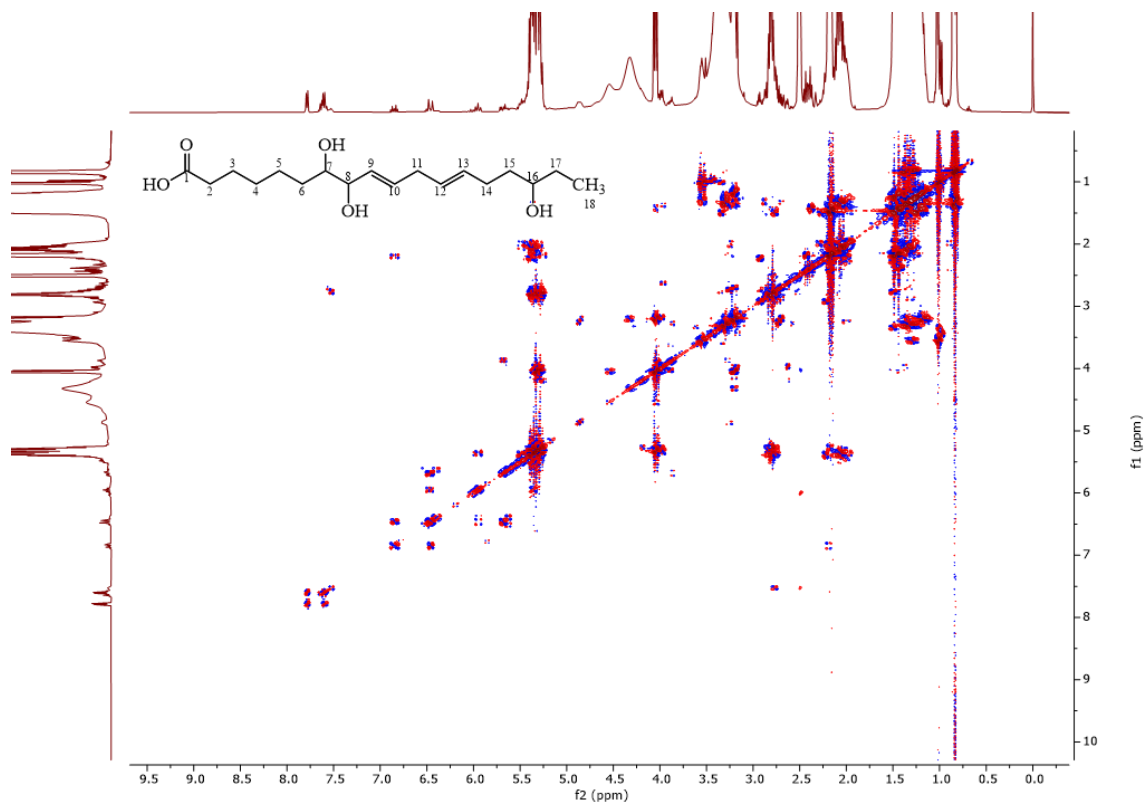
**Figure S 88** COSY spectrum of compound **3.17** in DMSO-d₆, 400 MHz.
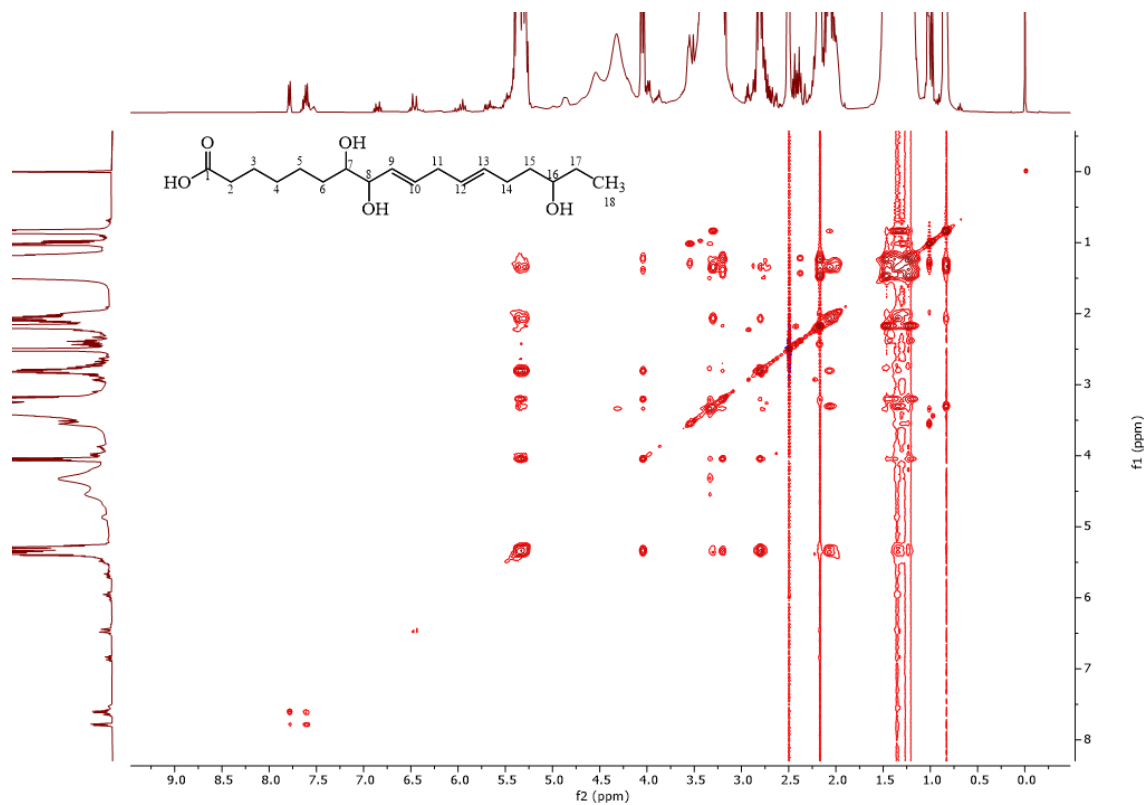
Figure S 89 TOCSY spectrum of compound **3.17** in DMSO-d$_6$, 400 MHz.
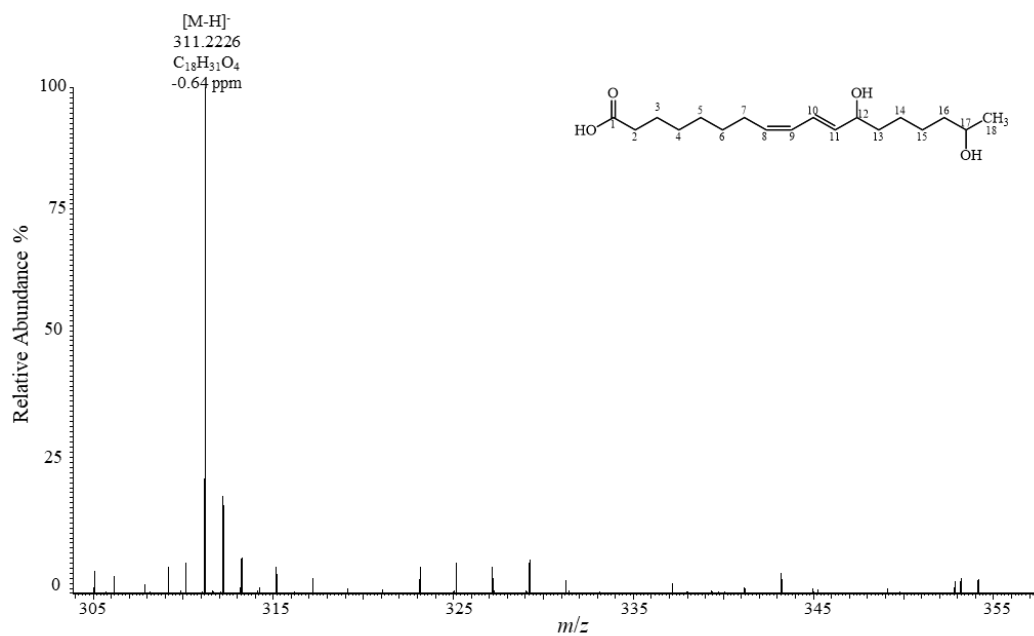
Figure S 90 (-)-ESI-HRMS spectrum of compound **3.18**.

Figure S 91 ^{13}C NMR spectrum of compound **3.18** in DMSO-d[6], 125 MHz.

Figure S 92 ^{1}H NMR spectrum of compound **3.18** in DMSO-d[6], 500 MHz.
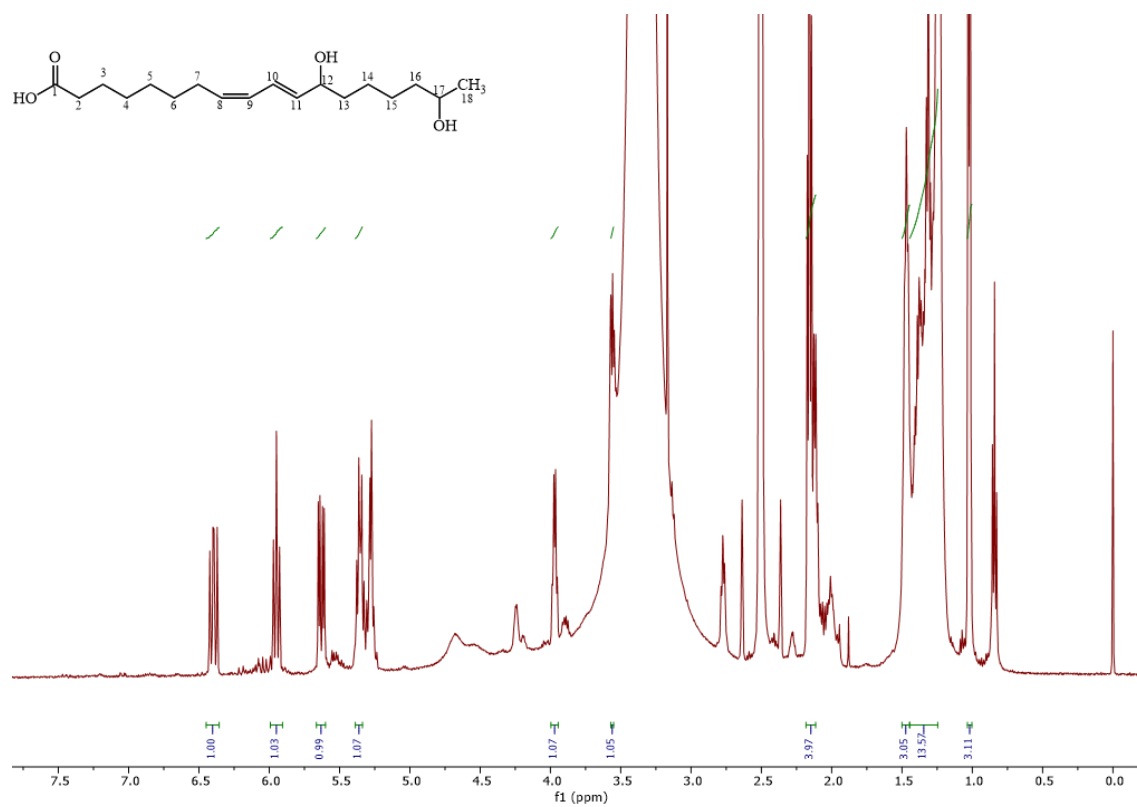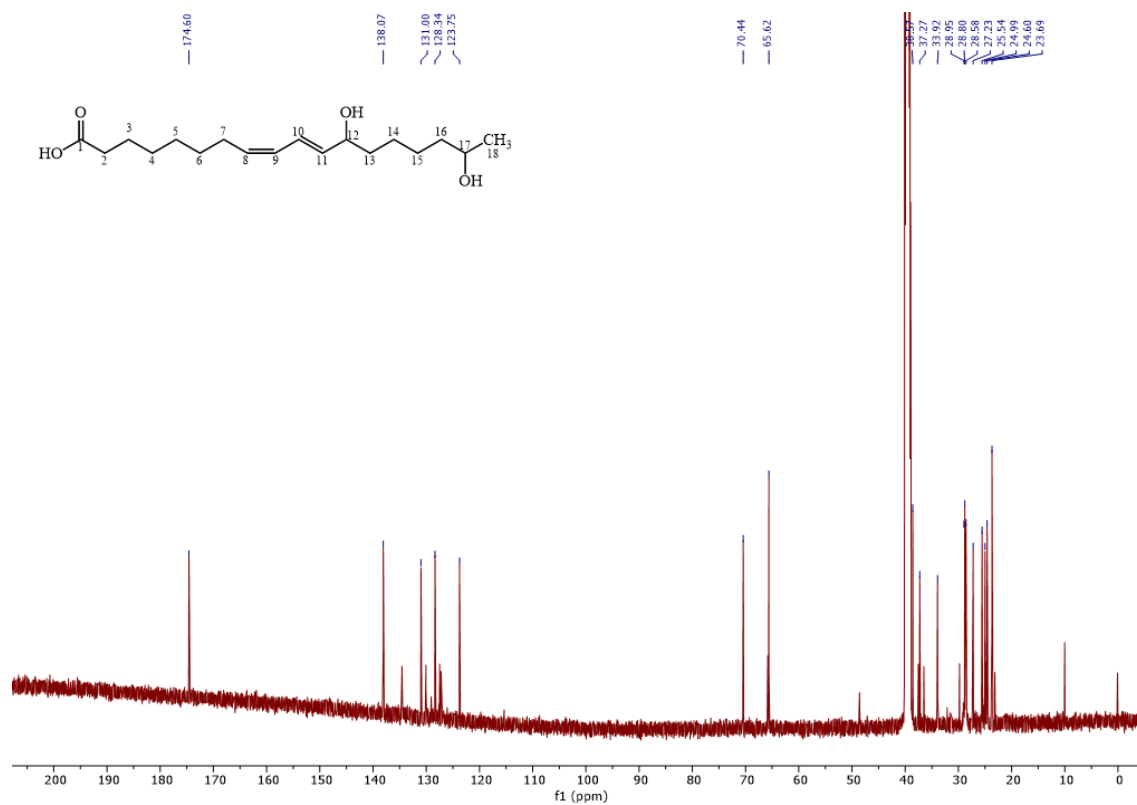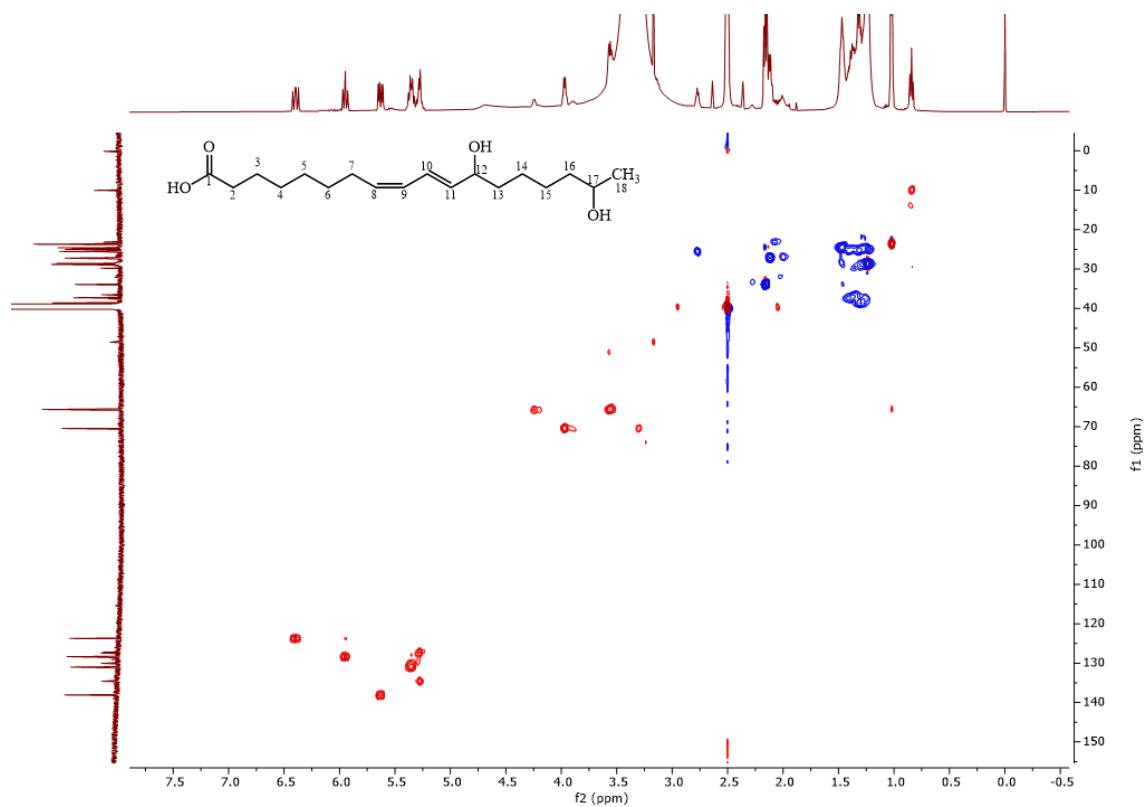
Figure S 93 HSQC spectrum of compound **3.18** in DMSO-d$_6$, 500/125 MHz.
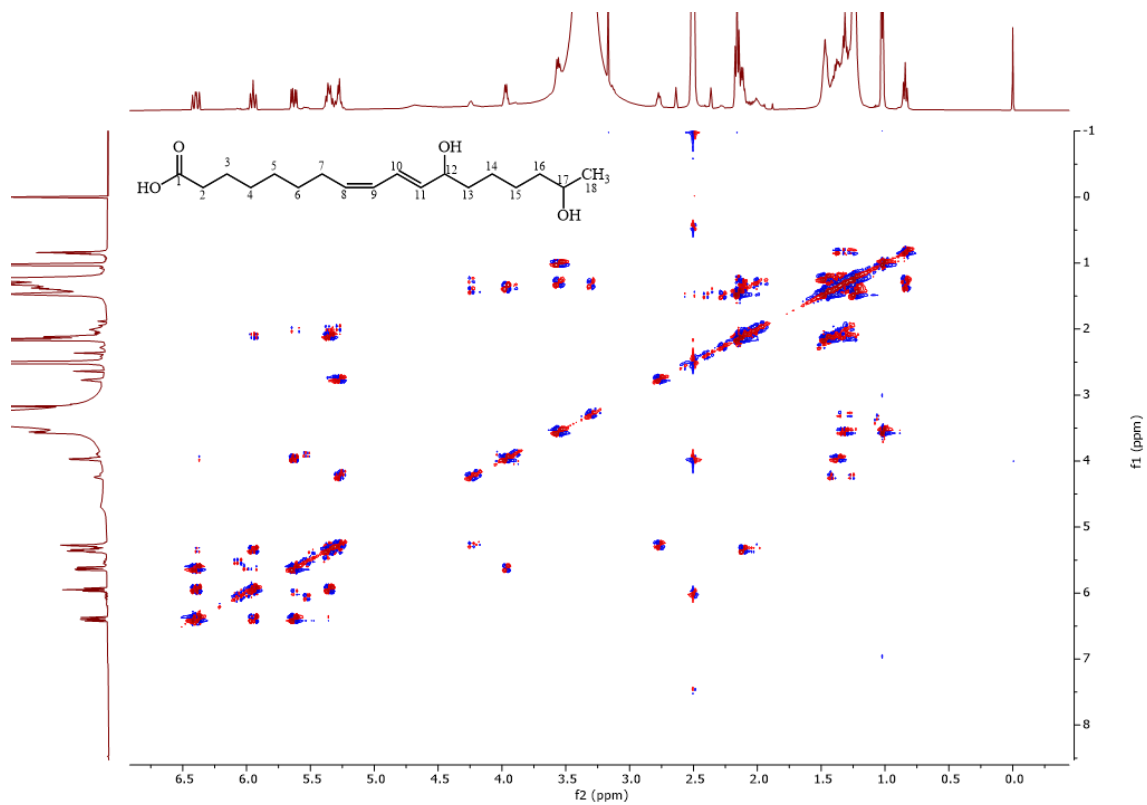
Figure S 94 COSY spectrum of compound **3.18** in DMSO-d$_6$, 500 MHz.
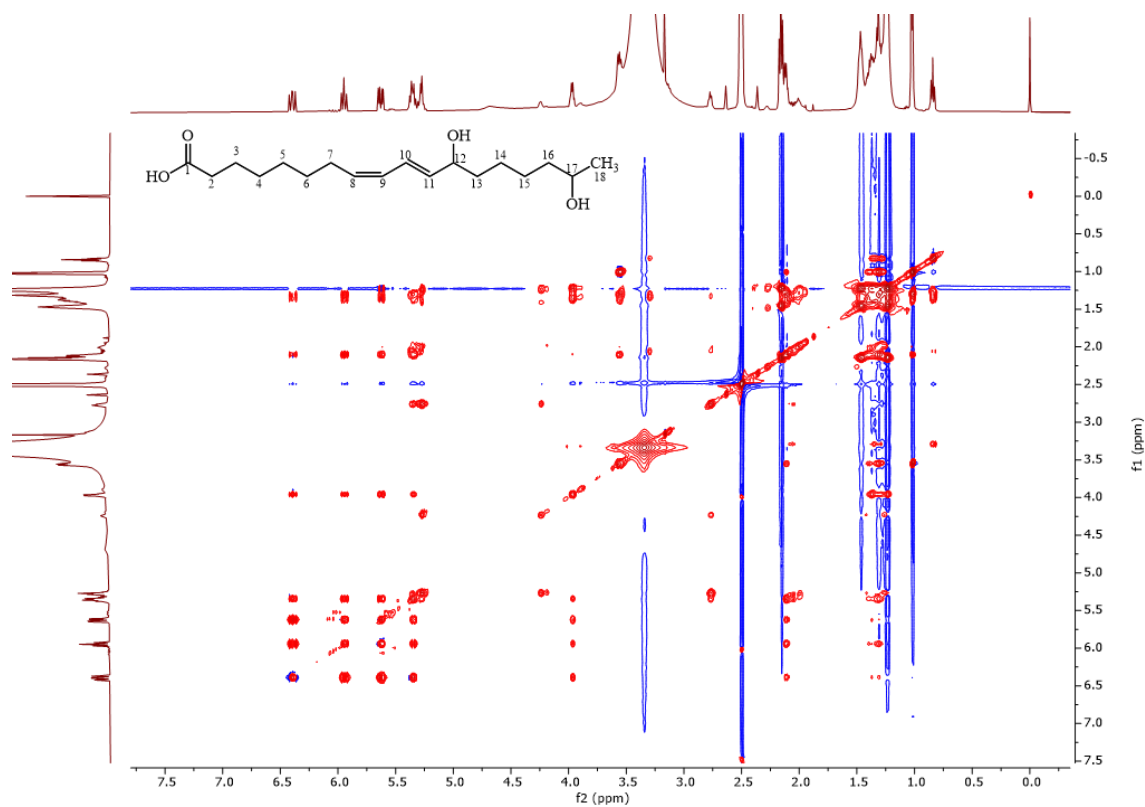
Figure S 95 TOCSY spectrum of compound **3.18** in DMSO-d$_6$, 500 MHz.

[M-H]$^-$
111.0199
C$_4$H$_3$N$_2$O$_2$
-0.90 ppm
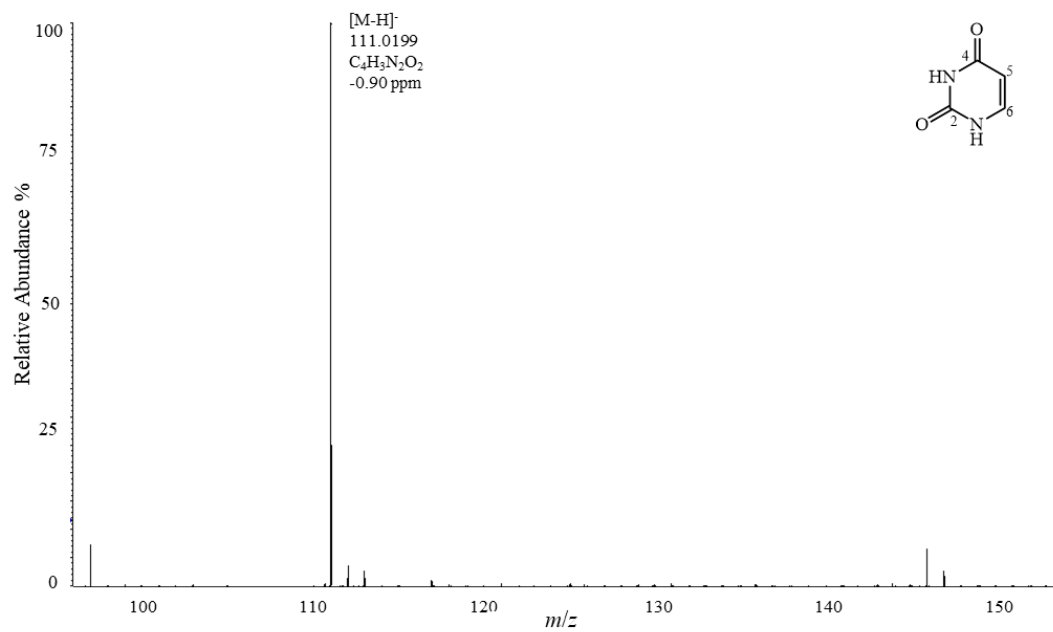
Figure S 96 (-)-ESI-HRMS spectrum of compound **3.19**.
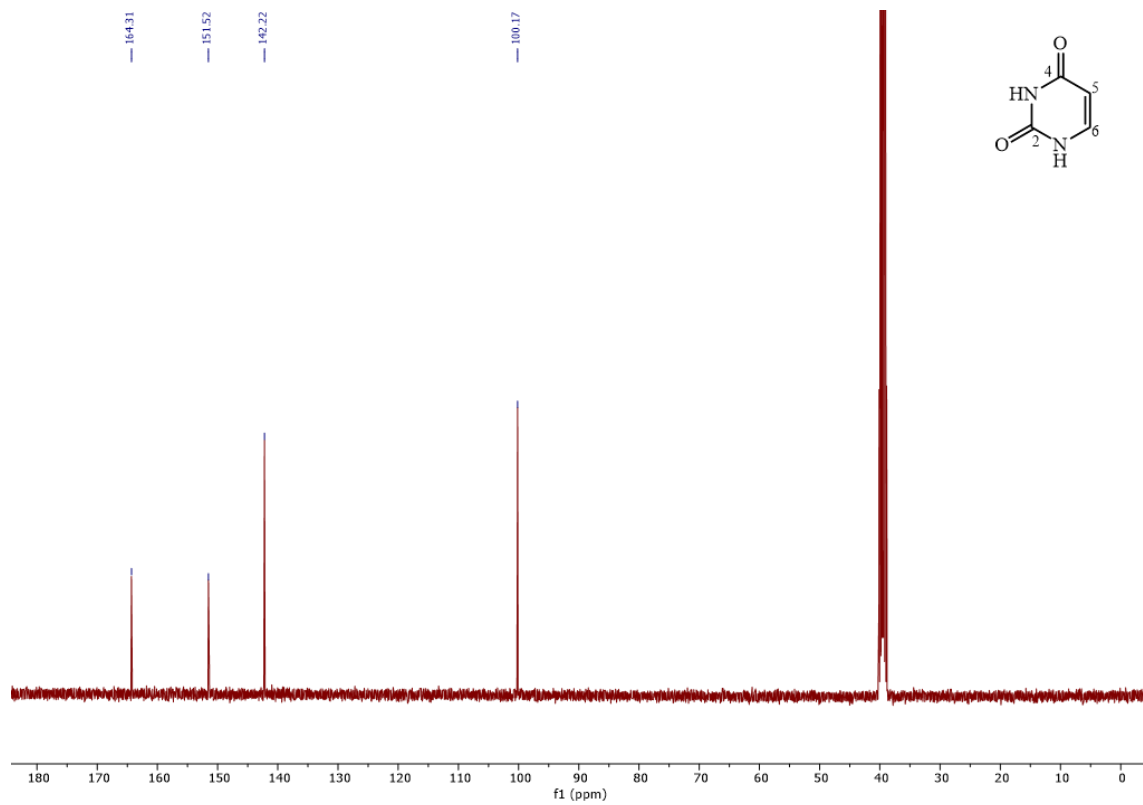
Figure S 97 ^{13}C NMR spectrum of compound **3.19** in DMSO-d$_6$, 125 MHz.
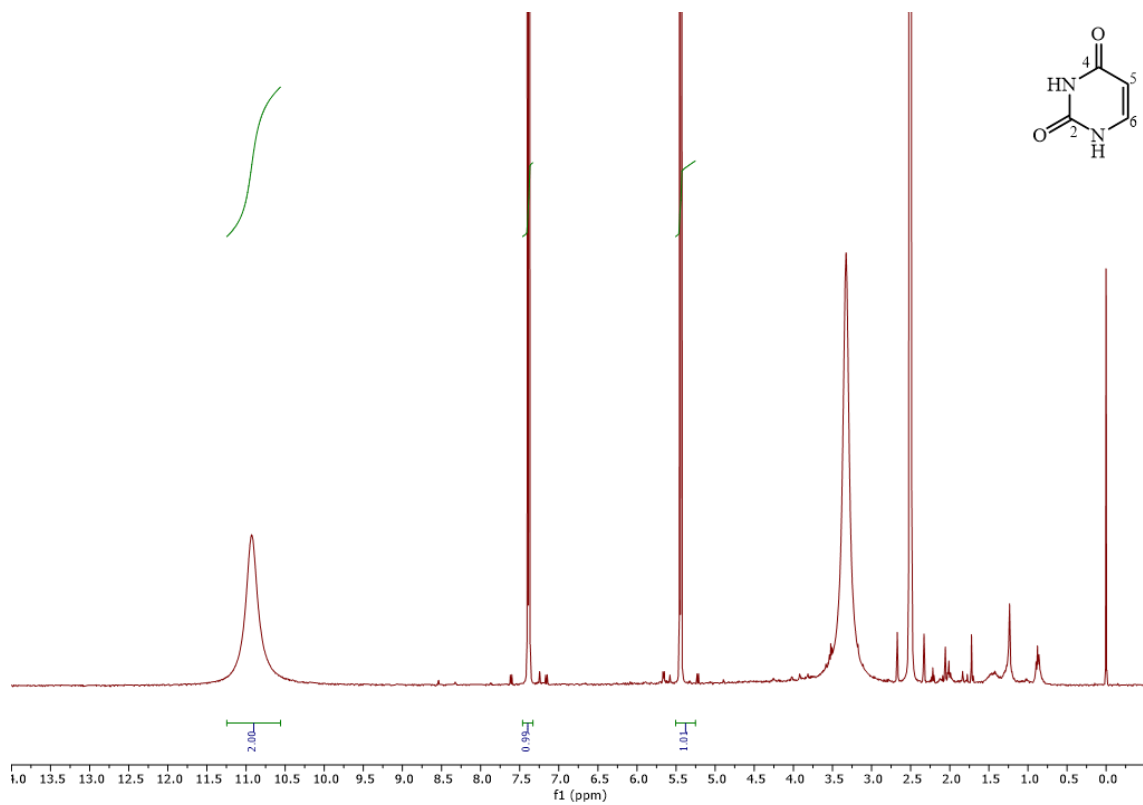
Figure S 98 ^{1}H NMR spectrum of compound **3.19** in DMSO-d$_6$, 500 MHz.
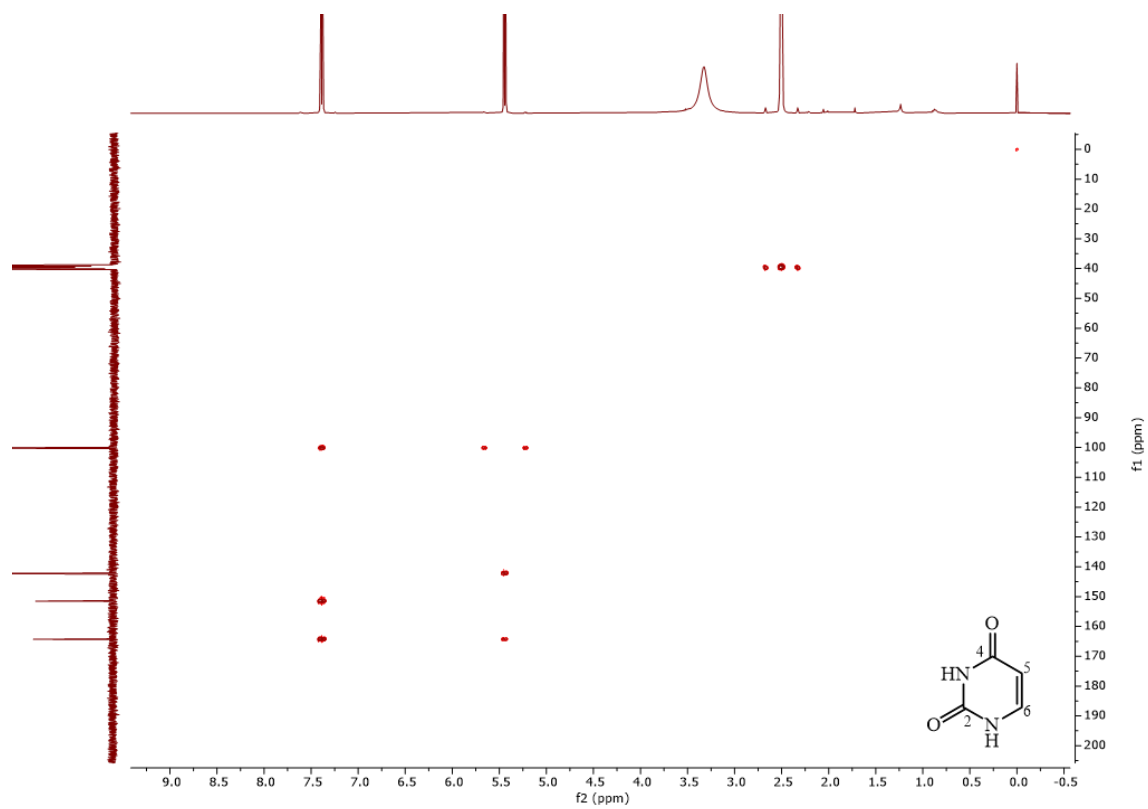
Figure S 99 HMBC spectrum of compound **3.19** in DMSO-d$_6$, 500/125 MHz.

Compound	100 mM	50 mM	20 mM	10 mM
3.1	-			-
3.2	-			
3.3	-			
3.4	-			-
3.5	-			
3.6				-
3.7	-			
3.8	-			
3.9	-			

3.10	-	-	-	-
3.11				
3.12	-	-	-	-
3.13		-	-	-
3.14		-	-	-
3.15		-	-	-
3.16	-	-	-	-
3.17	-			-
3.18	-			**-**
3.19	-		-	-
Blank				
Paraquat (0.1 mM)				

Figure S 100 Pictures of leaf-spot assay of compounds **3.1** – **3.19**.
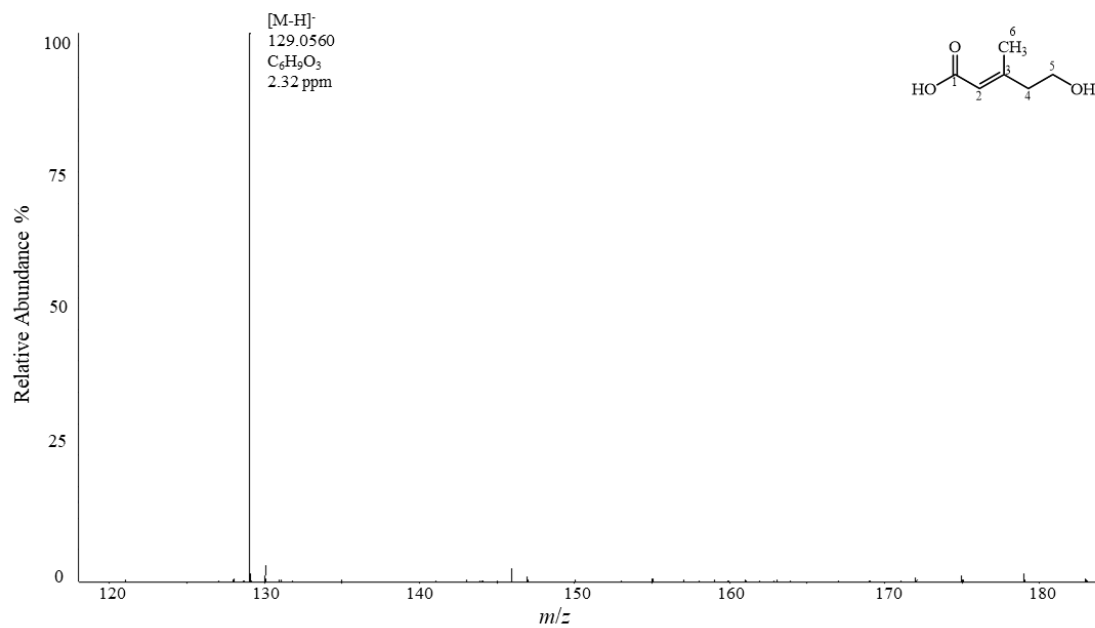
Figure S 101 (-)-ESI-HRMS spectrum of compound **4.1**.
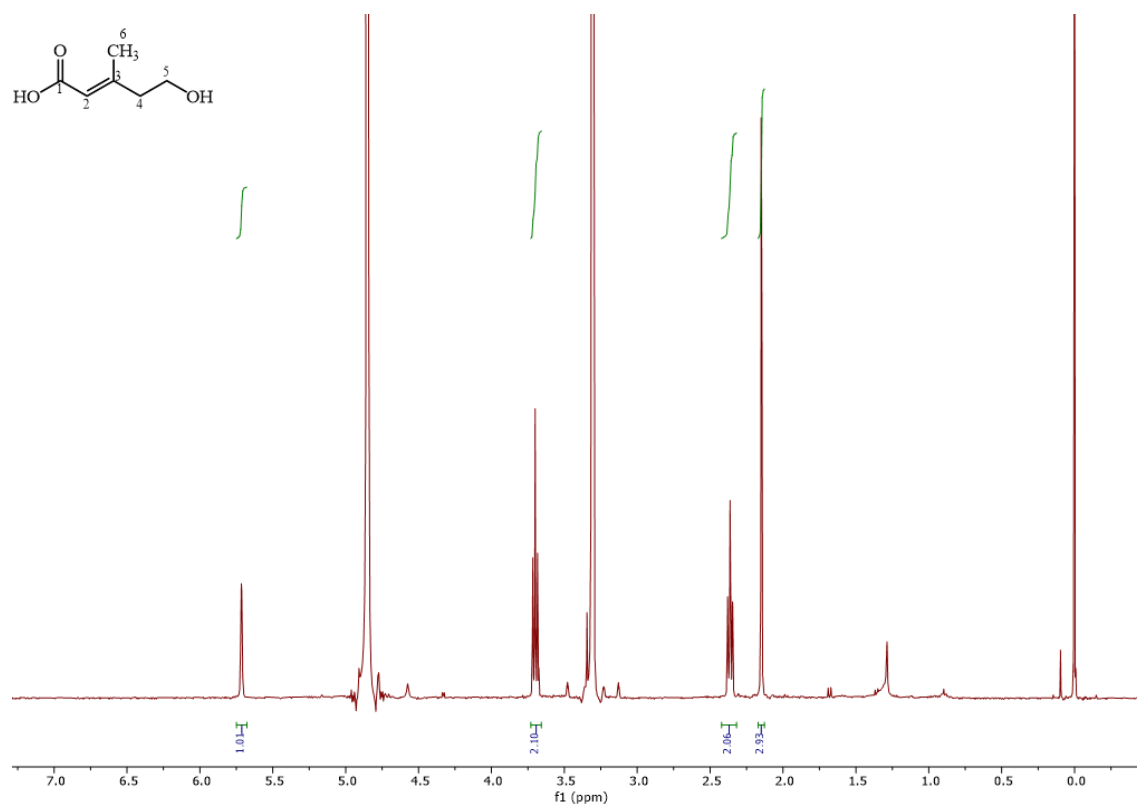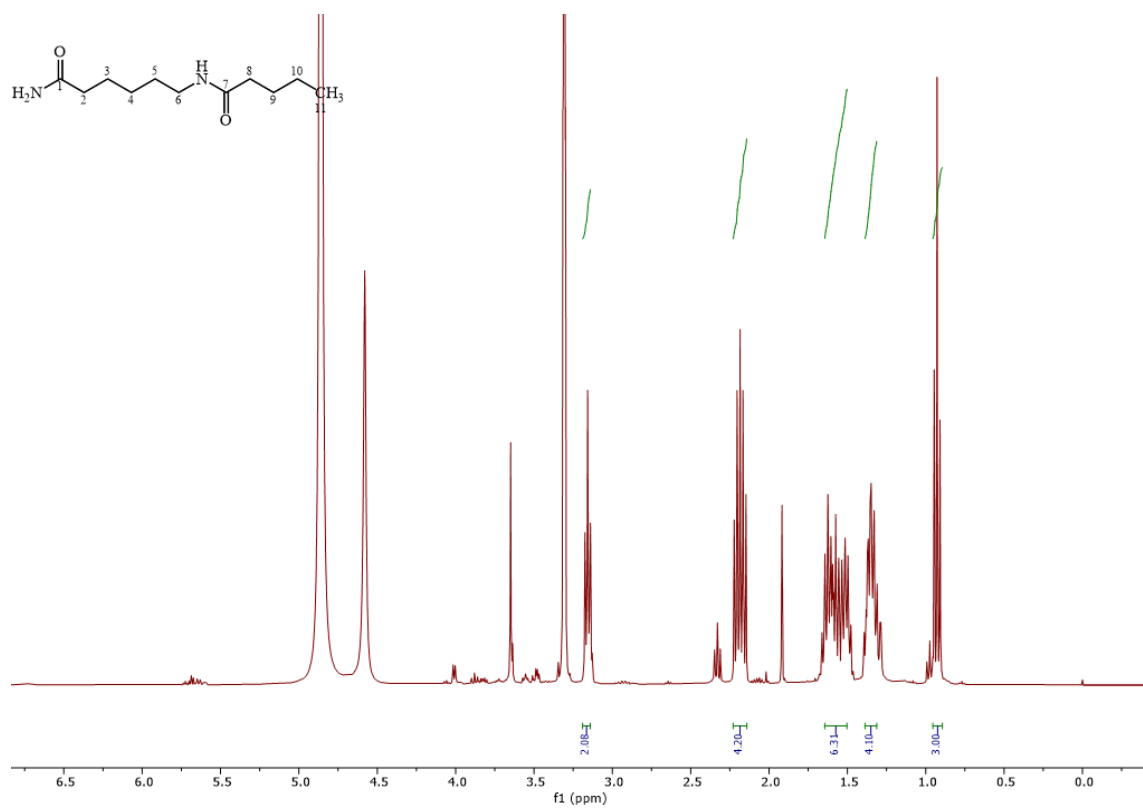

Figure S 102 ^{1}H NMR spectrum of compound **4.1** in methanol-d$_4$, 400 MHz.
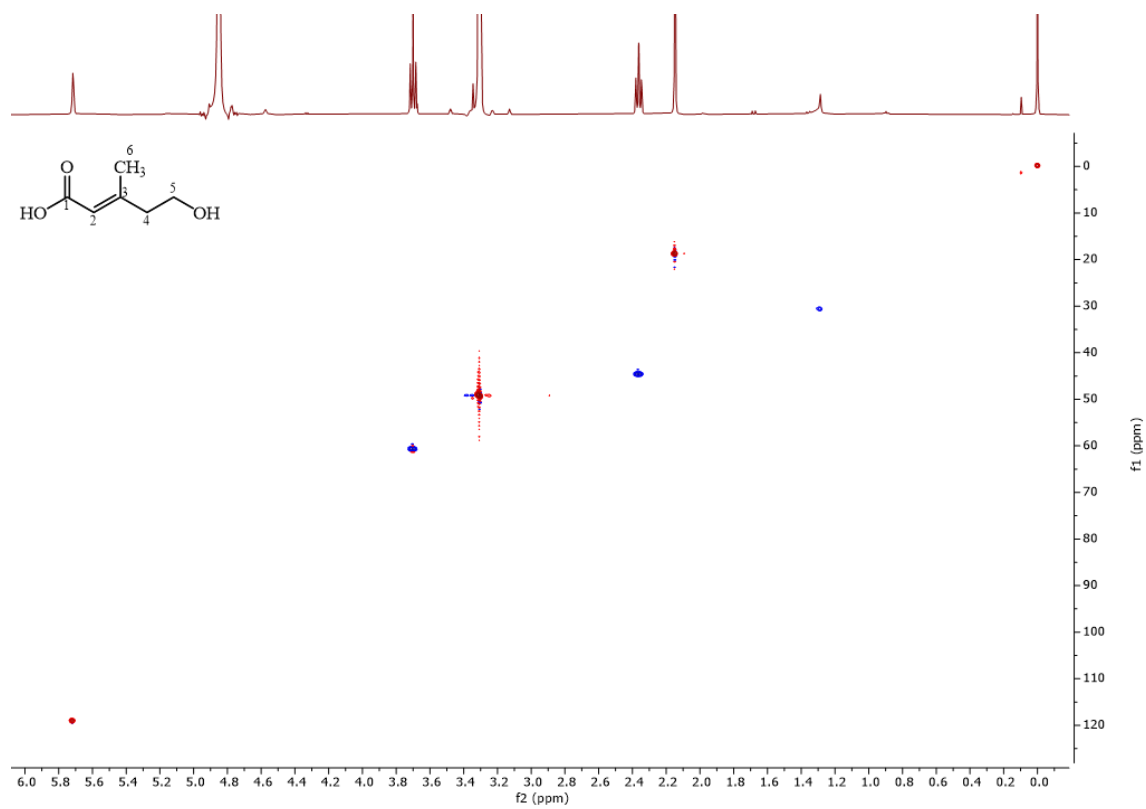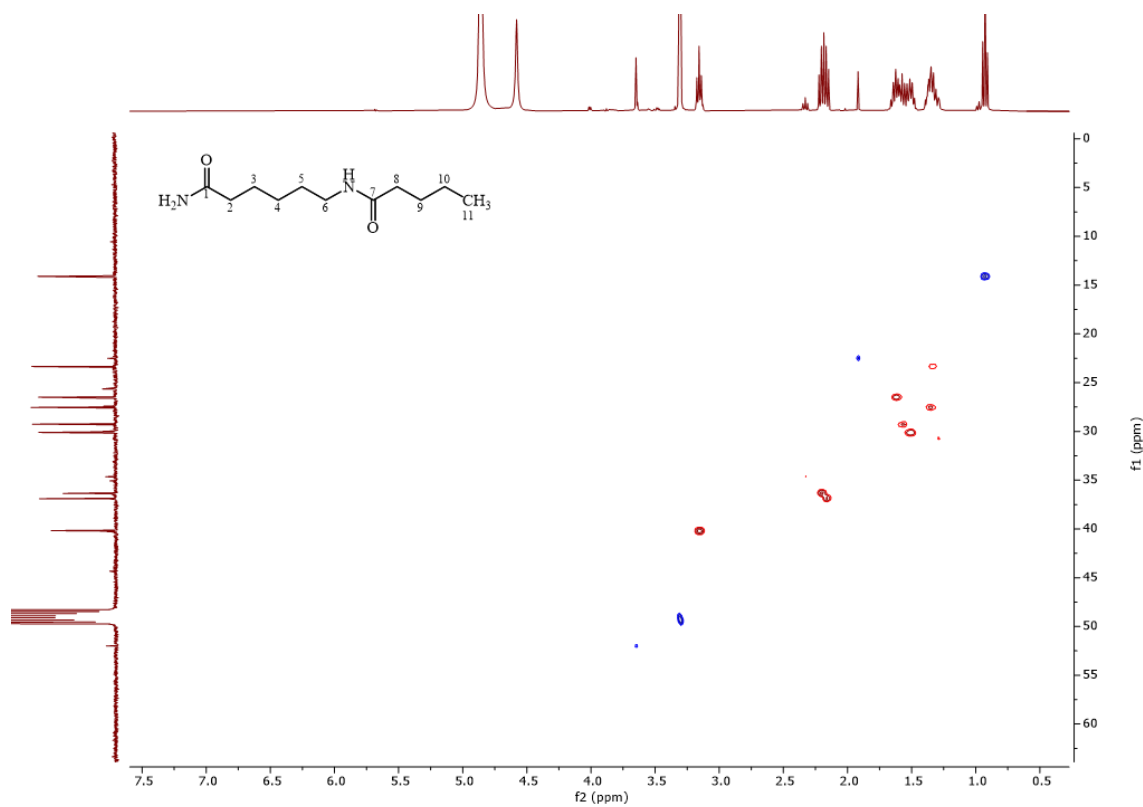
Figure S 103 HSQC spectrum of compound **4.1** in methanol-d$_4$, 400/100 MHz.
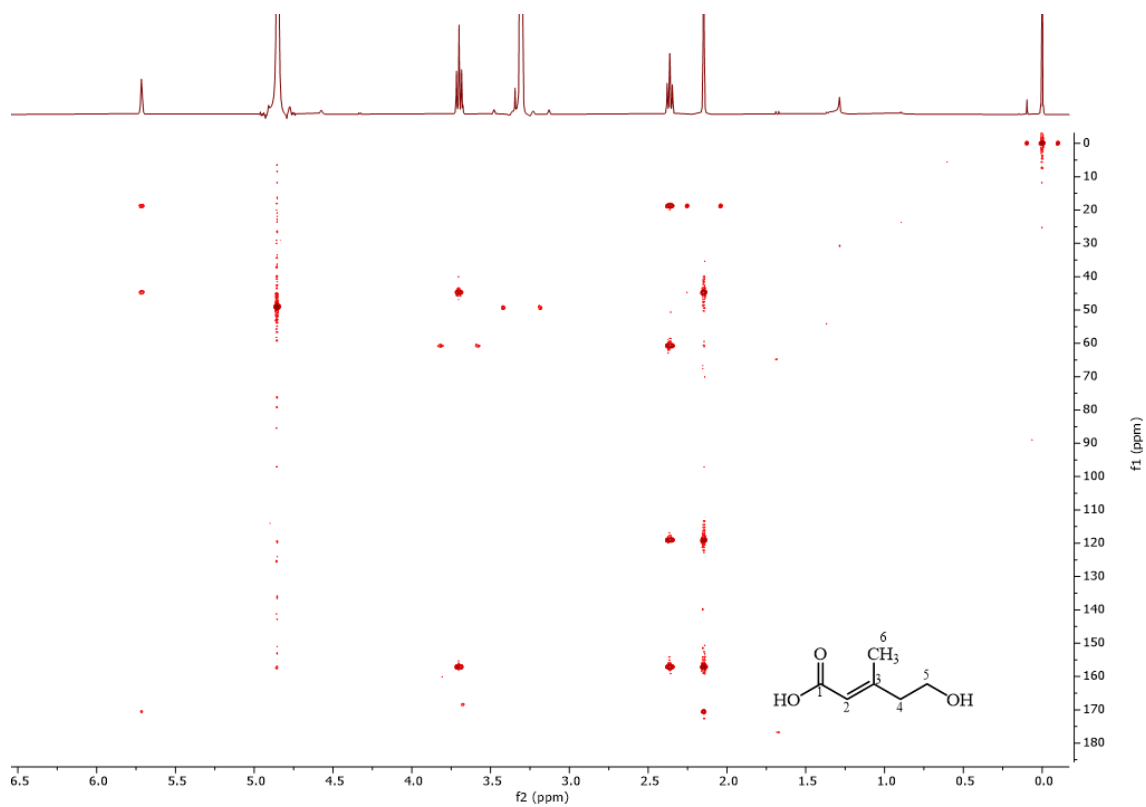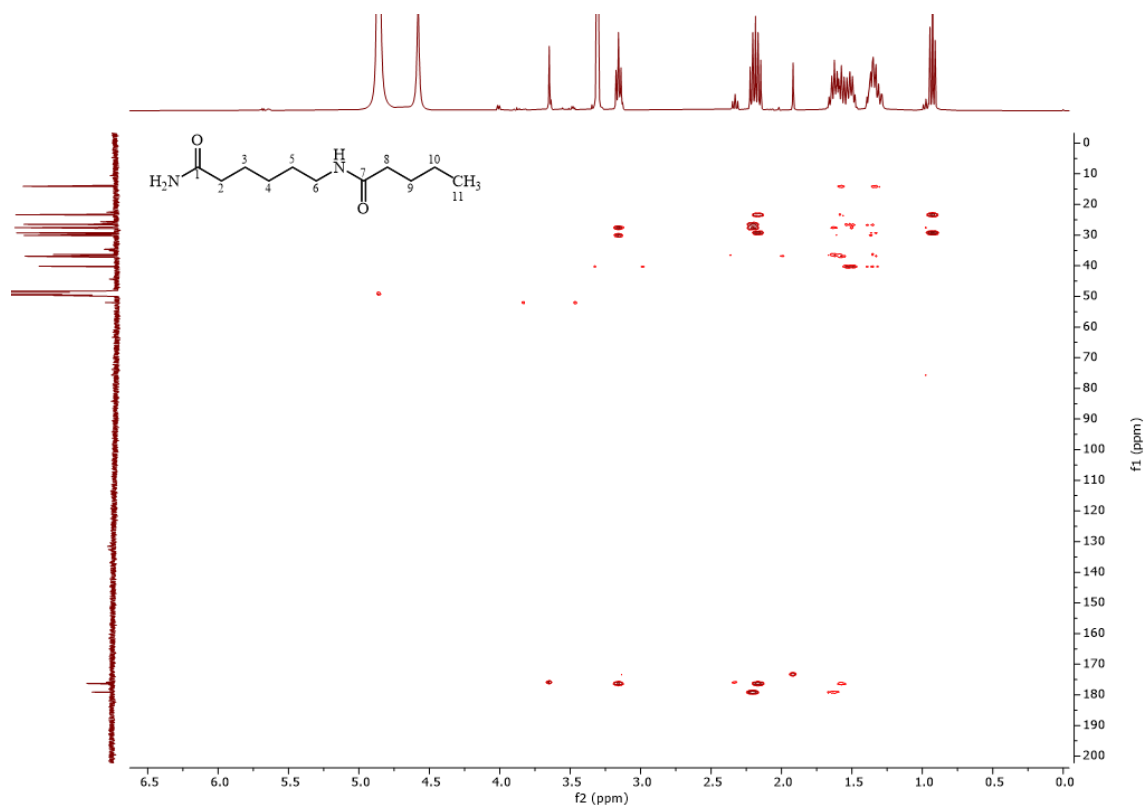

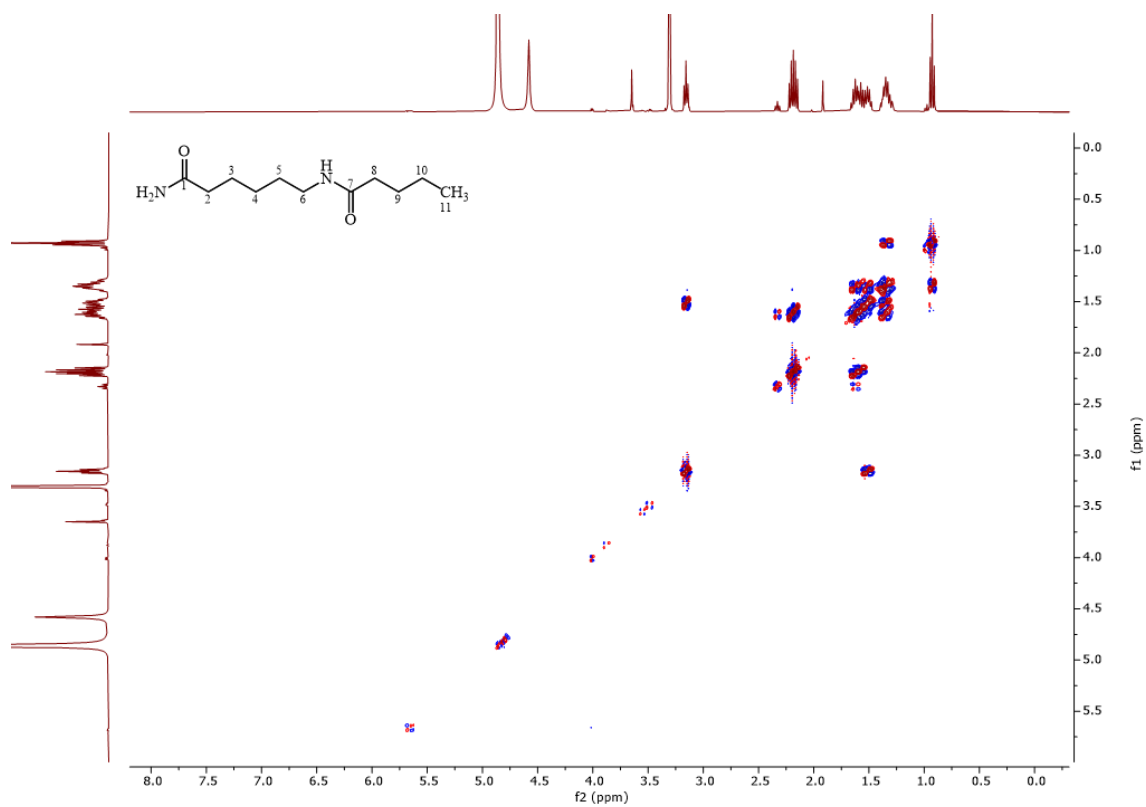**Figure S 104** HMBC spectrum of compound **4.1** in methanol-d$_4$, 400/100 MHz.
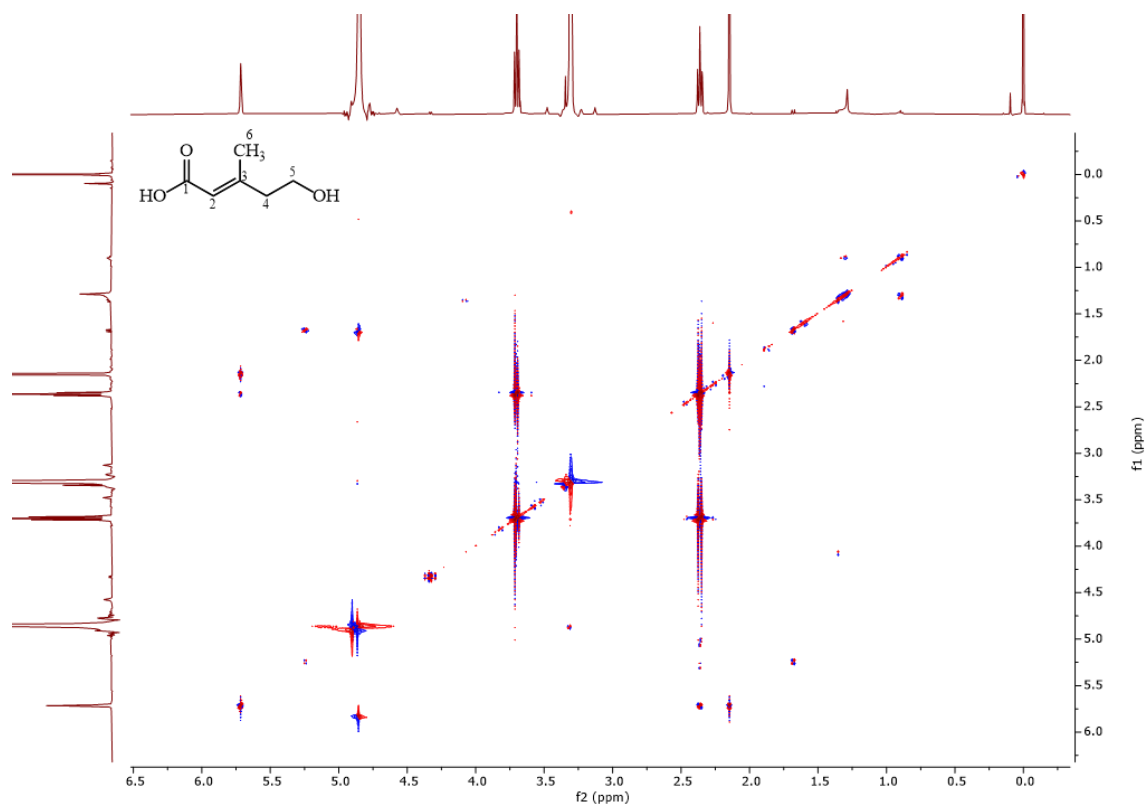
Figure S 105 COSY spectrum of compound **4.1** in methanol-d₄, 400 MHz.
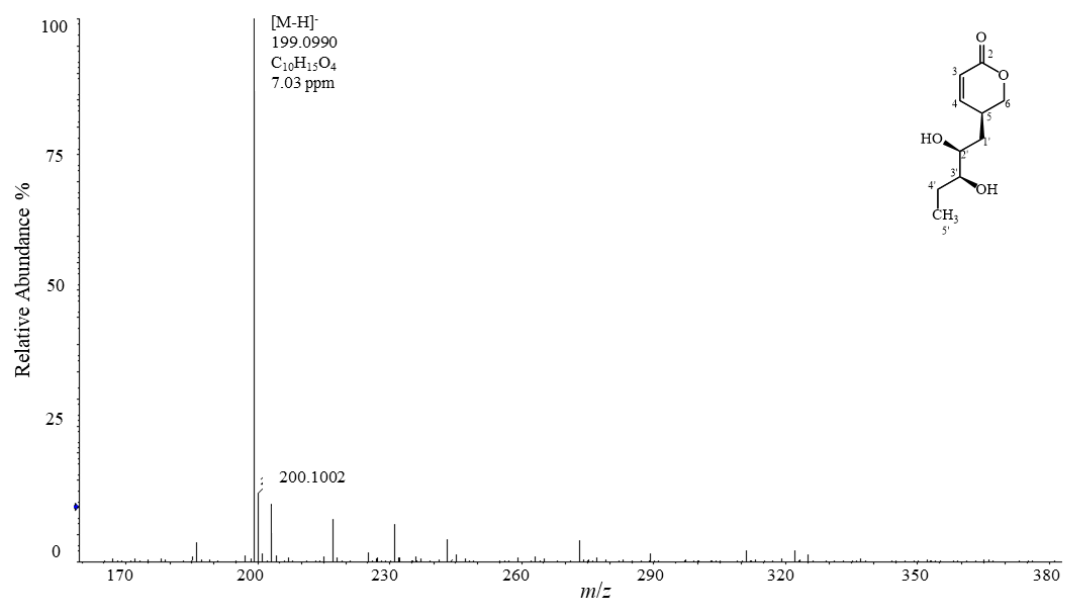
Figure S 106 (-)-ESI-HRMS spectrum of compound **4.2**.
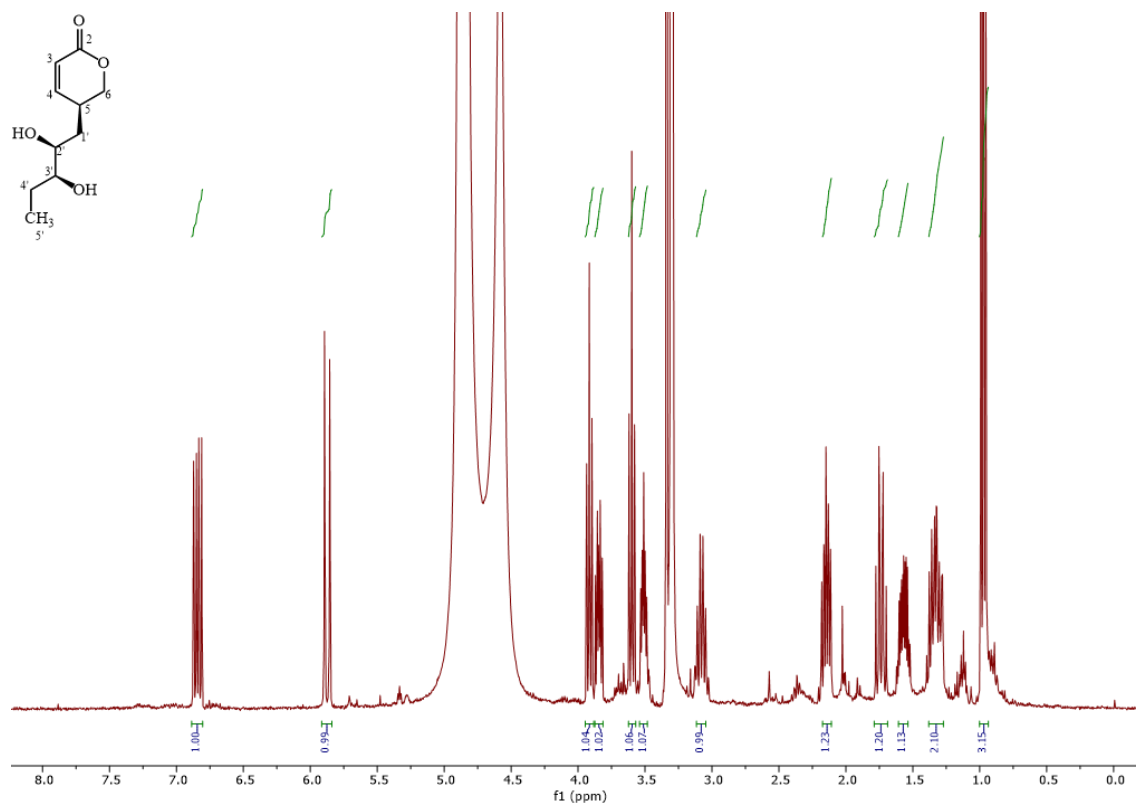
Figure S 107 ^{1}H NMR spectrum of compound **4.2** in methanol-d$_4$, 400 MHz.
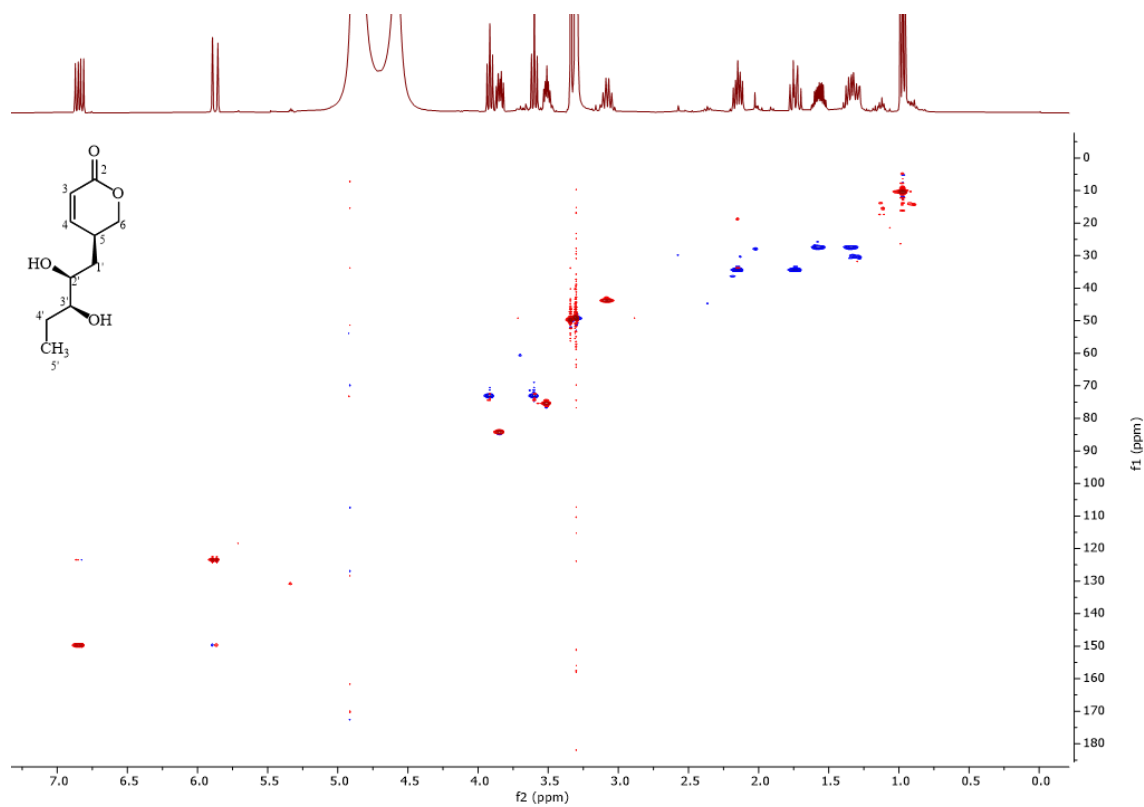
Figure S 108 HSQC spectrum of compound **4.2** in methanol-d$_4$, 400/100 MHz.
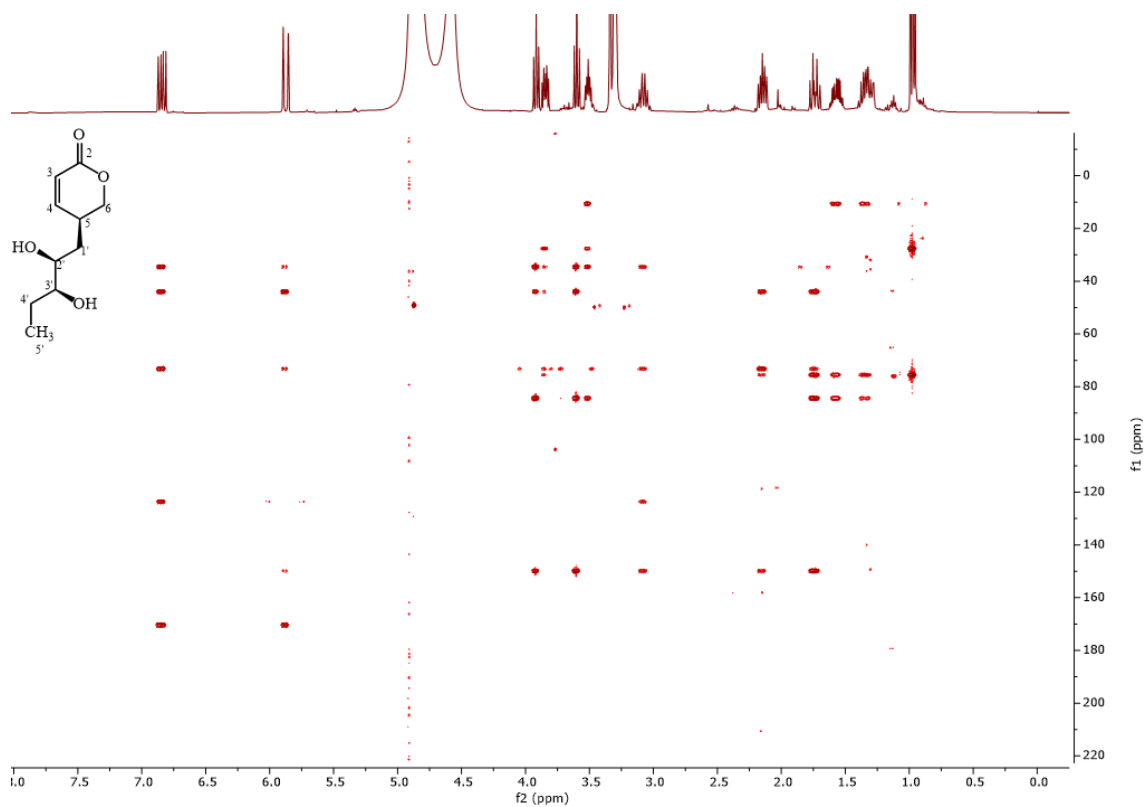
Figure S 109 HMBC spectrum of compound **4.2** in methanol-d₄, 400/100 MHz.
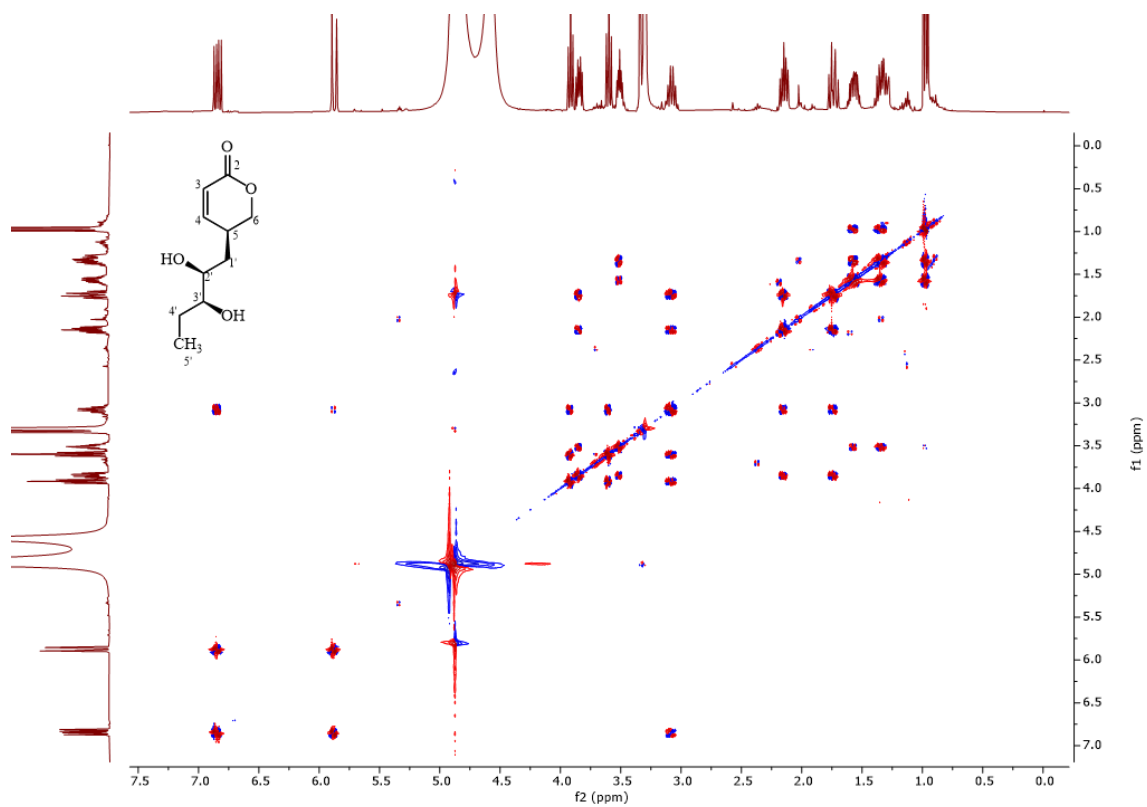
Figure S 110 COSY spectrum of compound **4.2** in methanol-d₄, 400 MHz.
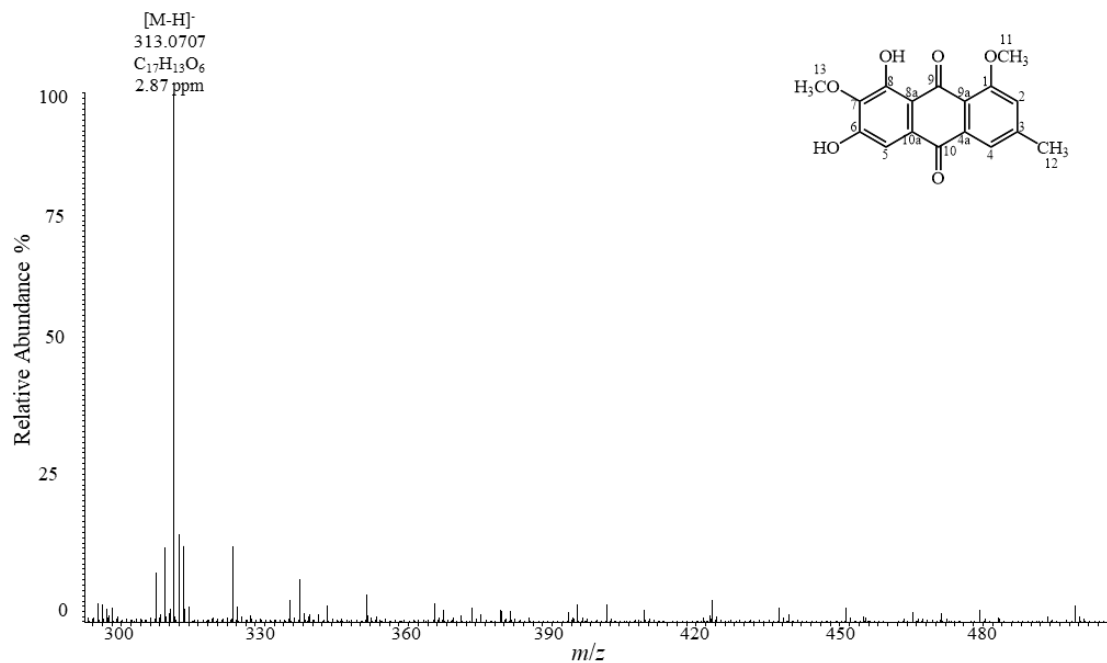
Figure S 111 (-)-ESI-HRMS spectrum of compound **4.3**.
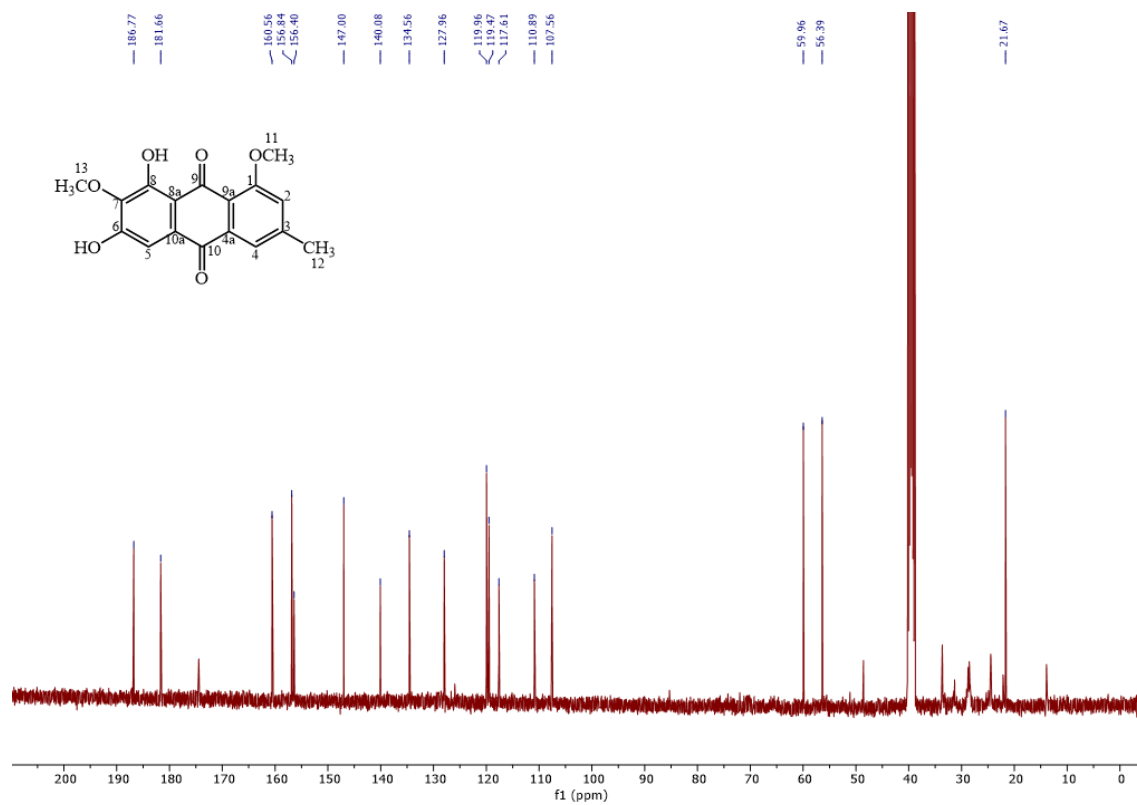
Figure S 112 ^{13}C NMR spectrum of compound **4.3** in DMSO-d$_6$, 125 MHz.
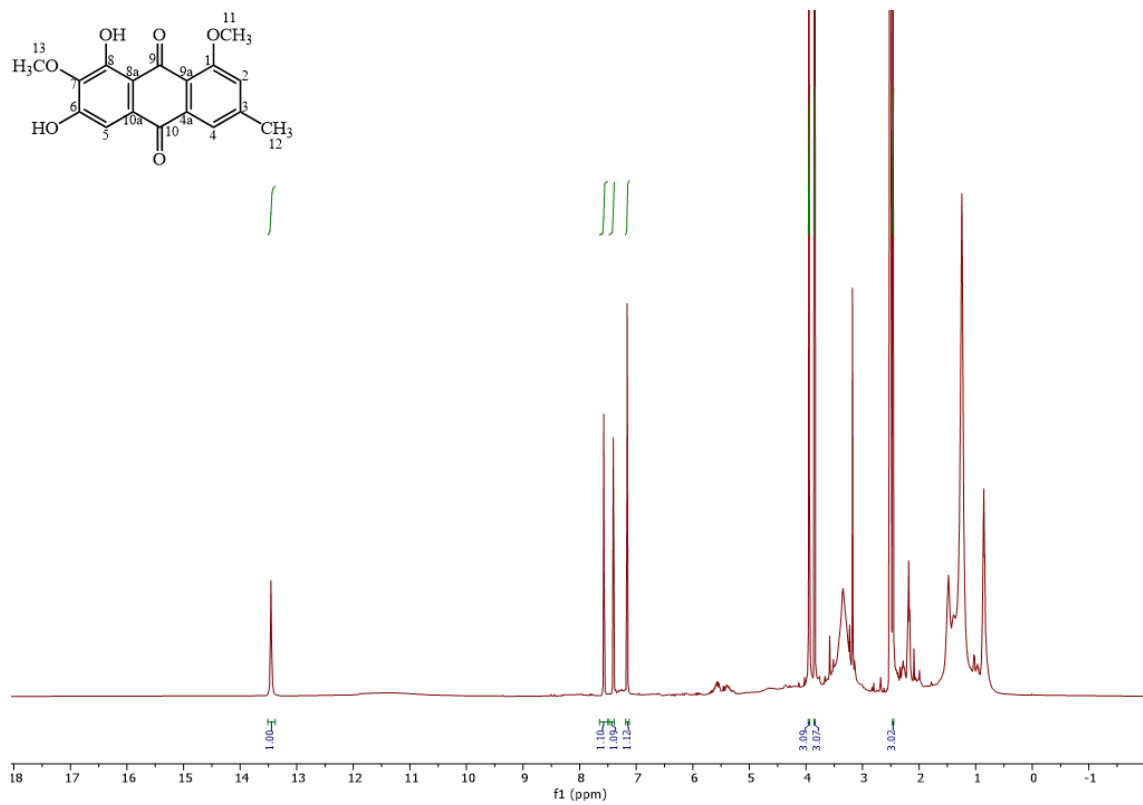
Figure S 113 ^{1}H NMR spectrum of compound **4.3** in DMSO-d$_6$, 500 MHz.

	Idps5871
Empirical formula	$C_{17}H_{14}O_6$
Formula weight/g·mol^{-1}	314.28
Temperature/K	170
Crystal system	monoclinic
Space group	$P2_1/c$
Unit cell dimensions/pm/° a =	757.23(5)
b =	1441.27(10)
c =	1275.47(9)
α =	90
β =	95.509(6)
γ =	90
Volume/nm^3	1,3856(17)
Z	4
Calculated density/g·cm^{-3}	1.507
Absorption coefficient m/mm^{-1}	0.115
Crystal size/mm^3	0.36x0.09x0.08
Ө range for data collection/°	4.726 – 51.998
Reflections collected	6957
R(int)	0.0469
Data/restraints/parameters	2708/0/213
Goodness-of-fit on F^2	1.017
R$_1$ (I>2s(I))	0.0559
wR$_2$ (all data)	0.1630
CCDC	2348292

Figure S 114 Crystal data and structure refinement for idps5871.
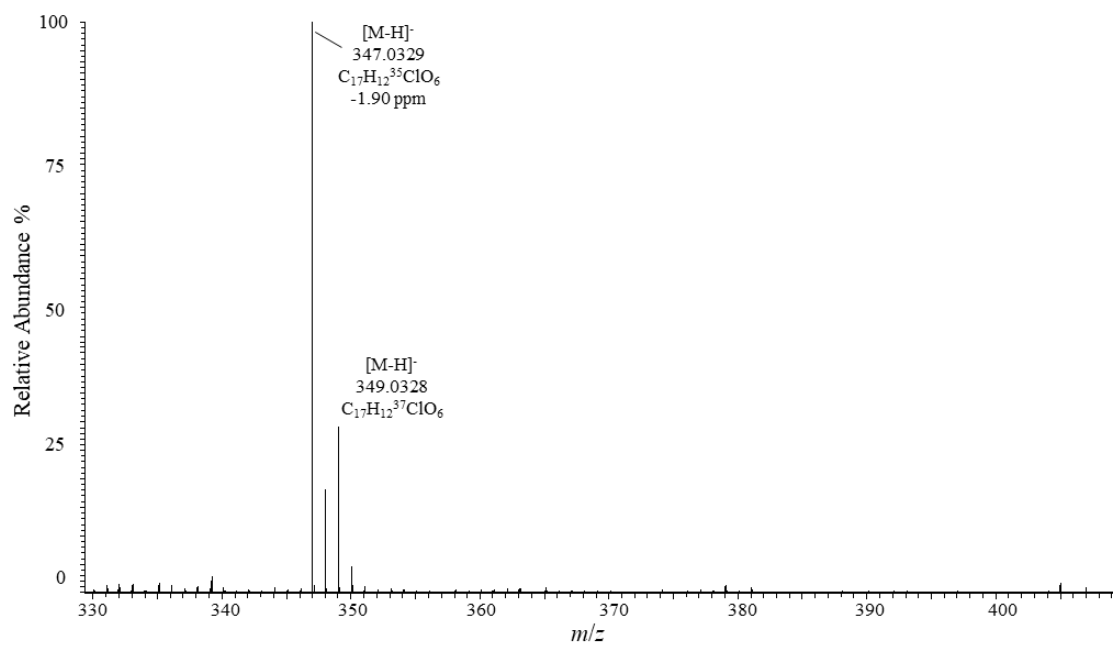
Figure S 115 (-)-ESI-HRMS spectrum of compound **4.4**
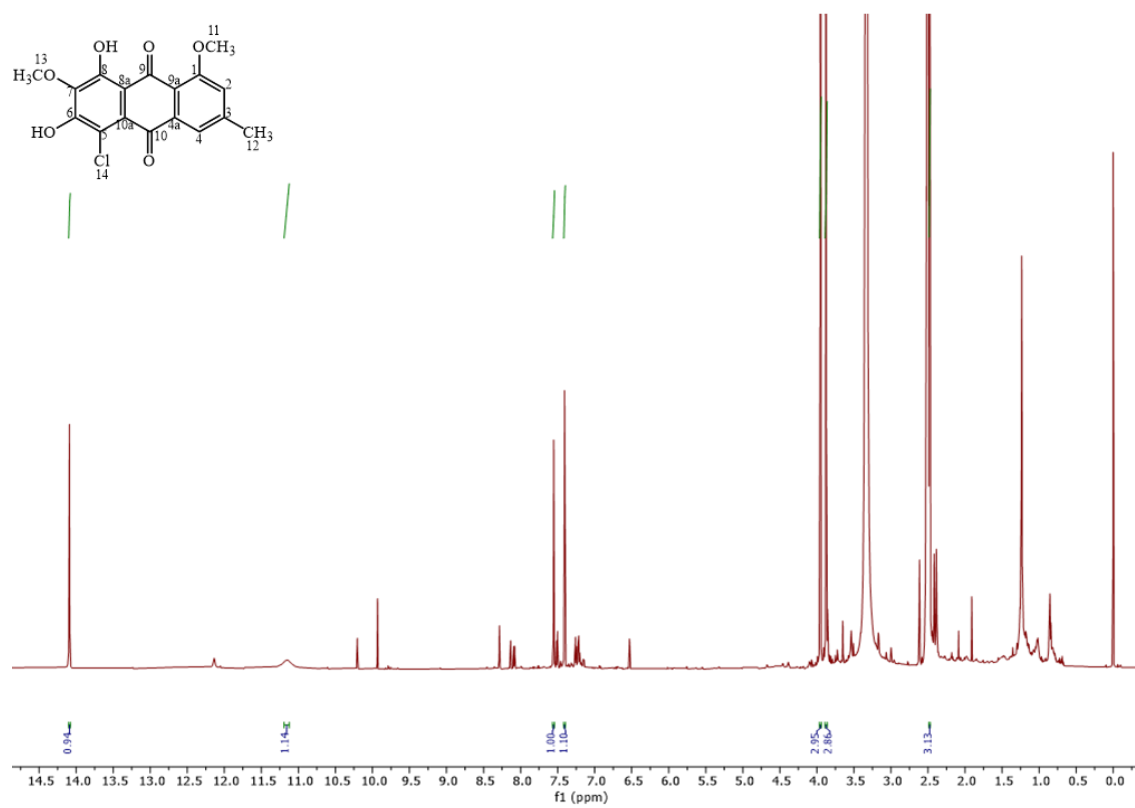
Figure S 116 ^{1}H NMR spectrum of compound **4.4** in DMSO-d$_6$, 500 MHz.
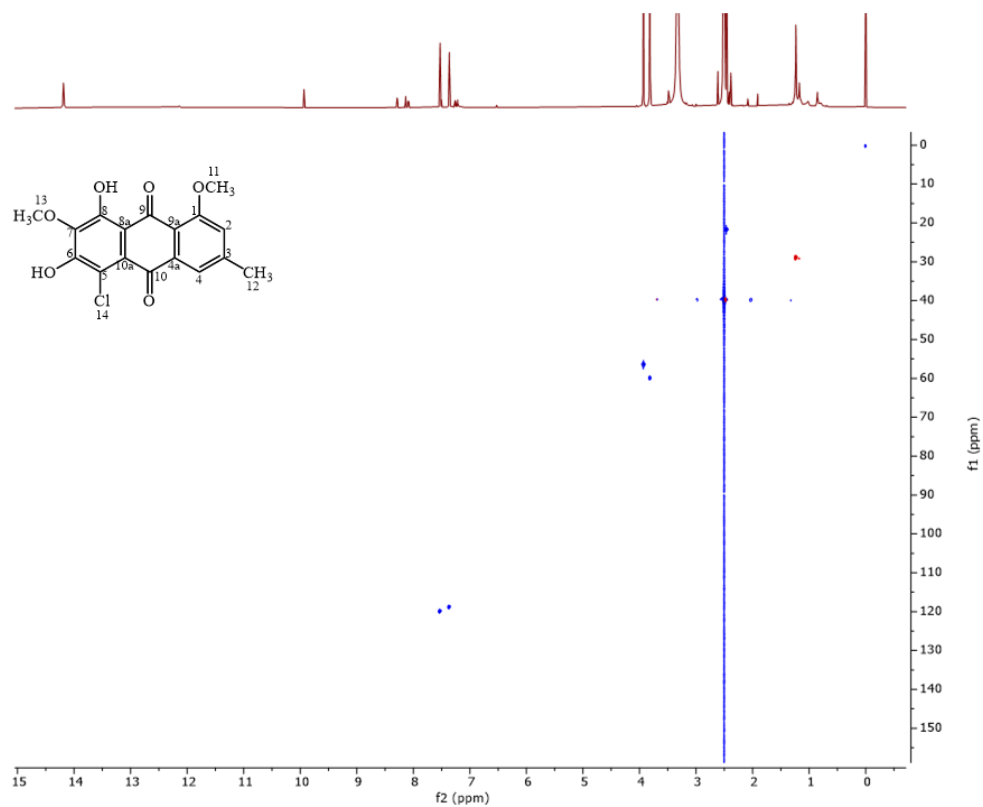
Figure S 117 HSQC spectrum of compound **4.4** in DMSO-d$_6$, 500/125 MHz.
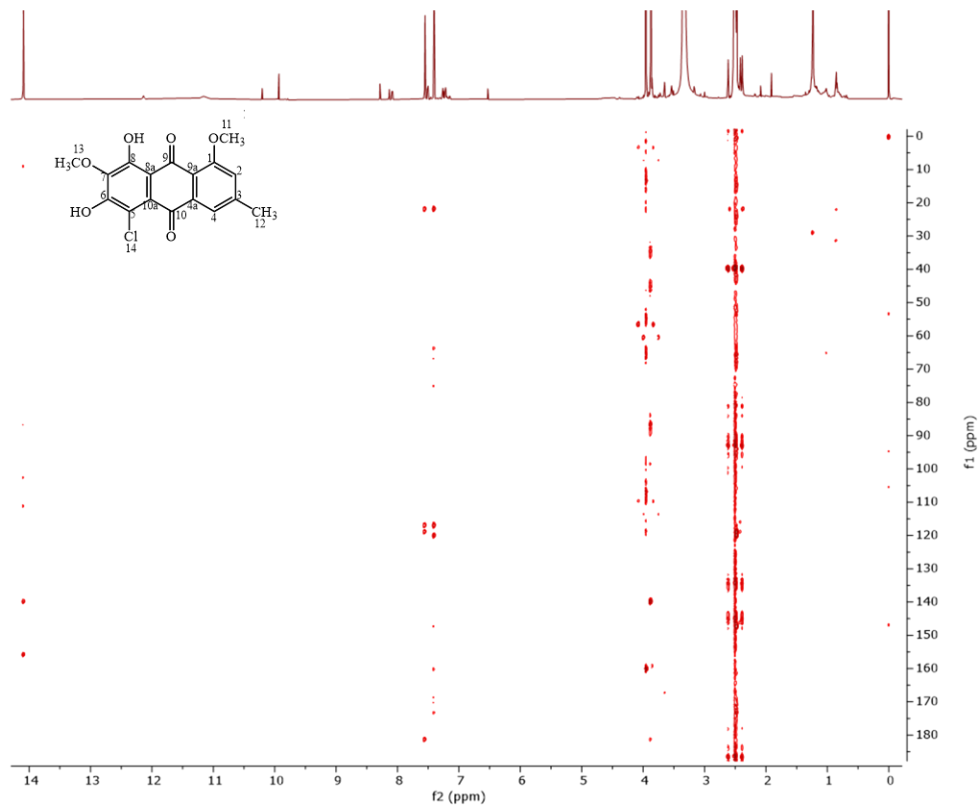
Figure S 118 HMBC spectrum of compound **4.4** in DMSO-d$_6$, 500/125 MHz.

183

	idps6481
Empirical formula	$C_{19}H_{19} \cdot ClO_7S$
Formula weight/g·mol^{-1}	426.85
Temperature/K	170
Crystal system	triclinic
Space group	P-1
Unit cell dimensions/pm/° a =	727.20(5)
b =	1065.57(7)
c =	1259.71(8)
α =	84.763(5)
β =	74.861(5)
γ =	75.973(5)
Volume/nm^3	0,913(11)
Z	2
Calculated density/g·cm^{-3}	1.551
Absorption coefficient m/mm^{-1}	0.365
Crystal size/mm^3	0.49x0.217x0.03
Ө range for data collection/°	3.35 – 58.524
Reflections collected	9946
R(int)	0.0393
Data/restraints/parameters	4897/0/260
Goodness-of-fit on F^2	1.021
R$_1$ (I>2s(I))	0.0377
wR$_2$ (all data)	0.1085
CCDC	2348291

Figure S 119 Crystal data and structure refinement for idps6481.
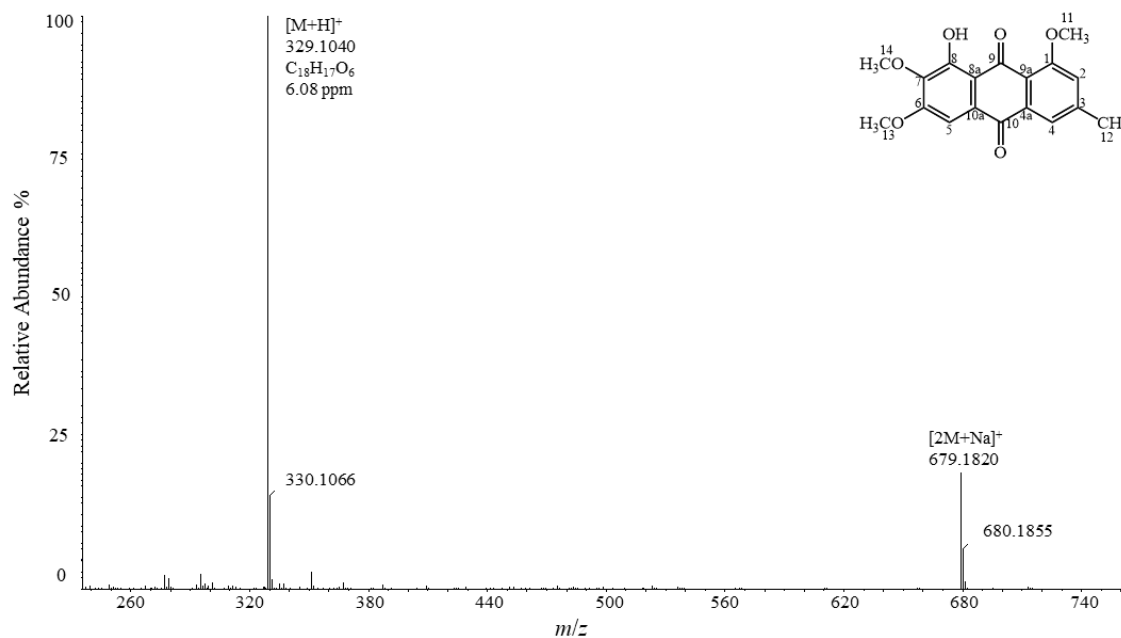
Figure S 120 (+)-ESI-HRMS spectrum of compound **4.5**.
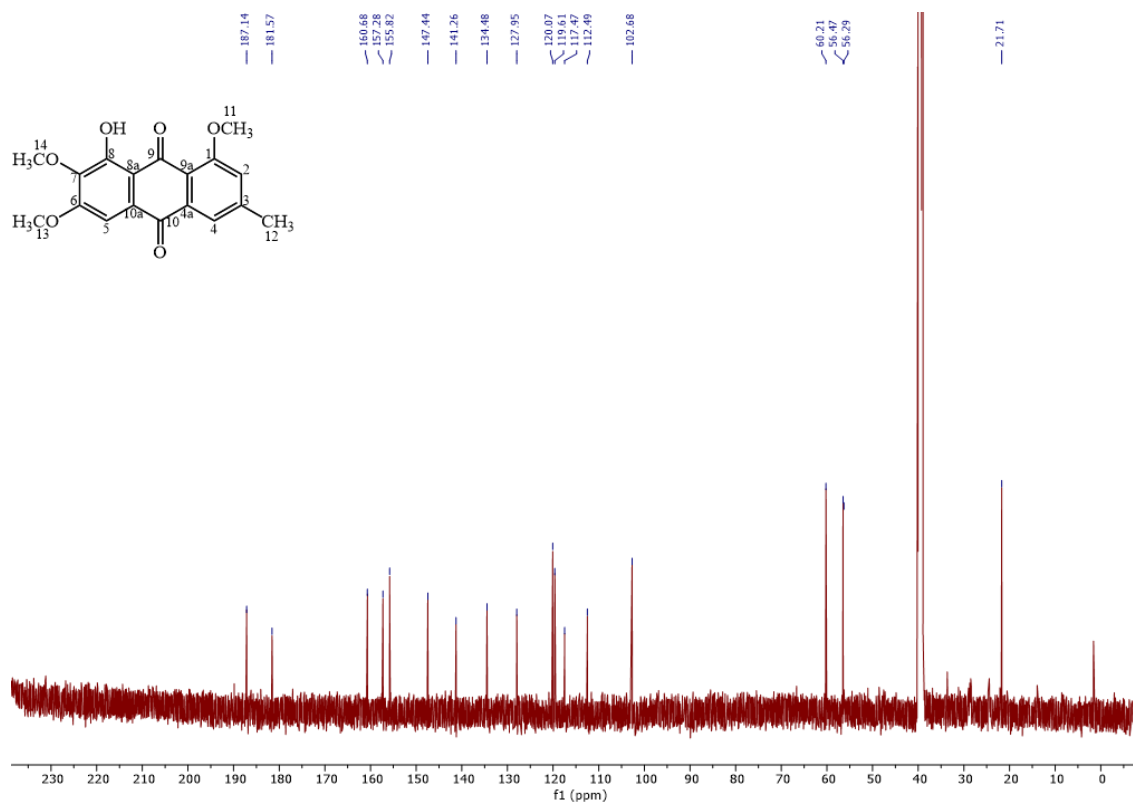
Figure S 121 ^{13}C NMR spectrum of compound **4.5** in DMSO-d$_6$, 125 MHz.
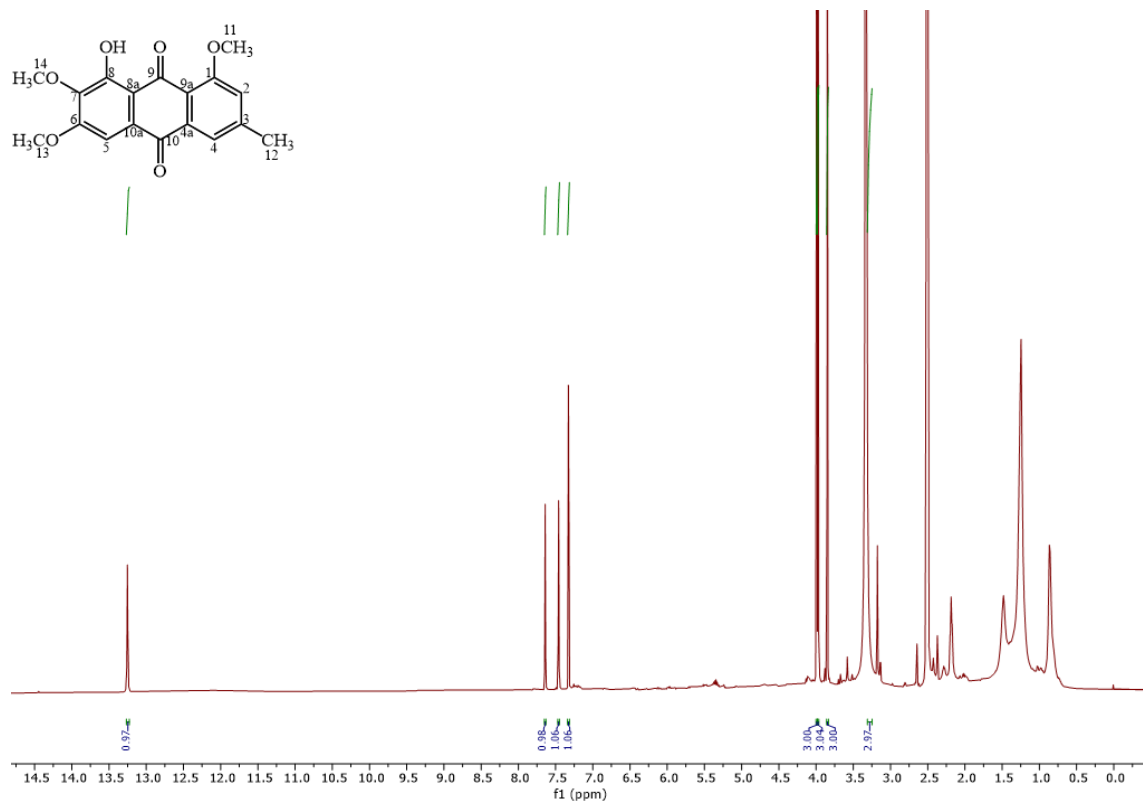
Figure S 122 ^{1}H NMR spectrum of compound **4.5** in DMSO-d$_6$, 500 MHz.
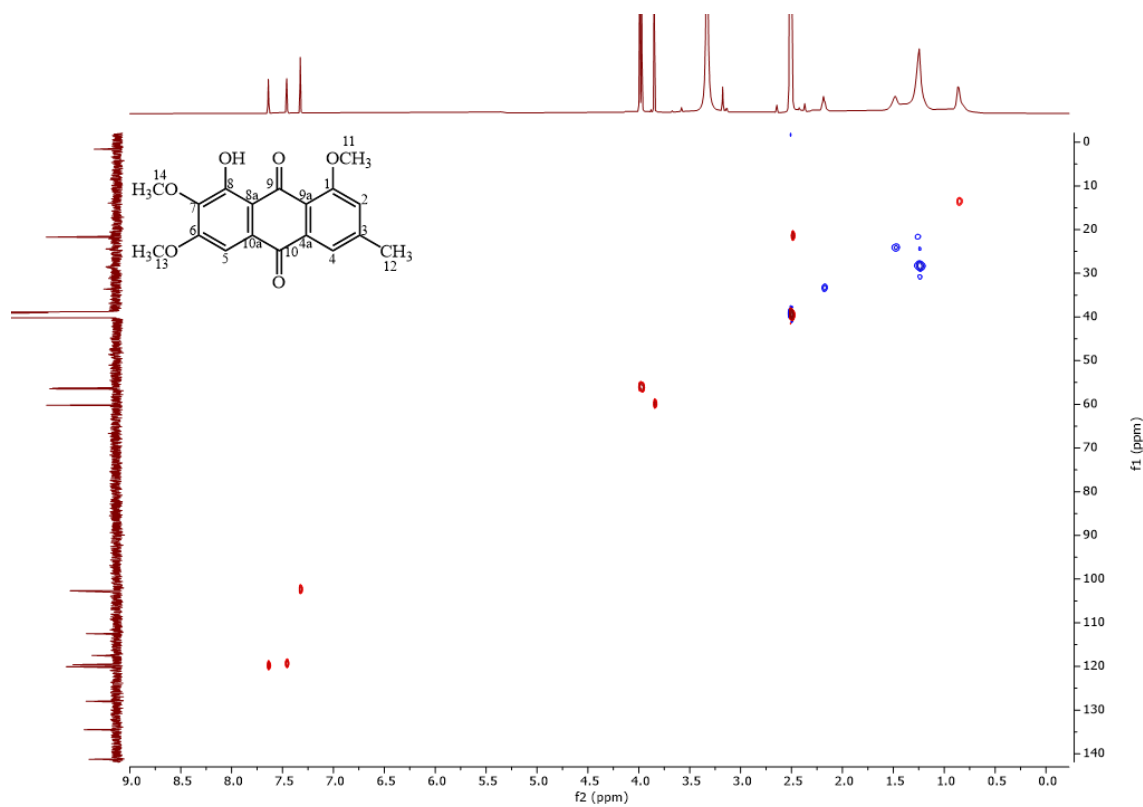
Figure S 123 HSQC spectrum of compound **4.5** in DMSO-d$_6$, 500/125 MHz.
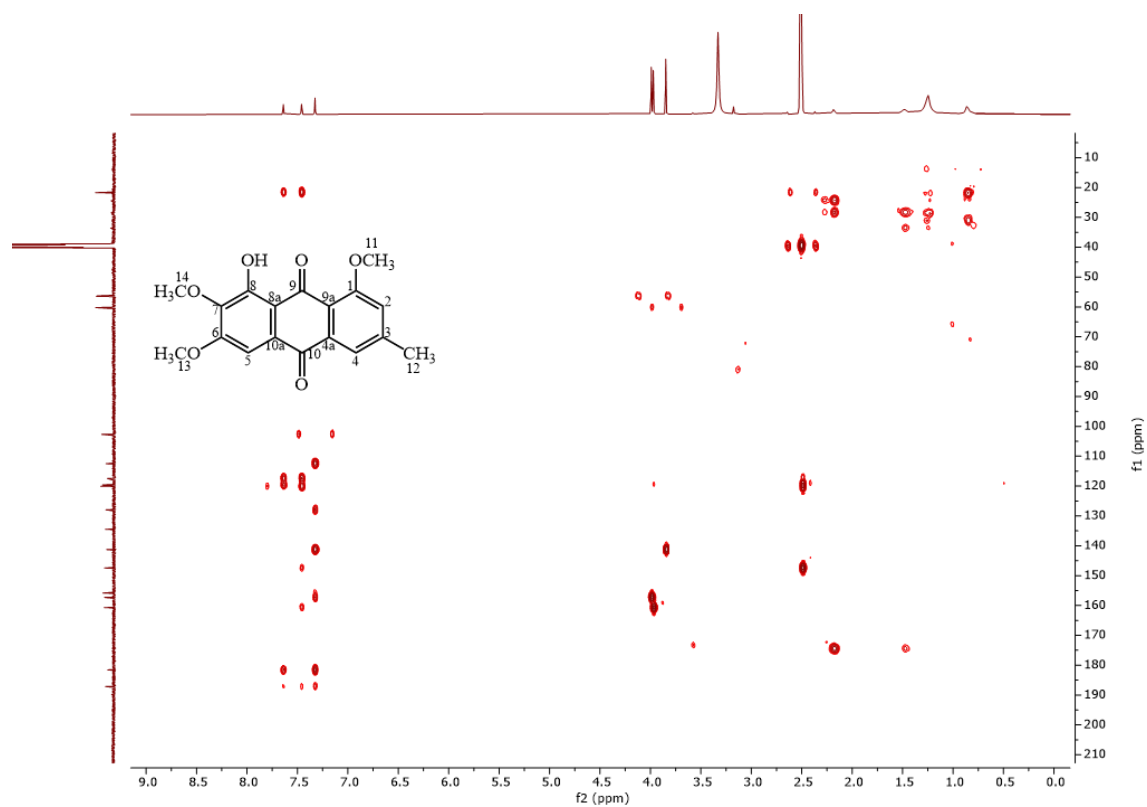
Figure S 124 HMBC spectrum of compound **4.5** in DMSO-d6, 500/125 MHz.
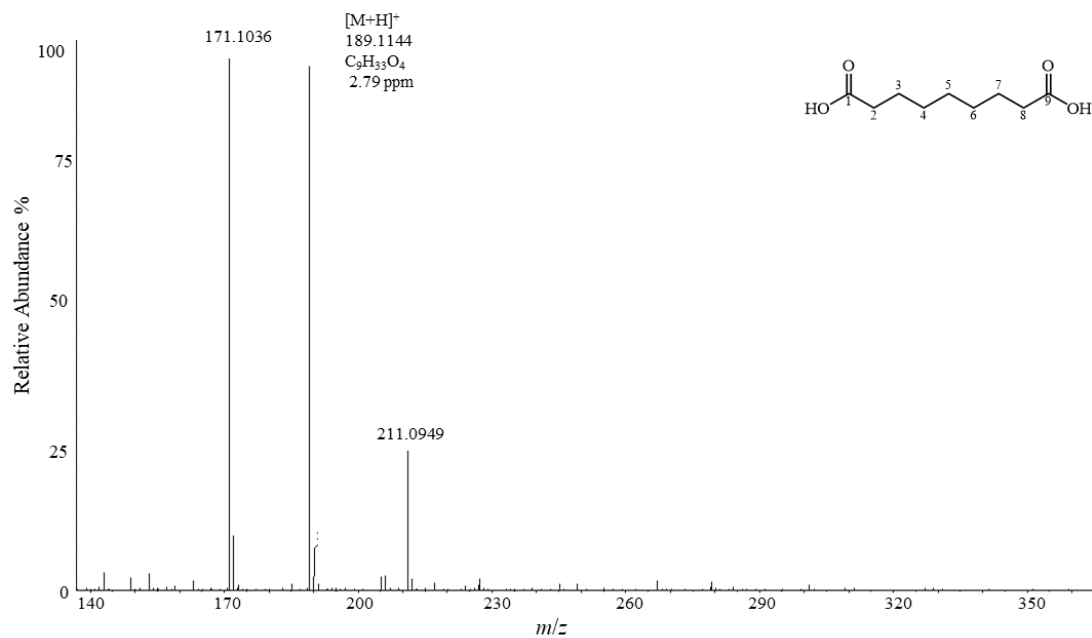
Figure S 125 (+)-ESI-HRMS spectrum of compound **4.6**.
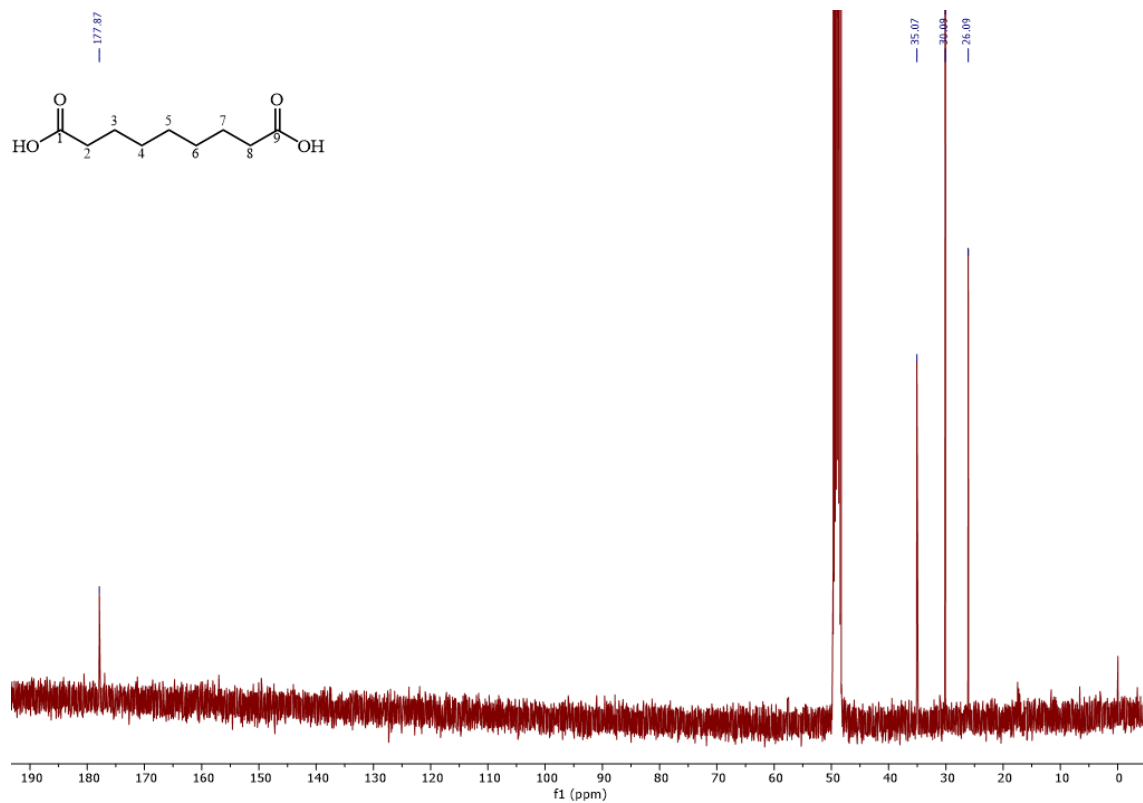
Figure S 126 ^{13}C NMR spectrum of compound **4.6** in methanol-d$_4$, 100 MHz.
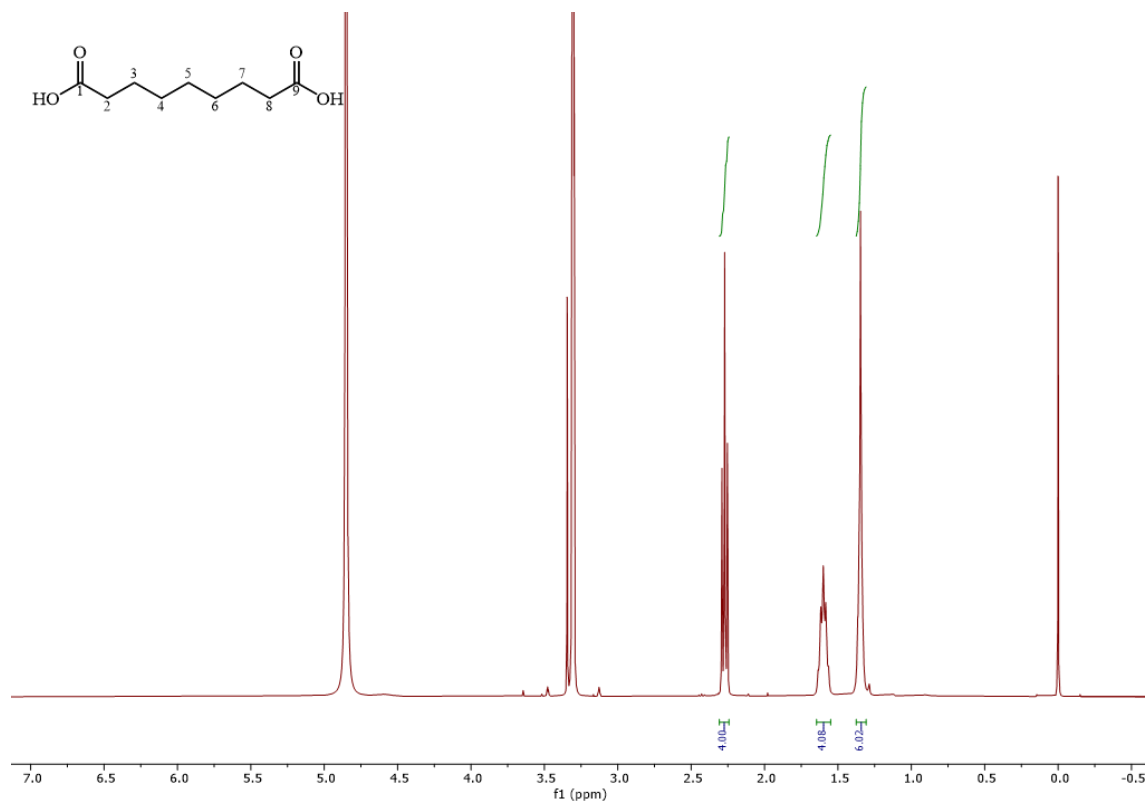
Figure S 127 ^{1}H NMR spectrum of compound **4.6** in methanol-d$_4$, 400 MHz.

Figure S 128 HSQC spectrum of compound **4.6** in methanol-d4, 400/100 MHz.

Figure S 129 HMBC spectrum of compound **4.6** in methanol-d4, 100 MHz.
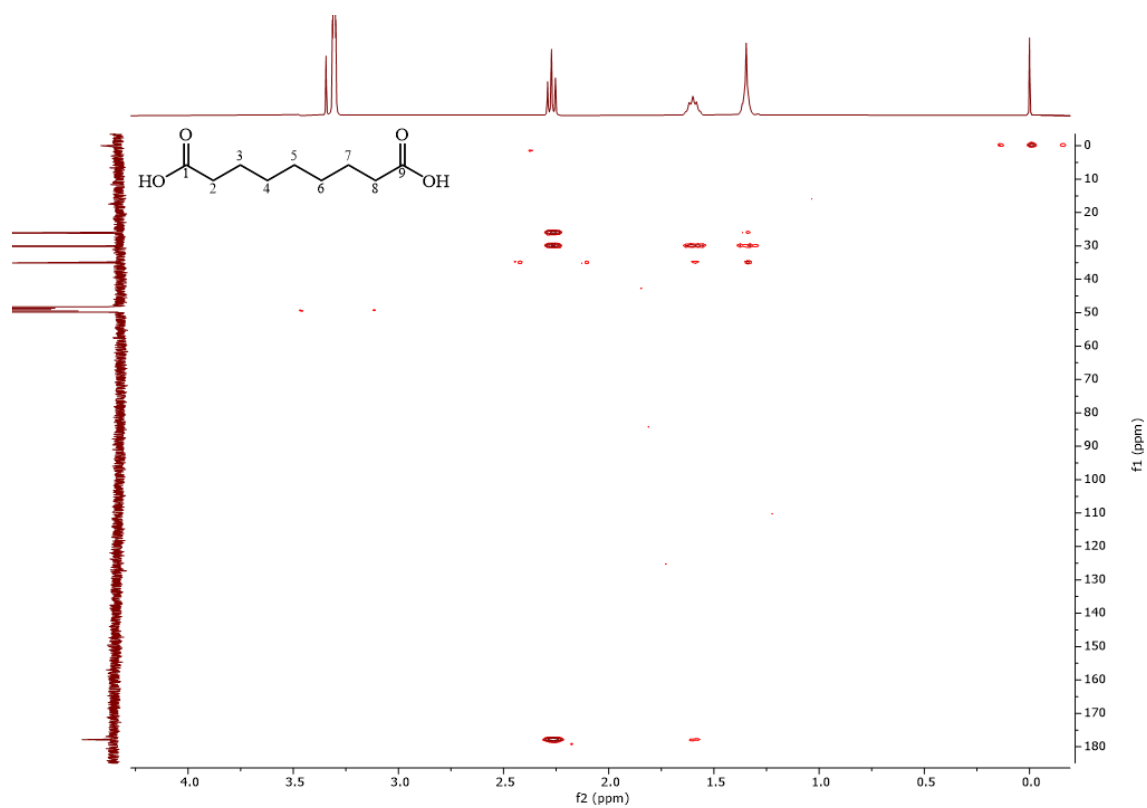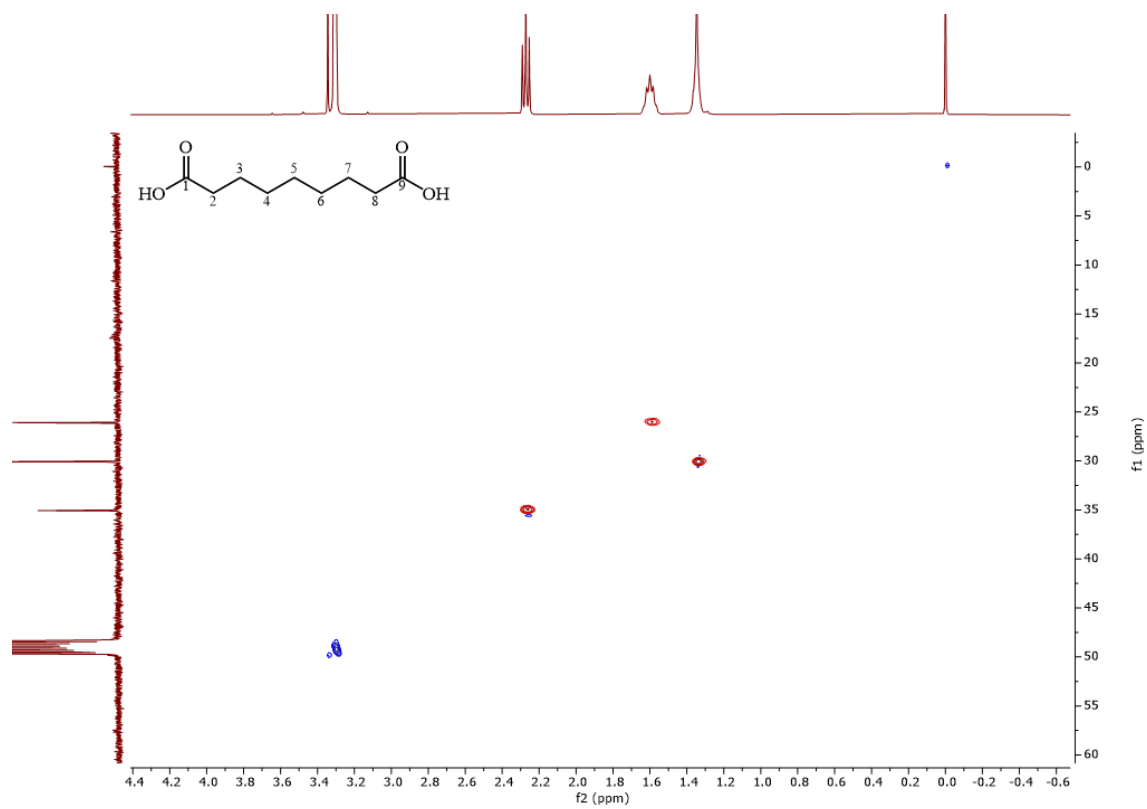
Figure S 130 (+)-ESI-HRMS spectrum of compound **4.7**.

Figure S 131 ^{1}H NMR spectrum of compound **4.7** in methanol-d$_4$, 500 MHz.
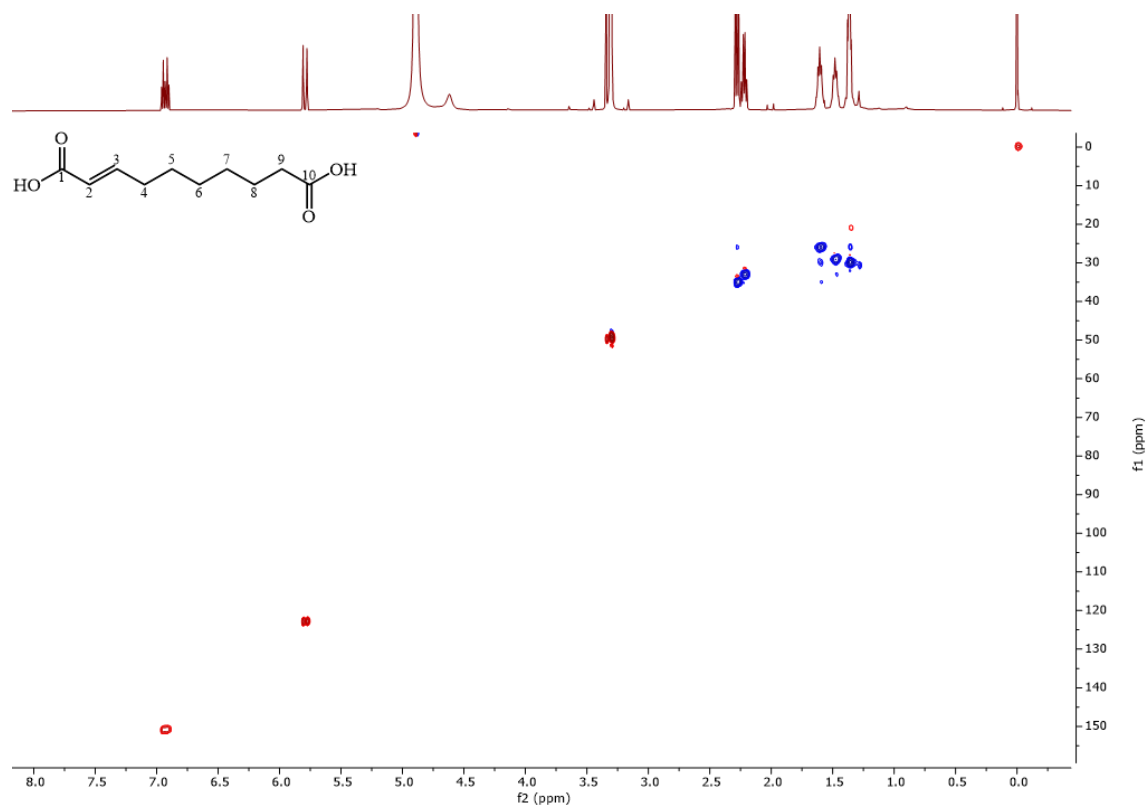
Figure S 132 HSQC spectrum of compound **4.7** in methanol-d4, 500/125 MHz.
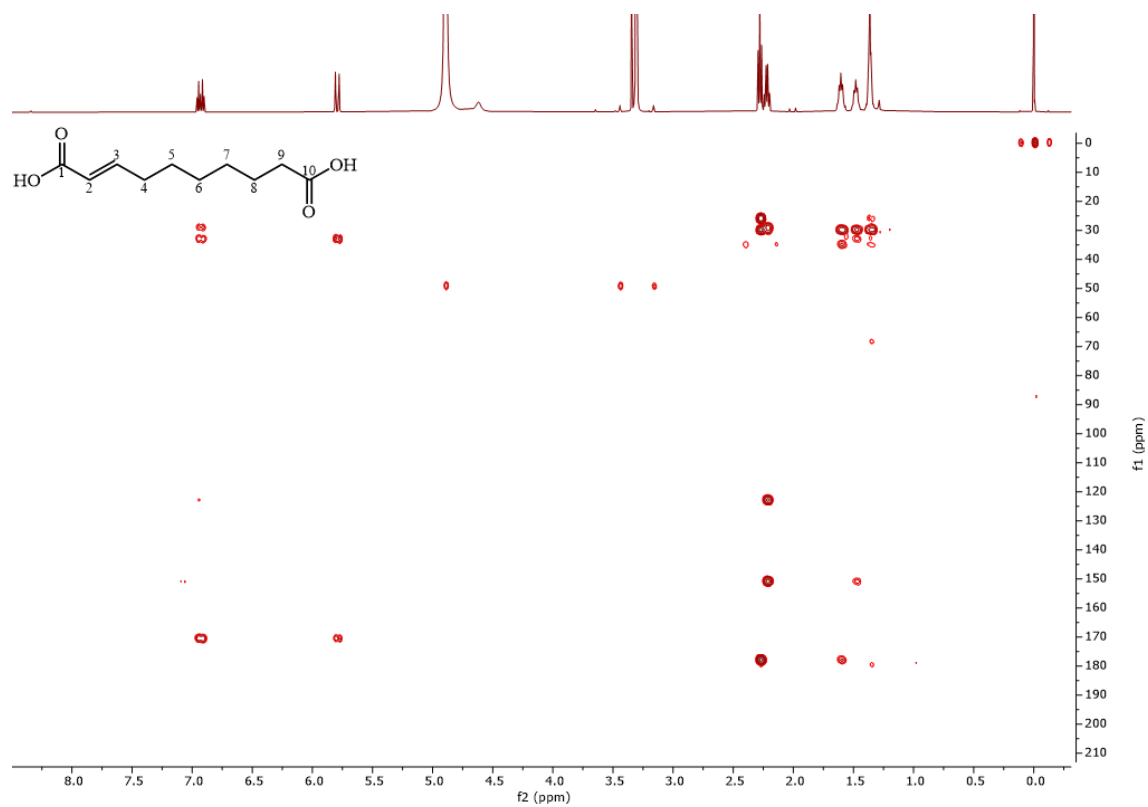
Figure S 133 HMBC spectrum of compound **4.7** in methanol-d4, 500/125 MHz.

Figure S 134 COSY spectrum of compound **4.7** in methanol-d$_4$, 500 MHz.

$[M+H]^+$
169.0976
$C_8H_{13}O_2N_2$
2.83 ppm
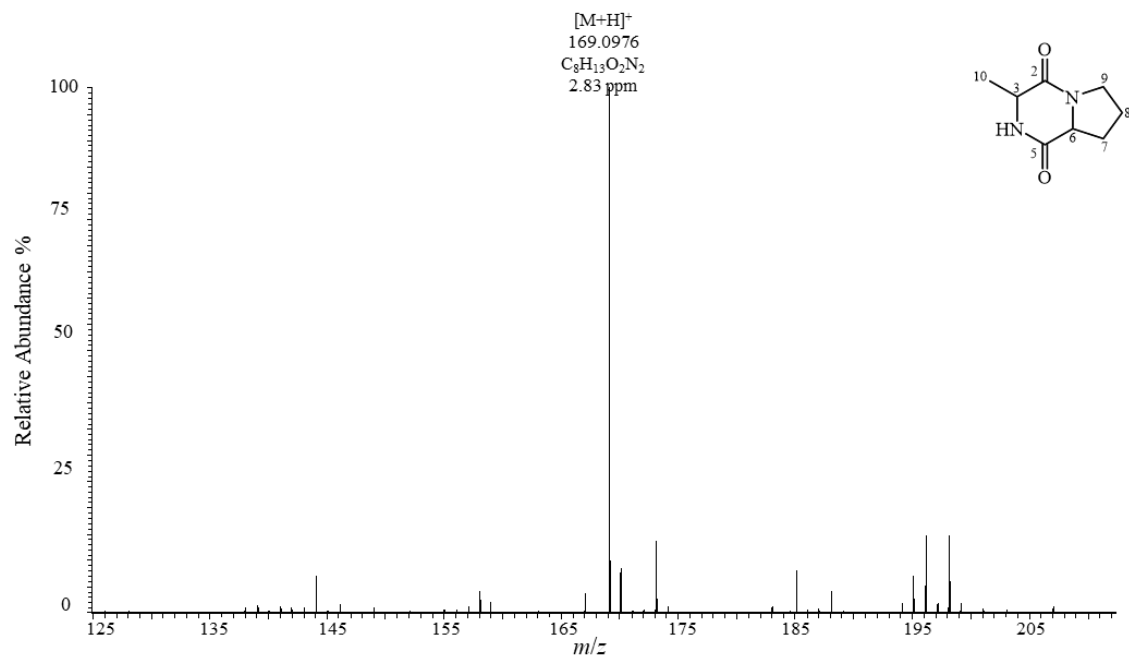
Figure S 135 (+)-ESI-HRMS spectrum of compound **4.8**.
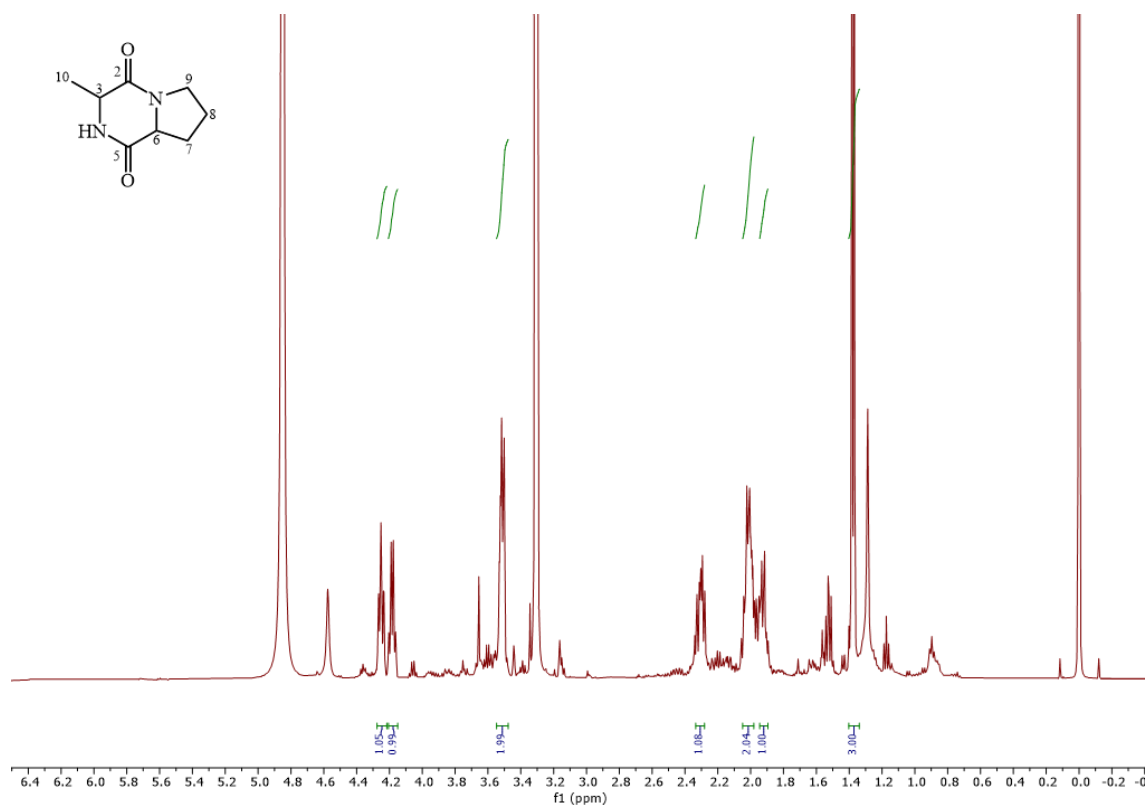
Figure S 136 ^{1}H NMR spectrum of compound **4.8** in methanol-d$_4$, 500 MHz.
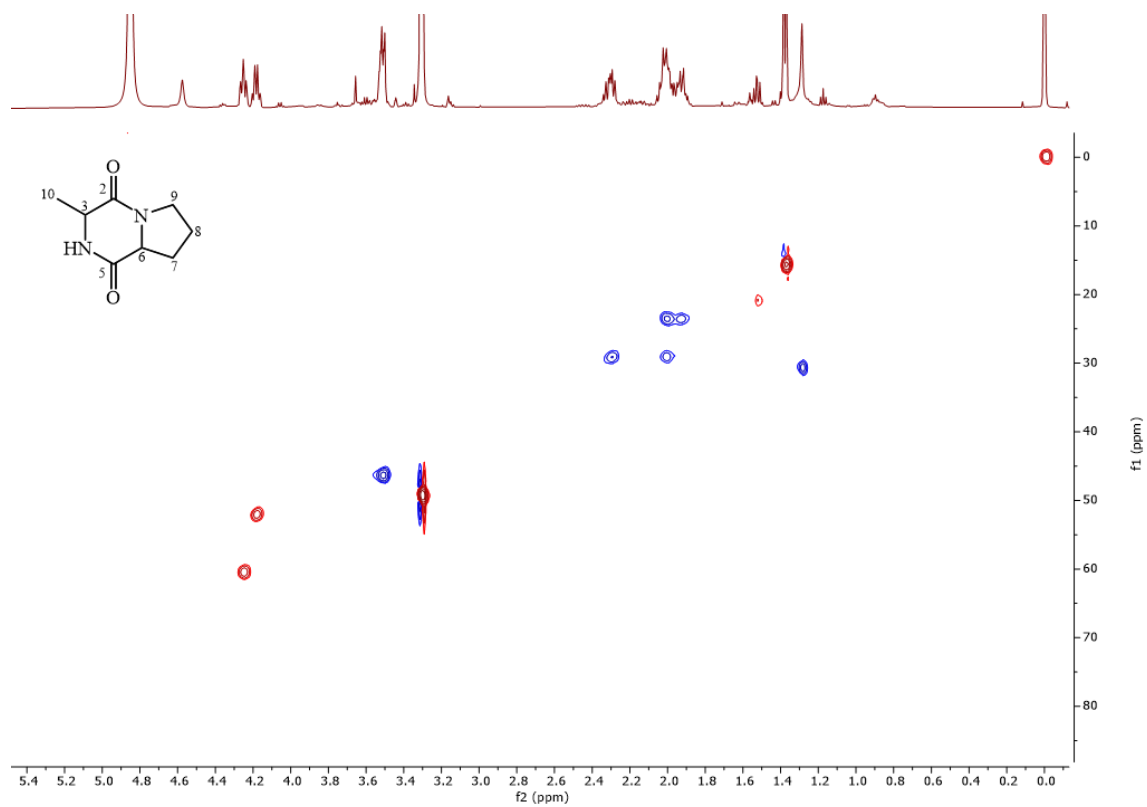
Figure S 137 HSQC spectrum of compound **4.8** in methanol-d$_4$, 500/125 MHz.
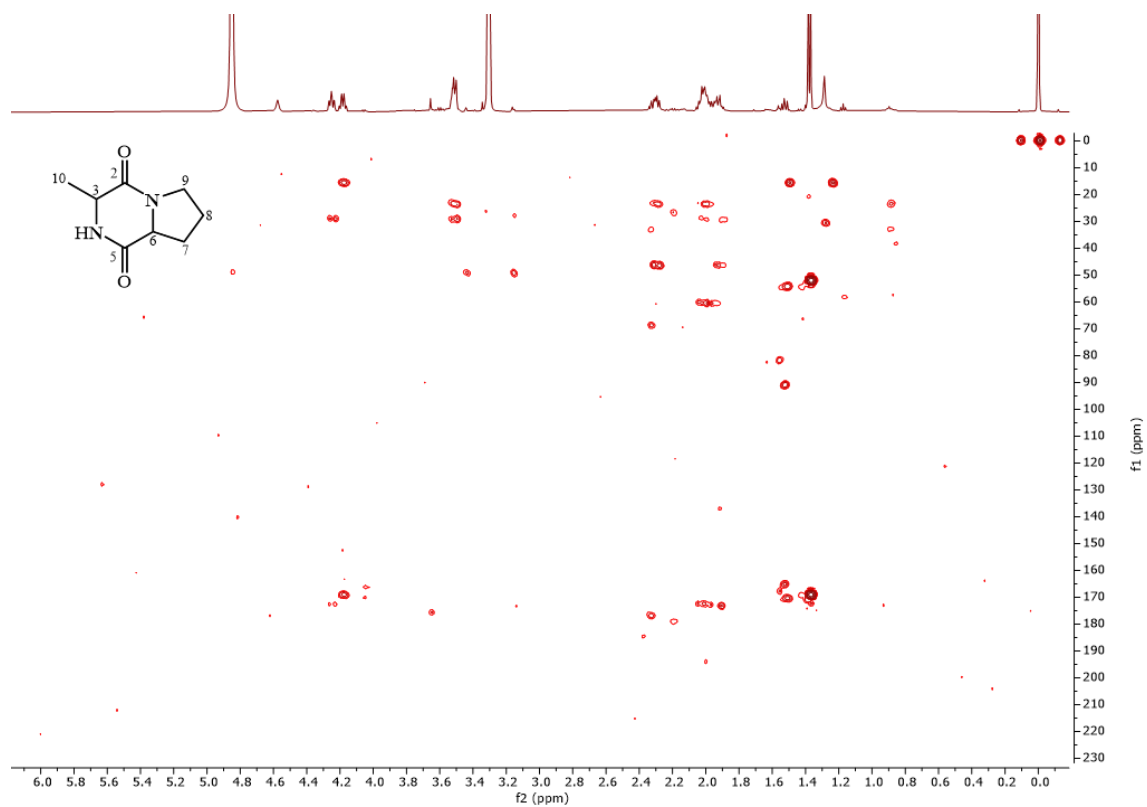
Figure S 138 HMBC spectrum of compound **4.8** in methanol-d4, 500/125 MHz.
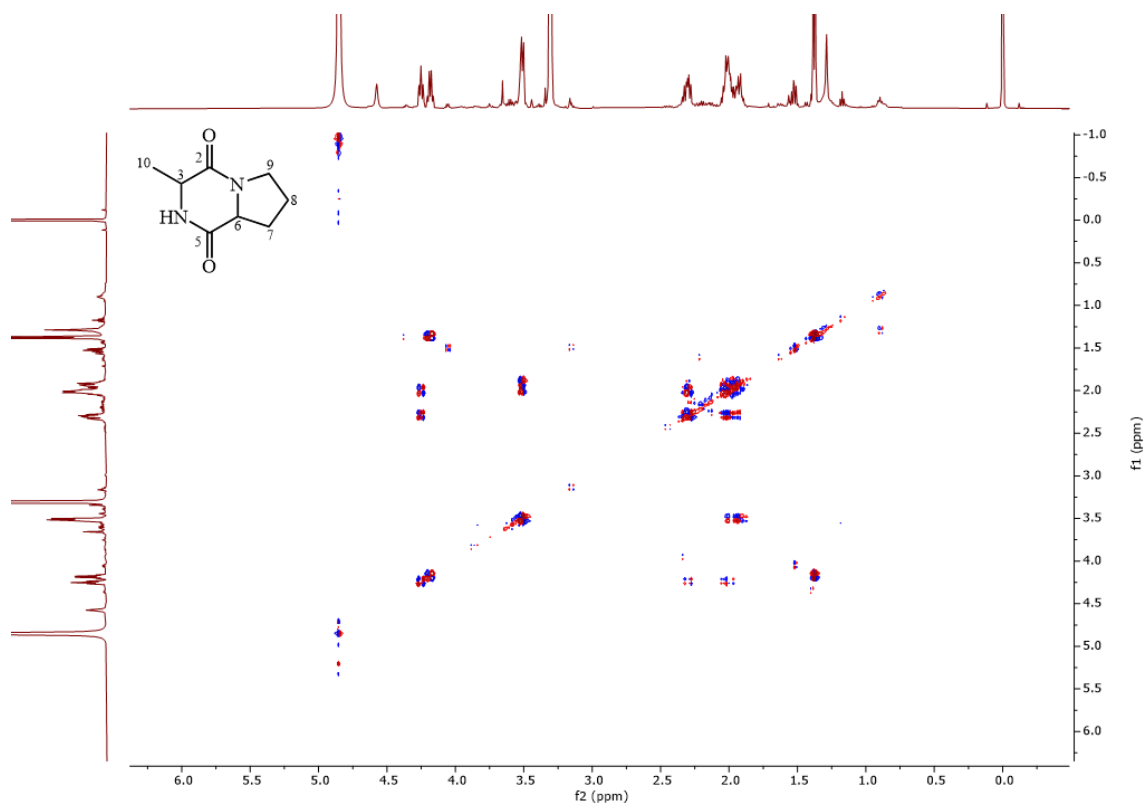
Figure S 139 COSY spectrum of compound **4.8** in methanol-d4, 500 MHz.
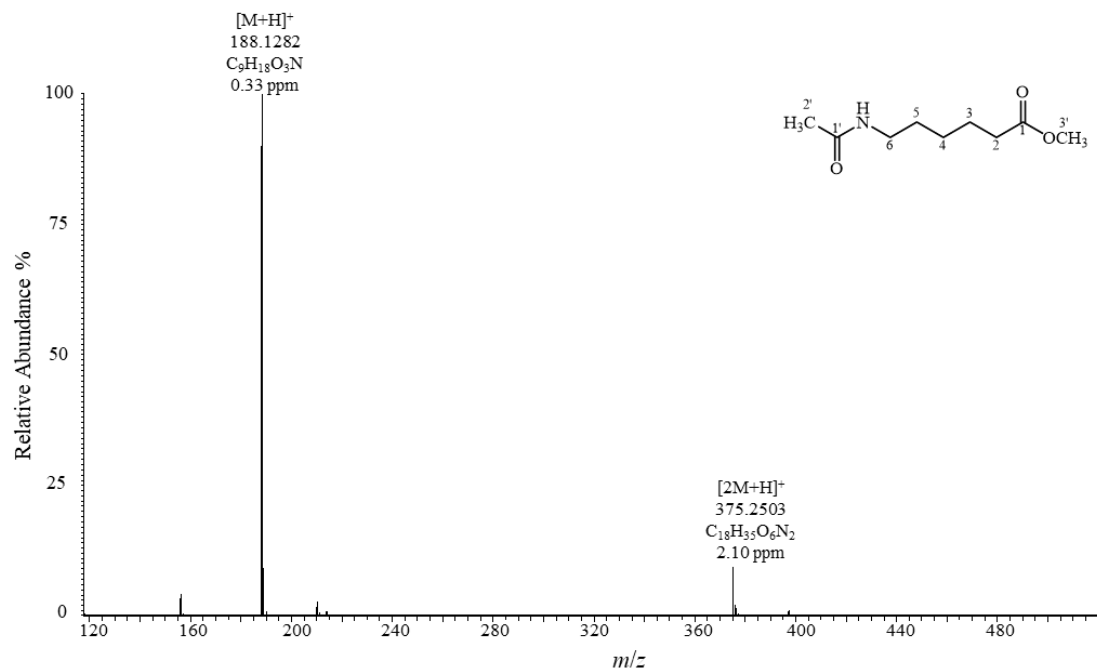
Figure S 140 (+)-ESI-HRMS spectrum of compound **4.9**.
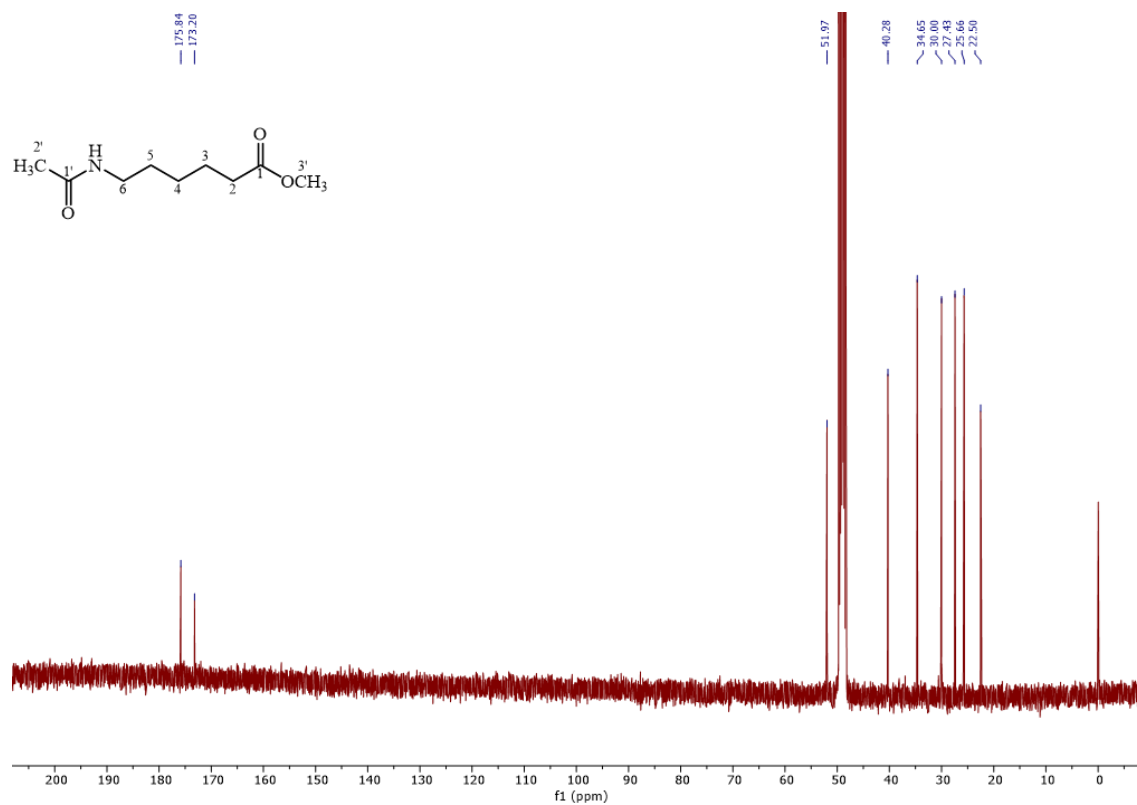
Figure S 141 ^{13}C spectrum of compound **4.9** in methanol-d$_4$, 100 MHz.

Figure S 142 ^{1}H spectrum of compound **4.9** in methanol-d$_4$, 400 MHz.

Figure S 143 HSQC spectrum of compound **4.9** in methanol-d$_4$, 400/100 MHz.
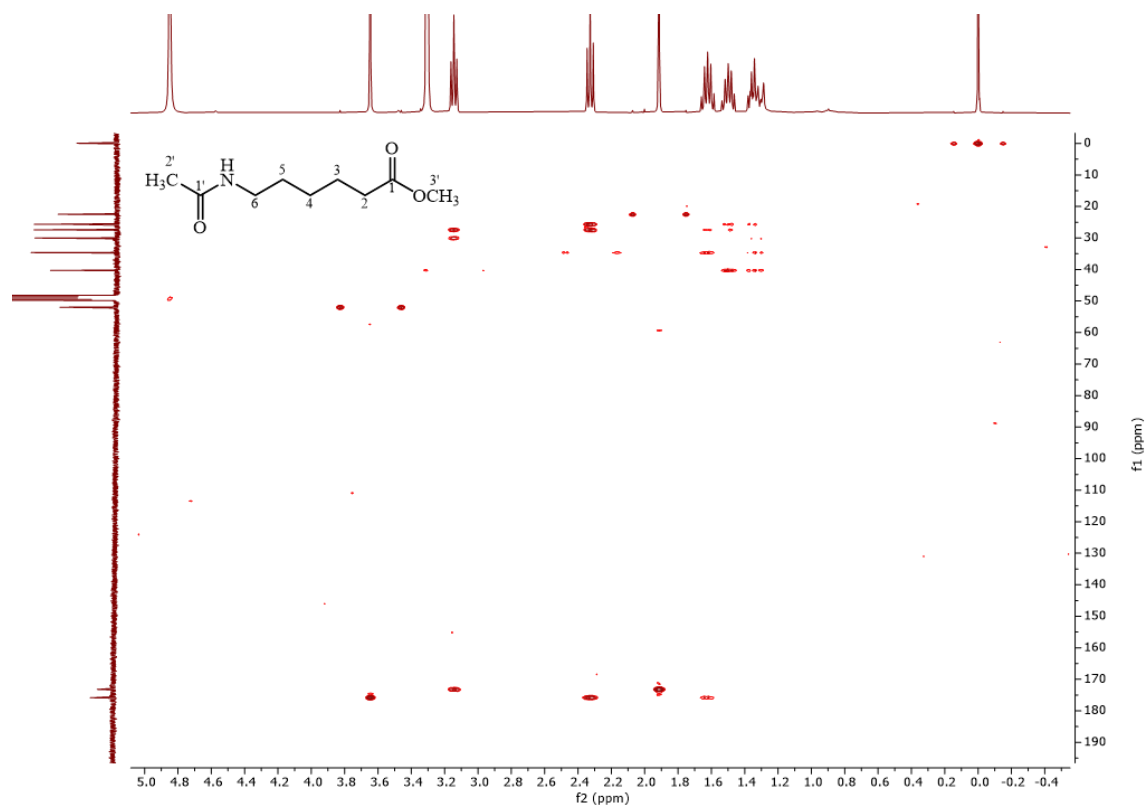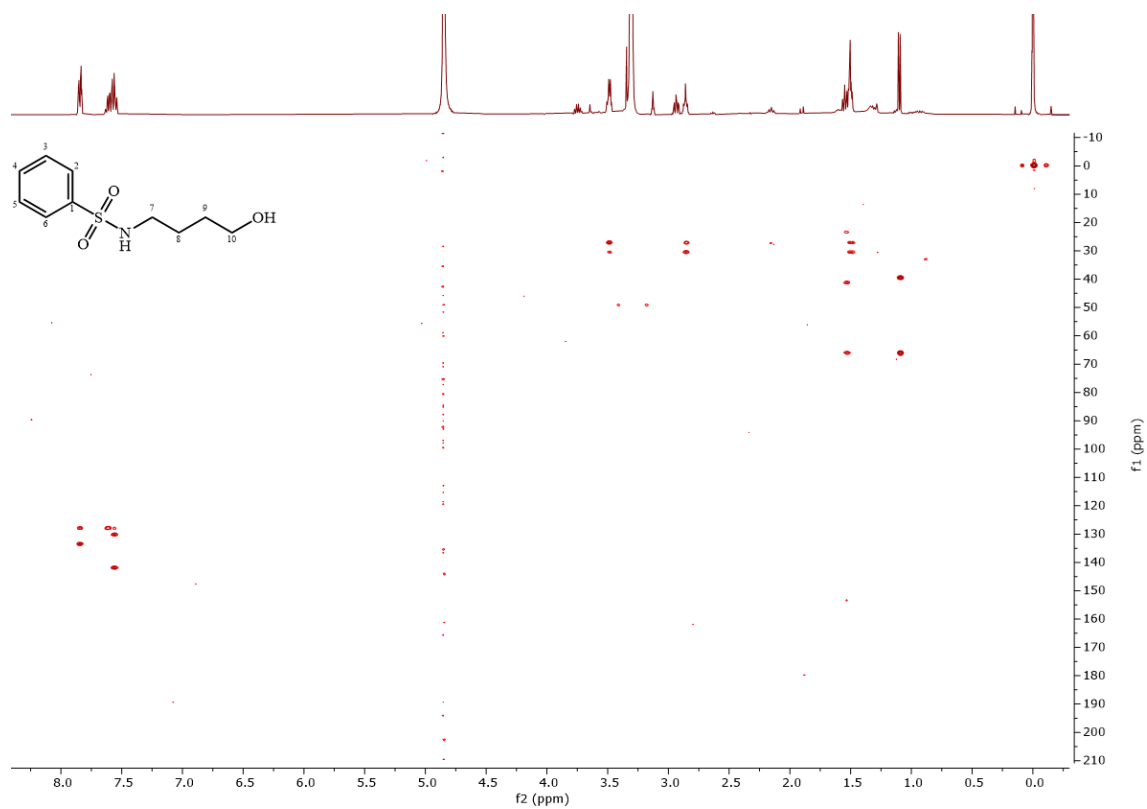
Figure S 144 HMBC spectrum of compound **4.9** in methanol-d4, 400/100 MHz.
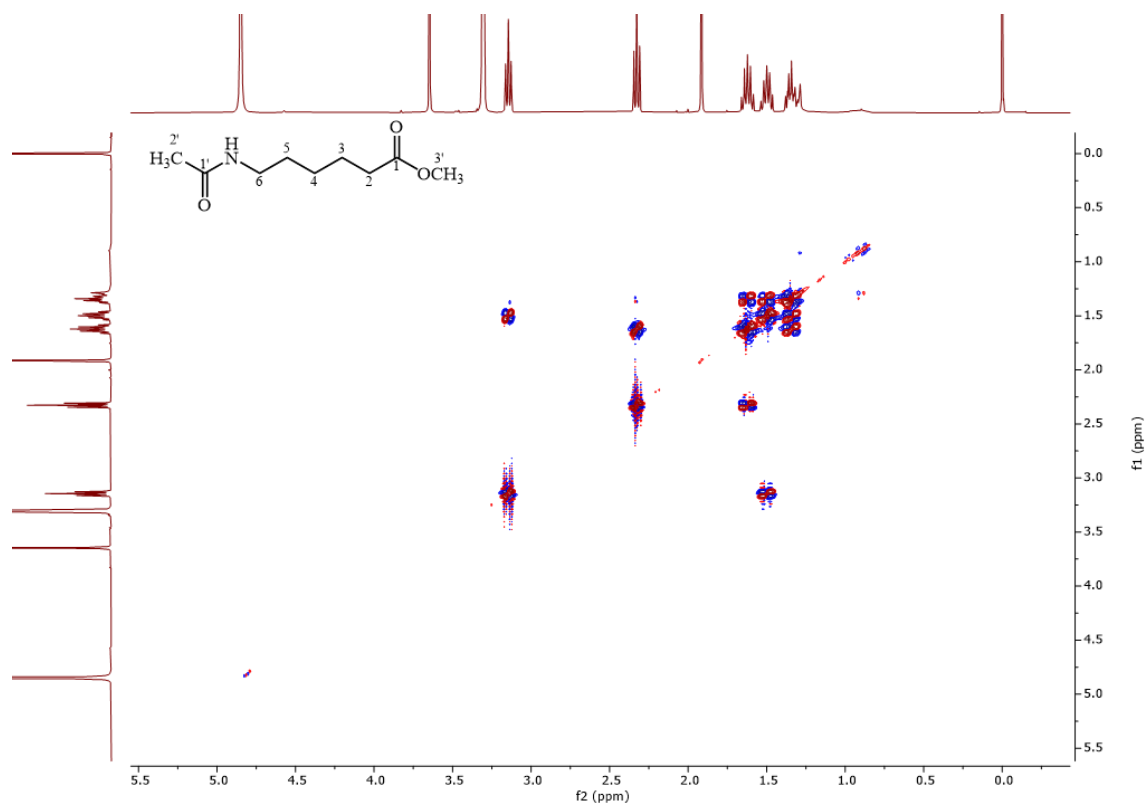
Figure S 145 COSY spectrum of compound **4.9** in methanol-d4, 400 MHz.
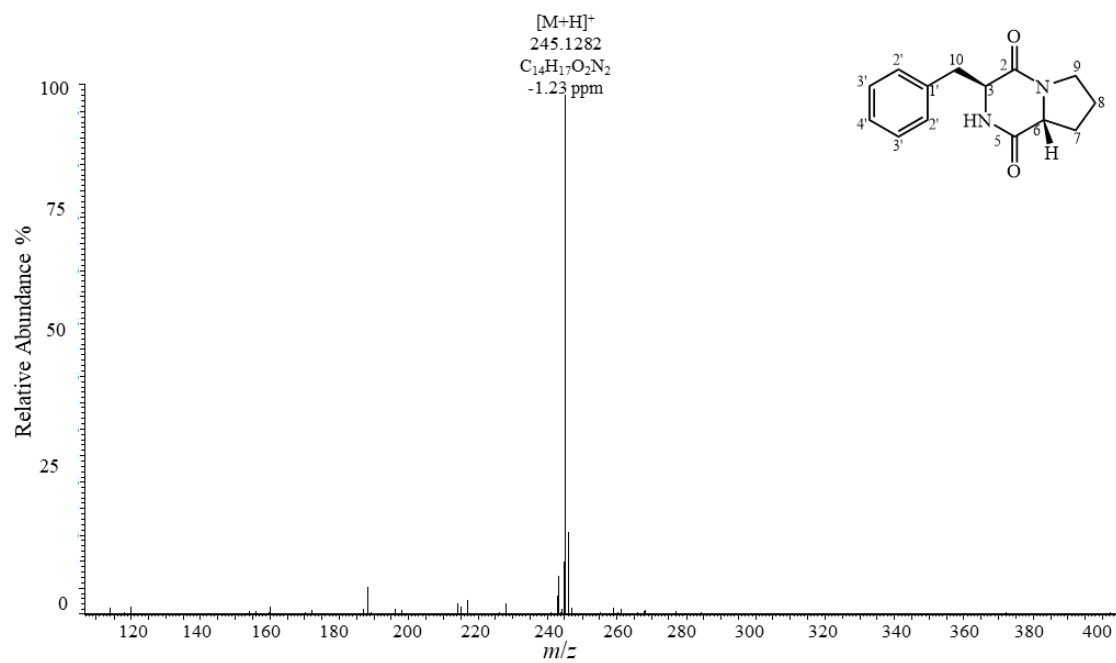
Figure S 146 (+)-ESI-HRMS spectrum of compound **4.10**.

Figure S 147 ^{13}C NMR spectrum of compound **4.10** in methanol-d$_4$, 125 MHz.

Figure S 148 ^{1}H NMR spectrum of compound **4.10** in methanol-d$_4$, 500 MHz.

Figure S 149 HSQC spectrum of compound **4.10** in methanol-d$_4$, 500/125 MHz.

Figure S 150 HMBC spectrum of compound **4.10** in methanol-d$_4$, 500/125 MHz.

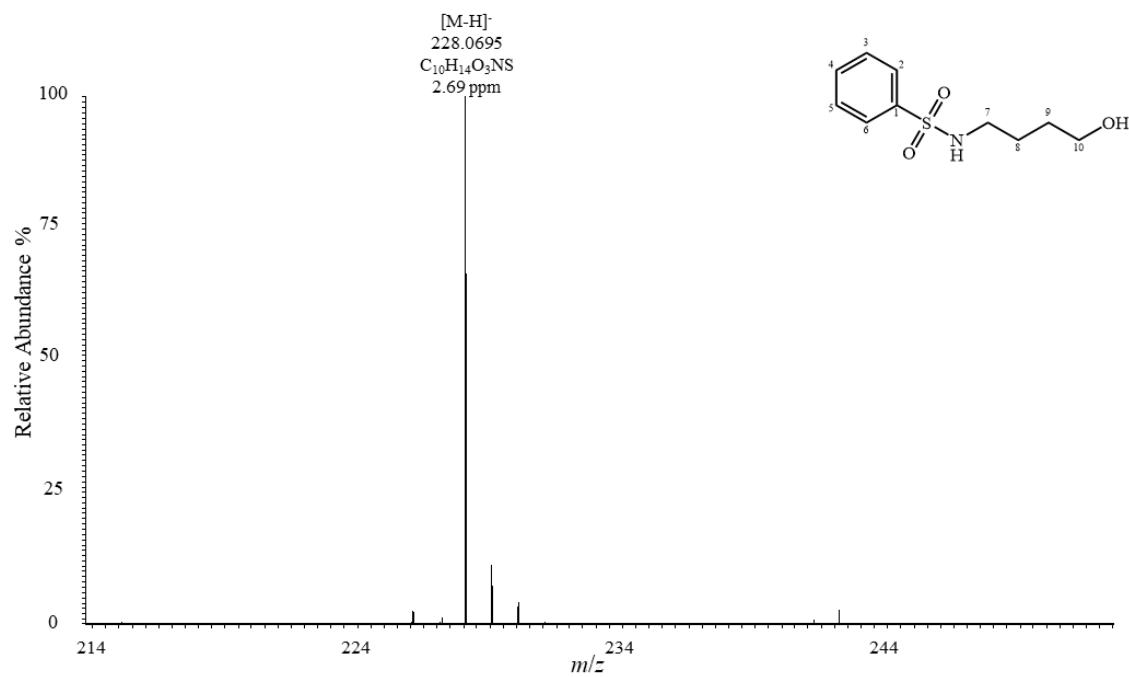**Figure S 151** COSY spectrum of compound **4.10** in methanol-d$_4$, 500 MHz.
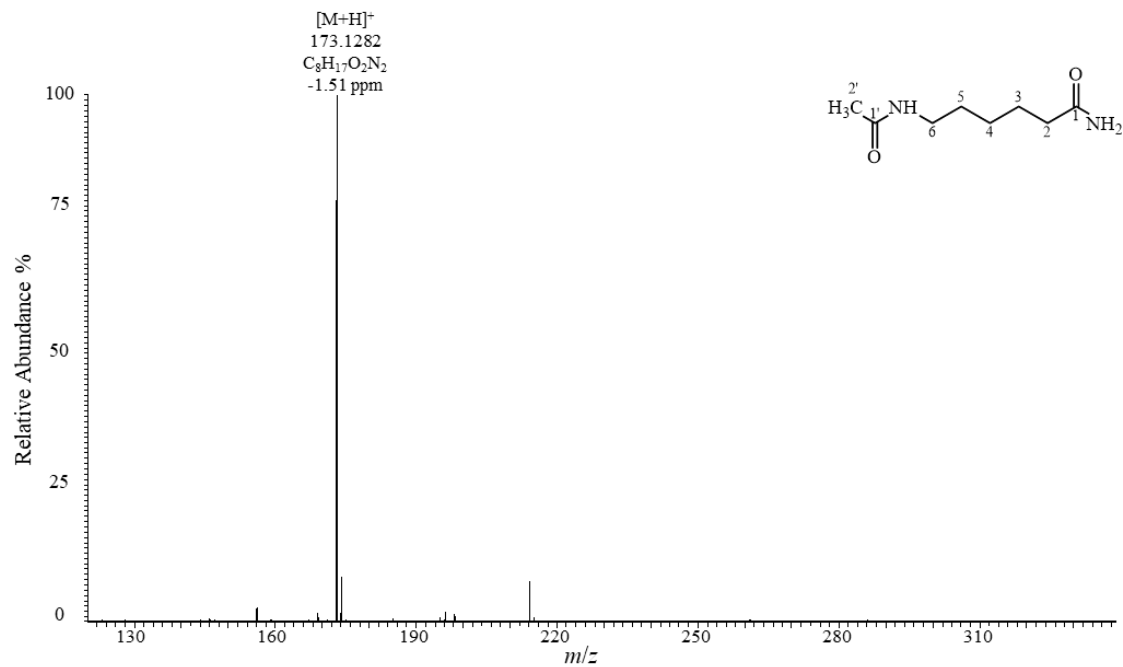
Figure S 152 (+)-ESI-HRMS spectrum of compound **4.11**.
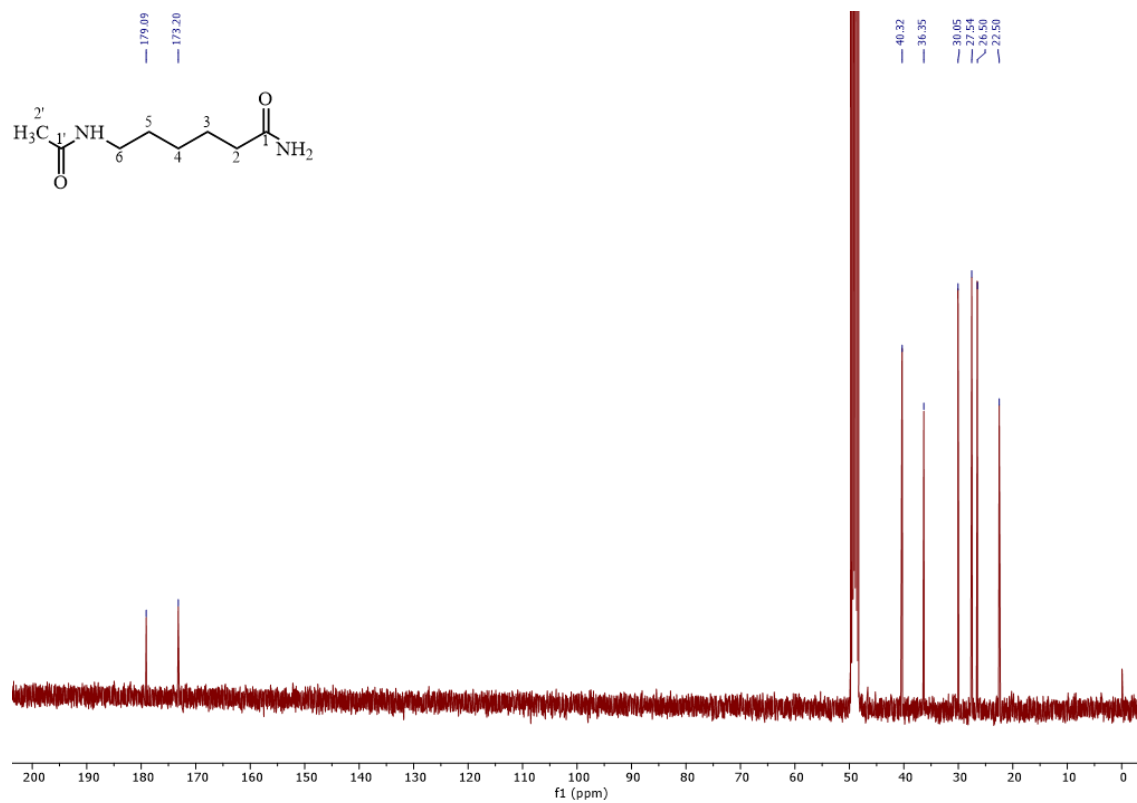
Figure S 153 ^{13}C spectrum of compound **4.11** in methanol-d4, 100 MHz.
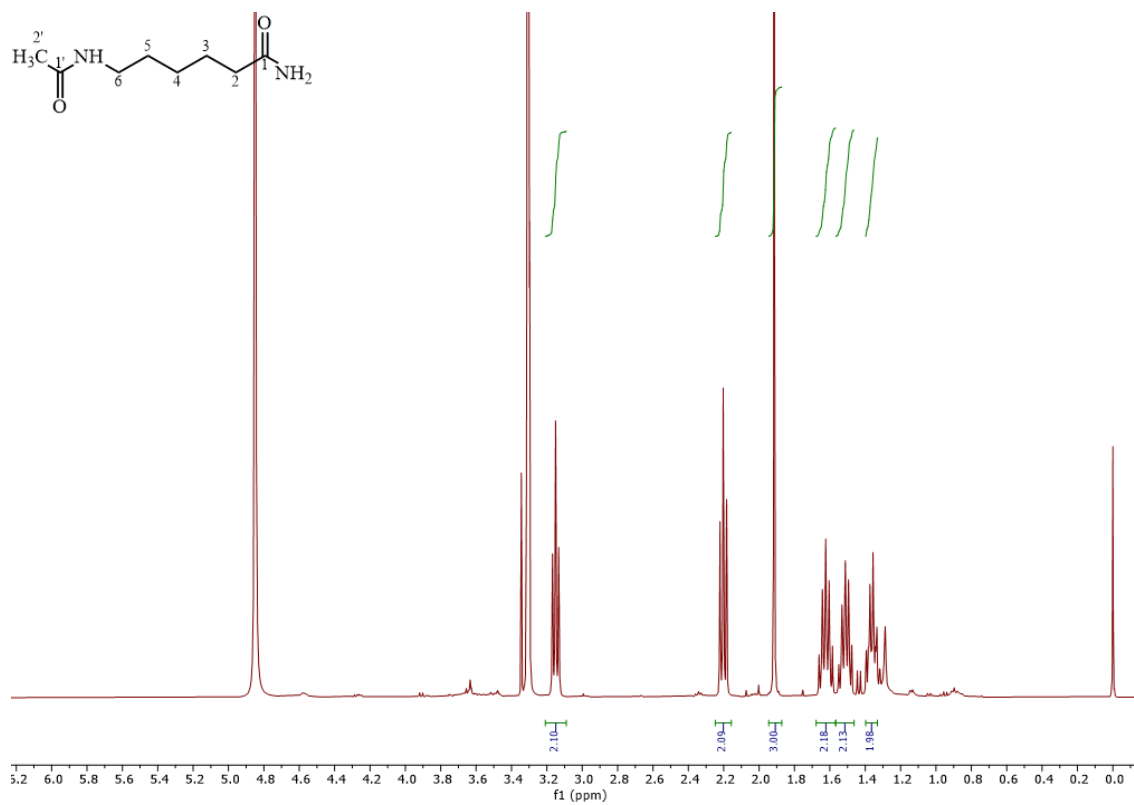
Figure S 154 ^{1}H spectrum of compound **4.11** in methanol-d$_4$, 400 MHz.

Figure S 155 HSQC spectrum of compound **4.11** in methanol-d$_4$, 400/100 MHz.

Figure S 156 HMBC spectrum of compound **4.11** in methanol-d$_4$, 400/100 MHz.

Figure S 157 COSY spectrum of compound **4.11** in methanol-d$_4$, 400 MHz.
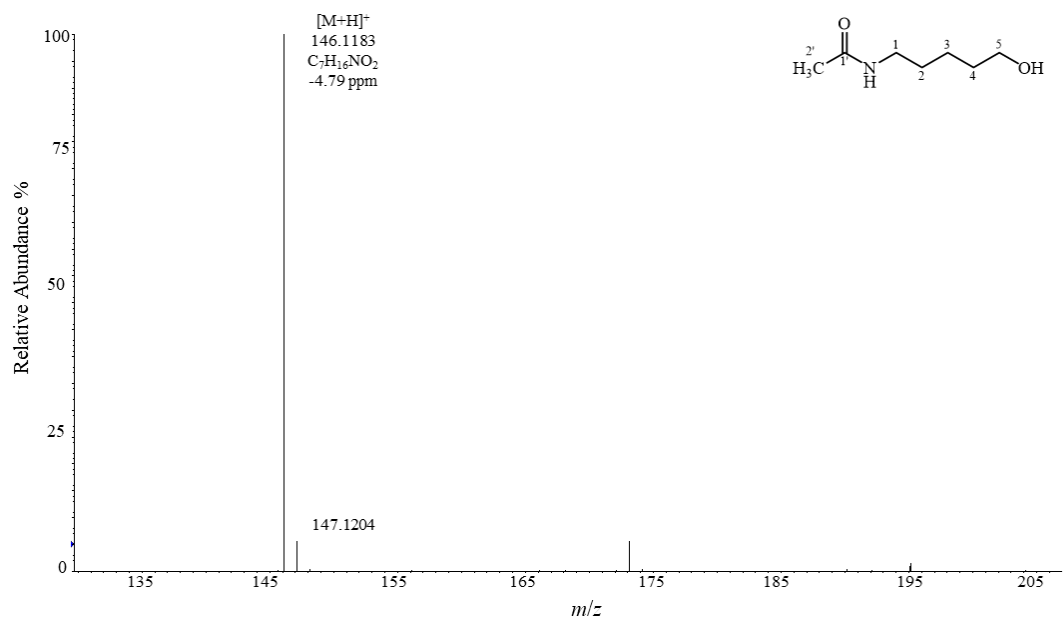
Figure S 158 (+)-ESI-HRMS spectrum of compound **4.12**.
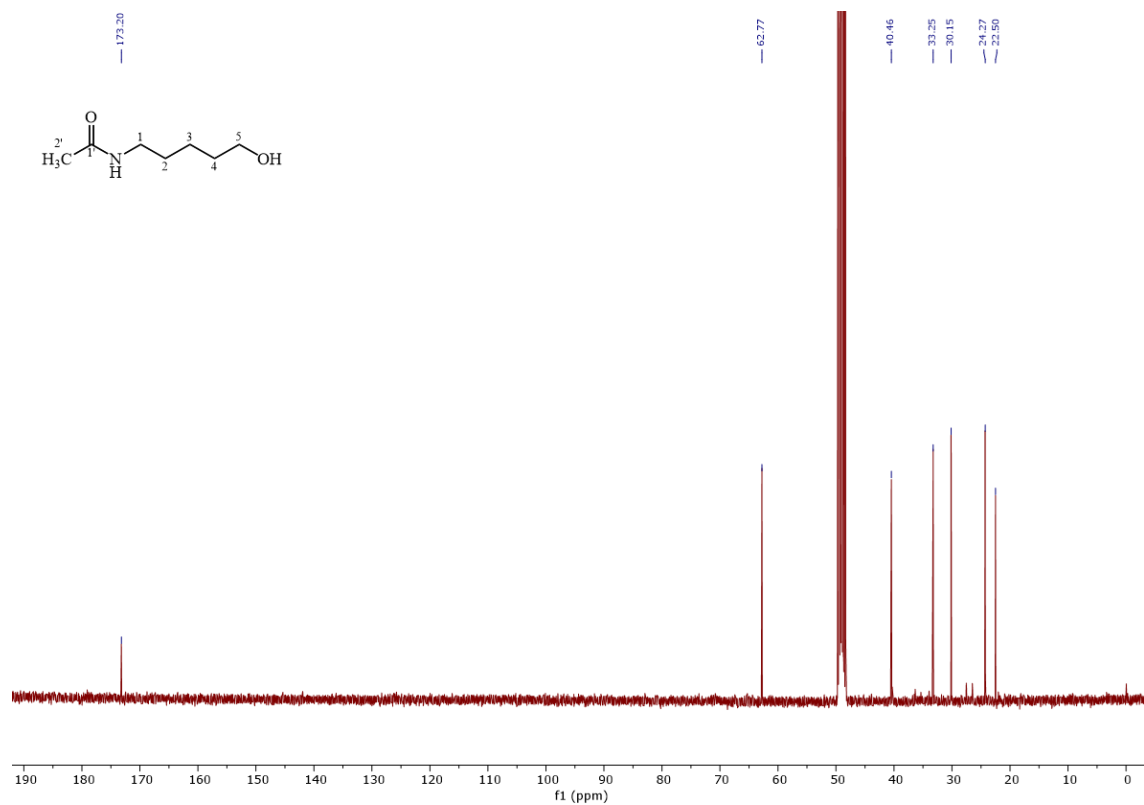
Figure S 159 ^{13}C spectrum of compound **4.12** in methanol-d$_4$, 100 MHz.
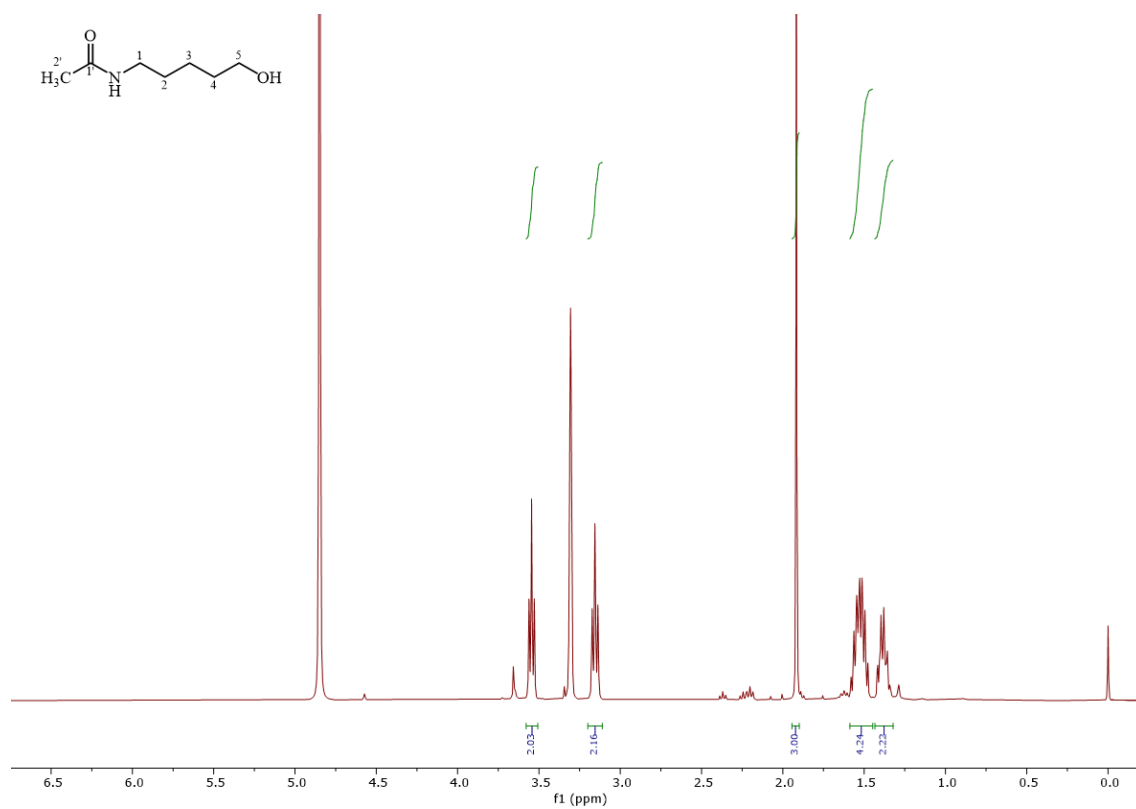
Figure S 160 ^{1}H spectrum of compound **4.12** in methanol-d$_4$, 400 MHz.
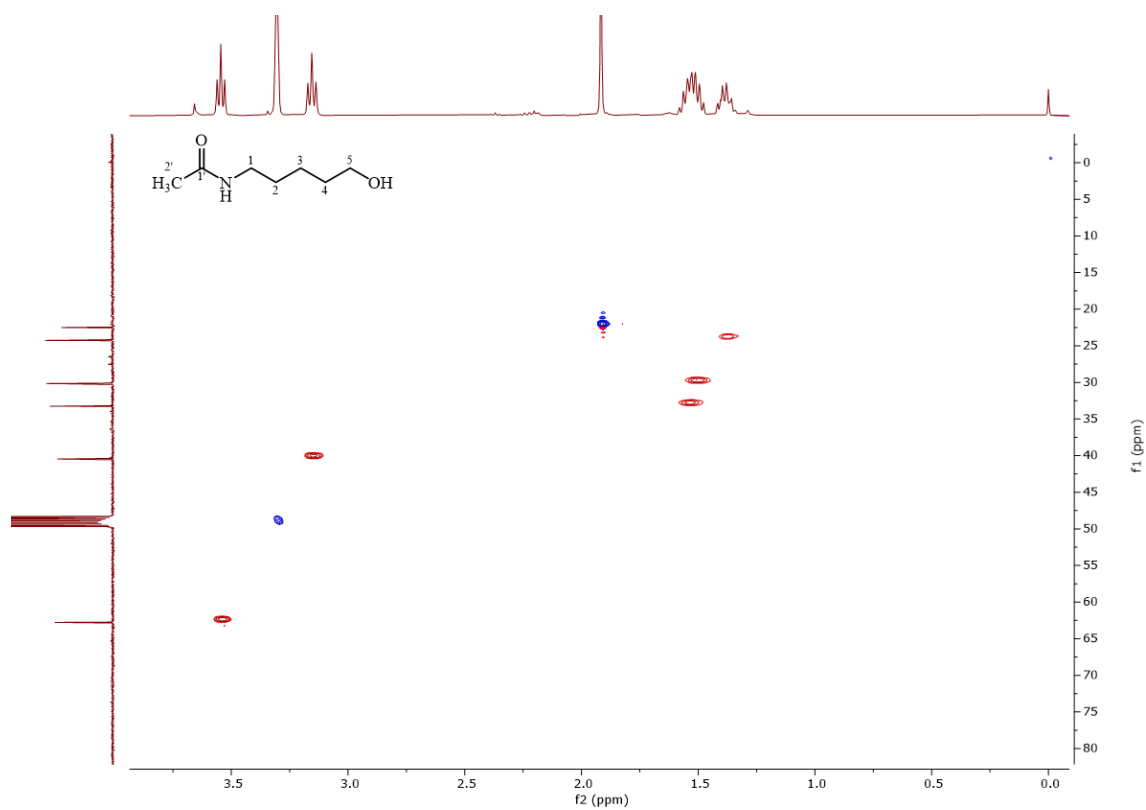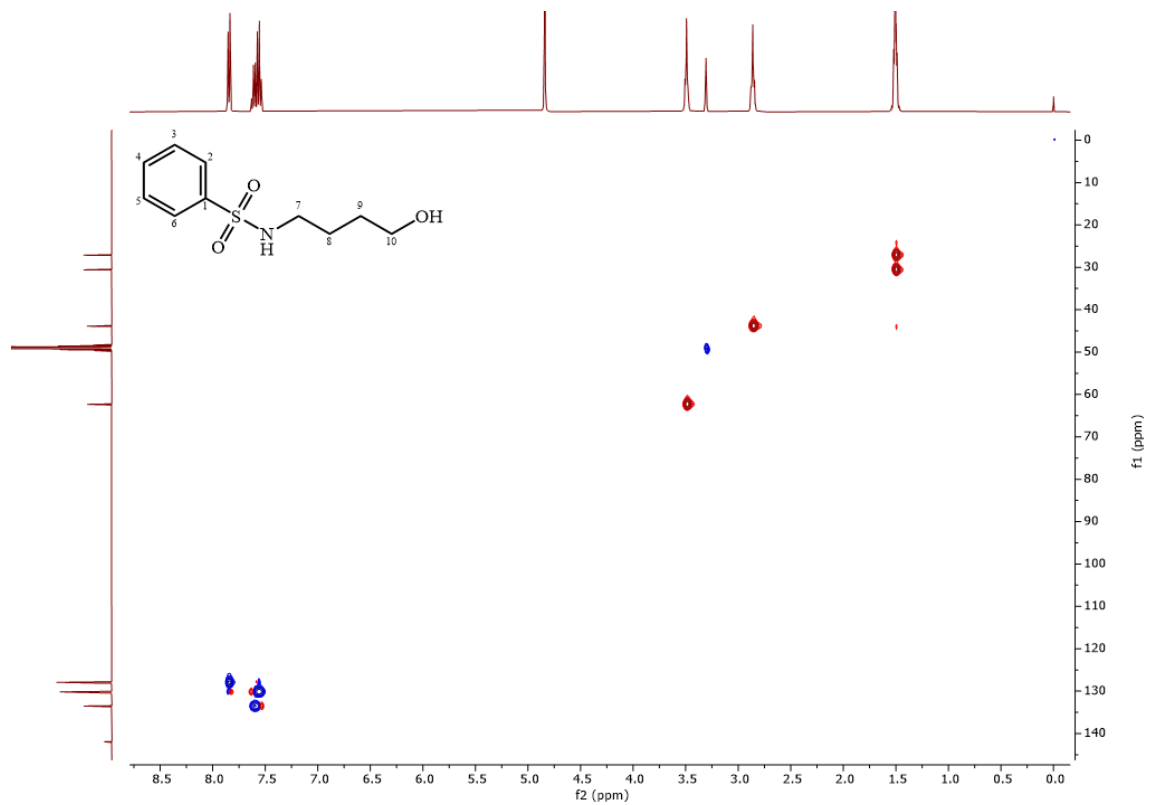

Figure S 161 HSQC spectrum of compound **4.12** in methanol-d$_4$, 400/100 MHz.
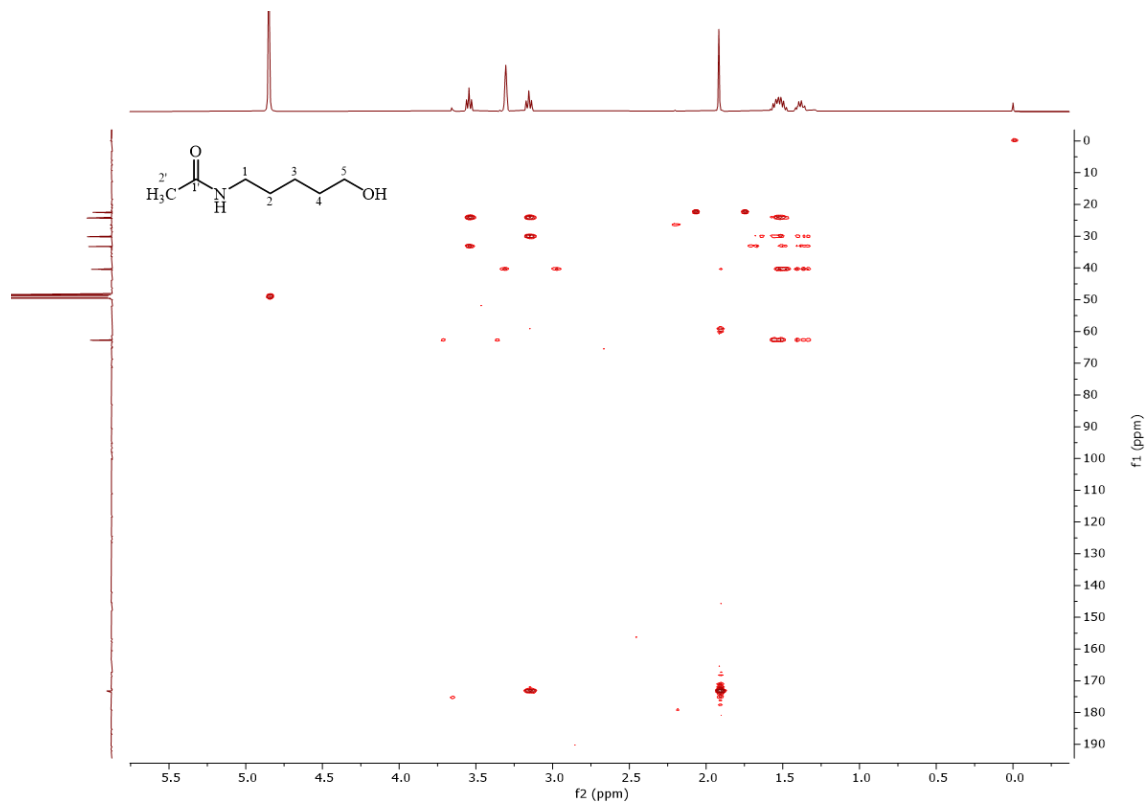
Figure S 162 HMBC spectrum of compound **4.12** in methanol-d$_4$, 400/100 MHz.
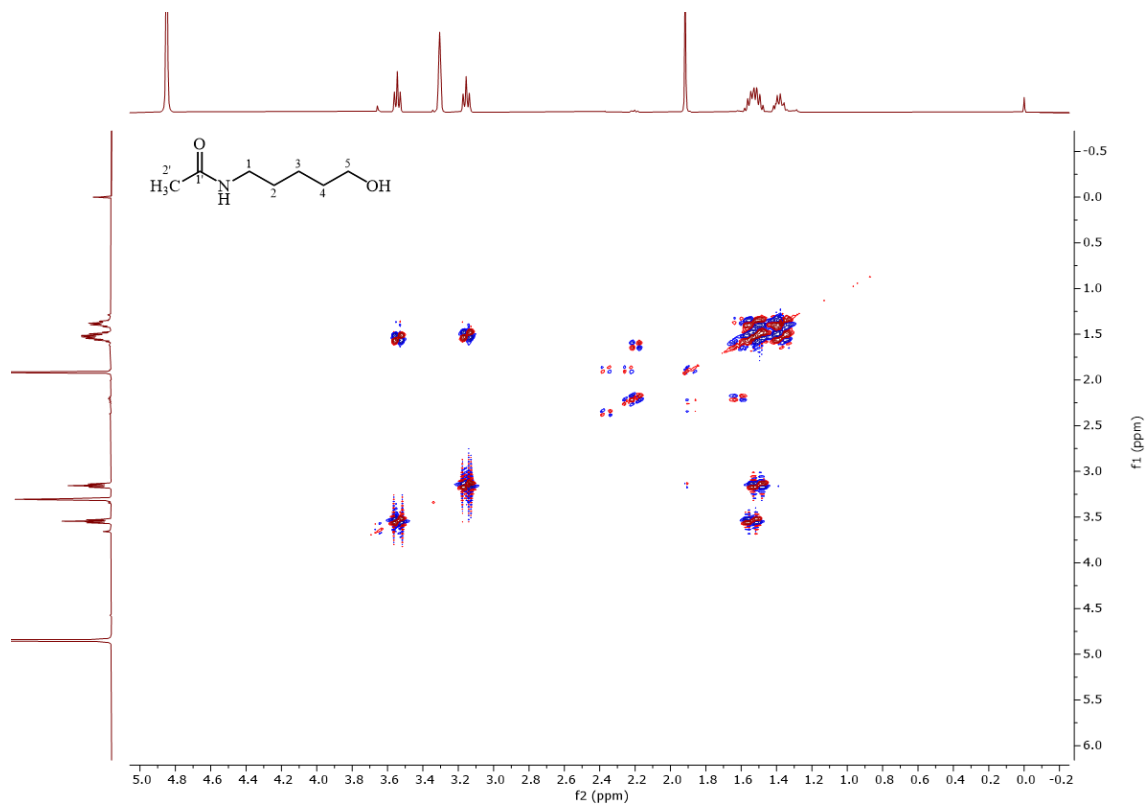
Figure S 163 COSY spectrum of compound **4.12** in methanol-d$_4$, 400 MHz.
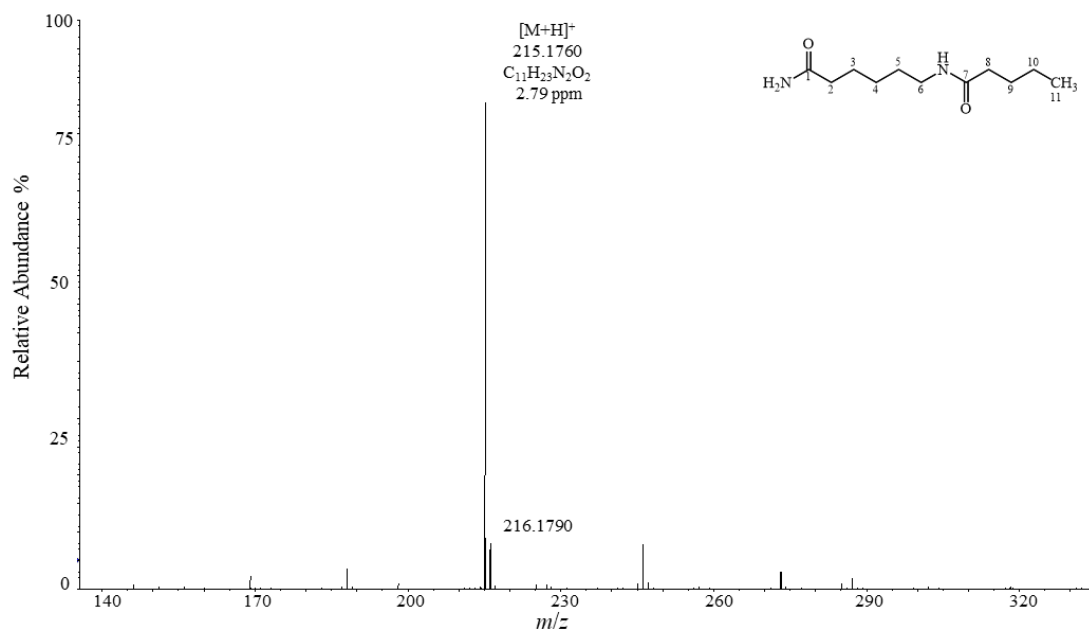
Figure S 164 (+)-ESI-HRMS spectrum of compound **4.13**.
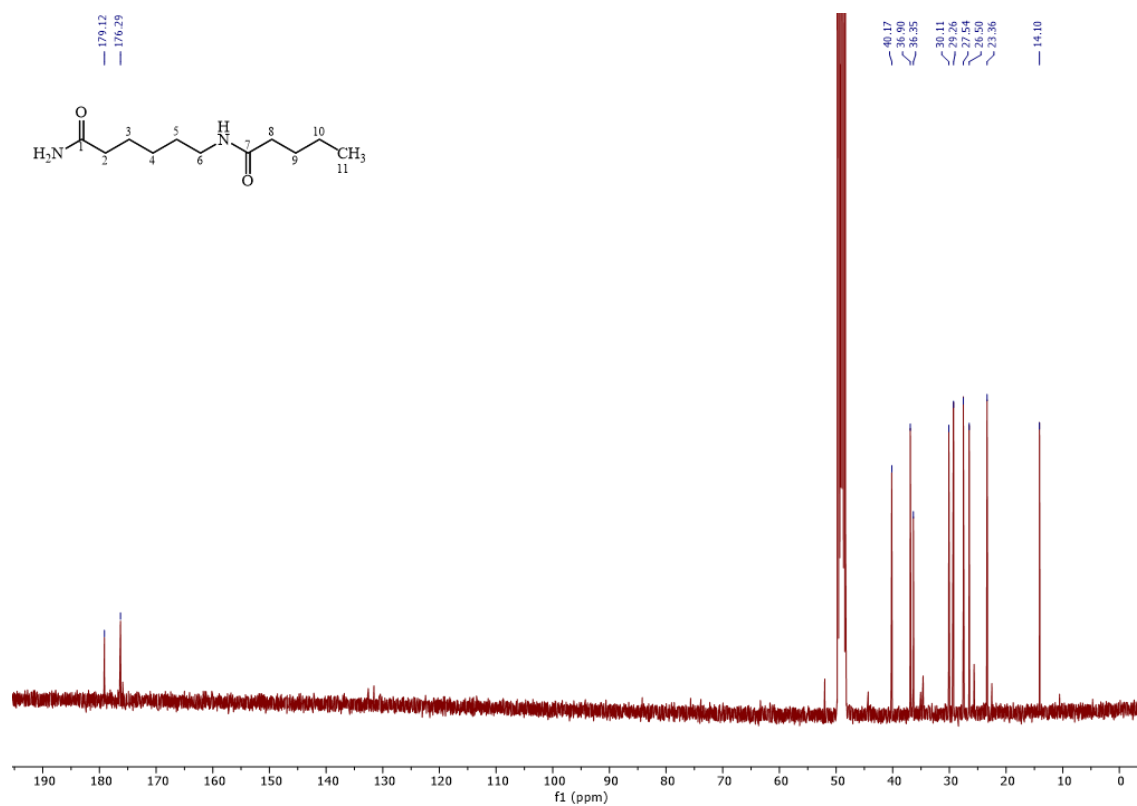
Figure S 165 ^{13}C spectrum of compound **4.13** in methanol-d$_4$, 100 MHz.

Figure S 166 ^{1}H spectrum of compound **4.13** in methanol-d$_4$, 400 MHz.

Figure S 167 HSQC spectrum of compound **4.13** in methanol-d$_4$, 400/100 MHz.

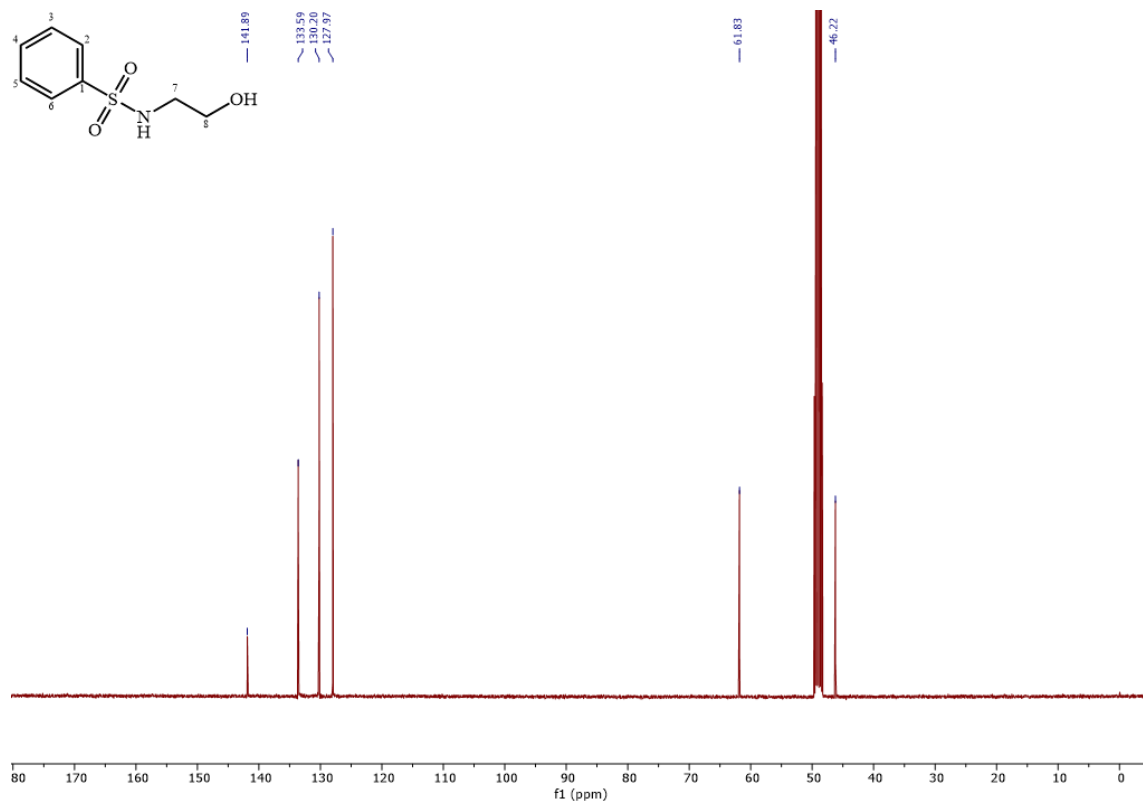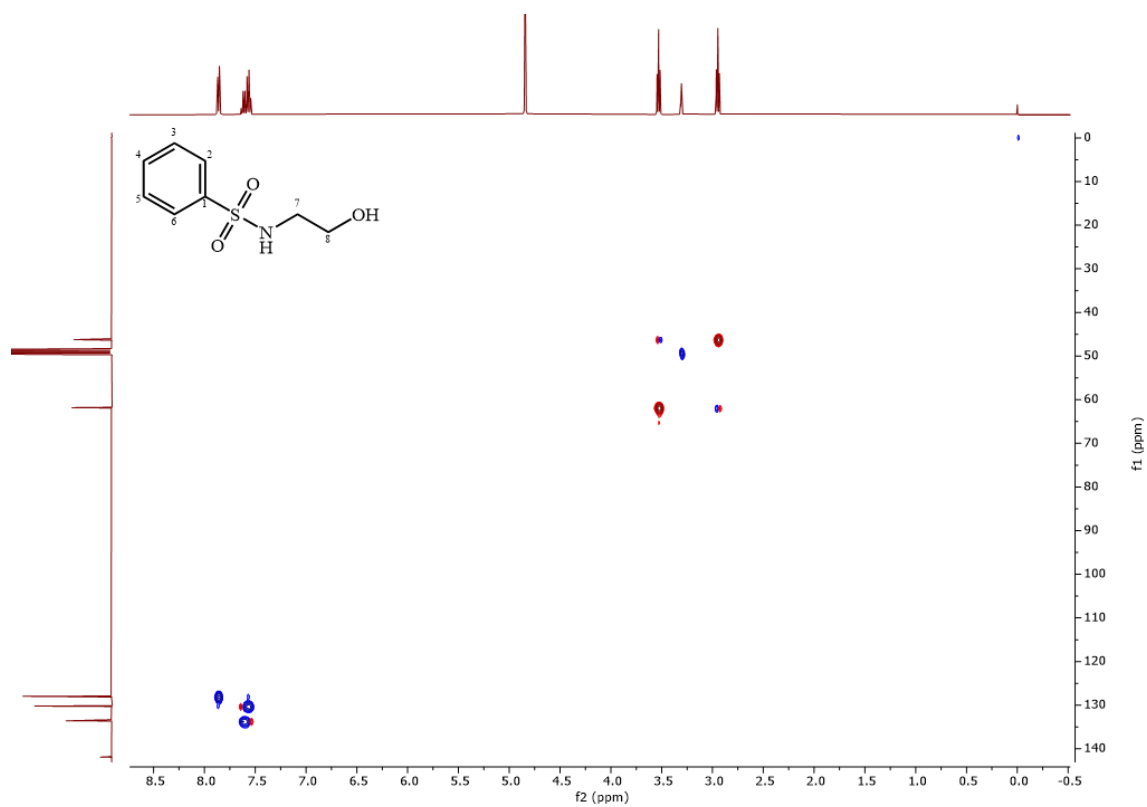**Figure S 168** HMBC spectrum of compound **4.13** in methanol-d4, 400/100 MHz.

Figure S 169 COSY spectrum of compound **4.13** in methanol-d4, 100 MHz.

Compound	100 mM	50 mM	20 mM	10 mM
4.1	-	-	-	-
4.2		-	-	-
4.3				
4.4	-	-	-	Figure S 205
4.5				
4.6				-
4.7				-
4.8				
4.9				
4.10				
4.11				
4.12				
4.13				
Blank				
Paraquat (0.1 mM)				

Figure S 170 Pictures of the leaf-spot assay of compounds **4.1** – **4.13**.

m/z	Intensity	Relative Intensity	Theo. Mass
228.0696	8501240	100	228.0696
229.0729	890761.7	10.48	229.0729
230.0653	346686.4	4.08	230.0653

[M-H]⁻
228.0696
$C_{10}H_{14}O_3NS$
3.19 ppm
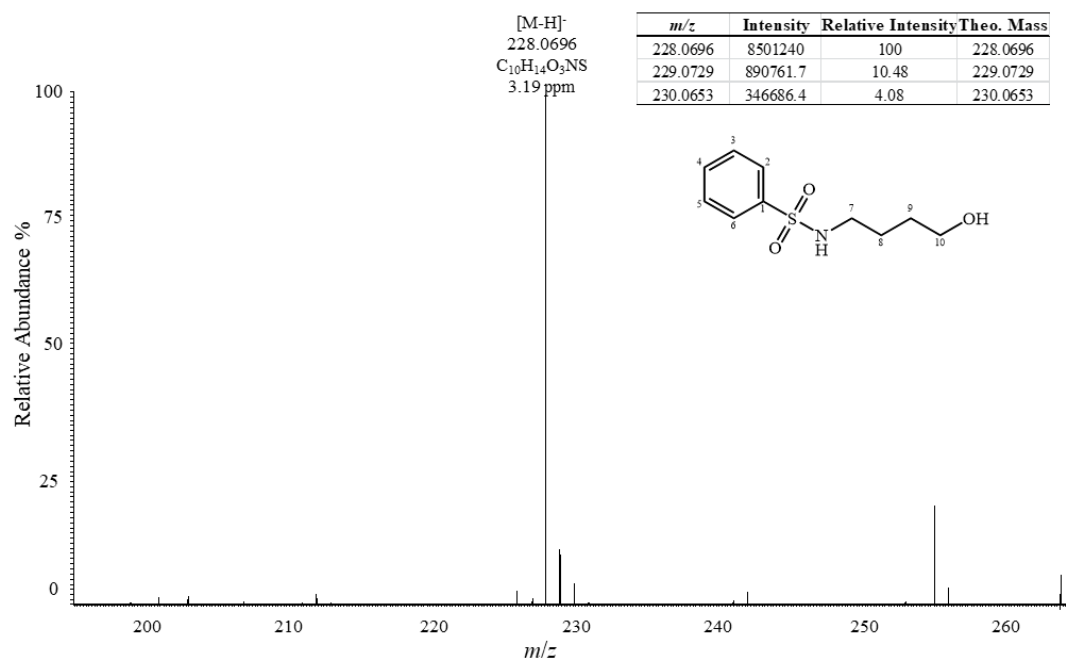
Figure S 171 (-)-ESI-HRMS spectrum of compound **5.1a**.
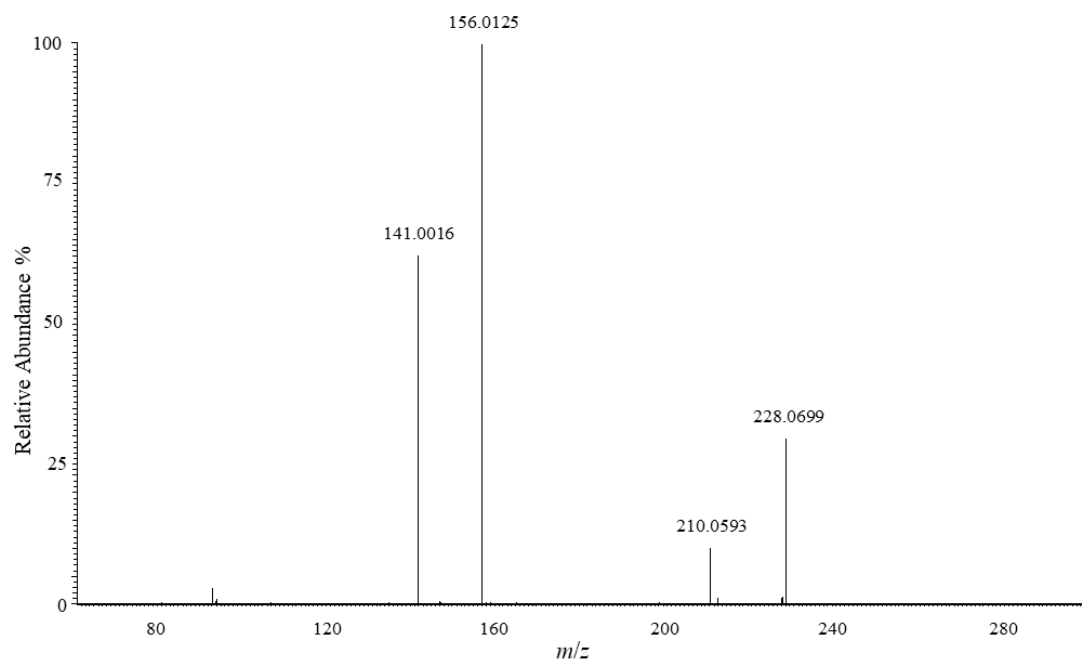
Figure S 172 (-)-ESI-HRMS^2 spectrum of compound **5.1a** [228.0696, CID 30.0].
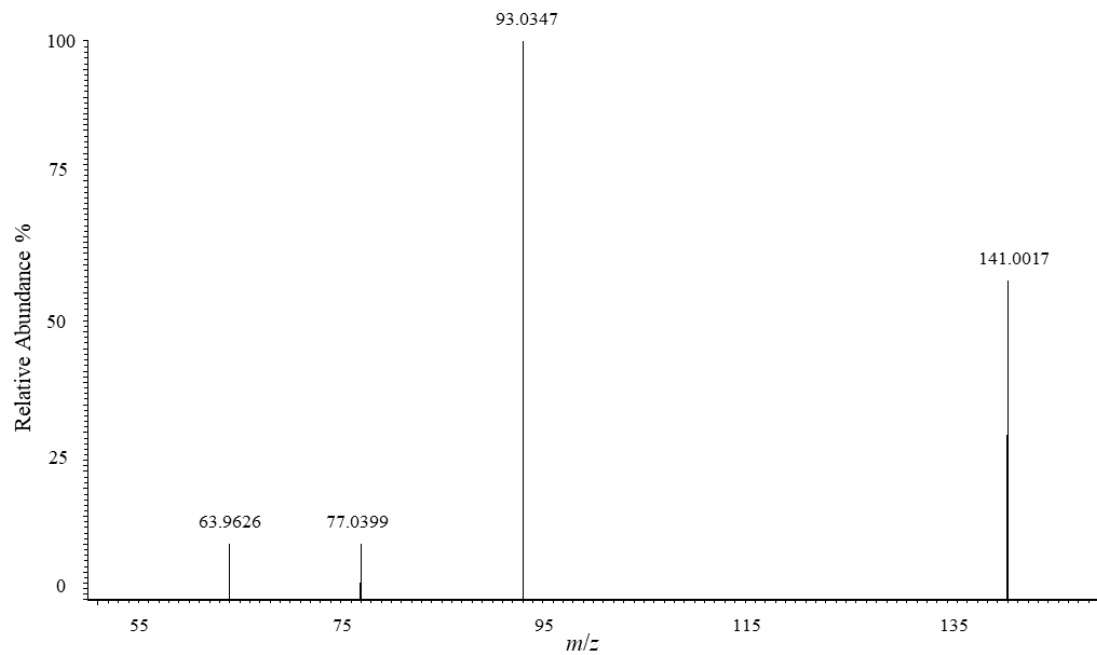
Figure S 173 (-)-ESI-HRMS[3] spectrum of compound **5.1a** [228.07, CID 30.0 – 141.00, CID 25.0].
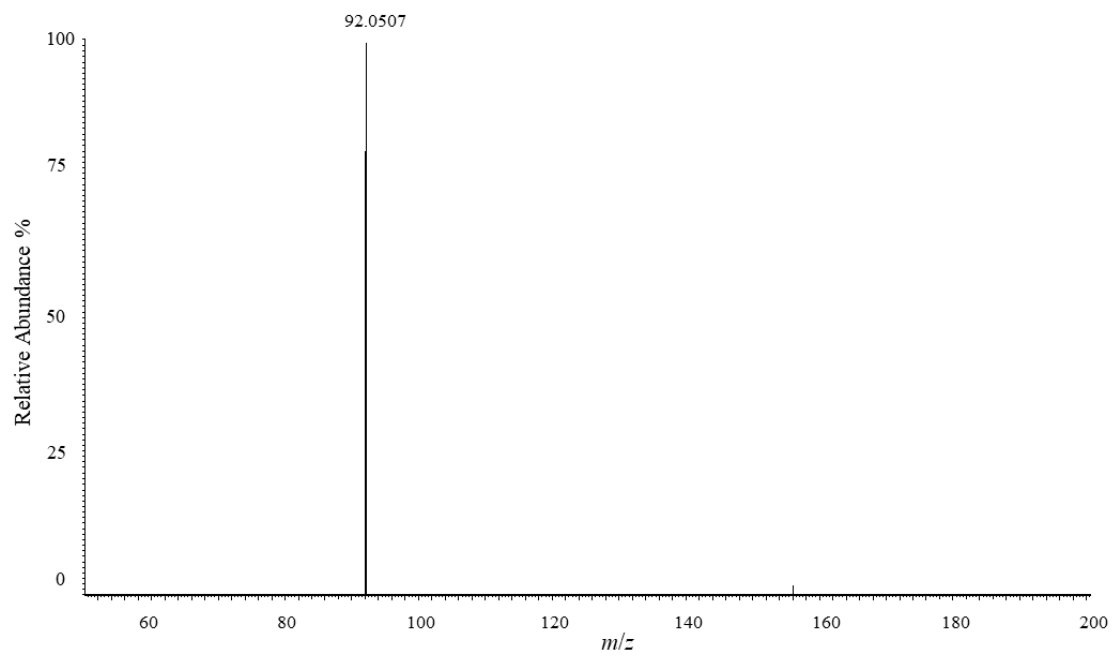
Figure S 174 (-)-ESI-HRMS[3] spectrum of compound **5.1a** [228.07, CID 30.0 – 156.00, CID 30.0].

Figure S 175 ^{1}H spectrum of compound **5.1a** in methanol-d$_4$, 400 MHz.

Figure S 176 HSQC spectrum of compound **5.1a** in methanol-d$_4$, 400/100 MHz.
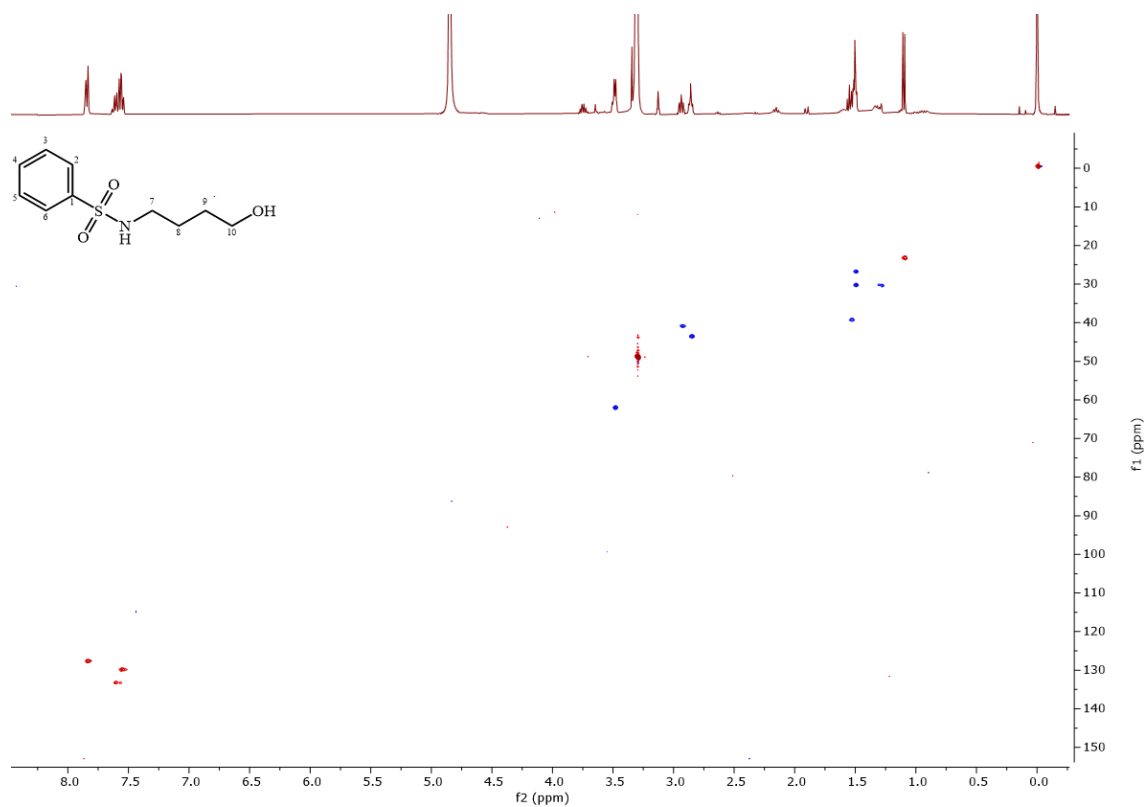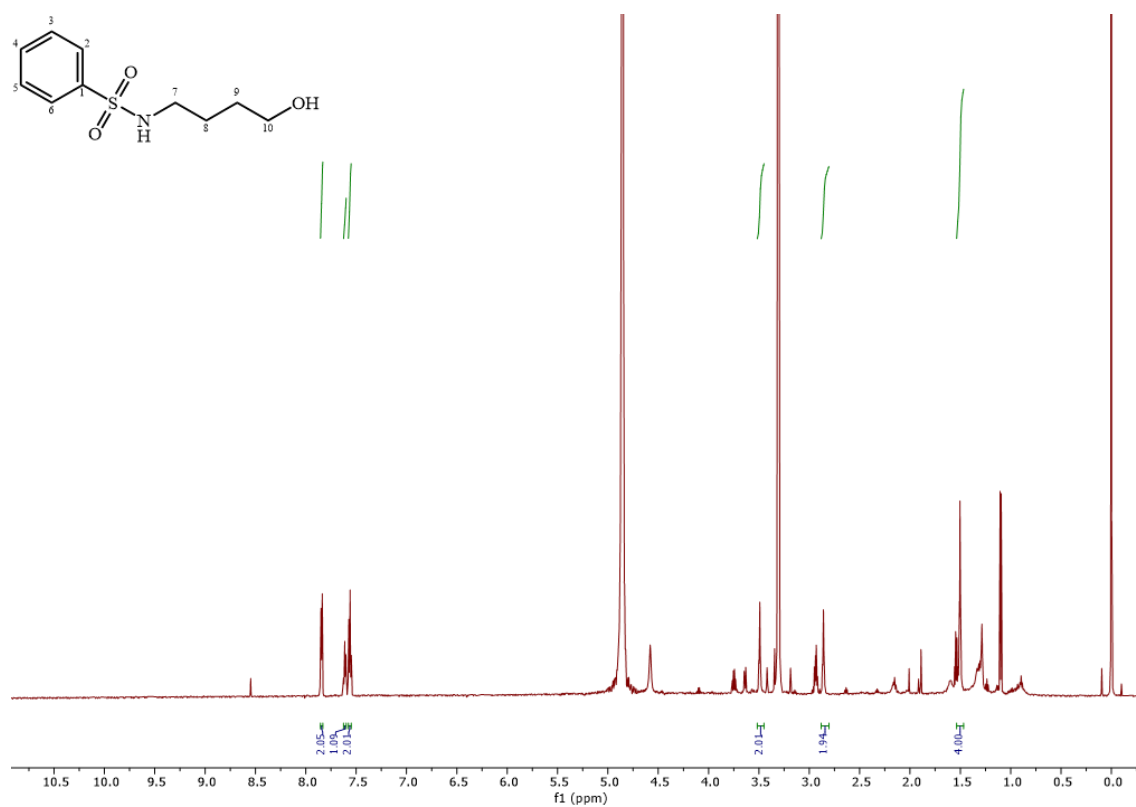
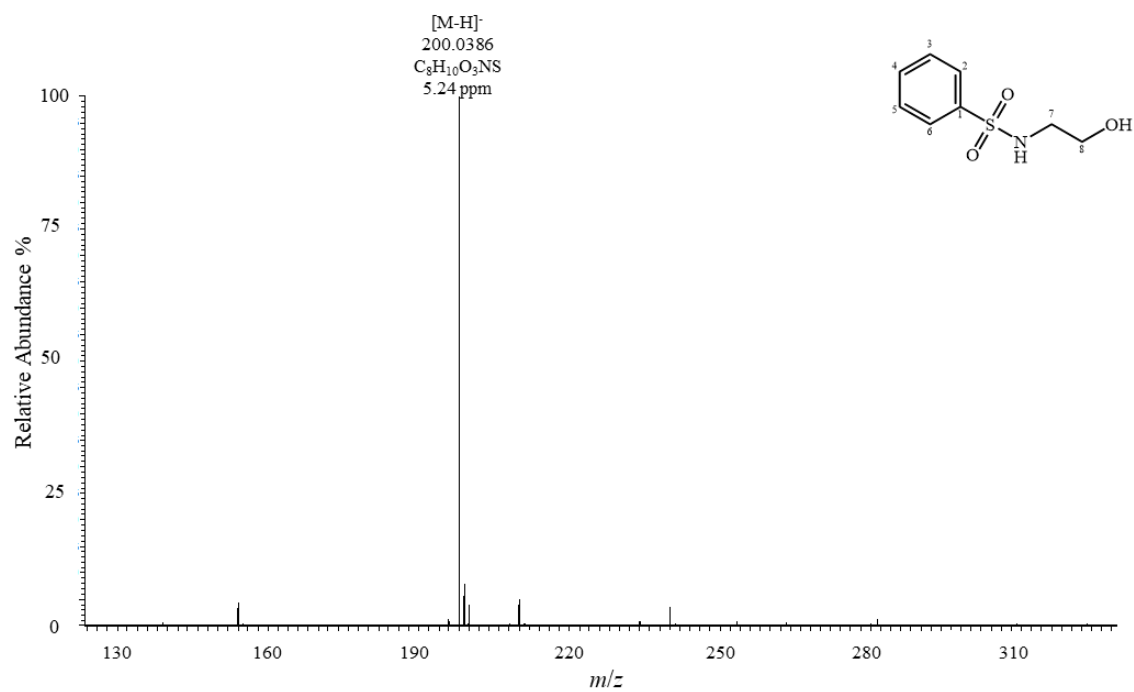**Figure S 177** HMBC spectrum of compound **5.1a** in methanol-d4, 400/100 MHz.
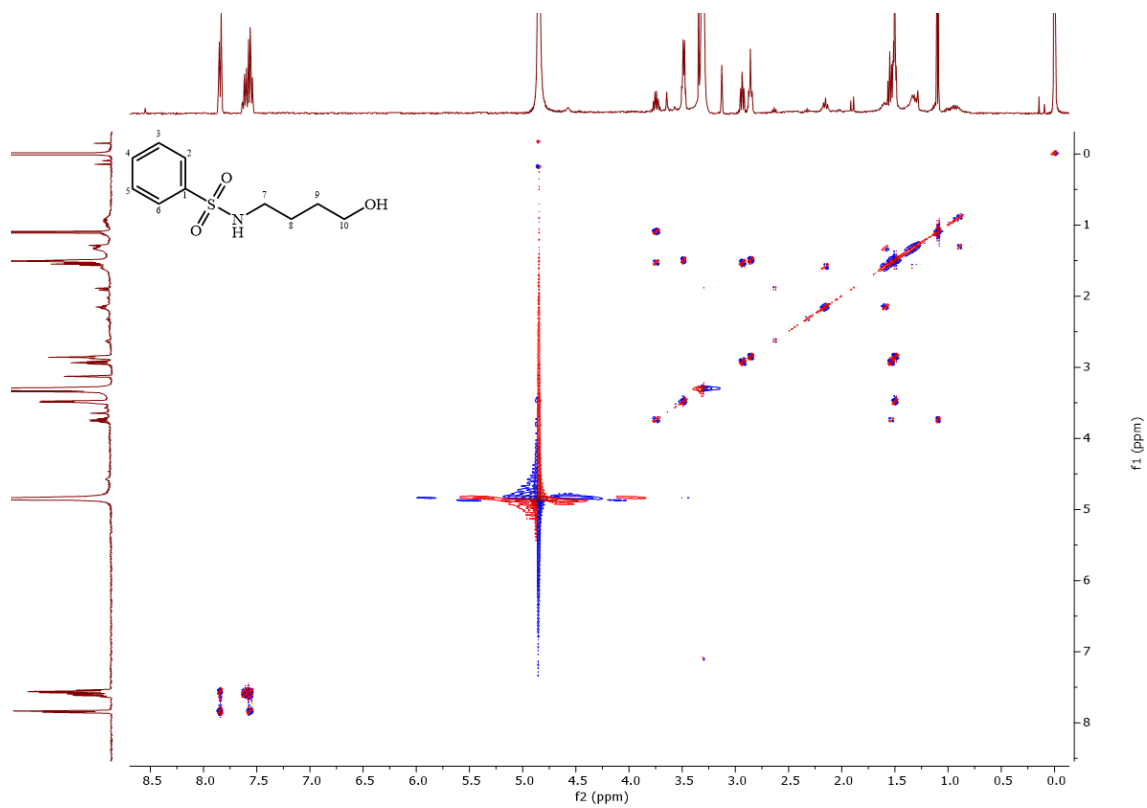
Figure S 178 COSY spectrum of compound **5.1a** in methanol-d4, 400 MHz.

Figure S 179 (-)-ESI-HRMS spectrum of compound **5.1b**.
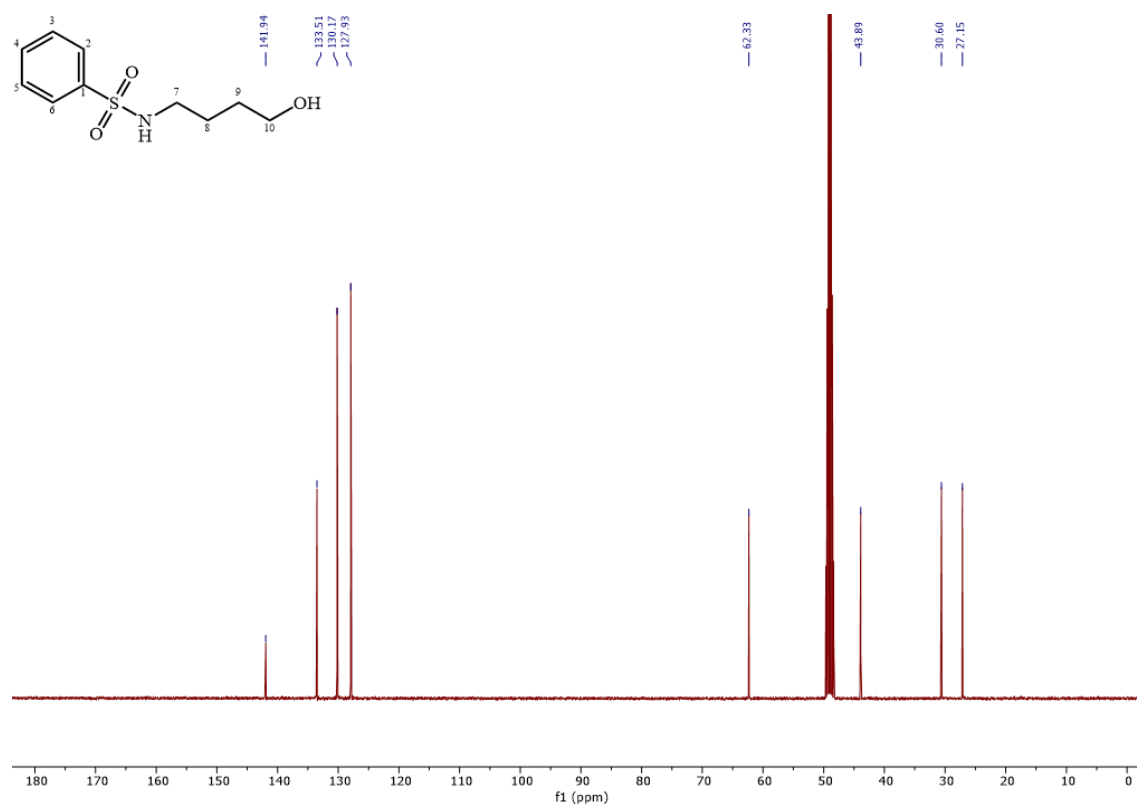
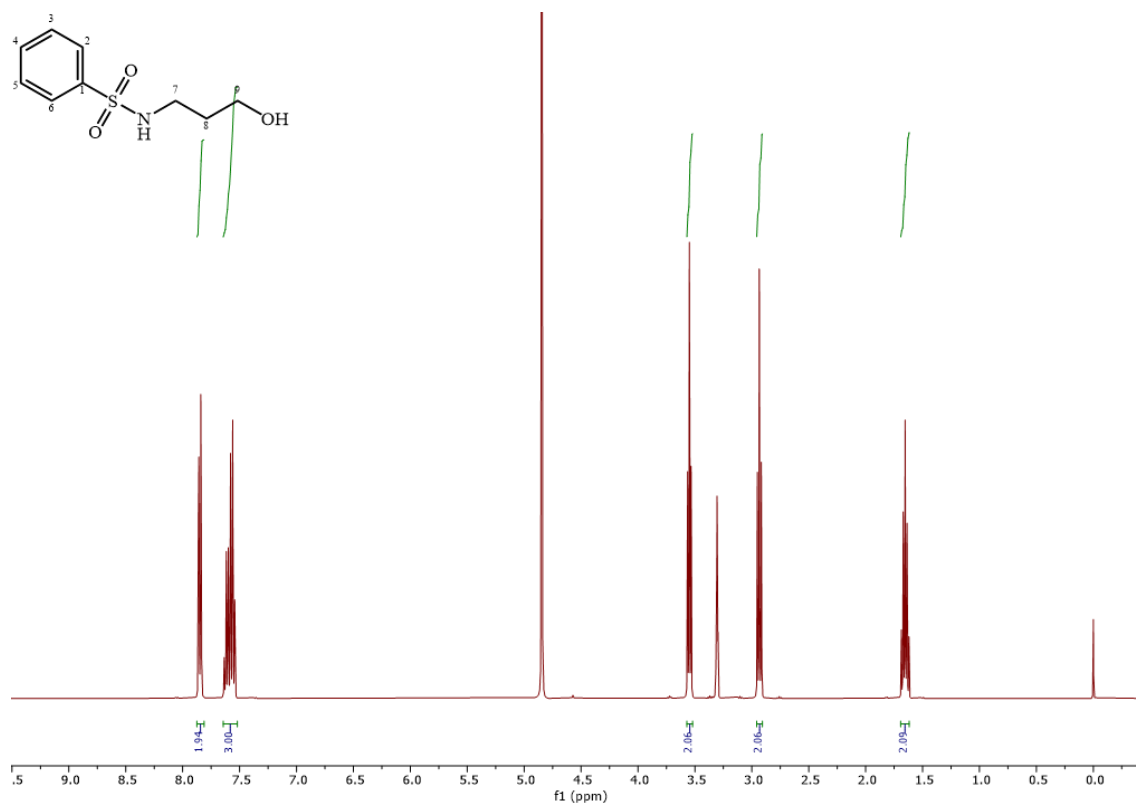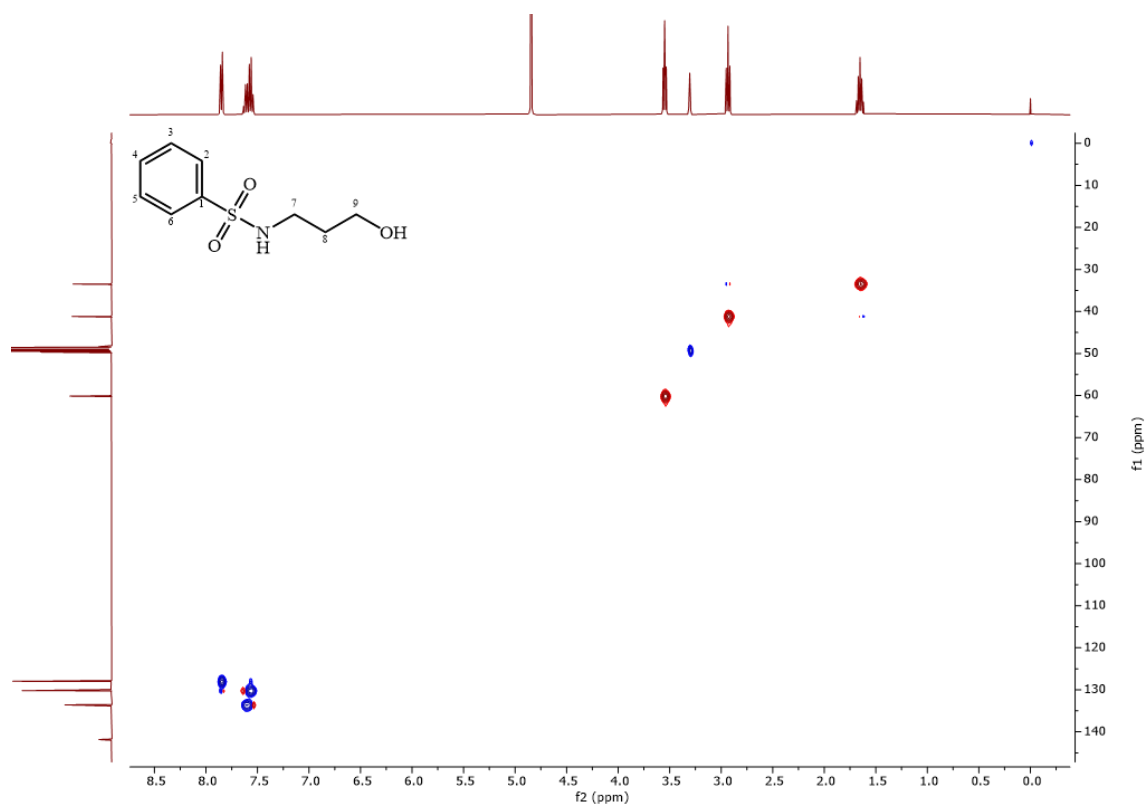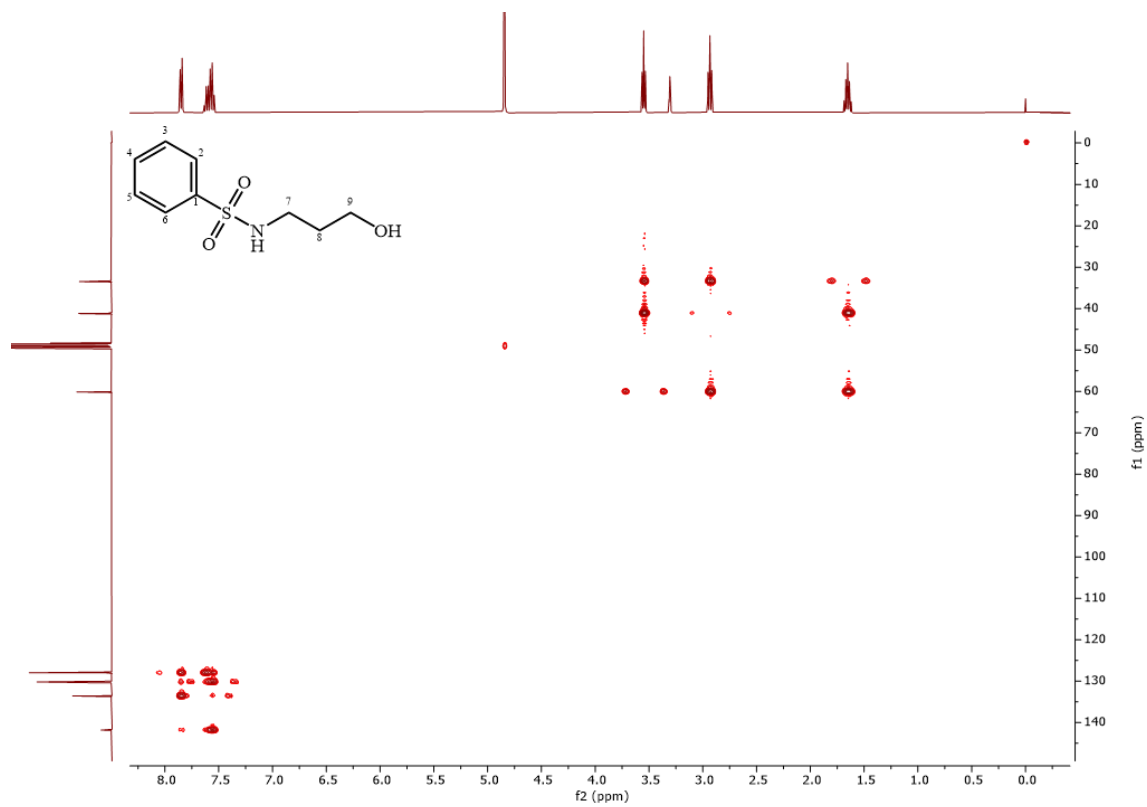**Figure S 180** ^{13}C spectrum of compound **5.1b** in methanol-d$_4$, 100 MHz.
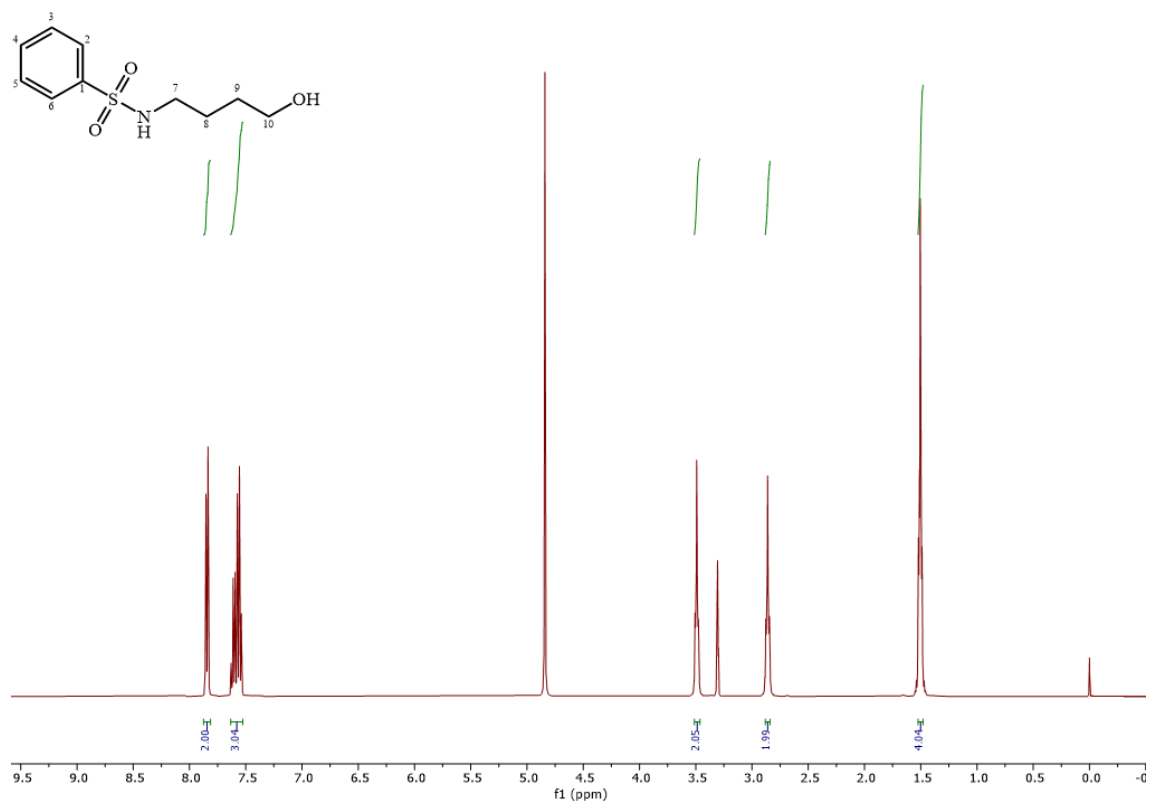
Figure S 181 ^{1}H spectrum of compound **5.1b** in methanol-d$_4$, 400 MHz.

Figure S 182 HSQC spectrum of compound **5.1b** in methanol-d$_4$, 400/100 MHz.

216

Figure S 183 HMBC spectrum of compound **5.1b** in methanol-d4, 400/100 MHz.
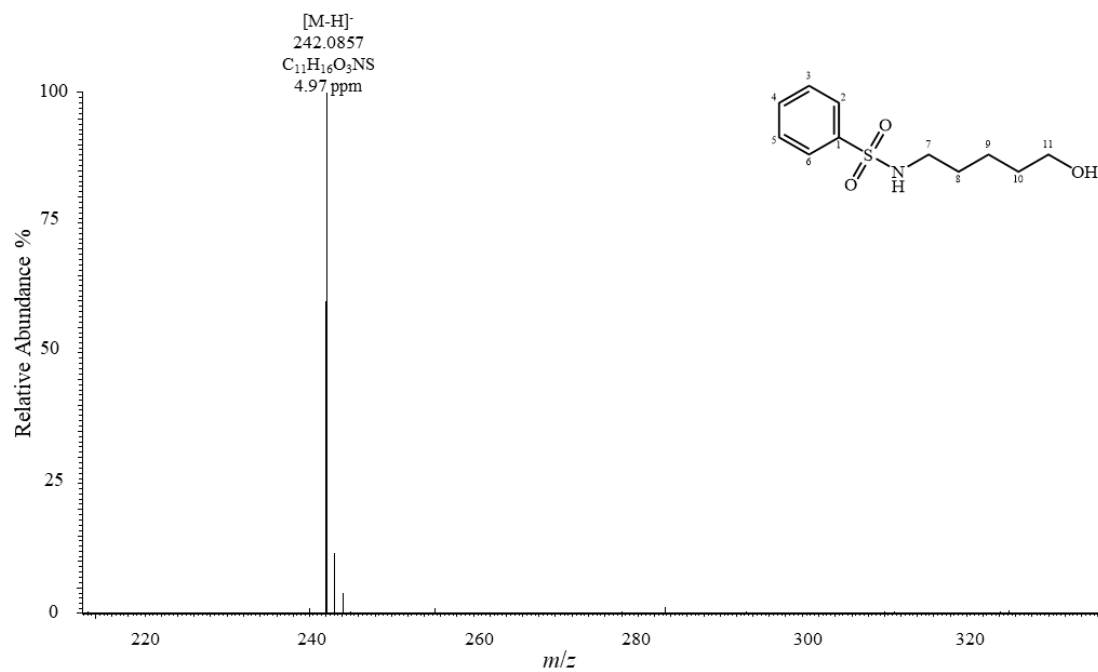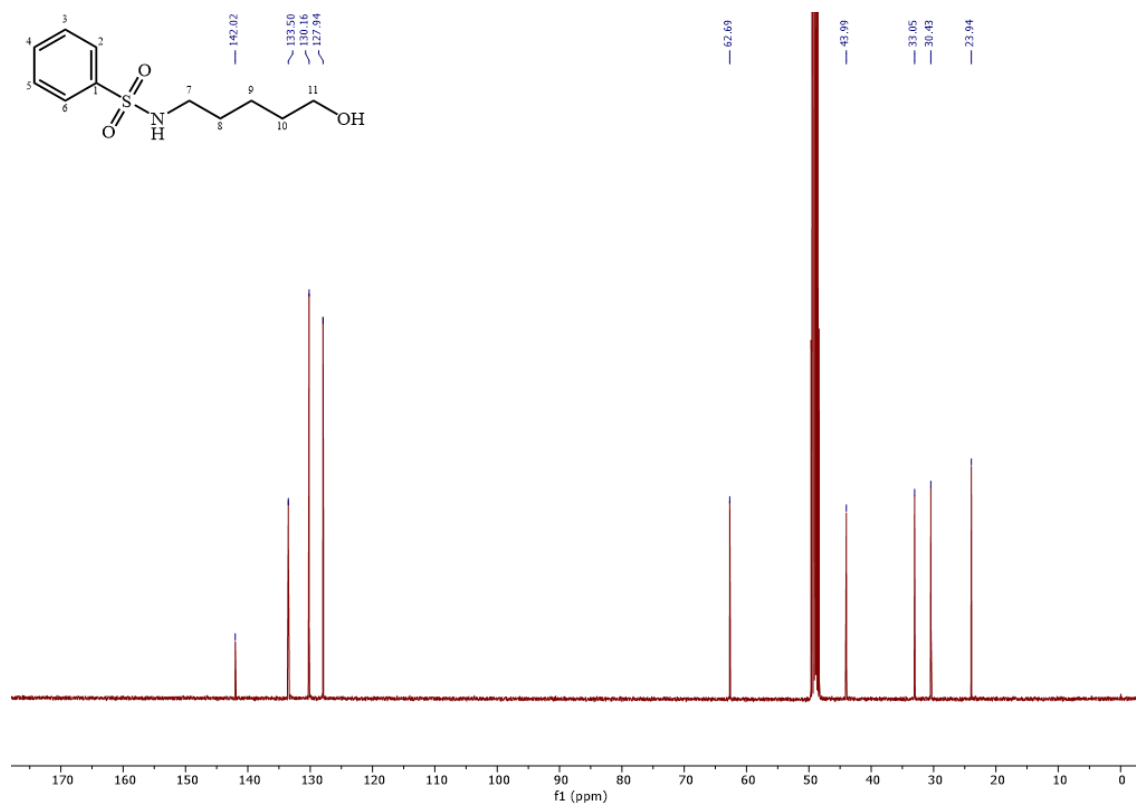

Figure S 184 (-)-ESI-HRMS spectrum of compound **5.2**.
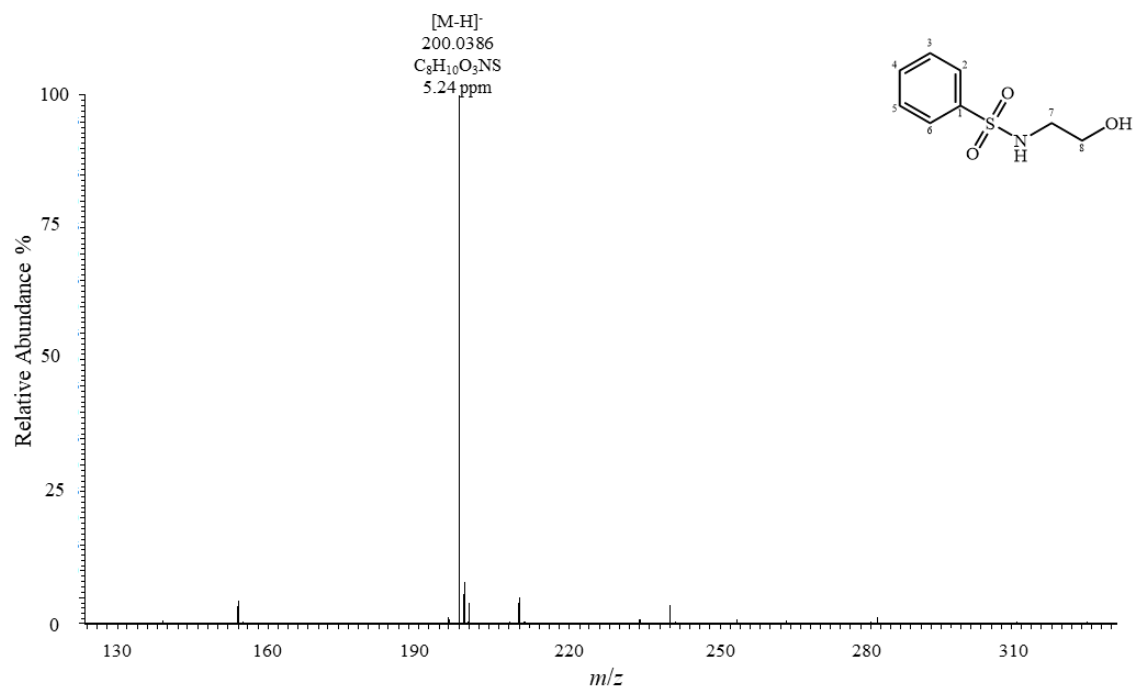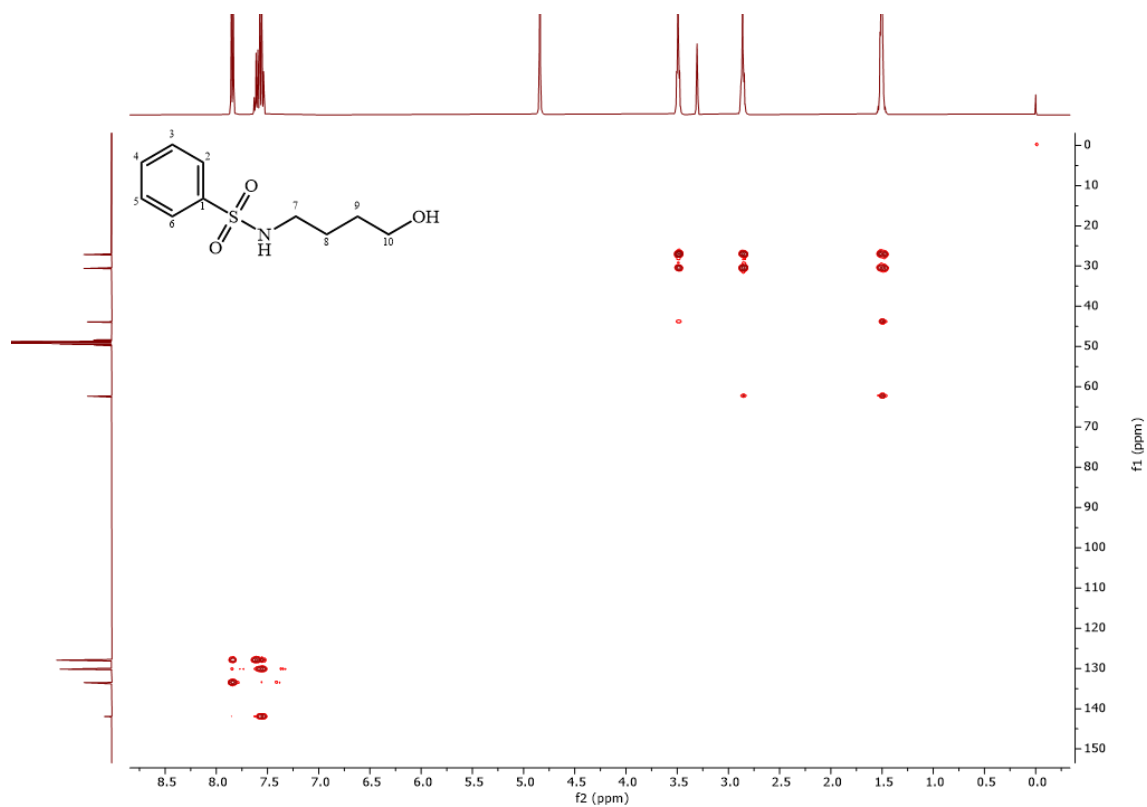
Figure S 185 ^{13}C spectrum of compound **5.2** in methanol-d$_4$, 100 MHz.
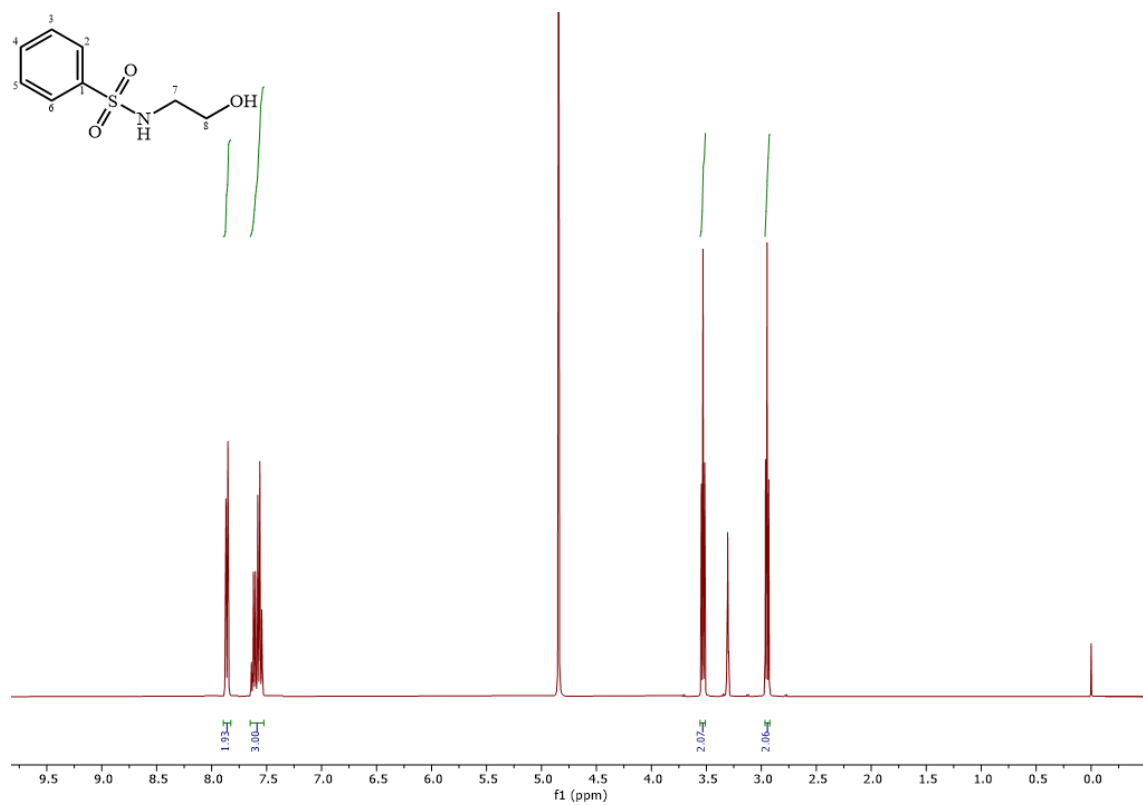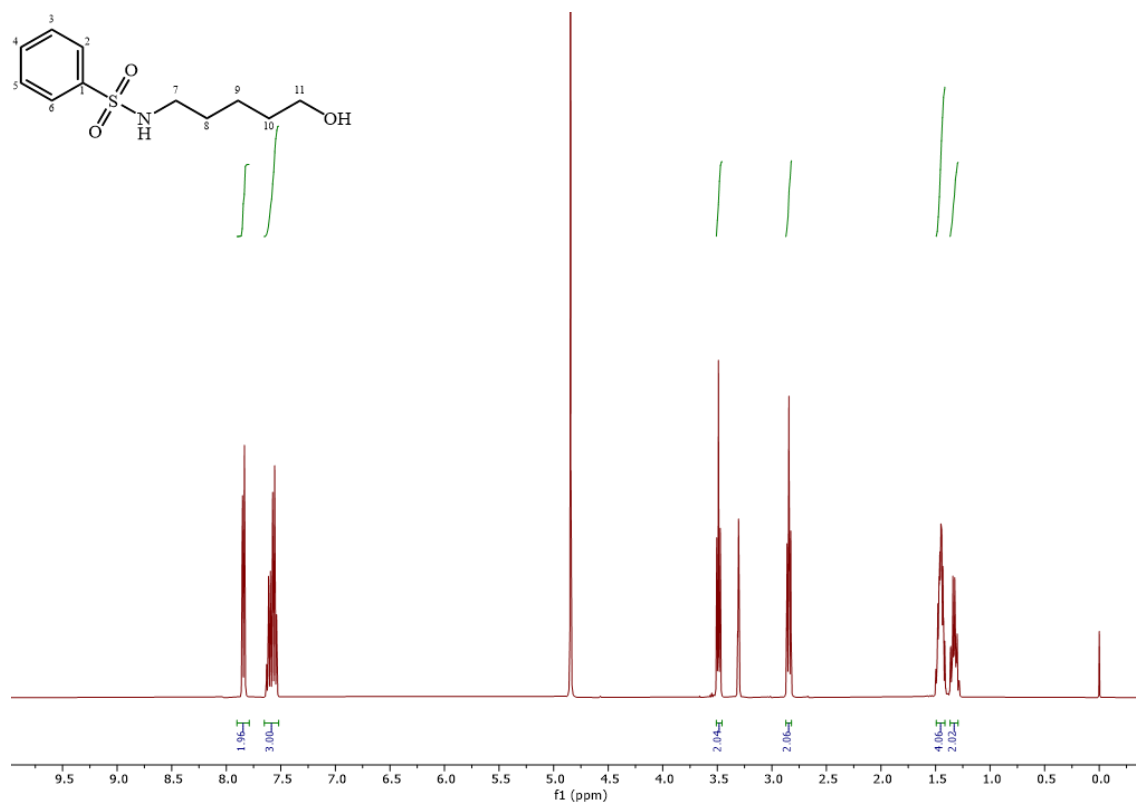

Figure S 186 ^{1}H spectrum of compound **5.2** in methanol-d$_4$, 400 MHz.

Figure S 187 HSQC spectrum of compound **5.2** in methanol-d$_4$, 400/100 MHz.
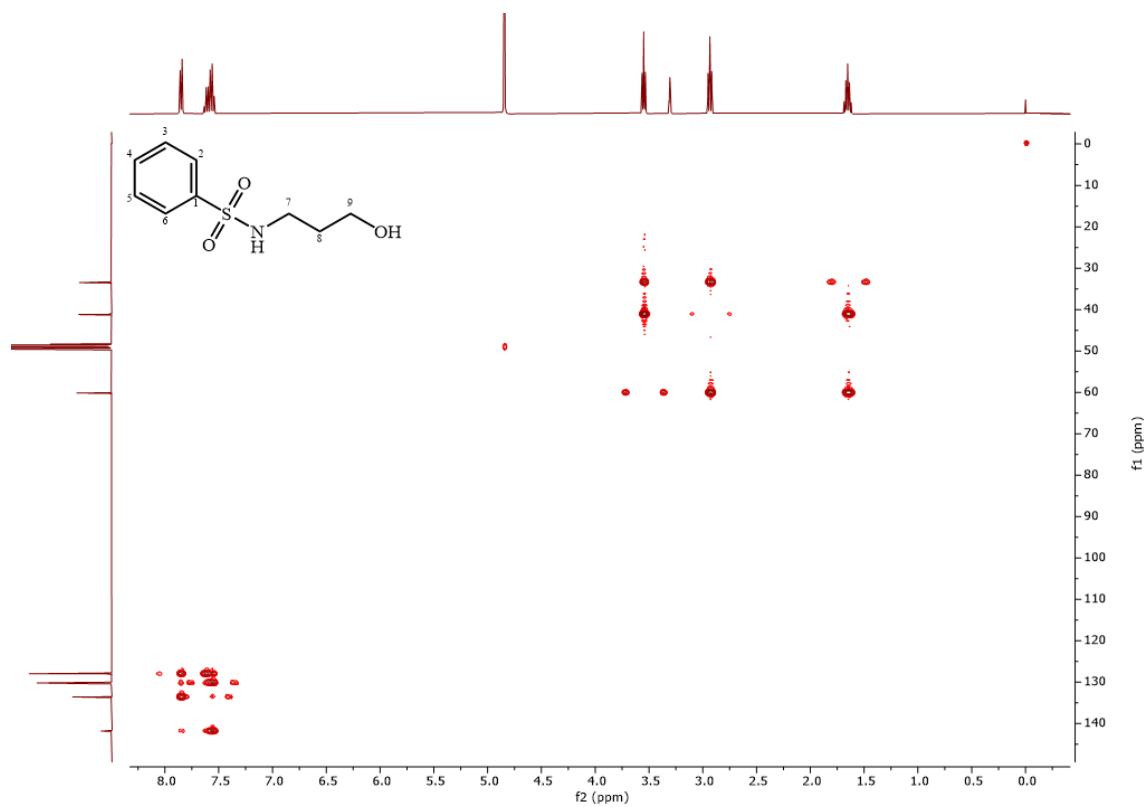
Figure S 188 HMBC spectrum of compound **5.2** in methanol-d$_4$, 400/100 MHz.

Figure S 189 (-)-ESI-HRMS spectrum of compound **5.3**.
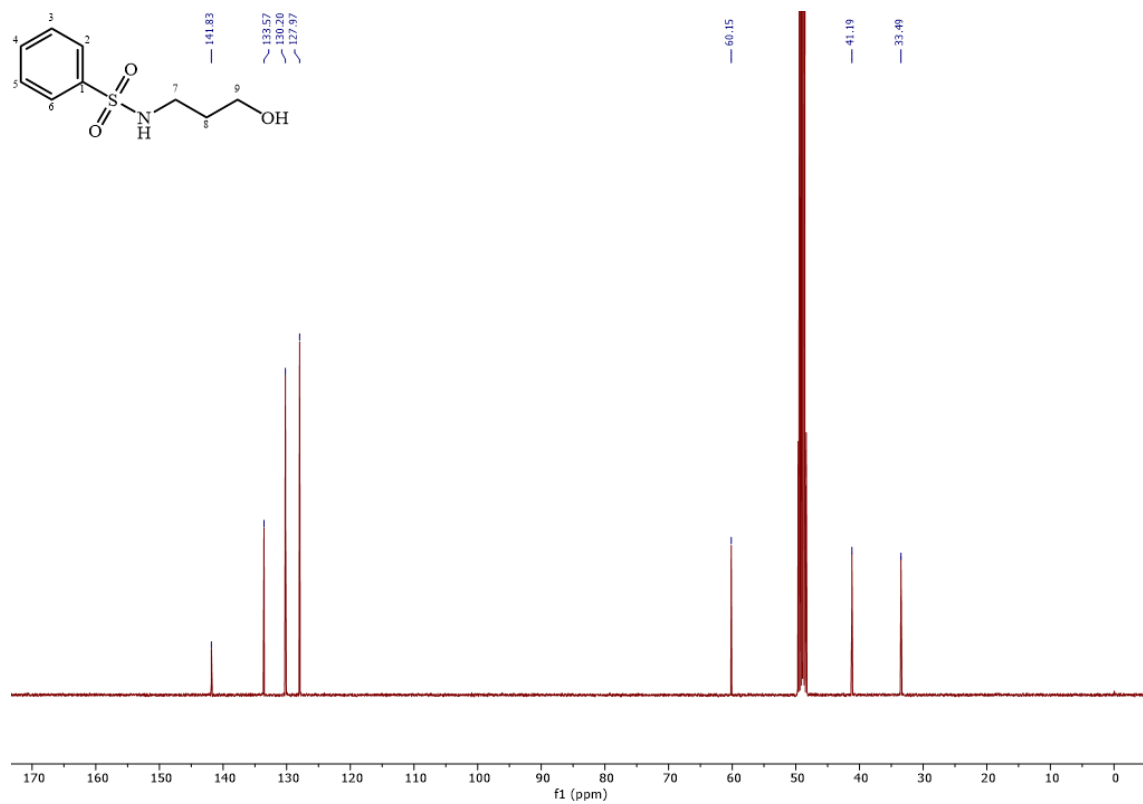
Figure S 190 ^{13}C spectrum of compound **5.3** in methanol-d$_4$, 100 MHz.

Figure S 191 ^{13}C spectrum of compound **5.3** in methanol-d$_4$, 400 MHz.
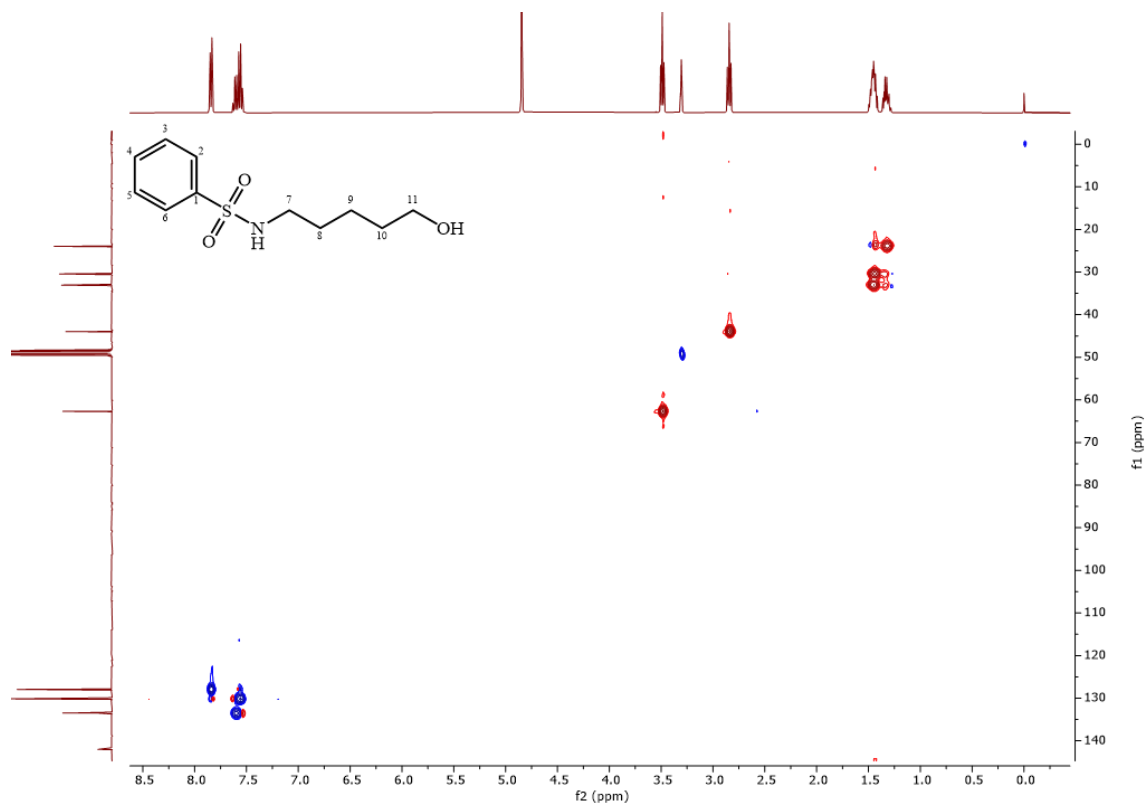

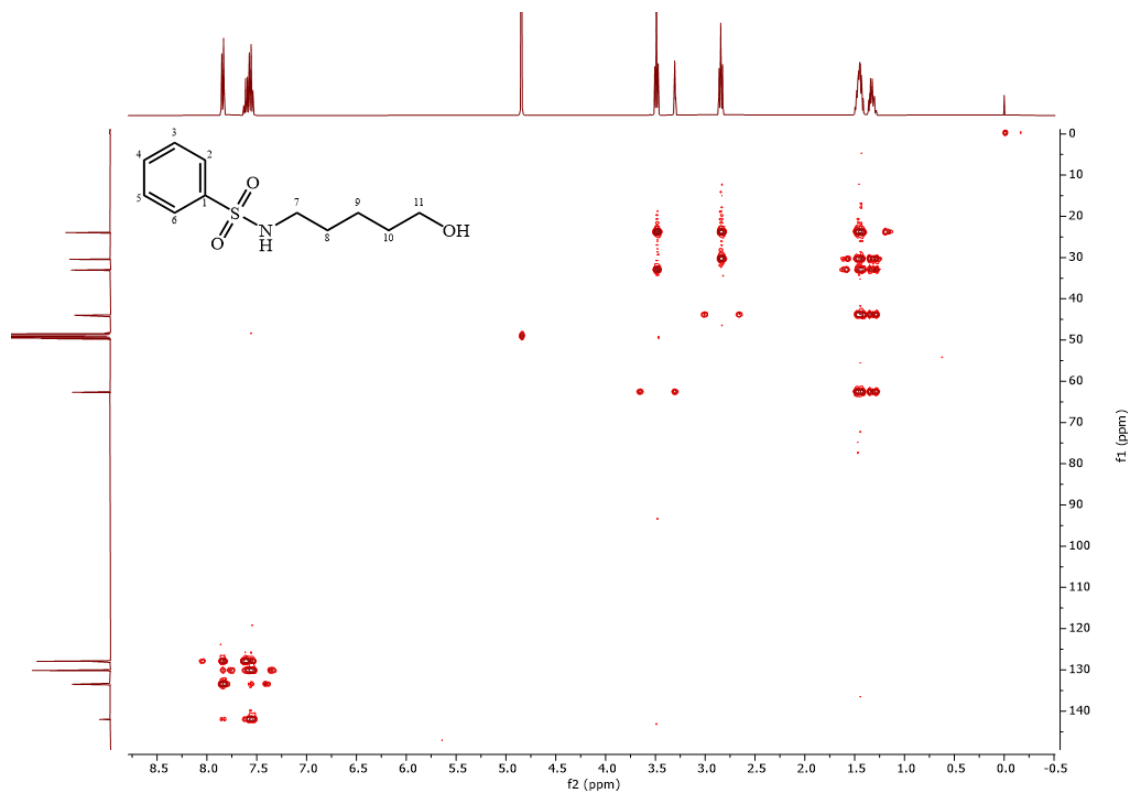**Figure S 192** HSQC spectrum of compound **5.3** in methanol-d$_4$, 400/100 MHz.

Figure S 193 HMBC spectrum of compound **5.3** in methanol-d4, 400/100 MHz.

[M-H]⁻
242.0857
$C_{11}H_{16}O_3NS$
4.97 ppm

Figure S 194 (-)-ESI-HRMS spectrum of compound **5.4**.

Figure S 195 ^{13}C spectrum of compound **5.4** in methanol-d$_4$, 100 MHz.

Figure S 196 ^{1}H spectrum of compound **5.4** in methanol-d$_4$, 400 MHz.

Figure S 197 HSQC spectrum of compound **5.4** in methanol-d₄, 400/100 MHz.

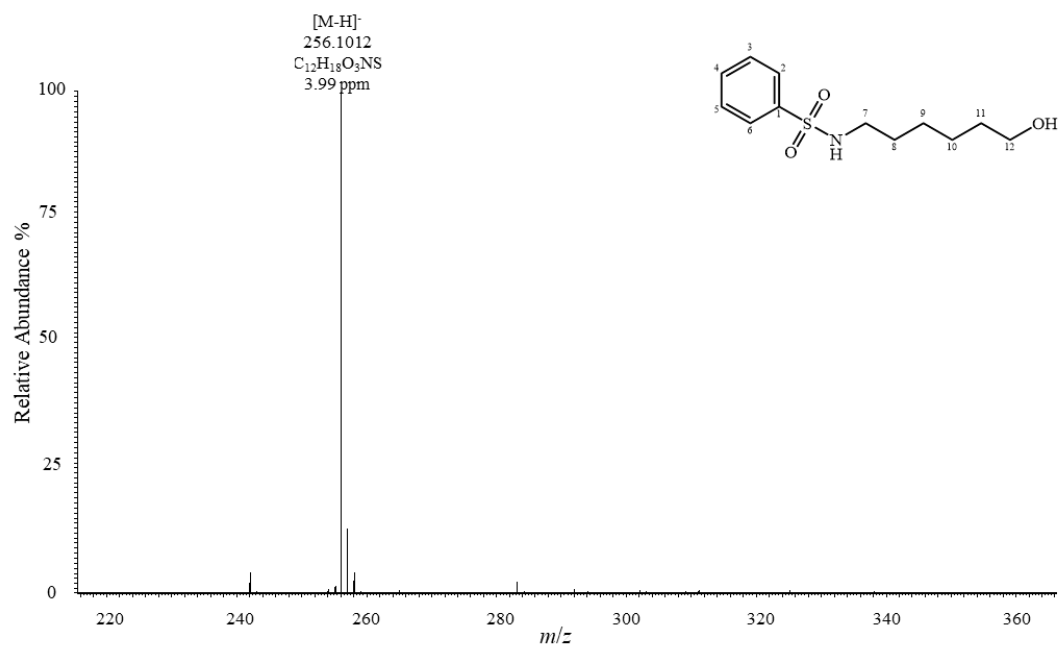**Figure S 198** HMBC spectrum of compound **5.4** in methanol-d₄, 400/100 MHz.

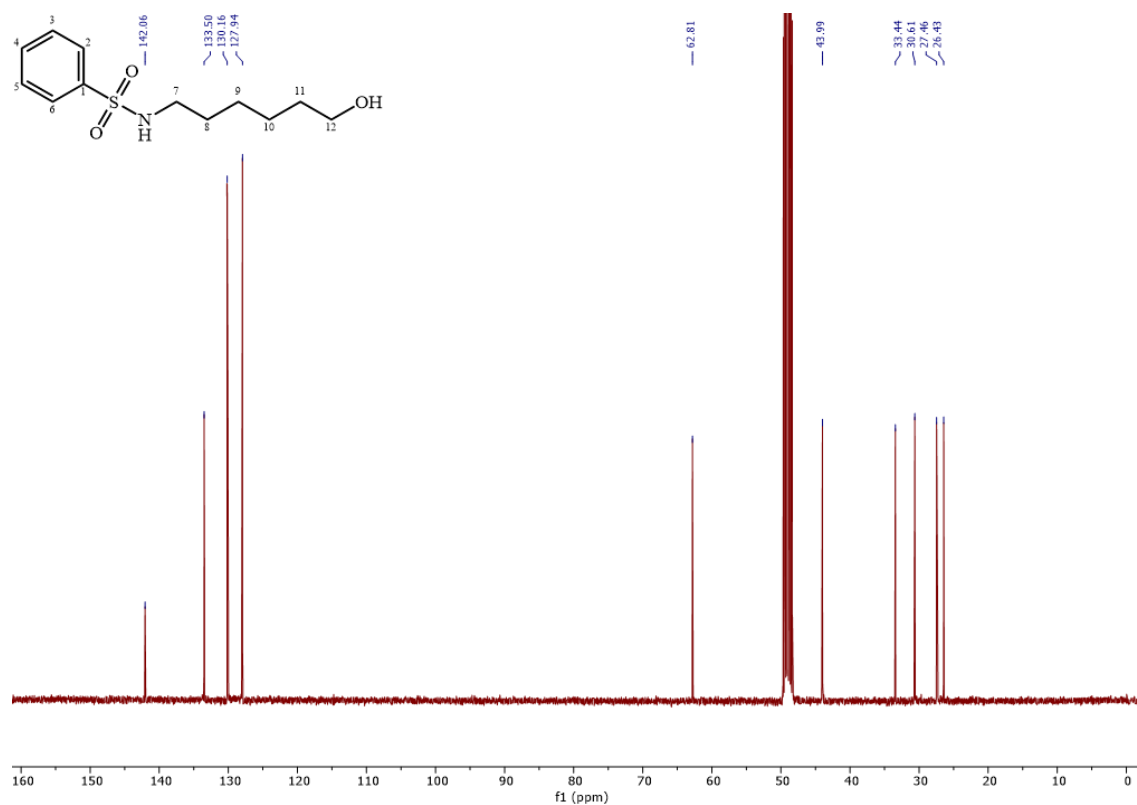**Figure S 199** (-)-ESI-HRMS spectrum of compound **5.5**.

Figure S 200 ^{13}C spectrum of compound **5.5** in methanol-d$_4$, 100 MHz.
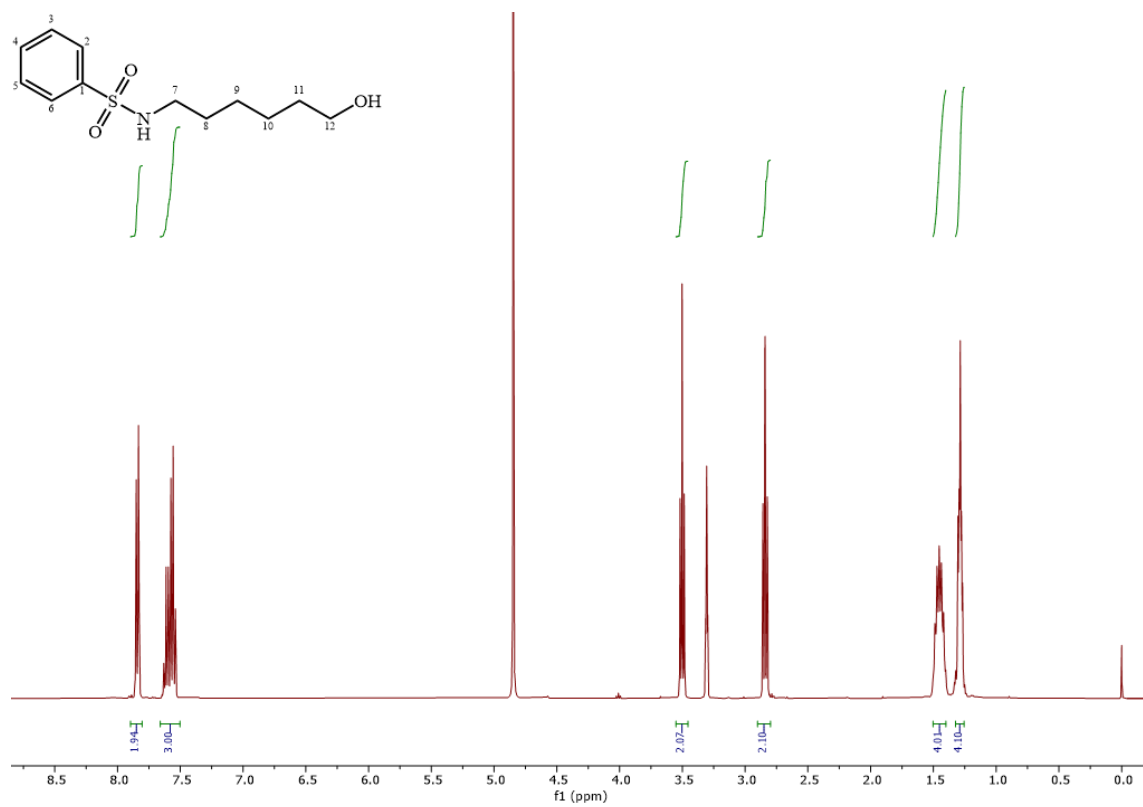
Figure S 201 ^{1}H spectrum of compound **5.5** in methanol-d$_4$, 400 MHz.
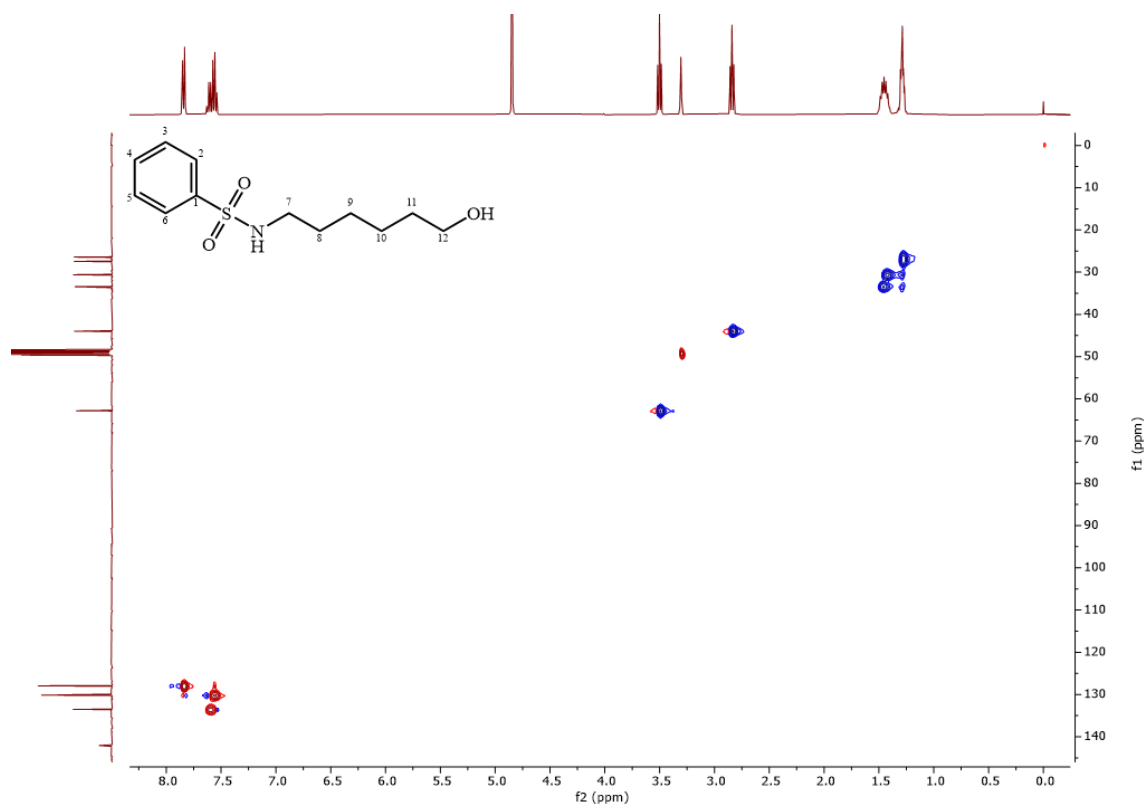

Figure S 202 HSQC spectrum of compound **5.5** in methanol-d$_4$, 400/100 MHz.
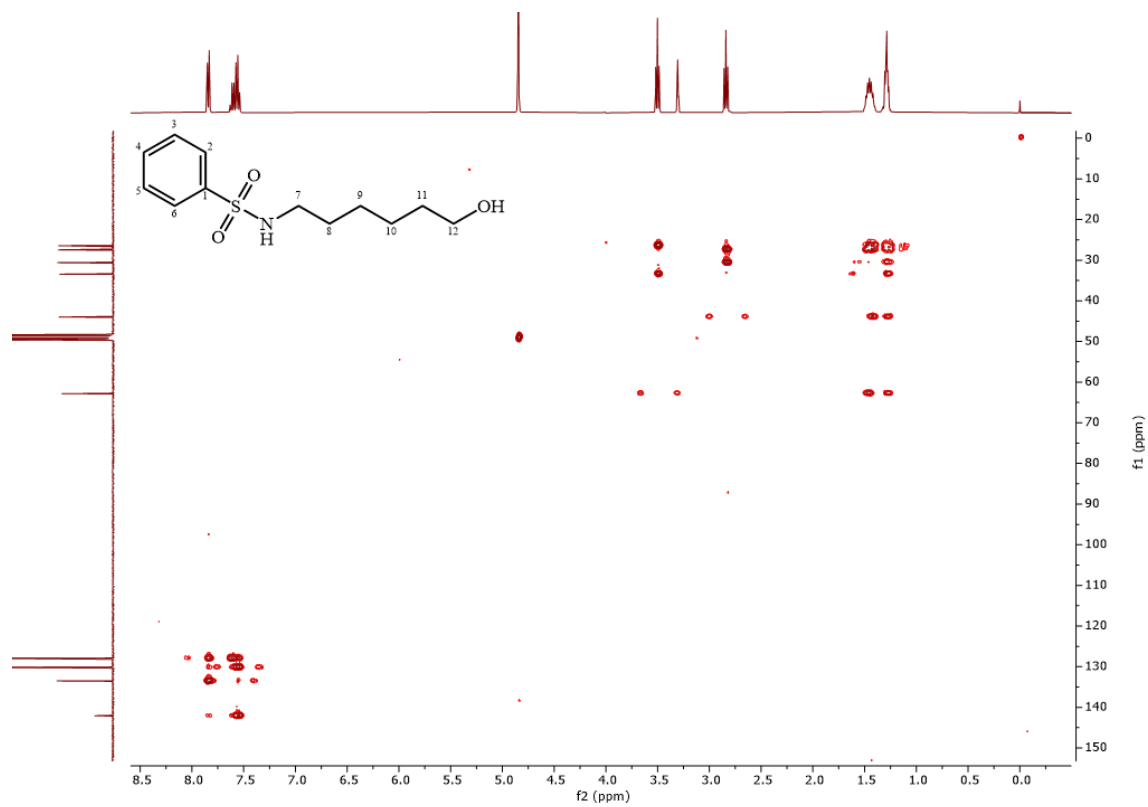
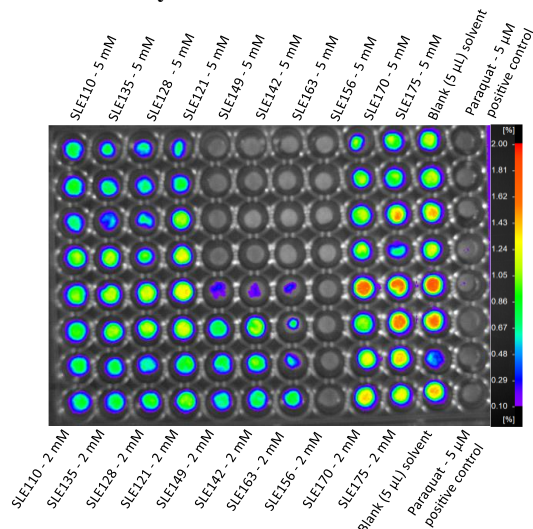**Figure S 203** HMBC spectrum of compound **5.5** in methanol-d4, 400/100 MHz.

3LC-IPB	Compound	3LC-IPB	Compound
SLE110	6.1a	SLE246	6.27
SLE111	6.1b	SLE247	6.28
SLE112	6.1c	SLE248	6.29
SLE113	6.1d	SLE249	6.30
SLE114	6.1e	SLE250	6.31
SLE115	6.1f	SLE160	6.12e
SLE116	6.1g	SLE161	6.12f
SLE117	6.1h	SLE162	6.12g
SLE118	6.1i	SLE163	6.11a
SLE119	6.1j	SLE164	6.11b
SLE120	6.1k	SLE165	6.11c
SLE121	6.4a	SLE166	6.11d
SLE122	6.4b	SLE167	6.11e
SLE123	6.4c	SLE168	6.11f
SLE124	6.4d	SLE169	6.11g
SLE125	6.4e	SLE170	6.2a
SLE126	6.4f	SLE171	6.2b
SLE127	6.4g	SLE172	6.2c
SLE128	6.6a	SLE173	6.2d
SLE129	6.6b	SLE174	6.2e
SLE130	6.6c	SLE175	6.3a
SLE131	6.6d	SLE176	6.3b
SLE132	6.6e	SLE177	6.3c
SLE133	6.6f	SLE178	6.3d
SLE134	6.6g	SLE179	6.3e
SLE135	6.5a	SLE180	6.32
SLE136	6.5b	SLE181	6.7a
SLE137	6.5c	SLE182	6.7b
SLE138	6.5d	SLE183	6.15a
SLE139	6.5e	SLE184	6.15b
SLE140	6.5f	SLE185	6.15c
SLE141	6.5g	SLE186	6.15d
SLE142	6.9a	SLE187	6.15e
SLE143	6.9b	SLE188	6.16c
SLE144	6.9c	SLE189	6.16e
SLE145	6.9d	SLE190	6.16f
SLE146	6.9e	SLE191	6.16g
SLE147	6.9f	SLE192	6.13a
SLE148	6.9g	SLE193	6.13b
SLE149	6.8a	SLE194	6.13d
SLE150	6.8b	SLE195	6.13e
SLE151	6.8c	SLE196	6.13f
SLE152	6.8d	SLE197	6.13g
SLE153	6.8e	SLE206	6.15f
SLE154	6.8f	SLE207	6.15g
SLE155	6.8g	SLE208	6.16a
SLE156	6.12a	SLE209	6.16b
SLE157	6.12b	SLE210	6.16d
SLE158	6.12c	SLE211	6.13c
SLE159	6.12d	SLE212	6.10a
SLE218	6.19b	SLE213	6.10b
SLE219	6.17a	SLE214	6.10c
SLE220	6.17b	SLE215	6.18a
SLE221	6.17c	SLE216	6.19a
SLE222	6.17d	SLE217	6.18b
SLE223	6.17e	SLE267	6.12h
SLE224	6.17f	SLE268	6.12i
SLE225	6.17g	SLE269	6.13h
SLE239	6.20	SLE270	6.13i
SLE240	6.21	SLE271	6.14a
SLE241	6.22	SLE272	6.14b
SLE242	6.23	SLE273	6.14c
SLE243	6.24		
SLE244	6.25		
SLE245	6.26		

Figure S 204 Internal IPB-code and compound number of sulfonamide derivatives in chapter 6.
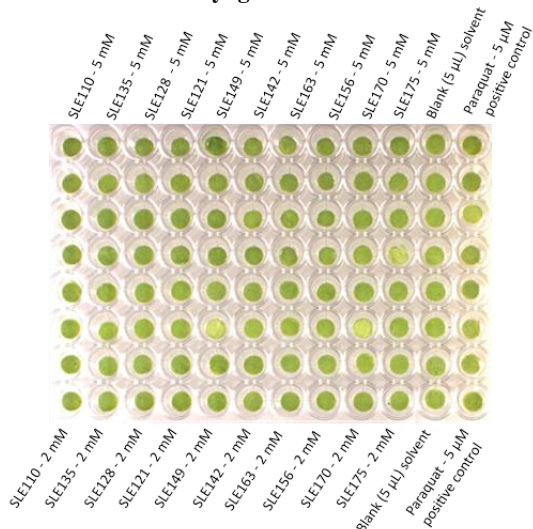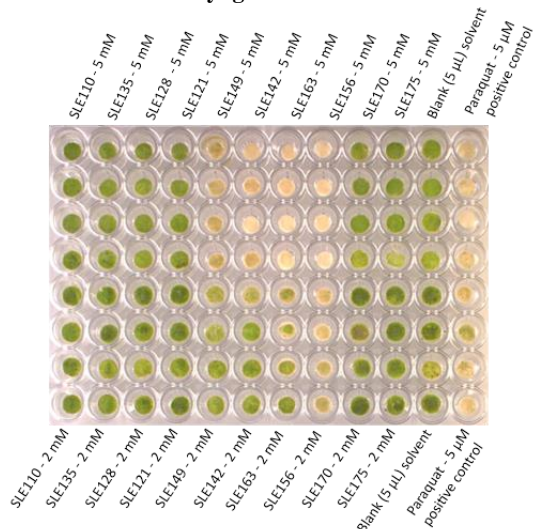
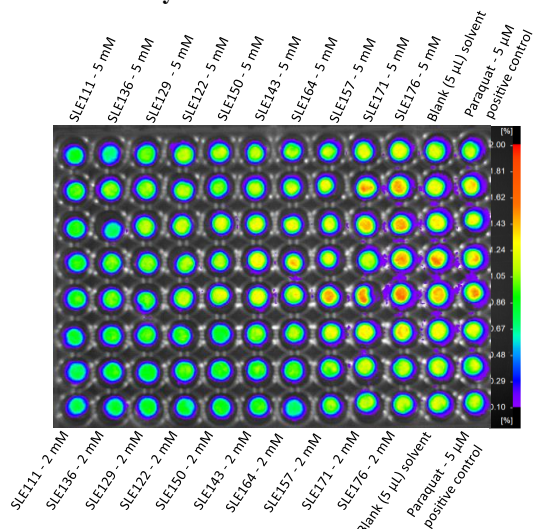**Delayed Fluorescence – t = 0 h**

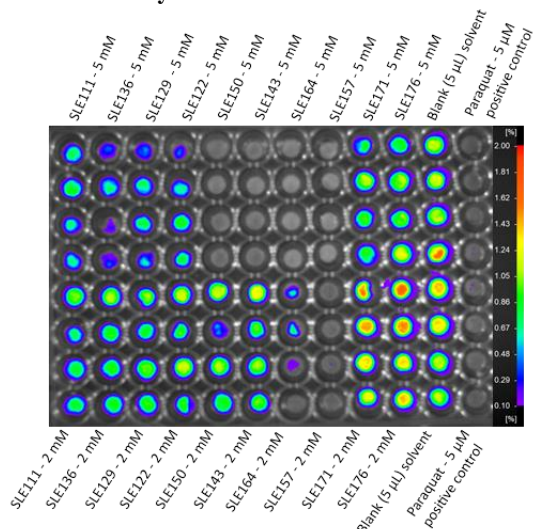
Delayed Fluorescence – t = 48 h
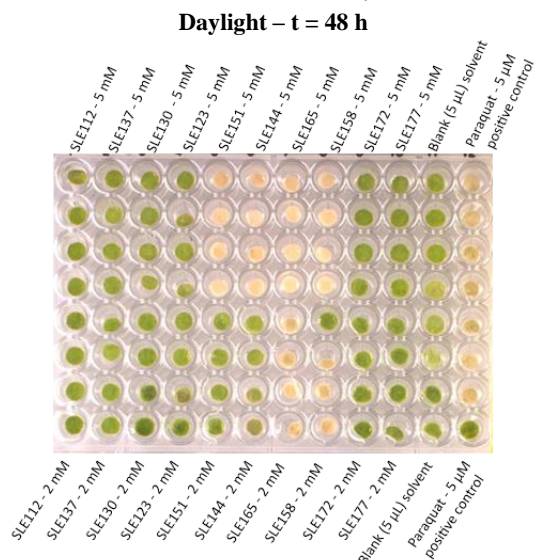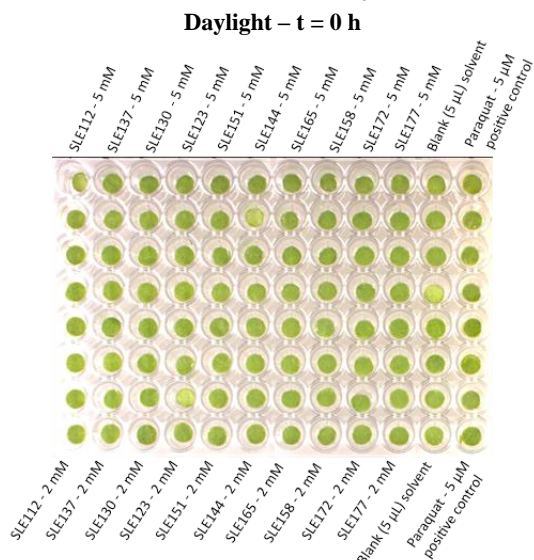

Daylight – t = 0 h

Daylight – t = 48 h

Delayed Fluorescence – t = 0 h

Delayed Fluorescence – t = 48 h

Daylight – t = 0 h

SLE111 - 5 mM, SLE136 - 5 mM, SLE129 - 5 mM, SLE122 - 5 mM, SLE150 - 5 mM, SLE143 - 5 mM, SLE164 - 5 mM, SLE157 - 5 mM, SLE171 - 5 mM, SLE176 - 5 mM, Blank (5 μL) solvent, Paraquat - 5 μM positive control

SLE111 - 2 mM, SLE136 - 2 mM, SLE129 - 2 mM, SLE122 - 2 mM, SLE150 - 2 mM, SLE143 - 2 mM, SLE164 - 2 mM, SLE157 - 2 mM, SLE171 - 2 mM, SLE176 - 2 mM, Blank (5 μL) solvent, Paraquat - 5 μM positive control

Daylight – t = 48 h

SLE111 - 5 mM, SLE136 - 5 mM, SLE129 - 5 mM, SLE122 - 5 mM, SLE150 - 5 mM, SLE143 - 5 mM, SLE164 - 5 mM, SLE157 - 5 mM, SLE171 - 5 mM, SLE176 - 5 mM, Blank (5 μL) solvent, Paraquat - 5 μM positive control

SLE111 - 2 mM, SLE136 - 2 mM, SLE129 - 2 mM, SLE122 - 2 mM, SLE150 - 2 mM, SLE143 - 2 mM, SLE164 - 2 mM, SLE157 - 2 mM, SLE171 - 2 mM, SLE176 - 2 mM, Blank (5 μL) solvent, Paraquat - 5 μM positive control
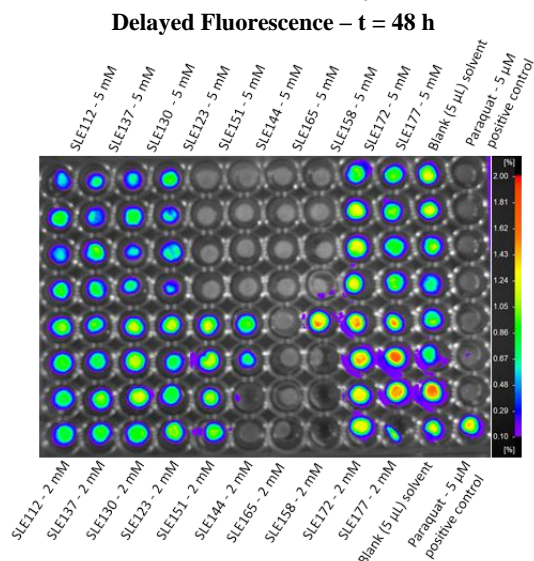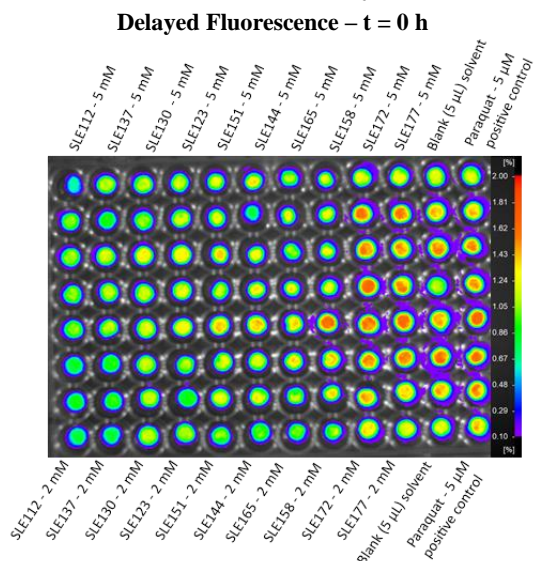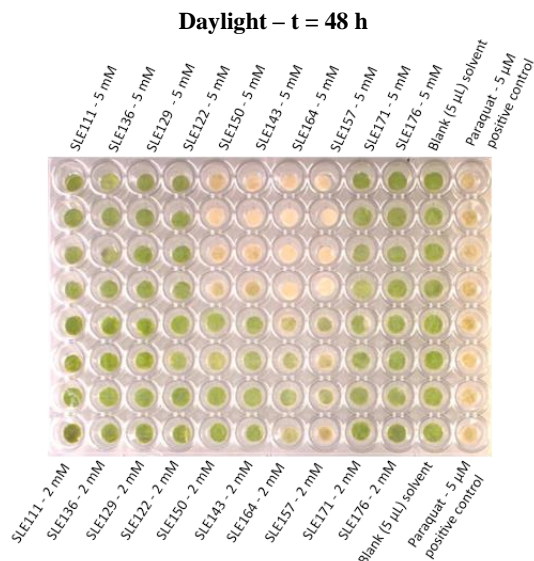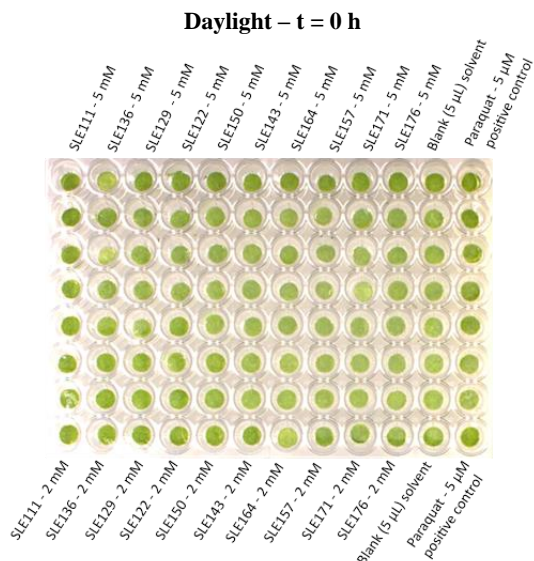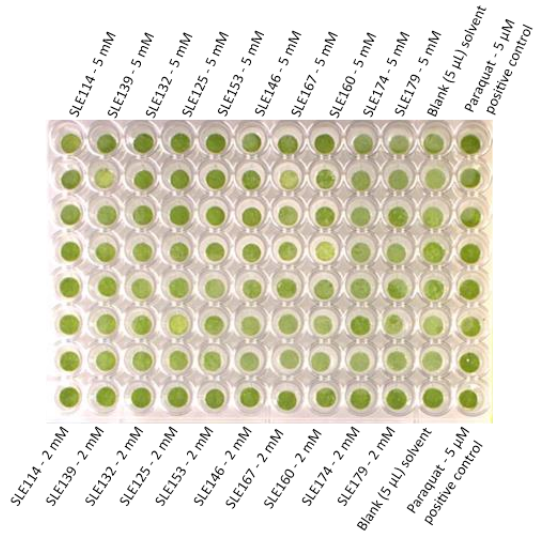
Delayed Fluorescence – t = 0 h

SLE112 - 5 mM, SLE137 - 5 mM, SLE130 - 5 mM, SLE123 - 5 mM, SLE151 - 5 mM, SLE144 - 5 mM, SLE165 - 5 mM, SLE158 - 5 mM, SLE172 - 5 mM, SLE177 - 5 mM, Blank (5 μL) solvent, Paraquat - 5 μM positive control

SLE112 - 2 mM, SLE137 - 2 mM, SLE130 - 2 mM, SLE123 - 2 mM, SLE151 - 2 mM, SLE144 - 2 mM, SLE165 - 2 mM, SLE158 - 2 mM, SLE172 - 2 mM, SLE177 - 2 mM, Blank (5 μL) solvent, Paraquat - 5 μM positive control

Delayed Fluorescence – t = 48 h

SLE112 - 5 mM, SLE137 - 5 mM, SLE130 - 5 mM, SLE123 - 5 mM, SLE151 - 5 mM, SLE144 - 5 mM, SLE165 - 5 mM, SLE158 - 5 mM, SLE172 - 5 mM, SLE177 - 5 mM, Blank (5 μL) solvent, Paraquat - 5 μM positive control

SLE112 - 2 mM, SLE137 - 2 mM, SLE130 - 2 mM, SLE123 - 2 mM, SLE151 - 2 mM, SLE144 - 2 mM, SLE165 - 2 mM, SLE158 - 2 mM, SLE172 - 2 mM, SLE177 - 2 mM, Blank (5 μL) solvent, Paraquat - 5 μM positive control

Daylight – t = 0 h

SLE112 - 5 mM, SLE137 - 5 mM, SLE130 - 5 mM, SLE123 - 5 mM, SLE151 - 5 mM, SLE144 - 5 mM, SLE165 - 5 mM, SLE158 - 5 mM, SLE172 - 5 mM, SLE177 - 5 mM, Blank (5 μL) solvent, Paraquat - 5 μM positive control

SLE112 - 2 mM, SLE137 - 2 mM, SLE130 - 2 mM, SLE123 - 2 mM, SLE151 - 2 mM, SLE144 - 2 mM, SLE165 - 2 mM, SLE158 - 2 mM, SLE172 - 2 mM, SLE177 - 2 mM, Blank (5 μL) solvent, Paraquat - 5 μM positive control

Daylight – t = 48 h

SLE112 - 5 mM, SLE137 - 5 mM, SLE130 - 5 mM, SLE123 - 5 mM, SLE151 - 5 mM, SLE144 - 5 mM, SLE165 - 5 mM, SLE158 - 5 mM, SLE172 - 5 mM, SLE177 - 5 mM, Blank (5 μL) solvent, Paraquat - 5 μM positive control

SLE112 - 2 mM, SLE137 - 2 mM, SLE130 - 2 mM, SLE123 - 2 mM, SLE151 - 2 mM, SLE144 - 2 mM, SLE165 - 2 mM, SLE158 - 2 mM, SLE172 - 2 mM, SLE177 - 2 mM, Blank (5 μL) solvent, Paraquat - 5 μM positive control

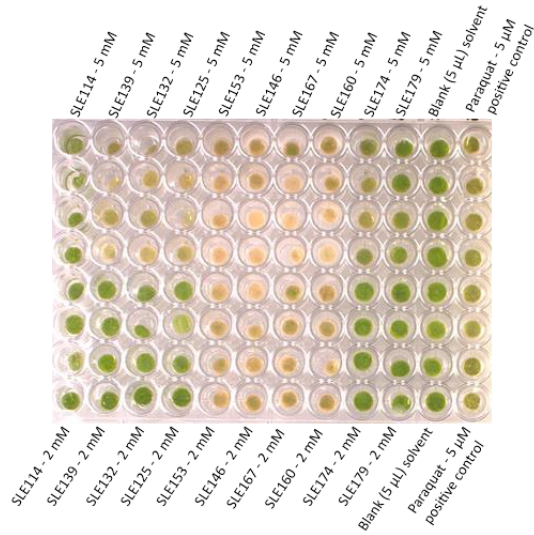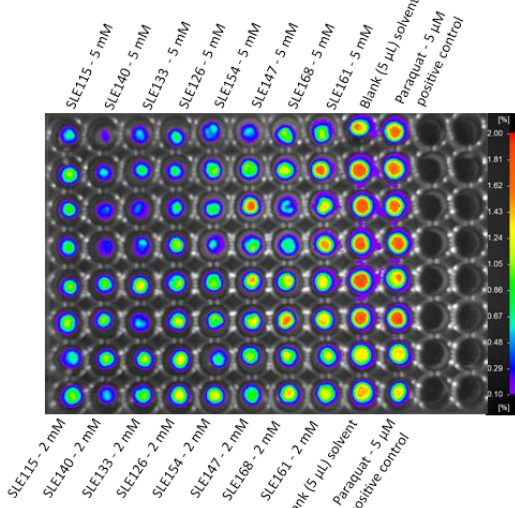**Delayed Fluorescence – t = 0 h**

Delayed Fluorescence – t = 48 h

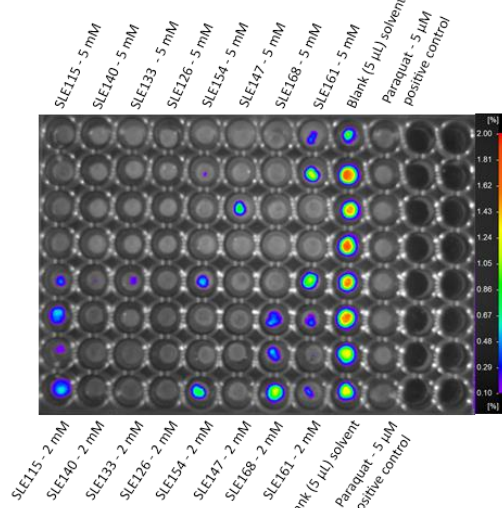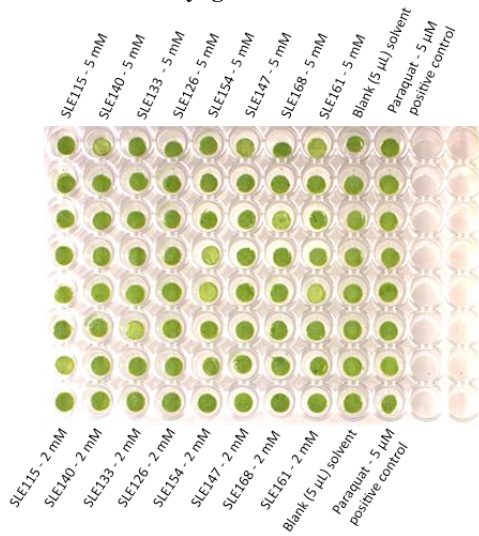**Daylight – t = 0 h**

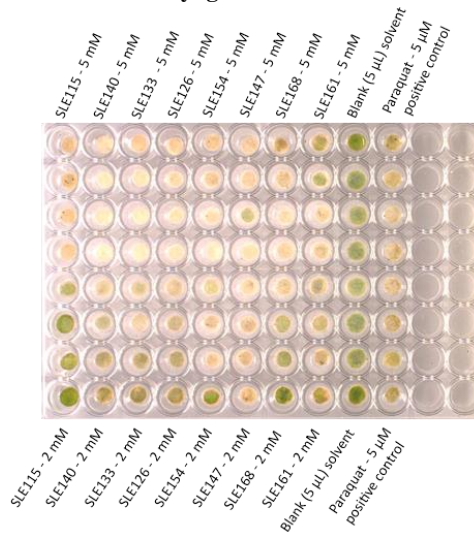
Daylight – t = 48 h

Delayed Fluorescence – t = 0 h
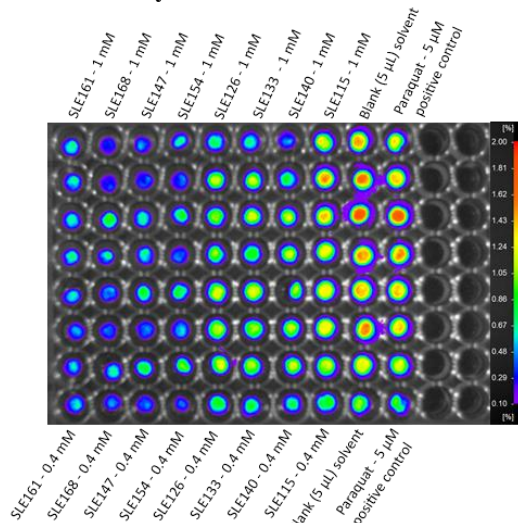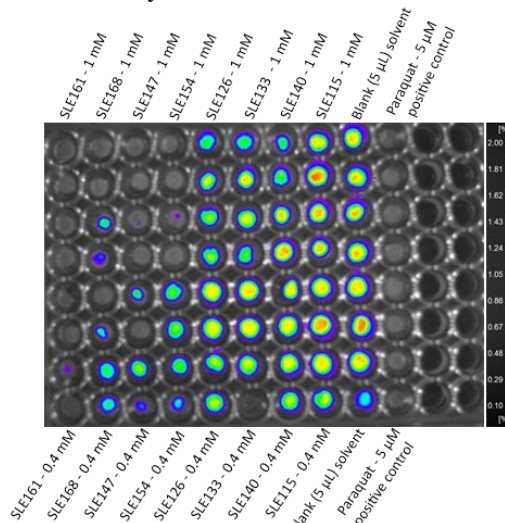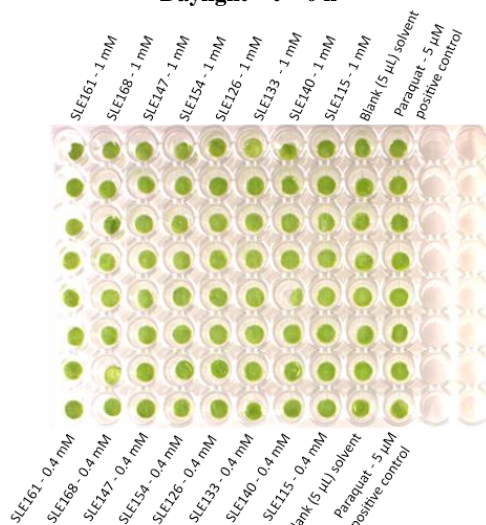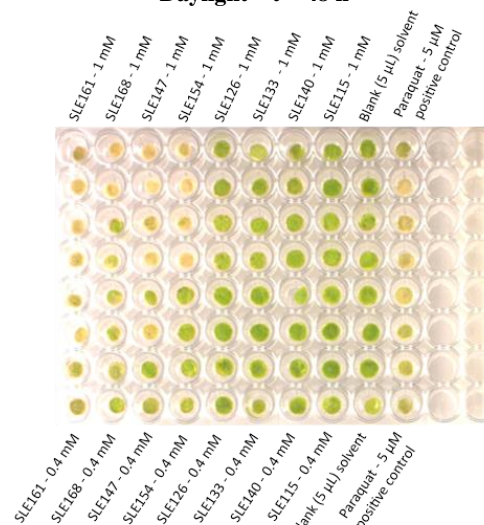

Delayed Fluorescence – t = 48 h

231

Daylight – t = 0 h

Daylight – t = 48 h

Delayed Fluorescence – t = 0 h

Delayed Fluorescence – t = 48 h

Daylight – t = 0 h

Daylight – t = 48 h

Delayed Fluorescence – t = 0 h
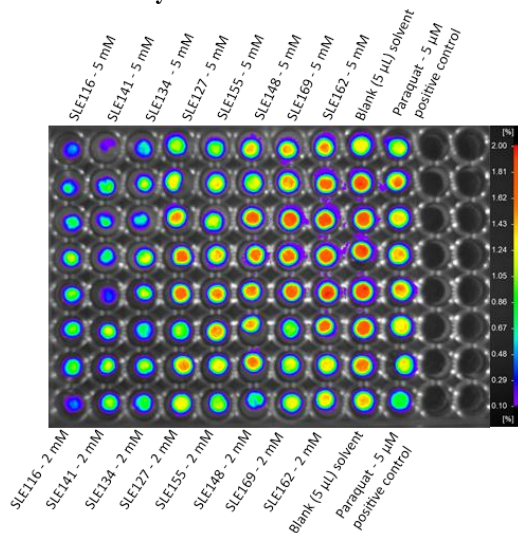

Delayed Fluorescence – t = 48 h

Daylight – t = 0 h

Daylight – t = 48 h

Delayed Fluorescence – t = 0 h

Delayed Fluorescence – t = 48 h

233

Daylight – t = 0 h

Daylight – t = 48 h

Delayed Fluorescence – t = 0 h

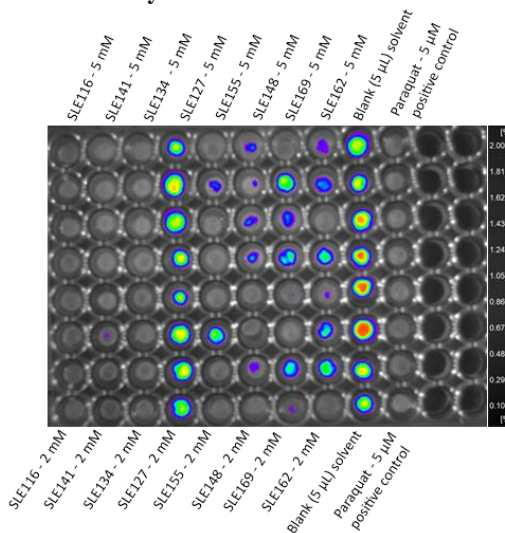**Delayed Fluorescence – t = 48 h**
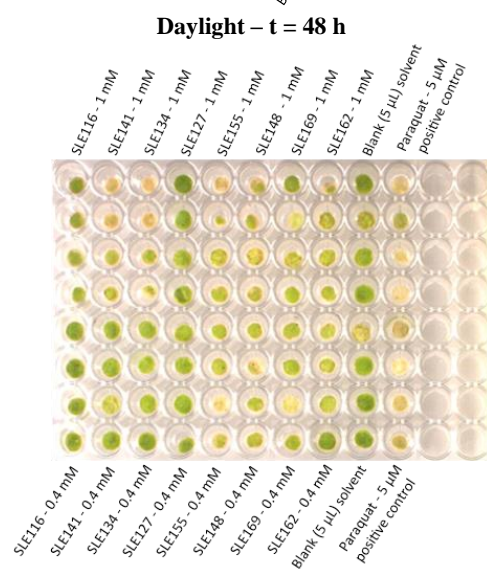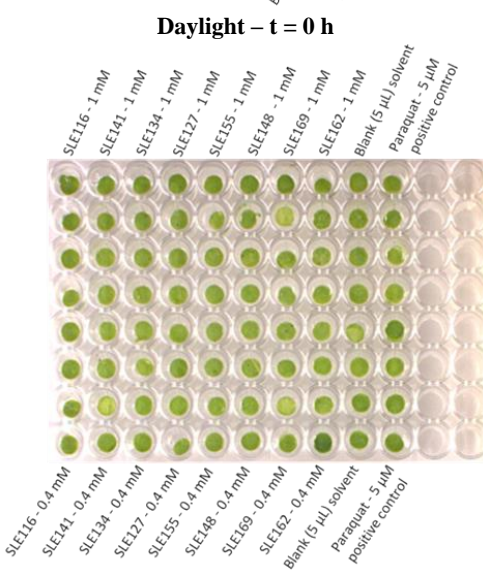
Daylight – t = 0 h

Daylight – t = 48 h

234

Delayed Fluorescence – t = 0 h

Delayed Fluorescence – t = 48 h

Daylight – t = 0 h

Daylight – t = 48 h

Delayed Fluorescence – t = 0 h

Delayed Fluorescence – t = 48 h

235

Daylight – t = 0 h

Daylight – t = 48 h

Delayed Fluorescence – t = 0 h

Delayed Fluorescence – t = 48 h

Daylight – t = 0 h

Daylight – t = 48 h

Delayed Fluorescence – t = 0 h

Delayed Fluorescence – t = 48 h

Daylight – t = 0 h

Daylight – t = 48 h

Delayed Fluorescence – t = 0 h

Delayed Fluorescence – t = 48 h

Daylight – t = 0 h

Daylight – t = 48 h

Delayed Fluorescence – t = 0 h

Delayed Fluorescence – t = 48 h

Daylight – t = 0 h

Daylight – t = 48 h

Delayed Fluorescence – t = 0 h

Delayed Fluorescence – t = 48 h

Daylight – t = 0 h

Daylight – t = 48 h

Delayed Fluorescence – t = 0 h

Delayed Fluorescence – t = 48 h

Daylight – t = 0 h

Daylight – t = 48 h

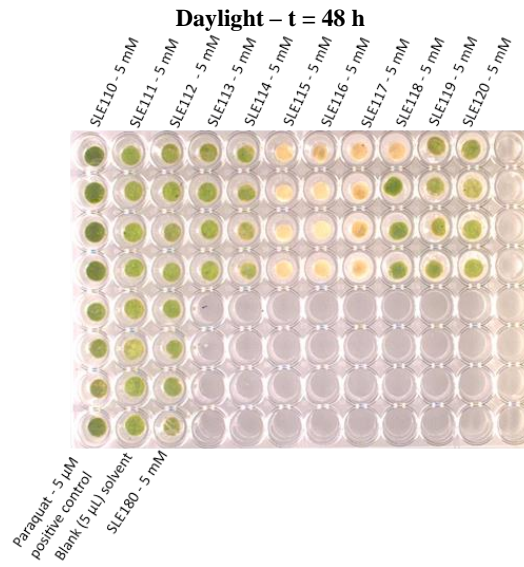missing

Delayed Fluorescence – t = 0 h
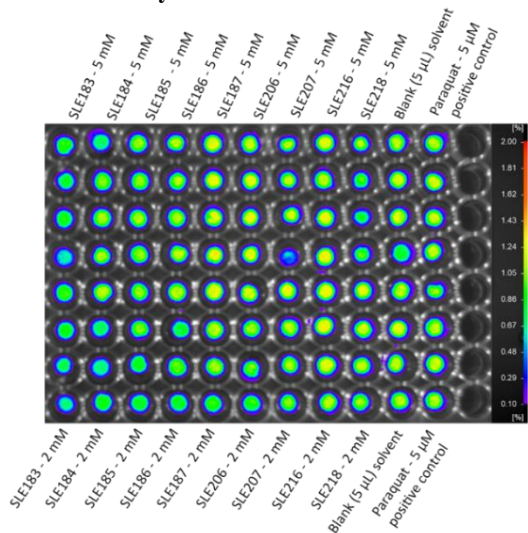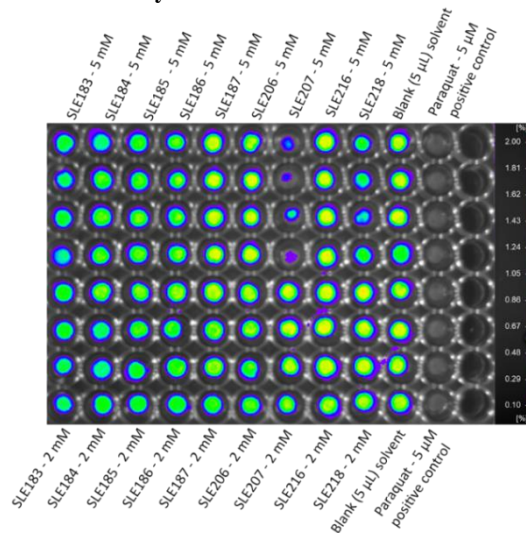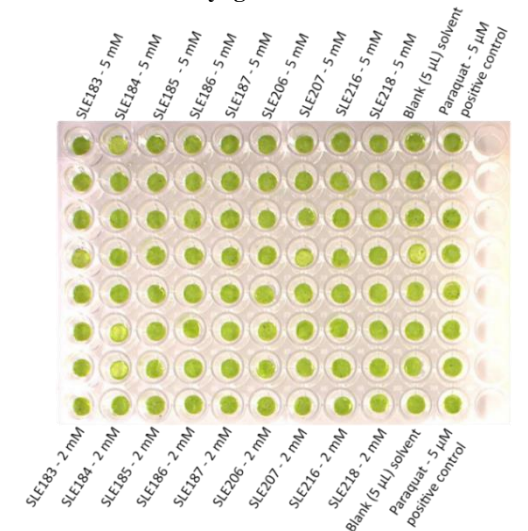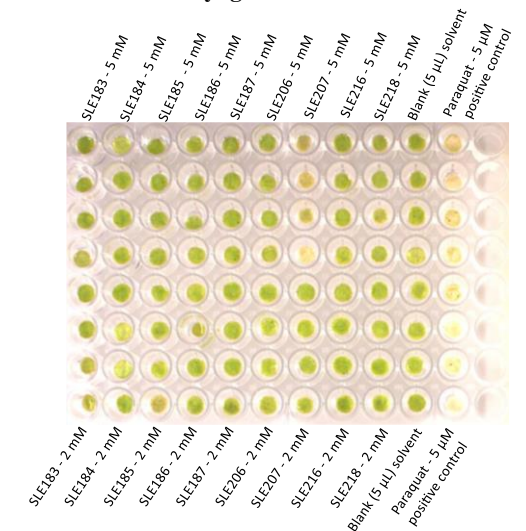
Delayed Fluorescence – t = 48 h

Daylight – t = 0 h

Daylight – t = 48 h

Delayed Fluorescence – t = 0 h
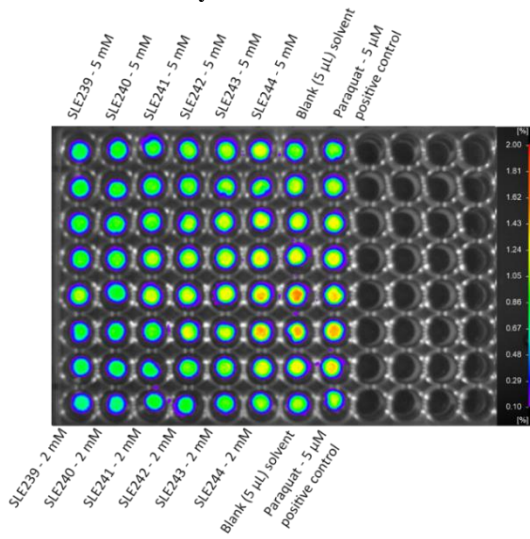
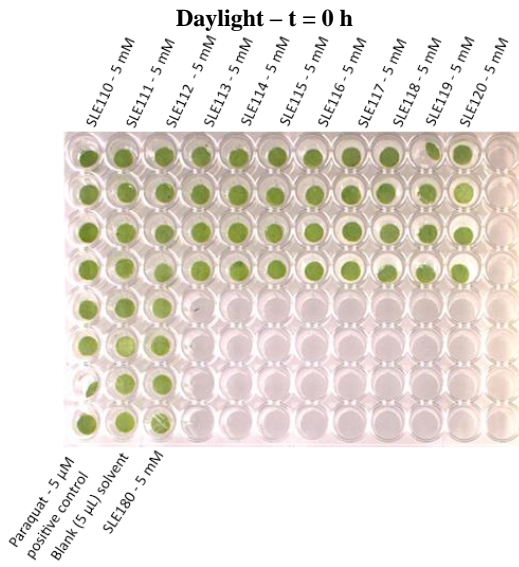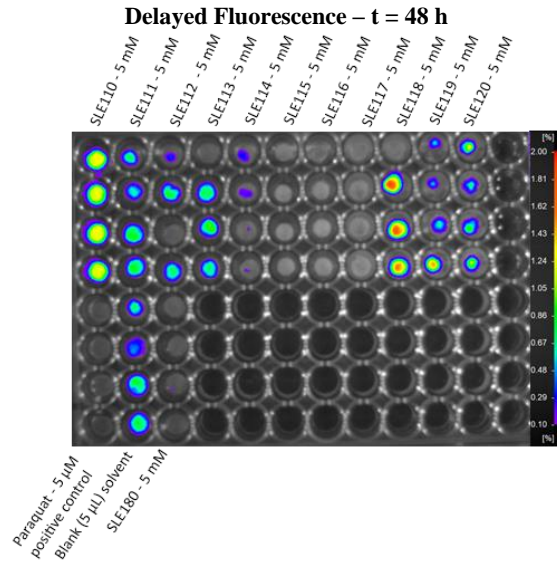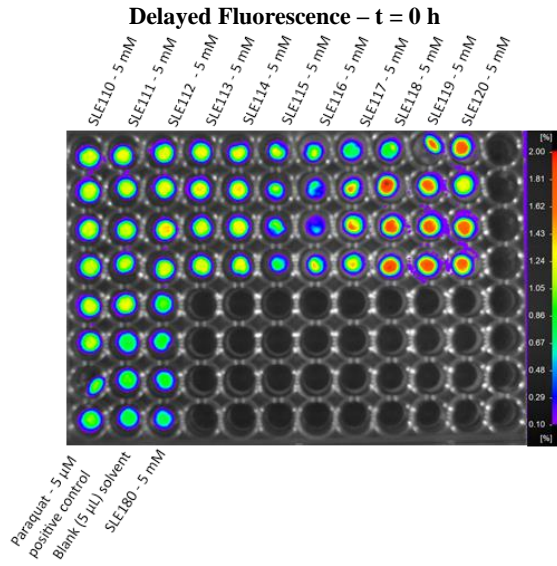**Delayed Fluorescence – t = 48 h**
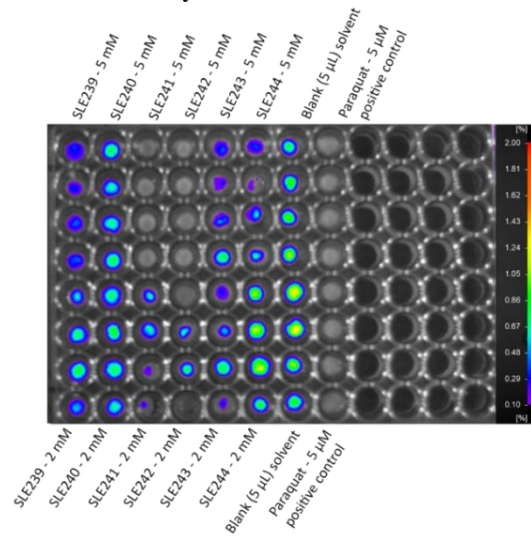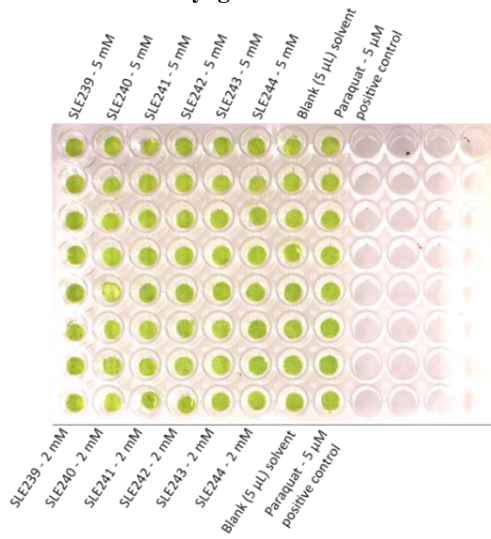
Daylight – t = 0 h
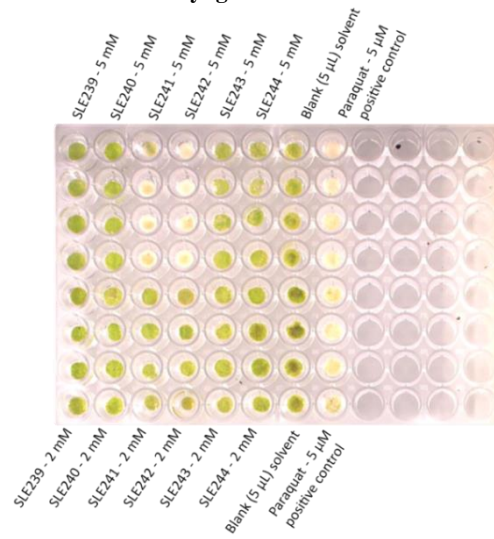
Daylight – t = 48 h

Delayed Fluorescence – t = 0 h
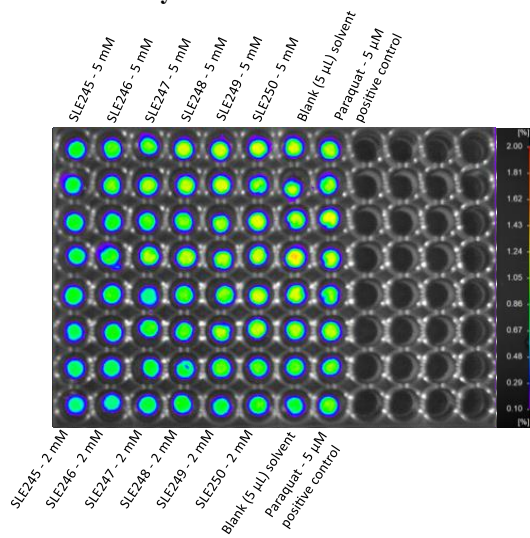
Delayed Fluorescence – t = 48 h
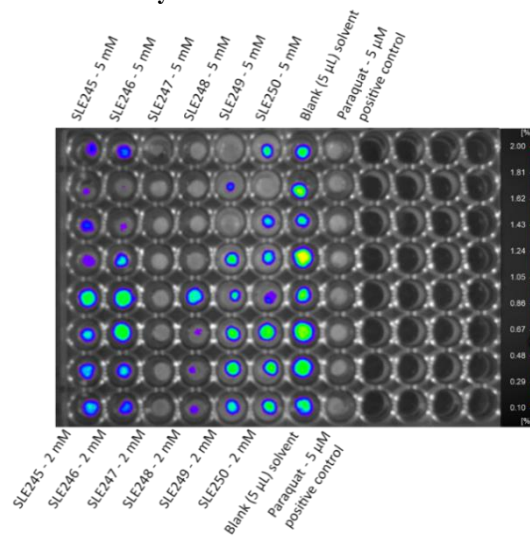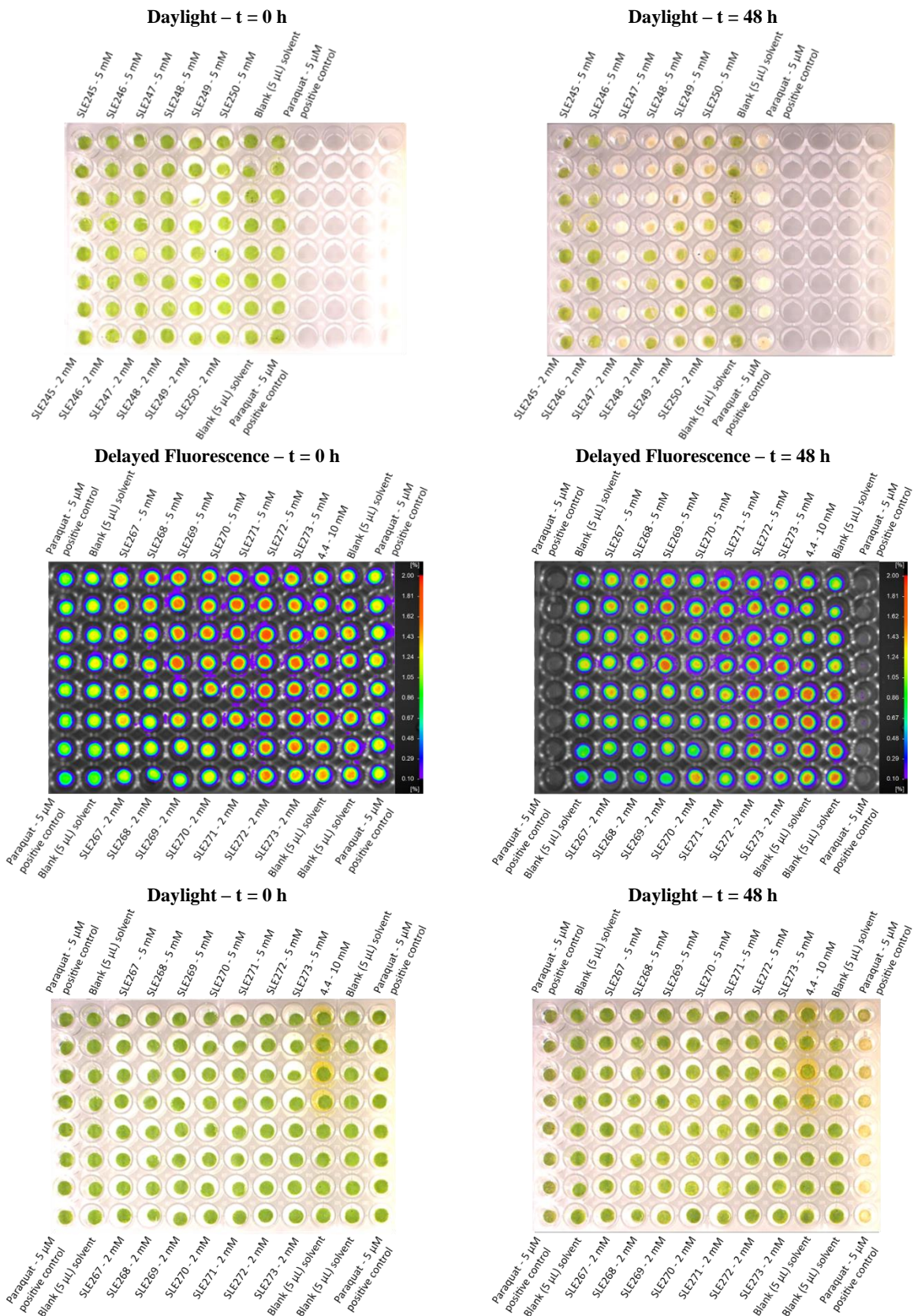
Figure S 205 Compounds **6.1 – 6.32** in the non-destructive leaf disk assay on *A. thaliana* Col-0 (DF and daylight images) at t = 0 h and t = 48 h. Red to yellow-green color of the leaf disks: strong DF; blue-purple color of the leaf disks: low DF; gray color of the leaf disks: no DF.

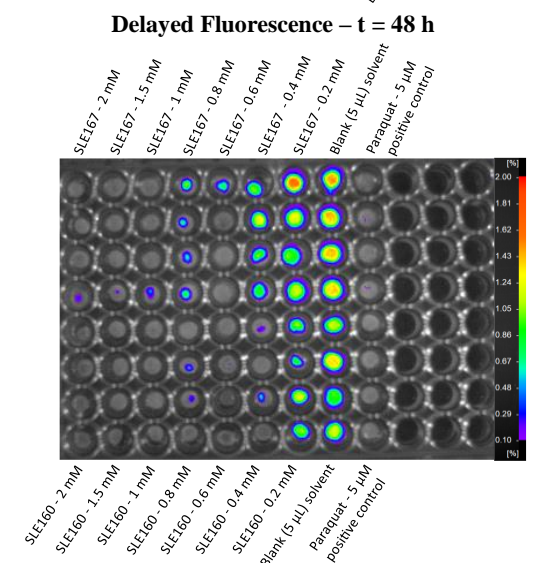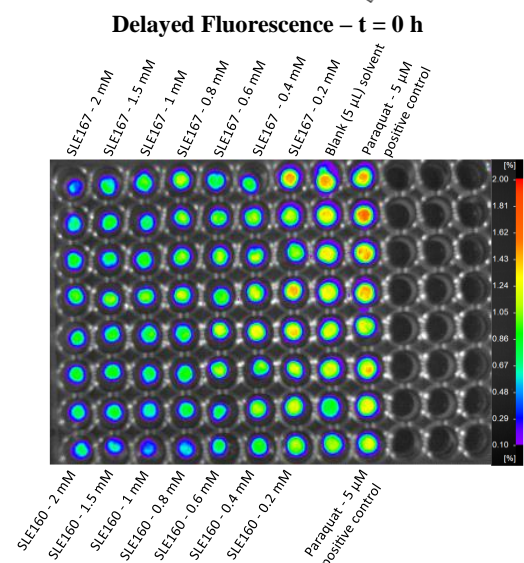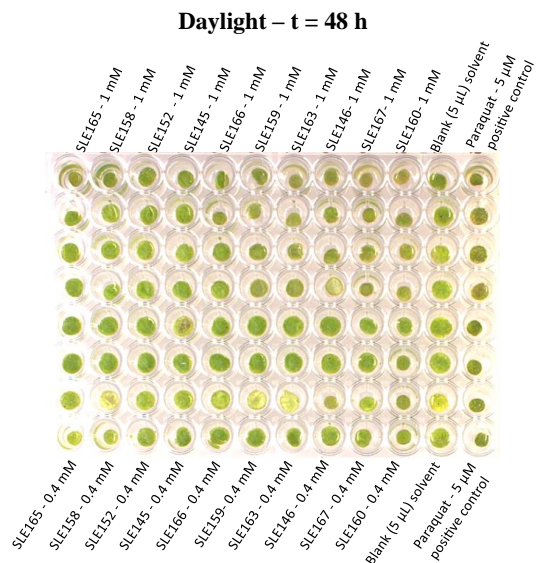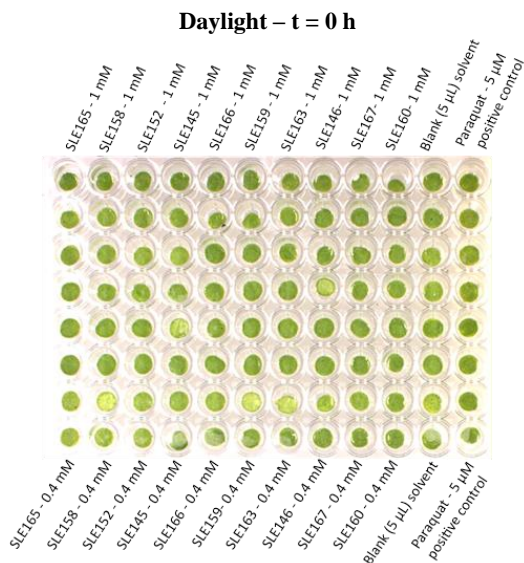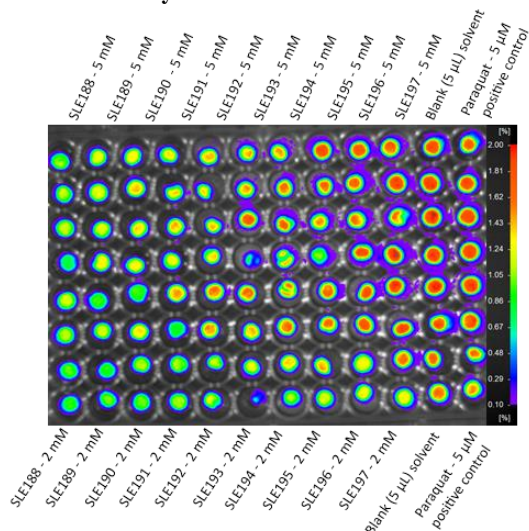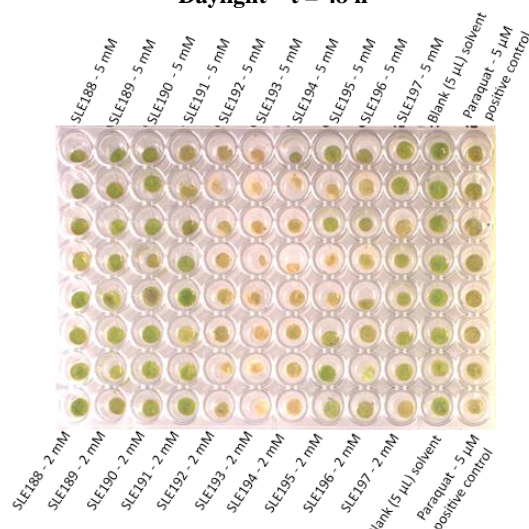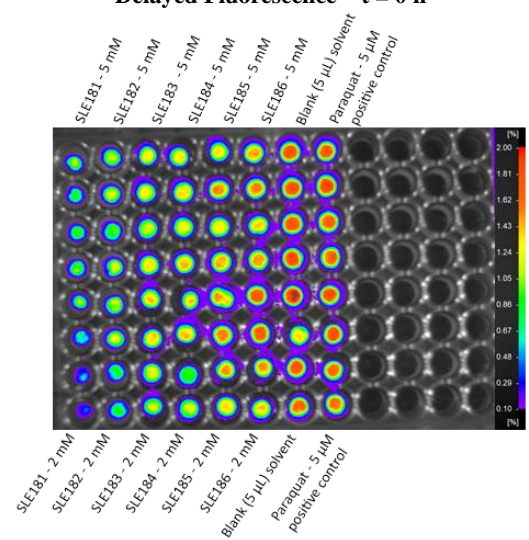| No.	[M+H]⁺	Rt (min)	formula	Δ ppm	Fragment ions (intensity)	Annotation
P1	175.1189	0.17	$C_6H_{15}O_2N_4$	-0.23	158.0920 (100), 130.0972 (42), 116.0703 (64)	Arginine
P2	104.1068	0.19	$C_5H_{14}ON$	-1.42	87.0438 (100), 85.0285 (46), 60.0805 (14)	Choline
P3	258.1095	0.20	$C_8H_{21}NO_6P$	4.07	104.1067 (100)	Glycero-phosphocholine
P4	118.0861	0.26	$C_5H_{12}O_2N$	-1.13	72.0806 (100)	
P5	268.1037	0.33	$C_{10}H_{14}O_4N_5$	-1.35	136.0615 (100)	Adenosine
P6	132.1016	0.35	$C_6H_{14}O_2N$	-2.13	86.0961 (100)	(Iso-)Leucine
P7	166.0861	0.58	$C_9H_{12}O_2N$	-0.87	120.0806 (100)	Phenylalanine
P8	693.4168	4.70	$C_{32}H_{55}O_8N_9$	-0.01	675.4066 (57), 581.3649 (29) 563.3544 (100), 435.2597 (54), 323.2076 (15)	Unknown
P9	301.0699	6.68	$C_{16}H_{13}O_6$	-0.81	286.0466 (100), 283.0596 (22), 273.0752 (13), 271.0595 (12), 255.0647 (25)	Unknown Anthraquinone
P10	351.2141	7.02	$C_{20}H_{31}O_5$	-7.01	333.2051 (9), 223.0938 (100)	Unknown
P11	195.1015	7.40	$C_{11}H_{15}O_3$	-0.52	177.0907 (6), 163.0753 (22), 149.0959 (10), 135.0803 (46), 107.0854 (100)	Colletopyrone
P12	315.0857	7.55	$C_{17}H_{15}O_6$	-3.71	300.0621 (100), 282.0517 (92)	Colletoquinone A
P13	277.2160	7.57	$C_{18}H_{29}O_2$	-0.84	259.2053 (77), 241.1948 (40), 195.1378 (18), 149.1323 (45), 135.1167 (100), 121.1010 (26)	Unknown
P14	295.2264	7.88	$C_{18}H_{31}O_3$	-1.12	277.2159 (100)	Unknown
P15	335.2189	8.86	$C_{20}H_{31}O_4$	-8.40	317.2078 (6), 195.0988 (100)	Unknown
P16	520.3393	9.64	$C_{30}H_{48}O_7$ $C_{29}H_{42}O_2N_7$	-0.30 -0.31	184.0731 (100)	Unknown
P17	1009.5316	9.80	$C_{44}H_{73}O_{15}N_{12}$	-0.34	979.5211 (20), 897.4794 (11)	Unknown

P18	391.2445	9.95	$C_{21}H_{33}O_4N_3$	-6.71	373.2340 (24), 317.2079 (100), 279.1608 (5), 149.0231 (8)	Unknown
P19	454.2919	10.13	$C_{23}H_{40}O_6N_3$	0.48	436.2816 (100), 393.2395 (5), 313.2734 (32)	Unknown
P20	496.3387	10.17	$C_{26}H_{46}O_6N_3$	1.21	478.3284 (100), 184.0732 (34)	Unknown
P21	933.6255	10.22	$C_{47}H_{83}O_{10}N_9$	-0.86	915.6158 (53), 821.5743 (40), 803.5635 (100), 677.3860 (6), 577.4210 (41), 548.3079 (13)	Unknown peptide
P22	481.2912	11.91	$C_{26}H_{41}O_4N_3Na$	-1.00	355.2236 (100)	Unknown
P23	425.2861	12.01	$C_{20}H_{40}O_5N_3Na$	0.70	-	Unknown

Figure S 206 UHPLC-HR-ESI-MS peak list of compounds annotated from *C. graminicola* cultivated in medium 1 (myzelium).

No.	[M+H]$^+$	Rt (min)	formula	Δ ppm	Fragment ions (intensity)	Annotation
P1	175.1189	0.17	$C_6H_{15}O_2N_4$	0.47	158.0920 (100), 130.0972 (42), 116.0703 (64)	Arginine
P2	104.1068	0.19	$C_5H_{14}ON$	-1.43	87.0438 (100), 85.0285 (46), 60.0805 (14)	Choline
P3	258.1099	0.20	$C_8H_{21}NO_6P$	-0.22	104.1067 (100)	Glycero-phosphocholine
P4	118.0862	0.26	$C_5H_{12}O_2N$	-0.78	72.0806 (100)	
P5	268.1039	0.33	$C_{10}H_{14}O_4N_5$	-0.54	136.0615 (100)	Adenosine
P6	132.1018	0.35	$C_6H_{14}O_2N$	-0.76	86.0961 (100)	(Iso-)Leucine
P7	166.0862	0.58	$C_9H_{12}O_2N$	-0.46	120.0806 (100)	Phenylalanine
P8	353.2296	7.22	$C_{20}H_{33}O_5$	-8.24	335.2191 (100), 317.2087 (6), 235.1307 (13), 195.0993 (40)	Unknown
P9	195.1016	7.40	$C_{11}H_{15}O_3$	-2.87	177.0907 (6), 163.0753 (22), 149.0961 (10), 135.0804 (46), 107.0854 (100)	Colletopyrone
P10	315.0861	7.56	$C_{17}H_{15}O_6$	-2.55	300.0624 (100), 282.0519 (92)	Colletoquinone A
P11	329.1019	8.42	$C_{18}H_{17}O_6$	-1.86	314.0781 (42), 296.0675 (100), 278.0570 (32), 268.0727 (65), 250.0622 (16)	Colletoquinone B
P12	335.2191	8.86	$C_{20}H_{31}O_4$	-9.20	317.2078 (4), 195.0988 (100)	Unknown
P13	344.3156	9.74	$C_{20}H_{42}O_3N$	-2.50	326.3052 (39), 300.2895 (100), 282.2790 (24)	Unknown
P14	1009.5325	9.84	$C_{44}H_{73}O_{15}N_{12}$	0.69	979.5211 (18), 897.4794 (10)	Unknown
P15	391.2452	9.96	$C_{21}H_{33}O_4N_3$	-4.85	373.2341(25), 317.2081 (100), 279.1608 (3), 149.0231 (7)	Unknown
P16	351.2524	9.97	$C_{21}H_{35}O_4$	-1.56	277.2158 (100), 167.1065 (60)	Unknown
P17	792.5664	10.02			748.5406 (9), 704.5145 (26), 660.4885 (57), 616.4622 (94), 572.4360 (100), 528.4098 (72), 484.3837 (35), 440.3575 (4)	Unknown
P18	496.3387	10.17	$C_{26}H_{46}O_6N_3$	1.20	478.3284 (100), 184.0732 (34)	Unknown
P19	718.5304	10.56			674.5038 (18), 630.4774 (62), 586.4512 (100), 542.4250 (72), 498.3990 (24)	Unknown
P20	481.2916	11.92	$C_{25}H_{41}O_7N_2$	0.39	355.2240 (100)	Unknown

Figure S 207 UHPLC-HR-ESI-MS peak list of compounds annotated from *C. graminicola* cultivated in medium 2 (myzelium).

No.	[M+H]+	Rt (min)	formula	Δ ppm	Fragment ions (intensity)	Annotation
P1	175.1190	0.17	$C_6H_{15}O_2N_4$	0.4658	158.0920 (100), 130.0972 (40), 116.0703 (64)	Arginine
P2	104.1068	0.19	$C_5H_{14}ON$	-1.735	87.0438 (100), 85.0285 (46), 60.0805 (14)	Choline
P3	258.1096	0.20	$C_8H_{21}NO_6P$	-0.51	104.1067 (100)	Glycero-phosphocholine
P4	268.1037	0.33	$C_{10}H_{14}O_4N_5$	-1.279	136.0615 (100)	Adenosine
P5	132.1018	0.35	$C_6H_{14}O_2N$	-0.9700	86.0961 (100)	(Iso-)Leucine
P6	166.0862	0.58	$C_9H_{12}O_2N$	-0.334	120.0806 (100)	Phenylalanine
P7	232.1541	0.99	$C_{11}H_{22}O_4N$	-0.968	173.0807 (100), 85.0282 (72)	Unknown
P8	301.0703	6.68	$C_{16}H_{13}O_6$	1.570	286.0467 (100), 283.0596 (22), 273.0753 (14), 271.0598 (12), 255.0647 (24)	Unknown anthraquinone
P9	351.0626	6.88	$C_{17}H_{16}O_6Cl$	-2.617	336.0392 (76), 334.0599 (69), 333.0522 (38), 319.0366 (100), 315.0861 (65), 305.0573 (15), 255.0648 (5)	Colletoanthrone
P10	195.1015	7.40	$C_{11}H_{15}O_3$	-2.932	177.0907 (6), 163.0753 (22), 149.0959 (10), 135.0803 (45), 107.0854 (100)	Colletopyrone
P11	315.0860	7.56	$C_{17}H_{15}O_6$	-2.647	300.0621 (100), 282.0517 (92)	Colletoquinone A
P12	365.0783	7.93	$C_{18}H_{18}O_6Cl$	-0.993	334.0600 (100)	Monorden
P13	319.0363	8.10	$C_{16}H_{12}O_5Cl$	-1.654	301.0258 (100), 291.0415 (89), 273.0310 (45)	Unknown
P14	567.1276	8.32	$C_{29}H_{18}O_9N_3$	-0.442	552.1047 (29), 535.1020 (100)	Unknown
P15	1009.5315	9.80	$C_{44}H_{73}O_{15}N_{12}$ $C_{59}H_{77}O_{14}$	-0.341 0.161	979.5211 (20), 897.4794 (11)	Unknown
P16	454.2921	10.15	$C_{23}H_{40}O_6N_3$	0.879	436.2819 (100), 393.2399 (5), 313.2736 (36)	Unknown
P17	496.3387	10.16	$C_{26}H_{46}O_6N_3$	-0.022	478.3284 (100), 184.0732 (33)	Unknown
P18	933.6255	10.22	$C_{47}H_{83}O_{10}N_9$	-0.856	915.6158 (53), 821.5743 (40), 803.5635 (100), 677.3860 (6), 577.4210 (41), 548.3079 (13)	Unknown peptide
P19	482.3233	11.13	$C_{25}H_{44}O_6N_3$	-0.425	464.3124 (100), 421.2704 (6),341.3043 (38)	Unknown
P20	524.3704	11.16	$C_{28}H_{50}O_6N_3$	1.807	506.3594 (100), 184.0731 (28)	Unknown

Figure S 208 UHPLC-HR-ESI-MS peak list of compounds annotated from *C. graminicola* cultivated in medium 3 (myzelium).

No.	[M+H]$^+$	Rt (min)	formula	Δ ppm	Fragment ions (intensity)	Annotation
P1	258.1093	0.11	$C_8H_{21}NO_6P$	-0.77	240.0976 (62), 196.1078 (37), 104.1068 (100)	Glycero-phosphocholine
P2	175.1188	0.17	$C_6H_{15}O_2N_4$	-1.09	158.0920 (100), 130.0972 (42), 116.0703 (64)	Arginine
P3	182.0811	0.32	$C_9H_{12}O_3N$	-0.62	165.0545 (100), 136.0756 (28)	Tyrosine
P4	132.1017	0.39	$C_6H_{14}O_2N$	-1.23	86.0961 (100)	(Iso-)Leucine
P5	166.0861	0.60	$C_9H_{12}O_2N$	-0.87	120.0805 (100)	Phenylalanine
P6	146.1175	0.65	$C_7H_{16}O_2N$	-0.63	128.1068 (100)	Unknown
P7	252.1227	4.17	$C_{13}H_{18}O_4N$	-1.25	206.1172 (100), 192.1016 (77)	Unknown
P8	485.2597	4.32	$C_{21}H_{41}O_{12}$	0.99	467.2492 (26), 373.2079 (4), 355.1966 (100), 243.1328 (9)	Unknown
P9	727.3859	4.63	$C_{30}H_{57}O_{15}N_5$	1.88	709.3757 (100), 691.3655 (16), 615.3341 (56), 597.3195 (90), 485.2608 (34), 467.2447 (34), 355.1955 (59), 243.1322 (19)	Unknown
P10	183.0915	4.63	$C_{12}H_{11}N_4$	-1.16	141.9583 (100)	Unknown
P11	741.4019	4.67	$C_{29}H_{57}O_{14}N_8$	4.10	723.3909 (38), 629.3494 (62), 611.3375 (98), 596.3282 (100), 467.2495 (18), 369.2015 (32), 257.1491 (11)	Unknown
P12	195.1013	7.39	$C_{11}H_{15}O_3$	-1.22	163.0751 (24), 149.0957 (10), 135.0802 (44), 107.0853 (100)	Colletopyrone
P13	315.0859	7.55	$C_{17}H_{15}O_6$	-1.38	315.0855 (9), 300.0620 (100), 282.0514 (92)	Colletoquinone A
P14	329.1015	8.41	$C_{18}H_{17}O_6$	-1.41	314.0780 (40), 296.0674 (100), 285.0757 (32), 268.0726 (63)	Colletoquinone B
P15	937.5847	9.36	$C_{45}H_{79}O_{12}N_9$	0.42	919.5737 (94), 825.5322 (48), 807.5192 (100), 695.4598 (18), 565.3844 (60), 467.2491 (16), 355.1973 (20)	Unknown peptide
P16	1009.5322	9.84	$C_{46}H_{75}O_{16}N_9$	-0.45	979.5228 (16), 897.4811 (10)	Unknown
P17	454.2924	10.14	$C_{23}H_{40}O_6N_3$	2.90	436.2814 (100), 393.2396 (4), 313.2733 (34)	Unknown
P18	496.3390	10.17	$C_{27}H_{40}ON_7$	-2.29	478.3278 (100), 184.0730 (34)	Unknown
P19	965.6147	10.22	$C_{46}H_{87}O_{16}N_5$	0.47	947.6047 (83), 835.5511 (100), 723.4917 (19), 593.4158 (68), 467.2486 (10), 355.1971 (22)	Unknown peptide
P20	1018.5273	10.43	$C_{55}H_{76}O_{15}N_3$ $C_{54}H_{70}O_{10}N_{10}$	0.23 0.24	1000.5165 (100), 888.4643 (42), 665.3453 (30), 489.2771 (28)	Unknown
P21	889.5632	11.41	$C_{44}H_{75}O_{10}N_9$	-0.37	871.5526 (90), 776.4792	Unknown peptide

(62), 629.4112 (100),
502.3117 (40), 388.2593
(14)

Figure S 209 UHPLC-HR-ESI-MS peak list of compounds annotated in *C. graminicola* cultivated in medium 4 (myzelium).

No.	$[M+H]^+$	Rt (min)	formula	Δ ppm	Fragment ions (intensity)	Annotation
P1	175.1189	0.17	$C_6H_{15}O_2N_4$	-0.24	158.0920 (100), 130.0972 (42), 116.0703 (64)	Arginine
P2	204.1229	0.20	$C_9H_{18}O_4N$	-0.86	145.0494 (81), 85.0282 (100)	Acetyl carnitine
P3	104.1069	0.22	$C_5H_{14}ON$	-1.35	87.0439 (100), 86.0599 (55)	Choline
P4	118.0861	0.23	$C_5H_{12}O_2N$	-1.60	72.0806 (100)	Glycine betaine
P5	132.1018	0.39	$C_6H_{14}O_2N$	-0.43	86.0961 (100)	(Iso-)Leucine
P6	166.0863	0.60	$C_9H_{12}O_2N$	-0.87	120.0805 (100)	Phenylalanine
P7	252.1955	6.49	$C_{15}H_{26}O_2N$	0.32	234.1850 (100)	Pyrrolidone derivative
P8	270.2063	6.67	$C_{15}H_{28}O_3N$	-0.15	292.1879 (100), 252.1954 (100), 234.1850 (68)	3-(6-hydroxy, 2,6-dimethyl-octanonyl)-5-methylpyrrolidin-2-one (**3.10**)
P9	252.1955	7.40	$C_{15}N_{26}O_2N$	-0.02	292.1879 (100), 252.1954 (100), 234.1850 (68)	Pyrrolidone derivative
P10	315.0862	7.56	$C_{17}H_{15}O_6$	-0.24	300.0624 (100), 282.0519 (94)	Colletoquinone A
P11	329.1015	8.41	$C_{18}H_{17}O_6$	-1.41	314.0780 (40), 296.0674 (100), 285.0757 (32), 268.0726 (63)	Colletoquinone B
P12	254.2110	9.20	$C_{15}N_{28}O_2N$	-1.92	236.2002 (100), 211.2051 (9)	3-(2,6-dimethyl-octanonyl)-5-methylpyrrolidin-2-one (**3.1**)
P13	254.2109	9.26	$C_{15}N_{28}O_2N$	-2.10	236.2002 (100), 211.2051 (9)	3-(2,6-dimethyl-octanonyl)-5-methylpyrrolidin-2-one (**3.1**)
P14	520.3394	9.65	$C_{29}H_{42}O_2N_7$	-0.18	502.3283 (63), 184.0731 (100)	Unknown
P15	520.3391	9.81	$C_{29}H_{42}O_2N_7$	-0.77	502.3283 (63), 184.0731 (100)	Unknown
P16	1009.5317	9.84	$C_{46}H_{75}O_{16}N_9$	-0.88	979.5223 (20), 879.4806 (12)	Unknown
P17	517.3628	9.88	$C_{30}H_{49}O_5N_2$	-1.56	499.325 (100), 481.3420 (13), 347.2326 (10)	Unknown
P18	517.3549	10.11	$C_{27}H_{49}O_8N_4$	0.66	539.3445 (100), 514.3483 (55), 496.3380 (32), 344.1826 (30), 306.1671 (29), 289.1639 (26)	Unknown
P19	522.3550	10.22	$C_{29}H_{44}O_2N_7$	-0.23	504.3445 (100), 184.0733 (64)	Unknown
P20	555.3393	10.23	$C_{27}H_{47}O_8N_4$	0.81	537.3289 (28), 512.3336	Unknown

No	[M+H]$^+$	Rt (min)	Molecular formula	Δ ppm	Fragments (Intensity)	Annotation/ Compound Class
					(39), 494.3231 (17), 304.1511 (14)	
P21	501.3682	10.45	$C_{30}H_{49}O_4N_2$	-0.99	347.2323 (100), 329.2218 (6), 252.1955 (6)	Unknown
P22	517.3630	10.52	$C_{30}H_{49}O_5N_2$	-1.20	499.325 (100), 481.3420 (13), 347.2326 (10)	Unknown
P23	501.3678	11.38	$C_{30}H_{49}O_4N_2$	-1.82	347.2323 (100), 329.2218 (6), 252.1955 (6)	Unknown

Figure S 210 UHPLC-HR-ESI-MS peak list of compounds annotated from *C. graminicola* cultivated in medium 5 (myzelium).

No	[M+H]$^+$	Rt (min)	Molecular formula	Δ ppm	Fragments (Intensity)	Annotation/ Compound Class
P1	252.1221	4.18	$C_{11}H_{16}O_3N_4$	1.69	206.1168 (100), 192.1012 (77)	Unknown
P2	485.2586	4.31	$C_{20}H_{35}O_7N_7$	-1.31	467.2483 (28), 355.1959 (100), 243.1322 (8)	Unknown
P3	258.1149	6.36	$C_{18}H_{14}N_2$	-0.03	240.1043 (100)	Unknown
P4	252.1952	6.67	$C_{15}H_{26}O_2N$	-2.44	234.1846 (100), 178.1222 (2)	Pyrrolidone derivative
P5	425.2857	12.02	$C_{22}H_{39}O_5N_3$	-4.52	-	Unknown

Figure S 211 UHPLC-HR-ESI-MS peak list of compounds annotated in the culture filtrate of *C. graminicola* cultivated in medium 1.

No	[M+H]$^+$	Rt (min)	Molecular formula	Δ ppm	Fragments (Intensity)	Annotation/ Compound Class
P1	252.1223	4.18	$C_{11}H_{16}O_3N_4$	2.41	206.1168 (100), 192.1012 (77)	Unknown
P2	485.2586	4.31	$C_{20}H_{35}O_7N_7$	-1.31	467.2483 (28), 355.1959 (100), 243.1322 (8)	Unknown
P3	258.1149	6.36	$C_{18}H_{14}N_2$	-0.03	240.1043 (100)	Unknown
P4	351.0624	6.88	$C_{17}H_{16}O_6Cl$	-1.66	336.0392 (76), 334.0599 (69), 333.0522 (38), 319.0366 (100), 315.0861 (65), 305.0573 (15), 255.0648 (5)	Colletoanthrone
P5	272.2216	8.15	$C_{15}H_{30}O_3N$	-2.24	254.2108 (100)	Unknown

Figure S 212 UHPLC-HR-ESI-MS peak list of compounds annotated in the culture filtrate of *C. graminicola* cultivated in medium 2.

No	[M+H]$^+$	Rt (min)	Molecular formula	Δ ppm	Fragments (Intensity)	Annotation/ Compound Class
P1	252.1223	4.18	C$_{11}$H$_{16}$O$_3$N$_4$	2.41	206.1168 (100), 192.1012 (77)	Unknown
P2	727.3860	4.63	C$_{45}$H$_{51}$O$_5$N$_4$	-0.03	709.3757 (100), 691.3655 (16), 615.3341 (56), 597.3195 (90), 485.2608 (34), 467.2447 (34), 355.1955 (59), 243.1322 (19)	Unknown
P3	741.4014	4.68	C$_{46}$H$_{53}$O$_5$N$_4$	0.44	723.3909 (38), 629.3494 (62), 611.3375 (98), 596.3282 (100), 467.2495 (18), 369.2015 (32), 257.1491 (11)	Unknown
P4	453.3423	5.24	C$_{26}$H$_{47}$O$_5$N	-5.79	435.3315 (100), 336.2271 (8), 209.1643 (10)	Unknown
P5	443.0966	5.51	C$_{22}$H$_{19}$O$_{10}$	-2.31	425.0851 (14), 397.0903 (10), 381.0955 (100), 341.0643 (6)	Unknown
P6	425.0857	6.01	C$_{22}$H$_{17}$O$_9$	-1.24	367.0439 (6), 341.0647 (100)	Unknown
P7	252.1951	6.49	C$_{15}$H$_{26}$O$_2$N	-1.96	-	Pyrrolidone derivative
P8	445.0676	6.57	C$_{26}$H$_{11}$O$_5$N$_3$	-3.94	409.0909 (100)	Unknown
P9	252.1953	6.68	C$_{15}$H$_{26}$O$_2$N	-2.19	-	Pyrrolidone derivative
P10	268.1902	6.75	C$_{15}$H$_{26}$O$_3$N	-1.77	250.1795 (100), 232.1690 (50), 208.1691 (17)	Pyrrolidone derivative
P11	351.0623	6.88	C$_{17}$H$_{16}$O$_6$Cl	-2.00	336.0390 (76), 334.0599 (69), 333.0519 (38), 319.0363 (100), 315.0858 (65), 305.0570 (15), 255.0645 (5)	Colletoanthrone
P12	407.0752	6.97	C$_{22}$H$_{15}$O$_8$	-2.24	389.0653 (100), 347.0547 (10)	Unknown
P13	195.1012	7.40	C$_{11}$H$_{15}$O$_3$	-1.84	177.0907 (6), 163.0753 (22), 149.0959 (10), 135.0803 (45), 107.0854 (100)	Colletopyrone
P14	274.2369	7.91	C$_{15}$H$_{32}$O$_3$N	-2.77	256.2263 (100)	Pyrrolidone derivative
P15	343.2947	8.08	C$_{19}$H$_{39}$O$_3$N$_2$	-2.36	240.2315 (100)	Unknown
P16	272.2213	8.15	C$_{15}$H$_{30}$O$_3$N	-2.61	254.2111 (100)	Pyrrolidone derivative

P17	371.3259	9.02	$C_{21}H_{43}O_3N_2$	1.13	268.2626 (100)	Unknown
P18	399.3569	9.96	$C_{23}N_{47}O_3N_2$	0.39	296.2942 (100)	Unknown
P19	427.3883	10.90	$C_{25}H_{51}O_3N_2$	0.61	324,3251 (100)	Unknown
P20	425.2864	12.02	$C_{22}H_{39}O_5N_{31}$	-4.80	$C_{22}H_{39}O_5N_3$	Unknown

Figure S 213 UHPLC-HR-ESI-MS peak list of compounds annotated in the culture filtrate of *C. graminicola* cultivated in medium 3.

No	$[M+H]^+$	Rt (min)	Molecular formula	Δ ppm	Fragments (Intensity)	Annotation/ Compound Class
P1	252.1223	4.18	$C_{11}H_{16}O_3N_4$	2.41	206.1169 (100), 192.1013 (77)	Unknown
P2	485.2584	4.31	$C_{20}H_{35}O_7N_7$	-1.83	467.2485 (28), 355.1962 (100), 243.1322 (8)	Unknown
P3	727.3849	4.63	$C_{45}H_{51}O_5N_4$	-0.69	709.3743 (100), 691.3655 (16), 615.3331 (56), 597.3187 (90), 485.2608 (34), 467.2444 (34), 355.1950 (59), 243.1318 (19)	Unknown
P4	741.3995	4.67	$C_{46}H_{53}O_5N_4$	-2.11	723.3912 (38), 629.3497 (62), 611.3375 (98), 596.3282 (100), 467.2499 (18), 369.2016 (32), 257.1496 (11)	Unknown
P5	282.2784	11.93	$C_{18}H_{36}NO$	2.17	265.2518 (100), 247.2413 (76)	Unknown
P6	425.2855	12.02	$C_{22}H_{39}O_5N_3$	-6.97	281.1720 (6)	Unknown

Figure S 214 UHPLC-HR-ESI-MS peak list of compounds annotated in the culture filtrate of *C. graminicola* cultivated in medium 4.

No	[M+H]$^+$	Rt (min)	Molecular formula	Δ ppm	Fragments (Intensity)	Annotation/ Compound Class
P1	252.1951	6.50	$C_{15}H_{26}O_2N$	-2.76	234.1834 (100)	Pyrrolidone derivative
P2	252.1952	6.54	$C_{15}H_{26}O_2N$	-2.44	234.1834 (100)	Pyrrolidone derivative
P3	268.1902	6.62	$C_{15}H_{26}O_3N$	-1.99	250.1793 (100), 232.1689 (50), 208.1690 (18), 178.1221 (10)	Pyrrolidone derivative
P4	252.1951	6.67	$C_{15}H_{26}O_2N$	-2.92	234.1837 (100)	Pyrrolidone derivative
P5	268.1900	6.75	$C_{15}H_{26}O_3N$	2.44	250.1793 (100), 232.1689 (50), 208.1690 (18), 178.1221 (10)	Pyrrolidone derivative
P6	502.3106	7.49	$C_{24}H_{44}O_8N_3$	-3.41	484.3003 (100), 474.3158 (30), 385.1958 (22), 276.1434 (58), 262.1278 (40)	Unknown

Figure S 215 UHPLC-HR-ESI-MS peak list of compounds annotated in the culture filtrate of *C. graminicola* cultivated in medium 5.

Declaration on author contributions

Chapter 3:   **Isolation of phytotoxic compounds from *Colletotrichum graminicola* cultivated in HMG medium**

Lea M. Schmitz, Dana Kibbhen, Erik Siefke, Dilara Balci, Mehdi Davari, Holger B. Deising, René Csuk and Norbert Arnold.

In this work, LMS developed the methods, planned, and performed the isolation and structure elucidation of secondary metabolites. DK and ES contributed to the isolation of phytotoxic compounds. Parts of this work are published in the diploma theses of DK and ES. HBD provided the fungal strain. DB and MD performed ECD calculations. LMS wrote the manuscript. The project was planned, coordinated, and supervised by HBD, RC and NA. The work was edited by RC and NA.

Chapter 4:   **Isolation of phytotoxic compounds from *Colletotrichum graminicola* cultivated in CM medium**

Lea M. Schmitz, Noelle Raschke, Dilara Balci, Mehdi Davari, Wolfgang Brandt, Christoph Wagner, Holger B. Deising, René Csuk and Norbert Arnold.

In this work, LMS developed the methods, planned, and performed the isolation and structure elucidation of secondary metabolites. NR contributed to the isolation of phytotoxic compounds. Parts of this work are published in the diploma thesis of NR. HBD provided the fungal strain. DB, MD and WB performed ECD calculations. X-ray measurements were performed by CW. LMS wrote the manuscript. The project was planned, coordinated, and supervised by HBD, RC and NA. The work was edited by RC and NA.

Chapter 5:   **Phytotoxic sulfonamide from *Colletotrichum graminicola*: isolation and synthesis**

Lea M. Schmitz, Holger B. Deising, René Csuk and Norbert Arnold.

In this work, LMS performed the isolation, structure elucidation, synthesis, activity testing and writing of the manuscript. HBD, RC and NA acted as supervisors of the project. The work was edited by RC and NA.

Chapter 6:   **Studies on quantitative structure-activity relationship (QSAR) of phytotoxic sulfonamides**

Lea M. Schmitz, Toni Denner, Holger B. Deising, René Csuk and Norbert Arnold.

LMS performed the testing of bioactivity, interpretation, and visualization of the results, and wrote the manuscript. TD performed the synthesis of all sulfonamide derivatives. The project was supervised by HBD, RC and NA. Study design and editing was done by RC and NA.

Chapter 7:   **LC-HR-ESI-MS based comparison of extracts of *Colletotrichum graminicola* grown in different cultivation media**

Lea M. Schmitz, Renata Amorim, Holger B. Deising, René Csuk and Norbert Arnold.

LMS planned and performed the experiments, data interpretation, data visualization, and wrote the manuscript. HBD provided the fungal strain. RA cultivated the fungus. The project was supervised by HBD, RC and NA. Editing was performed by RC and NA

Curriculum vitae

Personal details

Name	Lea Maleen Schmitz
Nationality	German

Formal education

2005 – 2013	Albertus-Magnus Gymnasium, Viersen
	Degree: General qualification for University entrance
2013 – 2018	Study of Food Chemistry, Martin-Luther University Halle-Wittenberg, Halle (Saale)
	Graduation as Diplom food chemist (Dipl.-LMChem.)
	Title: "Synergistisch antioxidative Effekte von Carotinoiden während der Lipidperoxidation"
	Supervisor: Prof. Dr. Marcus Glomb, Dr. Thomas Heymann
2018 – 2019	Vocational training as a state-certified food chemist at the State Office for Consumer Protection Saxony-Anhalt (LAV), Halle (Saale)
	Degree: State-certified food chemist
2019 – present	PhD candidate (Dr. rer. nat.), Leibniz Institute of Plant Biochemistry, Department of Bioorganic Chemistry, Halle (Saale)
	Title: "Weed control by biological compounds identified in necrotizing plant pathogenic fungi"
	Supervisor: Prof. Dr. René Csuk
	Mentor: Dr. Norbert Arnold

Work experience:

09/2019 – present	Research Assistant, Leibniz Institute of Plant Biochemistry, Department of Bioorganic Chemistry, Halle (Saale)

Publications

Publications in peer-reviewed journals

Heymann, T.; **Schmitz, L.M.**; Lange, J.; Glomb, M.A., Influence of β-carotene and lycopene on oxidation of ethyl linoleate in one and disperse phase model systems, *J. Agric. Food Chem.* **2020**, *68*, 2747-2756, doi: 10.1021/acs.jafc.9b07862.

Deising, H.B.; Amorim, R.; De Oliveira Silva, A.; Raschke, A.; Eisermann, I.; Wirsel, S.G.R.; Csuk, R.; **Schmitz, L.M**.; Arnold, N., Antagonistic microorganisms in plant protection: Consumers' friends or foes?, *Modern fungicides and antifungal compounds* IX, Deising, H.B.; Fraaije, B.; Mehl, A.; Oerke, E.C.; Sierotzki, H.; Stammler, G. (eds.), DPG, Braunschweig, **2020**, ISBN: 978-3-941261-16-7.

Kappen, J.; Manurung, J.; Fuchs, T.; Vemulapalli, S.P.B.; **Schmitz, L.M.**; Frolov, A.; Agusta, A.; Muellner-Riehl, A.N.; Griesinger, C.; Franke, K.; Wessjohann, L.A., Challenging structure elucidation of lumnitzeralactone, an ellagic acid derivative from the mangrove *Lumnitzera racemosa, Mar. Drugs* **2023**, *21*, 242, doi: 10.3390/md21040242.

In peer-review process:
Lam, Y.T.H.; **Schmitz, L.**; Huymann, L.; Dhar, D.; Morgan, I.; Rennert, R.; Davari, M.; Peitner, U.; Palfner, G.; Arnold, N., *Cortinarius steglichii*, a taxonomical and chemical novelty from Chile, *Mycol. Progess*.

Patent
Schmitz, L., Denner, T.C., Amorim, R., Deising, H., Csuk, R., Arnold, N., Pilzbasierte Biozide. European Patent application (pending).

Oral presentations
Schmitz, L.M., Phytopathogenic fungi as a source of new potential herbicides, Plant science students conference (PSSC), Gatersleben, 04th July 2023.

Schmitz, L.M., Phytopathogenic fungi as a source of new potential herbicides, 60. Naturstofftreffen, Würzburg, 06th October 2023.

Poster presentations
Schmitz, L.M.; Kibbhen, D.; Arnold, N.; Deising, H.B.; Csuk, R.; Wessjohann, L.A., Phytotoxic compounds from fungi, Plant science students conference (PSSC), online, 14th – 17th June 2022.

Eidesstattliche Erklärung

Ich erkläre, dass ich die vorliegende, unter der Betreuung von Herrn Prof. Dr. rer. nat. René Csuk und Herrn Dr. rer. nat. Norbert Arnold, angefertigte wissenschaftliche Abschlussarbeit selbstständig verfasst habe.

Andere als die angegebenen Hilfsmittel wurden von mir nicht benutzt. Alle angeführten Zitate wurden kenntlich gemacht.

Halle (Saale), den 20.11.2024

Lea Schmitz